

International conference

Diagnostika '13

Conference on Diagnostics in Electrical Engineering CDEE 2013

held by
**The Department of Technologies and Measurement, Section of
Electrotechnology of the Faculty of Electrical Engineering, University
of West Bohemia in Pilsen.**

Parkhotel Pilsen, September 2 – 4, 2013

ISBN 978-80-261-0210-6

Published by University of West Bohemia

Conference, of which proceedings you have just opened, is 11th in line of Diagnostics conferences, which became part of our professional life.

Diagnostika '13

Following the tradition of the previous conferences the main aim of the conference is to interchange the experiences and present the results of the scientific activities of participants. Objective of the conference is to create environment for creating new, and deepen current contacts of the colleagues working in the area of diagnostics of electrical appliances, electrical material science and other field of electrotechnics.

This conference is a priority action in the organizing activities of our Department - Department of Technologies and Measurement, Faculty of Electrical Engineering, University of West Bohemia in Pilsen, Czech Republic.

Conference is traditionally based on the cooperation of our department with companies working in the area of electrical engineering. This year is therefore in its program included traditional block entitled "Cooperation in Research". This section is focused on presentation of R&D of BRUSH SEM s. r. o., Pilsen, COGEBI a. s., Tábor, ČEPS a. s., Prague, ETD Transformátory a. s., Pilsen, ORGREZ a. s., Brno, 1.SERVIS-ENERGO s. r. o., Pilsen, ŠKODA Electric s. r. o., Pilsen, VÚKI a. s. Bratislava, The program of the conference contains the presentations of the companies.

Printed proceedings (ISBN 978-80-261-0210-6) contain accepted papers for the conference. All papers were reviewed by International Technical Program Committee.

DIAGNOSTIKA `13 is held in Parkhotel Pilsen, in Pilsen Czech Republic. We believe that once again all of you who have accepted our invitation to attend the conference DIAGNOSTIKA `13, will find in the program something that interests you, what you will find a new, interesting, helpful and inspiring in your future activities. We expect this year conference as creative and friendly as in the last years.



Doc. Ing. Pavel Trnka, Ph.D.
Executive chair



prof. Ing. Václav Mentlík, CSc.
Honorable chair

INTERNATIONAL TECHNICAL PROGRAM COMMITTEE

prof. Ing. Milan Dado, Ph.D., Faculty of Electrical Engineering, University of Žilina, Slovakia
Rainer Haller, Em. Univ. Prof. Dipl. Ing. Dr. techn., Regensburg University of Applied Sciences, Germany
Stefan Kornhuber, Dr., ABB AG, Germany
Doc. Ing. Jozef Kuchta CSc., EVPÚ a.s., Slovakia
Doc. Ing. Pavel Mach, CSc., Faculty of Electrical Engineering, Czech Technical University in Prague, Czech Republic
Michael Muhr, Em. Univ. Prof. Dipl. Ing. Dr. techn. Dr.h.c., Institute of High Voltage Engineering and System Management, Technical University Graz, Austria
prof. Ing. Alena Pietriková, CSc. Faculty of Electrical Engineering and Informatics, Technical University of Košice, Slovakia
Doc. Ing. Radek Polanský, Ph.D., Faculty of Electrical Engineering, University of West Bohemia, Czech Republic
Ing. Dr. Ladislav Sobotka, Škoda Electric a.s., Czech Republic
Anurag Srivastava, Ass. Prof., Director, School of Electrical Engineering and Computer Science, Washington State University, USA
Doc. Ing. Pavel Trnka, Ph.D. , Faculty of Electrical Engineering, University of West Bohemia, Czech Republic
Christian Weindl, PD Dr.-Ing. habil., Lehrstuhl für Elektrische Energiesysteme, Friedrich-Alexander-Universität Erlangen-Nürnberg, Germany
Andreas Welsch, Prof. Dr.-Ing., Regensburg University of Applied Sciences, Germany

INTERNATIONAL STEERING COMMITTEE

Doc. Ing. Eva Kučerová, CSc., University of West Bohemia, Pilsen, Czech Republic
Pavel Kupilík, Kabelovna KABEX, a.s., Holýšov, Czech Republic
Doc. Ing. Jaroslav Lelák, Ph.D., Slovak University of Technology in Bratislava, Slovakia
Ing. Pavel Lukeš, MSc., Brush SEM s.r.o., Czech Republic
Ing. Jiří Málek, COGEBI a. s., Tábor, Czech Republic
prof. Ing. Karol Marton, DrSc., The Technical University of Kosice, Slovakia
prof. Ing. Václav Mentlík, CSc., University of West Bohemia, Pilsen, Czech Republic
prof. Ing. Ján Michalík, Ph.D., EVPÚ a.s., Nová Dubnica, Slovakia
Pavel Novák, I. SERVIS-ENERGO s.r.o., Pilsen, Czech Republic
Ing. František Říšský, ETD Transformátory s. r. o., Pilsen, Czech Republic
Ing. Lumír Šašek, CSc., ETD Transformátory s. r. o., Pilsen, Czech Republic
Ing. Jaromír Šilhánek, Škoda Electric s. r. o., Pilsen, Czech Republic
Ing. Juraj Šmatlík, BEZ Transformátory, a.s., Bratislava, Slovakia
Ing. Jiří Velek, ČEPS a.s., Prague, Czech republic
Ing. Otto Verbich, Ph.D., VÚKI a.s., Bratislava, Slovakia

CONFERENCE CHAIR

Honorable

Prof. Ing. Václav Mentlík, CSc.

Executive

doc. Ing. Pavel Trnka, Ph.D.

ORGANIZING COMMITTEE

Ing. Josef Pihera, Ph.D.
Ing. Pavel Prosr, Ph.D.

Table of contents

Invited lecture

Reliability aspects of lead-free solders applied in electronics	9
<i>A. Pietrikova</i>	

Laboratory Methods of Diagnostics

Diagnostics of Electrical Properties of Electrically Conductive Adhesives	14
<i>P. Mach, M. Plaček, J. Kolář, D. Bušek</i>	
Electrically Conductive Adhesives Usability for Power Electronics Packaging	18
<i>P. Mach</i>	
The use of artificial neural networks in SW STATISTICA for classification analysis of samples that have passed mechanical tests	22
<i>L. Kupka, O. Tůmová, T. Langhammer</i>	
Power devices cooling using heat pipes	26
<i>R. Janiš, J. Kuba</i>	
The proposition of low frequency filter in electrical machines diagnostics	30
<i>J. Poliak, D. Korenčiak</i>	
Analysis model of transformer by PDC method	33
<i>D. Korenčiak, M. Gutten, M. Kučera, T. N. Koltunowicz</i>	
Effect of Asymetry on Reliability of a Distribution Transformer in Star-Delta Configuration	37
<i>M. Kučera, M. Šebök, D. Korenčiak, P. Zhukowski</i>	
Comparison of accuracy of precision LCR meter during dielectric properties measurement	41
<i>J. Ulrych, R. Polanský, J. Pihera, A. Voborník</i>	

On-Site Testing of Electrical Appliances

Utilization of digital protection and terminal communication for power plant electrical equipment testing	45
<i>O. Mareček, M. Kaška</i>	
Application of SFRA method to the transformer with Yz winding connection without a neutral terminal	49
<i>M. Brandt, R. Seewald, J. Michalík</i>	
Reliability of Various PWB Materials in High Frequency Area	53
<i>A. Pietrikova, T. Rovensky, K. Ruman, J. Gamec</i>	
In-situ Assessment and Monitoring of PV Systems Operation	57
<i>M. Váry, E. Firický, M. Perný, V. Šály, J. Packa</i>	

Electrical Insulation Properties and Structural Changes

Influence of humidity on glass transition of thermosetting epoxy laminate	62
<i>P. Prosr</i>	

Comparison of temperature limits of cable sheaths measured by Dynamic Thermo Mechanical Analysis <i>M. Pinkerová, M. Bartůňková, R. Polanský</i>	66
HFFR Power Cables Testing and Certification <i>R. Nejd, V. Mentlík</i>	70
Diagnostics of Alternative Insulating Liquids Using Monitoring the Thermal Characteristics <i>J. Souček, M. Širůček, P. Trnka</i>	74
Partial discharge behaviour of special shaped protrusions in different gases and gas mixtures <i>A. F.X. Welsch, S. Irlbacher</i>	78
Study of electrical properties of plant oils and their compounds derived from plants <i>M. Spohner, K. Liedermann, M. Klampar</i>	82
Dielectric measurement of a nanocomposite material at an early stage of accelerated ageing <i>M. Klampar, K. Liedermann</i>	86
Effect of moisture on the insulation condition of twisted coils <i>B. Kotlárík, R. Vaňková, Z. Filová</i>	90
Influence of Firing Process on LTCC Characteristic <i>A. Pietrikova, J. Durisin, I. Vehec</i>	94
Comparison of basic properties of insulating liquids for electrical purposes <i>J. Brázdil, J. Sládek</i>	98
 Other Diagnostic Methods	
Stator Core Fault Diagnostics of Turbo Generators <i>V. Zábranský, O. Tůmová</i>	102
AC voltage tests on production lengths of LV cables <i>P. Voda</i>	106
Oxidative degradation of insulating oils <i>J. Černý, N. Ladyka</i>	110
Sustainability and performance of technical systems <i>P. Ponický, V. Zamarský</i>	113
Application of the combined voltage impedance spectroscopy for insulation diagnostics <i>V. Ďurman, J. Lelák, V. Šály</i>	117
 Theories, Methods and Models	
Non-statistical measurement uncertainties <i>T. Panc, O. Tůmová, Z. Mačičková</i>	120
Evaluation of mechanical parameters by the software for quality control <i>M. Růžková, O. Tůmová</i>	124
Mathematical analysis of transformer insulation state <i>M. Gutten, D. Korenčiak, M. Šebök, M. Bartłomiejczyk</i>	128

Analysis of Ignition Systems	132
<i>M. Šebök, M. Gutten, L. Ostrica, D. Korenčiak</i>	
Acoustic investigation of magnetic fluid based on transformer oil TECHNOL	136
<i>J. Kúdelčík, P. Bury, M. Šebök</i>	
Possibility of using simulation tools for the development of new nanocomposite materials	140
<i>M. Čermák, R. Polanský</i>	
Implementation of Lean management for diagnostic processes	144
<i>J. Šimota, K. Bandžáková, J. Tupa</i>	
The influence of nano- and micro- fillers on heat transfer in electrical insulation system	148
<i>T. Tomášková, M. Svoboda, P. Trnka</i>	
PD Series Prediction Based on Surface Charge Distribution Measuring by Matrix Method	152
<i>P.N.Bondarenko, O.A.Emelyanov, A.P.Gorlov, J.V.Shabanov, M.V.Shemet, I.N.Sorokoletov</i>	
Influence of technological factors on thermal and electrical properties of insulation systems for large rotating machines	156
<i>A. Bezborodov, T. Shikova</i>	
Condition Monitoring	
Insulating liquids without negative impact on the environment	160
<i>V. Mentlik, P. Trnka, J. Černý</i>	
Influence of the Electrical and Environmental Test-Conditions on the Characteristic Parameters of Return Voltage Curve	164
<i>I. Mladenovic, Th. Scharrer, Ch. Weindl</i>	
Comprehensive Approach to Management of Service Lifetime of Power Generation Equipment	168
<i>P. Cvešpr</i>	
Detection and Visualisation of SF ₆	172
<i>V. Straka</i>	
Online Hot Spot Calculation in Power Transformers	176
<i>M. Svoboda, P. Trnka</i>	
Temperature Correlation of C and Tg δ Based on Real Response of Measured Object	180
<i>V. Straka</i>	
Experiences in Online Condition Monitoring System for Power Transformers	184
<i>B. Dolata, J. Dončuk, F. Mamutov, J. Velek</i>	
Intelligent measuring diagnostic system for estimation of operational state of high voltage rotating and non-rotating electrical machines	189
<i>P. Ryška, P. Justiz</i>	
Transformer Fleet Management as Approach for Risk Based Asset Management	193
<i>S. Kornhuber, O. Kouzmine, S. Schreiter</i>	
Electric Machines and Devices	
Influence of end corona protection on dissipation factor	198
<i>J. Stauber, T. Birner, J. Bezděkovský, P. Krupauer P.</i>	

Aspects of partial discharge behaviour – voltage dependence	202
<i>P. Mráz, V. Mentlík, J. Pihera, R. Haller</i>	
Electrical field distribution along stator bars in dependence of lengths semiconductive stress grading tapes	207
<i>O. Krpal, E. Kučerová</i>	
VPI process optimization	211
<i>M. Rok, R. Zahradníček, T. Barták, L. Kousal</i>	
DC Diagnostics of Solar Cell Parameters	215
<i>O. Szabó, Milan Perný, J. Lelák, V. Šály, M. Váry, S. Flickyngerová, E. Vavrinský</i>	

Reliability aspects of lead-free solders applied in electronics

Alena Pietrikova

Technical University of Kosice, Slovakia, <http://www.tuke.sk/>
tel: +421 55 602 3194, email: alena.pietrikova@tuke.sk

Abstract— This paper gives its reader a review of reliability aspects of lead-free solders applied in electronics and provides information on possible developments and suitability for the SAC solder usage in electronic devices.

Keywords— Lead-Free, alloys, Tin-Silver-Copper, reliability

I. INTRODUCTION

In 2006, the European Union Restriction of Hazardous Substances Directive has revolutionized the use of electronic packaging materials: Tin-lead solders were replaced with lead-free solders. Exemptions from the substitution requirement were permitted if it is not possible from scientific and technical point of view or where scientific evidence demonstrates that their use does not result in any significant risk to health or the environment. Some already exempted products are as follows:

- Pb in high melting temperature type solders (i.e. tin-lead solder alloys containing more than 85% Pb),
- lead in glass in electronic components,
- lead in piezoelectric devices,
- lead in solders for network infrastructure equipment for switching, signalling, transmission as well as network management for telecommunication.

Experience of manufacturers in the field of lead-free alloys from this time help us for modelling and predicting the reliability of lead-free solder. Sn-Ag-Cu (SAC) solders are widely used as lead-free replacements but their coarse microstructure and formation of hard and brittle intermetallic compounds (IMCs) have limited their use in high temperature applications. From the perspective of manufacturability, cost, availability, and reliability, SAC series solder alloys have become the standard for lead-free applications. SAC alloy composition (with or without the addition of a fourth element) has also been chosen to be the benchmark, with SnPb being the baseline, for testing any other alloys to be included in the listing to be provided to the industry. Wettability or solderability is an important parameter in characterizing these solders alloys. Important idea is that smaller solder joints are generally impacted more by the thickness and morphology of intermetallic compounds (IMCs) and the composition of the bulk solder alloy than larger solder joints surface tensions, wetting forces and contact angles measurements were made at 250°C and 260°C. Extensive knowledge and understanding of the mechanical behaviour of lead-free solders is required to satisfy the demands of structural

reliability. Higher processing temperatures and compatibility with lead bearing finishes is typical for this type of alloys. Metals costs for this alloy are about 2.2 to 2.7 times that of SnPb eutectic at current market values. Process considerations must be addressed with this alloy, which has a higher melting temperature than most SAC alloys. At current market values, this alloy is 1.5 times more expensive than SnPb eutectic as well. As the electronics industry begins to focus upon SAC family of alloys as a viable replacement for tin-lead solders, research needs to be done to determine if any particular alloy is best suited for the broadest range of applications.

SAC series of alloys have a great deal of positive response from various industry consortia and organizations in recent years and the majority of manufacturers plan on implementing one of these alloys. The most popular of SAC alloys are Sn96.5/Ag3.0/Cu0.5, Sn95.5/Ag3.8/Cu0.7 and Sn95.5/Ag4.0/Cu0.5. Tab. 1 shows solder alloys used most often by companies in electronics.

TABLE I THE MOST OFTEN USED SOLDER ALLOYS

Solders	Melting Range (°C)	Industry	Company
SnAg	221 - 226	Automotive	Visteon (Ford)
SnAgBi	206 - 213	Military/Aerospace	Panasonic
		Consumer	Hitachi
SnAgBiCu		Military/Aerospace	Panasonic
SnAgBiCu Ge		Consumer	Sony
SnAgBiX	206 - 213	Consumer	Panasonic
SnAgCu	217	Automotive	Panasonic
		Telecommunications	Nokia
			Nortel
			Panasonic
			Toshiba
SnBi	138	Consumer	Panasonic
SnCu	227	Consumer	Panasonic
		Telecommunications	Nortel
SnZn	198.5	Consumer	NEC
			Panasonic
			Toshiba

II RELIABILITY OF LEAD-FREE SOLDER JOINTS

Solder joints perform three functions: electrical, mechanical, and thermal. The successful functioning of electronic products depends on the reliable joints provided by these tiny and numerous solder joints, over the life of

the product, under vastly different use conditions. The physics of failure (directly related to reliability) represents a critical topic still under intense investigation for lead-free solders. The reliability of the joints for a PWB assembly depends on the reliability of the components, the PWB, and the solder joints. Lead-free solders based on SAC alloys (with melting temperature usually under 220°C) are extensively used as solder materials in the electronic industry. Numerous studies have revealed that additions of transition metals in SAC alloys result generally in improvement of mechanical properties and important microstructure modification [1, 7]. Solder joint microstructure of final electronic devices is generally influenced by applied solder alloy, process of soldering, composition of soldered materials and utility of the final device. Each of the four factors has a significant impact on the phase transformations in solder joints, consequently influencing their properties. Solder joint formation is based on melting of the solder alloy, reaction of the alloy with soldered surface, and solidification of the solder alloy. Microstructure of the most widespread SAC305 off-eutectic alloy dominantly consists of large β -Sn dendritic crystals ($\approx 10^1$ - $10^2 \mu\text{m}$). In interdendritic regions, crystal phases are excluded from eutectics, i.e. again β -Sn and fine Ag_3Sn precipitates (≈ 1 - $10^1 \mu\text{m}$) [5, 6].

The trend of miniaturization, light weight, high speed and multifunction are common in electronic assemblies, especially, for electronic products. In particular, board-level solder joint reliability, in term of both mechanical (e.g. drop impact) and thermo-mechanical (e.g. thermal cycling) loads is of great concern for electronic products. In electronic products, the transition to lead-free solder happened to coincide with a dramatic increase.

Today, the reliability becomes one of the most important parameters of any successful product. Most companies understand that the reliability must be built in the design phase and then during the whole manufacturing process. The reliability issues must be taken into account in the design of the process/product (the so-called design for reliability), with a special care for thermal design (because the temperature is the main enemy of a good reliability) and also during the manufacturing (process reliability). Special attention must be given to screening, the last step of the manufacturing process.

This is highlighted by the fact that for the reliability, not only the number of elements of the first series that fail is important, but also the deviations of their characteristics. It is necessary to know for what time period the initial characteristics are preserved, how big the time variation of the deviation is, what are the percentages of failures during the first operation hours, what is the failure speed for the operation time, what is the shape of the survival function, and finally, what statistical distribution can it be associated with. All these characteristics are represented in the Fig. 1. [1].

One must be aware that the user can have an important contribution to shorten or to prolong the lifetime of the component. Previously, the system designers imposed drastic quality conditions, trying to acquire a higher

certitude, so that the constructive elements satisfy the specifications of the certificate of guarantee. Today, the designers demand acceptable tests completing the quality inspection.

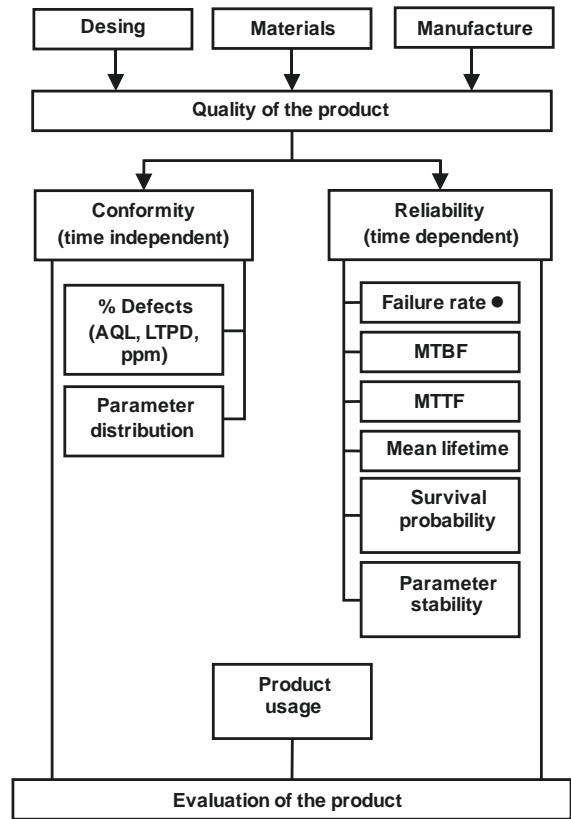


Fig. 1. The elements of product quality (AQL - Acceptable Quality Level, LTPD - Lot Tolerance Percent Defective, MTBF - Mean Time Between Failures, MTTF - Mean Time to Failure)

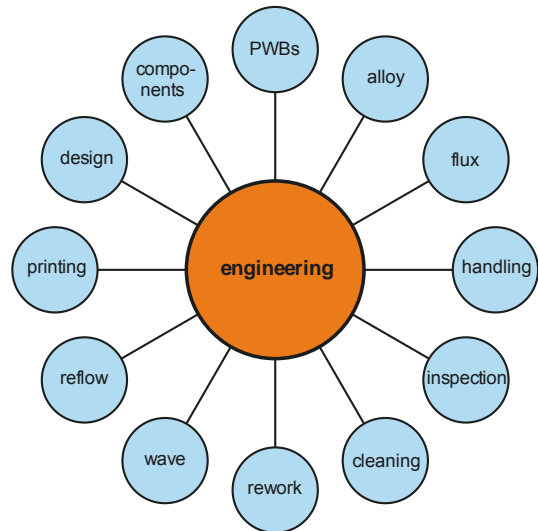


Fig. 2. Parameters influencing reliable lead-free electronics assembly

This is requested to ascertain the manufacturer's specifications are valid and applicable initially, at input inspections, but also later, after a longer operation time. In the planning phase or in the design phase of a new

product, still a maximization of the probability that the desired product will be in the limits of the general planned costs must be taken into account.

Lead-free electronics assembly is achievable, but it requires a strong understanding of the changes required by each person involved in the manufacturing process. This pertains to considerations regarding design, components, PWBs, solder alloys, fluxes, printing, reflow, and wave soldering, rework, cleaning, equipment and inspection. Engineering personnel have to pay a close attention to design, components, PWBs, solder alloys, fluxes, and the printing, reflow, wave soldering, rework and cleaning processes and equipment (Fig. 2).

Both the amount and size of IMC in the microstructure affect the issue of solder joint reliability, being a detrimental factor in both crack initiation and propagation. For its analysis, the most often form is represented by accelerated ageing test. A typical temperature cycling test condition of -40°C to 125°C is required to ensure a reliable package performance [3]. Then, solder joints should be cross-sectioned and inspected for cracks. Although there is only a few of them, yet there are publications related to integrated design analysis of board-level solder joint reliability, with consideration of both drop impact load and thermal cycling load performance simultaneously. Comprehensive solder joint reliability is determined by the combination of service environment and system design. The service environment will determine the temperature extremes which the product must endure, the frequency of power on / off cycling, and the possibility of specific mechanical shocks (for example, drop impact) stresses. Where the system design is concerned, a series of factors that include component and substrate physical properties, solder joint geometry, bulk solder alloy microstructure and mechanical properties, the nature of the IMC layer formed and their structure at the solder joint / pads interfaces are important. Cost limitations add additional restrictions, consequently forcing hard choices to be made [3]. The robustness of a solder joint subjected to both drop impact load and temperature cycles load is affected by a complex combination of IMC layer properties and bulk solder alloy properties [10]. For bulk solder alloys, eutectic tin-lead, with its long established history, has been replaced with the complexity of a multitude of new and unfamiliar lead-free alloys.

III MICROSTRUCTURE ASPECTS OF LEAD-FREE SOLDER JOINTS

In the electronics industry, SAC is now recognized as the standard lead free solder alloy for packaging interconnects. However, SAC alloys are not enough to meet high solder joint reliability under different loading conditions. This study presents direct correlation between mechanical and microstructure properties of SAC bulk solder alloy and the reliability of SAC solder joints in term of both drop impact and thermal cycling loading conditions.

The fact that the microstructural characteristics of an alloy determine its mechanical performance is widely known [14]. The alloy system and process conditions during solder joint formation affect the microstructure development of a solder joint [15]. Therefore, understanding the micro-structural characteristics of the SAC ternary system is essential to understanding the mechanical performance and reliability of SAC solders (Fig. 3). These properties provide necessary information to design and manufacturing engineers when deciding on a solder alloy for their specific application.

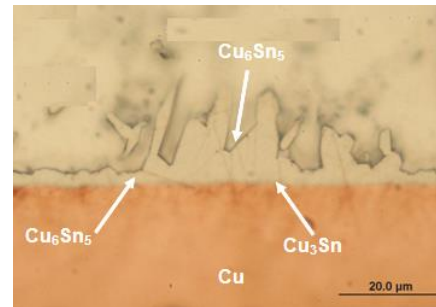


Fig. 3. Typical phase interface of solder joint based SAC have two layers of IMCs: thick and irregular in thickness Cu_6Sn_5 , and very thin and uniform Cu_3Sn .

An essential element in SAC composition is silver which can have different effects on the solder joint reliability, depending on the loading conditions. Depending on the application, package and reliability requirements, the content level of silver in SAC solder alloys can be an advantage or a disadvantage [24], e.g. the best level of silver content for drop performance is not definitely the best level for optimum temperature cycling reliability [25]. Thus, the SAC alloys are limited in their potential applications in the portable electronic products in which thermal cycling and impact/drop are the primary requirement for board level solders joint reliability. Currently, a wide range of SAC solders containing different levels of silver, and maintaining a Cu level to manage substrate dissolution, such as Sn-1Ag-0.5Cu (SAC105) and Sn-3Ag-0.5Cu (SAC305), have been studied and are used in the electronics industry for a wide variety of applications. They found that the microstructures of Sn-x Ag-Cu alloy consisted of a β -Sn matrix with dispersoids of fine Ag_3Sn and coarsened Cu_6Sn_5 intermetallic compounds (IMC particles) [16]. The size of the IMC particles ranged from submicron to several microns for all alloys, which is known to be a common feature of the Sn-xAg-Cu alloys [17]. Volume fraction of the Ag_3Sn IMC particles in the microstructure tends to increase with increasing silver content. In the microstructure of SAC105, relatively large primary Sn grains and the Ag_3Sn IMC particles appeared within the matrix [18]. The SAC205 contains cell-like primary Sn grains, and the grains include very fine Ag_3Sn IMC particles. In the SAC305, the Ag_3Sn IMC particles formed a network structure around the primary Sn grains, of which the sizes are larger than that of the 2Ag solder. In

the SAC405 alloy, the Ag_3Sn IMC particles compounds are dispersed within the matrix, and the inter-particle distance is smaller as in other alloys [18].

In electronic products, all commonly base materials, coatings, and metallization, such as Cu, Ni, Ag, Ag-Pd, and Au, form IMCs with Sn. Therefore, chemical reactions occur between solders and conductor metals during soldering (i.e., component metallization's, board surface finishes, and underlying conductors), and IMCs nucleate and grow at the solder/conductor interfaces.

The soldering process can be divided in three stages [21]: spreading, base metal dissolution, and formation of an IMC layer. For most solders, diffusivity is an important property. Further, good wetting is required for good solders. Hence, interfacial reactions with substrates are usually important not only at the solid/liquid contacts, but also at the solid/solid contacts at high operation temperatures [22]. Strength of the solder joint is controlled by the land pattern design and a good metallurgical bond between the component and the board. A reliable solder connection must have a solderable surface in order to form a good metallurgical bond between the solder and the components to be joined. In the fabrication of electronic products, interfacial reactions at the solder joints are key factors.

Fig. 4 depicts the interfacial reaction of SAC305/Cu during solder reflow. When heat is applied, the solid SAC305 solder melts, and the contacted Cu substrate starts to dissolve to the molten SAC305 solder (Fig. 4(a)). The layer of molten SAC305 solder near the SAC305/Cu interface becomes supersaturated with dissolved Cu (Fig. 4(b)). The solid IMC begins the formation of the interfacial zone. Cu_6Sn_5 with a scallop structure was first formed (Fig. 4(c)), followed by thin layer-like Cu_3Sn (Fig. 4(d)) [19].

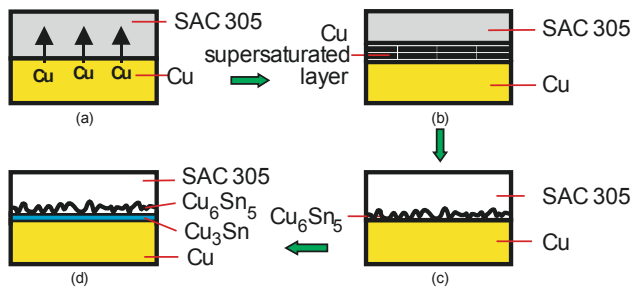


Fig. 4. Scheme of the interfacial reaction of SAC305/Cu during solder reflow: (a) dissolution of the Cu substrate, (b) super saturation of the molten solder layer with Cu, (c) formation of the scallop-type Cu_6Sn_5 at the interface, and (d) Cu_3Sn emerges between Cu_6Sn_5 /Cu with prolonged soldering.

Two intermetallic layers are commonly found at the interfacial zone of SAC and the Cu substrate, that is, Cu_6Sn_5 and Cu_3Sn . While Cu_6Sn_5 forms first and possesses a scallop-like structure, Cu_3Sn emerges at the Cu_6Sn_5 /Cu interface and has a layered structure as well. However, the thickness of Cu_3Sn is much smaller than of Cu_6Sn_5 , and its formation requires longer contact times. Morphological transformations may occur depending on

the phase stability. With increasing reflow temperature and time, both Cu-Sn IMCs grow [19].

In this context of improved reliability of power electronic devices, question of packaging technologies for higher operating and ambient temperatures might be interesting.

Diffusion soldering process for power semiconductors to form a high melting bond between chip and substrate [20 - 22] has been developed. Depending on the choice of chip metallisation and the soft solder material in standard soldering, Cu-Sn or Ni-Sn intermetallic are usually formed as thin interfacial layers. All these intermetallic compounds have a much higher melting point than the Sn-based soft solders. For example, depending on the process parameters in the Cu-Sn system either Cu_3Sn with $T_m=676^\circ C$ or Cu_6Sn_5 with $T_m=415^\circ C$ is formed during the soldering process. In diffusion soldering, this solidification process is exploited to create pure intermetallic joints with a remelting temperature $T_m > 400^\circ C$ from Sn-Ag solder.

Fig. 5 illustrates a schematic comparison between a standard and a diffusion soldered joint. Both joints are formed from a Sn-rich solder, whereas in the standard joint only a fraction of the Sn is transferred into a high melting intermetallic. By contrast, in the diffusion soldered joint, the entire volume of low melting solder is consumed by the solidification process. The result is a high melting bond between substrate and chip. Depending on the ratio between the two different intermetallic phases formed in the Cu-Sn system, the homologous temperature for these joints ranges from $T_H=0.52-0.65$.

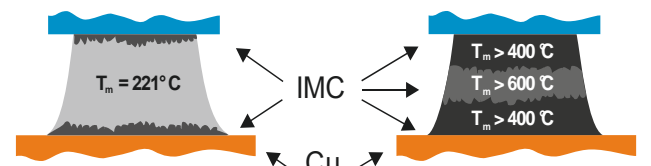


Fig. 5. Schematic comparison of a standard solders joint (left) and a diffusion soldered joint (right). The diffusion soldered joint consists of two different intermetallic phases.

TABLE 2 HOMOLOGOUS TEMPERATURES OF SnAg SOLDER VS. SnCu AND Ag [23].

Material	SnAg3.5	Cu_6Sn_5	Cu_3Sn	Ag
Melting temp.[$^\circ C$]	221	514	638	961
T_H for $125^\circ C$	0.81	0.58	0.44	0.32
T_H for $150^\circ C$	0.86	0.61	0.46	0.34
T_H for $200^\circ C$	0.96	0.69	0.52	0.38
T_H for $250^\circ C$	1.06	0.76	0.57	0.42

Solder exhibits different mechanical behaviours, depending on whether the upper dwell temperature (T_{op}) exceeds or not a homologous temperature (defined as $T_H = T_{op}/T_m$) of approx. $0.74 T_m$. When T_{op} is below this value, shear strain variations remain in relatively small range values, and shear stress variations have a linear dependence with the temperature variation. If $T_H < 0.4 T_m$, there is no or small influence on behaviour of materials, if

$T_H > 0.4 T_m$, it is typical for creeping, and finally, if $T_H > 0.7 T_m$, there is strong decrease of mechanical strength (Tab. 2.)

Reliable power electronic devices require emerging packaging technologies for higher operating and ambient temperatures: copper wire bonding, diffusion soldering or micro Ag-sintering for die attach, DBC (Direct bonded copper substrate) for baseplate.

Solder joints with intermetallic compounds growth may be the solution for high temperatures die attaches. Challenges for diffusion soldering are long process time, voiding in area soldering and brittleness of IMC. In the future, packaging technologies for power electronic devices will require:

- Foil sintering and foil ultrasonic wedge bonding,
- low temperature current – assisted sintering of nanosilver for die attach,
- micro channel cooling in DBC baseplate.

Isothermal solidification during diffusion soldering of Cu-Sn interface conduct to IMC growth: During initial stages both Cu_6Sn_5 and Cu_3Sn phases grow. After consumption of every available Sn, the Cu_3Sn phase grows reactively at the expense of Cu and Cu_6Sn_5 . Finally, solder joints are obtained, consisting of only Cu_3Sn (T_m is $638^\circ C$). It is recommended to re-melt paste (reflow soldering) and keep the temperature until IMC growth is completed [23].

IV. CONCLUSION

This paper reviews the function and importance as well reliability aspects of Sn-Ag based solder alloys in electronics industry and the interfacial reaction of Sn-Ag/Cu solder joint at various solder forms and various processing conditions.

ACKNOWLEDGMENT



MINISTERSTVO ŠKOLSTVA,
VEDY, VÝSKUMU A ŠPORTU
SLOVENSKEJ REPUBLIKY



Európska únia
Európsky fond regionálneho rozvoja



This paper was developed with support of operating program Research and development for the project: "Univerzitný vedecký park Technicom pre inováčné aplikácie s podporou znalostných technológií" (University Science Park Technicom for innovative applications with support of knowledge technologies), code ITMS: 26220220182, co-financed from European funds.

REFERENCES

- [1] Băjenescu, T. I., and M. Băzu, Reliability of Electronic Components. A Practical Guide to Electronic Systems Manufacturing, Berlin and New York: Springer, 1999.
- [2] Tee, T. Y., H. S. Ng, et al. (2003). Design for enhanced solder joint reliability of integrated passives device under board level drop test and thermal cycling test, IEEE.
- [3] Tu, K. (2007). Solder joint technology: materials, properties, and reliability, Springer Verlag
- [4] Ye, L., Z. Lai, et al. (2001). "Microstructure investigation of Sn-0.5 Cu-3.5 Ag and Sn-3.5 Ag-0.5 Cu-0.5 B lead-free solders." Soldering & surface mount technology 13(3): 16-20.
- [5] R. J. Fields, S. R. L. "Physical and mechanical properties of intermetallic compounds commonly found in solder joints." Retrieved April 20, 2011, 2011, from http://www.metallurgy.nist.gov/mechanical_properties/solder_paper.html.
- [6] Pang, H., K. Tan, et al. (2001). "Microstructure and intermetallic growth effects on shear and fatigue strength of solder joints subjected to thermal cycling aging." Materials Science and Engineering: A 307(1-2): 42-50.
- [7] Che, F., W. Zhu, et al. (2010). "The study of mechanical properties Ag content and Ni doping under different strain rates and temperatures." Journal of Alloys and Compounds.
- [8] Anderson, I. E. (2007). "Development of Sn-Ag-Cu and Sn-Ag-Cu-X alloys for Pb-free electronic solder applications." Lead-Free Electronic Solders: 55-76.
- [9] Frear, D., L. Ramanathan, et al. (2008). Emerging reliability challenges in electronic packaging. Annual International Reliability Physics Symposium, IEEE.
- [10] Grafe, J., R. Garcia, et al. (2008). "Reliability and Quality Aspects of FBGA Solder Joints." FORSCHUNG & TECHNOLOGIE 10: 2224-2234.
- [11] Henshall, G., R. Healey, et al. (2009). Addressing opportunities and risks of pb-free solder alloy alternatives, IEEE.
- [12] Hosford, W. F. (2005). Physical metallurgy. Boca Raton, FL USA, CRC Press, Taylor and Francis Group.
- [13] K. Nimmo (2004). Alloy selection. New York, Marcel Dekker.
- [14] Allen, D. K. (1969). Metallurgy theory and practice. Homewood, IL USA, American Technical Publishers.
- [15] Moon, K. W., W. Boettinger, et al. (2000). "Experimental and thermodynamic assessment of Sn-Ag-Cu solder alloys." Journal of electronic materials 29(10): 1122-1136.
- [16] Terashima, S., T. Kohno, et al. (2009). "Improvement of thermal fatigue properties of Sn-Ag-Cu lead-free solder interconnects on Casio's wafer-level packages based on morphology and grain boundary character." Journal of electronic materials 38(1): 33-38.
- [17] Kariya, Y., T. Hosoi, et al. (2004). "Effect of silver content on the shear fatigue properties of Sn-Ag-Cu flip-chip interconnects." Journal of electronic materials 33(4): 321-328.
- [18] Terashima, S., Y. Kariya, et al. (2003). "Effect of silver content on thermal fatigue life of Sn-xAg-0.5 Cu flip-chip interconnects." Journal of electronic materials 32(12): 1527-1533.
- [19] LiuMei Lee and Ahmad Azmin Mohamad, Interfacial Reaction of Sn-Ag-Cu Lead-Free Solder Alloy on Cu: A Review, Hindawi Publishing Corporation, Advances in Materials Science and Engineering, Vol. 2013, Article ID 123697, 11 pages, <http://dx.doi.org/10.1155/2013/123697>
- [20] S. Bader, W. Gust, H. Hieber, Rapid formation of intermetallic compounds by interdiffusion in the Cu-Sn and Ni-Sn Systems, Acta. metall. mater. 43 (1), 329 (1995)
- [21] D. M. Jacobson, G. Humpston, Diffusion soldering, Soldering & Surface Mount Technol. 10, 27 (1992).
- [22] A. Ciliox et al, New module generation for higher life-time, paper submitted to PCIM Conference, Nuremberg, Germany (2010).
- [23] Klaus-Jürgen Wolter, Reliable Power Electronics for Electric Vehicles, 36th International Spring Seminar on Electronics Technology, Alba Julia "Automotive Electronics – invited lecture
- [24] Henshall, G., R. Healey, et al. (2009). Addressing opportunities and risks of pb-free solder alloy alternatives, IEEE.
- [25] Syed, A., J. Scanlan, et al. (2008). Impact of package design and materials on reliability for temperature cycling, bend, and drop loading conditions. IEEEECTC, IEEE

Diagnostics of Electrical Properties of Electrically Conductive Adhesives

Pavel Mach, Martin Plaček, Jiří Kolář, David Bušek

Czech Technical University in Prague, Faculty of Electrical Engineering, Department of Electrotechnology,
Technická 2, 166 27, Prague 6, Czech Republic

¹⁾ tel: +420 2 2435 2214, email: mach@fel.cvut.cz ,

Abstract— Electrically conductive adhesives are used instead of lead-free solders in some types of electronics assembly. Unlike solders adhesives are composite materials consisting of two components, insulating matrix and electrically conductive filler. Diagnostics of these materials should provide information about their basic electrical and mechanical properties. The paper presents different types of diagnostics of electrical properties of adhesive joints. Presented is measurement of the resistance and impedance of the joints, noise measurement and nonlinearity of the current vs. voltage characteristic measurement. The methods are documented by measurements of adhesive joints formed of adhesives with isotropic electrical conductivity of epoxy type.

Keywords— *electrically conductive adhesives;; resistance measurement; nonlinearity measurement; noise measurement*

I. INTRODUCTION

Electrically conductive adhesives are used as a substitution of solders for applications where heat sensitive components must be electrically connected. An LCD display is, for example, such a component. If lead-free soldering would be used for formation of an electrically conductive joint, the component could be damaged. Therefore an adhesive joint formed of electrically conductive adhesive must substitute a soldered one.

Adhesive assembly must also be used for assembly of electronic components with small gaps between terminations. The use of lead-free soldering for such the assembly is usually associated with occurrence of bridges between some adjacent contacts and malfunction of an integrated circuit.

Two types of electrically conductive adhesives (ECAs) are used in electronics: adhesives with isotropic electrical conductivity (ICAs) and adhesives with anisotropic electrical conductivity (ACAs). Both the types consist of an insulating matrix and electrically conductive filler [1-2].

ICAs have the same electrical conductivity in all directions. These adhesives are filled with metal flakes (silver flakes usually) and the concentration of these filler particles in adhesive is in the range of 60 – 80 % (by weight) [3]. Flakes are manufactured by different ways, e.g. by milling or as a metal glasses (an amorphous material). The shapes of flakes in one adhesive are different and their dimensions are in the range of 5 to 30 μm . Silver is mostly used as a materials of flakes. Other

metals such as gold or palladium were also tested as fillers in some special applications. Due to high concentration of filler in ICAs, these adhesives are substantially more expensive than lead-free solders. As for the price in general, it can be said that the price of ICAs with silver filler is comparable with the price of silver on the market. If gold or palladium is used, the price dramatically increases.

The structure of an adhesive joint formed of ICA is shown in Fig. 1.

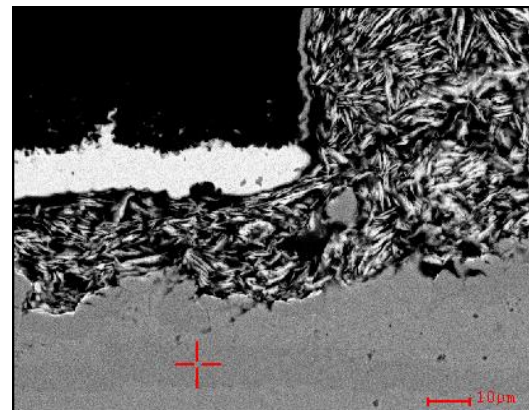


Fig. 1 Scanning figure of adhesive joint of SMT resistor. Body of the component is in the left upper corner, light bar is metallization of a component, lower part of the figure is metallization of a pad the right upper corner and the bar under metallization of a component is ICA. Flakes are good visible here.

Adhesives with anisotropic electrical conductivity are filled with metal balls or with balls of plastic materials covered with an electrically conductive metal film. Some of these “plastic” fillers have the top electrically conductive film covered with a very thin insulating film. The principle of anisotropic electrical conductivity of ACA is as follows: the concentration of filler particles in the ACA is, in difference with the ICA, very low (7 – 15 % b.w. usually). Filler particles are balls with diameter of 5 - 15 μm . One adhesive has balls of one diameter usually. The assembly is carried out at the curing temperature and under the pressure. The adhesive is applied on the pad, then lead of a component is attached to the pad and the adhesive is cured by the simultaneous application of the pressure perpendicularly to the plane of a PCB. The balls

are clamped between the pad and the component lead. Because the balls concentration in adhesive is not so high that the balls touch, the adhesive joint has the electrical conductivity in the direction perpendicular to the PCB (in direction of the axis z) and its conductivity in the directions of axes x and y is near to zero. Therefore ACAs are also known as adhesives with “ z conductivity” or “ z conductive adhesives.”

Diagnostics of electrically conductive adhesives is very significant for monitoring of their properties and changes of these properties. The paper is focused on diagnostics of electrical properties of adhesive joints formed of ICAs.

II. THEORY AND RESULTS OF SELECTED DIAGNOSTIC METHODS

A. Methods of the Joint Resistance and Impedance Measurement

The resistance of an adhesive joint formed of ECA consists of the tunneling resistance and the constriction resistance [4].

The tunneling resistance is caused by a very thin insulating film in contacts (2 – 3 nm) between filler particles. These films can be formed in air as oxide, nitride, sulfide, hydride or carbide.

The constriction resistance is caused by high narrowing of the cross section of a conductor through which the current flows. As for the ICAs, the constriction resistance is usually neglected and it is assumed, that the tunneling mechanism dominates. The reason is that ICAs are filled with flakes and there are many contacts between two flakes (see Fig. 1).

On the other hand the constriction resistance can be a significant part of the total resistance of the joints formed of ACAs. The filler of these adhesives are balls and a contact between two balls is a circle with very low diameter.

The most frequently measured electrical parameter of adhesive joints is the joints resistance. A four point method is used for this measurement usually.

The value of the resistance of an adhesive joint is, according to the adhesive type, in the range of 8 to 140 mΩ for assembly of SMD components with the package 1206 (the dimension of a contact on the component is 0,5 x 1.6 mm). For comparison, the resistance of the soldered joint of the same dimensions is approximately 20 – 120 μΩ.

A three point method is also used for the joint resistance measurement (see Fig. 2). I is a current source, A is an ammeter, mV is a millivoltmeter. The measurement is carried out as a DC one or as a low frequency measurement. An example of the resistance of adhesive joints formed of different types of adhesives is in Fig. 3. The joints were aged at combined climatic ageing (85 °C / 85 % RH) [5] for 700 and 1000 hours. All adhesives presented in this paper are ICAs formed of an epoxy matrix filled with silver flakes and produced by Amepox.

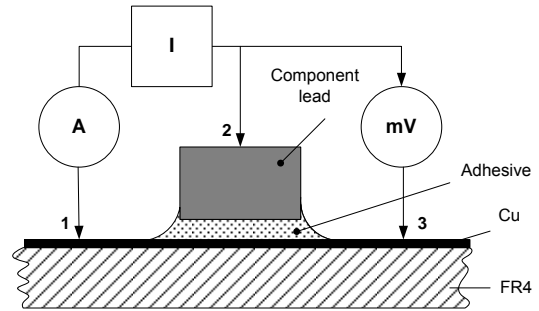


Fig. 2 Three point method for the adhesive joint resistance measurement

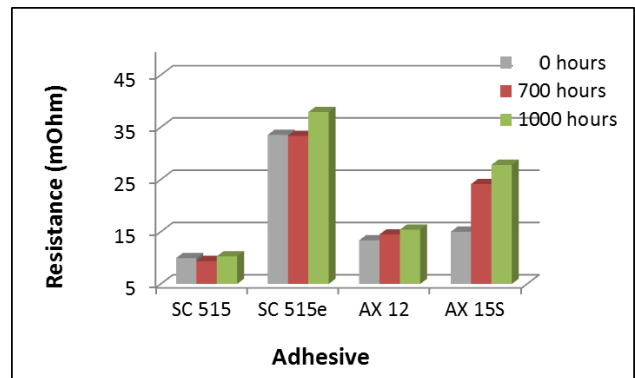


Fig. 3 Resistance of adhesive joints formed of different types of ICAs. Adhesives were aged at 85 °C / 85 % RH for 700 and 1000 hours. Starting values are presented for 0 hours ageing

The next type of electrical diagnostics of adhesive joints is impedance measurement in dependence on the measuring frequency [6]. Different types of precision LRC meters are usable for these measurements (in our case an RLC meter HP 4284A was used). Frequency dependence of adhesive joints formed of different ICAs with bis-phenol epoxy matrix is shown in Fig. 4. The dependence fully corresponds with [7].

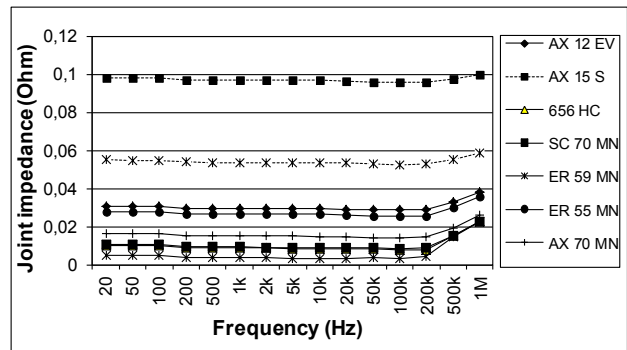


Fig. 4 Impedance of adhesive joints formed of different types of ICAs in dependence on frequency in the frequency range of 20 Hz – 1 MHz

The measurement of adhesive joints in higher frequencies is also carried out sometimes. This measurement is more complicated. One possibility is to use for such the measurement a high-Q triplate stripline.

B. Noise Measurement

Next significant method of electric diagnostics of adhesive joints is noise measurement.

The current flowing through adhesive must overcome barriers between filler particles and contacts adhesive/pad and adhesive/component termination. This process generates current noise. Therefore it is possible to use noise measurement as a tool for analysis changes in the adhesive after some tests, e.g. after climatic ageing.

Noise measurements were carried out in arrangement shown in Fig. 5. The workplace for noise measurement consists of following parts:

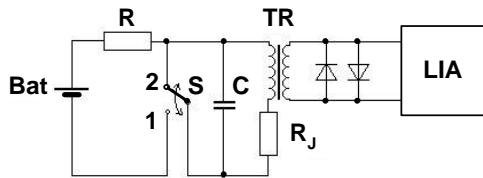


Fig. 5 Noise measurement of adhesive joints

- Current source is composed of an accumulator battery Bat and a resistor R.
- Measuring transformer TR.
- Measured adhesive joint R_j joined in series with a primary winding of a measuring transformer TR.
- Lock-in amplifier LIA used in a mode micro-voltmeter. Lock-in amplifier was protected by protective diodes.
- Switch S.

The measuring process was carried out in two steps: at first the switch was in position 1 and the capacitor C was charged. Then the switch was switched to position 2 and the capacitor was discharged through the adhesive joint and the primary winding of the measuring transformer. Due to very low amplitude of noise signal the equipment must be carefully screened. It is also necessary to avoid ground loops. An example of noise measurements of adhesive joints formed of some types of adhesives with epoxy matrix filled with silver flakes is presented in Fig. 6.

C. Nonlinearity of Current vs. Voltage Characteristic Measuring

The last of significant electrical parameters is nonlinearity of a current vs. voltage characteristic (I/V characteristic) of adhesive joints [8].

The basic measuring method is based on powering of an adhesive joint with the sinusoidal current and measuring of harmonics of the periodic voltage on the joint. If the I/V characteristic is of a type of an even parabola, the even harmonics of the voltage will occur on the junction, if the I/V characteristic is of a type of an odd parabola, the odd harmonic will occur on the junction [9].

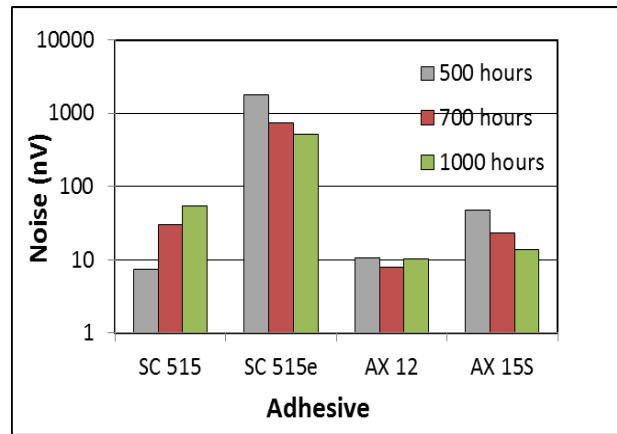


Fig. 6 Noise of adhesive joints formed of different types of ICAs. Adhesives were aged at 85 °C / 85 % RH for 700 and 1000 hours. Starting values are presented for 0 hours ageing

The measurement of the even harmonics (the second one usually) is carried out using measuring equipment whose principle is shown in Fig. 7.

An oscillator OSC powers the joint with a sinusoidal signal, battery is used to set the operating point; A is a DC amplifier and LIA Lock-in amplifier.

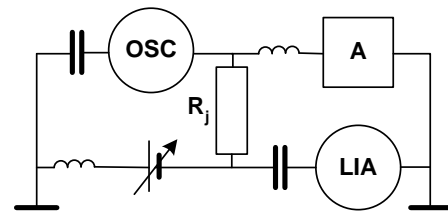


Fig. 7 Measurement of nonlinearity of I/V characteristic if the characteristic is of a type of even parabola

The operating point is slowly moved during the measurement and the level of the second harmonics is measured using LIA. The frequency of OSC is low and it has to be chosen different from the power net harmonics frequencies. The measured voltages are very low. Therefore the equipment has to be carefully screened and grounded.

The measurement of an odd harmonic component, third one usually, is carried out using equipment based on two possible principles. The first one is shown in Fig. 8.

The adhesive junction R_j is powered with the sinusoidal current from a current source. The source is formed of a generator G1 and a wire resistor R. The frequency is 10 kHz usually. The voltage of the first harmonics is measured with the selective millivoltmeter U1 and the third harmonics with the selective millivoltmeter U3. The result of the measurement can be expressed as an index of third harmonics THI.

$$THI = 20 \log \frac{U_3}{U_1^3} \quad (1)$$

Where $U_3 \dots$ voltage of the third harmonics (μV), $U_1 \dots$ voltage of the first harmonics (V). THI is expressed in dB.

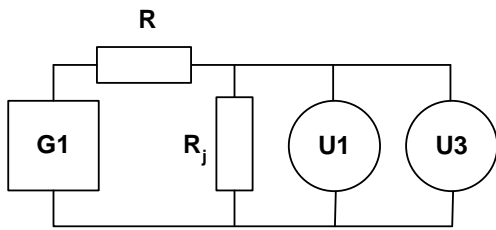


Fig. 8 First method of measurement of nonlinearity of I/V characteristic if the characteristic is of a type of odd parabola

The second method of the measurement of the third harmonics is shown in Fig. 9. The measuring equipment is based on powering of the adhesive junction with two sinusoidal currents. Nonlinearity of the junction causes intermodulation and generation of different types of intermodulation products. One of intermodulation products of the third order is measured using a spectral analyzer.

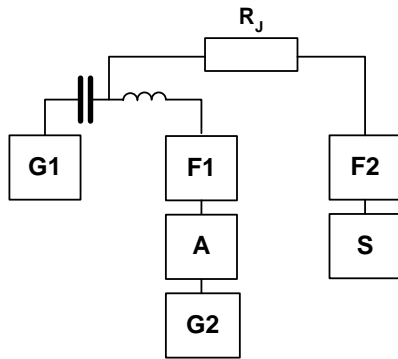


Fig. 9 Second method of measurement of nonlinearity of I/V characteristic if the characteristic is of a type of odd parabola. $R_j \dots$ adhesive joint, G1 ... generator of a sinusoidal signal with the frequency of 4.1063 MHz, G2 ... generator of the sinusoidal signal with the frequency of 150 kHz, A ... low frequency amplifier, F1 ... low pass, F2 ... band pass, S ... spectral analyzer

An example of results of nonlinearity measurement is in Fig. 10. The measurement of nonlinearity is useful for studying of adhesive joints ageing, nonlinearity changes during ageing in dependence on influence of different types of mechanisms of electrical conductivity.

III. CONCLUSION

Basic methods for diagnostics of electrical properties of electrically conductive adhesives were presented. The measuring methods of the adhesive joints resistance, joints impedance in a wide frequency spectrum, joints noise and nonlinearity of the current vs. voltage characteristic were presented and documented by measured data.

The diagnostic methods for electrically conductive adhesives and adhesive joints are specific due to the very low resistance values of adhesive joints.

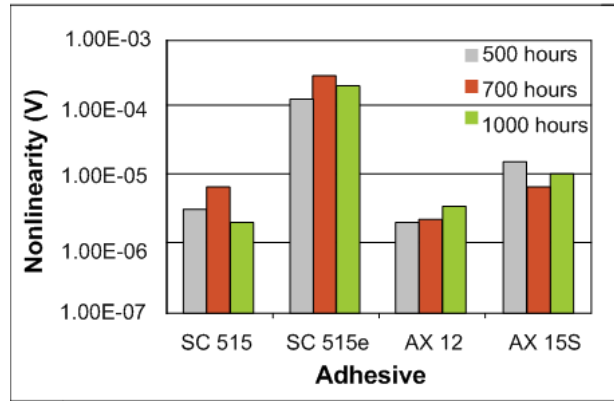


Fig. 10 Nonlinearity of adhesive joints formed of different types of ICAs. Adhesives were aged at 85 °C/85 % RH for 700 and 1000 hours. Starting values are presented for 0 hours ageing

When examining the electrical properties of joints their resistance is usually measured only. The paper showed more diagnostic methods of joints electrical properties that can provide highly interesting and significant information. Measurement of I/V characteristic nonlinearity is one of such the methods. that can provide information about the change of the type of conductive mechanism in adhesive.

ACKNOWLEDGMENT

Authors thank the Ministry of education, youth and sports for financial support under the project "Diagnostics of Materials", number MSM6840770021

REFERENCES

- [1] Luyckx, G., Dreezen, G., "Electrically Conductive Adhesives as Solder Alternative: A Feasible Challenge." In E. Zschech, C. Whelan and T. Mikolajick, *Materials for information Technology*. Springer London, 2005, pp. 363-375
- [2] Li, Y., Wong, ChP., "High performance conductive adhesives for lead-free interconnects." *Advanced Electronic Packaging Symposium*, Boston, MA, USA. 2006, pp. 169-74
- [3] E. Sancaktar, L. Bai, „Electrically conductive epoxy adhesives,“ *Polymers*, Vol. 3, pp. 427-466, 2011
- [4] Su, B., "Electrical, Thermomechanical and Reliability Modeling of Electrically Conductive Adhesives." Doctoral thesis, *Georgia Institute of Technology*, pp. 1 – 36, 2006
- [5] R. Gomatam, E. Sancaktar, „A novel cumulative fatigue damage model for electronically conductive adhesive joint under variable loading,“ *J. Adhes. Sci. Technol.*, Vol. 20, pp. 53-68, 2006
- [6] P. Mach, V. Papez, A. Duraj, "Frequency Dependence of Impedance of Adhesive Joints,“ *ESTC Germany*, pp. 812-817, 2006
- [7] Agilent, "Imp. Measurement Handbook", 4th edition, pp. 1-5, 1-6. <http://cp.literature.agilent.com/litweb/pdf/5950-3000.pdf>
- [8] P. Mach, D. Busek., "Theoretical and experimental background of resistance and nonlinearity measurements of adhesive conductive joints,“ *SIITME*, pp. 272-275, 2008
- [9] P. Mach, V. Papež, D. Bušek, A. Duraj, "Equipment for measurement of nonlinearity of nominally linear components,“ *ISSE, Germany*, pp. 238.240, 2006

Electrically Conductive Adhesives Usability for Power Electronics Packaging

Pavel Mach

Czech Technical University in Prague, Faculty of Electrical Engineering, Department of Electrotechnology,
Technická 2, 166 27 Prague 6, Czech Republic,
tel: +420 2 2435 2214, email: mach@fel.cvut.cz ,

Abstract—Electrically conductive adhesives (ECAs) are used, in parallel with lead-free solders, as a nature-friendly substitution of tin-lead solders in electronics packaging. Adhesives with isotropic electrical conductivity are mainly used for assembly of components with low resistance to heat; adhesives with anisotropic electrical conductivity for assembly of components having fine-pitch and ultra-fine-pitch packages. Limits of using of ECAs in power electronics assembly are discussed. The application of these materials at the higher temperature causes their additional curing and changes of their properties, they have low resistivity against humidity, worse mechanical properties and higher noise in comparison with lead-free solders, current pulses of higher amplitude changes their electrical properties etc. Yet they are tested for tabbing ribbons joining in photovoltaic panels assembly.

Keywords— *electrically conductive adhesives;; resistance measurement; nonlinearity measurement; noise measurement*

I. INTRODUCTION

When the use of tin-lead solders was prohibited by RoHS directive from July 1, 2006, it was necessary to find some new types of environmental friendly materials for conductive joining in electrical engineering, which would substitute tin-lead alloy. These new materials must not contain lead. Many lead-free alloys were tested for this substitution, but many problems occurred during this testing. These problems were joined with changes of mechanical properties of soldered joints especially during some types of climatic testing and with stability of the joints properties in general, with wettability and of different types of surfaces by various solder, with the level of the soldering temperature and many others. Finally, as the alloy with optimum properties, the alloy SAC ($\text{SnAg}\alpha\text{Cu}\beta$, where α and β differ in different countries, α is in the interval 3.0 - 3.8 % b.w. and β in the interval 0.5 - 0.7 b.w.) was chosen as a dominant alloy for lead-free soldering [1/2]. The main disadvantage of this alloy is higher soldering temperature in comparison with the tin-lead alloy by 20 °C approximately.

It appeared that a prospective alternative to soldering can be adhesive joining using electrically conductive adhesives (ECAs). These composite materials consist of two components, of a resin, e.g. epoxy or silicone resin, which forms and insulation matrix and of electrically conductive filler. Electrically conductive particles of different shapes and dimensions are used as filler.

ECAs can be of different types. In terms of the number of adhesive components, a one-component type and a two-component type are used

In terms of the curing temperature, snap cure conductive adhesives, heat cure conductive adhesives and room cure conductive adhesives are available on the market [3-4].

In terms of the electrical conductivity, adhesives with isotropic conductivity (ICAs) and anisotropic conductivity (ACAs; „z-adhesives“) were developed. The filler concentration in ICAs is high, 60 – 80 % b.w., the filler concentration in ACAs is very low, 7 – 15 % b.w. usually. ACAs lead the current perpendicularly to the plane of PCB only and therefore it is possible to meet also with the designation „z – adhesives.“ Conductive particles of different shapes are as a conductive component in ECAs

The substitution of lead-free solders by ECAs is limited. The first limit is given by the price of the ECA and lead-free solder. ICAs filler is mostly composed of silver flakes. With respect to high concentration of filler in ICAs, the price of ICAs is substantially higher than the price of lead-free solder. As for electrical properties, the electrical conductivity of lead-free alloys is by two or three orders higher in comparison with adhesives, ECAs are composite materials and therefore they have higher electrical noise and nonlinearity of the current vs. voltage characteristic. As for mechanical properties such as the tensile strength and shear strength, they are worse in comparison with mechanical properties of lead-free solders. Climatic resistivity of adhesives is lower than solders; dangerous is their exposure in the environment with increased humidity

On the other hand, ECAs are indispensable when assembled components, which could be damaged by heat, which is necessary for a lead-free soldering process. Also some types of small outline integrated circuits packages with lead pitches down to 80 μm are offered on the market (e.g. flip chip, chip on board, fine-pitch, ultra-fine pitch and others). The limit for effective use of lead-free wave soldering is the lead pitch about 65 μm [5]. This limit is given by possible bridging between adjacent leads. Therefore ACAs have promising prospective in this area of electronics assembly.

Next possible application of ECAs is in assembly of photovoltaic (PV) panels. PV cells are interconnected by tabbing ribbons. The ribbons are joined by soldering usually, but joining using ECAs is also tested. The limits of ECAs using in electronic assembly are mentioned in this paper.

II. THEORY

ECAs are composite materials consisting of conductive filler and insulating matrix, binder. The resistance of an adhesive bond has two components: a tunnel resistance and a constriction resistance. As for ICAs the tunnel resistance dominates, as for ACAs the constriction resistance has significant contribution to the total joint resistance.

ECAs are applied by stencil printing or dispensing usually. The technology of adhesive application has no influence on properties of adhesive joints.

Heat cure conductive adhesives are used the most often. The curing process is carried in air circulated oven usually and the curing temperature and the curing time are recommended by an adhesive producer. The curing process has significant influence on adhesive joint properties. Unless the adhesive is fully cured, its properties are inferior to the cured one. The properties of an adhesive joint formed of not fully cured adhesive will have worse mechanical as well as electrical properties. The testing of nine types of electrically conductive adhesives with epoxy matrix showed that 6 of them were not fully cured, even though they were cured according to the manufacturer's recommendation [6].

Power electronics devices are often exposed to various climatic conditions. Therefore it is necessary, for analyzing of possible usability of ECAs for power electronics assembly, to focus on climatic endurance of ECAs at first.

Adhesive are sensitive to exposure in different climatic conditions. Ageing adhesives at the higher temperature, e.g. at the temperature of 100 °C or higher, improve their conductivity in the initial phase of ageing usually, when the adhesives are not fully cured. The longer time of ageing at the higher temperature causes adhesive degradation. Mechanical properties get worse due to breaking of chemical bonds in the resin. Electrical properties get also worse due to oxide, carbide and other types of film, which origin on the surface of filler particles and increase the resistance of the contacts among them.

Exposure of adhesive at the higher humidity changes the properties of these materials significantly, especially if epoxy resin is used as the insulating matrix of ECA. Just adhesives composed of epoxy resin filled with silver flakes are the most commonly used type of these adhesive due to their low price in comparison with adhesives based on silicon or other type of an insulating matrix. ECAs of an epoxy type are hygroscopic. Water molecules penetrate into adhesive and form oxides and hydrides on the surface of silver filler particles, which cause decrease of adhesive conductivity.

Electrically conductive joints in devices of power electronics connections are often subjected to mechanical stresses of different types. These stressed can mainly be caused by dilatations or vibrations. For testing of usability of ECAs for power devices assembly must be known possible changes of adhesive joints properties under the static and dynamic mechanical stress. It was found that mechanical stress can cause generation of micro-cracks in adhesive. The frequency of micro-cracks and their dimensions grow with

the growing time of mechanical load and with the level of this load. Electrical properties as well as mechanical properties of adhesive joints get worse. When there is a mechanical stress applied simultaneously with the climate load, the micro-cracks generated by the mechanical stress support penetration of water molecules into the adhesive and the changes of adhesive properties are faster than that when the mechanical stress is not applied.

ICAs are mostly filled with silver flakes. It is very good known that mobility of silver ions is very high. High currents or high current pulses occur in devices of power electronics very often. Therefore possible influence of such the currents and pulses must also be taken into account when usability of ECAs for application in power electronics is investigated.

When the adhesive will be dry, then application of high DC or AC currents or current pulses with high amplitudes should not cause movement of silver ions, because the current flowing through the joint flows through a conductive net formed by filler particles and the negligible current only will flow through the adhesive matrix. If the adhesive will be wet, the current will flowing through the matrix increases and supports the movement of silver ions. Result of such the movement can be formation of bridges of silver atoms inside adhesive. The bridges will be formed in parallel to contacts between filler particles and will improve electrical conductivity of adhesive. Such the effect was observed for some experiments when the adhesive joints were loaded with short current pulses with high amplitude [7].

However, it is not possible to exclude other cause of improvement of adhesive conductivity when the short current pulses of high amplitude (e.g. the frequency of the pulses 50 Hz, the pulse width 5 μ s, the pulse amplitude 60 A) are applied on the adhesive joint. The width of the pulses was so small to examine influence of the pulses without heat influence. The lost power for these pulses was very low and the heat generated by them was not possible to cause some changes in joints properties. The reason why the conductivity increases can be the dielectric breakdown of thin films in contact between filler particles and improvement of electrical conductivity of these contacts. It is a great problem to separate these reasons and to define which of them is more or less significant.

When the width of the pulses is higher, the lost power grows and the heat generated with this power can cause changes in properties of the joints. The second possible influence of the currents and pulsed having high amplitudes is heat generation in adhesive joints. The contact areas between filler particles are very small. If the current or current pulses of high intensity will flow through such the contact, the current density in the contact will be very high. Heat will be generated near area around the contact. Heat causes thermal degradation and decomposition of resin around the contact. Decomposition products can react with the filler particles and the particles will start to cover with thin films of products of these reactions and quality of contacts get worse.

A. Samples preparation

Experiments were carried out with adhesives of company Amepox. All adhesives were ICAs with epoxy matrix and silver flakes used as filler. The temperatures used for adhesives curing were in the range of 120 to 180 °C, the curing time was between 15 to 120 minutes in an air flowing oven according to the recommendation of a producer. One-component as well as two-component adhesives were tested.

TABLE I ADHESIVES USED FOR EXPERIMENTS

Adhesive	Components	Adhesive parameters		
		Resistivity ($\mu\Omega m$)	Curing temper. (°C)	Curing time (min)
Ecosolder SC 65MN	1	4.0–6.5	180	40-60
Elpox AX 12EV	2	4.0–6.0	120	120
Elpox AX 15S	2	1.7-1.8	140	100
Elpox SC 24D	1	2.0–5.0	20	24 hours
Elpox SC 24D	1	2.0–5.0	150	15
Elpox SC 24D	1	2.0–5.0	140	30
Elpox SC 24D	1	2.0–5.0	170	5
Elpox SC 515 (e)	1	6.0-30.0	150	120
Elpox SC 515 (e)	1	6.0-30.0	200	5

The adhesive joints were formed by SMT assembly of jumpers of the type 1206 on the test PCB. The board made a four point measurement of the joints resistance possible. Surface finish of the pads was Cu, the jumper terminations had NiCr-Cu-Ag surface finish, which is recommended for adhesive assembly. Seven jumpers were assembled on one test board; the adhesive was applied by dispensing.

B. Measuring equipment

Changes of adhesive joints were monitored by the measurement of the joint resistances. This measurement is the most used one for electrical properties of adhesive joints inspection. The adhesive joint resistance was measured using a four-point method. A measuring device LCR meter HP 4284A was used for the resistance measurements. The measuring frequency was 1 kHz, the measuring voltage 5 to 20 mV.

C. Environmental ageing

Environmental ageing of adhesive joints was carried out in a climatic chamber Weiss Technik and in a climatic chamber WTB Binder. Conditions of climatic ageing were as follows: heat ageing 120 °C for 1000 hours, climatic combined ageing temperature/humidity at 85 °C /85 % RH for 1000 hours and humidity ageing at in 98 % RH for 1000 hours.

IV. RESULTS AND DISCUSSION

Results of climatic ageing are shown in Fig. 1 to Fig. 3.

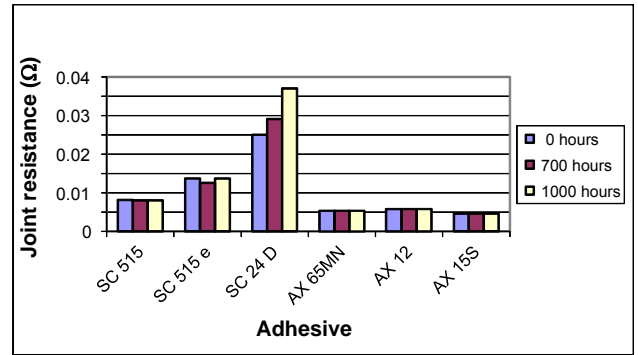


Fig. 1 Resistance of adhesive joints during heat ageing at the temperature of 120 °C

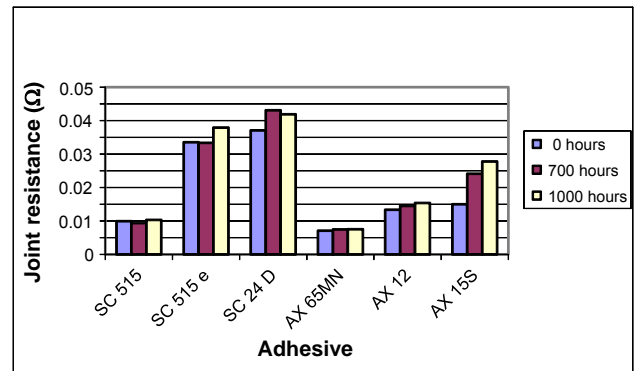


Fig. 2 Resistance of adhesive joints during combined climatic ageing at 85 °C / 85 RH

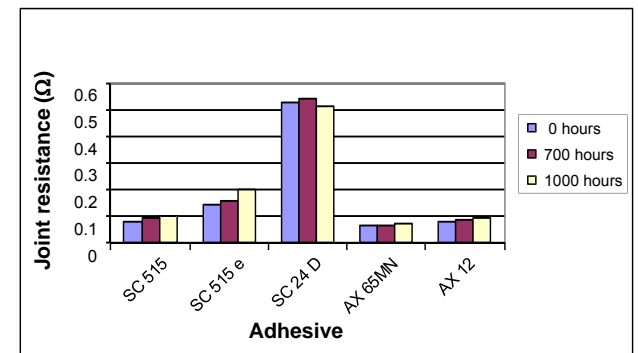


Fig. 3 Resistance of adhesive joints during humidity ageing at 98 % RH

A measuring device for ageing of adhesive joints under the static mechanical load is shown in Fig. 4. Results of adhesive joints ageing under the static mechanical load are presented in Fig. 5.

Fig 6 shows results of loading of adhesive joints with current pulses (the frequency 50 Hz, the pulse width 5 μs , the pulse amplitude 10, 20 or 50 A, the time of loading 60 min).

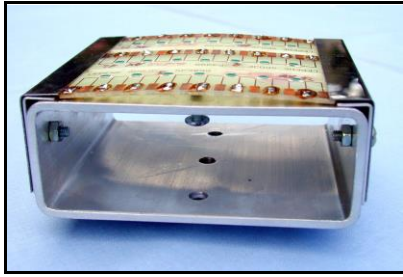


Fig. 4 Ageing of adhesive joints under the static mechanical load. The test board with assembled jumpers was deflected and the stresses in individual adhesive joints calculated. Adhesive joints resistances were measured using a four-point method

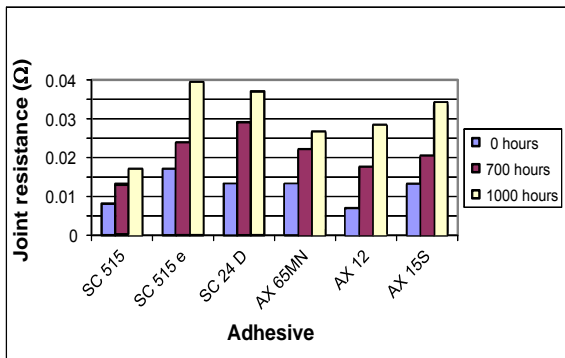


Fig. 5 Resistance of adhesive joints during ageing under the static mechanical load

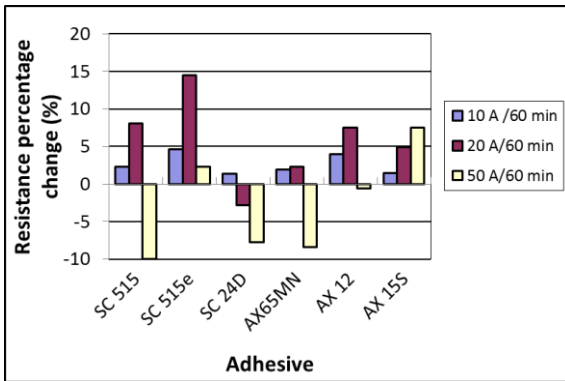


Fig. 6 Resistance percentage change of adhesive joints loaded with short current pulses (50 Hz, amplitude 10, 20 or 50 A, pulse width 5μs, time of loading 60 min)

It was found that changes caused by temperature and humidity ageing are smaller than those caused by ageing in combined climatic conditions temperature/moisture. When the joints are exposed at the higher temperature, at the beginning of ageing their properties can improve. The reason is that such the type of ageing influences as additional curing, which improves electrical as well as mechanical properties of the joints. When the ageing is too long or the ageing temperature too high, the resin starts to degrade and reaction products deteriorate the contacts quality and conductivity. Changes of the adhesive joints aged in

humidity were not significant. Exposition of the joints in combined climatic conditions temperature/humidity changes electrical properties of adhesive significantly more. It means that penetration of water molecules into adhesive, if it is supported by the increased temperature, is faster than their penetration at the normal temperature.

Mechanical load causes high changes of the adhesive joints resistance (see Fig. 5). The reason is formation of microcracks, which are generated by this type of the load.

Loading of adhesive joints with short current pulses of high intensity causes resistance increase at first and then its decrease. The starting increase can be caused by the temperature increase of the contact and following decrease by piercing of insulating barrier in a contact.

V. CONCLUSION

Resistivity of adhesive joints formed of 6 types of ECAs against climatic, mechanical and electrical load (electrical pulses) was examined. The goal of the work was to find possible areas of using of electrically conductive adhesives in power electronics. It was found that adhesive joining can be used for devices intended for small climatic and mechanical load. As for the electrical load it is necessary to accept that the adhesive joint resistance is approximately 100 – 1000 times higher than the resistance of a soldered joint of the same area.

ACKNOWLEDGMENT

Authors thank the Ministry of education, youth and sports for financial support under the project "Diagnostics of Materials", number MSM6840770021

REFERENCES

- [1] Y. Toyoda, "The latest trends in lead-free soldering," International Symposium on Electronic Packaging Technology, Beijing, China, August, 2001, pp. 434-438
- [2] Challenges and Efforts Toward Commercialization of Lead-Free Solder – Road Map 2000 for Commercialization of Lead-Free Solder, Japan Electronic Industry Development Association, (JEIDA), version 1.3, 2000
<http://www.jeida.or.jp/english/information/pbfree/roadmap.html>
- [3] Henkel, „Electrically conductive adhesives,“
<http://www.henkel.com/electrically-conductive-adhesives-27427.htm>
- [4] Dow Corning, „Electrically conductive adhesives“
http://www.dowcorning.com/content/etronics/etronicsdieadh/etronics_daa_ecov.asp
- [5] J. C. Jagt, P. J. M. Beris, G. F. C. M. Litjen, „Electrically conductive adhesives: A prospective alternative for SMD soldering?“, IEEE Trans. Comp. Pack. and Manuf. Tech., Part B, Vol. 18., 1995, pp. 292-298
- [6] P. Mach, E. Povolotskaya, „Study of Curing Process of Electrically Conductive Adhesives using Differential Scanning Calorimetry,“ International spring seminar on electronics technology, Romania, 2012, pp.
- [7] P. Mach, V. Papež, D. Bušek, „Current Loading of Adhesive Joints Aged in Environment with High Humidity,“ ASEM 2013, in press

The use of artificial neural networks in SW STATISTICA for classification analysis of samples that have passed mechanical tests

Lukáš Kupka¹⁾, Olga Tůmová²⁾, Tomáš Langhammer³⁾

University of West Bohemia, Faculty of Electrical Engineering, Univerzitní 26, Pilsen, Czech Republic, www.fel.zcu.cz

¹⁾ tel: +420 377 634 565, email: lkupka@ket.zcu.cz ,

²⁾ tel: +420 377 634 563, email: tumova@ket.zcu.cz ,

³⁾ tel: +420 377 634 578, email: tlangham@ket.zcu.cz

Abstract— The aim of this paper is to design and train artificial neural networks for classification analysis of samples that have passed mechanical tests. Samples of materials are Relanex, Relastic, Lamplex and paperboard. Based on the mechanical tests results (temperature, exposure time, bending resistance and impact resistance) neural networks can identify the type of material with great precision. All samples are used for networks training, validation process is based on medians of groups. For this purpose are used Multilayer perceptron networks (MLPN) and RBF networks.

Keywords— artificial neural networks; classification analysis; mechanical tests; multilayer perceptron networks; RBF networks

I. INTRODUCTION

The use of artificial neural networks is useful in many fields. There are three basic types of analysis where we can use the artificial neural networks (i.e. prediction, regression, classification analysis). This paper focuses on a classification analysis by the artificial neural network. This artificial neural network can recognize (classifies) isolation materials based on the results of mechanical tests. The whole analysis has been performed by the STATISTICA v 7.1 software.

II. MECHANICAL TESTS

The mechanical test has been performed on Relastic 45.013, Relanex 45.010, Lamplex FR4 and on the paperboard L05. The paperboard L05 is a natural solid organic insulator based on compressed cellulose layers. Relastik 45.013 is a thermosetting insulating material, flexible at room temperatures, plastic and sticky at elevated temperatures. It is made of calcinated mica paper Remika (Muscovite) and a polyethyleneterephthalate (PETP) foil, Binder together with epoxy-novolac resin. Relanex 45.010 is three-component insulator. Three components are calcined mica paper and glass fiber glass and epoxinovolac resin. Lamplex FR4 is a composite material composed of woven fiberglass cloth with an epoxy resin binder that is flame resistant [3]. Test specimens (dimensions 15 x 100 mm) were inserted into the laboratory furnace Venticell (Fig. 1). For each material, 10 samples were analysed by single methods. They were

exposed to constant temperature stress at a fixed time. Temperature and times were chosen by EN 60216-1:2001 standard and they are shown in Tab. 1.



Fig. 1. Test specimens placement in furnace Venticell

TABLE I. SUMMARY OF TEMPERATURES AND TIMES FOR ACCELERATED AGING OF MATERIALS

Type of material	Temperature [°C]	Time [h]
paperboard L05	24	0
	170	24, 48, 72, 96, 120, 144
	180	16, 37, 61, 80, 96
	190	6, 13, 23, 32, 40
	200	2, 7, 13, 19, 24
Relastic 45.013	24	0
	170	96, 192, 288, 384, 480, 600
	178	24, 48, 72, 96, 120
	186	2, 10, 15, 20, 25
	194	1, 1,5, 2,5, 3
Relanex 45.010	24	0
	170	96, 192, 288, 384, 480, 600
	175	48, 96, 144, 192, 240
	180	8, 16, 24, 32, 48
	186	2, 4, 6, 8, 10
Lamplex FR4	24	0
	170	96, 192, 288, 384, 480, 600
	180	48, 96, 120, 144, 168
	190	24, 48, 60, 72, 84
	200	10, 15, 20, 25, 30

Then all specimens were removed from the furnace and cooled to ambient temperature. Two thirds of samples were subsequently mounted in a rack. Material was deformed by the steel thorn. The steel thorn was placed at the centre of the sample. The test is terminated by decreasing of resistance which puts the material to the thorn. The maximum pressure caused by thorn per sample was recorded. Procedure is described in detail in the standard CSN EN ISO 178. The intact third of samples were tested by the impact stress. The sample was clamped to Charpy hammer where it was fractured subsequently. The force required for fracturing was recorded. Procedure is described in the detail in the standard ČSN EN ISO 179.

III. ARTIFICIAL NEURAL NETWORKS

The Artificial neural networks are based on biological neural networks. The basic building block of every artificial neural network is a mathematical model of neuron [1]. In cases where is not the algorithm to solve the problem well known but there is a sufficiently data amount of correct results or we are working with incomplete or broken data, there we can use artificial neural networks.

A. Mathematical model of neuron

The mathematical model of neuron was published in 1943 by McCulloch & Pitts. In the mathematical model there are dendrites and axons considered for perfect lossless lines. Synapses are regarded as memory elements and placed in a confluent. The artificial neural network provides the aggregation of operations, thresholding and nonlinear displaying. The basic mathematical model of neuron is shown in Figure 2 [1].

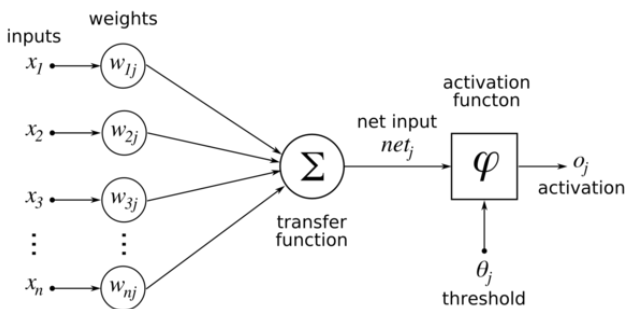


Fig. 2. Mathematical model of neuron

Synapses are represented by “the synaptic weights”. The synaptic weights are expressed by real numbers. Depending on the information that comes into a neuron, than can be the size of these numbers continuously varied. The neuron becomes trained. Mathematically synapses occur in the operation of confluency of current inputs and synaptic weights. Scales size can be changed by the setting of neuron [1]. Three mathematical operations are developed in the body of the neuron (soma). Signals which come from all synapses are aggregated. The aggregated value is compared with the threshold. When a non-linear function of the aggregate value shows then neuron signal appears at the output if the threshold is exceeded.

According to non-linear functions we can distinguish different types of neurons and neural networks. Neural

network can be defined as a parallel distributed system of executive elements which are suitably arranged so as to be able to process the requested information [1]. Each of the neural networks is characterized by its paradigm i.e. structure, type of neurons and function of the neural network. There are large amount of paradigms of neural networks. Selecting of the right type of paradigm for a given task is very important.

B. Distribution of networks according to the learning method

The artificial neural networks are divided into the groups by criteria. One of the most important criteria is based on the method of network self-education. There are three basic groups i.e., supervised learning, assessment of learning and competitive learning [1].

- In the case of *supervised learning* method, the network expects for each input pattern the corresponding output pattern. The network weights are adjusted by the difference between the desired output and the actual output. Supervised learning is used for regression, prediction and classification networks. They are represented by perceptron multi-layer networks (MLPN) and networks with radial basis (RBF) [1] in the STATISTICA software.
- *Evaluated learning* requires less information than supervised learning. This method evaluates an adequacy of the level between desired output and real output. It is not performed for each input pattern, but at regular time intervals [1]. This method does not use STATISTICA software.
- *Competitive learning* requires a minimum of information. There is no output pattern. The network organizes input patterns to outputs itself. The network clustered inputs in groups [1], Kohonen’s network is a typical representative and is also used by the STATISTICA software.

C. Distribution network's architecture

- Multi-Layer Perceptron Network (MLPN) - This is the most common type of network and It is basic building block is called a perceptron. MLPN networks use an adaptive learning cycle for supervised learning. MLPN is suitable for solving regression, prediction and classification tasks. STATISTICA software uses three-layer MLPN network. Generally, the hidden layer can be formed by more layers than one. The network is fully connected but without lateral connections – i.e. the output of the single layer perceptron is distributed to all perceptron in the following layers. [1]. The activation functions of neurons are optional in the hidden and output layer. Example MLPN topology is shown in Figure 3 [1].

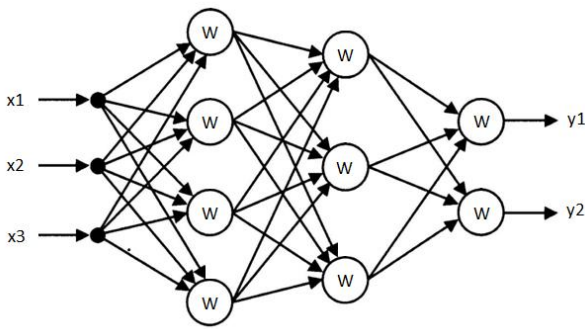


Fig. 3. Topology of MLPN

- Radial basis function (RBF) network - principle of RBF networks is the data coverage of data areas which can be assimilated to the circles (in two-dimensional space). The centers of the circles are located in the center of clusters. The radius of these circles are given by activation functions of individual neurons. RBF network is always three-layer, unlike MLPN-layer networks. The number of neurons is optional in the hidden layer. The network is completely connected, the same as the adhesion MLPN, but without lateral connections. Neurons in the hidden layer are called radial neurons type, it means that the distance from the input vector to the vector of weights is calculated, instead of the weighted sum of inputs (as is the case MLPN networks). The activation functions of the hidden neurons have Gaussian character. The output layer consists of neurons with linear activation function. [1]
- Kohonen's network - This network is a typical representative of competitive learning. Network approximates the probability distribution of the presented training data. The network has two layers, the input layer and the executive layers. Input neurons and executive layers are completely interconnected. Executive layer is composed of neurons arranged in a grid. That is called topological map with lateral connections. The weights of neurons in competitive layer can be seen as the coordinates which indicates the location of the neuron in the topological map. Competitive neurons in the layer consists of so-called formal neurons. The competitive neurons usually have binary output - active or inactive. The input pattern is compared with vectors stored in individual neurons during learning. Neuron is selected as a winner when the vectors setting is most similar to input pattern. Then the setting of the weights is adjusted. There is always only one active winning neuron for any design [1].

IV. CLASIFFICATION ANALYSIS

This chapter focuses on training of the network which can recognize the type of tested material by using the input variables. The variables are: temperature stress, exposure time, bending and impact. As the training set there are

used all the measured values. For the subsequent verification of sets medians groups are used.

The samples were divided randomly during network training into the training set, the validation set and the testing set in the ratio of 2:1:1. As the most suitable networks related on RBF network and MLPN were selected. These two networks were selected because of their suitability for the classification type of tasks in the method of supervised learning.

The result of the training is a comparison of network input material of their prediction errors based on output variables. The results of classification errors and abilities of the best four networks are found in Tab. 2 and 3.

TABLE II. RESULTS OF CLASSIFICATION ERRORS OF THE WINNING NETWORKS

Index	1	2	3	4
Net name	MLPN 4-15-4	MLPN 4-28-4	MLPN 4-14-4	MLPN 4-22-4
Training Perf.	100,000	100,000	99,773	99,773
Test Perf.	100,000	100,000	100,000	100,000
Validation Perf.	99,091	98,181	97,727	98,636
Training Algorithm.	BFGS 31	BFGS 32	BFGS 20	BFGS 78
Error function	Entropy	SOS	Entropy	SOS
Hidden activation	Logistic	Tanh	Tanh	Exponential
Output Activation	Softmax	Logistic	Softmax	Exponential

TABLE III. RESULTS OF CLASSIFICATION ABILITIES OF THE WINNING NETWORKS

Sample	Target material	Output material			
		1. MLPN 4-15-4	2. MLPN 4-28-4	3. MLPN 4-14-4	4. MLPN 4-22-4
Lpk t170 e48	paperboard	paperboard	paperboard	paperboard	paperboard
Rnx t175 e144	Relanex	Relanex	Relanex	Relanex	Relanex
Rnx t186 e8	Relanex	Relanex	Relanex	Relanex	Lamplex
Lmx t170 e0	Lamplex	Lamplex	Lamplex	Lamplex	Lamplex
Rsk t170 e384	Relastik	Relastik	Relastik	Relastik	Relastik
Lmx t190 e24	Lamplex	Lamplex	Lamplex	Lamplex	Lamplex
Lpk t180 e80	paperboard	paperboard	paperboard	paperboard	paperboard
Rnx t24 e0	Relanex	Relanex	Relanex	Relastik	Relanex
Lmx t170 e480	Lamplex	Lamplex	Lamplex	Lamplex	Lamplex
Lpk t200 e13	paperboard	paperboard	paperboard	paperboard	paperboard
Rsk t186 e2	Relastik	Relastik	Relastik	Relastik	Relastik
Lmx t24 e0	Lamplex	Lamplex	Lamplex	Lamplex	Lamplex
Rnx t186 e4	Relanex	Relanex	Relanex	Relanex	Relanex
Lmx t170 e600	Lamplex	Lamplex	Lamplex	Lamplex	Lamplex
Lpk t200 e7	paperboard	paperboard	paperboard	paperboard	paperboard
Rnx t175 e95	Relanex	Relanex	Relanex	Relanex	Relanex
Lmx t200 e25	Lamplex	Lamplex	Lamplex	Lamplex	Lamplex

The winning networks were subjected to testing on the data created from medians of material groups. Results of classification are presented in Table 4.

TABLE IV. FINAL RESULTS OF CLASSIFICATION

		Material-Lamplex	Material-paperboard	Material-Relanex	Material-Relastik
1. MLPN 4-15-4	Total	220,0000	220,0000	220,0000	220,0000
	Correct	220,0000	220,0000	219,0000	219,0000
	Incorrect	0,0000	0,0000	1,0000	1,0000
	Correct (%)	100,0000	100,0000	99,0000	99,0000
	Incorrect (%)	0,0000	0,0000	0,0000	0,0000
2. MLPN 4-28-4	Total	220,0000	220,0000	220,0000	220,0000
	Correct	218,0000	220,0000	219,0000	219,0000
	Incorrect	2,0000	0,0000	1,0000	1,0000
	Correct (%)	99,0000	100,0000	99,0000	99,0000
	Incorrect (%)	0,0000	0,0000	0,0000	0,0000
3. MLPN 4-14-4	Total	220,0000	220,0000	220,0000	220,0000
	Correct	219,0000	220,0000	216,0000	219,0000
	Incorrect	1,0000	0,0000	4,0000	1,0000
	Correct (%)	99,0000	100,0000	98,0000	99,0000
	Incorrect (%)	0,0000	0,0000	1,0000	0,0000
4. MLPN 4-22-4	Total	220,0000	220,0000	220,0000	220,0000
	Correct	218,0000	220,0000	218,0000	220,0000
	Incorrect	2,0000	0,0000	2,0000	0,0000
	Correct (%)	99,0000	100,0000	99,0000	100,0000
	Incorrect (%)	0,0000	0,0000	0,0000	0,0000

The results show that some of the networks are classified with hundred percent success rates in the verification on the medians of groups. However, this success should be taken with caution. To verify the quality of the classification would be more appropriate to use data from measuring of the different material samples and impact measurement performed on the same types of materials. It is interesting to note there is no RBF network in the final five successful networks. Probably, it is because the RBF networks use many times more neurons in the hidden layer than the MLP network. For this particular case the complexity of RBF network is unnecessary and counterproductive.

A gains chart in Figure 4 shows the strength and quality of forces classification of the best neural network which was found - MLPN 4-15-4.

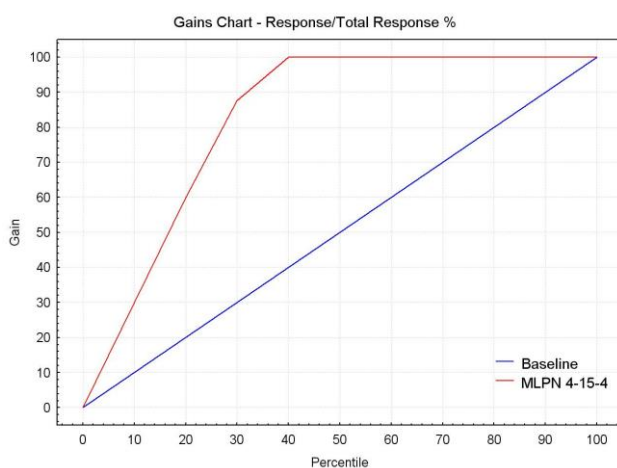


Fig. 4. Gains chart of best found network (MLPN 4-15-4)

V. CONCLUSION

The goal of classification by artificial neural networks was the use of different materials samples (paperboard L05, Relastik 45.013, Relanex 45.010 and Lamplex FR4) to train neural networks. Trained neural networks can recognize a sample of material when the values of

individual variables are entered. The final error rate of the networks given by the results of training cycles was less than three percent after training. The best neural network for this purpose is Multi-layer Perceptron Network 4-15-4 with 1 hidden layer.

Afterwards, the trained networks were tested on medians of groups of samples. There was demonstrated a very high classification accuracy in the tests. These medians were used as the representative value of each group of samples. Generally, the classification of artificial neural networks leads to the very accurate and practically meaningful results.

REFERENCES

- [1] M. Novák, Umělé neuronové sítě: teorie a aplikace, Praha: C. H. Beck, 1998.
- [2] M. Jiřina, Rozdělování dat do trénovacích a testovacích množin, Biomedicínské inženýrství před námi [online]. Praha: ARSCI, 2007, [cit. 2011-05-08]. From WWW: <<http://www.marceljirina.cz/index.php?s=marcel-jirina-jr&page=2>>.
- [3] V. Mentlík, R. Polanský, P. Prosr, Termické analýzy a elektrotechnický design [online], Plzeň ZČU, 2009, [cit. 2011-05-08]. From WWW: <www.icpf.cas.cz/ehlt/oscht/KS2009_Mentlik.ppt>.
- [4] M. Meloun, J. Militký, Kompendium statistického zpracování dat: metody a řešení úlohy analýza experimentálních dat, 2. ed., Praha, Academia, 2006. pp. 140-166, 255-275, 479-519.
- [5] M. Meloun, Statistická analýza vícerozměrných dat [online], Pardubice, 2002, [cit. 2011-05-08]. From WWW: <<http://meloun.upce.cz/docs/research/chemometrics/methodology/4gmetody.pdf>>.
- [6] M. Meloun, J. Militký, Přednosti analýzy shluků ve vícerozměrné statistické analýze [online], Pardubice, 2006, [cit. 2011-05-08]. From WWW: <<http://meloun.upce.cz/docs/publication/152.pdf>>.
- [7] I. Křivý, E. Kindler; Simulace a modelování [online], Ostrava, 2001, [cit. 2011-05-08]. From WWW: <<http://prf.osu.cz/kip/dokumenty/Msm.pdf>>.
- [8] J. Hanuš, Shluková analýza a její aplikace [online], Plzeň, ZČU, 2009, Bachelor thesis.
- [9] How to work with neural networks in SW STATISTICA, users manual, StatSoft ČR, 2004
- [10] Help SW STATISTICA

Power devices cooling using heat pipes

Roman Janiš¹⁾, Jan Kuba²⁾

FEE CTU in Prague, Technická 2, 166 27 Prague 6, Czech Rep., <http://www.fel.cvut.cz/>

¹⁾ tel: +420 224352198, email: janisrom@fel.cvut.cz ,

²⁾ tel: +420 224352164, email: kuba@fel.cvut.cz

Abstract— Authors are dealing with the possibilities of power devices cooling using heat pipes. Two basic types of the heat pipes, this is gravitational and capillary heat pipes are mostly used in practice. Mentioned various construction modifications of heat pipes including their characteristic behaviors are described in this paper. A disadvantage of the heat pipes in some applications is the restriction of the possibility to control their thermal conductivity. More detail the authors mention a little known management options of the thermal conductivity of heat pipes with an external static magnetic field. Some knowledge and the experiences especially the behavior of heat pipes with magnetically active nanodispersions as a working fluid are presented in this paper.

Keywords— cooling; heat pipe; magnetic fluids; thermal conductivity

I. INTRODUCTION

Heat pipes are used as devices to highly efficient heat transport in the direction of its longitudinal axis and are used in a wide number of the technical applications. Currently, heat pipes have a common alternative to conventional methods of heat transfer in many devices used in various areas of life, such as elements of power electronics cooling, heat recovery, ensuring the thermal dynamics of selected technological and biological processes, cooling of solar panels and many others. The heat pipe function is based on the closed two phase cycle of a working fluid (liquid and steam phase) located inside the pipe. In principle, the heat pipe consists of a hermetically sealed outer casing in which the special working fluid. Sheath material, its shape and size and type of working fluid is chosen especially with regard to the range of operating temperatures and aggressive environments, in which a heat pipe is used. Operating temperature range may be very large, of the order of 1 K to 1000 K. Outwardly, the heat pipe behaves as a solid body made of a material of extremely high thermal conductivity (of the order to $10^4 \text{ W}\cdot\text{m}^{-1}\cdot\text{K}^{-1}$), significantly higher than for example pure copper ($380 \text{ W}\cdot\text{m}^{-1}\cdot\text{K}^{-1}$). Some of heat pipe advantages are:

High thermal conductance (high heat flux), almost isothermal along the whole length, passive device (no power feeding necessary), can work as a thermal transformer (small area heat in - large area heat out), heat source - heat sink separation, simple construction and build in flexibility, quiet operation, no moving parts, long life and reliability (even in a hard environment).

Some of heat pipe disadvantages are:

Operation temperature range limited by a used working fluid, position limitations, possible complications at start-up, could be more expensive compared to conventional systems, limited ability to control heat transfer.

II. BASIC TYPES OF HEAT PIPES

According to the method of the internal arrangement of the heat pipe is divided into two basic types - gravitational and capillary. To ensure the return of the working fluid condensate is the gravitational heat pipes required vertical position and location of the condenser above the evaporator. Capillary heat pipes containing inside the specially made capillary system (wick) by flowing condensate in particular due to capillary forces, and therefore the correct function of this pipe on orientation in space little dependent, it depends on the type and design of the capillary system. Basic types of capillary systems are shown in Fig.1.

The principle suggested by its function of gravitational or capillary heat pipe provides intensive, but mostly unregulated heat transfer. In some applications it is desirable or necessary to heat flow in the pipe be to regulate. These are cases where it is required, for example the temperature to stabilize at some level or heat transfer completely interrupt.

III. EXPERIMENTAL METHOD

The heat transport ability of the selected capillary heat pipe company Thermacore was experimentally verified depending on its position. The pipe diameter of 9.5 mm and a length of 400 mm was on one side (evaporator) provided with a heating coil. The heating coil was connected to a controllable DC source, performance measurement was maintained power $P = 10 \text{ W}$. On the other hand pipe (condenser) was attached heat sink. Temperatures were measured at the evaporator and condenser with digital thermometers GTH1170 and type K thermocouples, the distance between them was 300 mm or by the thermal camera type FLIR IR7. The pipe was mounted in a holder which allowed its positioning in the range 0° to 180° . All measurements were realized at normal temperature of air. Some results are shown in Fig. 2. and Fig. 3.

We designed, implemented and experimentally verified a controllable heat pipe with an external static magnetic field. This pipe is a gravity type and was

designed for temperatures close to the ambient temperature. In this case, the sealed casing pipe consideration of non-ferromagnetic material (Cu) and the working fluid is magnetically active nanodispersions.

A solution of distilled water and a magnetic fluid, water-based type Ferrotec EMG 304 in ratio 1:1, the total amount of the working fluid 3 ml was used. A pressure in the pipe at normal temperature was set by using vacuum pump to about 2.5 kPa. The outer and inner diameter of the pipe were 8 mm / 6 mm and a length of 400 mm was on one side (evaporator) provided with a heating coil. On the other hand pipe (condenser) was attached heat sink. Heating the pipe $P = 10 \text{ W}$ and the temperature measurement was performed as in the case of a capillary pipe as given before. From the outside of the heat pipe was located source of static magnetic field between the evaporator and condenser.

A principle of a heat pipe arrangement controllable by an external magnetic field is shown in Fig. 4.

Position 1 is Cu sheath of the pipe, 2 is evaporator equipped with a heating coil, 3 is a condenser provided with a ribbed heat sink, 5 is a magnetic working fluid and position 4 is a source of static magnetic field. Two permanent NdFeB magnets 40x20x10 mm oriented opposite poles facing each other were used. The pipe was placed in a gap between the magnets, the gap width was 12 mm, the induction $B \text{ app. } 0.5 \text{ T}$, the vector perpendicular to the axis of the pipe. Was also tested alternative to NdFeB permanent magnet in the shape of a toroid with dimensions 42x22x10 mm. Induction inside the toroid was about 0.35 T, the vector was longitudinal to the axis of the pipe in this case. Some results are shown in Fig. 5. and Fig. 6. and Fig. 7.

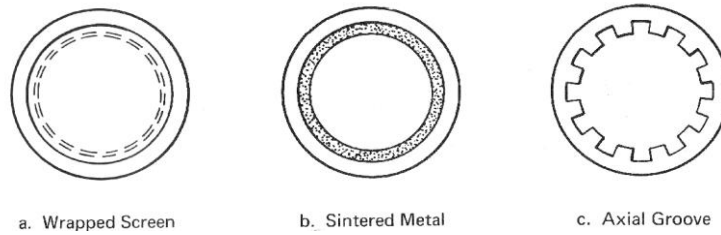


Fig. 1. Basic types of capillary systems.

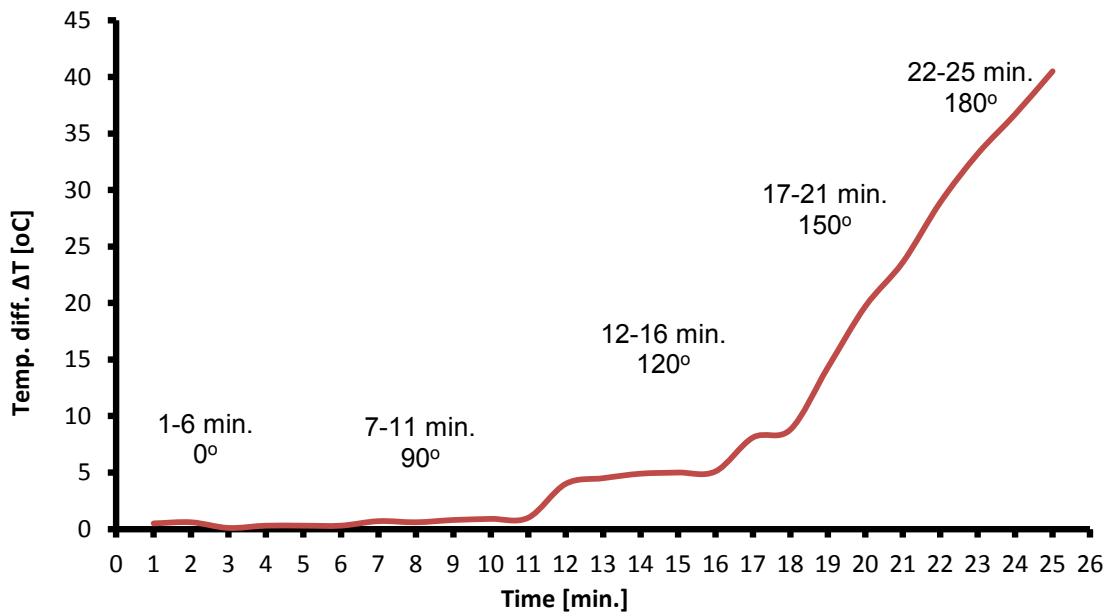


Fig. 2. Time dependence of the temperature difference ΔT between the ends of the pipe at positioning.

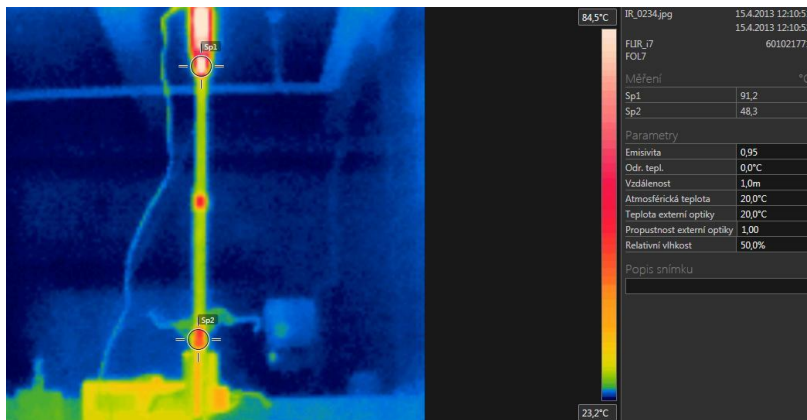


Fig. 3. Temperature distribution along the pipe during a rotation of 180°.

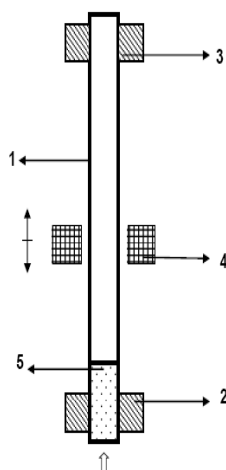


Fig. 4. Heat pipe arrangement with ferrofluid controllable by an external magnetic field.

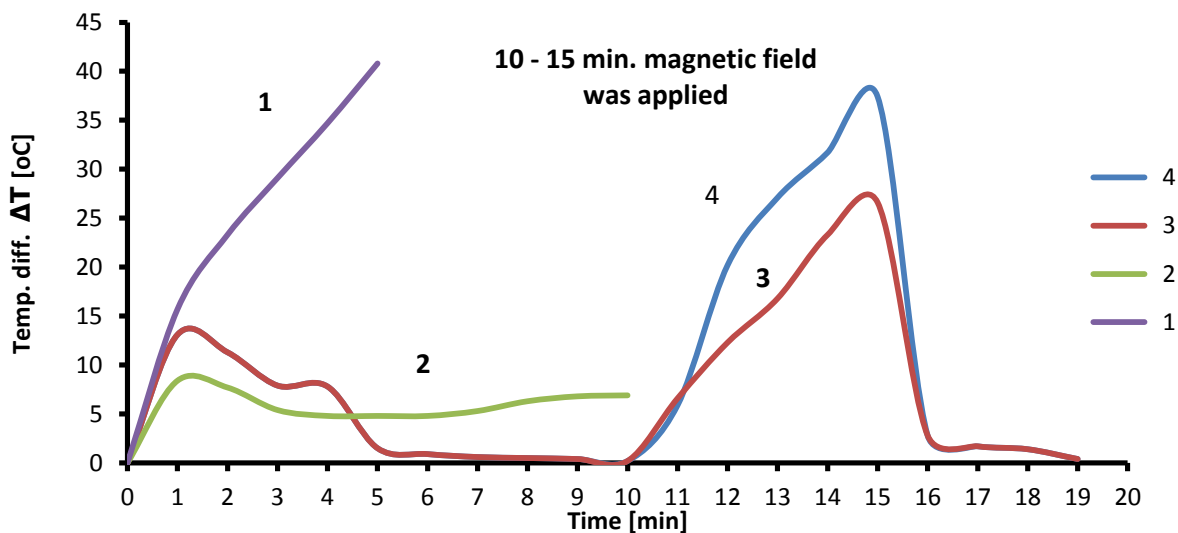


Fig. 5. Time dependence of the temperature difference ΔT between the ends the pipe – empty pipe (1), with clean water (2), with ferrofluid with longitudinal MF(3), with ferrofluid and with transverse MF(4).

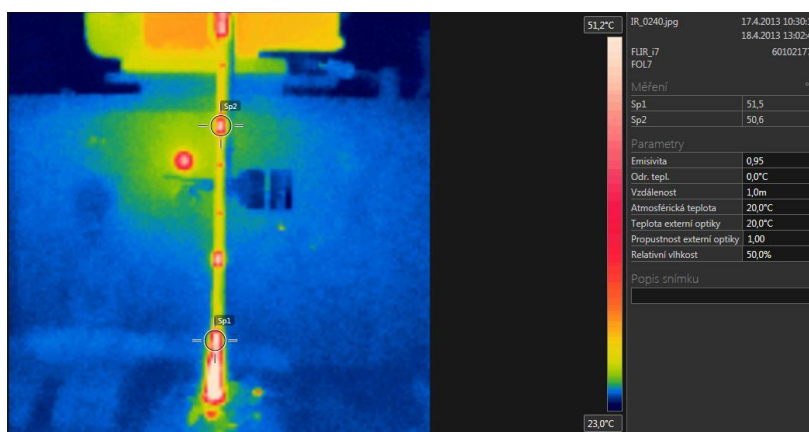


Fig. 6. Temperature distribution along the pipe with ferrofluid in the steady state and without MF.

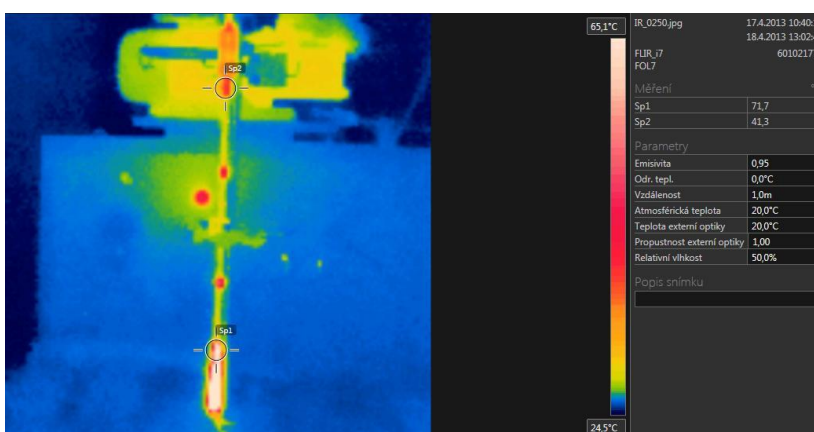


Fig. 7. Temperature distribution along the pipe with ferrofluid in the steady state and with longitudinal MF.

IV. CONCLUSION

From the results of the measurements with the standard capillary tube Thermacore we can say that its transport capacity is highest in an ideal vertical position (0° - evaporator down, condenser above). Good capability is maintained in a horizontal position, too. The next filming begins procedures to decrease and at the angle of 120° is already a significant reduction. When complete rotation of the pipe is made (180° - evaporator above, condenser down) the pipe is virtually non-functional. Measurements made on the gravitational heat pipe filled with magnetic fluid showed that influence its ability to heat transport an external magnetic field is very effective. It is possible to apply an external magnetic field in the transverse or longitudinal direction of the axis of the pipe, as well. Using magnetic fluid as the working fluid in heat pipes with controlled heat transport an external magnetic field is still under-researched area, but due to the possibilities of widespread use in practical applications, a very promising area.

ACKNOWLEDGMENT

This paper is based on the research program for students No. **SGS13/071/OHK3/1T/13** “Magnetic fluids and their use in heat pipes“ of CTU in Prague.

REFERENCES

- [1] Reay, D., A., Kew, P., A.: Heat pipes Theory and Practice, Elsevier, London 2006
- [2] Cingroš, F., Hron T., Kuba, J.: Magnetic Field Control of Cryogenic Heat Pipes. In *Proceeding of the International Conference ISSE 2009*. Brno (Czech Republic), 2009.
- [3] Kuba, J., Janiš, R.: Heat Pipe with Controlled Heat Transport, The Utility Model, No. 24730, Czech Industrial Property Office, Prague 2012
- [4] Janiš, R., Kuba, J.: The Possibility of Cooling of Electronic Equipment , In *Transaction on Electrical Engineering*, Vol.1., ISSN 1805-3386, Prague 2012
- [5] <http://www.thermacore.com>

The proposition of low frequency filter in electrical machines diagnostics

Ján Poliak¹⁾, Daniel Korenčiak²⁾

Department of Measurement and Application Electrical engineering, Faculty of Electrical Engineering, University of Žilina, Univerzitná 1, 010 26 Žilina, Slovakia

¹⁾ tel: +421 41 513 2127, email: jan.poliak@fel.uniza.sk ,

²⁾ tel: +421 41 513 2135, email: daniel.korenciak@fel.uniza.sk

Abstract— In the paper are introduced the criteria for low frequency filters measurement which must be satisfied by filter in electric machines diagnostics. Also contains its design procedure and calibration.

Keywords— bandpass; amplifier; low frequency; low cost

I. INTRODUCTION

In electric machine diagnostics are multiple methods which are based on low frequency measurement so this is very important to eliminate higher frequencies than 10Hz.

As an example, here is one such measurement method FDS (Fig. 1), which is used for assessing of moisture and is monitoring of frequency dependence of insulation parameters transformer paper and oil (capacity, permittivity, $\tan \delta$) from tens of mHz to 10 kHz. This is so called dielectric spectroscopy, where the principle is monitoring of response (polarization) of particles based on frequency changes in a broad band. The biggest problem with measurement method is the preparation of FDS source of lower frequency.

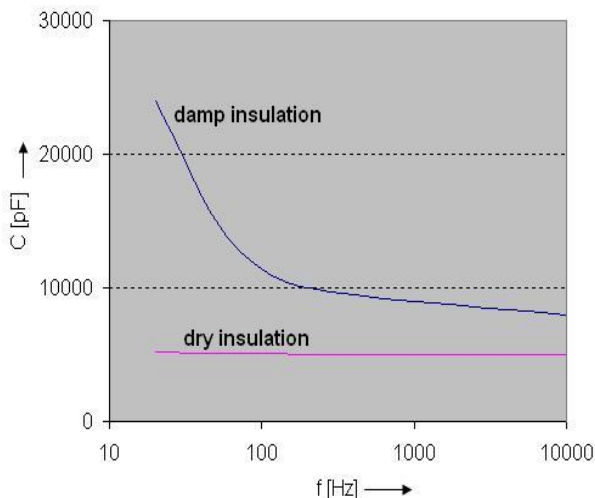


Fig. 1. Frequency dependences of capacity at dry and damp insulation of electrical machine [9]

So this problem not always as simple as it seems and each filter is not suitable for this purpose. Many suitable

filters are expensive. For this reason was designed, constructed and calibrated a simple filter.

II. IMPORTANT FILTER CRITERIA

The filter must be tunable in the range from 0 Hz to 100 Hz, and should be transmitting only the tuned frequency, other frequencies should be suppressed. This implies that the filter were bandpass with a very narrow pass band. Because the filter will operate at very low frequencies, it is necessary to use a variant of the active elements we had to use a large coil inductance in passive filter at low frequencies.

III. DESIGN PROCEDURE

We can proceed in two ways in the design. One way is complete filter proposition. In this way we must determine the width of the pass band, all the required frequencies f_1, f_{-1}, f_2, f_{-2} , in the next were chosen minimal and maximal values of specific level for not very big filter level, and use these values to design new filter. This process is very tedious and difficult. An easier way is to use the already proposed filter is adapted it for our requirements for required frequencies. It is close Tunable BP with quality constant Q , which schematic is on Fig. 2.

At the upper limit position of the potentiometer of this filter (the runner is at the end connected on output of the previous amplifier) is the center frequency given by

$$f_0 = \frac{1}{2\pi R_1 C_1} \quad (1)$$

where $R_1 = R_2 = R_3 = R_4 = R_5$ and $C_1 = C_2$. To determine the center frequency is fundamental capacitor C_1 .

If we want value 100 Hz, capacitor C_1 should have a value

$$C_1 = C_2 = \frac{1}{2\pi R_1 f_0} = 1,591549 \mu F \quad (2)$$

For a limited component base (1.5 μF capacitor is not in shop offer), I need to use capacitors $C_1 = C_2 = 1 \mu F$. At the upper limit position potentiometer was calculated value $f_0 = 159.155$ Hz.

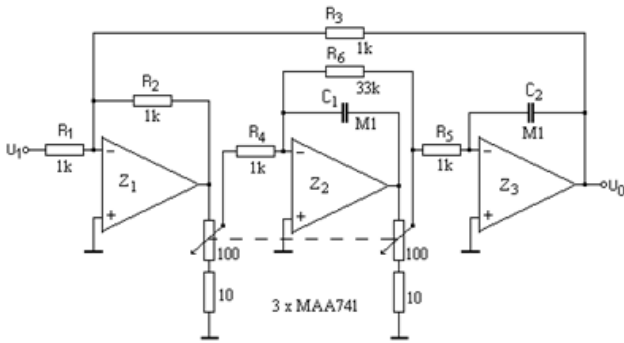


Fig. 2. Tunable BP with quality constant Q.

The upper frequency is given by upper potentiometer limit position. Also is necessary to achieve a lower frequency at 0 Hz. From the diagram is evident that the frequency is given by the size of the potentiometer resistance, runner in the lower limit position. This was experimentally made for 20 kΩ potentiometer, in which were found lower frequency $f_0 = 1.44$ Hz.

In next were been found that the passing frequency dependence of the position of the runner is exponential. This excludes using a potentiometer with a linear resistance taper, because the frequencies higher than 50 Hz were very difficult to tune. For compensation this phenomena was used a potentiometer with logarithmic resistance taper.

Finally, the proposal of the BP was replenished with a simple amplifier with two OZ type MAA 501, the scheme is shown in Fig. 3.

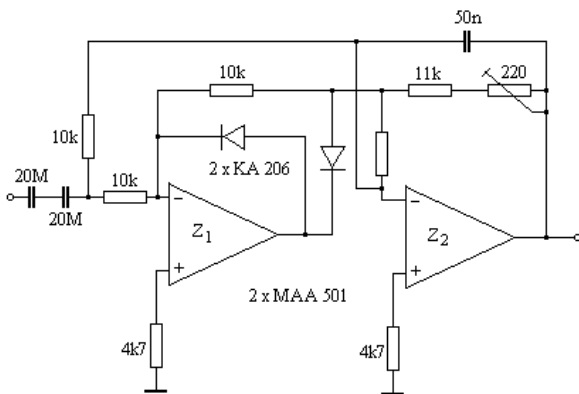


Fig. 3. Involvement of a single amplifier.

IV. REALISATION

A. Printed circuit board design

For the proposed connection of BP amplifier was necessary to design the PCB. For simplicity, it was decided to propose a separate board for the BP and the separate for an amplifier. This variant is better to eliminate any errors. The several programs were used for the proposal. They were “Editor Schémat of Formica 4.2 system”, “Ferda Mravenec 3.50”, “Editor plošných spojov and Autorouter of Formica 4.2 system”.

Using Editor schémat Formica 4.2 was drawn schematic and BP amplifier. The reason was program function called Netlist creation, which is a joint list of points, circuit elements and pins OA, which was been used in the other programs.

On the default component layout was used program Ferda Mravenec 3.50, because is easy to define and edit non-standard size components (potentiometers) in this program. This program also includes Autorouter (program for automatic design of joints), but it does not contain Undo function, the design was rather completed in the Editor plošných spojov and Autorouter system in Formica 2.04 program.

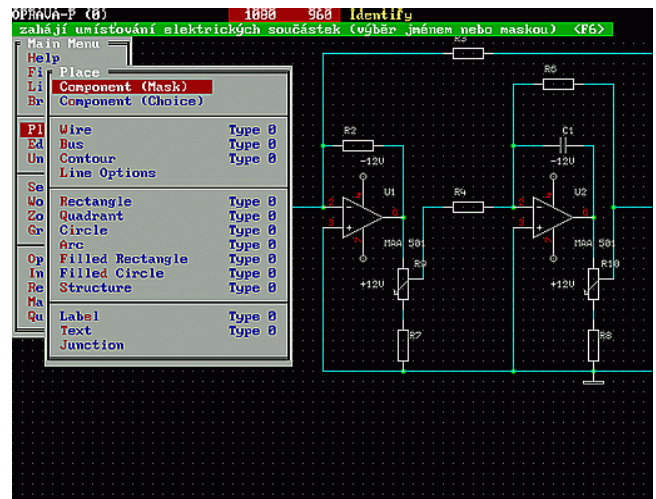


Fig. 4. The Editor schémat Formica 4.2 program .



Fig. 5. The Ferda Mravenec 3.50 program .

This program contains multipass optimizing Autorouter based on Lee's algorithm which is operating on any two conductive layers and it is able to design wires in eight directions. Input for the Autorouter are arrangement of the objects on board, especially (hand) spaced component and list of missing components and connections which are made by comparing the list of connections - the netlist with the actual involvement of the PCB. For selected connection is suffice board with one conductive layer.

The Autorouter setting is based on the current size of elements and insulation distances. It operates on a pair of layers A and B, or on only one layer and create connecting lines with preselected settings. Autorouter function is configurable using several parameters and weights.

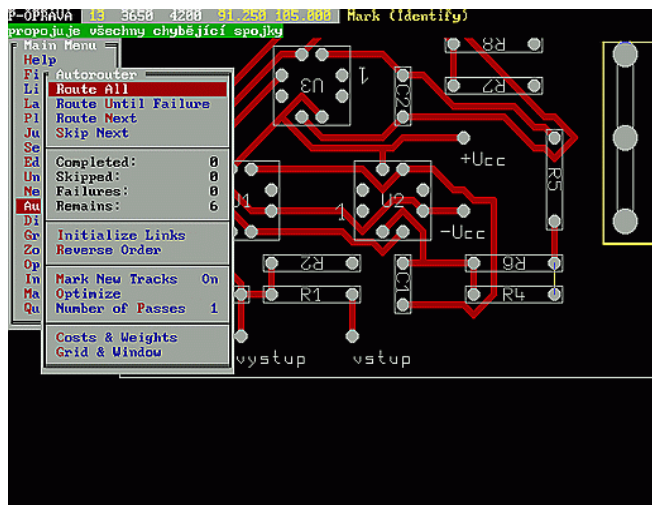


Fig. 6. The Editor plošných spojov Formica 4.2 program .

The problem was to find the optimal layout of components for better wiring realization for Autorouter. Dimensions parts were considered by [6] and [7]. The advantage of this program is manual connection implementation for some components. Thus were created connections for power, inputs, outputs and ground. For convenience, a separate PCB for BP, a separate PCB for amplifier and a simple PCB for potentiometer was created, which is tuned frequency in BP. Potentiometer connection with BP board is realized by wire.

Using Editor schémat Formica 4.2 was drawn schematic and BP amplifier. The reason was program function called Netlist creation, which is a joint list of points, circuit elements and pins OA, which was been used in the other programs.

V. CALIBRATION

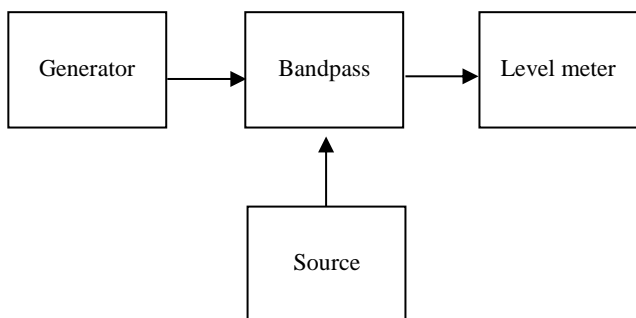


Fig. 7. Block diagram of BP connections at calibration.

To power the Bandpass was used external laboratory source (Fig. 4). On the input of Bandpass were given signal from tunable pulse generator. The conditions were as precise as possible tuned frequency. On Bandpass output was connected level meter. Potentiometer is at the lower limit position.

The generator was set at 2 Hz, which is the lower limit frequency of Bandpass. Then the potentiometer was rotated and the deflection was monitored by the level meter. The position, which level meter showed the highest value of the deflection circuit was tuned to a frequency of 2 Hz. This was repeated for frequencies 10, 20, 30 ... 100 Hz.

VI. CONCLUSION

The tasks of design were not only proposal but also assemble and calibrate type of tunable bandpass filter. Its frequency range should be from 0 to 100 Hz. Based on used schematic and the most accessible component base were implemented tunable filter at range from 2 Hz to 150 Hz, which the BP is calibrated only to 100 Hz. The advantage of the filter is simple parameter modification by modifying some parts. The whole device is very simple to operate and economically is inexpensive.

ACKNOWLEDGMENT

This work was supported by the Grant Agency VEGA from the Ministry of Education of Slovak Republic under contract 1/0624/13.

References

- [1] Křišťan, L., Machala, V. , Příručka pro navrhování elektronických obvodů, vydalo SNTL – nakladatelství technické literatury, Praha, 1982
- [2] Boreš, P., Volner, R., Tichá, D., Teória obvodov - syntéza a simulácia, vydala Žilinská univerzita v Žiline, 1997
- [3] Čajka, J., Kvasil, J., Teorie lineárních obvodů, vydalo SNTL – nakladatelství technické literatury a Alfa, Praha, 1979
- [4] Hrubý, J., Novák, M., Mikroelektronické filtry RC se zesilovači, vydala Academia, Praha, 1976
- [5] Kolombet, E., Jurkovič, K., Zodl, J., Využitie analógových integrovaných obvodov, vydala Alfa, Bratislava, 1990
- [6] Nečásek, S., Janeček, J., Rambousek, J., Elektronické a elektroakustické součástky, vydalo SNTL – nakladatelství technické literatury a Alfa, Praha, 1985
- [7] Taurek, J. a kol., Technické údaje polovodičových součástek, vydalo SNTL –nakladatelství technické literatury, Praha, 1980
- [8] Amatérské rádio, rada B, č. 6/1977, Aktivne filtre
- [9] Gutten, M., Korenčiak, D.: Analysis of humidity influence in a transformer model, In: PRZEGLĄD ELEKTROTECHNICZNY= Electrical Review, Vol. 88, No. 12a, 2012, ISSN 0033-2097, pp. 302-304

Analysis model of transformer by PDC method

Daniel Korenčiak¹⁾, Miroslav Gutten²⁾, Matej Kučera³⁾, Tomasz N. Kołtunowicz⁴⁾

Department of Measurement and Application Electrical engineering, Faculty of Electrical Engineering, University of Žilina, Univerzitná 1, 010 26 Žilina, Slovakia

¹⁾ tel: +421 41 513 2135, email: daniel.korenciak@fel.uniza.sk

²⁾ tel: +421 41 513 2127, email: miroslav.gutten@fel.uniza.sk ,

³⁾ tel: +421 41 513 2126, email: matej.kucera@fel.uniza.sk ,

⁴⁾ Politechnika Lubelska, Faculty of Electrical Engineering and Computer Science, Department of Electrical Apparatus and High Voltages Technology, Nadbystrzycka 38a, 20-618 Lublin, Poland, Email: t.koltunowicz@pollub.pl

Abstract— Paragraph is containing mathematical interpretation of transformer insulation system. This system is basically composed by two elements oil and pressboard. Simulation of this complex system is necessary for more precisely results from measurement. We mathematically describe how to calculate relaxation currents and how that currents are generated. This is the first step to compare measured and computed values.

Keywords— Insulation, oil, paper, winding, transformer, polarization, depolarization, diagnostics.

I. INTRODUCTION

Many power transformers around the world are approaching the end of their operation time. Transformer is very expensive to replace. We need to clearly know its conditions. For this reason is necessary precision fast and cheap diagnostic. The diagnostic important part of transformer operation. We need to know how transformer insulation cooperates between elements and how it works for running of the diagnostic system in ideal conditions.

These allow us to mathematic explanation individual parameters. Mathematical calculation is too difficult in system like transformer. We describe a small part of mathematical simulation of this system for this reason. We focus on simulation of the polarization depolarization current and its behaviour. We analyze generation of this currents and we shows from what the currents are made in this method. [1]

II. THEORY BASES

In last few years several diagnostic techniques have been developed and used to determine the power transformer insulation. That means this techniques must determine insulator composed from transformer oil and paper in main. Most of these techniques have been in use for many years, such as the measurement of insulation resistance (IR), dielectric loss factor (DLF), partial discharges (PD), interfacial polarization (IP) using anomalous IR and frequency dispersion capacitance, oil quality, moisture content, dissolved gas analysis (DGA), viscometric degree of polymerization (DPV) . and tensile strength of cellulosic paper and pressboard. [2]

For PDC analysis is fixed DC voltage step applied across the test insulation for testing time t_p , the so-called polarization duration. Thus a charging current of the transformer capacitance so-called polarization current is measured. It is a pulse-like current during the application which decreases during the polarization duration to a certain value given by the conductivity of the insulation system. Then voltage is removed and the object is short circuited. The previously charging current jumps to a negative value, which goes gradually towards zero. The charging and discharging currents are influenced by the properties of insulation material and its geometrical structure. This measurement system is shown in Fig.1. [3]

Next picture (Fig.2) shows polarization current and its response in this measurement system.

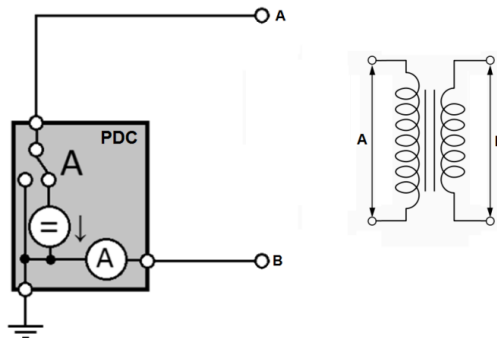


Fig. 1. Simply PDC measurement system

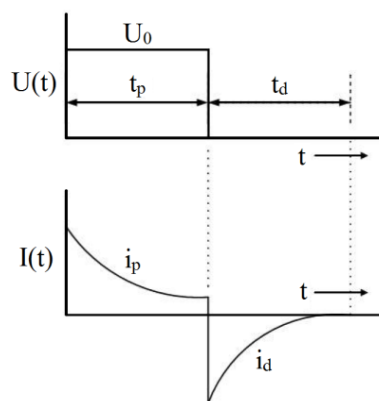


Fig. 2. Principle waveform of relaxation currents [4]

III. MATHEMATICAL INTERPRETATION OF POLARIZATION PROCESS IN DIELECTRIC MATERIAL

Assuming a homogenous electric field $E(t)$ is applied to the dielectric material the current density through the surface could be expressed as following:

$$J(t) = \sigma \cdot E(t) + \frac{dD}{dt} \quad (1)$$

Where, $J(t)$ is current density which is the sum of the conduction current and the displacement current, σ is DC conductivity, $D(t)$ is electric displacement, which has the following relationship between polarization and the electric field vector:

$$D(t) = \varepsilon_0 \cdot E(t) + P(t) \quad (2)$$

where ε_0 is vacuum permittivity and observed dielectric polarization, $P(t)$, contain two element parts:

$$P(t) = P_{\text{rapid}}(t) + P_{\text{slow}}(t) \quad (3)$$

where $P_{\text{slow}}(t)$ is slow polarization, $P_{\text{rapid}}(t)$ represents instantaneous polarization processes in the material, which can follow the changes of electric field, so $P_{\text{rapid}}(t)$ can be expressed as:

$$P_{\text{rapid}}(t) = \varepsilon_0 (\varepsilon_r - 1) \cdot E(t) \quad (4)$$

where ε_r is the relative permittivity of the insulation (typically is ostensible at power frequency with value 4.5 for cellulose and 2.2 for oil).

In general, a material cannot polarize instantaneously in response to an applied field. Therefore, the slow polarization process is delayed response polarization due to dipolar and interfacial polarization processes. The polarization is a convolution of the electric field $E(t)$ with time-dependent dielectric response function $f(t)$.

For any arbitrary electric field $E(t)$, the show polarization processes can be given as:

$$P_{\text{slow}}(t) = \varepsilon_0 \cdot \int_0^t f(t-\tau) \cdot E(\tau) d\tau \quad (5)$$

where $f(t-\tau)$ represents the degree of delay.

Therefore, the observed polarization can be rewritten as:

$$P(t) = \varepsilon_0 \cdot (\varepsilon_r - 1) \cdot E(t) + \varepsilon_0 \cdot \int_0^{\infty} f(t-\tau) \cdot E(\tau) d\tau \quad (6)$$

By combining (1), (2) and (6), the total current density $J(t)$ due to a constant electric field can be written as follows:

$$j(t) = \sigma \cdot E(t) + \varepsilon_0 \cdot \varepsilon_r \cdot \frac{dE(t)}{dt} + \varepsilon_0 \cdot \frac{d}{dt} \left\{ \int_0^t f(t-\tau) \cdot E(\tau) d\tau \right\} \quad (7)$$

Moreover, according to (7), we can find that the behavior of the dielectric material is characterized by

conductivity σ , high frequency dielectric permittivity ε_r and the dielectric response function $f(t)$ in the time domain. Three characteristic quantities provide important information of insulating material. [5]

IV. SHAPE OF POLARIZATION CURVE AND SIMULATION

In (Fig.2.) we can see the polarization (charging) current. This current can be expressed as:

$$i_{\text{pol}}(t) = C_0 \cdot U_0 \cdot \left[\frac{\sigma_r}{\varepsilon_0} + f(t) \right] \quad (8)$$

where C_0 is the geometric capacitance, σ_r is the average conductivity of the composite insulation system, ε_0 is the vacuum permittivity and $f(t)$ is the dielectric response function of the composite insulation, U_0 is the applied charging voltage.

It can also be shown that the depolarization current can be expressed as:

$$i_{\text{depol}}(t) = C_0 \cdot U_0 \cdot [f(t) + f(t+t_c)] \quad (9)$$

where t_c is the time during which the fixed step voltage was applied to the insulation system. So we are able to dismantle real shape of curve of dielectric response to base equations. The equations could be calculated by simulating program. [5]

We use extended Debye model for calculating the current for the best result in simulation. Many factors affect the polarization process of oil-paper insulation, such as aging, moisture and temperature of insulation, which can cause a series of different relaxation time constant. So single RC circuit cannot follow measured dielectric response exactly. Thus, it is difficult to reflect the complex polarization by the equivalent circuit with single Debye relaxation time. This is the reason why we need extended model (Fig.3.). But for simplicity of calculation we use model with three relaxation elements.

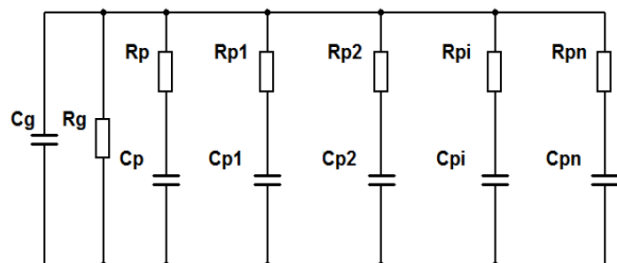


Fig. 3. Principle circuit for simulating relaxation currents

We picked-up current through this circuit and then we obtain curves which are shown in Fig.4. Values of parameters used in simulation are measured from tested object (transformer TESLA 230V~24V; 16,8VA; 50Hz - Fig.4.).

This transformer is old transformer in a good condition. Transformer was selected as a sample for value of a direct current. Measured value of direct current is bigger because the old insulation had lower insulation resistance. For this

case the measured curve is better for analyzing. Measured parameters are in Table 1.

TABLE I. MEASURED PARAMETERS OF TRANSFORMER

	R_1 [M Ω]	C_1 [nF]	R [M Ω]	C_{50} [nF]
1	12	45	50	90
2	16	7,5		
3	30	6		

These values are substituted in equations and draw a curve consequently.

The result of simulation of polarization and depolarization current with extended Debye model is shown in Fig.5. Fig.5 shows the charge and the discharge currents obtained on transformer using parameters of Table 1. Calculated value of maximal voltage of simulated curve is $\pm 4,287$ V. The calculated value of direct current was 0,433 V. Now we had dielectric model for a real transformer. In the next we need to measure real curve from the simulated transformer. [9]



Fig. 4. Measured transformer TESLA 230V~24V

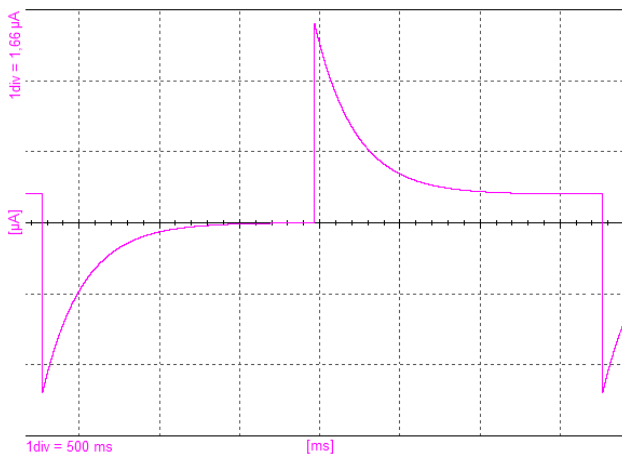


Fig. 5. Simulation of PDC with extended Debye model.

V. EXPERIMENTAL MEASUREMENT

For PDC measurement a step-like dc charging voltage of magnitude U_c is applied to the test object. Dielectric memory of the test object must be cleared before PDC

measurement. Charging voltage should be free of any ripple and noise, in order to measure the small polarization current. Then a polarization current $i_{pol}(t)$ through the test object can be recorded. The charging process takes a long time until the polarization current becomes either stable or very low. Immediately following the polarization, the depolarization current $i_{dpol}(t)$ can be measured by subsequent short circuiting of the test object.

The setup is equipped with high voltage source and picoammeter, which is composed by oscilloscope and shunt resistor which was sensed by a personal computer. All measurements were carried out at 300 V after lacquer-paper moisture equilibrium was achieved. Before the test began, the specimen remained in short circuit case until very low-level detectable current was achieved in order, to ensure similar condition for the measurements. Principle scheme of measuring device is showed on Fig.6.

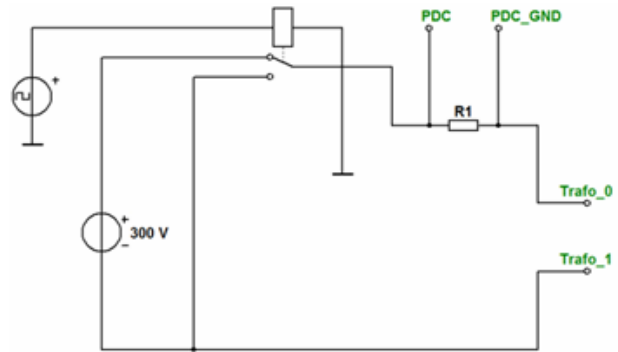


Fig. 6. Principle circuit for measuring relaxation currents

For measurement purpose the switch is switched like on Fig.6, so that the polarization current flows in insulation specimen and decreases to zero during application of voltage. For the investigated samples the current decreases from some mili ampere to some micro ampere. After polarization duration, which takes for example 1000s, switch was flipped and the specimen is short circuited. Similar to polarization duration, depolarization current in this stage flows, but in another direction. Both currents are stored for analysis in computerized measuring system.

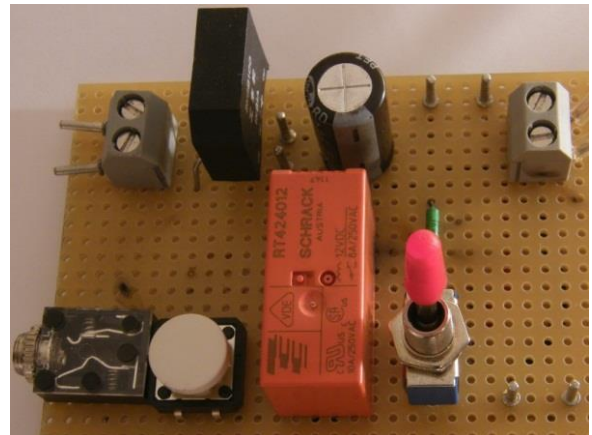


Fig. 7. Principle circuit for measuring relaxation currents

Connection of simple measurement circuit is showed on Fig.7. When the circuit is connected to the PC and to the measured specimen, we obtain time response of polarization and depolarization current (Fig.8, 9). Then we are able to compare measured and simulated value of polarization (depolarization) current.

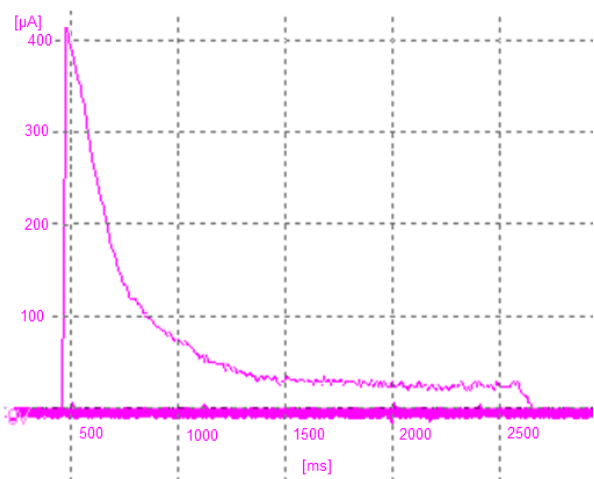


Fig. 8. Measured curve of polarization current

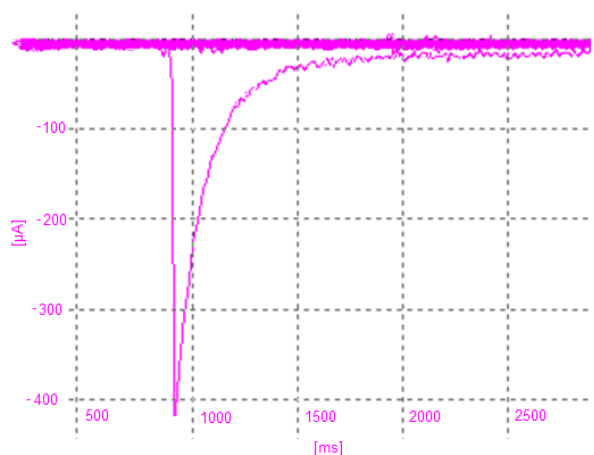


Fig. 9. Measured curve of depolarization current

When we connect specimen to polarization voltage $U=300V$ we measured maximal voltage on shunt resistor. This voltage was 4,158V at maximum. It corresponds to 4 mA at maximum peak value. The direct current is corresponding to a 468µA in stable state. Shape of curve of polarization current is showed on Fig.8.

Now polarization voltage is disconnected and measured transformer is connected to ground, depolarization current flows through the circuit. Measured voltage on sample was -4,202V at maximum peak. It corresponds to 4 mA at maximum peak value. Shape of curve of polarization current is showed on Fig.9.

VI. CONCLUSION

Depolarization current analysis shows important information about insulation which is moisture content or ageing status of transformer.

Difference between measured and calculated values was 0,085V which correspond to a 0,5% of a maximum peak value of a measured current. Direct current difference of a polarization process was 7% of stabilized curve. That means the lacquer and paper conductivity must be corrected for further calculation.

PDC measurement is important and exact method for diagnostic the state of transformer insulation. This method could be used in small transformer or in distribution transformer with oil-paper insulation.

ACKNOWLEDGMENT

This work was supported by the Grant Agency VEGA from the Ministry of Education of Slovak Republic under contract 1/0624/13.

REFERENCES

- [1] Patsch, R., Kouzmine, O.: Return Voltage Measurements - the Step from Experimental Data to a Relevant Diagnostic Interpretation, In: Proceedings of International Symposium on Electrical Insulating, zv. B6, pp. 889-892, 2005.
- [2] Shayegani, A., A., Hassan, O., Borsi, H., Gockenbach, E., Mosheni, H.: PDC Measurement Evaluation On Oil-Pressboard Samples, In: International Conference on Solid Dielectrics, zv. 4, pp. 50-62, 2004.
- [3] Leibfried, T., Kachler A., J.: Insulation Diagnostics on Power Transformers using the Polarisation and Depolarisation Current (PDC) Analysis, In: International Symposium on Electrical Insulation, zv. 10, pp. 170-173, 2002.
- [4] Saha, T., K., Purkait, P.: Some Precautions for the Field Users of PDC Measurement for Transformer Insulation Condition Assessment, In: IEEE, zv. 3, pp. 2371-2376, 2003
- [5] Chen, M., Hu, S., Mo, Z.: Fault Diagnosis Model of Oil-immersed Transformer Based on Return Voltage Measurement, In: CIED, zv. 1, pp. 1-5, 2008
- [6] Saha, T., K., Pradhan, M., K., Yew, J., H.: Optimal Time Selection for the Polarisation and Depolarisation Current Measurement for Power Transformer Insulation Diagnosis, In: IEEE, zv. 7, pp. 1-7, 2007
- [7] Gutten, M., Kučera, S., Kučera, M., Šebök, M.: Analysis of power transformers reliability with regard to the influences of short-circuit currents effects and overcurrents, In: PRZEGLĄD ELEKTROTECHNICZNY, p.62-64, R. 85 NR 7, 2009
- [8] Šimko, M., Chupáč, M.: Non-destructive method of measurement of radio transmitters antenna systems, In: Elektronika ir elektrotechnika = Electronics and electrical engineering, Vol. 107, No. 1, 2011
- [9] Jurčík, J.: Analysis of insulating state on transformer model using PDC method. In: Proceedings 9th International Conference ELEKTRO 2012, Rajecké Teplice, ISBN 978-1-4673-1178-6

Effect of Asymmetry on Reliability of a Distribution Transformer in Star-Delta Configuration

Matej Kučera¹⁾, Milan Šebök²⁾, Daniel Korenčiak³⁾, Pawel Zhukowski⁴⁾

Department of Measurement and Application Electrical engineering, Faculty of Electrical Engineering, University of Žilina, Univerzitná 1, 010 26 Žilina, Slovakia

¹⁾ tel: +421 41 5132118, email: matej.kucera@fel.uniza.sk,

²⁾ tel: +421 41 5132129, email: milan.sebok@fel.uniza.sk,

³⁾ tel: +421 41 513 2135, email: daniel.korenciak@fel.uniza.sk

⁴⁾ Politechnika Lubelska, Faculty of Electrical Engineering and Computer Science, Department of Electrical Apparatus and High Voltages Technology, Nadbystrzycka 38a, 20-618 Lublin, Poland, Email: pawel@elektron.pol.lublin.pl

Abstract— This article describes analysis of frequent faults on 630kVA, 22/04kV transformer which is connected in star - delta configuration (Dyn1). Multiple breakdowns in a short (eight months) period made us to analyse its operation with a view to completely resolve or at least diminish this issue which subsequently cause considerable financial loss.

Keywords— Reliability, asymmetry, transformer, harmonic analysis.

I. INTRODUCTION

Reliability of a technical device cannot be set with an absolute certainty. Reliability can be considered as a quality time fragment which is affected by technological discipline and a level of personnel qualification.

In all applications we can see that decreasing level of reliability comes with:

- higher levels of sophistication of an equipment,
- harsh work environment.

Reliability of distribution transformers is highly dependent on their type of use. One of the significant factors affecting its operational life is temperature, which can be influenced by:

- degradation of insulation systems,
- effects of short currents,
- symmetric overload over nominal value of a transformer,
- asymmetric overload at the transformer output.

II. ANALYSIS OF DISTRIBUTION TRANSFORMER FAILURES

The area of analysis and synthesis of a closed electroenergetic system supplied from a distribution transformer is from the reliability point of view, whilst providing a non-stop operation, one of the most crucial tasks.

In current practise of prophylactics of power transformers dominate methods evaluating dielectric-electric parameters focused on insulation system or on transformer coiling.

From point of view of mechanical state in active transformer (630 kVA) parts that were measured, we had very little information about strength of this power transformer. (In some cases, as mentioned in [1], deformation of a transformer coiling and its age had as a result decommissioning of a unit)

From a theoretical analysis a probability of faultless operation can be defined by means of fault intensity as follows:

$$R(t) = e^{-\int_0^t \lambda(t) dt} \quad (1)$$

Where λ is fault intensity,

t is time in operation.

In a period of random faults of a system, if assumed that λ is constant, formula (1) can be simplified to

$$R(t) = e^{-\lambda t} \quad (2)$$

Presumption stemming from formulas (1) and (2), has a rational basis. Value λ is affected by physical,

mechanical, chemical and technological factors, under which influence λ can exponentially change. To solve this problem it is particularly suitable to apply analysis of current passing through windings which cause losses. These losses significantly affect operation of a transformer. The losses are mainly transformed to heat. Overheating minimises use of active materials and hence the overall output as well. Short time overheating is for insulation much less detrimental than prolonged overheating. However it is not the average temperature of winding, oil etc, but a temperature of transformer hottest point that we should bear in mind.

In present days, the second but equally important identification is EMC, which historically used to be used mainly to protect equipment from radio signals, but now involves a broad spectrum of electronic and electrical engineering principles. Investigating EMC one always the basic EMC flowchart, depicted in Fig.1.



Fig. 1. Analysis of Transformer Consumption

Consumer is connected to 22kV public distribution network through distribution transformer 22/0,4 kV with nominal output of 630 kVA. Supply of electrical energy is measured at the secondary side of a transformer via current measuring transformers 1500/5A incorporated within bus system 400V – in own distribution plant. Connection of distribution plant from mast transformer station is realised with AYKY cable.

Analysis of electrical energy consumption with focus on minimising reordered ¼ hour maximum was carried out by The Slovak Republic Energy Inspectorate. The method and its principles of this measurement are documented in [7]. From the energetic point of interest are important mainly ¼ hour maxim and their values in the investigated period. What amount and in what particular times was consumed to maintain continuous and smooth operation is depicted in graphs in Fig.2.

After the analysis carried out by The Slovak Republic Energy Inspectorate in the establishment we did this work, installed output was not increased. The survey recommended the consumer to install means of ¼ maxim regulation, utilizing electronic regulator EKS.

After instalment of EKS regulator, thermal overload occurred again and so did faults on transformer 630 kVA.

		ASANA Period Values			
		VT-area		NT-area	
Monday 15.6.					
Ch 1	Maximum:	79 kW	9.45	241 kW	22.00
	Energy:	248 kWh		2076 kWh	
Time	Ch 1				
7:00 - 7:15	46.4	*****			
7:15 - 7:30	40.2	*****			
7:30 - 7:45	30.4	*****			
8:00 - 8:15	33.4	*****			
8:15 - 8:30	45.0	*****			
8:30 - 8:45	47.2	*****			
8:45 - 9:00	48.0	*****			
9:00 - 9:15	46.4	*****			
9:15 - 9:30	34.4	*****			
9:30 - 9:45	76.2	*****			
10:00 - 10:15	45.6	*****			
10:15 - 10:30	40.0	*****			
10:30 - 10:45	42.4	*****			
10:45 - 11:00	73.0	*****			
Tuesday 16.6.					
Ch 1	Maximum:	229 kW	8.30	580 kW	16.15
	Energy:	767 kWh		4928 kWh	
Time	Ch 1				
7:00 - 7:15	180.0	*****			
7:15 - 7:30	171.2	*****			
7:30 - 7:45	187.2	*****			
8:00 - 8:15	194.4	*****			
8:15 - 8:30	228.4	*****			
8:30 - 8:45	214.4	*****			
8:45 - 9:00	181.4	*****			
9:00 - 9:15	190.4	*****			
9:15 - 9:30	227.2	*****			
9:30 - 9:45	204.4	*****			
10:00 - 10:15	174.0	*****			
10:15 - 10:30	192.0	*****			
10:30 - 10:45	174.4	*****			
10:45 - 11:00	173.2	*****			

Fig. 2. Consumed Electrical Power 2 Days (1/4 hour maxim)

III. POWER ANALYSIS AT THE TRANSFORMER OUTPUT

A well known phenomenon of asymmetry was analyzed by measuring current and voltage on phases L₁, L₂ and L₃. Currents on the secondary side of the transformer were measured via measuring transformers 1500/5A, phase voltages were recorded directly from bus bars.

Flowchart and schematics of electro-energetic feed of our technology equipment, its recording, and measuring equipment used are depicted in Fig.3.

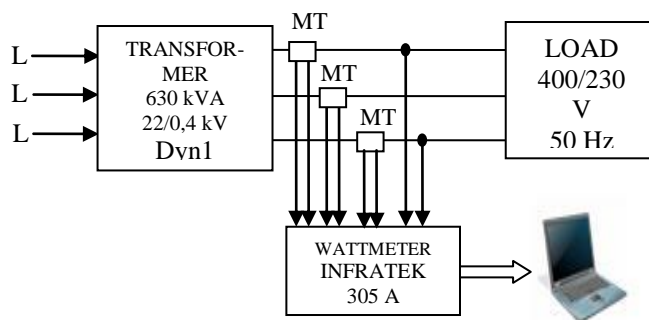


Fig. 3. Flowchart and Schematics of Electro-energetic Feed of technology Equipment and its Measurement

At the experimental analysis especially stresses point of interest was on measuring currents in phases. Up to date measuring equipment allowed us to carry out our measurements without interrupting technology operation. Recording was in 1 minute intervals over a period of 1 week. A graph representing results of this measurement is in Fig.4.

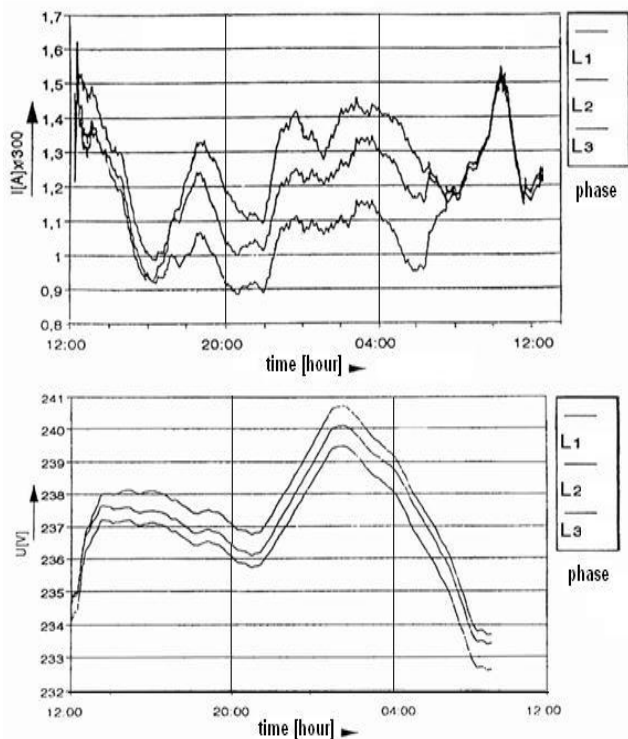


Fig. 4. Output Currents and Voltages at the Output Side of a Distribution Transformer

IV. HARMONIC ANALYSIS AT THE OUTPUT SIDE OF A TRANSFORMER

Application of fully regulated electric drives requires watching parameters of energy network also from the point of harmonic analysis. The problem of clear function of electric energy is important chiefly because of:

- effect of a non-sinus function on an inherent equipment,
- effect of a non-sinus function on other electrotechnical equipment.

The effect of a non-sinus function is caused by power semiconductors and its negative impacts can be seen in all bands:

- Energy spectrum: 0 - 200 Hz
- Acoustic spectrum: 15 Hz - 20 kHz
- Radio spectrum: 150 kHz - 300 kHz

In higher bands impacts for power application are minimal and for this reason we concentrated on the analysis of energy spectrum only. Graphical presentation of this analysis for $f = 0 \div 2000$ Hz is in Fig.5. It is obvious to see interphase asymmetry, which comes from comparison of phases and their limit values.

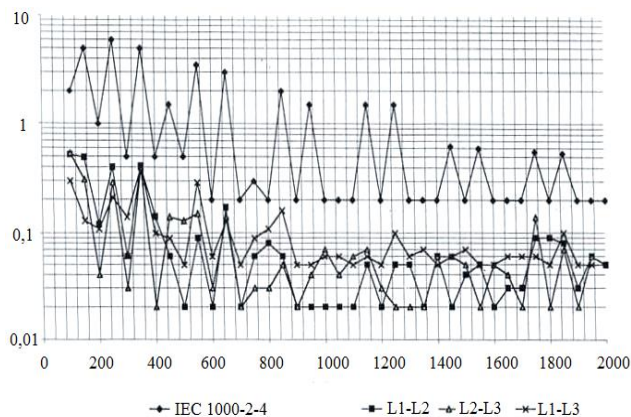


Fig. 5. Harmonic Analysis

V. CONCLUSION

In this paper we showed 2 different analysis carried out on the same distribution transformer 630 kVA 22/0,4 kV, Dyn1 with the same characteristics of consumed power. One analysis is from the point of optimisation of ¼ hour maxim and the second investigates the symmetry of load on L₁, L₂ and L₃.

While at the optimisation of ¼ hour maxim we measured the mean value and the results suggested a fault (with automatic regulation), analysis of load symmetry showed deviations up to 35% between phases L₁, L₂ and L₃. Such asymmetric load for a transformer connected in Dyn1 is quite large. (For similar asymmetric loads over 20% it is more advisable to use connection Yzn1).

Asymmetric load on phases is accompanied by greater losses. By higher power usage of a transformer, the overloaded phase causes overheating of coiling, faster ageing of insulation and hence higher fault frequency. Anomalies we found were caused by unbalanced 1-phase load.

In order to achieve results of electroenergetical state as accurate as possible, in our measuring period of 1 week (which means 20 technological cycles) both voltage and current were measured on primary and secondary side too.

From the results found in our analysis we can say that if the same technology operation is maintained and the energy distribution balanced is tuned more finely – this distribution transformer is able to provide reliable operation and fulfil EMC criteria at the same time.

ACKNOWLEDGMENT

This work was supported by the Grant Agency VEGA from the Ministry of Education of Slovak Republic under contract 1/0624/13.

REFERENCES

- [1] Kováčik, J.: Nová diagnostická metóda v oblasti výkonových transformátorov. Vedecká konferencia, Nové smery v diagnostike a opravách elektrických strojov a zariadení, areál VŠDS, Žilina 28.-29.5.1996
- [2] Jezierski, E.: Transformátory, Academia Praha 1973 (kniha)
- [3] Rada, J.: Symetrizační členy pro trojfázové sítě. Elektrotechnický obzor 1978/7
- [4] Kosa, P.: Technická správa, ŠTI pre Slovensko, august 1992
- [5] Kučera, S., Kučera, M., Líška, M., Vaňko, D.: Expertízna správa, analýza odberu el. energie, dis. traf. 630 kVA VŠDS, február 1996
- [6] Kučera, S.: Vypracovanie posudku k norme „ Požiadavky na zariadenia pripájané do elektrizačnej sústavy z hľadiska harmonických a účinníka “ PČ EF /14/1999, ŽU v Žiline -EF
- [7] Gutten, M., Kučera, S., Kučera, M., Šebök, M.: *Analysis of power transformers reliability with regard to the influences of short-circuit currents effects and overcurrents*, In: PRZEGLĄD ELEKTROTECHNICZNY= Electrical Review, Vol. 85, 2009, ISSN 0033-2097, No. 7, p. 62-64
- [8] Jurčík, J., Gutten, M.: *Analysis transformer insulation by PDC method*, In: PRZEGLĄD ELEKTROTECHNICZNY= Electrical Review, Vol. 89, 2013, No. 1a, p. 169-171, ISSN 0033-2097
- [9] Gutten, M.: *Diagnostic of Distribution Transformers by SFRA Method*, In: PRZEGLĄD ELEKTROTECHNICZNY= Electrical Review, Vol. 83, 2007, No. 4, p. 144-146, ISSN 0033-2097

Comparison of accuracy of precision LCR meter during dielectric properties measurement

Jiří Ulrych¹⁾, Radek Polanský²⁾, Josef Pihera³⁾, Aleš Voborník⁴⁾

^{1,4)} University of West Bohemia/ Faculty of Electrical Engineering/ KET, Univerzitní 8, 306 14 Pilsen, Czech Republic

^{2,3)} University of West Bohemia/ Faculty of Electrical Engineering/ RICE, Univerzitní 8, 306 14 Pilsen, Czech Republic

¹⁾ tel: +420 377 634 558, email: ulrychj@ket.zcu.cz

²⁾ tel: +420 377 634 517, email: rpolansk@ket.zcu.cz

³⁾ tel: +420 377 634 520, email: pihera@ket.zcu.cz

⁴⁾ tel: +420 377 634 571, email: vobornik@ket.zcu.cz

Abstract—The paper deals with the accuracy of measurement of precision LCR meter. Dielectric spectroscopy was used for evaluation of this test. The main aim of the paper is to compare the accuracy of measurement with measuring voltage of 1 V and 5 V in the frequency range from 200 Hz to 2 MHz. Two types of electrical insulating materials commonly used in many applications in high voltage engineering as a part of insulation system of large rotating machines (turbo or hydro generators) were used for this measurement. Expressive beta relaxation in measured dielectric spectra has been recorded and the accuracy of the measurement of the measured dielectric properties for used materials was compared for both measuring voltages.

Keywords—relative accuracy, precision LCR meter, dielectric test fixture, relative permittivity, loss factor

I. INTRODUCTION

The real (actual) value of the required characteristic can never be obtained by measurement precisely. The accuracy of the entire process of measurement consists of the accuracy of measuring instrument, the method of measurement and the operator. The results of measurement therefore have to be taken as approximate values. This paper is dealing with determination of relative accuracy of precision LCR meter during measuring of relative permittivity and loss factor. It is necessary to take into account that during the measurement of LCR meter accuracy further inaccuracies are caused by the measurement circuit (test fixture, cables, etc.) [1].

The measurement of dielectric properties was performed by the method of dielectric spectroscopy. Dielectric spectroscopy belongs to standard methods used for diagnostics. It is based on monitoring of the response of particles polarization due to frequency changes of the external electrical field. [2]

II. EXPERIMENT

A. Description of measured materials

Two solid materials commonly used for insulation of large turbo-generators and hydro-generators were chosen for measurement. The glass fibre material (F class) is

based on glass fibre, calcined mica paper and epoxy-novolac resin [3]. The polyethyleneterephthalate (PETP) foil material (F class) is based on PETP foil, calcined mica paper and epoxy-novolac resin [4]. We can assume that the dielectric properties of the above mentioned materials will be different, because their carrier components are different.

B. The description of measurement and measuring equipment

The relative accuracy of relative permittivity and loss factor measurement of the precision LCR meter (Agilent E4980A) was determined for effective values of 1 and 5 volts. The examined LCR meter belongs to the group of digital measuring instruments functioning on the principle of auto-balancing bridge method [5]. This instrument operates within the range from 20 Hz to 2 MHz. All detail information concerning this equipment is given in the technical documentation of the manufacturer. [6, 7]

The accuracy of measurement is also influenced by the utilized dielectric test fixture (in this case type 16451B), which is based on the so called parallel plate method. Parallel plate electrodes together with the measured material form a capacitor. All detail information concerning this equipment is given in the technical documentation of the manufacturer. [1, 5, 8]

The measurement was carried out on square samples (100 mm), one of each material given above. LCR meter was connected to dielectric test fixture and the results were recorded by connected computer. The measurement frequencies were in the range from 200 Hz to 2 MHz.

C. Tables and formulas used for calculations of relative accuracy

The procedure of calculation of permittivity and loss factor relative accuracy measurement and conditions of this calculation are given in the technical documentation of the respective LCR meter and test fixture. [1, 7] The measurement was carried out in the MED (medium) measurement time mode, which is related to the measurement speed [6]. The loss factor was measured and the relative permittivity was calculated by the following relation:

$$\varepsilon_r' = \frac{t \cdot C_p}{\pi \cdot \left(\frac{d}{2}\right)^2 \cdot \varepsilon_0} \quad (1)$$

where: $\varepsilon_r'(-)$ is relative permittivity, C_p (F) is measured parallel capacity, d (m) is the diameter of measuring electrode, ε_0 (F/m) is vacuum permittivity and t (m) is the sample thickness. The average material thickness of the glass fibre based material was 0.396 mm and the average thickness of the PETP foil based material was 0.291 mm. Parallel capacity means the sample capacity in parallel equivalent. The parallel equivalent circuit was chosen because it is a convenient model for determination of dielectric losses of sample caused by electrical conductivity in a broad frequency band [9, 10]. The relative accuracy of relative permittivity measurement was calculated by the following relation:

$$\pm A_c + 0.04 \cdot f^2 \cdot \varepsilon_r' \cdot \varepsilon_0 \cdot \left(\frac{\pi \cdot \left(\frac{d}{2}\right)^2}{t}\right) + \frac{100 \cdot (\varepsilon_r' - 1)}{\left(\varepsilon_r' + \frac{t}{0.01}\right)} \quad (2)$$

where: f (Hz) is frequency, t (mm) is the sample thickness and A_c (%) is the LCR meter accuracy for the capacity measurement which was calculated by the following relation:

$$A_c = \left[A_b + \frac{Z_s}{Z_m} \cdot 100 + Y_0 \cdot |Z_m| \cdot 100 \right] \cdot K_t \quad (3)$$

where: A_b (%) is the basic accuracy of measurement. V_s (Vrms) represents effective values of measuring voltage and F_m (Hz) is the frequency during the measurement. $|Z_m|$ (Ω) is the absolute impedance value of the sample. This value was calculated by the following relation:

$$|Z_m| = \frac{1}{2 \cdot \pi \cdot f \cdot C_p} \quad (4)$$

In some cases, the value given in the documentation was added to the calculated absolute impedance. Z_s (Ω) is short offset of the instrument. In this measurement, 1 m long cable was used between the LCR meter and the test fixture; therefore a certain value had to be added to Z_s . Y_0 (S) is open offset. This admittance value had to be multiplied by a certain value, corresponding with the cable length used (1 m). K_t is temperature coefficient (3). [7] The temperature during the measurement was 23 °C. For the calculation of the relative loss factor accuracy of measurement the following formula was used:

$$\pm A_d + E_a + E_b \quad (5)$$

where: A_d is the LCR meter accuracy for the loss factor measurement. Following equations are valid for calculating of A_d , E_a and E_b :

$$A_d = \pm \frac{A_c}{100} \quad (6)$$

$$E_a = 0.005 + 0.0004 \cdot f^2 \cdot \varepsilon_r' \cdot \varepsilon_0 \cdot \left(\frac{\pi \cdot \left(\frac{d}{2}\right)^2}{t}\right) \quad (7)$$

$$E_b = \frac{\tan \delta}{100} \cdot \left[A_c + 0.04 \cdot f^2 \cdot \varepsilon_r' \cdot \varepsilon_0 \cdot \left(\frac{\pi \cdot \left(\frac{d}{2}\right)^2}{t}\right) + \frac{100 \cdot (\varepsilon_r' - 1)}{\left(\varepsilon_r' + \frac{t}{0.01}\right)} \right] \quad (8)$$

where: $\tan \delta (-)$ is the measured value of loss factor. [1]

Equations (3) and (6) are given in the LCR meter documentation and they are valid for $\tan \delta \leq 0.1$ [7]. Equations (2), (5), (7) and (8) are given in the dielectric test fixture documentation and they are valid for $\tan \delta < 0.1$ [1]. The measured values of loss factor fulfilled these conditions. The calculated values of relative permittivity accuracy (2) and loss factor (5) were added to, or subtracted from the measured or calculated values of loss factor and relative permittivity, thus providing possible deviations from actual value. [1, 7]

III. RESULTS AND DISCUSSION

The loss factor and relative permittivity dependences on the frequency for both the examined materials are given in the Figures 1, 2, 3 and 4. Continuous line shows the measured or calculated values of the explored dielectric property and both the dash lines show the maximum deviations.

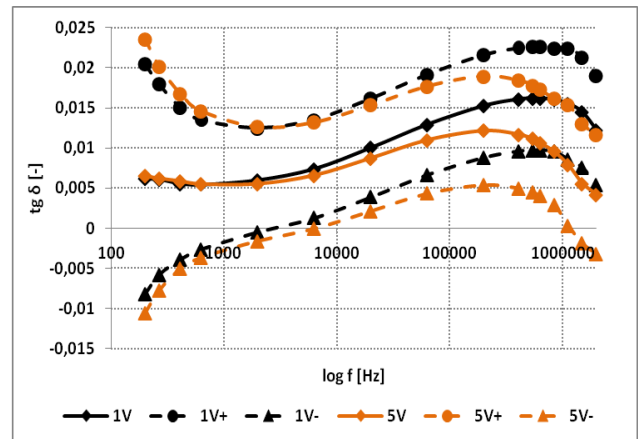


Fig. 1. Dependence of loss factor on frequency for glass fibre based material

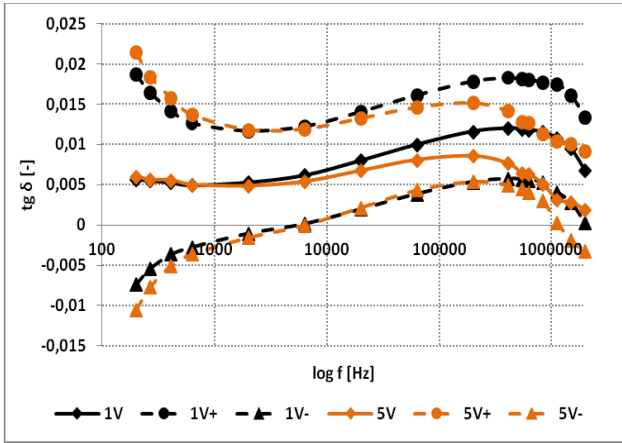


Fig. 2. Dependence of loss factor on frequency for PETP foil based material

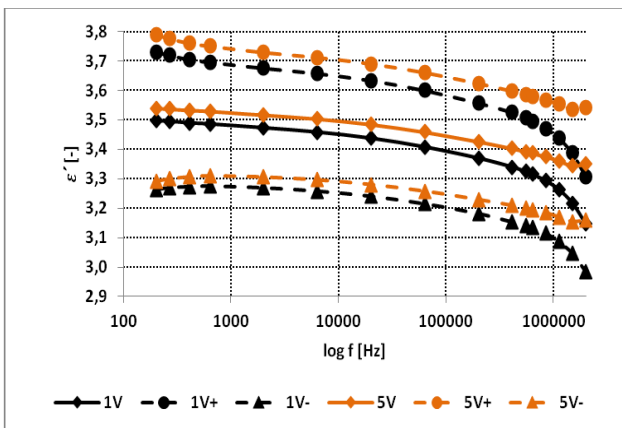


Fig. 3. Dependence of relative permittivity on frequency for glass fibre based material

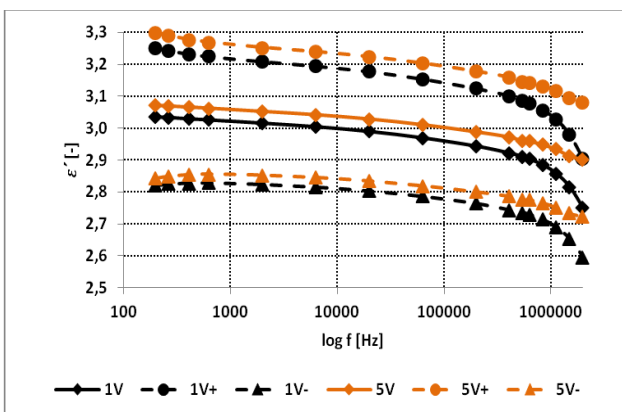


Fig. 4. Dependence of relative permittivity on frequency for PETP foil based material

considerably higher than the accuracy of the whole measurement system (LCR meter + test fixture). With the measurement using 1 V the maximum loss factor shows frequency shifting compared with 5 V measurement (Fig. 1 and 2). This is caused probably by the fact, that the measured values are already situated in the area of frequency limits of the instrument, which brings further inaccuracies.

Table 3 shows relative accuracy development of relative permittivity for 1 V and 5 V depending on the frequency of LCR meter itself and its connection with dielectric test fixture. The relative accuracy grows with increasing frequency.

The measurements also showed that the results of relative accuracy measurement under the same conditions were better for 1 V than for 5 V.

In Figures 1 and 2 only β polarization peaks are observed. The influence of α polarization and conductivity is shown in [11]. In our study the influence is missing due to the limited measurement range from 200 Hz to 2 MHz.

The α polarization is caused by segmental motions of the polymer main chain resulting in the rotation of dipoles around the polymer main chain. The β polarization is associated with local movement of specific molecular group relaxations.

TABLE I. DEVELOPMENT OF LOSS FACTOR ACCURACY MEASUREMENT OF GLASS FIBRE BASED MATERIAL

f (Hz)	The accuracy of tan δ measurement			
	1 V	5 V	1 V	5 V
	LCR meter (\pm)	LCR meter (\pm)	Measurement system (\pm)	Measurement system (\pm)
200	0,008935	0,011609	0,014347	0,017068
267	0,006472	0,008512	0,011865	0,013931
411	0,004102	0,005530	0,009447	0,010908
632	0,002697	0,003763	0,008026	0,009107
2000	0,001114	0,001772	0,006466	0,007106
6325	0,000683	0,001230	0,006111	0,006628
20000	0,000559	0,001074	0,006133	0,006594
63246	0,000522	0,001028	0,006253	0,006675
200000	0,000556	0,001071	0,006407	0,006781
410705	0,000531	0,001030	0,006433	0,006709
547684	0,000524	0,001030	0,006421	0,006676
632456	0,000522	0,001022	0,006417	0,006640
843394	0,000518	0,001018	0,006409	0,006583
1124684	0,001041	0,002050	0,006919	0,007544
1499790	0,001037	0,002044	0,006875	0,007437
2000000	0,001034	0,002040	0,006791	0,007416

Tables 1 and 2 show the trend in relative accuracy of loss factor depending on the frequency of LCR meter itself and its connection with dielectric test fixture (for 1 V and 5 V). Relative accuracy of loss factor measurement changes in all cases in accordance with the frequency range. The lowest accuracy of measurement is typical for high and low frequencies areas approaching the range limits of the instrument. As we can see in the tables, the accuracy of loss factor measurement of the LCR meter itself is

TABLE II. DEVELOPMENT OF LOSS FACTOR ACCURACY MEASUREMENT OF PETP FOIL BASED MATERIAL

f (Hz)	The accuracy of tan δ measurement			
	1 V		5 V	
	LCR meter (±)	LCR meter (±)	Measurement system (±)	Measurement system (±)
200	0,007639	0,009983	0,013043	0,015431
267	0,005555	0,007360	0,010936	0,012765
411	0,003548	0,004835	0,008900	0,010220
632	0,002360	0,003339	0,007684	0,008678
2000	0,001020	0,001654	0,006359	0,006972
6325	0,000655	0,001195	0,006046	0,006545
20000	0,000550	0,001063	0,006052	0,006500
63246	0,000519	0,001023	0,006138	0,006539
200000	0,000548	0,001060	0,006261	0,006602
410705	0,000526	0,001025	0,006269	0,006511
547684	0,000521	0,001026	0,006251	0,006436
632456	0,000519	0,001018	0,006245	0,006428
843394	0,000515	0,001015	0,006231	0,006344
1124684	0,001034	0,002042	0,006724	0,007292
1499790	0,001031	0,002038	0,006669	0,007301
2000000	0,001029	0,002034	0,006564	0,007313

TABLE III. DEVELOPMENT OF RELATIVE PERMITTIVITY ACCURACY MEASUREMENT OF GLASS FIBRE AND PETP BASED MATERIAL

f (Hz)	The accuracy of ε' measurement			
	Glass fibre based material		PETP based material	
	1 V	5 V	1 V	5 V
	LCR meter (±%)	Measure. system (±%)	LCR meter (±%)	Measure. system (±%)
200	6,69	7,05	7,10	7,44
267	6,44	6,73	6,89	7,17
411	6,19	6,43	6,67	6,90
632	6,04	6,24	6,54	6,75
2000	5,85	6,02	6,38	6,55
6325	5,78	5,93	6,31	6,47
20000	5,72	5,88	6,26	6,42
63246	5,65	5,81	6,19	6,36
200000	5,57	5,75	6,12	6,30
410705	5,57	5,69	6,12	6,25
547684	5,47	5,67	6,02	6,22
632456	5,45	5,66	6,00	6,21
843394	5,40	5,63	5,95	6,18
1124684	5,39	5,71	5,92	6,25
1499790	5,29	5,67	5,80	6,19
2000000	5,14	5,69	5,61	6,16

IV. CONCLUSION

As already mentioned above, no measurement can determine values of the examined properties with absolute accuracy. The results of measurement have to be regarded as approximate values. Resulting from the calculated values we can see that determination of relative accuracy with measurements of dielectric characteristics by means

of precision LCR meter is depending on many circumstances, which have to be taken into account. These circumstances include the inaccuracies of dielectric test fixture, the influence of temperature, the cable length between LCR meter and test fixture, frequencies, etc. The highest inaccuracies are caused by the test fixture system and it is necessary to take this fact into consideration.

ACKNOWLEDGMENT

This research has been supported by the European Regional Development Fund and the Ministry of Education, Youth and Sports of the Czech Republic under the Regional Innovation Centre for Electrical Engineering (RICE), project No. CZ.1.05/2.1.00/03.0094 and by the Student Grant Agency of the West Bohemia University in Pilsen, grant No. SGS-2012-026 "Material and Technology Systems in Electrical Engineering".

REFERENCES

- [1] Agilent Accessories Selection Guide For Impedance Measurements. In: Agilent Technologies [online]. December 2008 [cit. 2012-04-14]. Available from: <http://cp.literature.agilent.com/litweb/pdf/5965-4792E.pdf>
- [2] Microwave Dielectric Spectroscopy Workshop: Measure the difference. In: Agilent Technologies [online]. © 2004 [cit. 2013-04-14]. Available from: http://www.home.agilent.com/upload/cmc_upload/All/MWDielectricSpectroscopyWS.pdf?&cc=CZ&lc=eng
- [3] Relanex 45.011: Flexible Mica Tapes and Foils. In: FKA [online]. [cit. 2012-04-14]. Available from: http://www.fkaeng.com/userfiles/45011RLX_cogebi1.pdf
- [4] Relastik 45.013: Flexible Mica Foils. In: FKA [online]. [cit. 2012-04-14]. Available from: http://www.fkaeng.com/userfiles/45013REL_cogebi1.pdf
- [5] Agilent Impedance Measurement Handbook: A guide to measurement technology and techniques. In: Agilent Technologies [online]. 4th Edition. © 17.6. 2009 [cit. 2013-04-14]. Available from: <http://cp.literature.agilent.com/litweb/pdf/5950-3000.pdf>
- [6] Agilent: E4980A Precision LCR Meter 20 Hz to 2 MHz Setting a new standard for low frequency impedance measurements. In: Agilent Technologies [online]. © 2004 [cit. 2013-04-14]. Available from: <http://cp.literature.agilent.com/litweb/pdf/5989-4235EN.pdf>
- [7] Agilent E4980A Precision LCR Meter 20 Hz to 2 MHz: Data Sheet. In: Agilent Technologies [online]. © 26.7 2011 [cit. 2013-04-14]. Available from: <http://cp.literature.agilent.com/litweb/pdf/5989-4435EN.pdf>
- [8] Agilent: Solutions for Measuring Permittivity and Permeability with LCR Meters and Impedance Analyzers. In: Agilent Technologies [online]. Application Note 1369-1. © 2004 [cit. 2013-04-14]. Available from: <http://cp.literature.agilent.com/litweb/pdf/5980-2862EN.pdf>
- [9] COOMBS, Clyde F. Electronic Instrument Handbook. New York: McGraw-Hill, Inc., © 1995, ISBN 0-07-113880-3.
- [10] MENTLÍK, Václav. Dielektrické prvky a systémy <in Czech>. Praha: BEN-technická literatura, 2006, 235 s. ISBN 80-7300-189-6.
- [11] LIEDERMANN, K.; POLSTEROVÁ, H. , "Dielectric relaxation in Relanex insulation during aging," Conduction and Breakdown in Solid Dielectrics, 1995. ICSD'95., Proceedings of the 1995 IEEE 5th International Conference on , vol., no., pp.124-128, 10-13 Jul 1995

Utilization of digital protection and terminal communication for power plant electrical equipment testing

Ing. Oto Mareček¹⁾, Ing. Miloš Kaška²⁾

TES s.r.o., Pražská 597, 67401 Třebíč, Czech republic, WWW.TES.EU

¹⁾ tel: +420 381 105 518, email: marecek@tes.eu ,

²⁾ tel: +420 568 838 429, email: kaska@tes.eu

Abstract— Digital protections and terminals are used for protective and automatic systems in new and modernized power plants nowadays. Analogue and binary data is provided via IEC61850 standard of data communication this digital protections and terminals .This article contains results of analogue and binary data applicability exploration for test, fast transients and failures analysis.

Keywords— busbar; disturbance; motor; overcurrent; protection; record; signal; start; start-up; terminal; trip;

I. INTRODUCTION

Electrical equipment is one of the most important parts of power plant blocks. Electrical equipment is used for electrical energy production (generator), electrical energy transmission into power system (generator switch, block transformer, switch gear) and power supply of technological equipment (water pumps, fans, instrumentation and control etc.). These electrical facilities are equipped by digital terminals and protections. The digital terminals and protections are primarily determined to perform the basic function – control and protection. A recording of analogue and binary data is the next function too. This data are provided via communication according to IEC61850 standard between the terminal or the protection and a monitoring system. The monitoring system is used for test analysis or analysis of malfunction processes in the electrical facilities.

The TES company has investigated how to use analogue and binary recordings of these terminals and protections for monitoring of electrical facilities in Temelín nuclear power plant.

II. DATA RECORDING REQUIREMENTS

Basic requirements have been defined on the basis of experience with the test analysis or the analysis of malfunction processes in the electrical facilities in Dukovany and Temelín nuclear power plant. The recording of analogue and binary data has to meet basic quality and accuracy requirements.

The recording of analogue data requirements:

- data acquisition allowing to record voltage and current sinus waveform of 50 Hz,

- sampling rate of 1000 samples/s minimum,
- length of the record 30 s minimum, ability to store a data for pre-set period of time before and after the incident,
- adjustment of triggering conditions upon a change of the signal character,
- acquisition of data of all monitored signals at the same time – mathematical operations among signals,
- accuracy 1% or better.

The recording of binary data requirements:

- acquisition of data of all monitored signals at the same time,
- sampling rate of 100 samples/s minimum,
- recording of signal changes (0, 1) with the time stamp,
- memory buffer for 100 000 signal change records minimum.

Acquisition analogue and binary signals has to be synchronised – difference 50 ms or less. The terminals and protections have to be synchronised with the monitoring system – difference 10 ms or less.

III. Monitoring system MOSAD[®]-5

Monitoring system MOSAD[®]-5, developed in TES laboratories, has been based on the proven MOSAD[®]-4 system. It has been designed to continuous has been focused on monitoring of electrical signals (analogue and binary signals). The system functions has been focused on monitoring of power system condition and performance, emphasizing transients and failures. The system operates fully automatically without permanent operator presence. The system is of a modular design. It allows to adjust the actual system composition and configuration according to specific requirements and character of the monitored equipment. If needed, the system configuration can be easily modified anytime. The MOSAD[®]-5 system may be synchronized with the GPS standard as well as with all systems using this standard. The system resolution is better than $\pm 100 \mu\text{s}$.

MOSAD[®]-5 monitoring system functions:

- monitoring of analogue signals at the sampling frequency from 10 ksamples/s per input (for 120 input channels used) to 200 ksamples/s per input (for 8 input channels used),
- monitoring of binary signals with the sampling period of 0,1 ms (for 480 input channels used),
- pulse counting with the maximum frequency of 10 MHz,
- event timing accuracy of 1 ms at all system modules,
- recording only time periods when the monitored analogue signals change (events occur) to effectively use the system storage capacity,
- recording of relevant changes of the monitored binary signals,
- automatic removal of permanently oscillating binary signals from recording to protect system memory from saturation; if pre-defined criteria are satisfied, the removed signals automatically return to the monitoring process,
- synchronisation of the MOSAD[®] – 5 system time with the GPS time standard,
- maintaining the system in operation at least 10 minutes after the normal power supply is lost; acquired data are stored automatically before the system is switched off.

Monitoring system MOSAD[®]-5 is primarily used for direct measurement of analogue and binary signals in Dukovany and Temelin nuclear power plant. The measuring / monitoring system is connected to standard sensors equipped with electrical output (voltage/current transformers, operational instrumentation), connecting to contacts of switching elements (circuit breakers, switches, relays...). Analogue signals are sampled with the rate of 2000 samples/s and the accuracy of 0,5%, binary signals 1000 samples/s.

The example of directly measured analogue and binary signals is displayed in the figure No. 1. It is a start-up procedure of the water pump motor 1RM54 D001:

- current of the motor in the phase L2 (1RM54 D001 IL2),
- current of the busbar in the phase L2 (1BDb IL2),
- voltage of the busbar in the phase L2 (1BDb UL2),
- switch status (1RM54 D001),
- overcurrent protection start F112 (1RM54 D001-F112).

Event timing accuracy between analogue and binary signals is better than 50 ms.

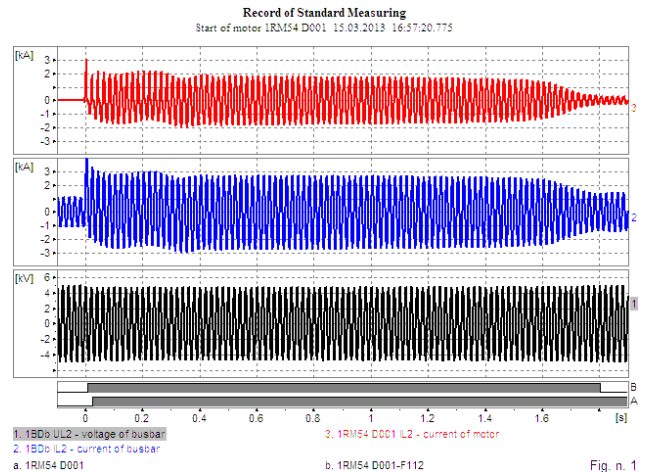


Fig. 1. Record of Standard Measuring – Start of motor 1RM54 D001

IV. TERMINAL AND PROTECTION DATA COMMUNICATION - IMITATION

A data communication between the REC 670 terminal (ABB product) and monitoring system MOSAD[®]-5 has been investigated in a Temelin nuclear power plant laboratory according to the IEC61850 standard. Acquisition of the analogue and binary signals has been executed with the sampling rate 1000 samples/s, accuracy of the analogue measurement has been better than 1%. The conditions met the requirements mentioned in the chapter “Data recording requirements”.

The record of data communicated analogue and binary signals is displayed in the figure No. 2. It is a trip imitation of the overcurrent protection F111 of the motor 1YD10D01:

- current of the motor in the phase L1 (1YD10D01 IL1/D),
- overcurrent protection start in the phase L1 (1YD10D01-F111-L1S/D),
- overcurrent protection trip (1YD10D01-F111-T/D).

Event timing accuracy between data communicated analogue and binary signals has been met too.

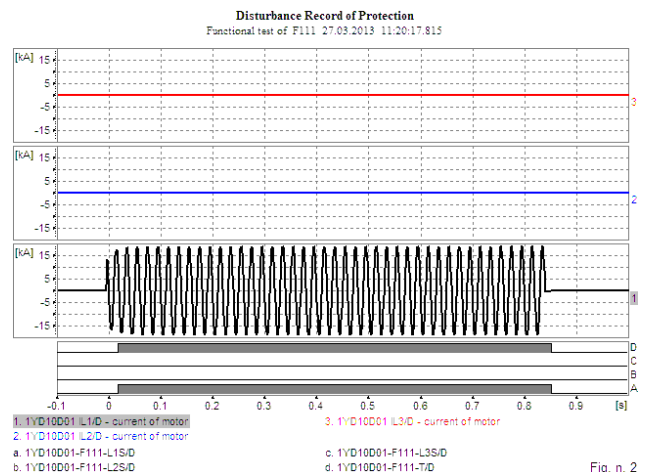


Fig. 2. Disturbance Record of Protection – Functional test of F111

V. TERMINAL AND PROTECTION DATA COMMUNICATION – REAL TEST

A data communication between the REC 670 terminal (ABB product) and monitoring system MOSAD®-5 has been investigated in a Temelín nuclear power plant switchgear 6 kV.

The record of directly measured analogue and binary signals is displayed in the figure No. 3. It is a start-up procedure of the water pump motor 1RM52 D001:

- current of the motor in the phase L2 (1RM52 D001 IL2),
- current of the busbar in the phase L2 (1 BBb IL2),
- voltage of the busbar in the phase L2 (1 BBb UL2),
- switch status (1RM52 D001),

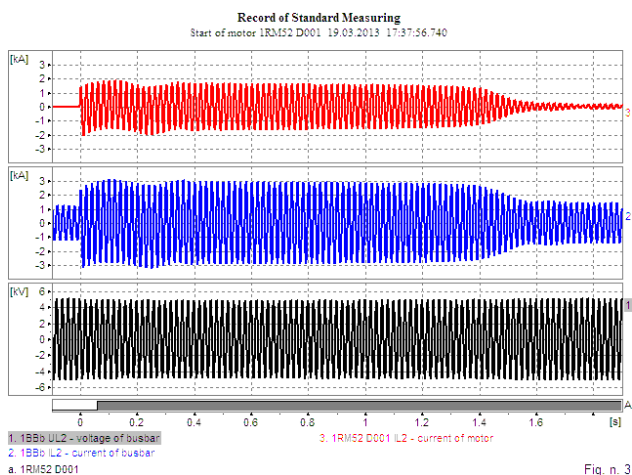


Fig. 3. Record of Standard Measuring – Start of motor 1RM52 D001

The record of data communicated analogue and binary signals is displayed in the figure No. 4:

- current of the motor in the phase L1 (1RM52 D001 IL1/D),
- current of the motor in the phase L2 (1RM52 D001 IL2/D),
- current of the motor in the phase L3 (1RM52 D001 IL3/D),
- voltage of the busbar in the phase L2 (1BBb UL2/D),
- overcurrent protection start in the phase L1 (1RM52D001-F112-L1S/D)
- overcurrent protection start in the phase L2 (1RM52D001-F112-L2S/D),
- overcurrent protection start in the phase L3 (1RM52D001-F112-L3S/D),
- switch status (1RM52D001-QM1 ZAP/D).

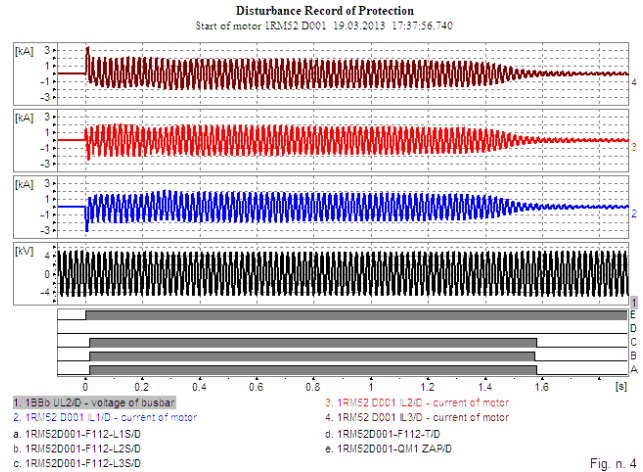


Fig. 4. Disturbance Record of Protection – Start of motor 1RM52 D001

The comparison between records of directly measured analogue and binary signals and the data communicated analogue and binary signals is displayed in the figure No. 5:

- current of the motor in the phase L2 (1RM52 D001 IL2/D) – data communication,
- current of the motor in the phase L2 (1RM52 D001 IL2) – direct measurement,
- current of the busbar in the phase L2 (1BBb IL2) – direct measurement,
- overcurrent protection start in the phase L1 (1RM52D001-F112-L1S/D) – data communication,
- overcurrent protection start in the phase L2 (1RM52D001-F112-L2S/D) – data communication,
- overcurrent protection start in the phase L3 (1RM52D001-F112-L3S/D) – data communication,
- switch status (1RM52D001-QM1 ZAP/D) – data communication.

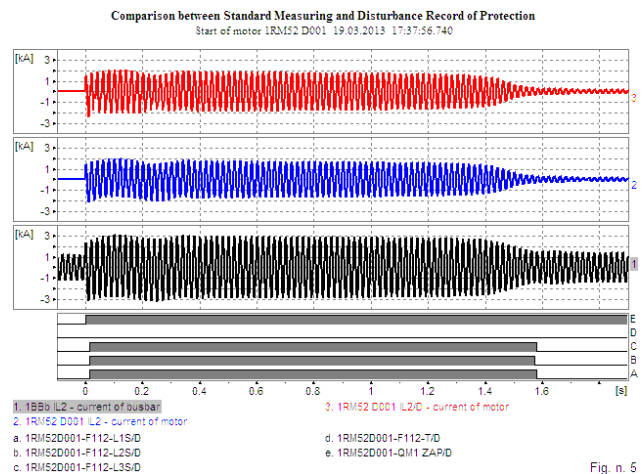


Fig. 5. Comparison between Standard Measuring and Disturbance Record of Protection – Start of motor 1RM52 D001

Event timing accuracy between the REC 670 terminal (data communicated signals) and the monitoring system MOSAD[®]-5 (directly measured signals) has been met too.

VI. CONCLUSION

Tests published in this paper have proved that data obtained via the IEC61850 communication standard are suitable for test analysis or analysis of malfunction processes in the electrical facilities of power plants. Records of the analogue and binary data communication signals have fully met quality and accuracy requirements.

ACKNOWLEDGMENT

The research described in the paper is financially supported by grant Czech ministry of industry and trade (MPO) No. FR-TI3/016.

REFERENCES

- [1] Mareček O., Solution of project FR-TI3/016 in annual report of 2011, arch. n. TES-Z-11-214,
- [2] Mareček O., Project FR-TI3/016, period E1: Research of using components, equipments and systems in the electrical area, arch. n. TES-Z-12-158.

Application of SFRA method to the transformer with Yz winding connection without a neutral terminal

Ing. Martin Brandt, PhD. ¹⁾, Ing. Róbert Seewald, PhD. ²⁾, prof. Ing. Ján Michalík, PhD. ³⁾

Faculty of Electrical Engineering, University of Žilina, Univerzitná 8215/1, 010 26 Žilina, Slovakia, www.fel.uniza.sk

¹⁾ tel: +421 41 513 5064, email: martin.brandt@fel.uniza.sk,

²⁾ tel: +421 41 513 5064, email: robert.seewald@fel.uniza.sk,

³⁾ tel: +421 41 513 5063, email: jan.michalik@fel.uniza.sk,

Abstract — In most cases the SFRA method it is usually used on the three phase power transformers with YNyn, Ynd, Dyn windings connection, but many of oil distribution transformers up to 300 kVA of power are made in Yzn winding connections without the neutral terminal on the primary side. This paper focuses exactly on this type of transformer, which has to be measured as transformer with delta connection of the primary winding. It is necessary to establish the SFRA methodology for this connection type. The results evaluation is often difficult, because of often disunited measurement procedure (according to IEC 60076-18). And, there is always a noise in output characteristics which make result interpretation more difficult.

Keywords — SFRA; transformer; interturn short circuit fault;

I. INTRODUCTION

As it was already mentioned in the abstract, we will focus on the diagnostic measurement with SFRA method of the distribution transformer (Tab. 1) whose connection is Yzn1 without a primary neutral terminal. The connection Yz (Star, zig-zag connected windings) of transformer is used in place where electricity consumption is asymmetrical. The internal connection of the transformer is shown in Fig. 2.

All measurements (for research purposes) including reference measurements were made on transformer pulled up from the transformer tank (Fig. 1).

Sweep frequency response analysis (SFRA) theory is a method which can indicate some damage or change in the winding or in the core of the transformer. The fundamentals of this type of measurements is to supply input winding of transformer by low voltage frequency impulses and the response in output winding is displayed as an amplitude frequency characteristics [1]:

$$H_U(j\omega) = \frac{U_{out}(j\omega)}{I_{in}(j\omega)} \quad (1)$$

$$A(dB) = 20 \log_{10}[H(j\omega)] \quad (2)$$

The frequency response change depends on the total transformer impedance, which depends on the equivalent circuit of transformer parameters: primary and secondary resistances of windings, magnetizing, leakage inductance and the capacity of windings given by transformer design or FEA [3]. The changes in frequency responses measured with SFRA determine if any mechanical changes in the windings occurred and if investigation of defect is needed. The most significant defects in the windings can occur during often short-circuit operation and high current stress, which can lead to the axial or radial deformation. The forces in the windings can cause radial shift and consequently axial deformation of windings. There are forces in radial direction have to be taken into account during the design of transformer core, but considering the case of the forces position in axial way is more important. This difference is the most useful at identifying a defect of transformer.

TABLE 1. NAMEPLATE DATA OF MEASURED TRANSFORMER.

Manufacturer	BEZ, v.č. 231160
Year of manufacture	1983
Type	aT0294/22
Connection	Yzn1
Frequency	50 Hz
Nominal voltage	22/0,4 kV
Nominal power	100 kVA
Position of tap switch	3



Fig. 1. The tested transformer pulled up from the transformer tank

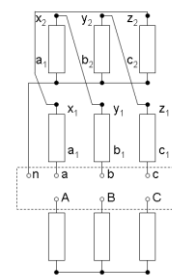


Fig. 2. Internal transformer connection

II. SFRA MEASUREMENTS

It is necessary to know all factors influencing the shape of frequency responses for exact interpretation of frequency responses and identification any mechanical damage that may occur during running of the transformer. As the primary winding has not neutral terminal it is not possible to measure winding according to the methodology A-N, B-N and C-N, but we have to use a methodology for measuring according to the delta connection. Another factor that influences the shape of frequency responses is secondary windings connection in zig-zag.

The impedances, which constitute measured circuit of primary winding (as determined by the methodology of measurement), are in this case always windings consist of two phases. The impedances of the third phase of the primary winding (the one that is not currently measured) and impedances of secondary winding coils have also the influence on the shape of the frequency responses. The compilation of a complete spare scheme required to simulate in wide range of input frequencies would be therefore very difficult. And that is why in this article we will focus on practical measurement and correct interpretation of the frequency responses measured on the transformer.

The basic methodology SFRA measurements is based on measuring described in [1]. The measurement of the primary winding is different, due to the fact that the star connected winding has not neutral terminal. Therefore, we have to measure as though it was connected to the delta winding (Tab. 2). It is important to note which impedances impact on the measured frequency responses at the interpretation of them.

TABLE 2. TABLE OF SFRA MEASUREMENTS

1. Open circuit					
22 kV			400 V		
Test 1	Test 2	Test 3	Test 4	Test 5	Test 6
A – B	B – C	C – A	a – n	b – n	c – n
2. Short circuit					
shorted a – b – c (ssek)			shorted A – B – C (sprim)		
Test 7	Test 8	Test 9	Test 10	Test 11	Test 12
A – B	B – C	C – A	a – n	b – n	c – n
3. Interwinding measurement					
Test 13	Test 14	Test 15			
A – a	B – b	C – c			

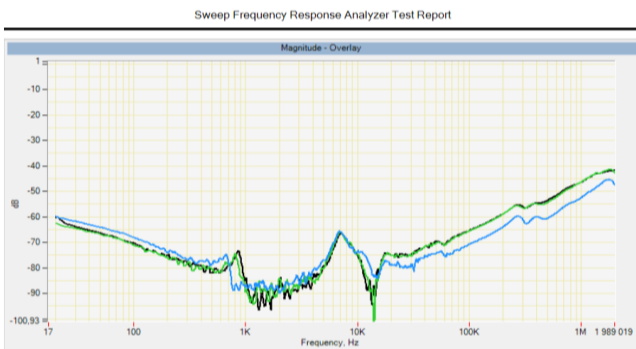


Fig. 3. Open circuit tests of primary windings A-B (black), B-C (green), C-A (blue).

From Fig. 3 it can be seen that the course of frequency responses has not a standard shape, the waveform is characterized with distortion and major signal noise to the frequency of 10 kHz. An inexperienced technician could evaluate waveforms as fault at a glance, or he would their shape attributed to the internal noise of measurement device. However, this may not be true. For this type of distribution transformer it is very problematic to assess if the fault was measured or not.

We have a look for additional assessment at the courses measured for the secondary winding with open circuit methodology (Fig. 4).

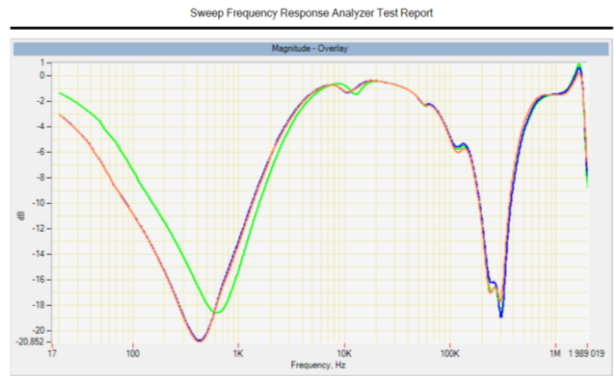


Fig. 4. Open circuit measurements of secondary winding: a-n (green), b-n (blue), c-n (red)

As the secondary winding is connected to the zig-zag and the frequency responses are the same for phase b and phase c. This situation results from the arrangement of the transformer windings on its core (Fig. 2). The coil of phase (a) is loaded on the first and third column of the core. The junction of both parts of the coil phase (a) has longer conducting way as the coils of phases (b) and (c). Therefore the impedance of phase (a) has a different value and a different shape over the frequency range up to 10 kHz. We have found by measurement of six same transformer with secondary winding connected to the zig-zag that the frequency responses are identical with the frequency responses on the Fig. 4 in the case when the transformer is without fault. Then the frequency response for phase (b) and phase (c) to 10 kHz are identical and frequency response for the phase (a) is different. If there is difference between all the phases, it means an internal fault. When the fault on transformer occurs, the frequency responses are reflected in other measured responses.

For the exact measurement of the transformer is useful interwinding methodology according to the article 2.8 of norm IEC 60076-18. The measurement results are shown in Fig. 5. The waveforms are in frequency range up to approx. 550 Hz characterized with distortion and major signal noise. It is due to the fact that impedance of the circuit of the measured transformer consists of winding resistance, which is in this case infinitely large, because the primary and secondary windings are not conductively connected. The frequency responses in this case are influenced by inductive and capacitive couplings between windings. The inductive and capacitive couplings will

begin to manifest in the bandwidth of frequencies higher than 550 Hz.

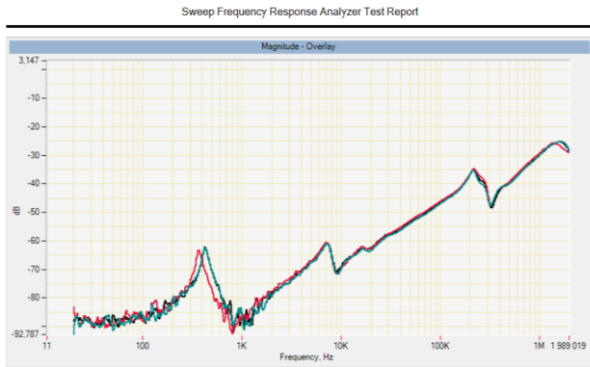


Fig. 5. Interwinding measurement A-a (black), B-b (red), C-c (blue)

The geometric structure of primary winding influences to the shape of frequency responses in the way, that first resonance maxima and frequency responses are the same for outer phases (A and C). The middle phase (B) has the values of frequency dependent impedance to frequency 5.7 kHz different. There are from the frequency 5.7 kHz the frequency responses identical in the frame of adjusted correlation (0.95 - 1). In the case of the fault of interturn short circuit or winding axial displacement it will be change the capacity of the winding coils and the mutual inductance. This state will influence the frequency dependent impedance and then amplitude of frequency responses according to [1].

Many of mechanical failures on the experimental transformer were simulated for the correct interpretation of measured results (much types failures that occur during operation of the transformer). The first results are described in the following chapter.

III. INTERTURN SHORT CIRCUIT - AXIAL

The creating of fault interturn short circuit axial on the phase A is shown in Fig. 6.



Fig. 6. The created interturn axial short circuit on the phase A

The interturn short circuit was created at the bottom (the lowest) segment of the primary winding on the phase A in agreement with following procedure:

- We removed the insulating coat from winding wires.
- We cleaned the place with acetone.
- It was applied on the aluminum winding wire the tin with high power solderer.

We used the same waveforms as in the first part of this paper for interpretation the frequency responses (Fig. 3, 4 and 5).

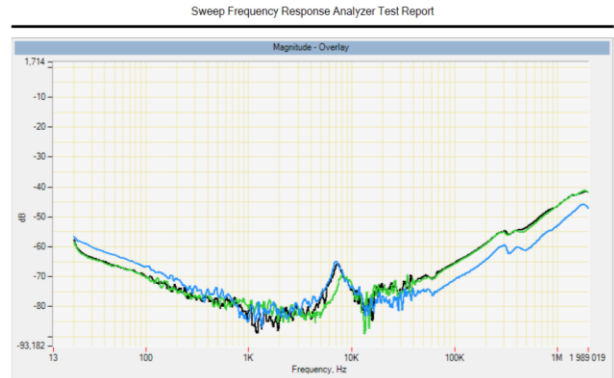


Fig. 7. Open circuit tests of primary windings A-B (black), B-C (green), C-A (blue) after axial interturn fault.

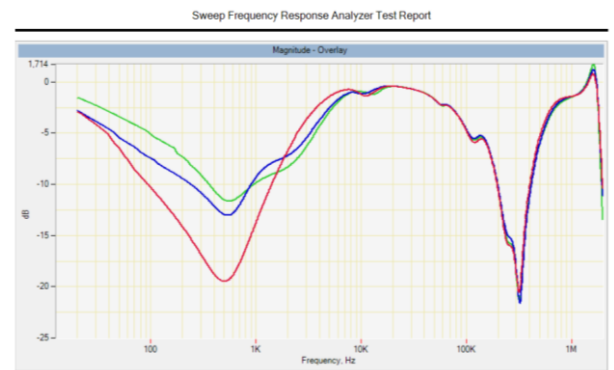


Fig. 8. Open circuit tests of secondary windings a-n (green), b-n (blue), c-n (red) after axial interturn fault.

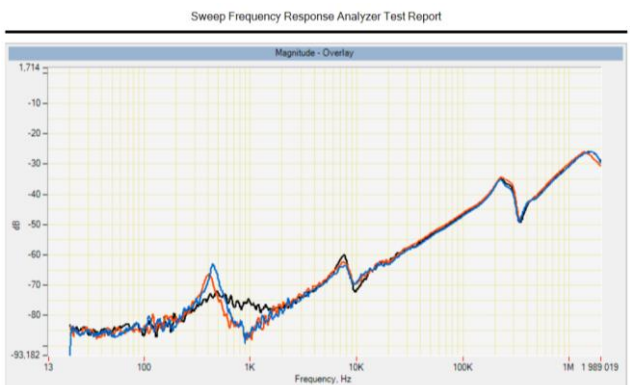


Fig. 9. Interwinding measurements A-a (black), B-b (red), C-c (blue) after axial interturn fault.

IV. CONCLUSION

It is very difficult to identify a fault in the transformer (according Fig. 7) when we do not have the reference frequency responses of transformer. On Fig. 7 may be the frequency responses of standard characteristics. According to the theoretical knowledge should be the primary winding frequency responses of A-B and B-C approximately equivalent and the frequency response of C-A is different. On Fig. 8 are shown frequency responses for open circuit tests of secondary windings and these responses are not equivalent to frequency responses at 10 kHz. These differences in frequency responses signalize the fault. The interwinding

measurement phases of the primary and secondary windings confirm the failure of the transformer. The measured frequency responses are shown on Fig. 9. The response of the phase A-a is different from the other two measurements. After this manner there was confirmed the fault of the transformer, which is related to the first phase of the primary or secondary winding. For next step the transformer must be completely shut down and subjected to repair if it is economically advantageous.

When we want detected specific type of fault we have to evaluate the measurement methodology short circuit tests and then we can use Cross Correlation Coefficient's analysis [2]. Identifying faults we are dealing with the assessment of the results of simulations of the transformer parametric model, in which are considered all self and mutual inductances, magnetic circuit of transformer and all capacities, which are published in the articles [3] and [4].

ACKNOWLEDGMENT

This paper was done within the project APVV-0703-10 – Analysis and diagnostic measurements of power transformer by Sweep Frequency Response Analysis.

REFERENCES

- [1] Brandt M., Michalik J., Seewald R., Sedlák J.: Diagnostic measurements of 3-phase 25MVA transformer and their analysis, In: Logistika : príloha Logistika - nauka : ISSN 1231-5478. - Nr. 6 (2011)
- [2] Kennedy, G., M., McGrail, A., J., Lapworth, J., A.: Using Cross-Correlation Coefficients to Analyze Transformer Sweep Frequency Response Analysis (SFRA) Traces. IEEE PES Power Africa 2007, 1-4244-1478-4/07
- [3] Brandt, M., Rafajdus, P., Peniak, A., Michalik, J.: Diagnostics System of Power Transformers Supported by Finite Element Analysis, Speedam 2012 Proceedings, IEEE Catalog Number: CPF1248A-CDR, ISBN: 978-1-4673-1300-1
- [4] Sedlák, J., Seewald, R.: Influence of remanent magnetization on the diagnostic of transformer by SFRA method, DESAM 2012 Proceedings, GEORG, 2012 , ISBN 978-80-89401-69-7

Reliability of Various PWB Materials in High Frequency Area

Alena Pietrikova¹⁾, Tibor Rovensky²⁾, Kornel Ruman³⁾, Jan Gamec⁴⁾

^{1),2),3)} Department of Technologies in Electronics, Technical University of Kosice, Slovak Republic,
<http://web.tuke.sk/fei-kte/>

⁴⁾ Department of Electronics and Multimedia Communications, Technical University of Kosice, Slovak Republic,
http://www.kemt.feit.tuke.sk/index_sk.html

¹⁾ tel: +421 55 602 3194, email: alena.pietrikova@tuke.sk,

²⁾ tel: +421 55 602 3017, email: tibor.rovensky@tuke.sk,

³⁾ tel: +421 55 602 3010, email: kornel.ruman@tuke.sk,

⁴⁾ tel: +421 55 602 4180, email: jan.gamec@tuke.sk

Abstract— This paper deals with HF (High Frequency) measurements of dielectric characteristics in changing working conditions. We simulated various environments using thermal shock chamber as well as temperature humidity chamber. We investigated behavior of five different substrates (Rogers RO3003C, Rogers RO4003C, RT/duroid 5880, RT/duroid LM and FR4) with microstrip structures – narrowband notch filter and transmission lines that were loaded up to 6 GHz. Temperature cycling tests were provided by changing temperature in thermal shock chamber from -55°C to 125°C. Temperature humidity chamber simulated “HTOL” (High Temperature Operation Life) tests with constant temperature 125°C. In situ measurements of scattering parameters up to 6 GHz were done by VNA (Vector Network Analyser) and present dependences of dielectric characteristics on temperature and humidity changes. This paper refers how extreme environment conditions influence behavior of dielectric properties in HF area.

Keywords— high temperature operation life tests, dielectric properties, PWB, temperature cycling tests,

I. INTRODUCTION

With evolution of information technology, the frequency applied to electronic devices has become higher to handle the growing volume data. These devices are used in various types of environments and higher frequency brings important problem – how to reduce the transmission loss on PWBs. According to temperature changes there is need of validation these PWB materials in various environments by specified comprehensive procedures e. g. “HTOL” and temperature cycling tests.

This article deals with influence of temperature, temperature changes and humidity on behavior of four different dielectric substrates (Rogers RO3003C, Rogers RO4003C, RT/duroid 5880 and RT/duroid LM).

In this paper reliability of various PCB materials in HF area was analyzed and gave overview about stability of filter up to 6 GHz.

The aim of this paper is find out impact of environment on dielectric substrates according to scattering parameters of microstrip filter and determine which of used PWB

materials is the most resistant to extreme surroundings conditions [1].

II. DIELECTRIC MATERIALS

Behavior of four different dielectric substrates was investigated after high temperature operation life tests and temperature cycling tests. Conventional substrate based on FR4 was excluded from this experiment due to unsuitability for microstrip structures in HF area. The main factor causing this disadvantage is higher content of inorganic (glass) fillers in epoxy and increasing water absorption, declined heat resistance and electrical insulation. New PWB substrates from Rogers corp. based on PTFE and hydrocarbon that can contain various inorganic fillers were analyzed.

A. Substrates

Rogers RO3003C HF circuit laminates are ceramic-filled PTFE composites. These substrates were developed for commercial microwave and RF applications and offer exceptional electrical and mechanical stability. Dielectric constant versus temperature of these materials is very stable. Advantages of these materials are: low dielectric loss – laminates can be used up to 77 GHz; excellent mechanical properties versus temperature; volume manufacturing process – competitive prices relative to other similar materials; stable dielectric constant versus temperature and frequency – ideal for bandpass filters and microstrip patch antennas. These materials are used in automotive radar applications, global positioning satellite antennas, patch antennas for wireless communications etc. [2].

Rogers RO4003C are glass reinforced hydrocarbon and ceramic (not PTFE) laminates. These materials offer superior HF performance and low losses. Circuits from these materials can be fabricated by standard epoxy/glass processes and offered competitive prices of fabrication. These materials provide properties needed to design RF microwave circuits, controlled impedance transmission lines and matching networks. Temperature coefficient of dielectric constant is one of the lowest from HF materials. Advantages of these materials are: stable electrical properties versus frequency; low dielectric tolerance and

low losses – ideal for broadband applications; low thermal coefficient of dielectric constant. Typical applications of these materials are RF identification tags, automotive radar and sensors etc. [3].

TABLE I. PROPERTIES OF DIELECTRIC SUBSTRATES RO3003C, RO4003C, RT/DUROID5880 AND RT/DUROID6010LM

Property	Typical Value (Units)			
	RO3003C	RO4003C	RT/duroid 5880	RT/duroid 6010LM
Substrate	RO3003C	RO4003C	RT/duroid 5880	RT/duroid 6010LM
Dielectric Constant	3	3.38	2.2	10.2
Dissipation Factor Tan	0.0013	0.0027	0.0009	0.0023
Dielectric Thickness	0.51 mm	0.51 mm	0.51 mm	0.632 mm
Resistivity Compared to Copper	1	1	1	1
Copper Thickness	17 μ m	17 μ m	17 μ m	17 μ m
Volume Resistivity ($M\Omega \cdot cm$)	1×10^7	1.7×10^{10}	2×10^7	5×10^6
Surface Resistivity ($M\Omega \cdot cm$)	1×10^7	4.2×10^9	3×10^7	5×10^5
Melting Temperature ($^{\circ}C$)	>280 ($^{\circ}C$ DSC)	>280 ($^{\circ}C$ DSC)	>260 ($^{\circ}C$ DSC)	>260 ($^{\circ}C$ DSC)

RT/duroid 5880 from Rogers Corporation are glass microfiber reinforced PTFE designed for microstrip and stripline circuit applications. To maximize benefits of fiber reinforcement glass fibers are randomly oriented in the direction most valuable to circuit application. The dielectric constant is stable over a wide frequency range. According to low dissipation factor usefulness of these materials is extended to area from 12 GHz and above. Advantages of these materials are: excellent chemical resistance; isotropic; lowest electrical loss for reinforced PTFE material; low moisture absorption. These materials are typically used for military radar systems, missile guidance systems, millimeter wave applications etc. [4].

RT/duroid6010LM from Rogers Corporation are ceramic-PTFE composites microwave materials intended to use for electronic and microwave circuit applications requiring a high dielectric constant. These materials is easy to fabricate and stable in use. According to low losses they are ideal to use up to 12 GHz. Advantages of these materials are: high dielectric constant for circuit size reduction; low moisture absorption; tight dielectric constant and thickness – repeatable circuit performance. Typical applications of these materials are space saving circuitry, patch antennas, aircraft collision avoidance systems etc. [5].

B. Copper foils

Copper foils deposited on HF materials are designed to achieve great performance in high reliability applications. Many types of copper foils exist and they could be divided depending on thickness and manufacturing process. Copper foil on both sides of substrate is deposited by an electrodeposited copper manufacturing process or rolled.

Copper material is electrolyzed by means of high current density in the electrolytic equipment. Copper foil is deposited on titanium drum (cathode) which is rotating.

Rolled copper is made by successive cold rolling operations to reduce thickness. Length starting with a billet of pure copper is extended.

RO3003C, RO4003C, RT/duroid6010LM have electrodeposited copper foil and RT/5880 has rolled copper foil [6].

C. Microstrip structure

HTOL tests and temperature cycling test were tested on dielectric materials with microstrip structure. These structures represent narrow-band notch filters from 2.4 GHz to 2.5 GHz. Dimensions of filter are various according to used dielectric material, principally dielectric constant of these materials, which value is in range from 2.2 to 10.2.

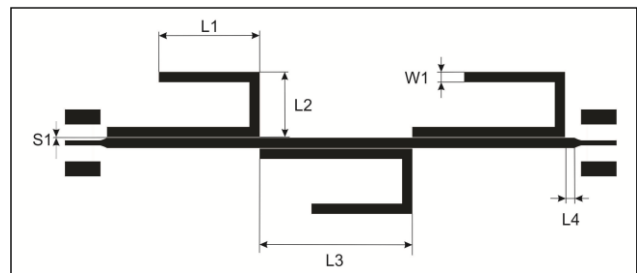


Fig. 1. Microstrip structure of narrow-band notch filter from 2.4 GHz to 2.5 GHz with pads for connector.

According to simulations of designed filter frequency tuning was made to achieve required scattering parameters and to compensate tolerance for fabrication. Dimensions of fabricated PCB with connectors are from 50.3 mm x 11.3 mm (RT/duroid6010LM) to 84 mm x 23.5 mm (RT/duroid5880). Width of structure is different for all materials and it is matched to 50 Ω characteristic impedance.



Fig. 2. Fabricated microstrip filter with soldered connectors (RT/duroid6010LM).

III. TESTING PARAMETERS

HTOL tests and temperature cycling tests were done according to commercial available standards which are usually used for testing various types of materials.

A. Temperature cycling tests

Temperature cycling tests were done according to standard JEDEC JESD22-A104-B and soak mode 3 (soak time 10 minutes). Four different substrates with microstrip structure were exposed to quick temperature changes, from -55 $^{\circ}C$ to +125 $^{\circ}C$. Interval between changes of

temperature was 10 minutes. Behavior of filter (frequency domain characteristic) was measured after 150, 300, 600 and 1300 cycles.

B. High Temperature Operation Life “HTOL” test

“HTOL” tests were done based on test method standard JEDEC JES22-A108. Four microstrip filters fabricated using different substrates were exposed to constant temperature +125 °C. Scattering parameters of filters were measured after 200 and 400 hours [8].

IV. TEST RESULTS

Vector Network Analyser (VNA) with two ports was used for measurements in frequency range from 10 MHz to 6 GHz. Test port cables were ended with SMA female connectors and SMA male connectors were soldered after each period of tests.

A. Results of temperature cycling tests

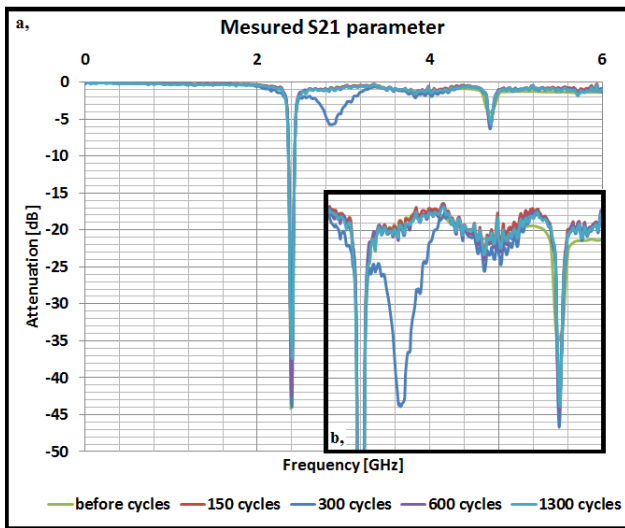


Fig. 3. a, Forward transmission coefficient (S21) of filter on substrate RO3003C after temperature cycling tests; b, Zoomed characteristic in range from 2 GHz to 5.2 GHz (0 dB to -7 dB)

Frequency domain characteristic of notch filter on dielectric substrate RO3003C, shown in Fig. 3a, are slightly changed after temperature cycles. In Fig. 3b frequency characteristic is zoomed, after 300 cycles attenuation up to -6 dB in range from 2.6 GHz to 3.1 GHz is achieved. This attenuation may be caused by re-soldering of connectors, because after 600 and 1300 cycles it is not measured.

In Fig. 4a measured forward transmission coefficient of filter based on RO4003C is shown. After 150, 600 and 1300 cycles attenuation up to -8 dB is measured in range from 3 GHz to 4.1 GHz. After 300 hours attenuation in “Wi-Fi” area is decreased from -42 dB to -34 dB. Zoomed characteristic is shown in Fig. 4b. Change of attenuation which appeared after 150, 600 and 1300 cycles is not measured after 300 temperature changes. Thus, it is supposed, that inaccuracy in process of connectors re-soldering could cause it.

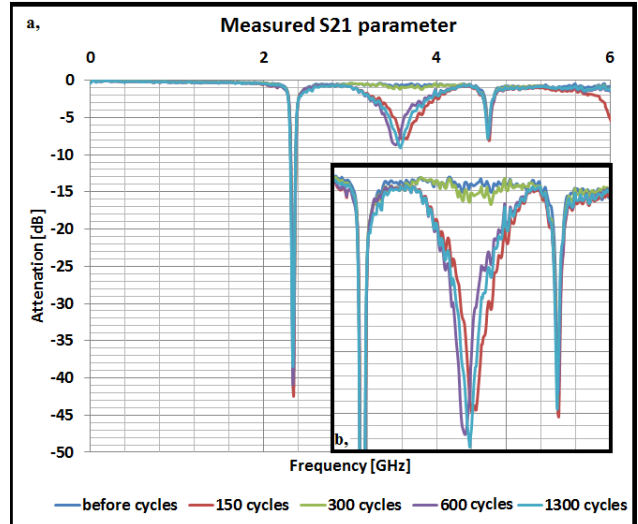


Fig. 4. a, Forward transmission coefficient (S21) of filter on substrate RO4003C after temperature cycling tests; b, Zoomed characteristic in range from 2 GHz to 5.2 GHz (0 dB to -9 dB)

Properties of notch filter fabricated on dielectric material RT/duroid5880, shown in Fig. 5, are significantly changed after temperature cycles. Frequency domain characteristic of microstrip notch filter after temperature cycling tests does not have bandstop properties.

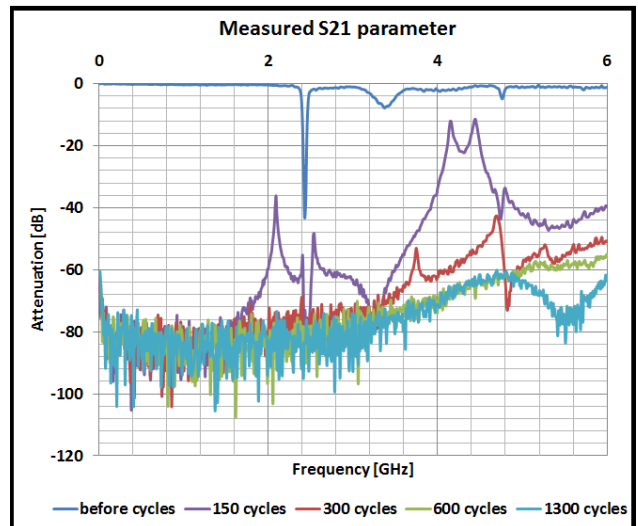


Fig. 5. Forward transmission coefficient (S21) of filter on substrate RT/duroid5880 after temperature cycling tests.

In Fig. 6a forward transmission coefficient of notch filter made from dielectric substrate RT/duroid6010LM is shown. Properties of microstrip filter after temperature cycles are changed. In Fig. 6b zoomed frequency characteristic is presented. Beyond 2.5 GHz attenuation is noticeable up to -13 dB. These similar attenuated bands appear periodically and they are spread over frequency from 2.5 GHz to 4 GHz.

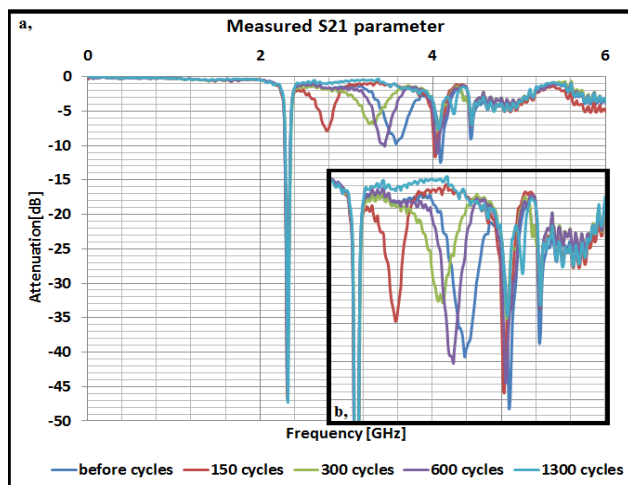


Fig. 6. a, Forward transmission coefficient (S21) of filter on substrate RT/duroid6010LM after temperature cycling tests; b, Zoomed characteristic in range from 2 GHz to 5.2 GHz (0 dB to -14 dB)

B. Results of “HTOL” tests

Frequency domain characteristic of filter using RT/duroid5880 is shown in Fig.7. After 400 hours of “HTOL” testing frequency domain characteristic of filter changed significantly.

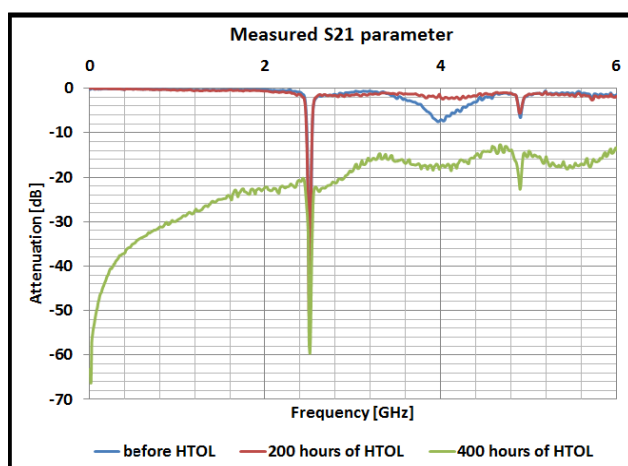


Fig. 7. Forward transmission coefficient (S21) of filter on substrate RT/duroid5880 after “HTOL” tests

Properties of other used materials (Rogers RO3003C, Rogers RO4003C and RT/duroid6010LM) after tests were not changed or changed insignificantly.

C. Summary

Repeatable temperature changes and temperature had impact on frequency domain characteristic of notch microstrip filter. These changes became significant from 2.5 GHz, up to this frequency changes of S21 parameter is insignificant. Process of re-soldering connectors could cause undesirable attenuation and changes of forward transmission coefficient.

V. CONCLUSION

We fabricated filters using four different materials and measured forward transmission coefficient (S21) of these structures by VNA. Behavior of microstrip notch filters on four different dielectric substrates were tested by temperature cycling tests and “HTOL” test. Results measured before tests were found to be correlated to the simulations. All of used materials were influenced by temperature, temperature changes and humidity significantly in HF area, beyond 2.5 GHz.

New laminates based on thermosetting resin, low polar and rigid linear polymer and low dielectric constant inorganic filler (besides glass), e.g. Rogers RO3003C, Rogers RO4003C, and RT/duroid6010LM have proved to be reliable materials for good transmission and achieved good stability after reliability tests. Dielectric substrate RT/duroid5880 doesn't achieved good properties presumably due to probability of creating agglomerates of glass fibers inside the resin that is tending to increase in water absorption and to decline in heat resistance.



ACKNOWLEDGMENT

This paper was developed with support of the project "Centrum excelentnosti integrovaného výskumu a využitia progresívnych materiálov a technológií v oblasti automobilovej elektroniky", ITMS 26220120055, that is co-financed from Structural Funds EU ERDF within Operational programme Research and Development OPVaV-2009/2.1/03-SORO and preferred axis 2 Support of Research and Development.

REFERENCES

- [1] Jia-Sheng Hong, "Microstrip Filters for RF/Microwave Applications," John Wiley & Sons, Inc., Hoboken, 2nd edition, New Jersey, 2011, 655.
- [2] RO3003, RO3006 and RO3010 High Frequency Laminates, Available on the Internet: 22.4.2013, <http://www.rogerscorp.com/documents/722/acm/RO3000-Laminate-Data-Sheet-RO3003-RO3006-RO3010.pdf>
- [3] RO4000 Series High Frequency Circuit Materials, Available on the Internet: 22.4.2013, <http://www.rogerscorp.com/documents/726/acm/RO4000-Laminates---Data-sheet.pdf>
- [4] RT/duroid 5870/5880 High Frequency Laminates, Available on the Internet: 22.4.2013, <http://www.rogerscorp.com/documents/606/acm/RT-duroid-5870-5880-Data-Sheet.pdf>
- [5] RT/duroid 6006/6010LM High Frequency Laminates, Available on the Internet: 22.4.2013, <http://www.rogerscorp.com/documents/612/acm/RT-duroid-6006-6010-laminate-data-sheet>
- [6] Copper Foils for High Frequency Materials, Available on the Internet: 22.4.2013, <http://www.rogerscorp.com/documents/749/acm/Copper-Foils-for-High-Frequency-Circuit-Materials.pdf>
- [7] JEDEC STANDARD, Temperature Cycling, JESD22-A104D, Available on the Internet: 22.4.2013, <http://www.jedec.org/sites/default/files/docs/22a104d.pdf>
- [8] JEDEC STANDARD, High Temperature Optimum Life, JEDEC JES22-A108, Available on the Internet: 22.4.2013, <http://www.jedec.org/sites/default/files/docs/22a104d.pdf>

In-situ Assessment and Monitoring of PV Systems Operation

M. Váry¹, E. Firický¹, M. Perný¹, V. Šály¹, J. Pačka¹

¹ Institute of Power and Applied Electrical Engineering, Faculty of Electrical Engineering and Information Technology, Slovak University of Technology Bratislava, tel: +421 905 981 652, michal.vary@stuba.sk

Abstract— Physical models of PV structures, cells, systems and experiments in laboratory conditions show adverse effects of some service factors (temperature, saturation due to high light intensity) on the parameters of PV systems, particularly on efficiency. Moreover, the value of this important property can be in real terms even lower. Proposed article deals with the theoretical analysis of these impacts and also provides data to measure the efficiency of PV grid-tied system in real-time with respect to operating conditions, such as temperature and intensity of incident solar radiation. In this paper the results from photovoltaic grid-tied system in-situ measurements and graphical interpretation are presented.

Keywords— PV system; solar irradiation; solar energy; energy production; efficiency;

I. INTRODUCTION

Photovoltaic (PV) module during the day, in outdoor working conditions, is exposed to changing irradiation level and module/cell temperature under real conditions. It is generally known that with regard to semiconductor and PN junction physics, PV module electric parameters are strongly affected by these factors. Well known physical models of photovoltaic structures, cells, systems and experiments in laboratory conditions show adverse effects of increased temperature and high light intensity particularly on the efficiency. Moreover, the value of this important property can be in real terms even lower.

On the other hand, long time monitoring of incident solar irradiation on the location can be helpful to optimize the performance of PV systems. The easiest and most accurate way to determine the amount of incident solar energy is a measurement of the intensity of solar irradiation in the given location. Necessary data on the availability of solar irradiation and its energy can in principle be obtained by pyranometric measurements. An important prerequisite for results of measurements of solar irradiation necessary to describe the actual relevancy of solar irradiation on the site is that the measurements represent averages for a long time, as recorded by pyranometer with digital recording devices with the possibility to collect suitable number of samples in chosen time period.

More difficult it seems to be processing and interpretation of measured data according to appropriate standards or internationally applicable methods. Moreover, if data acquiring device failure occurs, there is

a problem of data completion. In this paper, we will attempt to interpret the results obtained from measurements on experimental and educational PV system. Results shown in this paper were recorded and evaluated from 20th November 2011 to 26th March 2013.

II. TECHNICAL PARAMETERS AND MONITORING SYSTEM

Proposed photovoltaic system consists of two polycrystalline PV panel branches. Each branch consists of three panels of same type, first Solara ($U_m=18,0$ V, $I_m=4,72$ A, $P_m = 85$ W) and second SunTech ($U_m=17,6$ V, $I_m=4,8$ A, $P_m = 85$ W) connected in series. Total active surface area (A_a) is $1,587$ m² for SunTech panels and $1,687$ m² for Solara panels. Each branch is grid tied by support of GRIDFIT 250 LV solar inverter, with maximum peak power tracking function. The geographical parameters of the installed PV system are GPS 48.152925, 17.073229, orientation south, angle 45 °. This PV system with maximal theoretical power 2x255W was built for experimental and educational purposes on IP&AEE FEI SUT.

All physical quantities on the experimental photovoltaic system (incident solar irradiation energy, temperature, DC voltage and DC current in PV branches) are measured and processed by means of Prolog logging system.

Data logging device does the recording of the instantaneous average values of solar irradiation (pyranometer Kipp&Zonen CMP 6), voltage, current of illuminated panels and voltage drop on Pt100 in 5 minute time interval. Data logging device provides sending of measured values to on-line accessible back up server in selected time intervals (24 hours in our case). The device was described in [1,2].

III. THEORETICAL CONSIDERATIONS

Derived parameters related to the PV system performance may be calculated from recorded monitoring data using standard mathematical operations over reporting periods τ , which are longer than the recording interval τ_r (such an hours, days, weeks, months or years, but expressed in units of hours). To calculate any energy quantities from their corresponding measured power parameters over the reporting period τ , the following equation is used [3]:

$$E_{i,\tau} = \tau_r \sum_{\tau} P_i \quad (1)$$

where $E_{i,\tau}$ is expressed in [kWh] and P_i in [kW].

To calculate net energy from panel $E_{A,m}$ over the month m , the following equation was used:

$$\begin{aligned} E_{A,m} &= \tau_r \sum_m P_{A,m} = \tau_r \sum_m U_A I_A = \\ &= \frac{1}{12.1000} \sum_m U_A I_A \end{aligned} \quad (2)$$

where $E_{A,m}$ is energy expressed in [kWh] and $P_{A,m}$ in [kW].

The expression $E_{A,m}$ represent monthly energy production derived from measured PV output voltage U_A and current I_A . In our case the recording interval τ_r is set to 5 minutes, during which the sampled and average values of measured quantities were recorded.

Next, as it was mentioned above, long time monitoring of incident solar radiation on the location can be helpful to optimize the performance of PV systems [4], even this measurement and data are required to evaluate the PV system performance in working conditions. From the measurement of total irradiance G_I [$\text{W}\cdot\text{m}^{-2}$] in the plane of PV panel measured by pyranometer was also derived incident solar energy during each month of monitored period and equation was used:

$$H_{I,m} = \tau_r \sum_m G_I = \frac{1}{12.1000} \sum_m G_I \quad (3)$$

where $H_{I,m}$ is expressed in [$\text{kWh}\cdot\text{m}^{-2}$].

The expression $H_{I,m}$ represents monthly solar energy incident to 1 m^2 derived from measured irradiance G_I . To get the incident solar energy on the active plane the conversion to the active panel area A_a [m^2] must be calculated using equation:

$$H_{A,m} = H_{I,m} A_a \quad (4)$$

where $H_{A,m}$ is expressed in [kWh].

The average panel efficiency for period of each month was calculated using equation:

$$\eta_{A,m} = \frac{E_{A,m}}{H_{A,m}} \cdot 100 \quad (5)$$

where $\eta_{A,m}$ is expressed in [%].

The theoretical influence of temperature and illumination on PV cell/panel is described below. Basic parameters of solar cells (I_{sc} , U_{oc} , fill factor, efficiency) are temperature dependent.

- little increase in the I_{sc} due to reduction of forbidden gap (for Si cells $dE_g/dT = -2,3 \cdot 10^{-4} \text{ eV/K}$) is famous [5,6]. I_{sc} growth can be interpreted as:

$$\frac{1}{I_{sc}(T = 298K)} \frac{dI_{sc}}{dT} = 0,033\% / K \quad (6)$$

- increase in the I_{sc} comparing to U_{oc} reduction is

negligible (equations 6 and 7).

- temperature dependence of U_{oc} can be defined as:

$$\begin{aligned} U_{oc}(T) &= U_{oc}(T_0) - \left[\frac{E_{g0}}{e} - U_{oc}(T_0) \right] \left(\frac{T}{T_0} - 1 \right) - \\ &- \frac{3k_B T}{e} \ln \frac{T}{T_0} \cong U_{oc}(300K) - const(T - 300K) \end{aligned} \quad (7)$$

where T_0 is initial temperature, E_{g0} is band gap width at the T_0

- accordingly to equation (7) for crystalline silicon solar cells $dU_{oc}/dT = -2,45 \text{ mV/K}$ (it is decrease of 0,4 % per 1 K)

The change in cell voltage with temperature is due to a change in diode characteristics. Significant decrease of U_{oc} as a function of increased temperature leads to reduction of PV cell parameters (maximum power point, fill factor and efficiency).

The effect of light intensity on the solar cell output is slight increase of open circuit voltage (U_{oc}) with the intensity of the solar radiation and subsequent saturation can be seen. Linearly increasing short circuit current (I_{sc}) as a function of the intensity of solar radiation is clear. If X is concentration factor for incident solar irradiation, I_{ph1} is photo induced current (PIC) for standard illumination (100 mW/cm^2), I_{ph} is PIC for X fold increase of solar irradiation, assuming ($R_s \sim 0$, $R_{sh} \rightarrow \infty$) we can write [7,8]:

$$I_{ph} = X I_{ph1} \quad (8)$$

$$U_{oc} = U_{oc1} + \frac{nk_B T}{q} \ln X \quad (9)$$

where U_{oc} is open circuit voltage for non concentrated irradiation.

Increase in performance is observed until the certain limit value of solar light intensity is reached. Effect of series resistance and injection of charge carriers is applied and leads to reduction of performance above this limit value [9].

These theoretical findings can be easily verified for PV cell in laboratory conditions. The situation is different for real PV panels/systems of almost any size, because these parameters have to be measured in real working conditions. By means of described in-situ measurements, the temperature and light intensity dependence of PV systems efficiency in maximum power P_m can be obtained.

IV. EXPERIMENT AND DISCUSSION

The experimental data were logged and then results calculated from 20th November 2011 to 26th March 2013. It represents more than 1 300 000 experimental points of measured and logged parameters. These were statistically processed in Matlab environment.

Table 1 shows SunTech branch calculated values for each month – incident solar energy on an area of 1m^2 $H_{I,m}$ obtained from from measured solar irradiance G_I in the plane of panel using pyranometer, net SunTech branch energy $E_{A,m}$ and average monthly efficiency $\eta_{A,m}$ during power generation.

Tab. 1. SunTech branch monthly energy production, solar irradiance and average efficiency.

Month	$H_{I,m}$ [kWh.m ⁻²]	$E_{A,m}$ [kWh]	$\eta_{A,m}$ [%]
november '11	8.69	1.357	9.84
december '11	27.01	4.253	9.92
january '12	56.068	8.8	9.89
february '12	73.484	11.266	9.66
march '12	142.353	17.348	9.03
april '12	153.504	15.909	8.49
may '12	178.054	23.982	8.28
june '12	160.454	20.652	8.11
july '12	166.959	21.357	8.06
august '12	174.183	21.488	7.77
september '12	134.299	18.518	8.69
october '12	92.823	13.851	9.4
november '12	36.324	5.921	10.27
december '12	37.257	5.918	10.01
january '13	28.804	4.480	9.80
february '13	40.476	6.477	10.08
march '13	76.132	11.825	9.79

Figure 1 shows incident solar energy dependence during the monitored period and monthly average temperature with its standard deviation, measured on the back site of the panels. The year 2012 yielded the total solar energy 1406 kWh.m^{-2} in the given location. In February 2012 was recorded the lowest temperature ($-21.9\text{ }^\circ\text{C}$) and the highest temperature in August 2012 ($62.7\text{ }^\circ\text{C}$).

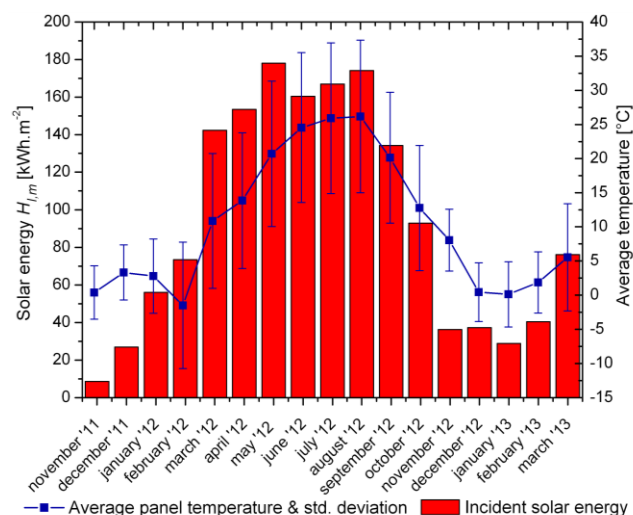


Fig. 1. Monthly incident solar energy on an area of 1 m^2 on the monitored PV system site and average monthly panel temperatures with standard deviation y-error bars.

Dependence on Figure 2 illustrates graphical comparison of monthly incident solar energy recalculated to active area and monthly energy production of SunTech branch. This ratio is the calculated average efficiency

stated in Table 1 for a given month. The year 2012 yielded the total solar energy incident on the active SunTech area 2231 kWh . Energy production of SunTech branch for year 2012 was approx. 185 kWh .

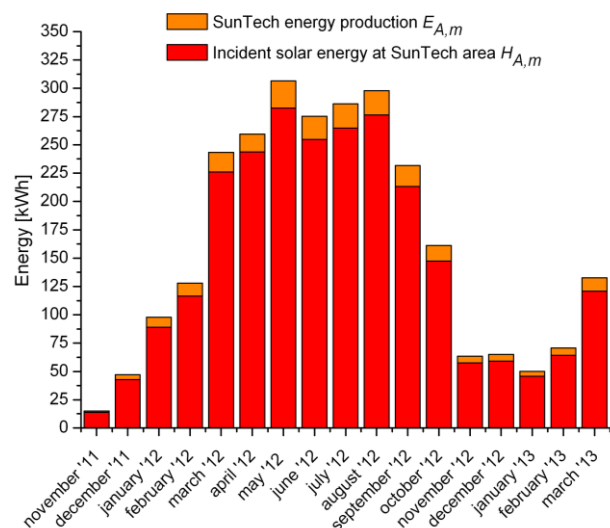


Fig. 2. Monthly incident solar energy at SunTech branch active area and energy production of SunTech branch.

Figure 3 and figure 4 shows temperature, energy production and average efficiency of SunTech branch during energy production for each month. According to this dependence it is clear, that the warm summer months reducing the efficiency of solar energy to electrical energy conversion, although the yield is still higher in sunny summer months (see Figure 5). Average efficiency values related to each month are shown in the Table 1. Minimum average efficiency was reflected in August 2012 (7.77 %) and maximum in November 2012 (10.27%). The maximum energy production of SunTech branch was in May 2012 (23.98 kWh) and the minimum in December 2011 (4.25 kWh). Maximum percentual energy production covers May 2012 (12.96 %). The evolution of SunTech energy production branch is shown on Figure 6.

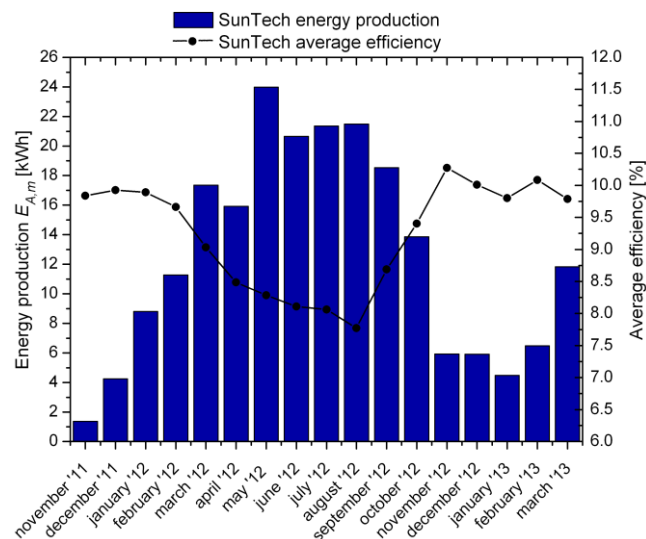


Fig. 3. Monthly energy production and monthly average efficiency.

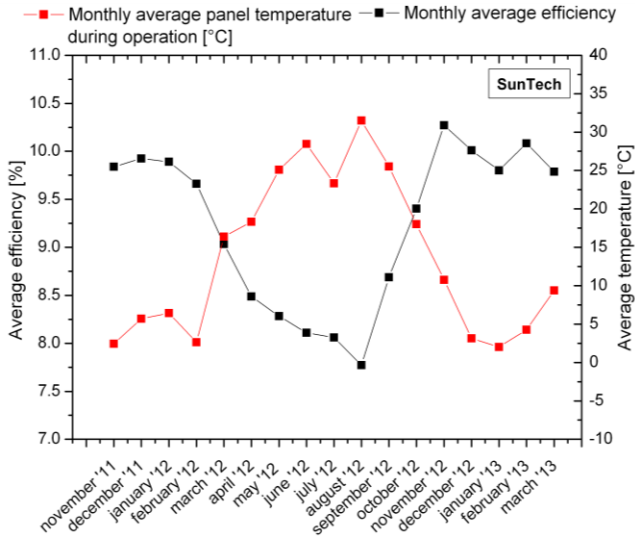


Fig. 4. Monthly average efficiency and average temperature during energy production.

Percentual SunTech energy production in 2012

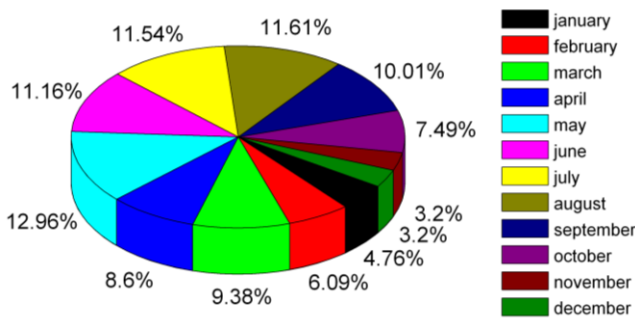


Fig. 5. Percentual SunTech branch energy monthly production during the year 2012.

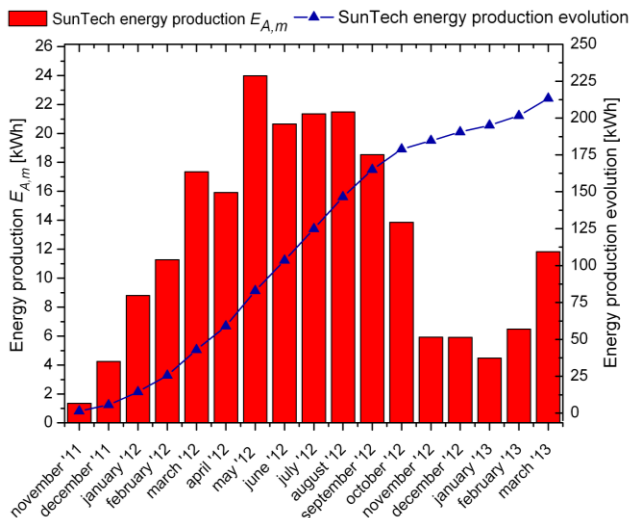


Fig. 6. Monthly and cumulative energy production of SunTech branch.

Figure 7 illustrates the temperature dependence of PV system efficiency (Solara and SunTech branches) at constant solar irradiation $800 \pm 10 \text{ W/m}^2$. The data of PV system performance (related to Figure 7) logged during

the first quarter of the year 2012 were statistically processed in Matlab.

Tab. 2. Parameters of PV system (Solara and SunTech branches) efficiency temperature dependence.

		Value	Std. Error
SunTech	Intercept	11,25 %	0,026 %
	Slope	-0,069 %/°C	0,0015 %/°C
Solara	Intercept	12,32 %	0,125 %
	Slope	-0,063 %/°C	0,007 %/°C

Table 2 shows the results of linear regression parameters of statistically evaluated data from Figure 7. Both panels are made of polycrystalline Si and the temperature dependence of efficiency is related largely with material used. The slope of the regression is $-0,069 \text{ \%}/^\circ\text{C}$ for SunTech branch and $-0,063 \text{ \%}/^\circ\text{C}$ for Solara branch (at solar radiation 800 W/m^2). According to fitted parameters, the efficiency for SunTech branch at $25 \text{ }^\circ\text{C}$ is 9,54 % and for Solara branch 10,74 %.

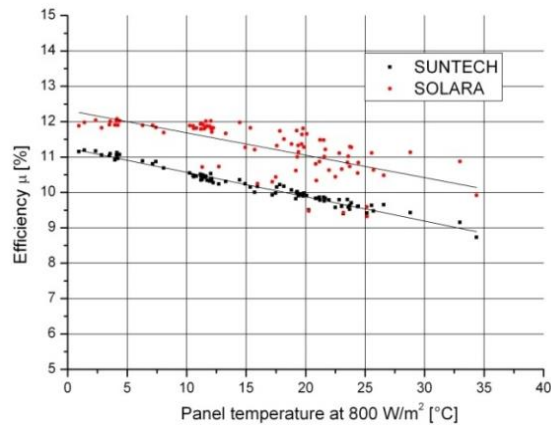


Fig. 7. Temperature dependence of PV system (SunTech and Solara

Figure 8 illustrates the monthly average panel temperature vs monthly average efficiency only of SunTech branch at various solar irradiation. Points on the plot were obtained from average panel temperatures and average efficiencies derived from each month values from 20th November 2011 to 26th March 2013.

Tab. 3. Parameters of SunTech branch average efficiency temperature dependence.

	Value	Standard Error
Intercept	10.26 %	0.144 %
Slope	-0.074 %/°C	0.008 %/°C

Table 3 shows the results of linear regression parameters of statistically evaluated data of SunTech branch from Figure 8. From these average efficiency and temperature values the slope of the regression is $-0.074 \text{ \%}/^\circ\text{C}$. The efficiency for SunTech branch at 25°C is 8,4 %. Total average efficiency for various solar irradiation and temperatures during the service period from 20th November 2011 to 26th March 2013 is 9,24 % (from Table 1).

branch) efficiency at solar irradiance 800 W/m^2 .

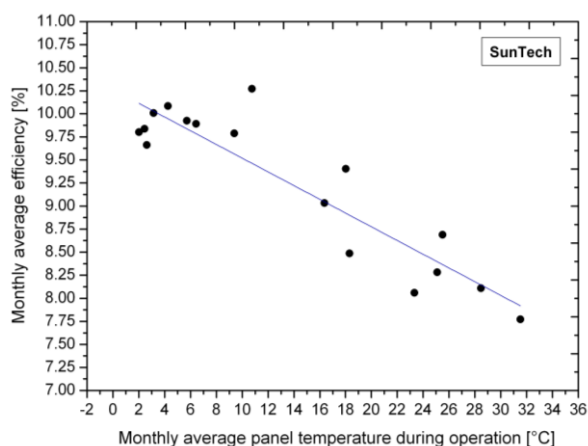


Fig. 8. Average panel temperature efficiency dependence of SunTech branch at various solar irradiance during energy production from 20th November 2011 to 26th March 2013.

V. CONCLUSION

Achievement of products final properties is determined by the knowledge of technological processes and input material properties. The overall performance of PV systems is determined by knowledge of working conditions and their optimization. Necessary data on the availability of solar radiation and its energy can in principle be obtained by pyranometric measurements. An important prerequisite for results of measurements of solar radiation necessary to describe the actual relevancy of solar radiation on the site is that the measurements represent averages for a long time, as recorded by pyranometer with digital recording devices with the possibility to collect suitable number of samples in chosen time period.

In this work system for monitoring parameters and working conditions of PV systems in real time was introduced and long time measurement results (above 1 300 000 experimental points) illustrated the perspective application of this appliance for in-situ monitoring.

The measurement of PV cell efficiency temperature dependence in laboratory conditions belongs to standard types of measurement. Proposed logging system allows measurement of this parameter in real working conditions (temperature, solar radiation) for small PV grid tied systems. Results illustrated in this paper are in good

compliance with theoretical assumptions. Similar temperature dependence of both panel types ($-0,069 \text{ \%/}^\circ\text{C}$ for SunTech branch and $-0,063 \text{ \%/}^\circ\text{C}$ for Solara branch, at solar radiation 800 W/m^2) is related with polycrystalline type of material used. The efficiency for SunTech branch at $25 \text{ }^\circ\text{C}$ is $9,54 \text{ \%}$ and for Solara branch $10,74 \text{ \%}$.

During the long-term in-situ measurements for various service conditions, solar irradiation and temperatures, the dependence of efficiency from monthly average temperature was shown for SunTech branch ($-0.07433 \text{ \%/}^\circ\text{C}$). The efficiency for SunTech branch at $25 \text{ }^\circ\text{C}$ was $8,4 \text{ \%}$. This methodology can be also used for estimation of PV system performance.

ACKNOWLEDGMENT

This contribution is the result of the project implementation: Finalization of Infrastructure of the National Centre for Research and Application of Renewable Energy Sources (ITMS: 26240120028), supported by the Research & Development Operational Programme funded by the EU.

REFERENCES

- [1] Váry M., Perný M., Firický E.: *Monitoring of Photovoltaic Systems Performance*, In: Elektroenergetika. - ISSN 1337-6756. - Vol. 4, No, 3 (2011), s. 11-13.
- [2] Váry M., Perný M., Firický E.: *Realtime Photovoltaic Systems Monitoring*, In: Power Engineering 2011. Renewable Energy Sources 2011 : Tatranské Matliare, Slovakia, June 7-9, 2011. - Bratislava : Slovak University of Technology in Bratislava, 2011. - ISBN 978-80-89402-38-0.
- [3] STN EN 61724: Photovoltaic system performance monitoring. Guidelines for measurement, data exchange and analysis, 2001.
- [4] Kittler, R., Mikler, J.: *Základy využívania slnečného žiarenia*, Vydala VEDA, vydavateľstvo Slovenskej akadémie vied v Bratislave v r. 1986, SÚKK 1729/1-85, ISBN 71-013-185.
- [5] Radziemska, E.: *Thermal performance of Si and GaAs based solar cells and modules: a review*, Progress in Energy and Combustion Science 29, 2003, str. 407-424.
- [6] Radziemska, E.: *Thermally affected parameters of the current-voltage characteristics of silicon photocell*, Energy Conversion and Management 43,2002, str. 1889-1900.
- [7] G. L. Aratijo: *Solar electricity*, Progensa, Ed. E. Lorenzo, 1994, str. 59-86.
- [8] H. J. Hovel: *Semiconductors and semimetals*, Ed. R. K. Willardson, A. C. Beer, Vol. 11, Solar Cells, Chap. 3, Academic Press, New York, 1975, str. 48-70.
- [9] Rauschenbach, H. S. (1980), *Solar Cell Array Design Handbook*, Vannostrand, Reinhold, NY.

Influence of humidity on glass transition of thermosetting epoxy laminate

Pavel Prosr

University of West Bohemia in Pilsen / RICE, Univerzitní 8, Czech Republic, www.zcu.cz
tel: +420 377 634 519, email: prosr@ket.zcu.cz,

Abstract— The main objective of this paper is to investigate the influence of the humidity on mechanical properties of thermosetting epoxy laminate. Glass transition and Young's modulus of elasticity measured by Dynamical mechanical analysis and bending tests using universal mechanical test machine were used to evaluate the mechanical properties of samples. The composite was exposed to thermal treatment at temperature 40 °C and humidity 93 %. Reductions in measured parameters were observed during the aging process.

Keywords— thermosetting epoxy laminate; glass transition; humidity; Young's modulus of elasticity

I. INTRODUCTION

Reliable operation of all materials depends critically on the integrity of its structure, which is disturbed by exposure to combination of thermal, mechanical, electrical and other environmental stresses. [1] Concerning on humidity influence of the insulating materials, the impact on electrical properties is well known. [2, 3, 4]

Reliability and lifetime of the insulating materials are affected not only by electric stress, but largely by action of mechanical stress (static and dynamic forces). Analysis of mechanical properties, with reference to their possible change due to a long time operation and excessive influence of humidity, should be done for complex evaluation of materials. Problem of humidity may play the significant role especially in areas, which are generally placed located closer to the equator or near coastal regions. [5]

Loading of the material by external force causes its mechanical stress and deformation. The temporary change in length, volume, or shape that is self-reversing after the force is removed is called elastic deformation. According to [6] relatively small deformations of an object, the displacement or size of the deformation is directly proportional to the deforming force or load. Under these conditions the object returns to its original shape and size upon removal of the load. This phenomenon is called Hooke's law and graphical dependence is visible on Figure 1.

Elastic behaviour of solids according to Hooke's law can be explained by the fact that a small displacement of their constituent molecules, atoms, or ions from normal positions, is also proportional to the force that causes the displacement [6].

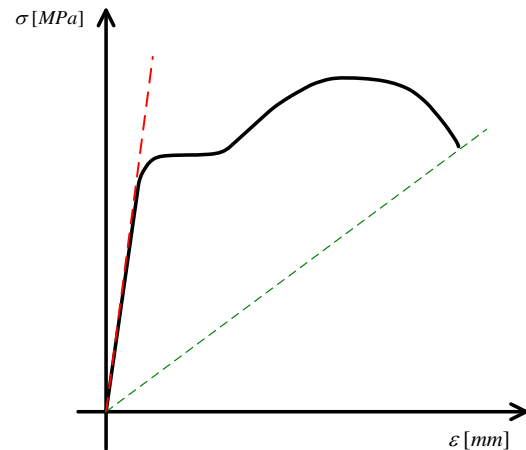


Fig. 1. Deformation curve according to Hooke's law - Young's Modulus E

For testing of the mechanical properties of material the different type of methods is possible to use. One of them represents single bend test. This method enables to estimate moduli of elasticity E . Another possibility of determination of mechanical properties allows application of Dynamical Mechanical Analysis (DMA). It is a technique that is especially used to characterize a material's properties as a function of different kind of parameters. The most frequently used parameters are temperature, time, frequency, stress or a combination of these parameters.

Generally the DMA is method, which is used for testing of the viscoelastic behaviour of material. Ideally stiff material is promptly deformed at strain activity and reversely, the elastic deformation is loosed at the same time with dropped strain. Actually there is necessary some time delay for transfer of atoms in real molecule. Deformation is therefore delayed under applied strain.

According to the chosen test method, mechanical properties may be expressed in terms of a dynamic storage modulus - E' [MPa], a dynamic loss modulus - E'' [MPa], and a mechanical damping term - $\tan \delta$ (Fig. 5) or Young's Modulus - the linear part of deformation curve (Fig. 1).

Viscoelastic behaviour of material is described using above mentioned parameters (storage and loss modulus). Remaining parameter ($\tan \delta$) is calculated using equation 1.

$$\tan \delta = \frac{E''}{E'} \quad (1)$$

II. EXPERIMENT

Two different test methods were applied by the reason of comparison of microscopic and macroscopic characterization of mechanical properties of thermosetting epoxy laminate. Dynamic mechanical analysis (DMA) and bending test using Labor Tech testing device were used, for this laboratory experiment. Changes of mechanical properties were observed during climatic aging.

Tested samples were prepared from one board of thermosetting material. Dimension of samples for bending test were, according to [8], chosen as 45, 15, 1.5 mm (length, width, thickness).

For DMA measurements, a rectangular shape of samples was prepared. Because the sample preparation is one of the most important factors in achieving of an accurate and reproducible results, the appropriate sample sizes were determined based on calculation of geometry factors (GF) using Equation 2.

$$GF = \frac{L^3}{48 \cdot I} \cdot \left[1 + \frac{12}{5} \cdot (1 + \nu) \cdot \left(\frac{t}{L} \right)^2 \right] \quad (2)$$

Where:

- GF = geometry factor
- L = sample length / mm
- I = geometric moment / mm⁴ (for rectangular samples = 1/12 · t³ · W)
- W = sample width / mm
- t = sample thickness / mm
- ν = Poisson's ratio (nominally 0,44)

The Equation 2 assumes that local deformation of the sample in the region of the supports are negligible and it can also help to determine if the properties of a sample of a particular size can be measured or if the sample dimensions will have to be changed.

The Fig. 2 displays the relationship between modulus range and the possible sample size range for the 3 point bending clamps. The modulus range is based on the range of stiffness over which the DMA can operate (10² to 10⁷ N/m).

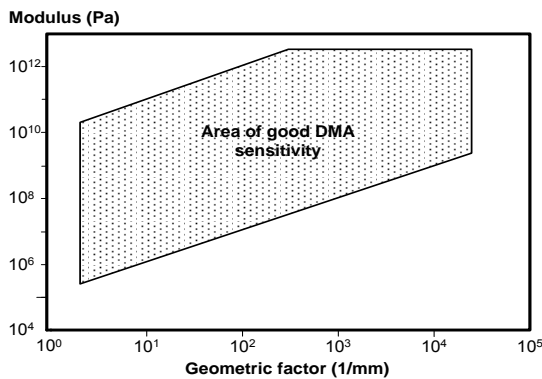


Fig. 2. Operating range of the 3-point Bending Clamps based on sample dimension and calculated Geometric Factor (Equation 1)

According to the precision specification, the length, height and thickness of the specimens were chosen as 50, 12 and 1.5 mm.

Specimens of tested thermosetting material were exposed to hot/wet conditions. Samples were aged for 624 hours at temperature 40 °C and relative humidity 93 %. Artificial aging, the “hot/wet” environment exposure, was carried out using a climatic chamber ILKA Feutron with digital temperature and humidity controls. All prepared samples were before placing to a climatic chamber dried for 24 hours at temperature 45 °C.

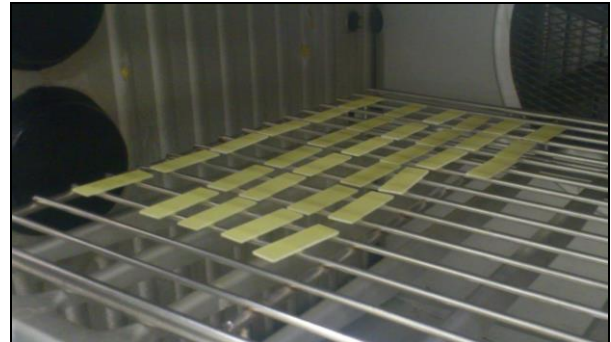


Fig. 3. Placement of samples in laboratory climatic chamber

III. RESULTS AND DISCUSSIONS

A. DMA results

The 3-point bending clamps, which are very sensitive to any sample malformation, were used for purpose of DMA measurement (see Fig. 4). Young's modulus and glass transition were analyzed for all measured materials.



Fig. 4. Placement of the sample in clamps during measuring by DMA method – 3 point bending mode of measurement

Young's modulus measures the resistance of a material to elastic (recoverable) deformation under load. It's the slope of the line for the elastic region of Stress / Strain graph. The stiffness of a component means how much it deflects under a given load. This depends on the Young's modulus of the material, but also on how it is loaded (tension, or bending) and the shape and size of the component. [6] A stiff material has a high Young's modulus and changes its shape only slightly under elastic loads (e.g. diamond). A flexible material has a low Young's modulus and changes its shape considerably.

Young's modulus of tested thermosetting samples was measured using stress/strain testing mode of DMA. Tested force was applied to 18 N at force ramp 3 N/min. The

results of measurement weren't repeatable. From this reason another parameter (glass transition) was used for analysis of the aging process using DMA.

TABLE I. RESULTS OF DMA MEASUREMENTS

Aging time / hours		0	168	456	624
DMA	T _g [°C]	130,79	126,77	123,69	123,55
	Standard Deviation [°C]	0,77	0,18	0,18	0,52
	Young's modulus E [MPa]	73,35	71,96	72,47	77,54

According to [7] the glass transition is the reversible transition in amorphous materials (or in amorphous regions within semicrystalline materials) from a hard and relatively brittle state into a molten or rubber-like state.

The glass transition of samples was taken by changing the temperature of specimens gradually under fixed vibrating frequency. The temperature raising speed was 3 °C/min, vibrating frequency 1 Hz, vibrating amplitude 15 μm and the range of heat sweep temperature 30-200 °C.

Three different values are possible to use for interpretation of the glass transition – storage, loss modulus and tan δ (Fig. 5). Dissipation factor (tan δ) representing mechanical damping of the material, was chosen for the purpose of this paper. The advantage of this factor (tan δ) consist in uniquely determined value. From the reason of analysis of mechanical properties, the storage modulus should be more suitable. However nonlinear initial part of this temperature dependence modulus could cause unneeded inaccuracies. Results of the dependence of glass transition with standard deviations on aging time are visible on Fig. 6.

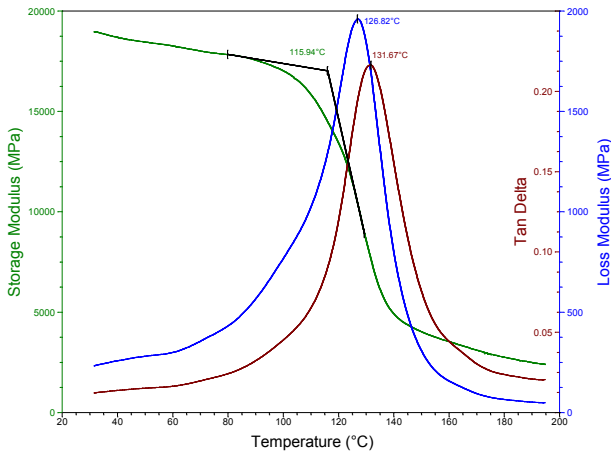


Fig. 5. DMA results – 3-point bending clamps

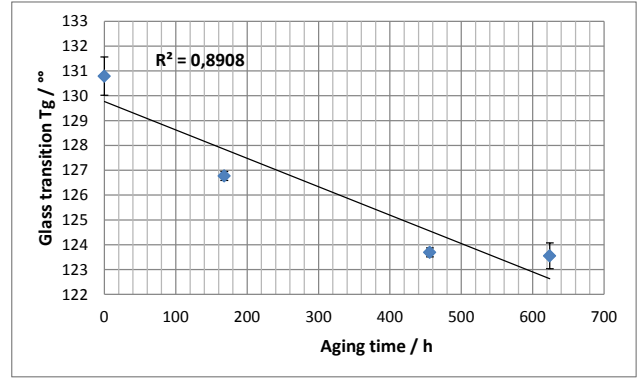


Fig. 6. Glass Transition changes in dependence on time of aging

B. Bending test (Labor Tech)

Measurements of bending strength were performed according to [8]. Three-point bending setup was used for mechanical test. The specimen was placed on two supports pins that were 30 mm apart. Force was applied in the exact middle of the two supports. The loading rate was set at 1.25 mm/min., corresponding to an average strain rate. Young's modulus and the maximal force needed for 80% deformation of the sample were analyzed (see Table II and Fig. 7 and 8).

TABLE II. RESULTS OF BENDING MACHINE MEASUREMENTS

Aging time / hours		0	168	456	624
Bending machine	F _{max} [N]	275,3	265,2	248	248,9
	Standard Deviation [N]	7,2	7,6	5,9	10,3
	Young's modulus E [MPa]	5495,5	5447,3	5166,2	5137,7
	Standard Deviation [MPa]	156,9	114,8	152,8	197,9

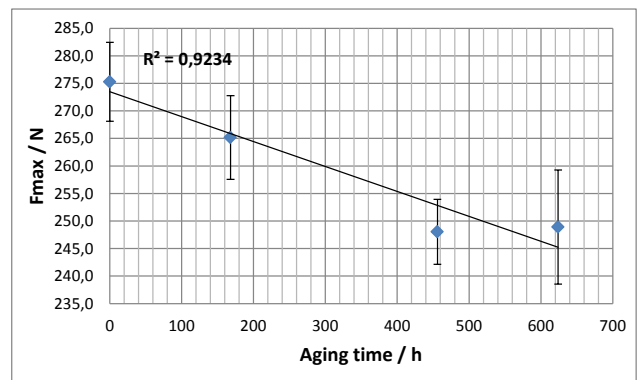


Fig. 7. Maximal force dependence using bending machine

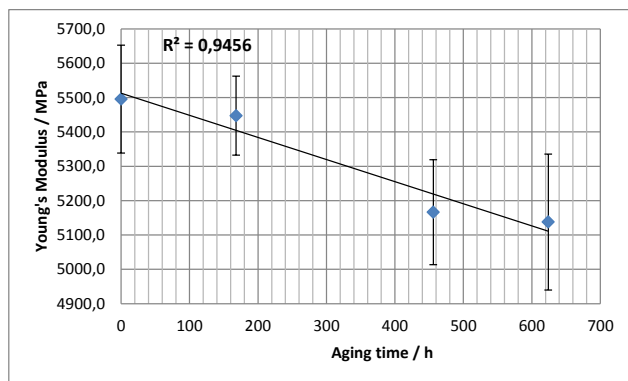


Fig. 8. Young's Modulus measured by bending machine

As we can see from previous figures, bending machine was sensitive to applied aging conditions. Maximal force and Young's modulus decrease depending on time of climatic stress.

C. Correlation

From the reason of using more count of samples for testing by the bending machine against DMA, correlations between these two diagnostics accesses were analyzed (Fig. 9 and 10).

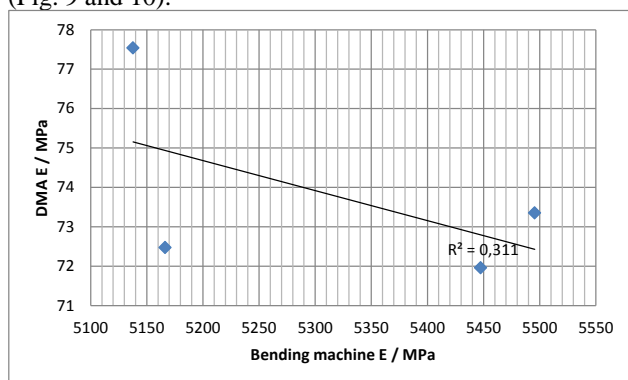


Fig. 9. Correlation between Young's modulus measured by DMA and bending machine

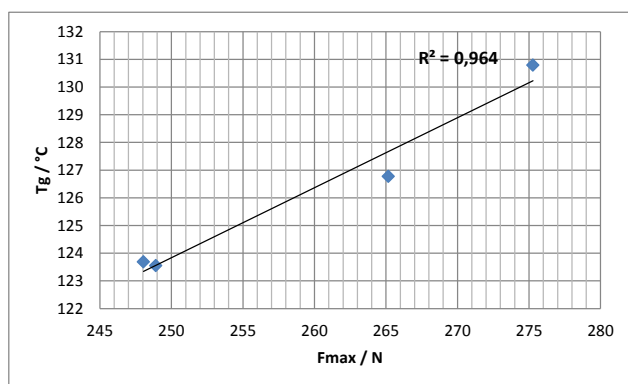


Fig. 10. Correlation between maximal force (bending machine) and glass transition (DMA)

As we can see, good correlation was proven between maximal force and glass transition. In the light of DMA, glass transition is well measurable parameter with great repeatability of measurement.

IV. CONCLUSION

The aim of this research is to study the impact of humidity on mechanical properties of a thermosetting epoxy laminate. These parameters (modulus or glass transition) are used as indicators of a material's stiffness.

According to presumption, correlation between glass transition and maximal force was proved. Almost linear dependence of these parameters leads to possibility of analyze of maximal force on the basis of glass transition. The second hypothesis based on liner dependence of Young's modulus measured by DMA and bending machine wasn't proved. The results of DMA measurement refer to causal character of measured data. The results of the bending test using DMA could be partly caused by partly imperfection of specimen preparation.

ACKNOWLEDGMENT

This research has been supported by the European Regional Development Fund and the Ministry of Education, Youth and Sports of the Czech Republic under the Regional Innovation Centre for Electrical Engineering (RICE), project No. CZ.1.05/2.1.00/03.0094.

REFERENCES

- [1] JIANCHENG, Song, Xie HENGKUN, Li HAIYING a Hao JUNFANG. Dynamic mechanical analysis of degradation of rotating machine composite insulation. *Acta Materiae Compositae Sinica* [online]. 2001 [cit. 2013-04-05]. ISSN 1000-3851. Available from: <http://ieeexplore.ieee.org/stamp/stamp.jsp?tp=&number=973777>.
- [2] GONON, P., A . SYLVESTRE, J. TEYSSEYRE a C. PRIOR. Combined effects of humidity and thermal stress on the dielectric properties of epoxy-silica composites. *Materials Science and Engineering: B* [online]. 2001, Vol. 83 [cit. 2013-04-16]. ISSN 0921-5107. Available from: <http://www.sciencedirect.com/science/article/pii/S0921510701005219>.
- [3] GONON, P., T. PHAM HONG a C. PRIOR. Influence of high levels of water absorption on the resistivity and dielectric permittivity of epoxy composites. *Materials Science and Engineering: B* [online]. 2001, č. 83 [cit. 2013-04-16]. ISSN 0921-5107. DOI: <http://dx.doi.org/10.1016/j.polymeresting.2005.02>. Available from: <http://www.sciencedirect.com/science/article/pii/S0142941805000267>.
- [4] THOMAS, P., K. DWARAKANATH, P. SAMPATHKUMARAN, S. SEETHARAMU a KISHORE. Influence of moisture absorption on electrical characteristics of glass-epoxy polymer composite system. *Proceedings of 2005 International Symposium on Electrical Insulating Materials, 2005. (ISEIM 2005)* [online]. IEEE, 2005, č. 83, 612-615 Vol. 3 [cit. 2013-04-16]. ISSN 0921-5107. DOI: 10.1109/ISEIM.2005.193443. Available from: <http://ieeexplore.ieee.org/lpdocs/epic03/wrapper.htm?arnumber=1496247>.
- [5] XUE, Yibin, David VEAZIE, Cindy GLINSEY, Meagan WRIGHT a Roger M. ROWELL. Mechanical Properties of Wood Fiber Composites Under the Influence of Temperature and Humidity. [online]. [cit. 2013-04-04]. Available from <http://www.fpl.fs.fed.us/docmnts/pdf2003/xue03a.pdf>.
- [6] Hooke's law." *Encyclopædia Britannica. Encyclopædia Britannica Online*. Encyclopædia Britannica Inc., 2013. Web. 04 Jun. 2013.
- [7] Property Information: Young's Modulus and Specific Stiffness. UNIVERSITY OF CAMBRIDGE. Materials Group [online]. [cit. 2013-04-16]. Dostupné z: <http://www-materials.eng.cam.ac.uk/mpsite/properties/non-IE/stiffness.html>
- [8] ČSN EN ISO 178. *Plastics – Determination of flexural properties*. 2003.

Comparison of temperature limits of cable sheaths measured by Dynamic Thermo Mechanical Analysis

Martina Pinkerová¹⁾, Monika Bartůňková²⁾, Radek Polanský³⁾

^{1,2)} University of West Bohemia/Faculty of Electrical Engineering/KET, Univerzitní 8, 306 14 Pilsen, Czech Republic

³⁾ University of West Bohemia/Faculty of Electrical Engineering/RICE, Univerzitní 8, 306 14 Pilsen, Czech Republic

¹⁾ tel: +420 377 634 528, email: mpinkero@ket.zcu.cz,

²⁾ tel: +420 377 634 528, email: mbartunk@ket.zcu.cz,

³⁾ tel: +420 377 634 517, email: rpolansk@ket.zcu.cz

Abstract— It is necessary to know temperature endurance of materials for using cable sheaths. Increasing temperature leads to softening of thermoplastics or even up to irreversible deformation of the shape and vice versa, decreasing temperature leads to gradual embrittlement and can cause the rupture of the material. The aim of the paper is to compare mechanical properties of sheathing materials used for cables during a broad temperature interval and recommend the right selection of material used for various applications. The paper is focused on a comparison of thermo-mechanical properties of six plastic insulation materials used for different cable sheaths made from: Polyurethane, Polyvinylchloride, Silicone rubber compound, Flexible elastomer based compound crosslinkable by exposure to moisture, Thermoplastic halogen-free flame-retardant (and low smoke emission) compound and Silane crosslinkable low-smoke low-toxicity halogen-free flame-retardant compound.

Keywords— plastics; cable sheath; dynamic mechanical analysis; glass transition.

I. INTRODUCTION

Polymers are considered to be a basic material of industrial manufacture. Their low price, simplicity of manufacture and wide modification flexibility of their properties are the main reasons for their rapid development. There are a lot of types of various polymer materials used in cable manufacture. For using cable sheaths is necessary to know temperature endurance of materials. Increasing temperature leads to the softening of the thermoplastics or even up to the irreversible deformation of the shape and vice versa, decreasing temperature leads to the gradual embrittlement and can cause the rupture of the material.

Plastic materials used in cable industry are divided into two main groups according to their physical and mechanical properties. Thermoplastics are materials that become pliable above a specific temperature, and returns to a solid state upon cooling. At cold temperature, thermoplastics are brittle (glassy). Upon heating, thermoplastics become soft and malleable, especially in the vicinity of their particular glass transition temperature. Further heating gradually transforms a thermoplastic mould into a viscous liquid. At that point, the plastic can

be moulded into a new shape for reuse. Thermoplastics are therefore easily recycled. [1] Elastomers are materials that can undergo much more elastic deformation under stress than most materials and still return to their previous size without permanent deformation. Vulcanization of these materials forms chemical bonds between adjacent elastomer chains and subsequently imparts dimensional stability, strength, and resilience. Vulcanized material is usually named rubber. Rubbers can therefore function as shock and vibration isolators and as dampers. [2] The last group, so-called “Thermoplastic elastomers” form a special group in this area. It is a class of copolymers or a physical mixture of polymers which consist of materials with thermoplastic and elastomeric properties. Thermoplastic elastomers show advantages typical of both rubbery materials (good mechanical properties) and plastic materials (easy processing and recycling). [3] It is obvious that all of the above mentioned groups of plastics behave differently at different temperatures. Therefore the main aim of the paper is to compare mechanical properties of selected cable sheathing materials (thermoplastics and elastomers) during a broad temperature interval and recommend the right selection of material used for various applications.

II. EXPERIMENT

A. Materials description

Six kinds of cables sheaths for various applications were analysed. The following materials were selected for a comparison:

- **PUR** is a thermoplastic polyurethane;
- **PVC** is a polyvinyl chloride compound for cable sheathing;
- **SIL** is a silicone rubber compound forming a stable ash on combustion;
- **EPR** is a flexible elastomer based compound crosslinkable by exposure to moisture for increased heat resistance of cable insulation;

- **HFRR** is a thermoplastic compound also filled by flame retardant; this material is designed for using in nuclear power plants. The cables made from materials like that can be used during accident of HELB (High-energy Line Break) [8].
- **XHFRR** is a chemically crosslinkable filled thermoplastic mixture whose structure is formed by spatial linking the chemical bonds, which create a three dimensional net. Material is designed for cable sheaths which are used in active zone of nuclear reactor. These cables should reliably work during LOCA (Loss of Coolant Accident) [9].

Table 1 shows comparison of the properties (density, tensile strength and elongation at break) of all materials used for experiment according to the supplier. These are the properties that dictate how polymers actually behave on a macroscopic scale.

TABLE I. PROPERTIES OF MATERIALS USED FOR EXPERIMENT [4-9]

Material	Specific gravity [g/cm ³]	Tensile Strength [MPa]	Elongation at Break [%]
PUR	1.22	42.5	390
PVC	1.49	15	240
SIL	1.31	10	340
EPR	0.89	8.5	300
HFRR	1.51	11	140
XHFRR	1.49	12	140

Bulk density is the weight per unit volume of the raw plastic material as it is purchased from the material supplier, usually in the form of small pellets or beads. Bulk density is useful as an incoming quality check on material. [10] The tensile strength of a material quantifies how much stress the material will endure before suffering permanent deformation. In general, tensile strength increases with polymer chain length and crosslinking of polymer chains. [11] The ultimate elongation at break of plastic material is the percentage increase in length that occurs before it breaks under tension. The combination of high ultimate tensile strength and high elongation leads to materials of high toughness. [12]

B. Measurement

The samples of materials were subjected to the thermomechanical analysis in a dynamic mode (DTMA). DTMA is a technique in which the viscoelastic behaviour of the sample under oscillatory load is monitored as a function of temperature while the sample is subjected to a controlled temperature programme [13]. It is used especially for very precise determination of glass transition temperature (T_g). The glass transition temperature describes the temperature at which amorphous polymers undergo a transition from a rubbery, viscous amorphous liquid, to a brittle, glassy amorphous solid. The glass transition temperature may be engineered by altering the degree of branching or crosslinking in the polymer or by the addition of plasticizer. [14]

DTMA was carried out on TA Instruments TMA Q400EM apparatus. Disk shape samples of diameter 3 mm were measured in a penetration mode. Static force of 0.3 N together with modulated force of ± 0.2 N at frequency of 1 Hz was applied. The samples were exposed to linear heating at a rate of 5 °C/min under air atmosphere in the temperature range from -150 to 100 °C.

C. Evaluation of results

As was already mentioned before, DTMA is very sensitive to measure T_g . Hence this technique is useful to use whenever T_g is undetectable by other thermal analysis (DSC, DTA, TMA). DTMA basic principle was described in the previous paragraph. Most important is the fact, that this technique allows separation of the viscoelastic material response to two components of complex modulus: a real part E' [MPa] and an imaginary part E'' [MPa]. Phase angle between these moduli is defined as a $\tan \delta$ [-] and is equal to: [16-18]

$$\tan \delta = \frac{E''}{E'}. \quad (1)$$

Graphical interpretation of all components (moduli E' , E'' and loss factor) as a function of temperature in the material EPR can be seen in Fig. 1.

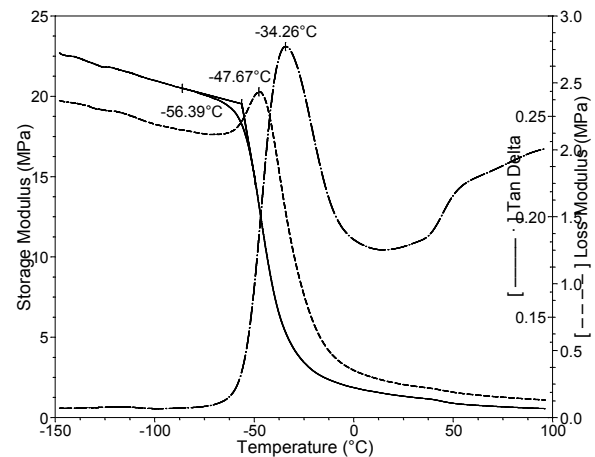


Fig. 1 Dynamic thermomechanical analysis of the sample EPR

The real part (E') represents a Storage Modulus, which characterizes elasticity of material. Higher absolute value of Storage Modulus adverts to better mechanical strength and conversely. Hence T_g can be analysed as an onset temperature of decrease of Storage Modulus. The imaginary part represents a damping part (Loss Modulus) which describes a viscosity of the material and T_g can be analysed as a peak maximum of the curve and the same principle (peak maximum) can be used to analyse T_g from the curve of Loss Factor (which characterized damping of the material). It is obvious that there are three different ways how to evaluate glass transition temperatures in terms of DTMA. This phenomenon was showed in the Fig. 1 where material EPR was analysed. The analysis gave three different values of T_g : -56 °C, -48 °C, -34 °C. Therefore is necessary to

adduce which curve was used for calculation always when is value of the T_g by DTMA evaluated. [15, 16]

III. RESULTS AND DISCUSSION

At first, the plot of the Storage Modulus versus temperature is shown in the Fig. 2 to determine the temperature limits of each material. The onset drop in the curve represents change in the mechanical strength of the material [15]. When the curve overstep T_g (from positive to negative temperatures), material starts to lose its elasticity.

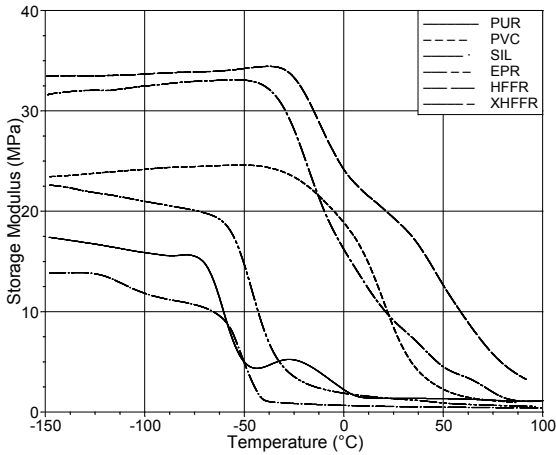


Fig. 2 DTMA - Storage Modulus vs. temperature of tested materials

According to the facts noted in the Introduction, Fig. 2 confirms presence of two main groups (thermoplastics and elastomers) of materials in the tested set of samples. Generally, thermoplastic materials have higher values of T_g than elastomers. [17] The highest value of T_g was recorded for material HFFR (-26 °C), while slightly lower T_g for PVC (-23 °C) and the lowest value (-36 °C) for crosslinked thermoplastic material XHFFR. The second group, elastomers, confirms general observation too and show lower values of T_g at all. Synthetic rubber EPR has glass transition temperature of -56 °C, a slightly lower T_g has silicone material (-55 °C) and the most temperature resistant material is supposed to be polyurethane (-69 °C).

Thanks to Storage Modulus it is possible to evaluate also the mechanical strength of material. Fig. 1 shows that thermoplastics have generally higher mechanical strength than elastomers (below T_g). Materials filled by flame retardant are the hardest at low temperatures. The lowest absolute value of the Storage Modulus has silicon that is associated with the low mechanical strength. It can be also seen how affects process of crosslinking material's mechanical properties from the presented results. Difference in T_g between HFFR and XHFFR is almost 10 °C. So, it is quite important to know the temperature range when the material can operate.

Loss Modulus measures the energy dissipated as a heat. The glass transition temperature can be usually taken from the peak in E'' (see Fig. 3). Characteristic behavior of various groups of materials is very similar as in the evaluation of Storage Modulus.

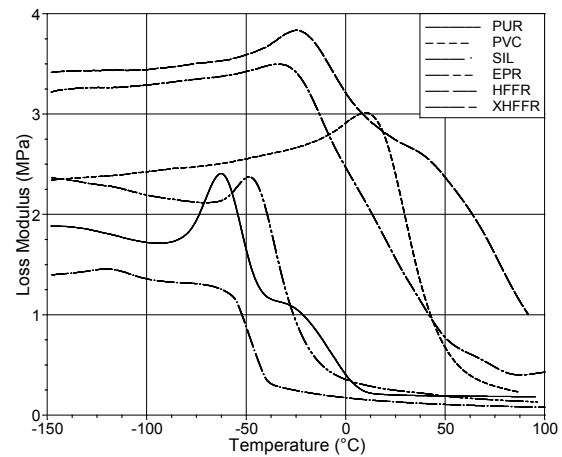


Fig. 3 DTMA - Loss Modulus vs. temperature of tested materials

As was mentioned above, Loss factor is a phase angle between Storage modulus and Loss modulus. In Fig. 4 Tan Delta curves of materials are plotted. Generally, if the value of $\tan \delta$ is low, material behaves more elastically than if the value is high. Materials are in the plastic state in this case.

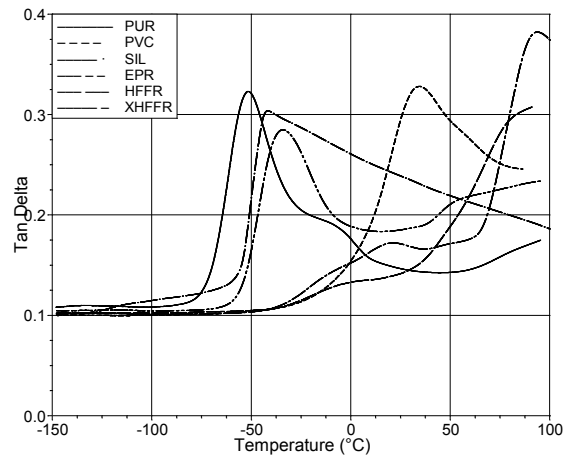


Fig. 4 Curves of Loss Factor dependence on material

Tan Delta curves of materials can be divided into two groups again, thermoplastics and elastomers. The Loss Factor of PVC approaches to its maximum at common service temperatures. It means that the damping increases and flexibility fade away. Material is starting to be soft in these temperatures, hence absorbs energy which was inserted to them. Other thermoplastic materials HFFR and XHFFR reach their maximum at higher temperatures (around 90 °C) contrary to elastomers which have peak maximum of Tan Delta in the temperature range from -52 °C (PUR) to -34 °C (EPR). The value of Tan Delta of elastomers is generally lower in comparison to thermoplastics at service temperatures. This fact results in lower damping which caused higher elasticity of elastomers. The energy inserted to them is returned back. [18]

DTMA is also sensitive to secondary transitions, Razmara observed this transition in material polyurethane

[19]. Secondary transitions can be seen mainly in the curves of materials PUR, SIL and EPR. The reason for these transitions can be related to the interactions and motions in the polymer structure. Secondary transitions may be associated with an accumulation of heat, vibration polymer structures, and especially also with the changes of electrical properties. Physical elements of secondary transitions across different materials are different. [20]

All of the T_g values calculated from curves of Storage Modulus, Loss Modulus and Loss Factor are summarized in the Table 2.

TABLE II. COMPARISON OF T_g VALUES

Material	T_g [°C]		
	Storage Modulus E' (on-set)	Loss Modulus E'' (peak)	Loss Factor $tg \delta$ (peak)
PUR	-69	-62	-52
PVC	-4	12	34
SIL	-55	-54	-42
EPR	-56	-48	-34
HFFR	-22	-25	91
XHFFR	-32	-31	93

IV. CONCLUSION

Six different insulation materials were analysed by dynamic thermo mechanical analysis (DTMA) in the temperature range from -150 to 100 °C to define the glass transition temperature. As mentioned above, T_g is an important phenomenon in the practical word because defines a temperature range of materials usage without losing their properties. Our analysis uncovered temperature limits of commonly use material.

Results showed that elastomers are materials which can be used without trouble in the negative temperatures. Hence, these materials are appropriate for cables which are installed in north areas and their mechanical properties will not be threatened. On the other hand, cables sheathed by thermoplastics have their operating limits at higher temperatures (starting from -32 °C for crosslinked compound XHFFR).

ACKNOWLEDGMENT

This research has been supported by the European Regional Development Fund and the Ministry of Education, Youth and Sports of the Czech Republic under the Regional Innovation Centre for Electrical Engineering (RICE), project No. CZ.1.05/2.1.00/03.0094 and by the Student Grant Agency of the West Bohemia University in Pilsen, grant No. SGS-2013-026 "Material and Technology Systems in Electrical Engineering".

REFERENCES

- [1] Aberdeen, Stan. Properties of a Thermoplastic. *EHow* [online]. 2012. Available from: http://www.ehow.co.uk/about_5545184_propertiesofthermoplastic.html. [cit. 10. 4. 2013]
- [2] Schaefer, Ronald J. *Harris' Shock and Vibration Handbook: Mechanical properties of rubber*. 6. Ed. 2009, pp. 33.1-33.18. ISBN 0071508198.
- [3] Thermoplastic Elastomers. Polymer Science Learning Centre, The University of Southern Mississippi [online]. 2005. Available from: <http://pslc.ws/macrog/tpe.htm>. [cit. 10. 4. 2013]
- [4] Material Safety Data Sheet [online]. Available from: <http://tpe-u.com/>. [cit. 10. 4. 2013]
- [5] Material Safety Data Sheet [online]. Available from: <http://www.matweb.com/search/GetMatlsByManufacturer.aspx?navletter=F&manID=611&manname=Fainplast+Compounds>. [cit. 12. 4. 2013]
- [6] Material Safety Data Sheet [online]. Available from: <http://www.biesterfeld-spezialchemie.com/>. [cit. 12. 4. 2013]
- [7] Material Safety Data Sheet [online]. Available from: <http://www.solvayplastics.com/>. [cit. 12. 4. 2013]
- [8] Material Safety Data Sheet [online]. Available from: <http://www.matweb.com/search/GetMatlsByManufacturer.aspx?navletter=F&manID=611&manname=Fainplast+Compounds>. [cit. 12. 4. 2013]
- [9] Material Safety Data Sheet [online]. Available from: <http://www.aecomponents.com/application-wire-and-cable/view/64/All-wire-and-cable-grades>. [cit. 12. 4. 2013]
- [10] Density of plastics. *Technical Articles* [online]. Available from: <http://www.steinwall.com/ART-density.html>. [cit. 15. 4. 2013]
- [11] Meyers, M. A., Chawla, K. K. *Mechanical Behavior of Materials* [online]. Cambridge University Press. (1999). ISBN 978-0-521-86675-0. [cit. 15. 4. 2013]
- [12] Tensile Property Testing of Plastics. *MatWeb: Material Property Data* [online]. 2012. Available from: <http://www.matweb.com/reference/tensilestrength.aspx.html>. [cit. 15. 4. 2013]
- [13] Vaniček, J. *Metody termické analýzy: Termická gravimetrie a termická mechanická analýza <in Czech>* [online]. pp. 3-4. Available from: <http://www.ft.vsl.cz/depart/ktm/files/20060106/prednaska6.pdf>. [cit. 16. 4. 2013]
- [14] Brandrup, J., Immergut, E.H., Grulke, E.A. *Polymer Handbook* (4 ed.). Wiley-Interscience. (1999). ISBN 0-471-47936-5.
- [15] *Handbook of Thermal Analysis and Calorimetry: Volume 3: Applications to Polymers and Plastics*. Stephen Z. D. Cheng. 1st edition, Amsterdam, The Netherlands: ELSEVIER SCIENCE B.V., 2002. ISBN 0-444-51286-1
- [16] Menard, K., P.: *Dynamic mechanical analysis: A practical introduction*, CRC Press, 1999. ISBN 0-8493-8688-8
- [17] Prokopová, I.: *Makromolekulární chemie <in Czech>*, VŠCHT v Praze, Praha 2007, ISBN 978-80-7080-662-3
- [18] Polanský, R.: *Influence of thermal treatment on the glass transition temperature of thermosetting epoxy laminate* [online], Polymer Testing 28 (2009) 428-436. [cit. 16. 4. 2013]
- [19] Razmara, M.: *DMA Investigation on Polyurethan* [online], FAME 2008 11-13. [cit. 18. 4. 2013]
- [20] Mentlík, V.: *Diagnostika elektrických zařízení <in Czech>*, BEN, Praha, 2008. ISBN 978-80-7300-232-9.

HFFR Power Cables Testing and Certification

Radek Nejd¹⁾, Vaclav Mentlík²⁾

Department of Technologies and Measurements, Faculty of Electrical Engineering

University of West Bohemia in Pilsen

Univerzitni 8, 306 14 Pilsen, Czech Republic

¹⁾ tel: +420 377 634 521, email: rnejdl@ket.zcu,

²⁾ tel: +420 377 634 513, email: mentlik@ket.zcu

Abstract— This paper deals with the HFFR (Halogen Free Flame Retardant) power cables. It describes methods and testing of the properties according to the valid standards which must be done to obtain the certification and CE conformity declaration from the Electrotechnical Testing Institute (ETI) which are necessary to offer these cables on the market.

Keywords— HFFR power cables, certification, CE conformity declaration, fire testing, mechanical and electrical properties

I. INTRODUCTION

Halogen-free flame retardant (HFFR) power cables for nominal voltage 0.6/1 kV are used in all locations where a high degree of protection against fire and fire damage has to be provided, including public buildings, telecommunication centers, industrial structures such as power plants, public transportation etc. Therefore these cables have to meet the requirements from the point of view of electrical and mechanical properties and fire safety. It includes increased fire retardation, low smoke emissions, low generation of corrosive and toxic gases and low fire propagation characteristics and maintaining circuit integrity during the fire.

Because the specific standards for any type of the cable do not exist, each manufacturer produces the cables according to its technical specifications which meet the requirements given by the corresponding standards. The technical specification contents code marking of cables, trade specifications, cable design, technical data, testing, production process quality, mounting, placing, transport and storing requirements and other appendix as a dimensions of the cable core and their properties. The cable design defines the materials and their properties which are used for cable core, insulation, cable filler, sheath and other possible parts of the cable design.

II. CERTIFICATION

Electrotechnical Testing Institute (ETI) is a leader in the Czech Republic in the area of certification practically all electrotechnical products because it has a long-term tradition, team of qualified specialists, excellent technical and personnel background. ETI is a member of practically all significant world and European certification systems therefore the manufacturers can export their products worldwide.

The internationally acknowledged certificates provides the basis for issuance of Statement of Conformance both in

accordance with the Act No. 22/97 Coll. and in accordance with EU Directives - CE marking and it is easy to obtain national certification marks of the system members. These certificates facilitate manufacturers their export to many countries of four continents and there is no need for further certification in the European Union countries and in many others.

ETI grants the ETI Certificate to products which have successfully passed the type tests according to the relevant technical standards. This certificate can be used as the basis for Statement of Conformance in accordance with the Act No. 22/97 Coll. and relevant orders-in-council. The validity of this certificate is usually restricted to three years.

If the manufacturer gains the ETI Certificate, it can mark the product with ESC mark. ESC mark represents the properties conformity of the product with the electrical safety standards. It is one of the oldest symbols for safe product in the world and this symbol is well-known and very required. The ESC mark is currently registered with the European Committee for Electrotechnical Standardization (CENELEC). The type tests of the product and the inspection at the manufacturer focused on the testing of the product safety during the production must be performed to gain this ESC mark

In accordance with the Act No. 22/97 Coll., the manufacturer or importer is bound to bring to Czech market only safe products. Before placing the particular product on the market, the manufacturer or importer is bound to issue a written Statement of Conformance based on the assessment of product properties together with safety requirements in accordance with the Act No. 22/97 and relevant technical rules - orders-in-council. The same is valid also in the area of the European Union where European Directives play the similar role as orders-in-council in the Czech Republic. The Declaration of Conformity must be issued for products and must be provided with the CE mark (Fig. 2).

The cable products have to meet the requirements set forth in the orders-in-council No. 17/2003 Coll. (technical requirements for low-voltage electrical equipment) and No. 163/2002 Coll. (technical requirements for building products).

Each product brought to the market of EU countries must be obligatory marked with the CE mark if such product is stipulated in some of EU Directives. The product meets all expectations as to the basic requirements

of all EU Directives which must be necessarily applied to such product. Deceptive placing of this mark on the product results in high penalties and disciplinary actions in the EU, which for example means: withdrawal of products from the market. Fig. 1 shows an example of the CE conformity declaration. [3]

CE CONFORMITY DECLARATION
Ref. No.: [redacted]

We, [redacted]

declare under our sole responsibility that
the product: [redacted]
type: [redacted]

to which this declaration relates is in conformity with the following standards:

EN 60332-1-1:04, EN 60332-1-2:04,
EN 50266-1:01, EN 50266-2-2:01,
EN 50267-1:98, EN 50267-2-3:98,
EN 61034-1:06, EN 61034-2:06,
IEC 60331-11:99, IEC 60331-21:99,
EN 60811-1-1:97, EN 60811-1-3:97, IEC60811-3-1:01,
EN 60228:05

Including amendments

following the provisions of Directive:
73/23/EEC - including amendment

Complementary information:
Certificate No.: [redacted]

issued by: Elektrotechnický zkušební ústav, Pod Lisem 129, 171 02 Praha 71, Czech Republic

The last two digits of the year in which the CE marking was affixed: 02

Place of issue: [redacted] Manufacturer representative: [redacted]

Date of issue: [redacted] Position: [redacted]

Issuer's address:
(if different from manufacturer)

Fig. 1. Example of the CE conformity declaration [1]

III. TESTING

A. Materials

For HFFR power cable certification, the cable 1-CXKE-V 3x1.5 was chosen because this cable is a representative specimen of the group of HFFR power cables and meets the requirements of the technical specification. Fig. 2 shows this type of cable.

As a power control cable it is used in circuits ensuring the function in case of fire, especially in circuits of fire systems (e.g. extinguishing systems, emergency lighting and ventilation power supply, circuits of emergency signals and operating of firewalls). The cables can be used everywhere that is insisted on personal protection, on the protection of equipment, constructions and materials (e.g. in public spaces, shopping malls, in hospitals, hotels or in tunnel constructions). It is possible to use them in dry or wet environment.

The construction meets the requirements of the standards of series HD 604 – special cable design for power stations. These cables are tested for service life of 40 years and the HELB accident. The cables can be placed in the environment with the explosion danger (zone 1, 2) providing compliances with the conditions of intrinsic safety according to IEC 60079-11. [2]

According to the technical specification of the manufacturer, the code marking of cables consists of a group of letters given in Table 1. Each manufacturer uses its own cable marking (it can be different) therefore the

code marking must be attached to a technical documentation or data sheets.



Fig. 2. Cable 1-CXKE-V 3x1.5

TABLE I. CABLE CODE MARKING [2]

Letter	Meaning	Marking	Meaning
1	nominal voltage	1-	0.6/1 kV
2	conductor material and design	C5	stranded round Cu conductor class 5
		S2	stranded round Cu conductor class 2
		S5	stranded round CuSn conductor class 5
		S2	stranded round CuSn conductor class 2
		C	Cu solid round conductor class 1
3	conductor insulation material	X	cross-linked PE type 2X11
		H	fire retarding PE type HJ2
4	cable design	F	cable fully screened by AIPET film + CuSn collector wire
		FO	cable fully screened by CuSn braiding with solid round wires diameter 0.2 mm + CuSn stranded collector wire
		K	cable
		KF	cable with a concentric wire including double wrapping by Cu film to achieve high screening effect
5	sheath material	E	fire retarding compound type HM4
6	fire resistance degree	R	fire retardant cable according to EN 60332-3-22
		V	fire retardant and fire resistant cable according to EN 60332-3-22 and IEC 60331-21
7	number of cores x conductor diameter	n_x x n_y	number of cores (or elements) x element conductor cross-section in mm ²

The conductor for this testing cable are wrapped by glass mica tape for created fire resistant barrier. The conductor insulation "X" is made of halogen-free PE type 2X11 according to DIN VDE 0207, part 22 (CSN 347660-5G, HD 604.5G S1). Above the stranded core assembly there is a wrapped tape of PET. Above the stranded elements there is the filler extruded from the same material as a sheath. The sheath is made of halogen-free, fire retardant PE type HM4 according to DIN VDE 0207, part 24 (CSN 347660-5G, HD 604.5G S1). [2]

B. Methods

The first parameter, which must be checked, is conductor construction. EN 60228:25 (conductors of insulated cables) describes materials, constructions, types, classes and values of resistance of the conductor. There is also mentioned electric resistance measurement at 20 °C. The sample must be placed in the laboratory conditions at least 12 hours before measurement.

Insulation resistance of the cable core is measured according to the CSN 347010-82 (electric cables – additional testing methods) at the ambient temperature with power supply of 500 V DC. The sample for volume resistivity must be at least 5 m long and placed in water.

The value of volume resistivity is counted according to relevant equation from the measured resistance. Dielectric strength of completed cable is measured in water at 20 °C with 2 kV AC power supply and the sample must be 10 m long.

Dimensions of insulations and sheath are important because thickness of these layers affects electrical properties. EN 60811-1-1 (insulating and sheathing materials of electric and optical cables - measurement of thickness and overall dimensions) deals with thickness measurements (Fig. 3) using a microscope.

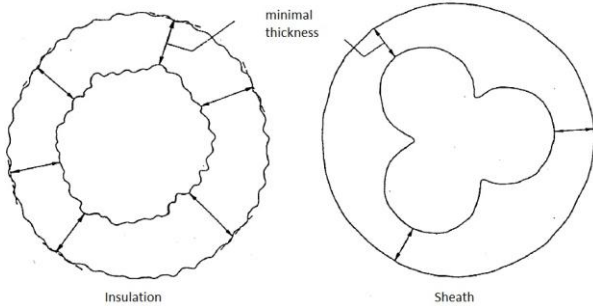


Fig. 3. Thickness measurements [6]

EN 60811-1-1 deals also with mechanical properties of the insulation and sheaths, specifically tensile strength and elongation at break. These parameters are the same important as electrical properties. Testing are performed after production and after heat-aging. Fig. 4 shows the shape and size of the testing sample.

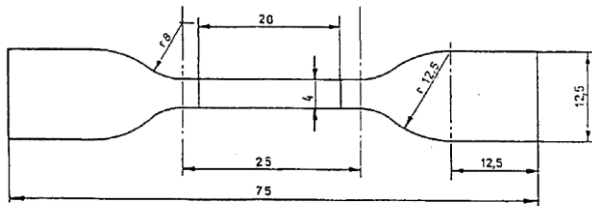


Fig. 4. The sample for mechanical testing [6]

As it is mentioned above, this testing cable has to meet requirements from the point of view of fire safety. Therefore these materials are tested according to EN 60332-3-22:2009 (tests on electric and optical fibre cables under fire conditions: test for vertical flame spread of vertically-mounted bunched wires or cables - Category A) and IEC 60331-21 (tests for electric cables under fire conditions - Circuit integrity - procedures and requirements - Cables of rated voltage up to and including 0.6/1.0 kV).

IV. RESULTS AND DISCUSSION

First of all measurements, the construction and dimensions tests were performed. Table 2 provides information and results about these tests. As you can see, the dimensions of all measured insulation thicknesses are higher than defined values. It is undesirable because the technology of production was not exactly observed and more plastic material (than was calculated) was used to manufacturing. The cross-section of the conductor is also

very important values because it affects the current load and heat stress during the operation.

TABLE II. CONSTRUCTIONS AND DIMENSIONS RESULTS

Test	Regulation	Measured		
Conductor construction		Core 1	Core 2	Core 3
EN 60228				
Type	solid round class 1	meets	meets	meets
Material	copper	meets	meets	meets
diameter	mm	1.370	1.373	1.373
cross-section	mm ²	1.48	1.48	1.48
Insulation thickness				
EN60811-1-1				
nominal	mm	0.7	-	-
medium	mm	-	0.87	0.77
minimal	mm	0.6	0.73	0.61
			0.61	0.69
Filler thickness				
EN60811-1-1				
nominal	mm	1.0	-	-
medium	mm	-	1.07	-
minimal	mm	0.75	1.02	-
Sheath thickness				
EN60811-1-1				
nominal	mm	1.2	-	-
medium	mm	-	1.24	-
minimal	mm	0.92	1.13	-
Total external dimensions				
EN60811-1-1, CSN 34 7010-82				
medium external diameter	mm	inf. 12.3	11.94	-
maximum diameter	mm	inf. 17.6	11.98	-

Table 3 gives information about electrical measurements. All requirements given by standards were fulfilled and insulation resistance and volume resistivity significantly exceed prescribed values.

TABLE III. ELECTRICAL TESTS

Test	Regulation	Measured		
Resistance of conductor		Core 1	Core 2	Core 3
EN60811-1-1, CSN 34 7010-82				
Resistance of conductor	Ω/km	11.700	11.712	11.745
at 20 °C				
max. 12.1				
Insulation resistance				
CSN 34 7010-82				
completed cable	GΩ/km	1 vs 2	2 vs 3	3 vs 1
at 20 °C, core vs core		104	7.99	57.8
min. 1.356				
Volume resistivity				
CSN 34 7010-82				
in water at 90 °C	Ω.cm	1.471x10 ²⁰	1.479x10 ²⁰	1.417x10 ²⁰
min. 10 ¹²				
Dielectric strength				
CSN 34 7010-82				
at completed cable	2kV	no breakdown	meets	
in water at 20 °C				

Table 4 is focused on fire safety testing. First measurement verifies circuit integrity during the fire when the system is supplied by minimal voltage of tested cable (in our case 1 kV). The other measurement investigates the height of carbonized of cable after burning (Fig. 5).

TABLE IV. TESTS IN FIRE CONDITIONS

Test	Regulation	Measured
Circuit integrity IEC 60331-21		
time of flame operation	hour 180 min.	meets
testing voltage	1000V no breakdown	
Vertical flame spread EN 60 332-3-22		
40 min./7l	max. 2.5 m	130 cm

Table 4 shows the measurements of mechanical properties for core insulation and cable sheath. The samples were tested after production and after heat-aging.

TABLE V. MECHANICAL TESTING

Test	Regulation	Measured		
		Core 1	Core 2	Core3
Mechanical pr. of insulation EN60811-1-1, EN 60811-1-2				
after production				
tensile strength	N/mm ² 12.5	13.43	13.17	12.84
elongation	% 200	395.4	386.3	371.2
after heat-aging (135 °C, 14 days)				
tensile strength	N/mm ² -	14.73	14.45	13.98
elongation	% -	393.2	390	385.9
change of				
tensile strength	% +25/-25	+9.69	+9.68	+8.83
elongation	% +25/-25	-0.57	+0.95	+3.97
Mechanical pr. of cable sheath EN60811-1-1, EN 60811-1-2				
after production				
tensile strength	N/mm ² 9	10.05		
elongation	% 125	172.2		
after heat-aging (110 °C, 14 days)				
tensile strength	N/mm ² -	10.44		
elongation	% -	159.7		
change of				
tensile strength	% -30/x	+3.94		
elongation	% +40/-40	-7.27		

V. CONCLUSION

If the manufacturer want to offer HFFR power (or other type) cables on the market, this product has to meet the electrical, mechanical and fire safety requirements which are necessary to obtain ETI certification and CE Fig. 5. A, B, C – vertical flame spread test; D – circuit integrity test

conformity declaration. Process of certification requests performance of many tests according to the corresponding standards which must be included in technical specification of each product.

Obtained results of measurements show that the chosen cable meets the requirements of construction, mechanical, electrical and safety fire properties and the group of HFFR power cables obtained ETI certification.

ACKNOWLEDGMENT

This work was supported by the Student Grant Agency of the West Bohemia University in Pilsen, grant No. SGS-2013-026 "Material and Technology Systems in Electrical Engineering".

REFERENCES

- [1] Internal material of the cable company
- [2] Technical specification of the cable company
- [3] Electrotechnal Testing Institute [online]. [cit. 2013-04-20]. Available at: <http://www.ezu.cz >.
- [4] EN 60228:25. Conductors of insulated cables.
- [5] CSN 347010-82. Electric cables – additional testing methods.
- [6] EN 60811-1-1:1995. Insulating and sheathing materials of electric and optical cables - Common test methods - Part 1-1: General application - Measurement of thickness and overall dimensions - Tests for determining the mechanical properties.
- [7] EN 60811-1-2:1995. Insulating and sheathing materials of electric cables - Common test methods - Part 1-2: General application - Thermal ageing methods.
- [8] EN 60332-3-10:2009. Tests on electric and optical fibre cables under fire conditions - Part 3-10: Test for vertical flame spread of vertically-mounted bunched wires or cables – Apparatus.
- [9] EN 60332-3-22:2009. Tests on electric and optical fibre cables under fire conditions - Part 3-22: Test for vertical flame spread of vertically-mounted bunched wires or cables - Category A
- [10] IEC 60331-11. Tests for electric cables under fire conditions - Circuit integrity - Part 11: Apparatus - Fire alone at a flame temperature of at least 750 °C.
- [11] IEC 60331-21. Tests for electric cables under fire conditions - Circuit integrity - Part 21: Procedures and requirements - Cables of rated voltage up to and including 0.6/1.0 kV.



Diagnostics of Alternative Insulating Liquids Using Monitoring the Thermal Characteristics

Jakub Souček¹⁾, Martin Širůček²⁾, Pavel Trnka³⁾

University of West Bohemia, Faculty of Electrical Engineering,
Univerzitní 8, 306 14 Pilsen, Czech Republic, www.fel.zcu.cz

¹⁾ tel: +420 377 634 516, email: mcsacek@ket.zcu.cz,

²⁾ tel: +420 377 634 516, email: msirucek@ket.zcu.cz,

³⁾ tel: +420 377 634 518, email: pavel@ket.zcu.cz

Abstract— The most commonly used insulating liquid is mineral oil. Mineral oil is characterized by high flammability and poor biodegradability. On the other hand, this oil has very good electrical properties. For reasons of environmental protection is an effort to replace the mineral oil by alternative insulating liquids. These alternative insulating liquids may be vegetable or synthetic oils. The different types of vegetable oils, which are modified in various ways, are investigated in this paper. The aim of this paper is to compare the electrical properties of these alternative insulating liquids with mineral oil. Dissipation factor was chosen as an important parameter, which was measured between periods of thermal aging at 110°C.

Keywords— *insulating liquid; vegetable oil; accelerated thermal aging*

I. INTRODUCTION

The most commonly used insulating liquid is mineral oil. The oil is used in transformers for cooling as well. For environmental reasons, these oils should be replaced by alternative fluids that would be friendly to the environment and organisms. As an alternative to mineral oils are used vegetable oils and synthetic organic esters. These fluids are perfectly biodegradable and have not a significant impact on the environment [1]. Biodegradability of insulating liquids is shown in Fig. 1.

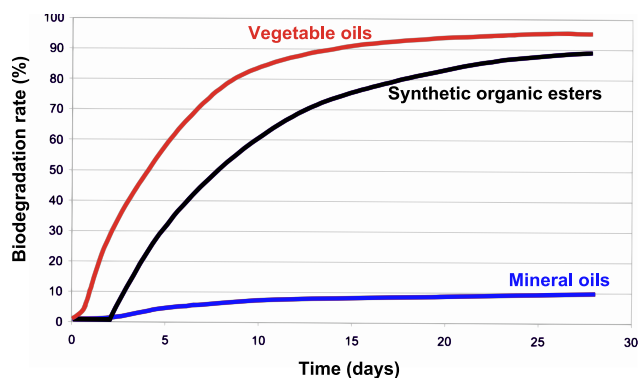


Fig. 1. Biodegradation rate of insulating liquids according to OECD 301 [1] - [3]

Biodegradability is a specific property of a substance or material that defines its complete biodegradability. This

occurs by means of biological reactions by microorganisms in nature. Rate of degradation depends on the composition of substances. Simpler and lighter substances are quickly degraded and do not pollute the environment [4]. The biodegradability of insulating liquids is defined as a decrease in the concentration of substances using microorganisms expressed as a percentage for 21 days. It is measured using the CEC L-33-A-93 "Biodegradability of Two-Stroke Cycle Outboard Engine Oils in Water" [5]. Test OECD 301 "Ready Biodegradability" is used for biodegradability of insulating oils in aerobic aqueous medium in 28 days [13].

In this paper will be described vegetable oils and synthetic organic esters. The advantage of these oils is their high flash-point. This property allows the use of these fluids in the most demanding conditions, such as transformers on high-rise buildings and oil rigs [3]. On the contrary, these oils have a lower freezing point, due to the higher viscosity [1], [2].

II. VEGETABLE OILS AND SYNTHETIC ORGANIC ESTERS

The development of biodegradable insulating liquids is most focused on vegetable oils and synthetic organic esters. Vegetable oils consist of a mixture of glycerol, esters, unsaturated and saturated fatty acids. These oils are extracted from oleaginous plants, which are then pressed. Properties of the oil are given by the kind of pressed plants. The Sunflower and canola are the most used in the Czech Republic. Composition of different types of vegetable oils are described in the TABLE I. The pressing can be done in two ways. The first is cold pressing. This pressing is done by a mechanical process. It is obtained a smaller amount of oil, but this oil has a very high quality. Contrary, the oil obtained by hot pressing has worse properties, but it is obtained greater amount of oil. Pressed oil is further refined to remove other undesirable substances [6], [7].

TABLE I. THE COMPOSITION OF OILS [4]

Name of acid	Canola oil	Palm oil	Soybean oil	Sunflower oil
palmitic	5%	45%	10%	4-9%
stearic	1,5%	5%	4%	1-7%
oleic	60%	38%	23%	14-40%
linoleic	20%	10%	51%	48-74%
linolenic	10%	-	8%	-
myristic	-	1%	-	-
lauric	-	-	-	-

These undesirable substances are free fatty acids, which cause a higher acidity of the oil. Deacidification is the most important refining process. This deacidification is performed by neutralization or esterification [6], [7].

A. Neutralization

Refining of free fatty acids of vegetable oils can be made by neutralization. Neutralization is a chemical reaction of carboxylic acids with the alkali. The products of this reaction are the salt and water. This reaction is described by equation (1). Formed precipitate must be filtered out and water must be dried [6], [8].



where R is a hydrocarbon radical.

B. Esterification

Another way to remove the free fatty acids is esterification. Esterification is the chemical reaction of an alcohol with a carboxylic acid. Products of this reaction are the esters and water. This reaction is described by equation (2). For the production of canola oil methyl ester is used transesterification. Transesterification is a process of mixing methanol with sodium hydroxide and then with pressed canola oil. A by-product of this reaction is glycerin [6], [7], [9].



where R is a hydrocarbon radical and R' is another hydrocarbon radical.

Synthetic organic esters are insulating liquids based on organic esters. These liquids are used as a substitute for mineral oil in transformers where is needed increased protection against the risk of fire or in places with increased requirements for environmental protection. Its composition is similar to vegetable oil. As a basis for

the production of synthetic organic esters are carboxylic acids. Organic esters are obtained using the esterification process which is described above by equation (2). These insulating liquids have better qualities than vegetable oil but their price is much higher [3], [7].

III. EXPERIMENT

The aim of this experiment was to find the best alternative insulating liquid based on natural esters. Commercially available sunflower and canola oil and insulating liquid based on synthetic organic esters MIDEL 7131 were selected as alternative insulating liquids. Mineral oil Shell Diala DX was selected as a comparison sample. These samples were aged in hot air ovens at a temperature of 110°C. Dissipation factor $\tan \delta$ was chosen as an important parameter, which was measured between periods of thermal aging at 110°C. The whole measuring of dissipation factor was performed according to standard EN 60247 [10].

Dissipation factor expresses the dielectric losses. These losses are proportional to the power that is converted into heat due to the alternating electric field. Resistivity is reduced and conductivity is increased by heating. Dissipation factor is defined by a dielectric conductivity for insulating liquids that do not contain impurities. For old electrical insulating liquids containing impurities is dissipation factor defined by dielectric conductivity, and polarization losses. The measuring principle is based on the location of the oil sample to the Schering Bridge. This Bridge is subsequently exported by a null indicator (NI), see Fig.2 [11].

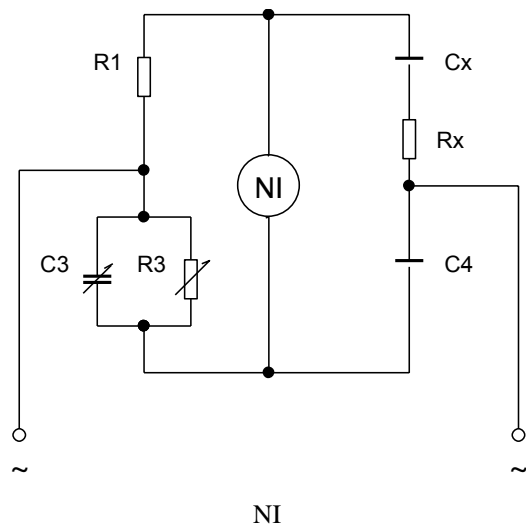


Fig. 2. Schering Bridge for measurement of dissipation factor [6]

The measuring instrument from the company Tettex AG Zurich was used to measure of the dissipation factor. The electrode system consists of a measuring system with a cylindrical capacitor with protective rollers.

It also contains a thermostat and thermometer. This electrode system is shown in Fig.3.



Fig. 3. Measuring system with a cylindrical capacitor

All insulating fluids were subjected to thermal aging at 110 °C for 1000 hours. The test voltage was set to 500 V at 50 Hz.

In the initial experiment, dissipation factor $\tan \delta$ was measured for MIDEI 7131, Shell Diala DX and sunflower and canola oil. The resulting chart is shown in Fig. 4.

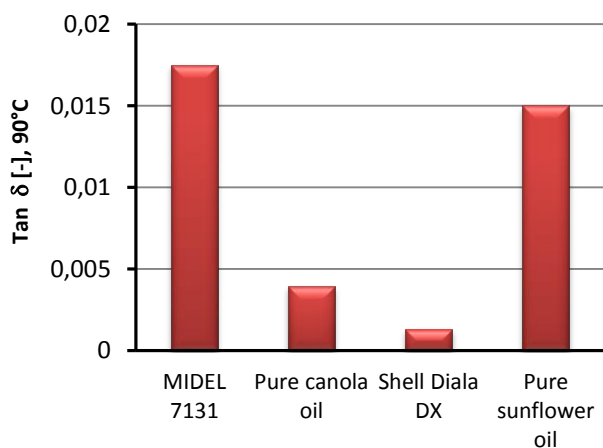


Fig. 4. Dissipation factor of selected oils in the initial experiment

From Fig. 4 it is seen that pure canola oil has a lower loss factor than sunflower oil. For this reason, we used a canola oil for the next experiment. This oil was subsequently transesterified and neutralized, see chapter II.

Neutralization was carried out using sodium hydroxide (NaOH). Each of ratio of NaOH was selected using study of [12] at a ratio of 0.6 mg and 0.18 mg NaOH·g⁻¹ of oil.

Crushed sodium hydroxide was mixed with oil using a magnetic stirrer. The turbid emulsion was formed, which was subsequently filtered through filter paper.

Ethanol 96% was used for the transesterification. First, sodium ethanolate was prepared by mixing 0.3 g of NaOH in 100 ml of ethanol. A mixture of sodium ethanolate and canola oil in a ratio of 2:1 was heated up by a magnetic stirrer with a controllable heater. Subsequently turbid emulsion was formed, which gradually passed to the clear liquid. Further, demineralized water is added to the mixture to form a separate liquid phases. Finally, the required transesterified oil was separated using a pipette.

All samples were subsequently exposed to thermal aging for 1000 hours. From the initial measurement is seen that transesterified canola oil had a high dissipation factor. For this reason, this oil was not further measured. Dissipation factor of insulating liquids was measured at 0, 250, 500 and 1000 hours of thermal aging. The resulting graph of the dissipation factor of these insulating liquids depending on the time of exposure to thermal aging is shown in Fig.5.

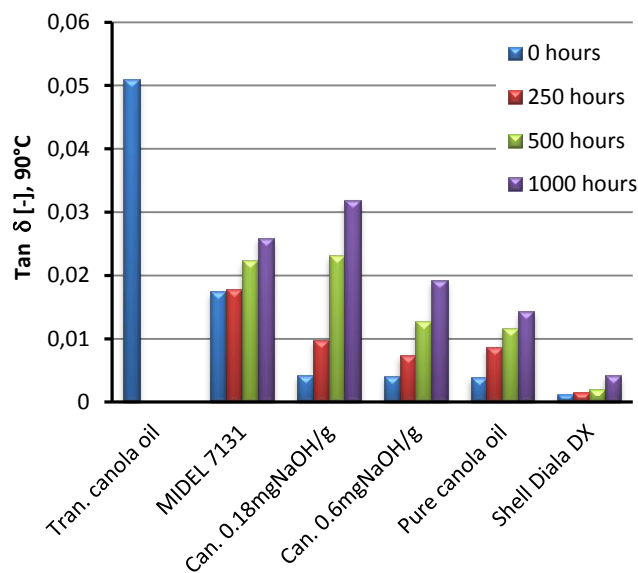


Fig. 5. Dissipation factor of modified insulating liquids for different times of aging

Finally, the dissipation factor was measured depending on the temperature. The system was heated from 20 °C to 100 °C in increments of 10 °C. Dissipation factor depending on the temperature of these oils was measured at 0 and 1000 hours of thermal aging. The resulting graphs are shown in Fig. 6 and Fig.7.

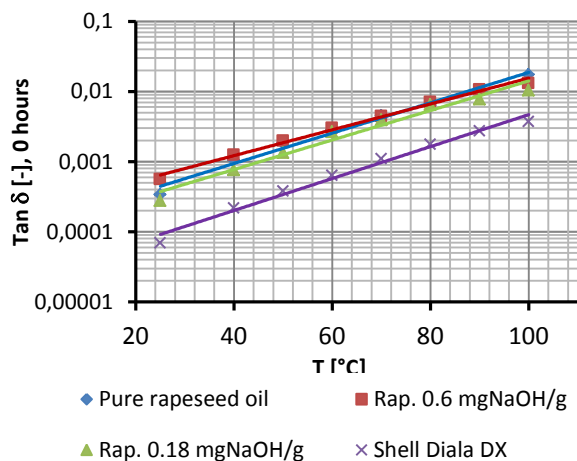


Fig. 6. Dependence of of the dissipation factor on temperature at 0 hours aging

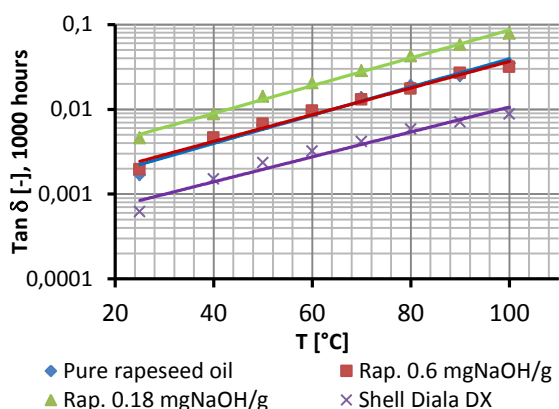


Fig. 7. Dependence of of the dissipation factor on temperature at 1000 hours aging

IV. CONCLUSION

As alternative insulating liquids were chosen canola and sunflower oil. From the initial experiment, it is seen that sunflower oil had a high dissipation factor, see Fig. 4. For this reason, the canola was used oil for further experiment. This oil was modified by neutralization and transesterification and then was aged for 1000 hours. Dissipation factor of insulating these liquids is shown in Fig. 5. This figure shows that transesterified canola oil had higher dissipation factor than was assumed before the start of the experiment. The higher dissipation factor could be caused by the rest of the alcohol in the resulting mixture. For this reason, the transesterified canola oil was not further measured. Fig. 5 shows that neutralized canola oil at 0 and 250 hours of aging had almost the same dissipation factor as pure canola oil. Change came at 500 and 1000 hours of aging, where neutralized canola oil with $0.18 \text{ mg NaOH} \cdot \text{g}^{-1}$ of oil had a significant increase in dissipation factor. Less amounts of sodium hydroxide probably cause insufficient neutralization and thereby increase the dissipation factor. At the end of the

experiment was carried out measuring of the dissipation factor depending on the temperature at 0 and 1000 hours aging, see Fig. 6 and Fig.7. These graphs show that neutralized canola oil and pure canola oil were an order of higher dissipation factor than mineral oil. This assumption is confirmed by a study [12]. The above measurements suggest that canola oil is applicable for example for distribution transformers and for applications at low operating temperatures.

ACKNOWLEDGMENT

This research has been supported by the European Regional Development Fund and the Ministry of Education, Youth and Sports of the Czech Republic under the Regional Innovation Centre for Electrical Engineering (RICE), project No. CZ.1.05/2.1.00/03.0094, project TA03020251 Environmentally friendly insulation liquids and supported by Student Grant Agency of the West Bohemia University in Pilsen, grant No. SGS-2012-026 "Material and Technology Systems in Electrical Engineering"

REFERENCES

- [1] Envirotemp FR3 Vegetable Oil-Based Insulating Dielectric Fluid. *California Environmental Protection Agency Department of Toxic Substances Control*. 2003, s. 1-8.
- [2] BIOTEMP Insulating Dielectric Fluid. *ETV Joint Verification Statement*. 2002, s. 1-8.
- [3] MIDEL 7135. In *MIDEL 7131 Complete Binder of Data Sheets* [online]. Manchester UK : M&I Materials, 2011 [cit. 2011-04-05]. Dostupné z WWW: <http://www.midel.com/uploads/midel/documents/technical/MIDEL_7131_Complete_Binder_of_Data_Sheets.pdf>.
- [4] Diaz E (editor). (2008). *Microbial Biodegradation: Genomics and Molecular Biology* (1st ed.). Caister Academic Press. ISBN 1-904455-17-4.
- [5] Directive No. 21-97. *Directive with the requirements for awarding the eco-friendly product*. Prague: Ministry of the Environment, 2008.
- [6] SOUČEK, Jakub. *Refinement and regeneration process for electro-insulating fluids, future horizons*. Plzeň, 2011. pp. 12-56, FEL ZČU, In Czech.
- [7] OKÉNKOVA, Eva. *Influence of refining on quality parameters and the stability of cold-pressed vegetable oils*. Zlín, 2006. 82 s. Univerzita Tomáše Bati ve Zlíně.
- [8] AHLUWALIA, V.K. *College Practical Chemistry*. Himayatnagar: Universities Press, 2005. ISBN 978-81-7371-506-8.
- [9] OTERA, Junzo. *Esterification: Methods, Reactions, and Applications*. 2nd. Weinheim: WILEY, 2009. ISBN 978-3-527-62763-9.
- [10] ČSN EN 60247. *Insulating liquids - Measurement of relative permittivity, dielectric dissipation factor (tan d) and d.c. resistivity*. Praha: UNMZ, 2005.
- [11] Mentlík,V., Polanský,R., Pihera,J., Prosr,P., Trnka,P.: *Diagnostika elektrických zařízení*, ISBN 978-80-7300-232-9, BEN technická literatura Praha 2008.
- [12] LI, Xiaohu. Properties of Transgenic Rapeseed Oil Based Dielectric Liquid. *SoutheastCon, 2006. Proceedings of the IEEE*. 2006, DOI: 10.1109/second.2006.1629328.
- [13] Test No. 301: Ready Biodegradability. *OECD Guidelines for the Testing of Chemicals, Section 3*. 1992, DOI: 10.1787/9789264070349-en

Partial discharge behaviour of special shaped protrusions in different gases and gas mixtures

Andreas F.X. Welsch¹⁾, Sabine Irlbacher²⁾

University of Applied Sciences Regensburg, Seybothstr. 2, 93053 Regensburg, Germany, www.hs-regensburg.de

¹⁾ tel: +49 941 943 1111, email: andreas.welsch@hs-regensburg.de

²⁾ sabine.irlbacher@stud.hs-regensburg.de

Abstract— The Partial Discharge (PD) measurement of medium voltage (MV) gas insulated switchgear becomes more important. A lot of manufacturers of MV gas insulated switchgears are going to introduce this measurement as a factory test for quality assurance to qualify the proper insulation of the switchgear. According to the discussion of prohibition of SF₆ other isolation gases were investigated in the last years for the usage in MV gas insulated switchgears. This paper presents characteristic external PD sources in MV GIS and the concerning PD behavior including the pattern in different isolation gases and gas mixtures. The presented failures are fundamental behavior. The presented failures show surprisingly characteristic shapes of the PD pattern, which allow the classification to types of PD sources. This method strongly supports the identification of the part concerned inside the MV GIS and should be very helpful in the daily work of a factory test bay. (Abstract)

I. INTRODUCTION

In the last years the research work in MV GIS is focused more and more on isolation gases or gas mixtures for the substitution of pure SF₆ gas. Meanwhile the breakdown behavior of such substitute gases is well known. To achieve the required voltage in some cases the gas pressure has to be strongly increased, up to several bars. However, a lot of manufacturers of MV GIS had introduced this measurement as a factory test for quality assurance to prove the proper insulation of the switchgear. So the requirement is now to know more about the PD behavior in such substitute gases. Many PD sources in GIS are defects, caused by external PD, which means shaped-edged metal parts rising up to the gas. These metal parts, generated during the production process, can be simulated by special shaped protrusions. The turning span e.g. can be reproduced by a sharp cone-shaped tip, fig. 1. The wedged-shaped tip (see fig. 2) simulates a cut off piece of wire and the sphere-shaped tip in fig. 3 a weld bead. As isolation gases an electronegative gas (oxygen), an electropositive gas (nitrogen) and air, as a mixture of these two gases (21% oxygen, 78% nitrogen) were investigated. To find out the changing in the PD behavior the mixture ratio was varied 10/90% to 90/10% nitrogen to oxygen. The characteristics describe PD, the inception and the extinction voltage over pressure and the PD pattern at 2 bar are chosen. In a tip-plate-arrangement with gas the PD occur first at the maximum of the negative half wave of the voltage. This was called the inception voltage 1. If the voltage is increased the PD inception takes place in the positive half wave (inception voltage 2), however mostly not in the maximum.

II. TEST SETUP AND ARRANGEMENT

The most usual method for detecting PD in MV GIS utilizes a coupling capacitor (Cc) that is placed in parallel with the test object, a standardized PD-test-circuit. The PD signals are measured via a measuring impedance (MI) connected between test object and ground. The extraction of the test voltage signal out of the measuring impedance is of great advantage, as it saves an additional voltage divider. The PD impulses are recorded and measured by means of a modern computer based PD measuring system according to IEC 60270 [1]. The measuring sensitivity was less than 0.1 pC, achieved by the Faraday-cage, in which the high voltage laboratory of the University of Applied Sciences Regensburg is encased. In fact, different protrusions lead to different PD characteristic and different PD

pattern. Therefore, three different special shaped tips that are connected on high voltage, are used. First of all, the cone-shaped tip, presented in fig. 1. This tip is a very sharp electrode. The electrode



Fig. 1 Cone-shaped tip

has a diameter of 2.4 mm and the height of the cone is about 10 mm. The smallest radius is smaller than 0.01 mm. Secondly, a wedged-shaped tip has been used. The wedged-shaped tip has the form of screw driver, see fig. 2. It has a height of approximately 11 mm and the diameter is also 2.4 mm. That the wedged-shaped tip has three different radiuses could be determined.

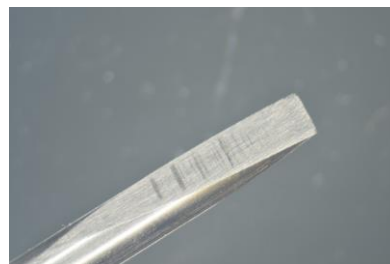


Fig. 2. Wedged-shaped tip

Last but not least, a sphere-shaped tip (fig. 3) has also been used. The spherical has a diameter of 3 mm and has been attached to an electrode that has a radius of 1.2 mm. Moreover, the spherical

has been attached to the electrode with a two-component adhesive. Apart from this, conductive varnish has also

been used in order to guarantee the electrical conductivity. For the test procedure each of the three electrodes has been connected to high voltage. Moreover, the counter electrode

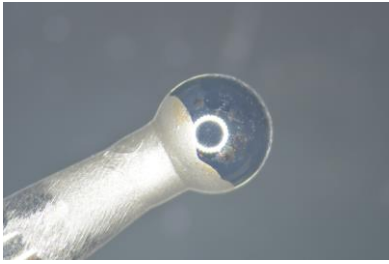


Fig. 3. Spherical-shaped tip

is a board that is connected to ground. By adjusting the space between tip and countertop and keeping it constant at 40 mm, a different characteristic of the PD inception voltages at which the pressure varies from 1 bar (ambient pressure) to 6 bar (5 bar gauge pressure) can be demonstrated. A space of 40 mm has been chosen for both the cone-shaped tip and the wedged shaped tip. For the spherical, however, a space between tip and countertop of 60 mm has been chosen, because corona discharges and lighting effects could be observed during the measurement at a space of 40 mm. Thereupon, high voltage has been increased until PD can be measured in the negative half wave first, as the tip is connected to HV. Afterwards, 1.1-times of the inception voltage has been adjusted and the PD pattern has been recorded over a time slot of twenty seconds. Moreover, the PD magnitude has been measured as well. After that, high voltage has been increased furthermore in order to measure the PD inception voltage in the positive half wave. After adjusting 1.1-times of the inception voltage, the PD pattern has been recorded once more and the PD magnitude has been measured. After measuring the PD inception voltage, the PD extinction voltage needs to be measured as well. Consequently, high voltage is decreased until no more PD can be measured in the positive half wave. This is the PD extinction voltage of the positive half wave. With continuing decreasing high voltage to the point where the partial discharges adjourn as well, the PD extinction voltage of the negative half wave can also be found. This test procedure has been executed for each of the three tips introduced above and has been repeated in three different isolation gases, i.e. air, oxygen and nitrogen. Apart from this, oxygen and nitrogen have been mixed where the volumetric content of nitrogen has been varied from 0 % to 100 %. A space of 40 mm has been adjusted for the cone-shaped tip. The pressure has been kept constant at 1 bar. Both the PD inception voltages and the PD extinction voltage of both half waves have been measured, as explained above.

III. TEST RESULTS

All of the three test setups have been tested in different isolation gases where pressure has been varied from 1 bar to 6 bar. For each of the three setups, the PD inception voltage in both the positive and the negative half wave have been plotted over pressure. The PD inception voltage 1 will be referred to as $V_{inc,1}$ (continuous line in all figures) and the PD inception voltage 2 will be denoted by $V_{inc,2}$ (dashed line in all figures). The PD extinction voltages are referred to as $V_{ext,1}$, respectively $V_{ext,2}$, as far as

the PD extinction voltage in the positive half wave is concerned.

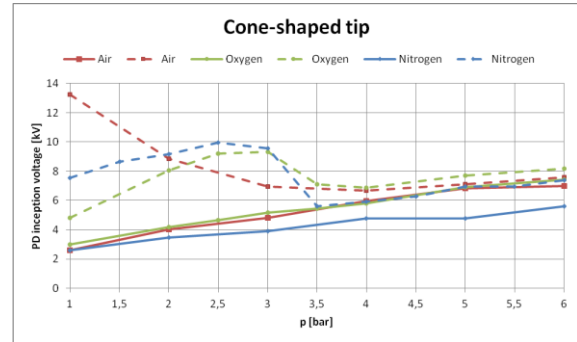


Fig. 4. Characteristic of PD inception voltages of a cone-shaped tip in different isolation gases under pressure

A. Cone-shaped tip in different isolation gases under pressure

The test results of the cone-shaped tip are presented in fig. 4. By varying the pressure, $V_{inc,1}$ in air (red continuous line) increases nearly linearly from about 2.6 kV to 7 kV. At ambient pressure $V_{inc,2}$ is approximately 13.3 kV. After that, $V_{inc,2}$ decreases up to a pressure of 4 bar. Then, PD occurs nearly simultaneously in both half waves. Starting with 3 kV, $V_{inc,1}$ rises linearly over pressure up to approximately 7.5 kV, just as in air. $V_{inc,2}$ at a pressure of 1 bar is about 4.8 kV. Then it rises slightly up to a pressure of 3 bar where it has its maximum of 9.3 kV. At 3.5 bar, PD occurs at around 7.1 kV, thereupon, starting from 4 bar, PD in both half waves begin simultaneously. In the negative half wave the PD inception voltage behaves in nitrogen just as in oxygen: it increases almost linearly. The inception voltage in the positive half wave starts at ambient pressure 7.5 kV. Thereupon it increases up to a pressure of 2.5 bar where a maximum of around 10 kV occurs. After that PD occur simultaneously in both half waves. Fig. 6 shows the PD pattern of the cone-shaped tip at a pressure of 2 bar at $V=1.1V_{inc,2}$ in oxygen, air and nitrogen. Both in the positive and in the negative half wave the PD pattern are very different in the different gases and can easily be distinguished.

B. Wedged-shaped tip in different isolation gases under pressure

While using the wedged-shaped tip, a quite another behavior of the PD inception voltages could be determined,

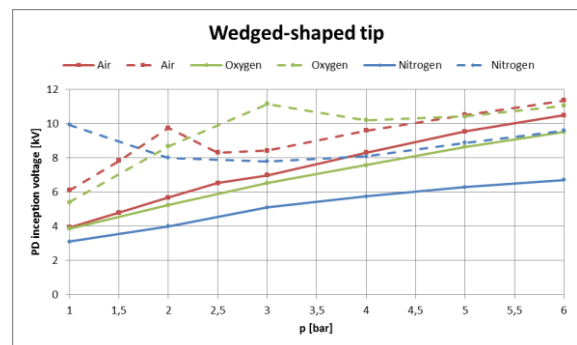


Fig. 5. Characteristic of PD inception voltages of a wedged-shaped tip in different isolation gases under pressure

as shown in fig. 5. In air $V_{inc,1}$ starts with approximately 3.9 kV at ambient pressure and increases linearly up to about 10.5 kV at 6 bar. In the positive half wave PD begin at 1 bar at around 6 kV. The inception voltage rises up to 9.7 kV at 2 bar, where it has its maximum. Thereupon, at 2.5 bar, the inception voltage decreases to 8.3 kV. From 3 bar to 6 bar, the inception voltage again increases nearly linearly. In oxygen, the PD inception voltage in the negative half wave ($V_{inc,1}$) starts with 3.8 kV at 1 bar. Thereupon it rises linearly up to a voltage of 9.5 kV at 6 bar. The PD inception voltage of the positive half wave ($V_{inc,2}$) is 5.4 kV at ambient pressure and rises linearly up to a pressure of 3 bar, where it has its maximum of 11.1 kV. At 4 bar the PD inception voltage only is 10.2 kV, thereupon the voltage rises from 10.4 kV (5 bar) to 11 kV (6 bar). In nitrogen, $V_{inc,1}$ nearly linearly from 3.1 kV (ambient pressure) to 6.7 kV (6 bar). $V_{inc,2}$, however, shows a totally different development in respect to air and oxygen.

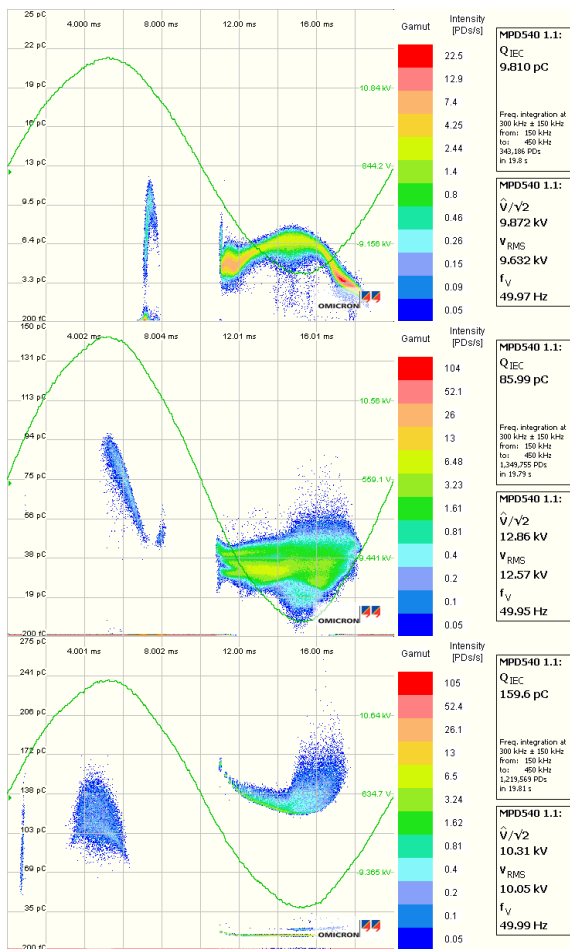


Fig. 6. PD pattern of the cone-shaped tip at a pressure of 2 bar at $V=1.1V_{inc,2}$ (upper: oxygen, middle: air, lower: nitrogen)

At ambient pressure, it is approximately 10 kV and decreases to 7.8 kV at 3 bar, where it has its minimum. Subsequently, the voltage rises from around 8 kV at 4 bar to 9.6 kV at 6 bar. Fig. 7 shows the PD pattern of the wedged-shaped tip at a pressure of 1 bar at $V=1.1V_{inc,1}$ in oxygen, air and nitrogen. The PD pattern in the negative

half wave in all three gases are very different and can easily be distinguished.

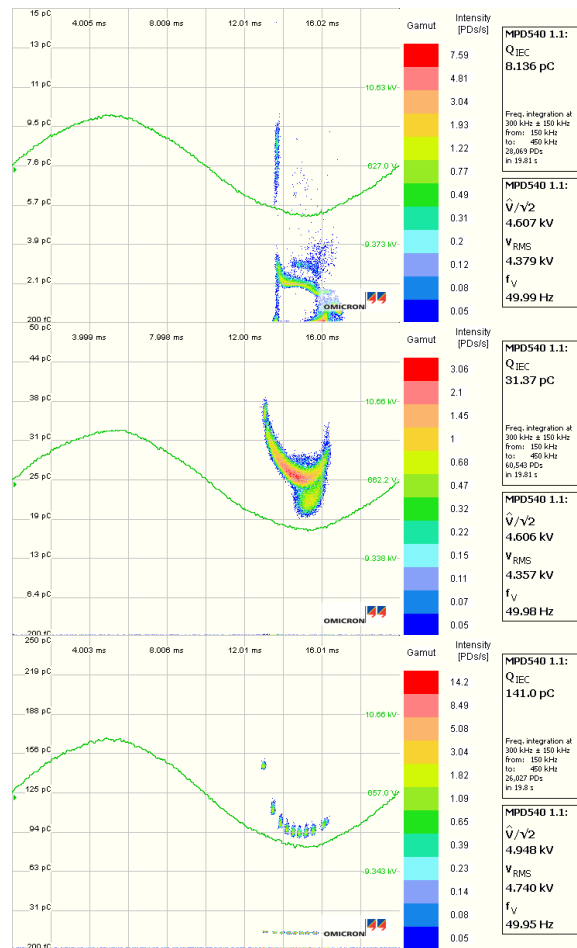


Fig. 7. PD pattern of the wedged-shaped tip at a pressure of 1 bar at $V=1.1V_{inc,1}$ (upper: oxygen, middle: air, lower: nitrogen)

C. Spherical in different isolation gases under pressure

Fig. 8 shows the test results of the spherical-shaped tip in different isolation gases under pressure. The characteristic of the PD inception voltages is totally different from the other two tips being used. Starting with about 12.5 kV in air at ambient pressure, $V_{inc,1}$ rises nearly linearly to approximately 49 kV. At 1 bar $V_{inc,2}$ is 15.8 kV and increases apparently parabolic to about 54 kV by rising the pressure. In contrast to the cone-shaped tip and the wedged-shaped tip, PD begin in oxygen both in the positive and the negative half wave at once. At ambient pressure $V_{inc,1}$ and $V_{inc,2}$ are 12.2 kV. After that, both rise linearly up to 43.7 kV at 5 bar gauge pressure. Only at a pressure of 1 bar in nitrogen $V_{inc,2}$ is 6 kV greater than $V_{inc,1}$. Thereupon, the PD inception voltages rise linearly to 51.1 kV at 6 bar.

D. Magnitude of PD

In table I. the magnitude of PD at $V > V_{inc,2}$ at a pressure of 2 bar is presented. For each of the three tips the highest PD values could be determined in nitrogen, and the lowest in oxygen. Apart from this, the cone-shaped tip has the lowest PD values in all isolation gases, and the spherical shaped tip has the highest ones.

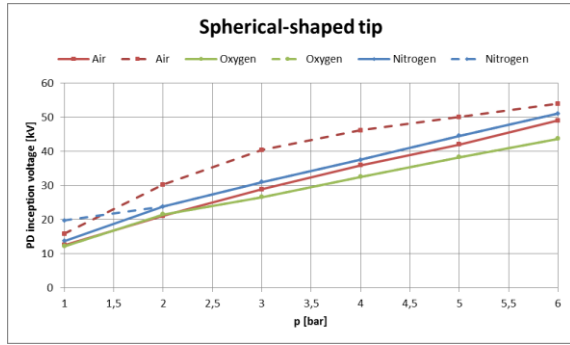


Fig. 8. Characteristic of PD inception voltages of a wedged-shaped tip in different isolation gases under pressure

In fact, the different tips have different radiuses. On account of that, the magnitude of PD can be explained due to the different smallest radiuses. As the smallest radius of the cone-shaped tip is less than 0.01 mm, the smallest PD occur. On the contrary, the highest PD occur while using the spherical-shaped tip, as it has the biggest radius of 1.5 mm. In fact, the different tips have different radiuses. On account of that, the magnitude of PD can be explained due to the different smallest radiuses. As the smallest radius of the cone-shaped tip is less than 0.01 mm, the smallest PD occur. On the contrary, the highest PD occur while using the spherical-shaped tip, as it has the biggest radius of 1.5 mm.

TABLE I. MAGNITUDE OF PARTIAL DISCHARGE

Tip	Isolation gas		
	Air	Oxygen	Nitrogen
Cone	85.99 pC	9.81 pC	156.6 pC
Wedge	98.32 pC	11.09 pC	280 pC
Sphere	1.702 nC	338.9 pC	18.35 nC

E. Cone-shaped tip in gas mixtures

In this test, the pressure has been kept at a constant value of 1 bar. As shown in fig. 8, the volumetric content of nitrogen has been varied from 0%, i.e. 100% oxygen, to 100%, i.e. 0% oxygen. Apart from this, the inception voltages in both half waves have been plotted over the volumetric content of nitrogen (fig. 9). At 0% of nitrogen, the $V_{inc,1}$ is 3 kV and $V_{inc,2}$ is 4.8 kV. These are the same values, just as in oxygen, see above. Up to 75% of nitrogen, the both PD inception voltages are more or less constant at around 2.8 kV, respectively at approximately 5 kV, as far as $V_{inc,2}$ is concerned. As the volumetric content in air is around 80%, both inception voltages rise to 3.2 kV, respectively 13.7 kV, just as in air at ambient pressure. From 85% to 100% nitrogen, $V_{inc,1}$ is again more or less constant at 2.6 kV. $V_{inc,2}$ first decreases to 10.7 kV at 85% nitrogen, and 10.6 kV at 90% nitrogen. At 100% nitrogen, $V_{inc,2}$ decreases furthermore to 9.8 kV. In fig. 10, the magnitude of PD, where $Q_{e,1}$ is the electric charge in the negative half wave and $Q_{e,2}$ in the negative half wave, is plotted over the volumetric content of nitrogen.

Starting in pure oxygen (0% nitrogen), $Q_{e,1}$ and $Q_{e,2}$ are only a few pC, more precisely, less than 10 pC. By raising

the volumetric content of nitrogen, $Q_{e,1}$ and $Q_{e,2}$ don't change very much.

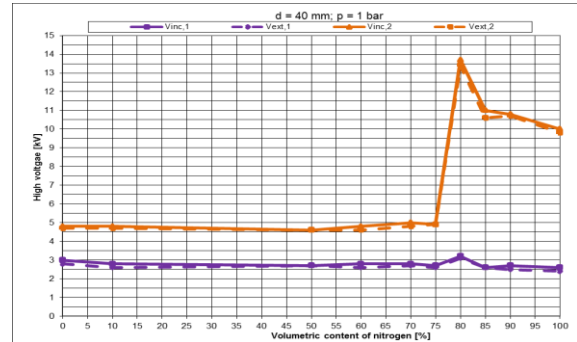


Fig. 9. Characteristic of PD inception and extinction voltages of a cone-shaped tip in gas mixture at ambient pressure [4]

At 75% nitrogen, both increase slightly to about 30 pC. At 80% nitrogen, $Q_{e,2}$ rises extremely fast to 1000 pC. $Q_{e,1}$ increases to 70 pC. Both magnitudes of PD have a maximum at 90% nitrogen: $Q_{e,1}$ is 100 pC and $Q_{e,2}$ is 1400 pC. Finally, in pure nitrogen, both $Q_{e,1}$ and $Q_{e,2}$ decreases. $Q_{e,1}$ now is 78 pC and $Q_{e,2}$ only is 800pC.

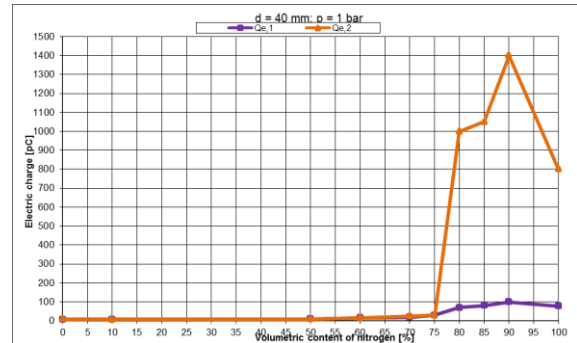


Fig. 10. Characteristic of magnitude of PD of a cone-shaped tip at ambient pressure in gas mixtures [4]

IV. CONCLUSION

The investigated protrusions in the chosen gases and gas mixtures lead to totally different PD behavior. The inception voltage 1 increases in all cases linearly with pressure. Contrary the developing of the inception voltage 2 with pressure depends on protrusion and gas type. In oxygen-nitrogen-mixtures the PD behavior till 75% nitrogen is comparable to pure oxygen. Remarkable is the very high PD magnitude for the sphere in nitrogen, which leads to high corona discharges and lighting effects. The PD patterns have such characteristic shapes, which allows the classification to types of PD sources and support the identification of the part concerned.

REFERENCES

- [1] IEC 60270, 2000, "Partial Discharge Measurements"
- [2] A. Welsch, R. Haller, "Partial Discharge Diagnostics for localisation of defect parts in gas insulated medium voltage switchgear"
- [3] A. Welsch, S. Ruhland, "PD Analysis of Gas Insulated Medium Voltage Switchgear during factory assembly and site commissioning", CIREN, Turin, 2005
- [4] A. Wehdanner, „Mustererkennung von Teilentladungen in Mischgasen“, Bachelor Thesis, 2012

Study of electrical properties of plant oils and their compounds derived from plants

Milan Spohner¹⁾, Karel Liedermann²⁾ Marian Klampar³⁾,

Department of Physics, Faculty of Electrical Engineering and Communication, Brno University of Technology
Technická 10, 616 00 Brno, Czech Republic, www.ufyz.feec.vutbr.cz

¹⁾ tel: +420 541 143 454, email: M.Spohner@phd.feec.vutbr.cz,

²⁾ tel: +420 541 143 453, email: liederm@feec.vutbr.cz

³⁾ tel: +420 541 143 395, email: marian.klampar@phd.feec.vutbr.cz,

Abstract — The subject of this work is the study of dielectric properties of perspective environmentally compatible electrical insulating fluids for electrical engineering and the relations with their chemical structure. Up to now, properties of the following natural oils have been experimentally studied: rapeseed and soybean oil. In addition, the same measurements were done on methylesters of fatty acids occurring in the natural oils, which include: methyl palmitate, methyl laurate, methyl stearate and methyl oleate. Measurements were performed on the HP 4284A and the ALPHA-A High Performance Frequency Analyzer by Novocontrol with high-resolution frequency range 0,01 Hz – 40 MHz in the temperature interval 263 K – 373 K.

Keywords— biodegradability, dielectric constant, dielectric loss, frequency dependence, temperature dependence, insulating liquids, methyl laurate, methyl oleate, methyl palmitate, methyl stearate, rapeseed oil, soybean oil, sunflower oil, vegetable oil.

I. INTRODUCTION

Mineral oils have been used in transformers in the USA since 1885. In the Czech Republic, the use of mineral oils dates back to 1897. Due to current environmental requirements for biodegradability (later disposal of oils, etc.) and for any accidents in transformers an alternative or a replacement in the available natural resources must be found. Mineral oils exhibit higher costs of environmental liquidation. Therefore, both in the USA and elsewhere, synthetic oils began to make inroads into use, primarily in transformers in large shopping centers, etc. for added safety. Synthetic oils were used as an alternative to mineral oil in the United States, Europe and even the Far East [1].

In the Czech Republic, the interest in using domestic natural products that can yield oil, has increased since 1985 and has also been accompanied by the decrease the use of mineral oils in electrical engineering. The causes were decreasing oil reserves, increasing mineral oils prices and greater interest in the environment in society. Another stimulus has come from some countries which wanted to reduce their dependence on imported oil products, which they do not get on their own territory (such as India and Brazil). After the political changes in the Czech Republic in 1989 and in connection with subsequent incorporation of the Czech Republic into the global economy the interest in the growing of oil plants for the production of oil for

food and technical applications has been increasing. Later farmers' subsidies within the framework of support from EU motivated for growing financially more lucrative plants, i.e. rapeseed and sunflower, which replaced the traditional crops, which included corn and potatoes. Other less oily plants are also grown in the Czech Republic: flax, poppy and soybean seeds [2].

Production of natural oils in the Czech Republic was in 20011/2012 as follows:

- rapeseed – 1 109 137 tons (oil yield = 37 wt%),
- soybeans – 13 149 tons of beans (oil yield = 14 – 20 wt%),
- sunflower seed – 56 943 tons (oil yield = 32 wt%),
- poppy seed – 12 814 ton (oil yield = 2 wt%),
- linseed – only 2 402 (oil yield = 38 – 44 wt%).

The analysis was undertaken by the Czech Statistical Office in the year 2012 [3].

II. PRESENT STATE AND BACKGROUND

A. Vegetable oil

Raw vegetable oils produced from oil seeds are usually darker and contain solid components such as protein and fiber and a liquid component which contains fats and oils. Presence of larger amounts of saturated triglycerides in the oil causes the solidification below ambient temperature. Oil component is usually liquid at a temperature around of 0 °C. If the oil contains more unsaturated fatty acids then it can remain liquid at temperatures down to -30 °C. The Fig. 1 shows the difference between the color and consistency of FAME at room temperature and at the temperature -20 °C. For long-term function, it is necessary to select the transformer oil with the highest stability parameters. Long-term thermal stability of natural oils is determined according to the degree of unsaturation. The stability of oil is reduced by its contact with copper surfaces in the transformer. Additional important parameter is the purity of oil that is not monitored in oils intended for food manufacturing industry. Scattered impurities increase the conductivity of oil. Antioxidants (inhibitors added in addition to improving and maintaining the required parameters) are used to increase the stability of oil. Oxidation inhibitors are additives of oil that reduces oil thickening and formation of acids and help to prevent

the sedimentation of sludge and carbon deposits caused by oxidation of oil and by oil aging [4].



Fig. 1. The difference in the appearance of Fatty Acid Methyl Ester at different temperatures (at left at 20 °C, at right at -20 °C)

B. Dielectric properties

Values of relative permittivity ϵ' (dielectric constant), loss number ϵ'' , dissipation factor $\tan \delta$, conductivity σ and volume resistivity ρ are important parameters for the characterization of electrically insulating fluids. All these quantities are strongly dependent on frequency and also on temperature.

In case dielectric losses are solely due to conductivity contribution the results acquired might be better analyzed using the conductivity formalism. Conductivity σ and dielectric loss ϵ'' are related to each other (1) as

$$\sigma = \omega \epsilon_0 \epsilon'' \tag{1}$$

where ω is angular frequency and ϵ_0 is permittivity of free space ($\epsilon_0 = 8.854 \times 10^{-12}$ F/m).

The activation energy was calculated under the assumption that the temperature dependence of conductivity satisfies Arrhenius equation (2):

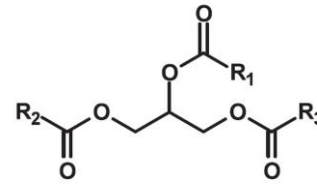
$$\sigma = \sigma_0 e^{\frac{W}{kT}} \tag{2}$$

III. SAMPLES

The range of oils selected for the measurement spanned both oils that are commercially available at the Czech oil market and pure chemical compounds contained in natural esters. Commercially available oils included synthetically produced vegetable oils (Ekolube CUT 80 P and Mogul Alfa Bio 68) and FAME (Fatty Acid Methyl Ester) that differed from each other in their chemical structure. FAME is formed from an acid molecule (here lauric acid, oleic acid, palmitic acid, stearic acid, linoleic acid, etc.) and methyl terminating group instead of triglycerides (Fig. 2) occurring in rapeseed oil. FAME is manufactured in the trans-esterification process, which uses sodium or potassium hydroxide as catalyst.

As for pure chemical compounds, four esters occurring in FAME were selected, namely methyl laureate (purity better than 98%), methyl oleate (purity better than 99%), methyl palmitate (purity better than 97%) and methyl stearate (purity better than 96%), supplied by Sigma Aldrich Co.

Triglyceride generic structure



R = fatty acid chain

Fig. 2. The difference in the appearance of Fatty Acid Methyl Ester at different temperatures

TABLE I. PERCENTAGE CONSTITUENTS OF FATTY ACIDS IN VEGETABLE OILS [5]

	sunflower oil	rape-seed oil	palm oil	soybean oil	olive oil
14:0	0	0.1	1.0	0.1	0
16:0	6.1	4.1	44.4	11	13.7
16:1	0	0.3	0.2	0.1	1.2
17:0	0	0.1	0.1	0	0
18:0	3.9	1.8	4.1	4	2.5
18:1	42.6	60.9	39.3	23.4	17.1
18:2	46.4	21.0	10.0	53.2	10
18:3	1	8.8	0.4	7.8	0.6
20:0	0	0.7	0.3	0.3	0.9
20:1	0	1.0	0	0	0

Comments on the table: 14:0 - myristic acid, 16:0 - palmitic a., 16:1 - palmitoleic a., 17:0 - heptadecyl a., 18:0 - stearic a., 18:1 - oleic a., 18:2 - linoleic a., 18:3 -k linolenic a., 20:0 - arachidic a., 20:1 - gondoic a..

IV. EXPERIMENTAL EQUIPMENT

Dielectric properties were measured using the precision LRC meter HP (Agilent) 4284A for the frequency range 20 Hz – 1 MHz and including dielectric liquid test fixture Agilent 16452A. The arrangement of dielectric measurement of oils is shown in Fig. 3. Communication between analyzers and a PC, i.e., analyzer control and data recording, made use of graphical language environment VEE Pro by Agilent. The test fixture Agilent 16452A was immersed into a water bath which was heated to required temperatures. The latest measurements of dielectric properties of soybean oil were implemented with the ALPHA-A High Performance Frequency Analyzer by Novocontrol with high-resolution frequency range 0,01 Hz – 1 MHz (Fig. 4).

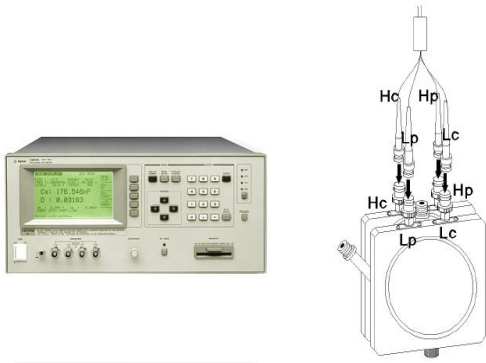


Fig. 3. Old measurement system (HP-Agilent) [6][7]



Fig. 4. New measurement system (Novocontrol)

The measurement results of two synthetically produced natural oils (Ekolube CTU 80 P, Mogul Alfa Bio 68) and two different sunflower oils showed approximately the same values of both sunflower oils. High dielectric constant and loss at 293 K was found in synthetic oil Ekolube CUT 80 P (Fig. 5 and Fig. 6).

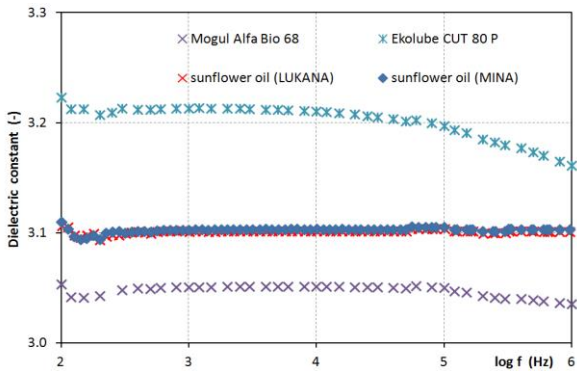


Fig. 5. Frequency dependence of dielectric constant of four different oil samples (Mogul Alfa Bio 68, Ekolube CUT 80P, sunflower oil LUKANA and sunflower oil MINA)

The measurement results of soybean oil (Fig. 9) have been obtained from the new measurement system (Fig. 4).

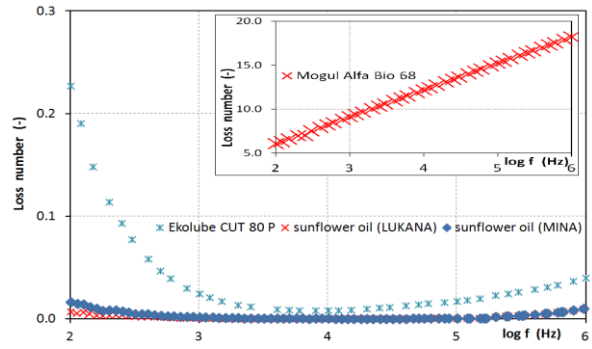


Fig. 6. Frequency dependence of loss number of four different oil samples (Mogul Alfa Bio 68, Ekolube CUT 80P, sunflower oil LUKANA and sunflower oil MINA) at 293 K.

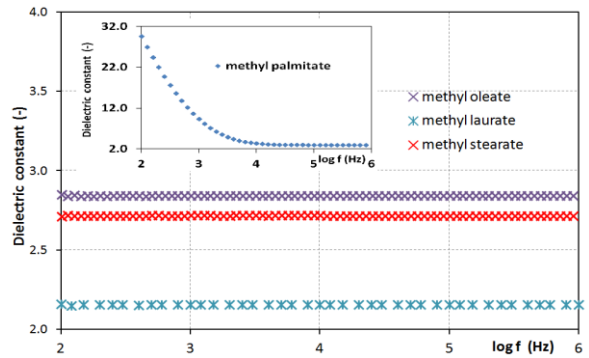


Fig. 7. Frequency dependence of dielectric constant of four samples of different methylesters at a temperature 323 K

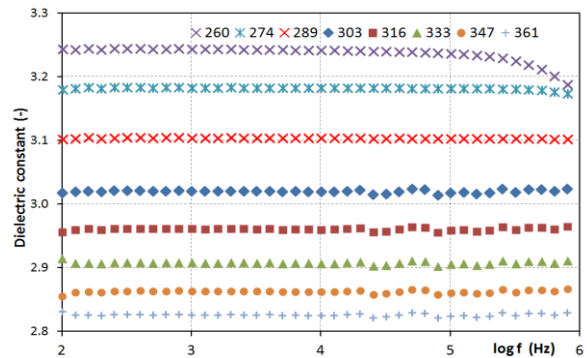


Fig. 8. Frequency dependence of dielectric constant of olive oil at a temperature from 260 to 361 K

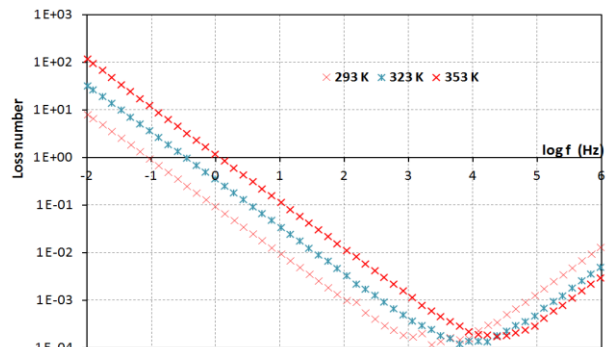


Fig. 9. Frequency dependence of loss number of soybean oil

V. RESULTS

Dielectric properties of methyl laureate and methyl oleate samples were analyzed in the temperature range 283 – 363 K. The methyl stearate sample, due to its melting point, was investigated in temperature range 323 – 363 K. In the observed temperature ranges, the values of relative permittivity decreased for methyl oleate from 3.11 to 2.49, for sample methyl laureate from 3.02 to 2.36 and for methyl stearate from 2.67 to 2.38. Dielectric losses exhibited a steady decrease without any hint for the presence of a relaxation peak (with exception of soybean oil). Dielectric losses can be described by the relation

$$\epsilon'' \sim \omega^{-n}, \tag{3}$$

which suggests that the predominant mechanism of dielectric losses is due to the conductivity component. Therefore, dielectric loss values were converted to conductivity values using Eq. (1); resulting conductivities are shown in Fig. 8. They were used for the calculation of activation energies for individual samples below.

Dielectric properties of olive oil sample were analyzed in the temperature range 260 – 361 K. The values of relative permittivity decreased for methyl oleate from 3.20 to 2.83 (Fig. 8).

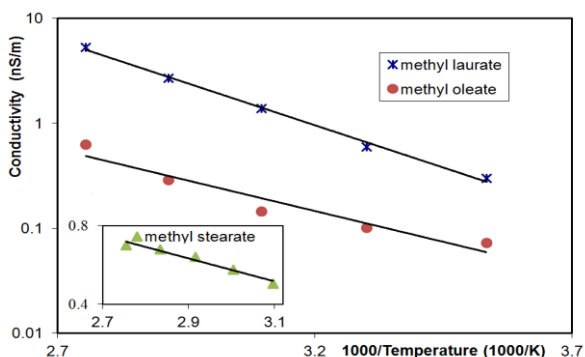


Fig. 10. Conductivity of methyl esters vs. inverse temperature

VI. CONCLUSION

Apparently, dielectric losses decrease with increasing frequency and increase with increasing temperature. This is in agreement with Eqs. (2) and (3).

Activation energies of three methyl esters contained in FAME differed from the activation energy of rapeseed oil. The temperature dependence of relative permittivity showed the following changes of values in temperature interval 283 – 363 K for samples: methyl laureate from 3.0 to 2.4, methyl oleate from 3.1 to 2.5. In an analogous manner, permittivity of methyl stearate slowly decreased in the temperature interval 323 – 363 K from 2.7 to 2.4. Frequency dependence of dielectric constant of these four

samples of different methyl esters at 323 K are shown in Fig. 7.

The value of activation energy E_A calculated according to equation (2) from the plot of conductivity vs. inverse temperature are 30.2 MJ/kmol for methyl laureate; 22.8 MJ/kmol for methyl oleate and is 8.7 MJ/kmol for methyl stearate. Methyl palmitate exhibited the highest value of the conductivity (64.1 MJ/kmol). Activation energies are summarized in Fig. 10.

TABLE II. ACTIVATION ENERGY OF SOYBEAN OIL AND FATTY ACIDS IN VEGETABLE OILS

type of oil	name of oil	activation energy E_A (MJ/kmol)
natural	soybean oil	27.2
acid methyl ester	methyl oleate	22.8
acid methyl ester	methyl laurate	30.2
acid methyl ester	methyl stearate	8.7
acid methyl ester	methyl palmitate	64.1

ACKNOWLEDGMENT

Research described in this paper was financially supported by the European Centre of Excellence CEITEC CZ.1.05/1.1.00/02.0068 and by European Regional Development Fund under projects Sensor, Information and Communication Systems CZ.1.05/2.1.00/03.0072 and Research and Utilization of Renewable Energy Sources CZ.1.05/2.1.00/01.0014.

REFERENCES

- [1] P. Thomas, S. Sridhar, K.R. Krishnaswamy, "Synthesis and evaluation of oleic acid esters as dielectric liquids", Conference Record of the 1996 IEEE International Symposium on Electrical Insulation, IEEE, 1996, pp.565-568.
- [2] P. Suchý, E. Straková, I. Herzig, "The quality of vegetable oils and their importance in terms of animal health and the possibility of influencing the nutritional value of foods of animal origin", Institute of Animal Science in Prag, v.v.i., 2008, pp. 1-59.
- [3] 2102-13, Definitive data on Farm Crops Harvest, contents [ČSU. [cit. 6. 5. 2013]. Available from: www.czso.cz/csu/2013edicniplan.nsf/p/2102-1320
- [4] T. V. Oomen, "Vegetable oils for liquid-filled transformers", IEEE, Electrical Insulation Magazine, vol. 1, Jan.-Feb. 2002, pp. 6-11.
- [5] L. M. De Espinosa, Michael M. A .R. Meier. "Plant oils: The perfect renewable resource for polymer science?!", European Polymer Journal. Vol. 47, No. 5, pp. 837-852.
- [6] Meander ~ Lab facilities. Agilent 4284A Precision LCR Meter. Agilent. [cit. 24. 4. 2012]. Available from: http://meander.uowm.gr/lab_facilities.html
- [7] 16452-90000.pdf. Agilent 16452A Liquid Test Fixture Operation and Service Manual. Agilent. 77 s. [cit. 10. 4. 2012]. Available from: <http://cp.literature.agilent.com/litweb/pdf/16452-90000.pdf>.

Dielectric measurement of a nanocomposite material at an early stage of accelerated ageing

Marian Klampar¹⁾, Karel Liedermann²⁾

Department of Physics, Faculty of Electrical Engineering and Communications, Brno University of Technology
Technická 10, Brno 61600, Czech Republic, www.feec.vutbr.cz

¹⁾ tel: +420 776 751 480, email: marian.klampar@phd.feec.vutbr.cz,

²⁾ tel: +420 541 143 453, email: liederm@feec.vutbr.cz

Abstract— This article discusses measurements of dielectric spectra in an electrical insulating nanocomposite at an early ageing stage. The focus of the research was on electrical and chemical changes, accompanied by the comparison of our results with those provided in the literature. The latest measuring technology available was used, most notably Novocontrol Alpha A analyzer, which was used to measure samples in the frequency range 0.1 Hz - 6 MHz, together with the Quatro Cryosystem, which allowed to measure samples under temperatures ranging from 120 K to 400 K. Partial changes of relaxation maxima during measurement were observed.

Keywords — dielectric measurement; epoxy resin; fast ageing; nanocomposite; Novocontrol

I. INTRODUCTION

Currently, one of the most popular tools for molecular dynamics analysis of material is dielectric relaxation spectroscopy (DRS) [1]. The result of advance in research and development of measurement instruments is that now it is possible to do measurements in the frequency range from 10^{-6} Hz to 10^{15} Hz and in the temperature range from some -260 °C to about 700 °C. DRS can indicate, which temperature, frequency or formulation ranges are suitable or not, for practical application. DRS can also elucidate microscopic mechanisms underlying the changes arising in the course of material aging [6].

Nanocomposites have been a subject of intense studies over the past twenty years [9], [10]. Currently there is a trend to a transition from the stage of purely scientific research to their practical application in engineering systems. Practical application requires stability in operation, absence of later defects and also an absence of substantial changes of their properties brought about by ageing under usual operating conditions (higher temperatures, humidity or presence of external electrical fields). One of the currently investigated application areas for nanocomposites is advanced electrical insulation [4].

The application of nanocomposites for electrical insulating purposes has both benefits and drawbacks. The benefits include an ability of the nanocomposite material to withstand electric discharges as nanoparticles in composites act as locally dispersed barriers against the propagating electrical trees [8]. For the illustration of the

electrical tree propagation prevention mechanism, see Fig 1 below:

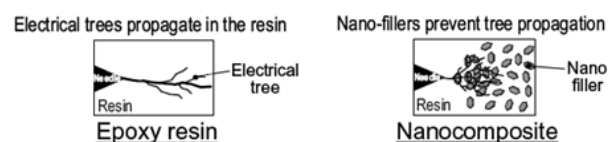


Fig. 1. Illustrative example of the increased resistance to electrical tree propagation in a nanocomposite, from [8]

One of the major drawbacks associated with the use of nanocomposites is a large area of internal oxide – epoxy interfaces. These large internal surface areas exhibit discontinuities between the properties of nanoparticles and surrounding matrix, and this may act as a source of defects. Moreover, the ageing, both thermal and electrical, may bring about an increase in defect concentration [7]. Therefore, it seems desirable to examine the properties of nanocomposites in the course of ageing prior to any large-scale deployment of them in electrical engineering industry. As ageing at standard operating conditions takes too much time, in this case it was replaced by an accelerated ageing at a higher temperature.

II. SAMPLES AND BACKGROUND

In this case, research was focused on epoxy resins with different additives, from non-conductive TiO_2 , Al_2O_3 , SiO_2 to conductive WO_3 . These samples were cast on a mold, specially made for this purpose. The mold had to be reheated as in the past, and can be seen in Fig. 2. Prior to manufacture, epoxy resin Araldite CY 228, hardener HY 918, flexibilizer DY 045 and curing accelerator DY 062 were mixed together in shares and steps set by the technical documentation of the supplier, Vantico Ltd. (formerly Ciba Specialty Chemicals, Oxford, UK) [2].

Two solutions were prepared: the first solution consisted of the mixtures of epoxy resin, flexibilizer, accelerator and nanofillers; the other solution consisted of pure hardener. One sample was left without the addition of nanofiller; in that case the first solution contained the mixtures of epoxy resin, flexibilizer and accelerator. Nanofillers TiO_2 , SiO_2 , Al_2O_3 and WO_3 were supplied by Sigma Aldrich. Their purities were different – TiO_2 was 99.7% pure, SiO_2 99.5%. Purity of Al_2O_3 and WO_3 were not mentioned in documentation. Even particle size was different among nanofillers – SiO_2 only 5 – 15 nm, TiO_2

approximately < 25 nm, Al₂O₃ roughly < 50 nm, WO₃ astonishing < 100 nm. The share of nanoparticles was set to 1.5 wt %.

Both solutions were stirred, placed in two different vessels in the same oven and heated to 60 °C, so that the uncured epoxy resin would be thinner and could be better put in the casting mold. Once a nanoparticle was added to the epoxy resin, nanoparticles aggregated to form flakes. The mixture was stirred mechanically and by ultrasound for 10 minutes. Ultrasound stirring was carried out using the Sonopuls ultrasonic homogenizer by Bandelin.

After breaking the aggregates, the mixture was again stirred by the laboratory mixer Model RW 16 by IKA and both solutions were mixed together, see Fig. 2.

Thorough mixing caused a development of a large number of air bubbles. Therefore, the oven was heated to 40 °C and subsequently evacuated to less than 0.05 bars so as to remove them.

The degassing was followed by the first phase of curing for some 1 to 2 hours at 80 – 90 °C. Once the epoxy resin with the hardener and nanoparticles added got rubbery, the casting mold was disassembled; samples were removed, loaded and hardened in the second phase so as to make them suitable for the measurement. The second phase of curing took about 12 – 14 hours at 140 °C.



Fig. 2. Stirring and homogenization

The preparation of thin samples was not as easy as it may seem from the above short description. Initially, samples were manufactured in a metallic original mold but the thickness of samples amounted to some 2 mm, i.e., samples were too thick for dielectric measurements, because the capacity of the sample reached the low limit of 10 pF. The next task was to create samples with thickness 350 – 550 μm. The only disadvantage was that their thickness was not even along whole area, which resulted in large deviations during measurement [3].



Fig. 3. Epoxy casting mold

However, this brought about problems with measurements, so this approach was abandoned.

Finally a method was developed that turned out to be successful: The mold was assembled of the metal sheets of thickness from 0.8 mm to 2 mm in vertical position, see Fig. 3.

This mold had separate inlet nozzle, through which it was filled with epoxy resin together with the hardener and nanofillers. Another hole was in the lower part, which allowed the material to spread evenly throughout the whole volume. Mold had a specific shape so that material could be poured in easily and air could vent out.



Fig. 4. Final nanocomposites samples at different stages of accelerated ageing

Dimensions of final nanocomposite samples were diameter 52 mm x thickness 0.8 mm, see Fig. 4. Various connections of samples to the measurement system were possible.

III. EXPERIMENTAL EQUIPMENT

Measurements were carried out on the Novocontrol Alpha A analyzer with Quatro cryosystem, manufactured by the same company.

The Novocontrol Alpha A analyzer exhibits a wide test frequency range 0.1 Hz – 1 MHz with basic accuracy 1 %. Duration of a single measurement did not exceed 15 ms and the measurement across the full frequency range 0.1 Hz – 1 MHz with 100 measuring points took about 35 minutes. The experimental setup is shown in Fig. 5.

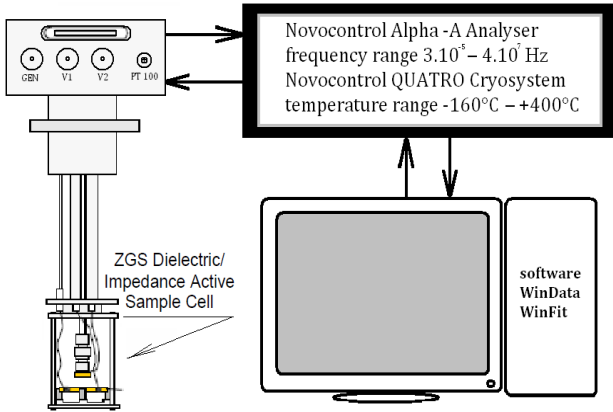


Fig. 5. Measurement setup

We used Quatro cryostatic system with temperature cycle, during which the sample was heated to 167 °C and slowly cooled in steps of 5 °C to 67 °C. In this point, temperature was quickly decreased to minimum value of 153 °C and was increased subsequently to 57 °C with 5 °C steps.

Using sample dimensions, the output from the Alpha A analyzer was provided in the form of material characteristics ϵ' and ϵ'' .

Temperature limits for the operation of the epoxy nanocomposite were determined by thermogravimetric analysis (TGA). Measurements of TG curves were carried out on the TA Q50 Thermogravimetric Analyzer.

IV. RESULTS AND DISCUSSION

Measurement results in terms of dielectric constant (permittivity) ϵ' and loss number ϵ'' (dielectric spectrum, $\epsilon'' = \epsilon' \cdot \tan\delta$) are shown in Figs. 6 to 8.

Fig. 5 shows imaginary permittivity (loss number) ϵ'' and loss factor $\tan \delta$ of the nanocomposite with Al_2O_3 , measured at 106.85 °C. The difference between the curves in Fig. 5 is the time of exposure of the samples to 200 °C, either 25 or 50 h.

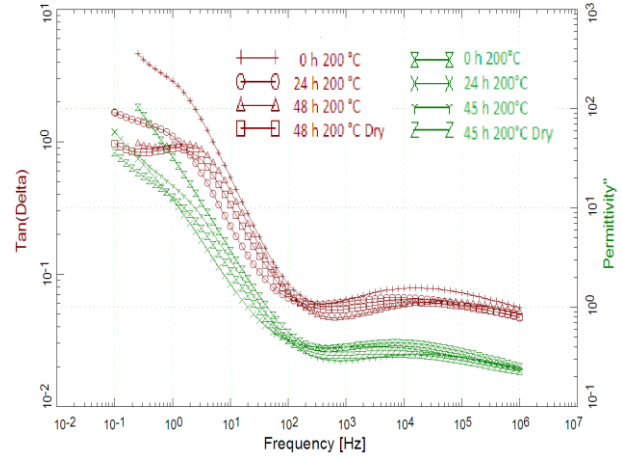


Fig. 6. Loss number ($\epsilon' \cdot \tan \delta$) [green], $\tan \delta$ [red]

Fig. 6 and 8 shows comparison between the pure epoxy and the nanocomposite with nanofillers Al_2O_3 and WO_3 (the behavior of epoxy nanocomposites with TiO_2 and SiO_2 was similar). We can see the behavior of samples before and after accelerated aging in times of 0 h, 25 h and 50 h at the frequency 0.1 Hz. As can be seen from the graphs in original state before aging, we can observe two maxima. After the exposure, the left-hand maximum gets smaller and finally disappears. This maximum is probably due to water or humidity presence in the sample, which evaporates after heating. Humidity is individual among samples, but after the aging process, all of them are equal and humidity level is so low that it can be barely measured. These graphs show a similar behavior as in paper [5], dealing with water evaporation.

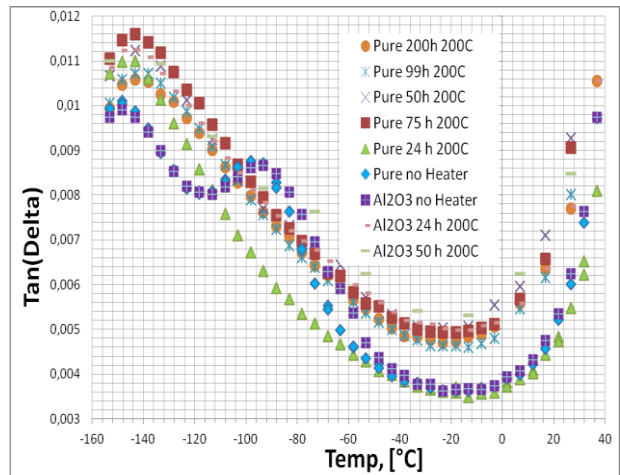


Fig. 7. $\tan \delta$ (-) Al_2O_3 red and Pure blue

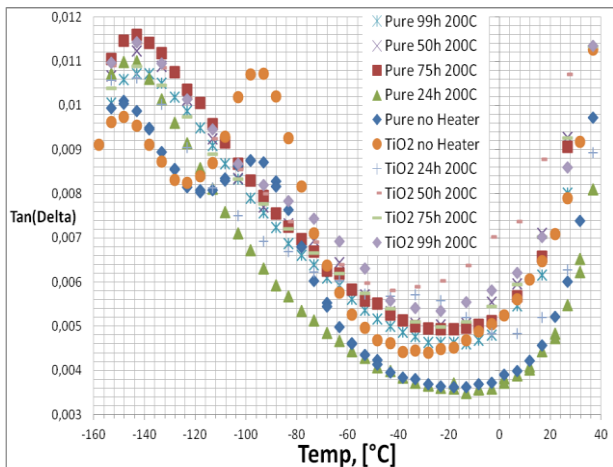


Fig. 8. $\tan \delta$ (-) TiO_2 red and Pure blue

TGA as seen on Fig. 9 shows pure epoxy damaged by rising temperature. Once temperature reaches 380 °C, the sample is burned and only dust remains.

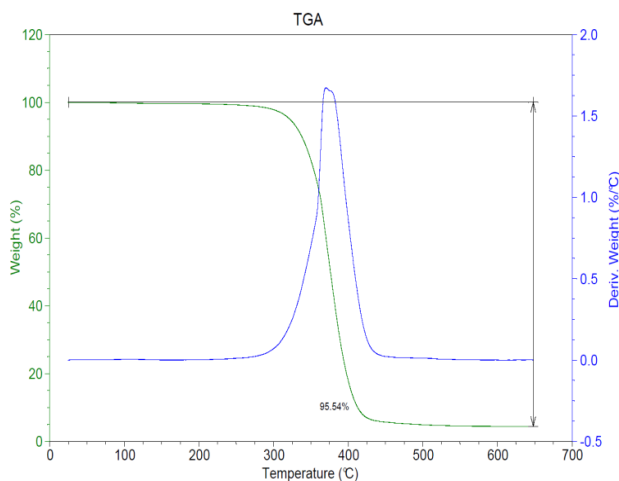


Fig. 9. TGA of pure epoxy

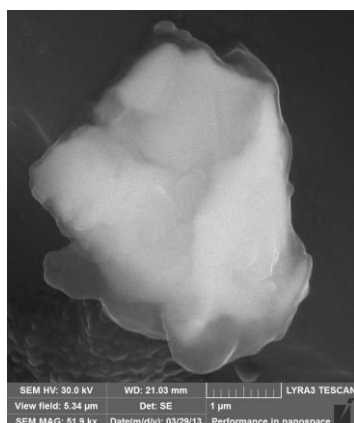


Fig. 10. Nanoparticles under electron microscope

V. CONCLUSION

To conclude, we confirmed the theory of sample ageing. Measurements provided notable knowledge of material quality and its ability to withstand temperature stress with temperatures reaching its limits. At about 300 °C, mechanical deterioration was observed on the surface of samples, which resembled human wrinkles. Another similarity with human skin was observed on certain samples, namely on surfaces from which bubbles developed, like blisters on burned skin. Despite it, dielectric attributes were not changed and material still shows very good electrical insulation properties (resistances still in excess of 100 MΩ). The above-mentioned effects were observed on pure epoxy, but were further confirmed on samples with nanocomposite as well.

ACKNOWLEDGMENT

The research described in the paper was financially supported by the European Centers of Excellence CEITEC CZ.1.05/1.1.00/ 02.0068, by project Sensor, Information and Communication Systems CZ.1.05/2.1.00/ 03.0072 and by the project OPVK-2-2.

REFERENCES

- [1] F. Kremer, A. Schönhal, Broadband Dielectric Spectroscopy, Springer, Heidelberg, Germany, 2002.
- [2] [http://www.lindberg-lund.com/files/Tekniske %20datablad/VAN-CY228-TD.pdf](http://www.lindberg-lund.com/files/Tekniske%20datablad/VAN-CY228-TD.pdf) [17.12. 2012]
- [3] M. Klampar, K. Liedermann, “Dielectric relaxation spectroscopy of epoxy resins with TiO_2 , Al_2O_3 , WO_3 and SiO_2 nanofillers under accelerated ageing conditions”, conference record of the 2012 IEEE international symposium on electrical insulation (ISEI) Pages: 637-640 Published: 2012 Porto Rico
- [4] F. Delor-Jestin, D. Drouin, P.-Y. Ceval, J. Lacoste, Thermal and photochemical ageing of epoxy resin – Influence of curing agents, (2005), France
- [5] S. Cerveny, S. Arrese-Igor, JS. Dolado, et al. “Effect of hydration on the dielectric properties of C-S-H gel”, J. Chem. Phys., Vol.: 134 Issue: 3 Article Number: 034509 DOI: 10.1063/1.3521481 Published: JAN 21 2011
- [6] Y. Cao, P. C. Irwin and K. Younsi, “The Future of Nanodielectrics in the Electrical Power Industry” IEEE Transactions on Dielectrics and Electrical Insulation Vol. 11, No. 5; October 2004, pp 797-807,
- [7] V. Mentlik, “Dielektrické prvky a systémy” BEN Praha, 2006, ISBN 80-7300-189-6
- [8] I. Takahiro, O. Tamon, S. Fumio, S. Toshio, H. Miyuki, O. Mitsukazu, T. Naoki, Y. Ohki and T. Tahala; Nanocomposite Insulating Materials for Environmental-conscious Heavy Electric Apparatuses, Proceedings of 2008 International Symposium on Electrical Insulating Materials, p. 674, September 7-11, 2008, Yokkaichi, Mie, Japan
- [9] By an international collective of scientists M. F. Fréchette, Editor; All Electrical Insulation Problems ?; 2010 International Conference on Solid Dielectrics, Potsdam, Germany, July 4-9, 2010, Nanodielectrics, A Panacea for Solving
- [10] T. Tanaka, G. C. Montanari and R. Mülhaupt; Polymer Nanocomposites as Dielectrics and Electrical Insulation-perspectives for Processing Technologies, Material Characterization and Future Applications; IEEE Transactions on Dielectrics and Electrical Insulation Vol. 11, No. 5; October 2004 763

Effect of moisture on the insulation condition of twisted coils

Bohumil Kotlárík, Ružena Vaňková, Zuzana Filová
 VUKI a.s., Rybníčná 38, 831 07 Bratislava, Slovakia, www.vuki.sk
 tel: +421 2 4488 1012, email: kotlarik@vuki.sk,

Abstract: It was observed influence of magnet wire type and impregnation on the insulation resistance of the twisted coil and the effect of moisture on the insulation resistance.

Keywords— *impregnation, insulation resistance, effect of moisture; (key words)*

During quality tests of impregnation of stators is used method IEEE 841 see Sub-clause.15, ČSN EN 60034-1:2005. Test of endurance to 100% humidity at 40°C for 168 h. This test is made on impregnated stators windings. Insulation resistance is measured between phases and between phase and frame, before humidity test, after it and after one and two hours after humidity test. Insulation resistance have to be over $5 \times 10^6 \Omega$. Reality that insulation resistance before humidity test was nearly the same between phases and between phases and frame and after humidity test was insulation resistance between phases 10 times lower as insulation resistance between phase and frame carry us to find what has influence on insulation resistance between phases. Between phases is insulation of magnet wire and impregnation resin. Used is magnet wire MW 35 or IEC 60317-13 what is Cu wire insulated by polyesterimid varnish (from 6-12 slots and with overcoat from amidimide varnish – two slots. Phases are wound from such magnet wire and after it are impregnated with impregnating resin. On insulation resistance has influence:

1. Insulation resistance of enamels on magnet wire – quality of enamelling and its curing.
2. Technology of winding – possible damage of insulation at winding.
3. Quality of impregnating resin, its insulating properties, degree of curing and influence on magnet wire enamel.

From these points we wanted to check influence of magnet wire and impregnating resin on insulation resistance before and after humidity test.

At first we tested influence of humidity (or water) on properties of impregnation resins. We measured volume resistivity according to STN EN 60093 of our resin NAB/UV-1K and resin of our competitor at temperature 23°C, 180°C, at 23°C after 96 h in water and after 168 h in 100% humidity at 40°C.

Results are in Table 1

After it we observed absorption of moisture on samples 55x60x2 mm. These samples we balanced before and after dipping to water for 168 h at room temperature. Results are in Table 2

Table 1

Impregnating resin	Volume resistivity after STN EN 60093 [Ω.m]			
	Temperature at test			
	23°C	180°C	23°C	
			96 h / water	168 h/40°C/water
NAB/UV-1K	1,1.10 ¹⁴	1,1.10 ⁹	1.10 ¹³	
Competitor resin	1,2.10 ¹¹	8,8.10 ⁸	5.10 ⁹	

Table 2

Impregnating resin	Weight before test	Weight after test (g)	Difference in (g)	Difference in %
NAB/UV-1K	9,5601	9,618	0,0579	0,61%
Competitor resin	9,4578	9,536	0,0782	0,83%

We impregnated Fe plates and gave them to water for 168 h at room temperature. We monitored rust formation. Result is on Fig.1



From results of volume resistivity, moisture absorption and rust resistance is our resin better as competitive resin. Our resin has 3500 times higher volume resistivity after influence of water as competitive resin. Absorption of moisture is about 35% lower as has competitive resin. Rusting of Fe plates is lower as has competitive resin.

After measuring influence of moisture on properties of resin we started testing of insulation system magnet wire and resin on humidity properties. We supposed that on insulation resistance have big influence magnet wire (quality of enamelling and winding) so we tested more types of magnet wires. Their properties are in Table 3.

Table 3

Magnet wire	Amider Gr.1 Ø 1,25	SH Therm 210 Gr.1 Ø 1,25	Gr.2 Ø 0,71	Gr.1 Ø 0,8	Gr.1 Ø 0,315
Overall dimensions of wire (mm)	1,308	1,308	0,764	0,85	0,347
Increase in	0,058	0,058	0,064	0,05	0,032

dimensions (mm)					
Mandrel winding test:1xd	C	C	C	C	C
Breakdown voltage at room temperature (V)	4482	3297	5097	4659	2709
Heat shock 210°C 0,5 h	C	C	C	C	C
Abrasion resistance (N)	17,1	13,23	11,76	13,71	6,57

C- convenient

Gr.2 is magnet wire type MW 35 with higher increase in dimensions, Gr.1 is magnet wire type MW 35 but with lower increase in dimensions.

From two parallel magnet wires with diameter 0,315 we prepared twisted coils. We made 36 windings which we turned on equipment for preparing twisted coils (in table 4. we marked it G1). Part of them we impregnated in resin NAB/UV-1K, part of them in NAB/UV-1K with higher reactivity (in table marked it NAB/UV-1K*) and part with competitors resin. Sample of winded twisted coil is on Fig. 2



For comparison we wound twisted coils from wire STN EN 60317-13 Gr.2 with diameter 0,71. We wound 15 coils, because diameter was bigger. These samples are in table 4 designed G2.

Table 4

Sample No:	Type of insulation	Insulation resistance before humidity test (Ω)
1	G1	6,0.10 ¹⁰
1	G1	2,0.10 ¹⁰
1	G1	1,50.10 ¹⁰
Average 1	G1	3,17.10¹⁰
2	G1+NAB/UK-1K	1,90.10 ¹⁰
2	G1+NAB/UV-1K	9,00.10 ⁹
2	G1+NAB/UK-1K	1,50.10 ¹⁰
Average 2	G1+NAB/UV-1K	1,43.10¹⁰
3	G1+comp.impr.	1,30.10 ¹⁰
3	G1+comp.impr.	1,50.10 ¹⁰
3	G1+comp.impr.	1,80.10 ¹⁰
Average 3	G1+comp.impr.	1,53.10¹⁰
4	G2	2,50.10 ¹¹
4	G2	3,50.10 ¹⁰
4	G2	2,50.10 ¹⁰
Average 4	G2	1,03.10¹¹
5	G2+NAB/UV-1K	7,00.10 ¹⁰
5	G2+NAB/UV-1K	1,60.10 ¹⁰
5	G2+NAB/UV-1K	3,00.10 ¹⁰
Average 5	G2+NAB/UV-1K	3,87.10¹⁰
6	G1+NAB/UV-1K*	2,10.10 ¹⁰
6	G1+NAB/UV-1K*	1,20.10 ¹⁰
6	G1+NAB/UV-1K*	1,20.10 ¹⁰
Average 6	G1+NAB/UV-1K*	1,50.10¹⁰

Samples No. 1 and 4 are without impregnation. In these samples was insulation resistance little higher as in impregnated samples. This reality we explain that insulation resistance of air is dependent on humidity of air and insulation resistance of sample is dependent on resistance of enamel, humidity of air and distance of holes in wire enamel. When space between wires fills impregnating resin, dispersion of insulation resistance is lower, because humidity has lower influence on insulation resistance of resin as has on insulation resistance of air.

After measuring insulation properties we gave samples to tin with water. All samples were dipped to water, tins were inserted to oven with temperature 40°C. See fig 3 and 4.

Fig.3



Fig 4



After 168 of influence 40°C water on samples we took them from water dry them with filter- paper and measured their insulation resistance immediately after test and after one and two hours after test in water. Results are in Tab.5

Table 5

Sample	Insulation resistance before test (Ω)	Insulation resistance after 168 h influence of 40°C water (Ω)	Insulation resistance after 1 h in room after 168 h influence of 40°C water	Insulation resistance after 2 h in room after 168 h influence of 40°C water
G1	6,00.10 ¹⁰	3,00.10 ⁵	6,00.10 ¹⁰	3,00.10 ¹¹
G1	2,00.10 ¹⁰	2,00.10 ⁵	3,00.10 ¹⁰	1,00.10 ¹¹
G1	1,50.10 ¹⁰	3,00.10 ⁵	2,00.10 ¹⁰	1,00.10 ¹¹
Average G1	3,17.10¹⁰	2,67.10⁵	3,67.10¹⁰	1,67.10¹¹
G1+NAB/UV-1K	1,90.10 ¹⁰	5,00.10 ⁵	2,00.10 ¹⁰	2,00.10 ¹⁰
G1+NAB/UV-1K	9,00.10 ⁹	6,00.10 ⁵	2,00.10 ¹⁰	2,00.10 ¹⁰

G1+NAB/UV-1K	1,50.10 ¹⁰	3,00.10 ⁵	2,00.10 ¹⁰	2,00.10 ¹⁰
Average G1+NAB/UV-1K	1,43.10 ¹⁰	4,67.10 ⁵	2,00.10 ¹⁰	2,00.10 ¹⁰
G1+comp.res.	1,30.10 ¹⁰	2,00.10 ⁵	3,00.10 ⁹	3,00.10 ⁹
G1+comp.res.	1,50.10 ¹⁰	2,00.10 ⁵	3,00.10 ⁹	3,00.10 ⁹
G1+comp.res.	1,80.10 ¹⁰	4,00.10 ⁵	3,00.10 ⁹	3,00.10 ⁹
Average G1+comp.res.	1,53.10 ¹⁰	2,67.10 ⁵	3,00.10 ⁹	3,00.10 ⁹
G2	2,50.10 ¹¹	2,00.10 ⁵	1,00.10 ¹¹	3,00.10 ¹¹
G2	3,50.10 ¹⁰	2,50.10 ⁵	3,00.10 ¹⁰	2,00.10 ¹¹
G2	2,50.10 ¹⁰	5,00.10 ⁵	5,00.10 ¹⁰	4,00.10 ¹¹
Average G2	1,03E.10 ¹¹	3,17.10 ⁵	6,00.10 ¹⁰	3,00.10 ¹¹
G2+NAB/UV-1K	7,00.10 ¹⁰	3,00.10 ⁵	1,00.10 ¹¹	1,00.10 ¹¹
G2+NAB/UV-1K	1,60.10 ¹⁰	2,20.10 ⁵	1,00.10 ¹¹	1,50.10 ¹¹
G2+NAB/UV-1K	3,00.10 ¹⁰	3,00.10 ⁵	1,00.10 ¹¹	1,50.10 ¹¹
Average G2+NAB/UV-1K	3,87.10 ¹⁰	2,73.10 ⁵	1,00.10 ¹¹	1,33.10 ¹¹
G1+NAB/UV-1K*	2,10.10 ¹⁰	5,00.10 ⁵	7,00.10 ¹⁰	3,00.10 ¹⁰
G1+NAB/UV-1K*	1,20.10 ¹⁰	7,00.10 ⁵	3,00.10 ¹⁰	3,00.10 ¹⁰
G1+NAB/UV-1K*	1,20.10 ¹⁰	3,00.10 ⁵	3,00.10 ¹⁰	3,00.10 ¹⁰
Average G1+NAB/UV-1K*	1,50.10 ¹⁰	5,00.10 ⁵	4,33.10 ¹⁰	3,00.10 ¹⁰

As we can see from Table 5, better insulation resistance has sample from wire G2. From comparison of insulation resistance used impregnating resins the best seems resin NAB/UV-1K*, then NAB/UV-1K and then competitive resin. Difference in insulation resistance between resins is very low, bigger difference is between insulation resistance dependence on used wire.

From two parallel wires type STN EN 60317-13 Gr.1 diameter 0,8 (Amider) we wound twisted coils with 15 coils. Part of them we did not impregnate and part of them we impregnated with NAB/UV-1K* and part with competitive resin. We measured increase of amount of resin in winding and insulation resistance before and after test in 40°C water. Results are in table 6.

Table 6

Sam. No.	Used resin	Increase of amount of resin (g)	Insulation resistance before test (Ω)	Insulation resistance after 168 h in 40°C water (Ω)	Insulation resistance after 1 h in room after 168 h influence of 40°C water	Insulation resistance after 2 h in room after 168 h influence of 40°C water
1	no	0	7,00.10 ¹¹	3,50.10 ⁶	2,00.10 ¹¹	2,60.10 ¹²
2	no	0	4,00.10 ¹¹	6,00.10 ⁶	2,20.10 ¹¹	4,20.10 ¹¹
3	no	0	2,00.10 ¹²	4,00.10 ⁹	4,70.10 ¹¹	1,20.10 ¹²
A			1,03.10 ¹²	1,34.10 ⁹	2,97.10 ¹¹	1,41.10 ¹²
4	NAB/UV-1K*	0,8498	3,50.10 ¹¹	8,00.10 ⁷	4,40.10 ¹¹	3,40.10 ¹¹
5	NAB/UV-1K*	0,8979	5,00.10 ¹¹	5,00.10 ⁸	2,00.10 ¹¹	3,20.10 ¹¹
6	NAB/UV-1K*	0,7859	4,00.10 ¹¹	6,00.10 ⁷	2,60.10 ¹¹	2,90.10 ¹¹
A		0,844533	4,17.10 ¹¹	2,13.10 ⁸	3,00.10 ¹¹	3,17.10 ¹¹
7	comp.res.	1,0951	3,00.10 ¹¹	1,20.10 ⁵	1,45.10 ¹¹	1,60.10 ¹¹
8	comp.res.	1,0759	1,20.10 ¹¹	3,00.10 ⁹	1,20.10 ¹¹	1,40.10 ¹¹
9	comp.res.	1,0419	2,20.10 ¹¹	6,00.10 ⁶	1,10.10 ¹⁰	5,00.10 ¹⁰
A		1,070967	2,13.10 ¹¹	1,00.10 ⁶	9,20.10 ¹⁰	1,17.10 ¹¹

A- Average

Increase of amount of impregnating resin in winding is about 22% higher in competitive resin as in our resin. This will cause higher consumption of competitive resin. Magnet wire with diameter 0,8 (Amider) has higher insulation resistance as wire G1 and G2, even G2 magnet wire has higher increase in dimensions and has higher breakdown voltage at room temperature (V). After test in 40°C water in one sample without impregnation we measured 3,50x10⁶ Ω which is under limit of standard, but two others are over limit 5 MΩ. All samples impregnated with our resin were over limit. From competitive resin one was under limit, but two were over limit. After 2 h in room temperature, after 168 h test in 40°C water is insulation resistance similar as before test.

From magnet wire SH Therm 210 and Amider both of diameter 1,25mm Gr. 1 we prepared twisted coils from 10 coils of parallel magnet wires. In table 7 is insulation resistance before and after test in 40°C water.

Table 7

Magnet wire	Used impregnating resin	Insulation resistance before test (Ω)	Insulation resistance after 168 h in 40°C water (Ω)
SH Therm	no	8,00.10 ¹¹	1,00E+06
SH Therm	no	2,80.10 ¹¹	5,00E+05
SH Therm	no	3,70.10 ¹¹	8,00.10 ⁴
Average SH Therm	no	4,83.10 ¹¹	5,27.10 ⁵
SH Therm	NAB/UV-1K*	4,60.10 ¹¹	7,00.10 ⁷
SH Therm	NAB/UV-1K*	3,70.10 ¹¹	2,10.10 ⁷
SH Therm	NAB/UV-1K*	2,60.10 ¹¹	1,00.10 ⁸
Average r SH Therm	NAB/UV-1K*	3,63.10 ¹¹	6,37.10 ⁷
SH Therm	Comp.res.	2,80.10 ¹¹	1,80.10 ⁸
SH Therm	Comp.res.	1,95.10 ¹¹	1,20.10 ⁹
SH Therm	Comp.res.	2,80.10 ¹¹	1,50.10 ⁷
Average SH Therm	Comp.res.	2,52.10 ¹¹	4,65.10 ⁸
AMIDER Gr.1	no	3,90.10 ¹¹	4,00.10 ⁵
AMIDER Gr.1	no	3,90.10 ¹¹	6,00.10 ⁶
AMIDER Gr.1	no	5,50.10 ¹¹	1,00.10 ¹¹
Average AMIDER Gr.1	no	4,43.10 ¹¹	3,33.10 ¹⁰
AMIDER Gr.1	NAB/UV-1K*	2,42.10 ¹¹	6,00.10 ⁶
AMIDER Gr.1	NAB/UV-1K*	2,25.10 ¹¹	8,00.10 ⁷
AMIDER GR.1	NAB/UV-1K*	4,30.10 ¹¹	2,00.10 ⁸
Average AMIDER Gr.1	NAB/UV-1K*	2,99.10 ¹¹	9,53.10 ⁷
AMIDER Gr.1	Comp.res.	1,30.10 ¹¹	8,00.10 ⁶
AMIDER Gr.1	Comp.res.	9,00.10 ¹⁰	1,80.10 ⁷
AMIDER Gr.1	Comp.res.	9,80.10 ¹⁰	4,80.10 ⁷
Average AMIDER Gr.1	Comp.res.	1,06.10 ¹¹	2,47.10 ⁷

Twisted coils from SH Therm without impregnation had after test insulation resistance 1,00x10⁶ Ω, 5,00x10⁵ Ω and 8,00x10⁴ Ω. All three samples were under limit of standard. Twisted coils from Amider without impregnation had only one sample under limit, it was 4,00x10⁵ Ω. After impregnation samples from both magnet wires had insulation resistance after test in 40°C water over limit of standard 5,00x10⁶ Ω

CONCLUSION.

From results we can see that insulation resistance of system before and after test in 40°C water depends not only on used impregnating resin, but mostly on quality of used magnet wire. Impregnating resins mainly decrease dispersion of insulation resistance. In case that between magnet wires is not high humidity, insulation resistance rises to 10^{10} - 10^{12} Ω.

On the end we would like to thank to our colleague Dr. G. Bínová, for suggestive expert assistance.

ACKNOWLEDGMENT

This work was supported by the Slovak Research and Development Agency (APVV) under the Contract No APVV-0 181-11.

Influence of Firing Process on LTCC Characteristic

Alena Pietrikova¹⁾, Juraj Durisin¹⁾, Igor Vehec¹⁾

¹⁾ Department of Technologies in Electronics, Technical University of Kosice, Slovak Republic,
http://web.tuke.sk/fei-kte/

¹⁾ tel: +421 55 602 3194, email: alena.pietrikova@tuke.sk,

¹⁾ tel: +421 55 602 3199, email: juraj.durisin@tuke.sk,

¹⁾ tel: +421 55 602 3016, email: i. vehec@tuke.sk,

Abstract— The paper describes results of investigations concerning the mechanical behavior and material characterization of different DuPont tapes. Firing is critical to the development of composite material characteristics. PEO 602 firing furnace with controlled atmosphere was used for firing two types of Low Temperature Co-fired Ceramics (LTCC from DuPont 951 and DuPont 9K7) using various firing profiles. This paper deals with X – Ray diffraction used for identification of crystallographic components and phases based on various firing profiles. In order to achieve crystallization in the material, LTCC samples were heated at a rate of 13.5 °C (or 0.7°C/ min) held at temperature 850°C (or 890 °C) within 20 min and cooled at a rate of 20.4 °C/ min (or 1.62°C/min). Additional mechanical testing methods were used to evaluate the composite material.

Keywords— LTCC, 951 DuPont, 9K7 DuPont, four-point bend test, X-ray analyse

I. INTRODUCTION

LTCC (low-temperature co-fired ceramic) is a multilayer platform technology that is used to make components, modules or packages for e.g. wireless, automotive, military, biomedical and photonic markets. This technology offers unique benefits and cost effective solutions for applications where high electrical performance, miniaturization, stability and reliability are key issues. Benefits of LTCC technology is flat frequency response and low loss up to millimeter waves, high conductivity metals (Ag, Au), integrated functions, excellent radiation management, low thermal coefficient of resonant frequency, high packaging density, high layer count, fine-line patterning and precise line definition, 3D structures, good CTE matching between the LTCC dielectric and semiconductors low temperature brazing for hermetic sealing, fine-line capability including screen-printing and photoimaging technologies. Our work in laboratory has focused on the development high-frequency application of the LTCC substrate for low loss stable dielectric requires the development of band pass filters for UWB radars. Investigation of mechanical properties in correlation with structure under various firing profile play important role.

The ceramic materials used in the work are two commercially available green tapes: DuPont 951 and DuPont 9K7. The GreenTape™ 9K7 ceramic tape dielectric represents a major technological advancement

for use in high frequency applications. Effect of multiple firing on microstructure and mechanical properties were undertaken to understand the differences in performance. X-ray diffraction analyze and investigation of responses of LTCC when subjected to 4-point bend were presented based on experimental results of this study.

II. EXPERIMENTAL PROCEDURE

Firing is critical to the development of composite material characteristics. The dissolution of the ceramic particles (Al_2O_3) in the glassy phase has an important influence on the viscosity of the melt during the firing. Sintering occurs through the viscous flow mechanism in which liquefaction of glass has a dominant role. We propose various firing profile for our experiments because it should have important role in mechanical and dielectric properties of LTCC. Our investigation is aimed to determination of density and micro strain and by this manner contributes to analyse of shrinkage of LTCC as unwanted property of LTCC.

Before sintering, 5 green tapes of 951 ceramic were laminated, and then cut from laminated sheet, using a steel rule cutting die. The laminating process follows the firing processes for each LTCC sample. Four types of firing profiles were applied for DuPont 951 ceramic: F1 – recommended standard profile under data sheet, F2 – double repeated firing profile, F3 – triple standard profile, F4 – adjusted standard profile with increasing max. temperature from 850 – to 890°C. DuPont 9K7 as a new type of LTCC was fired under data sheet recommendation (see Fig. 1).

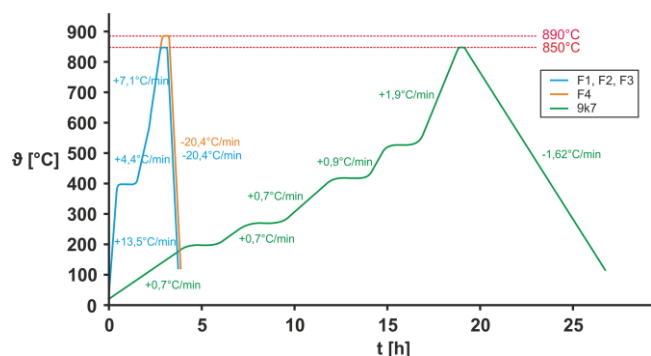


Fig. 1 Temperature profiles applied for 951 (F1, F2, F3 and F4) and 9K7 DuPont LTCC

III. MECHANICAL PROPERTIES OF LTCC

4-point dynamic bending (4PB) tests of LTCC were carried out in order to investigate the mechanical properties because it is suitable for evaluating strength of brittle materials. Response of any structure to mechanical loading depends on geometry, load and material. The 4PB test was performed at room temperature and pressure using a Testometric M250-2.5CT (Fig. 2).

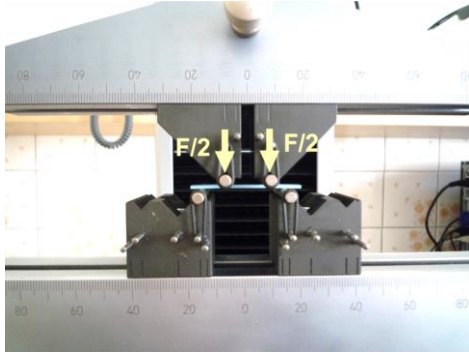


Fig. 2 Example of bend testing under a four-point bend

The loading rate for the test was set as 0.5mm/min. The dimension of LTCC samples was about 55mm x 6.35 mm x 1.1 mm. All bend test data are averaged from over 10 samples. The specimen was supported on two precision machined (stationary) anvils of a defined radius (4 mm). The force was applied at a defined distance either side of the center (4 point – see Fig. 2). The support beam is graduated lengthways in metric units for accurate positioning of the anvils, equally spaced to the center line. 4PB test arrangements are shown in the Fig. 2.

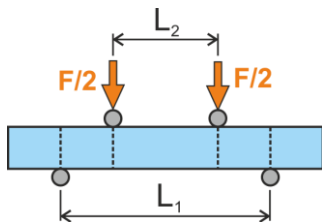


Fig. 3 Experimental setup of 4 point bend test

Bend strength is equivalent to the modulus of rupture in bending and can be calculated from the relation:

$$R_{mo} = \frac{3F_f(L1 - L2)}{2Bt^2} \quad (1)$$

R_{mo} – bend strength, B - the specimen width, t - thickness of the specimen, $L2$ – anvils distance, $L1$ – consoles distance

The results of the 4-point bend tests are in the Fig 4. Bend strength of 951 ceramic of F1 compared to the F2, F3 and F4 is approx. 20% lower. This indicates that repeated firing influence mechanical properties. The reason is that the densification of LTCC/Al₂O₃ system probably increases with increasing number of firing.

Microstructure of LTCC at F1 and F2 shows higher porosity. Porous was probably completely eliminated after sintered at firing process F3 (triple standard profile) and F4 (max. temp. 890°C – See Tab.1). The LTCC reached at F3 and F4 higher densification. Mechanical bend strength of 9K7 ceramic is bigger in compare with 951 ceramic.

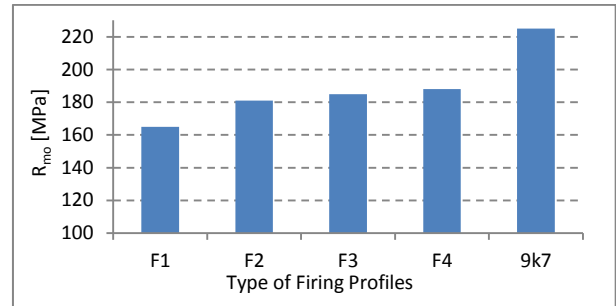


Fig. 4 Results of 4PB test of LTCC fired under various firing profiles (F1 – fundamental state, standard profile, F2 - repeated firing profile, F3 – triple standard profile, F4 – adjusted standard profile with increasing max. temperature from 850 – to 890°C)

TABLE I. CHANGE OF DENSITY AFTER VARIOUS FIRING PROCESS

Firing	Volume shrinkage %	Density (g/cm ³)
F1 – 951 ceramic	34,18	2,90
F2 – 951 ceramic	33,81	2,98
F3 – 951 ceramic	33,97	3,06
F4 – 951 ceramic	33,96	3,08
9K7 ceramic	24,33	2,94

Results of validation by the experimental indicate that this methodology developed in this study can be used to extract the details of stress and strain drop/impact loading. For brittle materials like LTCC having a linear stress-strain relation, the fracture stress can be determined from the fracture stress in bending. The fracture stress in bending is called the bend strength or flexure strength, which is equivalent to the modulus of rupture in bending. The bend strength is slightly different from the fracture stress obtained from the tensile test if failure takes place further away from yielding. However, brittle materials like LTCC possess higher strength in compression than in tension. The material failure under bending is therefore owing to the tensile stresses especially along the surface opposite to the load direction.

IV. X-RAY STRUCTURAL ANALYSIS

To evaluate the effect of multiple firing on microstructure of the 951 ceramic samples in more detail, specifically average crystallite size and average microstrain, we applied X-ray diffraction measurements. X-ray diffraction experiments were performed in Bragg-Brentano reflection regime by application of a laboratory diffractometer Philips X'Pert. As a source of primary X-ray radiation was used sealed Cu anode tube with K_{α} wavelength of 1.54187 Å (\approx 8 keV). Diffracted beam was consequently recorded by a position sensitive detector with angle range of $\Delta 2\theta \approx 2^{\circ}$, where 2θ is double of Bragg

angle θ . To obtain correct diffraction patterns, the flat ceramic samples were located in axis of the goniometer.

The following figure (Fig. 5) depicts a typical diffraction pattern of the 951 ceramic samples (here labeled by "F1" for fundamental state). As it is evident, dominant phase of the 951 ceramic is Al_2O_3 , therefore X-ray analysis of the ceramic is based on evaluation of Al_2O_3 microstructure.

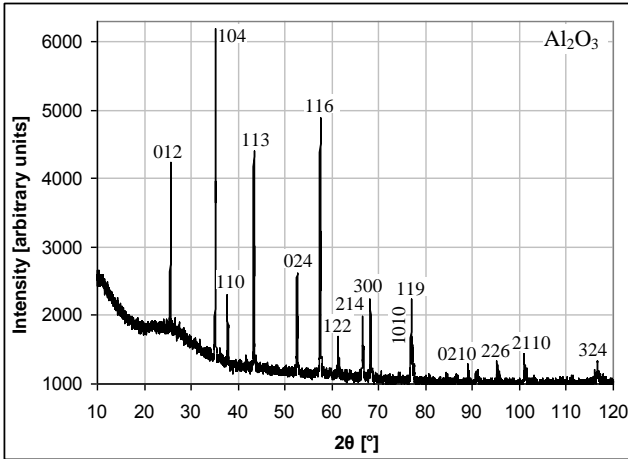


Fig. 5 Diffraction pattern of the 951 ceramic sample (Al_2O_3) labeled by standard firing profile "F1".

To analyze influence of the multiple firing on crystallite size and microstrain of the Al_2O_3 phase, we evaluated broadening of single peaks, i.e. full width at half maximum (FWHM - Full Width at Half Maximum) – Fig. 65; 951 ceramic dominant phases are Al_2O_3 and amorphous SiO_2 .

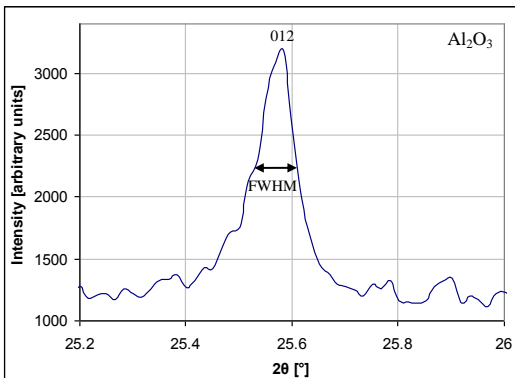


Fig. 6 FWHM of the 951 ceramic sample labeled by "F1" (012 peak of Al_2O_3 ; after $K_{\alpha 2}$ stripping).

We used the method proposed by Keijser et al. [1] enabling decomposition of the peak FWHM into Gaussian (instrumental) distribution and Cauchy distribution (sample: crystallite size, microstrain) broadening.

The results of the average crystallite size and the average microstrain ($\epsilon = \Delta d/d$, where d is interplanar distance) vs. multiple firing are depicted in Fig. 7. From Fig. 7 it is clear, that with multiple firing the average crystallite size slightly increases (from $\approx 173 \mu m$ to $\approx 184 \mu m$) and the average microstrain slightly decreases (from

$\approx 0.078 \%$ to $\approx 0.057 \%$). But in fact, value of the microstrain is overall negligible. If only microstructure modification of Al_2O_3 included, one can expect improved mechanical properties. However, considerable can be also effect of other minor compositions of the 951 ceramic (oxides of Na, Ca, Pb).

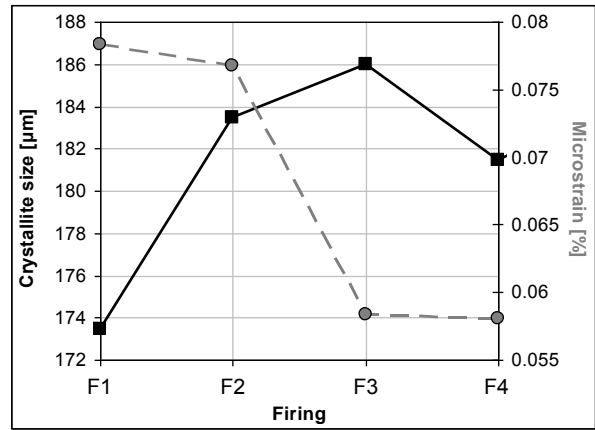


Fig. 7 Effect of multiple firing on the average crystallite size and the average microstrain of the 951 ceramic

In the case of the 9K7 ceramic dominant phase is Al_2O_3 only. Diffraction pattern of the ceramic is depicted in the Fig. 8.

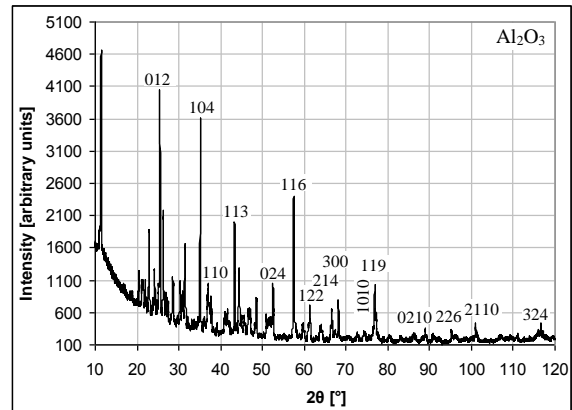


Fig. 8 Diffraction pattern of the 9K7 ceramic sample (dominant phase is Al_2O_3).

As it is clear from the figure, contrary to the 951 ceramic, the 9K7 ceramic contains significant amount of other types of oxides of B, Ca, La (i.e. the diffraction pattern shows presence of many peaks, which do not belong to the Al_2O_3 phase). Additionally, the oxides peaks significantly overlap. From the analysis of FWHMs of the major Al_2O_3 peaks results that the crystallite size is here roundly few tens of μm (from 30 to 50 μm). Microstrain of the 9K7 ceramic was negligible.

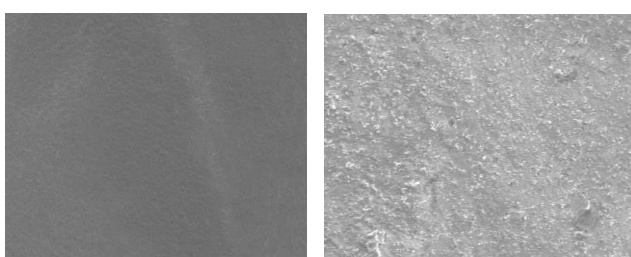
The data generated by EDX analysis consist of spectra showing peaks corresponding to the elements making up the true composition of the sample being analysed. Chemical element analyze realized by scanning electron microscope (EDX – Energy dispersive X-ray analyze) confirm that 951 green tapes contains Si and Pb

contrary to 9K7. Important is that glass content present inside the LTCC 951 the sample sintered at 850°C (Si – 11,38 weight % at F1) is higher than that of the 890°C - sample (Si - 5,67 weight % at F4 Tab II) .

TABLE II. CHEMICAL ELEMENT ANALYZE OF 9K7 AND 951 CERAMICS

9K7 ceramic		951 ceramic (F1)	
Element	Weight %	Element	Weight %
B	15.39	C	21.10
C	9.77	O	37.60
O	37.62	Na	1.10
Na	0.33	Al	20.53
Al	24.20	Si	11.38
Si	0.40	Cl	0.31
P	0.69	K	0.70
Ca	3.40	Ca	1.86
La	8.20	Cr	0.25
		Co	0.27
		Pb	4.90

Surface analysis realized by scanning electron microscope demonstrates on higher amount of in-homogeneities at 951 ceramic (F1 status) in compare with 9K7 ceramics (Fig. 9) .



a) 9K7 Ceramic

b) 951 Ceramic

Fig. 9 Surface analysis of a) 9K7 LTCC and b) 951 LTCC

V. CONCLUSION

While LTCC is known for its good electrical properties, mechanical strength of 951 DuPont LTCC has been identified as one of its main weaknesses (150 - 220 MPa) as compared to alumina (400–500 MPa). Various sintering profile of 951 DuPont LTCC, sintering of 9K7 DuPont LTCC, comparison mechanical and micro-structural analysis was realized.

Results of 4-point dynamic bending test for the assessment of LTCC were carried out to investigate the mechanical properties influenced by various firing profile. This test provides a method to quickly and effectively evaluate mechanical status and structure of material.

4-point dynamic bending test was established, analyzed and compared with X-ray diffraction analysis of LTCC. It is shown that 951 LTCC with higher density show higher mechanical properties. Repeated firing influences amount of glass content as well. Effect of multiple firing

influences average crystallite size and the average micro strain of the 951 ceramic. 951 DuPont LTCC dominant phases are Al_2O_3 and amorphous SiO_2 .

In the case of the 9K7 ceramic dominant phase is Al_2O_3 only. Long firing profile (25 hours) contributes to the effect that micro strain of the 9K7 ceramic was negligible. Long firing profile contributes to the smart surface without in-homogeneities.

As a final conclusion, it should be noted that the research of novel LTCC compositions (9K7 LTCC) have been very successful showing outstanding improvement of the materials properties.

ACKNOWLEDGMENT



This paper was developed with support of the project "Centrum excelentnosti integrovaného výskumu a využitia progresívnych materiálov a technológií v oblasti automobilovej elektroniky", ITMS 26220120055, that is co-financed from Structural Funds EU ERDF within Operational programme Research and Development OPVaV-2009/2.1/03-SORO and preferred axis 2 Support of Research and Development.

REFERENCES

- [1] Th. H. de Keijser, J. I. Langford, E. J. Mittemeijer and A. B. P. Vogels, "Use of the Voigt function in a single-line method for the analysis of X-ray diffraction line broadening", *J. Appl. Cryst.* (1982). 15, 308-314.
- [2] Rolf Grieselerl, Jens Mullerl, Stefan BarthS, Pawlowski. B., "Properties of high-k materials embedded in low temperature cofired ceramics" *Electronic-System Integration Technology Conference (ESTC)* (2010). Berlin. ISBN 987-1-4244-8554-3
- [3] Barth, S et ai, "Low sintering high k materials for LTCC application," *Proceedings of CICMT 2008*, Munich.
- [4] Yang-Fei Zhang, Shu-Lin Bai, Min Miao, Yu-Feng Jin, "Microstructure and mechanical properties of an alumina-glass low temperature co-fired ceramic" in *Journal of the European Ceramic Society* 29 (2009) 1007-1082
- [5] M. R. Gongora-Rubio, P. Espinoza-Vallejos, L. Sola-Laguna, and J. J. San- tiago-Aviles, "Overview of Low Temp-erature Co-Fired Ceramics Tape Technology for Meso-System Technology," *Sensor. Actuat. A*, 89 222–241, (2001)
- [6] W. K. Jones, Y. Liu, B. Larsen, P. Wang, and M. Zampino, "Chemical, Structural and Mechanical Properties of the LTCC Tapes," *Proceedings of the International Symposium on Microelectronics, IMAPS*, Boston, MA, 469–473, 2000
- [7] G. Ewsuk, C. B. DiAntonio, F. Uribe, and S. L. Monroe, "Materials and Process Control Technology for LTCC Microelectronics Packaging," *Pro-ceedings of the Ceramic Interconnect Technology Conference, IMAPS*, Denver, CO, 1–6, 2004
- [8] P. Espinoza-Vallejos, J. Zhong, M. Gongora-Rubio, L. Sola-Laguna, and J. J. Santiago-Aviles, "Meso (Inter-Mediate)-Scale Electromechanical Systems for the Measurement and Control of Sagging in LTCC Struct-Ures," *Mat. Res. Soc. Symp. Proc.*, 518 73–79 (1998)

Comparison of basic properties of insulating liquids for electrical purposes

Ing. Jiří Brázdil, MBA, PhD.¹⁾, Bc. Jan Sládek²⁾

Orgrez, a.s., Divize elektrotechnických laboratoří, Vítkova 17, 186 00 Praha 8 - Karlín, Česká republika, www.orgrez.cz

¹⁾ tel: +420 222 314 320, email: jiri.brazdil@orgrez.cz

²⁾ tel: +420 723 756 126, email: sladek_jan@centrum.cz

Abstract— This paper describes the properties of used insulating liquids for electrical purposes. At present, mineral oils (based on crude oil), man-made synthetic esters and natural esters (based on the processing of agricultural products) are used in practice. Mineral oils are the most common insulating liquids used in the electrical industry and their properties are verified in practice. Natural esters are characterized by high biodegradability but they are not fully examined with respect to their insulating properties. This paper deals with comparison of chosen electrical and quality parameters of individual types of insulating liquids for electrical purposes.

Keywords— *insulating liquid; mineral oil; silicone liquid; synthetic organic ester; natural ester; breakdown voltage; water content*

I. INTRODUCTION

Electrical insulating liquids form a large group of materials, widely used in the power energy sector. In electrical device they usually perform two functions:

- insulating – prevent current conduction between electrodes on different potential,
- cooling – transfer heat from active parts to the container.

Insulating liquids are commonly used in middle voltage (MV) and high voltage (HV) transformers. The ability to extinguish the arc is used in power switchgears. They are used as an impregnation of paper or dielectrics in capacitors and cables too.

Currently used insulating fluids can be divided into four groups according to their origin, as shown on Fig. 1.

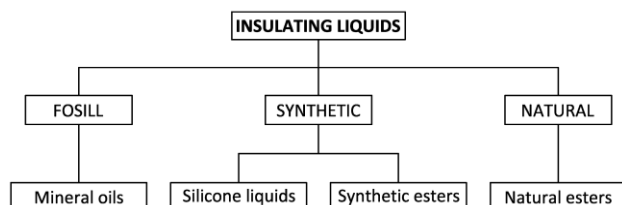


Fig. 1. Insulating liquids divided by the origin

A. Mineral oils

Mineral oils are traditional insulating fluids for more than 100 years. They are produced by fractional distillation of crude oil.

Mineral oils are characterized by their low viscosity, good thermo-oxidative stability and high pour point. They are inexpensive and can be regenerated. Other advantages are the facts, that they have been verified in practice operation and wide range of diagnostic tests is available. Main disadvantages include low flash and fire point, low water saturation limit and sludge forming during aging. The latest problem is the presence of corrosive sulfur, which has negative effects on materials in transformers. Also, the biodegradation is low.

B. Silicone liquids

Silicone fluids are synthetic polymeric materials based on silicon-oxygen bond. Polydimethylsiloxan is mostly used as an insulating liquid.

Silicones are characterized by high thermal resistance and pour point. During aging, the formation of sludge is reduced. On the other hand, they are relatively expensive and have very low biodegradability and high viscosity. Silicone fluids are slowly disappearing from the market due to price pressure.

C. Synthetic organic esters

Synthetic organic esters are artificially produced fluids, manufactured by esterification (reaction of polyol and carboxylic acid). Typical insulating fluid is an ester made from saturated acids and alcohol pentaerythritol.

These fluids have high flash point and fire point, good thermal stability and antioxidant properties. Biodegradability is very high, about 90 % (by OECD tests). They are able to absorb more water than other fluids without compromising the breakdown voltage. Higher viscosity and price are main disadvantages.

D. Natural esters

Natural esters, or vegetable oils, are naturally produced in living organisms. In the electrical engineering are mainly used oils pressed from the seeds of plants (canola, sunflower, soy). The main components are triglycerides, esters of glycerol and fatty saturated and unsaturated acids.

Natural esters are renewable, have high biodegradability (up to 97 %), high flash point and fire point. They can also dissolve large amount of water. Main disadvantages are higher viscosity and lower oxidation stability. While oxidizing, insoluble polymers are formed, which significantly increase the viscosity.

II. TECHNICAL STANDARDS REQUIREMENTS

Each group of insulating liquids has recommended parameters for the unused products, defined in the following technical standards:

TABLE 1: TECHNICAL STANDARDS FOR UNUSED INSULATING LIQUIDS

Insulating liquid	Standard
Mineral oil	ČSN EN 60296
Silicone liquid	ČSN EN 60836
Synthetic ester	IEC 61099
Natural ester	IEC 62770 *
* CDV Version, not published yet	

Specific requirements of the individual properties are summarized in Table 2.

TABLE 2: REQUIREMENTS OF TECHNICAL STANDARDS FOR UNUSED INSULATING LIQUIDS

Property	INSULATING LIQUID			
	Mineral oil [1]	Silicone liquid [2]	Synthetic ester [3]	Natural ester [4]
Physical				
Appearance	clear, free from water and suspended matter			
Density at 20 °C (kg/m ³)	≤ 895	955 – 970	≤ 1000	≤ 1000
Kinem. viscosity at 40 °C (mm ² /s)	≤ 12	40 ± 4	≤ 35	≤ 50
Kinem. viscosity at other temp. (mm ² /s)	≤ 1800 (-30 °C)	---	≤ 3000 (-20 °C)	≤ 15 (100°C)
Pour point (°C)	≤ -40	≤ -50	≤ -45	≤ -10
Flash point (°C)	≥ 135	≥ 240	≥ 250	≥ 250
Fire point (°C)	---	≥ 340	≥ 300	≥ 300
Chemical				
Acidity (mg KOH/g)	≤ 0,01	≤ 0,01 ^c	≤ 0,03	≤ 0,06
Water content (mg/kg)	≤ 30 ^a ≤ 40 ^b	≤ 50 ^c	≤ 200 ^c	≤ 200
Total additives (%)	U: <0,01 T: <0,08 I: ≤0,40	---	---	≤ 5
Oxidation stability				
Total acidity (mg KOH/g)	≤ 1,2	---	≤ 0,3	≤ 0,6
Total sludge (% mass)	≤ 0,8	---	≤ 0,01	---
DDF (tan δ) at 90°C (-)	≤ 0,5	---	---	≤ 0,5
Electrical				
Breakdown voltage (kV)	≥ 30 ≥ 70 ^d	≥ 40 ^c	≥ 45 ^c	≥ 35
DDF (tan δ) at 90°C (-)	≤ 0,005	≤ 0,001	≤ 0,03 ^c	≤ 0,05
DC resistivity at 90 °C (GΩ.m)	---	≥ 100	≥ 2	---
^a Delivery in a tank. ^b Delivery in a barrel or IBC container. ^c For untreated liquid, as received. ^d After laboratory treatment.				

III. PROPERTIES OF INSULATING LIQUIDS

Parameters of selected concrete new products of insulating liquids are presented in Table 3.

TABLE 3: PARAMETRES OF SELECTED UNUSED INSULATING LIQUIDS

Property	INSULATING LIQUID			
	Nynas Nytro Lyra X [5]	Xiameter PMX-561 [6]	M&I Midel 7131 [7]	M&I Midel eN [8]
	Mineral oil	Silicone liquid	Synthetic ester	Natural ester
Physical				
Appearance	clear, free from water and suspended matter			
Density at 20 °C (kg/m ³)	870	960	970	920
Kinem. viscosity at 40 °C (mm ² /s)	9,3	40 ± 4	28	37
Kinem. viscosity at other temp. (mm ² /s)	926 (-30 °C)	---	1400 (-20 °C)	9,3 (100 °C)
Pour point (°C)	-48	≤ -50	-60	-31
Flash point (°C)	152	260	260	327
Fire point (°C)	~ 170	370	316	360
Chemical				
Acidity (mg KOH/g)	≤ 0,01	0,008	≤ 0,03	≤ 0,03
Water content (mg/kg)	≤ 20	30	50	50
Total additives (%)	0,38	---	---	---
Oxidation stability				
Total acidity (mg KOH/g)	0,06	---	0,01	---
Total sludge (% mass)	≤ 0,02	---	≤ 0,01	---
DDF (tan δ) at 90°C (-)	≤ 0,02	---	---	---
Electrical				
Breakdown voltage (kV)	40 – 60 ≥ 70 ^b	50 ^a	≥ 75	≥ 75
DDF (tan δ) at 90°C (-)	≤ 0,001	0,0005	≤ 0,008	≤ 0,003
DC resistivity at 90 °C (GΩ.m)	---	1000	≥ 30	---
Environmental				
Biodegradability OECD 301 F (%)	---	---	89	97
Economical				
Relative price (-)	1	2 – 2,5	3	1,5
^a For untreated liquid, as received. ^b After laboratory treatment.				

IV. WATER IN INSULATING LIQUID

Negative property of all electrical insulating liquids is the ability to uptake moisture. Possible sources are ambient atmosphere, thermo-oxidative aging of insulating liquid and degradation of paper dielectrics. Less important source is residual moisture of materials, which have been dried during manufacturing.

Water in insulating liquid can exist in three states: free, dissolved and emulsified. The state depends on temperature, neutralization number and content of other impurities.

Solubility, total amount of dissolved water at specific temperature [9], extremely depends on the temperature. The increase of moisture is exponential as a function. Dependence of solubility of different insulating liquids on temperature is shown on Fig. 2. Moisture saturation level axis is logarithmic.

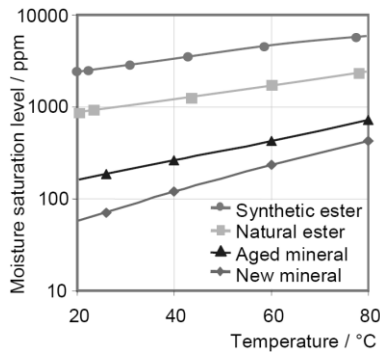


Fig. 2. Dependence of moisture saturation level on temperature [10]

If the water content in a liquid rises above the saturation limit, free or emulsified water could occur [9]. This situation is critical for an electrical device, because the breakdown voltage of liquid rapidly decreases.

V. EXPERIMENTAL MEASUREMENTS

Practical part of this article is focused on dependence of the breakdown voltage on the water content of insulating liquids. Moisture behavior in insulating fluids differs according to their solubility. Generally, synthetic and natural esters are able to dissolve much more water than mineral and silicone oils without compromising the breakdown voltage.

Measurements were performed on samples of natural ester Midel eN and synthetic organic ester Midel 7131. Data for mineral oil were extracted from the laboratory database, data for silicone fluids were copied from literature [11] (just for comparison).

A. Measurement procedure

- 600 ml of liquid was poured into a beaker
- Certain number of drops of distilled water was injected into the liquid. The aim is to artificially increase the water content. One water drop increases the water content in 0,5 l of liquid by approximately 100 ppm.
- A magnetic bar was inserted into a beaker and a beaker was placed on a magnetic stirrer. The liquid was stirred vigorously for at least 24 hours.
- In the case of natural ester, a liquid had been heated for 30 minutes at 50 °C – solubility of oil had increased and the dissolving process became more effective.

- Next step was a visual inspection whether the sample contains visible water droplets or impurities.
- Water content was measured according to IEC 60814.
- The breakdown voltage was measured on Baur PGO 90 A-2 (see Fig. 3), according to IEC 60156 with the following settings:
 - Spherispherical electrodes
 - 2,5 mm gap
 - 6 breakdowns
 - 5 minutes interval between breakdowns
 - Active stirring (25 mm magnetic stick)



Fig. 3. Measurement of the breakdown voltage – Baur PGO 90 A-2

B. Results

Dependence of the breakdown voltage on the water content of insulating liquids is shown on Fig. 4

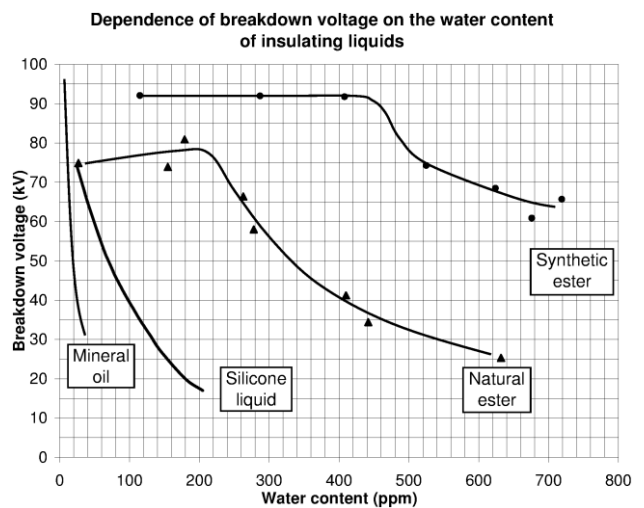


Fig. 4. Dependence of breakdown voltage on the water content of insulating liquids

VI. CONCLUSION

As insulating fluids in a power energy sector are no longer used just traditional mineral oils. New manufacturing methods and the effort to make the world more environmental friendly brought new insulating liquids based on silicon and esters.

Each group of liquids has slightly different physical and chemical parameters, which reflects in the requirements of specific standards.

Experimental measurement shows, that the best results were achieved on synthetic ester. The breakdown voltage is not affected by moisture approximately to 450 ppm of water content. The breakdown voltage is also very high, in some cases the breakdown didn't occur, because regulating transformer in the oil tester came to the end position and the experiment had been interrupted. Measuring on natural ester showed, that the breakdown voltage is slowly increasing with water content, peak of the curve is around 200 ppm. Dependence of the breakdown voltage on the water content of silicone and mineral oils is significant, because the solubility of both liquids is very low.

The reason of this behavior is the fact, that esters are more polar substances than mineral and silicone liquids and have the ability to form hydrogen bonds with water molecules. Water doesn't participate in a construction of a conductive bridge between electrodes and the breakdown voltage is unaffected. There is, of course, a certain limit, when the breakdown voltage begins to decrease.

ACKNOWLEDGMENT

This paper was created thanks to the support of the Technology Agency of the Czech Republic within the third ALFA sub-programme, project "Environment-friendly Insulating Liquids", No. TA03020251. The authors also thank Dr. Attila Gyore from M&I Materials, United Kingdom for sending samples of insulating liquids.

REFERENCES

- [1] ČSN EN 60296. *Kapaliny pro elektrotechnické aplikace - Nepoužité minerální izolační oleje pro transformátory a vypínače*. ed. 2. Praha: UNMZ, 2012.
- [2] ČSN EN 60836. *Specifikace nepoužitých silikonových izolačních kapalin pro elektrotechnické účely*. Praha: Český normalizační institut, 2006.
- [3] IEC 61099 *Insulating liquids--specifications for unused synthetic organic esters for electrical purposes*. Ed. 2.0. Geneva: International Electrotechnical Commission, 2010. ISBN 978-288-9121-601.
- [4] IEC 62770. *Fluids for electrotechnical applications - unused natural esters liquids for transformers and similar electrical equipment*. Committee Draft For Vote. Geneva: International Electrotechnical Commission, 2012.
- [5] Nytro Lyra X: Product Data Sheet. In: *Nynas AB* [online]. 2012 [cit. 2013-02-19]. Dostupné z: [https://nyport.nynas.com/Apps/1112.nsf/wnpds/Nytro_Lyra_X_IEC/\\$File/PDS_Nytro_Lyra_X_EN.pdf](https://nyport.nynas.com/Apps/1112.nsf/wnpds/Nytro_Lyra_X_IEC/$File/PDS_Nytro_Lyra_X_EN.pdf)
- [6] Xiameter PMX-561 Transformer Liquid: Technical Data Sheet. In: *Xiameter* [online]. 2009 [cit. 2013-03-11]. Dostupné z: <https://www.xiameter.com/EN/Pages/RetrieveDocument.aspx?type=PDS&DocumentId=090007c88031292a&s=56894>
- [7] Midel 7131: Dielectric Insulating Fluid Overview. In: *MIDEL: Natural and synthetic esters and transformer oils* [online]. 2010 [cit. 2013-03-12]. Dostupné z: http://static.mimaterials.com/midel/documents/technical/MIDEL_7131_Dielectric_Insulating_Fluid_Overview.pdf
- [8] Midel eN: Natural Ester Dielectric Insulating Fluid Overview. In: *Midel* [online]. 2012 [cit. 2013-03-13]. Dostupné z: http://static.mimaterials.com/midel/documents/technical/MIDEL_eN_Dielectric_Insulating_Fluid_Overview.pdf
- [9] LEWAND, Lance. Understanding Water in Transformer Systems: The Relationship Between Relative Saturation and Parts per Million (ppm). *Neta World Journal* [online]. 2002, Spring 2002 [cit. 2013-04-29]. Dostupné z: <http://www.netaworld.org/files/netajournals/NWsp02%20-%20ChemPersp.pdf>
- [10] TENBOHLEN, S., M. KOCH, D. VUKOVIC, A. WEINLÄDER, J. BAUM, J. HARTHUN, M. SCHÄFER, S. BARKER, R. FROTSCHER, D. DOHNAL a P. DYER. Application of vegetable oil-based insulating fluids to hermetically sealed power transformers. In: *CIGRE 2008* [online]. 2008 [cit. 2013-04-30]. Dostupné z: http://www.uni-stuttgart.de/ieh/forschung/veroeffentlichungen/2008_Cigre_Vukovic_Application_of_vegetable_oil-based.pdf
- [11] Midel 7131 Moisture tolerance. In: *Midel: Natural and synthetic esters transformer oils* [online]. 2010 [cit. 2013-04-30]. Dostupné z: http://static.mimaterials.com/midel/documents/technical/MIDEL_7131_Moisture_Tolerance%5B1%5D.pdf

Stator Core Fault Diagnostics of Turbo Generators

Vladimír Záborský¹⁾, Olga Tůmová²⁾

University of West Bohemia, Faculty of Electrical Engineering, Department of Technologies and Measurement,
Univerzitní 26, Plzeň, Czech Republic, www.fel.zcu.cz

¹⁾ tel: +420 776 791 013, email: vzabrans@ket.cz,

²⁾ tel: +420 377 634 563, email: tumova@ket.zcu.cz

Abstract — This paper is focused on the comparison of two stator core fault diagnostics. The first diagnostics is the flux test powered by a high power generator. The second diagnostics is performed by an instrument called an electromagnetic core imperfection detector (EL CID).

Keywords — stator; core; turbo generator; flux; diagnostics; lamination; infrared camera, EL CID

I. INTRODUCTION

The object of examination is a stator core of a turbo generator. The rotor creates a rotating magnetic field and then the voltage is induced into the stator winding.

The stator core is assembled of multitude of insulated laminations and pressed together with clamping plates at each side. The inter-laminar insulation is made by a thin layer of varnish. This design reduces eddy currents in the stator [1]. The magnetic flux excites voltage along the core. All the sheets are touching the key bars on the stator periphery. Therefore a fault of the insulation causes a short circuit connection among laminations. This thermal effect of flowing current could seriously damage a stator core.

The first introduced diagnostic method is a high power flux test. The function of a high power flux test is to warm up the core by losses in the stator core approximately to 10 – 15 °C above the ambient temperature. The temperature of the core is monitored during the test with an infrared camera. The fault in the core is signaled by the different color of warmer spots [2].

The second introduced diagnostic method is performed by an instrument called the electromagnetic core imperfection detector (EL CID). A low power excitation coil is tied around the stator core. The excitation of the coil is approximately 4 % of nominal value. The probe is moved axially along the stator core. The EL CID diagnostics instrument is connected with the probe and the excitation coil. The probe is highly sensitive to detect the change of active current and its phase in the stator core. The position and response of the probe is recorded and the increase of active current amplitude signals the fault [3].

The damage of inter-laminar insulation could happen during assembly of a stator core or during the operation of a machine. It is recommended to provide the

flux test or EL CID diagnostics of the core in the manufacturer's workshop before and after assembly of the winding. The core should be also checked during the regular inspection of the machine in a power plant and after every failure.

II. HIGH POWER FLUX TEST

A. Basic Fundamentals

The losses in the stator core raise the mean temperature of the core. They are created by eddy currents and changes of magnetic domain due to fluctuation of magnetic flux [4]. The short circuit among stator laminations increases the losses in stator core and the local temperature.

B. Measurement Procedure

Magnetic flux in the core should be 80 – 100 % of nominal magnetic flux. The excitation coil is wound around the stator core and connected to a high power generator with frequency 50 Hz. The core is watched during the test by an infrared camera. At the end of the test the temperature of the defect spots is compared with the mean temperature of the yoke. The investigation should be provided for a difference higher than 10 °C.

III. ELECTROMAGNETIC CORE IMPERFECTION DETECTOR (EL CID)

A. Basic Fundamentals

The stator core is excited by low power winding to produce the ring flux. In the core are circumferential magnetic field due to the excitation and the magnetic field due to fault currents [5]. The probe is then moved along the core to detect magnetically the presence of fault currents. The sensing probe is made by Chattock potentiometer to pick up the magnetic fields.

B. Measurement Procedure

The Chattock potentiometer is positioned on two neighbouring teeth and moved along the core, see Fig. 1. The part of the signal in phase with the reference signal is due to the magnetic flux resulting from the core excitation. The phase signal is present in the core whether the fault exists or not. Current induced in a fault circuit is shift an angle of 90° from the excitation field and is called a quadrature (quad) current.

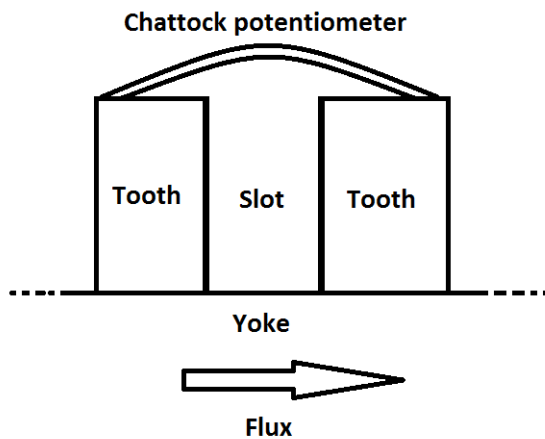


Fig. 1. EL CID measurement.

IV. COMMON FAULTS OF STATOR CORES

Faults of stator cores could be made during assembly or during operation of the machine by some accident. The faults could be separated to surface and sub-surface (deep-seated). The causes of the faults are mainly failures of inter-laminar insulation, debris in slots, loose coils and wedges [6].

V. COMPARISON OF DIAGNOSTICS

There are some advantages and disadvantages of both methods. In ideal case, both methods should be combined. The high power flux test could be dangerous for a seriously damaged stator core. The short circuit of a high amount of laminations raises the active current and the local warming. The core could melt down when the critical temperature is reached. If there is a serious suspicion of finding some faults, starting with the EL CID method is recommended.

The magnetic flux density during the flux test of the stator core is equivalent to the magnetic flux density during operation of the machine. The temperature rise of a damaged spot would be similar to the temperature rise in the loaded turbo generator.

EL CID measures the feedback to the excitation but doesn't show the temperature rise under real conditions. For a test engineer it is then difficult to decide how serious the fault would be for the operation of the machine.

For example a generator manufactured in the factory BRUSH Škoda Electrical Machines fell down from the trailer during transport and after the accident it was returned to the factory. It was decided to scrap the stator. It was an opportunity to create some induced damages in the core. Faults were created by a grinding machine and chisel in order to simulate the most common faults. Faults were recorded by infrared camera during the flux test and by EL CID probe and both diagnostic methods were compared.

The following rules are valid for all recorded EL CID diagnostics: the red curve represents shape of a quad current and the blue curve represents shape of a phase current. The horizontal axis shows the distance in meters,

the left scale is the magnitude of the quad current in milliamps and the right scale is the magnitude of the phase current also in milliamps.

A. Stator Core Without Induced Defects

- EL CID diagnostic was performed at the stator core without any defects to record the magnitude of interference. The value of quad current was up to 30 mA, see Fig. 2.

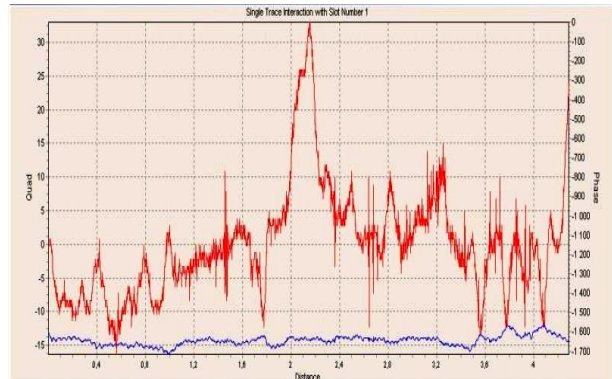


Fig. 2. EL CID record – no faults.

B. Defect Made by the Chisel

- The defect nr. 5 was made at the edge of a stator core tooth, see Fig. 3.
- EL CID record didn't show either a change of quad current or phase current.
- The temperature rise during the flux test was 5.3 °C after 30 minutes.



Fig. 3. Defect made by the chisel.

C. Light Defect Made by the Grinding Machine

- The defect nr. 9 was made by a gentle touch of the grinding machine, see Fig. 4.
- ELCID didn't show either a change of quad current or phase current.
- The temperature rise during the flux test was 18.1 °C after 30 minutes.



Fig. 4. Defect made by a gentle touch of the grinding machine.

D. Serious Defect Made by the Grinding Machine

- The defect nr. 8 was made by a heavy touch of the grinding machine. The cut was approximately 2 mm deep, see Fig. 5.
- The peak of quad current was 420 mA, see Fig. 6.
- The temperature rise during the flux test was higher than 77 °C after 30 minutes.



Fig. 5. Defect made by a grinding machine.

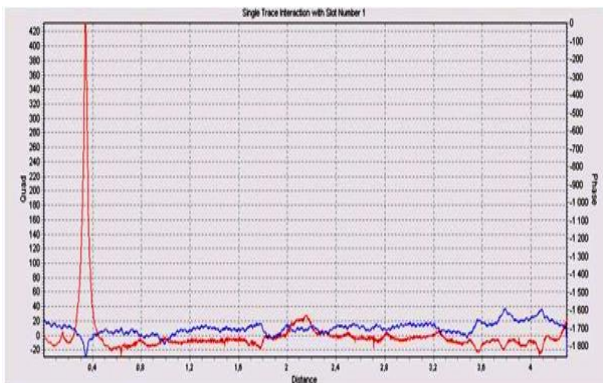


Fig. 6. EL CID record – serious defect made by the grinding machine.

E. Defect Made by the Grinding Machine at the side of the Tooth

- The defect nr. 11 was made by a touch of the grinding machine. The cut was approximately 1 mm deep, see Fig. 7.
- The peak of quad current was 140 mA, see Fig. 8.
- The temperature rise during the flux test was 60.1 °C after 30 minutes.



Fig. 7. Defect made by a touch of grinding machine at the side of the tooth.

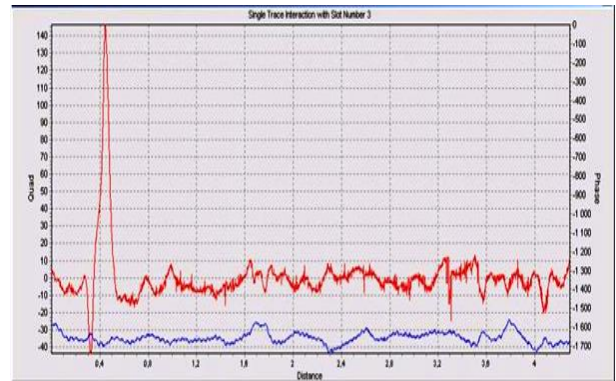


Fig. 8. EL CID record – defect made by the grinding machine at the side of the tooth.

F. Conclusion

The photograph from the infrared camera is in Fig. 9. The defect made by the chisel wouldn't be critical for the function of a turbo generator. The temperature rise of the damaged spot was only 5.3 °C after 30 minutes. The defects made by the grinding machine could cause serious damage to the turbo generator due to a high temperature rise. The comparison of both diagnostics is in table 1.

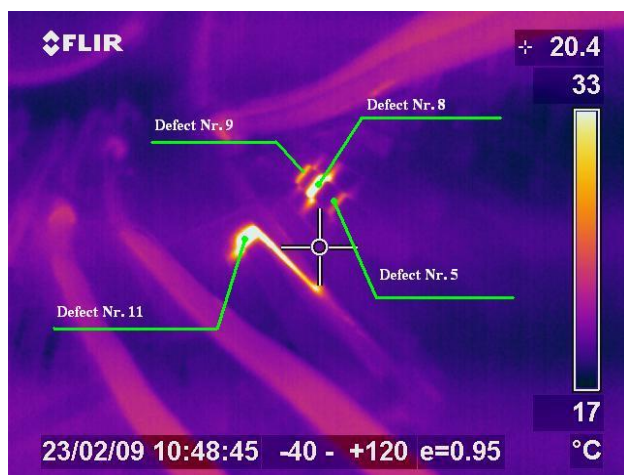


Fig. 6. Infrared thermal camera photo of defects nr., 5, 8, 9 and 11.

TABLE 1.

Defect nr.	EL CID – quad current [mA]	Flux test – temperature rise [°C]
5	-	5.3
9	-	18.1
8	420	77.0
11	140	60.1

VI. SUMMARY

This paper is an introduction to stator core fault diagnostics. There is an option of two basic methods. The high power flux test is demanding for supply and preparation of the test. It simulates the real operation condition, but could be dangerous for a seriously damaged

stator core. The test engineer should avoid overheating the core and carefully watch the increasing temperature of the core.

The EL CID diagnostics is suitable for on-site conditions where no sufficient supply is present. There was a good opportunity to compare both methods due to a stator accident during transport. The defects in the core were induced. The comparison of both methods demonstrated that light damage to the core wouldn't be recorded by EL CID and so the temperature rise taken by infrared camera would be less than 20 °C after 30 minutes.

The short circuit connection of the higher amount of laminations was detected by EL CID and the quad current was hundreds of milliamps. The temperature rise was more than 60 °C.

REFERENCES

- [1] Prof. Ing. Ivan Uhlíř DrSc., Ing. Lukáš Novák, PhD., Doc. Ing. Jiří Šťastný, CSc., Ing. Josef Vlček, CSc., "Elektrické stroje a pohony," České vysoké učení technické, Praha, 2007, pp. 95-102.
- [2] Prof. Ing. Stanislav Ďaďo, DrSc., Doc. Ing. Marcel Kreidl, CSc., "Senzory a měřicí obvody," České vysoké učení technické, Praha, 1996, pp. 211-216.
- [3] D. R Bertenshaw, "Digital EL CID," ADWEL International Limited, Watford, UK, 2004, pp.11-17.
- [4] O. Roubíček, "Elektrické motory a pohony," BEN – technická literatura, Praha, 2004, pp. 40-57.
- [5] G. K. Ridley, D. R. Bertenshaw, "A deeper insight into EL CID," The International Journal on Hydropower & Dams, Issue Four, 2005, pp. 87-91.
- [6] G. Klemptner, I. Kerszenbaum, "Operation and Maintenance of Large Turbo-generators," IEEE, New York, USA, 2004, pp. 469-484.

AC voltage tests on production lengths of LV cables

Petr Voda

Petr Voda Electronics, Zámecké schody 13, 594 01 Velké Meziříčí, Czech Republic
 tel: +420 566 524 819, email: vodaelectronics@vm.cz

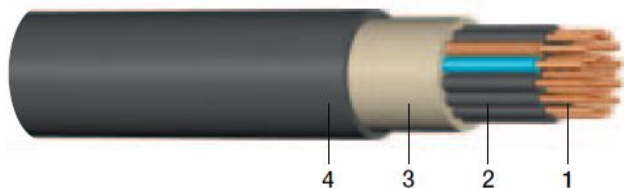
Abstract: AC voltage tests are common method to verify insulation integrity of cables and create a part of routine factory acceptance tests. Because cable lengths to be tested become longer and longer in order to maximize manufacturing productivity, there are some essential, up to this time not important phenomenon connected with execution of these applied voltage tests. Testing frequency is usually 50-60 Hz therefore cables under test could be considered as a concentrated element at the first look. But it will be more detailed in paper that longer cable lengths bring new problems which cannot be neglected.

Keywords: AC voltage test; LV cable; production length; power testing capacity; compensation; attenuation; inductance; capacitance

I. INTRODUCTION

Most of cable factories try to achieve maximum production efficiency in order to save labor and material costs at the present. Testing costs inside the manufacturing process are not negligible. Therefore leave the sheathing lines always longer lengths on larger drums. This enables to reduce number of AC applied voltage and conductor resistance tests (routine tests) which are essential tests on LV cables. Note, that manufacturing capacity of modern advanced sheathing lines amounts with 3-core LV cable to approx. 500 km/day.

LV unscreened installation cables usually consist of copper or aluminum conductors, PVC or XLPE insulation, filling layer and overall PVC or PE sheath. Rated voltage U_0/U is ranging from 300/500 V up to 0.6/1 kV. Test levels with AC applied voltage test are ranging from 2.5 kV up to 4.5 kV. Conventional construction of these cables is illustrated at Fig. 1 below.



- Construction**
- 1 Copper conductor
 - 2 PVC insulation
 - 3 Filling layer
 - 4 PVC sheath

Fig. 1. Construction of a typical LV cable according [1]

In the following will be more detailed AC voltage test on long cable lengths. The conductor resistance test (a part of routine tests) will not be discussed, because of different test circumstances.

II. POWER TESTING CAPACITY

Long cable line can be represented by equivalent $R-L-G-C$ circuit that is demonstrated at Fig. 2 and usually describes a never-ending homogeneous line. Cable parameters have following meaning: C – capacitance, L – inductance, R – resistance and G – conductance. Parameters L and G can be neglected for practical calculation and the equivalent circuit can be then simplified into a simple LP filter (RC , 1st order) [2].

Cable as a test object presents practically only a capacitance C that is linearly growing with cable length. All remaining cable parameters are not important for calculation of HV source capacity for AC voltage test with frequency 50 Hz. Test arrangement is so that one core is connected to test voltage and the others are connected together and earthed. It is generally known that unit cable capacitance increases with number of cores.

Let's consider that

- U is magnitude of applied voltage,
- I is current flowing through the cable capacitance C and
- ω is angular frequency.

These quantities are firmly bonded with AC voltage test of a LV cable by expression

$$I = U\omega C. \tag{1}$$

Because angular frequency is constant, required test current depends on magnitude of test voltage and cable capacitance respectively cable length.

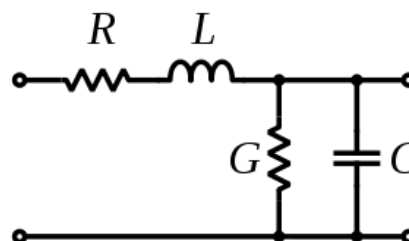


Fig. 2. Equivalent circuit of a long cable line [3]

PRACTICAL EXAMPLE A

Cable to be tested: Type CYKY 2x1.5, length on drum 18 km, capacitance 0.11 μF/km, resistance 13 Ω/km, test voltage 2.5 kV/50 Hz. Total cable capacitance C amounts to 1.98 μF. After introducing the numeric values into (1) we get

$$I = 1.554 \text{ A.}$$

It is obvious that HV testing source shall deliver at least 1.6 A in order to reach specified test voltage magnitude of 2.5 kV. If the cable length will be doubled then the available test current must be almost 3.2 A, and so can be continued. Required input power supply increases simultaneously.

III. UNSUFFICIENT POWER TESTING CAPACITY

HV test equipment which are working in cable factories in routine test fields of LV cables at the present have mostly historic origin (30 or more years old) and low power testing capacity. They are often upgraded with advanced control and adapted to new safety standards. But main components (HV transformer, HV divider, regulating transformer etc.) are usually in good condition and therefore they are not replaced. This behavior is also supported by quite high prices of new HV test systems.

Often happens that the HV test equipment is not able to deliver required test current. Simple solution is to connect a suitable inductance parallel to the HV transformer output and simultaneously to the capacitance of tested cable. This arrangement is schematically shown at Fig. 3 where used symbols have following meaning:

- I denotes current flowing from the HV transformer output (secondary winding)
- C is capacitance of tested cable
- L is suitable additional inductance and
- R is resistor which represents total losses of the test circuit, mainly in inductance and in cable

Current I can be divided into three parts. First component flows through the resistor R and is in phase with output voltage U . The remaining current components have phase shift – capacitance by +90° and inductance by -90°. Therefore these two current components can be mutually compensated, in ideal case to zero current – well known LC resonance condition.

Consider a fixed value of the compensation inductance. Because cable length can vary from few meters up to many kilometers (C is function of cable length), current through the compensating inductance may not exceed rated output current of the HV test transformer.

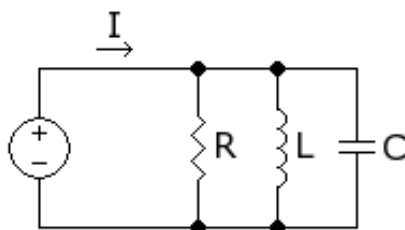


Fig. 3. Test circuit arrangement with additional inductive compensation

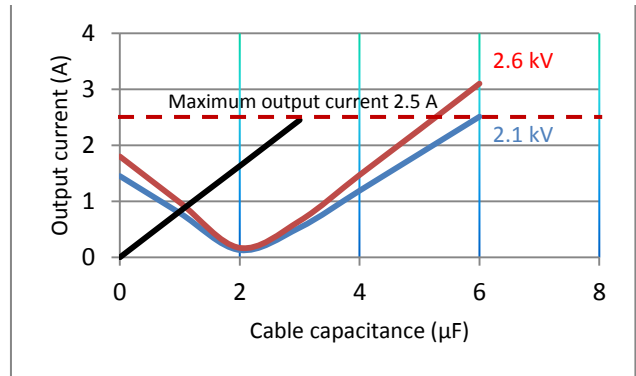


Fig. 4. Output characteristics with single stage inductive compensation

PRACTICAL EXAMPLE B

Existing HV test equipment (maximum output parameters 3 kV/2.5 A) was extended with fixed inductive compensation. Black line at Fig. 4 represents load diagram before installation if the inductive compensation. Maximum testable cable capacitance amounted to approx. 3 μF (test voltage 2.6 kV). Situation after installation is illustrated by red curve. It is obvious that maximum testable cable capacitance lies slightly above 5 μF now. Another advantage of the single stage compensation is handling free operation of the HV test equipment – permanent connection of the inductance.

If this single stage inductive compensation is not sufficient, there is possible to use two-stage compensation in this case. But the second inductance must be disconnected if cable capacitance falls below 3 μF. Disconnection can be done manually or better with help of a PLC unit and suitable HV switch. Absolutely, number of compensation stages can be enlarged. Practical limits are given by losses originating in cable (test object) and compensating inductances. It should be mentioned here, that better compensation results can be gained with PE insulated than with PVC insulated cables (significantly lower loss factor).

IV. OTHER TROUBLES WITH TESTING

Let's consider HV test equipment with sufficient testing capacity for long lengths of LV cables, for example 5 kV/10 A.

PROBLEM I: HIGH LOOP RESISTANCE

Test object is cable from practical example A, length on drum is 40 km. That means that loop resistance of the cable amounts to 1,040 Ω. If we connect such resistor at output terminals of the a.m. HV test equipment, no breakdown will be detected, because current flowing through the resistor (test voltage 2.5 kV) is slightly below 2.5 A. This value is deep below maximum output current (10 A).

The above described situation occurs if cable fault is located at the far end of the cable (near end is connected to terminals of the HV test equipment). Simulation was carried out by simple short-circuiting of conductors at the far end and no fault was detected during AC voltage test. The test obviously failed in this case – what to do?

As described, under certain circumstances the HV test equipment with high power testing capacity can bring troubles into the test procedure. To avoid failing the test, resonance test equipment with low active power should be used. Another possibility is to monitor phase relation between test voltage and test current flowing through the cable.

PROBLEM II: CABLE ATTENUATION

Equivalent circuit of a long cable line (Fig. 2) can be simplified with low frequency signals according to [2]. Then the equivalent circuit contains only R and C elements, the others primary elements are neglected. Specific attenuation β (in Np/m) can be expressed as

$$\beta = \sqrt{(\omega RC/2)} . \tag{2}$$

At the first look is clear that attenuation increases with cable length. Let us define that U_1 denotes voltage at near end of the cable (connected to HV test equipment), U_2 denotes voltage at far end of the cable (open) and l is cable length. Relationship of the above defined quantities is given by formula

$$U_2 = U_1 e^{-\beta l} . \tag{3}$$

PRACTICAL EXAMPLE C

Cable BS 2x1.5+1, length l on drum amounts to 30 km, cable construction is illustrated at Fig. 5. Test arrangement for AC voltage test (2 kV/300 s) can be carried out in two alternatives which differ in electric parameters:

- 1) Phase and neutral conductors are connected together and earthed, protective conductor is connected to high voltage output of the test equipment;
- 2) Phase or neutral conductor is connected with protective conductor and earthed, neutral respectively phase conductor is connected to high voltage output.

The first alternative was selected for real measurement. Primary line parameters (capacitance and loop resistance) for this arrangement of cable cores are (influence of ambient temperature was neglected):

$$C = 0.255 \mu\text{F/km} \text{ and } R = 24.5 \Omega/\text{km} .$$

After substitution of symbols for numeric values in Equation (2) can be calculated specific attenuation

$$\beta = 31.3 \text{ mNp/km} .$$

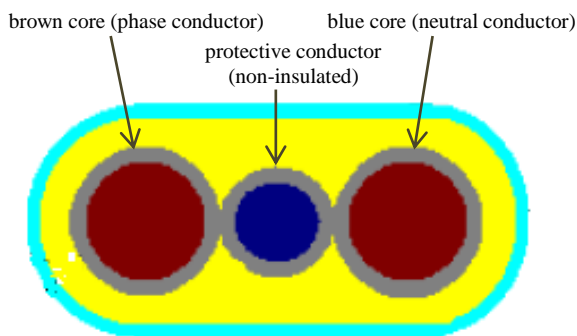


Fig. 5. Cable BS 2x1.5+1 – cross-section

From Equation (3) can be calculated test voltage U_2 at far end of the cable now. After substitution we get

$$U_2 = 0.391 U_1 . \tag{4}$$

It is obvious that voltages at both cable ends differ essentially and test proof of insulation integrity is not satisfactory for the far cable end, because the test voltage is much lower than the specified value and cable insulation is not enough stressed in this area.

The theoretical analysis above was verified by voltage measurement in cable factory (cable BS 2x1.5+1, length 30 km on wooden drum, applied AC voltage 2 kV, test arrangement according to 1)). Measured values for U_1 and U_2 determined relationship of these voltages as

$$U_2 = 0.818 U_1 . \tag{5}$$

Lowering of the test voltage along cable wound on a drum was confirmed, but there is great difference with comparing results form (4) and (5). Why?

Cable is not a straight line, but it is wound on the drum. Therefore the equivalent circuit according to Fig. 2 requires modification. Between layers exists two parasitic capacitances: C_s bridges part of the live conductor and C_p can be added to cable capacitance C . Moreover cable winding represents a multilayer tubular coil having its own inductance L_s . Modified equivalent circuit at Fig. 6 shows a simplified arrangement of these new elements. Accurate determination of numeric values for the new elements seems to be a little difficult, because they are function of cable construction (flat or round), insulating and sheathing materials, number of cores, thickness of insulation and sheath, drum material etc.

Nevertheless what to do with lower voltage at the far cable end? How secure proper voltage test?

We can increase test voltage in order to get correct value at the far cable end, but near part of the cable will be then overstressed. Test power demand will be raised simultaneously.

Another possibility is to connect both cable ends together. After that is not known condition in the middle of cable – requires further investigation through simulation with help of two equal cable lengths.

If two or more cable lengths are tested simultaneously, then parallel connection of individual cable lengths should be preferred (near ends connected together), because series connection creates a longer cable length.

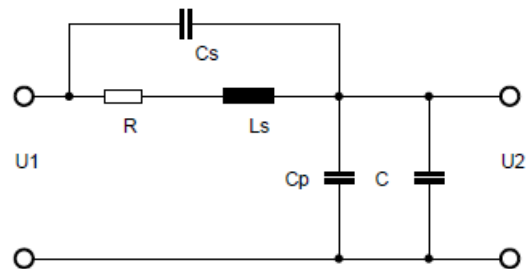


Fig. 6. Modified equivalent circuit of a long cable on drum

PROBLEM III: TIME CONSTANT

Routine tests of LV cables also include conductor resistance measurement. During this measurement current source in micro-ohmmeter supplies conductor and generates voltage at its ends that is measured. The conductor can be replaced by active resistance R and inductance L , because cable is wound on a drum. These two components create together time constant τ of the measuring circuit (LR circuit) and measurement conditions are very similar to conductor resistance measurements of transformer windings.

As derived in [2], time constant of LR circuit can be expressed by the following equation

$$\tau = L/R . \quad (6)$$

As was mentioned previously, cable on a drum represents a multilayer tubular coil. Inductance increases with drum size. Approximate calculations show that actual inductance values can reach up to a few H with drum's flange diameter 2.5 m and conductor cross-section above 150 mm². Similar results were calculated for time constant – max. 2 - 3 seconds. Note that time constant has higher value with copper conductors than with aluminum conductors under equal cable construction.

In order to keep measuring uncertainty as low as possible, a certain time delay is necessary, because transient component of current in measuring circuit has to decay. If measured voltage is taken earlier than measuring current reaches its correct value, the acquired voltage value contains additionally a small inductive component that produces a measuring error.

How eliminate required time delay and keep measuring uncertainty in acceptable limits? The only solution is to use maximum possible measuring current, because then the transient current component has lower percentage of steady value. Higher voltage of the current source can also reduce the time delay. If these possibilities are exhausted, waiting is necessary.

V. CONCLUSION

First part of the paper describes cable length as equivalent circuit consisting of concentrated elements. The circuit is used for calculation of required power testing capacity for AC voltage test.

Many existing test equipment have not sufficient power testing capacity. It is demonstrated that a simple inductive compensation can be helpful in this situation.

Problem comprising long cable lengths a small conductor cross-section is mentioned. Breakdown detection fails in some cases if power testing capacity is sufficient. Possible solutions are mentioned.

Furthermore is investigated both theoretically and practically influence of cable attenuation that causes voltage drop at the far cable end. It was found that theoretical and practical results are not in harmony. Therefore was developed a new equivalent circuit for cables which are wound on a drum. There are presented suggestions to eliminate impact of cable attenuation in this part.

Last part describes meaning of time constant during conductor resistance measurement on large drums. Some recommendations to reduce the time delay are given. More detailed information about conductor resistance measurement in cable factories can be found in [5].

ACKNOWLEDGMENT

The author would like to acknowledge the help of Mr. Lukas Fiala of Prysmian Draka Velké Meziříčí for preparation and support with measurements of LV cables in cable factory.

REFERENCES

- [1] Product Catalogue. Prakab, a.s., 2009.
- [2] Z. Trnka, Teoretická elektrotechnika. SNTL/ALFA, CZ: Prague, 1972.
- [3] http://en.wikipedia.org/wiki/File:Transmission_line_element.svg
- [4] http://en.wikipedia.org/wiki/File:RLC_parallel_circuit.png
- [5] P. Voda, K problematice měření činného odporu jader silových kabelů v kabelovnách. EKT 42 (1989), p. 77-81.

Oxidative degradation of insulating oils

Jaroslav ČERNÝ¹⁾, Nadia LADYKA²⁾

Institute of Petroleum Technology and Alternative Fuels, Institute of Chemical Technology
Technická 5, 16628 Prague, Czech Republic

¹⁾ phone: +420 220 443 780, email: jaroslav.cerny@vscht.cz

²⁾ phone: +420 220 444 238, email: nadiia.ladyka@vscht.cz

Abstract— Paper summarizes the basic knowledge about oxidation of petroleum oils with the emphasis on insulating oils. Composition and some properties of recent petroleum oils are discussed in relation to their oxidative stability. Effect of antioxidants is also shortly explained. Attention is also paid to diagnostics and maintenance of oils.

Keywords— petroleum oil, properties, oxidation

I. INTRODUCTION

Oxidation is a main reason for ageing and degradation of insulating and/or other industrial oils during their service. It is natural process proceeding in all systems when oils are accessible by air or other oxidizing agent. Increased temperature and some other conditions, such as access and increased intensity of light or catalysis by wear metals, can accelerate the oxidation rate.

Majority of insulating oils is produced from petroleum base oils similarly like other industrial oils. Petroleum base oils are composed of hydrocarbons and just the hydrocarbon bonds between carbon and hydrogen are the reactive sites for oxidation reactions. Increased intensity of light and increased temperature both factors promote the oxidation rate. It is often noticed that increase in temperature by 10 °C causes about two times faster oxidative ageing of oils. Oxidation is accompanied by a formation of oxidation products, such as ketones, aldehydes, ethers, acids, esters, etc. Such products can react in subsequent reactions and form condensation or polymerization reaction products. Such consecutive reactions can lead to an increase of acidity and viscosity of oils, and insoluble oxidation products start to be formed in the oils.

Beginning and further development of the oxidative ageing is mostly accompanied by a formation of cloudy appearance of the oils due to a presence of insoluble matter. So the cloudy appearance of oils cannot necessarily be caused by moisture but oxidation is more frequent reason for that oil behavior. When oil maintenance is not satisfactory then more severe oil oxidation can lead to a formation of varnish and sludge. Walls of the oil systems and oil filters can be covered by resin deposits as evidenced from Figures 1 and 2.

II. OIL QUALITY AND OXIDATION

Majority of insulating or other petroleum oils are complex mixtures of several types of hydrocarbons that have different susceptibility to oxidation due to differences in their structure:



Fig. 1 Oil filter covered by resin-like material of oxidation products



Fig. 2 Piece of black insoluble material formed by oil oxidation

- Saturated hydrocarbons (paraffins, isoparaffins, and naphthenes) are considered as the very stable part of petroleum oils. Most stable components are n-alkanes (n-paraffins). However, they are removed from oils due to their very unsatisfactory low temperature behavior. Isoalkanes (isoparaffins - branched paraffins) are the very valuable components of oils and their oxidative stability is also very good. However, petroleum oils also contain some portion of naphthenic hydrocarbons (cycloalkanes) and their oxidation stability can be somewhat lower, especially in the case of naphthenes with higher number of naphthenic rings in their molecule [1]. This can be the case of insulating oils which are mostly produced from naphthenic oils that have, in the other hand, very good low temperature behavior with very low pour point.

- Unsaturated hydrocarbons are very reactive during oxidation. They are undesirable in industrial fluids and lubricating oils. Low oxidative stability leads to an easy formation of resin-like material, a typical example can be utilisation of fluids based on vegetable oils.

- Aromatic hydrocarbons are mostly less stable during oxidation than paraffins and/or naphthenes while utilized in usual industrial systems. This fact is mirrored in lower oxidative stability of mineral oils that are less refined. Some aromatics have however very good oxidative stability and that is often utilized in usage of synthetic oil based on alkylbenzenes. The oxidative stability of aromatics is lower with increasing number or aromatic ring in their molecule [1].

It is evident from the above statements that a high content of saturated hydrocarbons (paraffins and naphthenes) and simultaneously a low content of aromatic hydrocarbons lead to increased oxidative stability of petroleum oils. In general, oxidative stability of oils decreases while the content of aromatic hydrocarbons increases. Content of saturated hydrocarbons is also one of the parameters that are important for classification of base oils. Quality of petroleum base oils according to API (American Petroleum Institute) classification is shown in Table I.

Table I: Classification of petroleum oils according to API

API group	Saturated hydrocarbons (wt. %)	Sulphur (wt. %)	Viscosity index
I	< 90	> 0,03	80-120
II	> 90	< 0,03	80-120
III	> 90	< 0,03	> 120

Oil composition and content of individual structural groups of hydrocarbons are responsible for behavior of oil in service. Especially important property of the oils is their oxidation stability that can be measured in a laboratory. Typical stability of petroleum oils is showed in the Figure 3 that was determined by using a common RPVOT test [2]. Very low oxidation stability is evident for the common

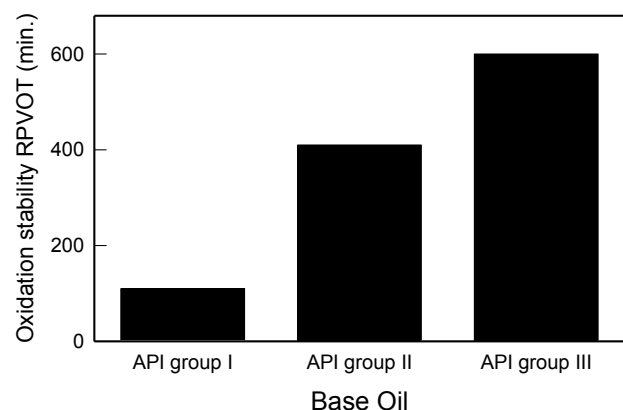


Fig. 3 Oxidation stability of base oils

relatively high content of aromatic hydrocarbons, mostly in the range 15-35 wt. %. The most valuable oils of the API group III have the best oxidation stability thanks to a very low content of aromatics [2,3].

III. SOLVENCY OF PETROLEUM OILS

Oxidation of petroleum hydrocarbons leads to a formation of oxidation products that have polar character in contrast to non-polar character of original hydrocarbons. Oxidation products formed in the early stages of oxidation are oil soluble molecules. However, oils start to get a typical reddish-brown color. While oxidation proceeds, oxidation products are of greater polarity, its molecules increase in dimensions due to their condensation and polymerization, and molecules tend to be less soluble in the oils. Such an effect is more and more pronounced in recent oils produced in advanced technological units based on severe hydrocracking. Oils produced in such units are of a high quality with excellent oxidative stability. However, when antioxidants are spent and oil started to oxidize then problems with a bad solvency of hydrocracked oils can emerge. Due to a low content of aromatics, hydrocracked oils can only solubilize small amount of polar oxidation products. Such amount is much lesser than that which can easily be solubilized in formerly often used mineral oils [4,5]. Oxidative degradation of hydrocracked oils can therefore appear suddenly. So, this phenomenon emphasizes an importance of oil monitoring and analysis, which should be performed regularly.

Insulating oils are a specific group of petroleum oils because other than usual lubricating properties are required. Insulating oils are of low viscosity, and they also should have very good low temperature properties as they often are exposed to environment and cold weather. Good low temperature properties of oils are already ensured by a selection of so called naphthenic petroleum raw for production of base oils. Such base oils have then increased amount of naphthenic hydrocarbons with very good low temperature behavior. Oils of such a composition also have relatively good solvency compared to common paraffinic oils. On the other hand, higher content of naphthenes can decrease their oxidation stability.

IV. ANTIOXIDANTS IN INDUSTRIAL OILS

History of antioxidants utilization comes back to 1930's. Antioxidants for the industrial application are usually the so called „low temperature“ antioxidants. That reflects conditions under which oils usually works, i.e. under temperatures below 120 °C. At higher temperatures, effectivity of the low temperature antioxidants is usually lower. On the other hand, high temperature antioxidants are usually utilized in motor oils that are working at temperatures as high as 200 °C and more. Both types of antioxidants have different mechanism of the antioxidative action.

The low temperature antioxidants are commonly exploited in the insulating oils. The phenolic type compounds are utilized for a long time, and their effectivity was confirmed in many applications. Phenolic antioxidants forms very stable radicals, scavenge free radicals from oils formed in early stages of oxidation, and

interrupt thus the oxidation reactions and inhibit therefore oil oxidation. Antioxidants are of course spent during their action and when they are depleted the oil start to readily oxidize. Early stages of oxidation are relatively slow and oxidation of hydrocarbon molecules is not dangerous for the oil system. However, oxidation rate gradually increases and oil is oxidized to a remarkable extent. Oil start to look dark and later a cloudy appearance is to be seen in the oil as the insoluble oxidation products are formed. When an insufficient attention is paid to oil in this stage the oil degradation can lead to aspects showed in Figures 1 and 2.

V. DIAGNOSTICS AND PREDICTIVE MAINTENANCE

Appropriate oil maintenance comprises good storage conditions on the one hand as well as good oil maintenance during the oil service on the other hand. It means that oils should be regularly checked for their appearance and color, and oilers and opening for oil top-uping should be kept clean. Oil properties should be checked in regular intervals, and oil samples should be analyzed for some selected parameters keeping in mind recommended warning limits. Checking the oxidation degradation of oils and estimation of remaining oil life is always highly recommendable.

Checking the oxidation degradation has been frequently done by FTIR analysis determining the phenolic antioxidant content. Decay of the antioxidant was a measure for the oil health. When concentration of antioxidant was sufficiently high then the oil can further be serviced without any concern for the oil health.

Problems have arisen in past few years when the phenolic antioxidants start to be replaced by the aminic ones. Amines give very weak signals in FTIR spectra and determination of their concentration therefore failed. Reliable replacement of the FTIR spectroscopy by another suitable analysis is a goal of many projects during past few years. Perhaps the best new method seems to be the cyclic voltammetry. However, there are only few references about its usage in plant practice.

Another possibility for evaluation of the remaining oil life can be direct determination of oxidation stability of the oil. There are suitable oxidation tests for each type of industrial oil. In such cases, decreasing oxidation stability of oil means that the remaining oil life also decreases. Any oxidation test can be based on about two approaches. One possibility is blowing air through the oil sample at given temperature and for a given time. Catalyst to accelerate oxidation can also be used. At the end of the test some appropriate properties are measured.

Another possibility can be oxidation of oil sample in a pressure cell. The most frequently used test is the RPVOT test (Rotating Pressure Vessel Oxidation Test). Oils are oxidized in a pressure cell by oxygen at 150 °C and oxidation is catalyzed by a copper wire. Formerly, this test was known under an abbreviation RBOT (Rotation

Bomb Oxidation Test) and procedure is given by a standard ASTM D 2272. Test is time consuming and another disadvantage of the method is also relatively high scattering of results obtained. Duration of the test can be as long as 10-15 hours for advanced oils and experimental error as high as 22 % according to statistical data of ExxonMobil Corporation [6].

Some years ago a new oxidation tester was developed and distributed under the name PetroOxy Tester. Tester has primarily been designed for testing automotive fuels, and it can also be used for testing industrial oils. Tester is relatively user friendly. However, testing procedure should only be developed [7].

VI. CONCLUSION

Oxidation stability is a basic process that degrades petroleum and other oils, whether they are used as lubricating, insulating or other industrial oils. Oxidation cannot be avoided but it can be inhibited by using a high quality antioxidants. Another way to control the oxidation stability is a primary choice of base oil as different quality of base oils within the API Groups gives the lubricating oil quite different properties with respect to oxidation stability as well as oil solvency.

Appropriate care about oils and predictive maintenance can help to keep lubricating and other oils in health and precede thus serious damage of industrial facilities. Choosing the appropriate method for checking the remaining useful life of oils is very important. Some ways to the best diagnostic practice were shown in this paper

ACKNOWLEDGMENT

The work was supported by the project of grant agency TAČR under the agreement No. TA 03020251, and the project of MŠMT dealing with a specific institutional research No. 21/2012.

REFERENCES

- [1] Černý J., "Principles of low- and hightemperature oxidation of hydrocarbon mixtures", Proc. 7th Conference Reotrib 2001, Velké Losiny, May 2001, pp. 45-54. (In Czech)
- [2] Lok B.K., Sztenderowicz M.L., Kleiser W.M., "Global Base Oil Trends", ICIS LOR World Base Oil Conference, London, February 2000.
- [3] Václavíková I., Černý J., "Quality of Industrial Lubricants Based on Hydrocracked Base Oils", 42nd Conference Lubricants, October 2009, Rovinj, Croatia.
- [4] Černý J., Ladyka N., "Oxidation and formation of varnish and sludge in oil systems", Proc. 18th Conference Reotrib 2012, Velké Losiny, May 2012, pp. 55-61.
- [5] Kamchev B., A Bad Mix Deposits Hamper Industrial Lubes. Lubes&Grease, EMEA Magazine, September 2012, pp. 18-22.
- [6] "Developing Turbine Oils. Beyond RPVOT", Technical Topic, ExxonMobil, 2009. <http://www.mobilindustrial.com/IND/English/files/tt-developing-turbine-oils.pdf>
- [7] Ladyka N., Černý J., "Laboratory testing of oxidation stability of turbine oils", Paliva 2012, 4(3), pp. 61-65. (In Czech)

Sustainability and performance of technical systems

Peter Ponický¹, Vítězslav Zamarský²

¹ Department of Quality and Environment, Business School Ostrava plc, email: peter.ponicky@vsp.cz

² Michálkovická 1810/181, 710 00 Ostrava – Slezská Ostrava, email: vitezslav.zamarsky@vsp.cz

Abstract – Seemingly unrelated concepts, ergo for some are these more contradictions. Nowadays in manufacturing organizations increase performance achieves technological and organizational innovations. To assess their performance is necessarily used monitoring, metrology and statistical processing of measured data. With the range and intensity of innovation, in our opinion, significantly has linked to their source (human, material, energy, financial, etc.) and social sustainability. Why is this happened? Just because of this the technical, technological and production systems are not independent, but they create a multi-processing chain with multi-polarity structures. Each even a trivial change raises a series of chain changes transforming the whole system, in principle, as in the case of the balloon under external pressure (just because it's a system). Today, it is very often used metaphors and parables with biological systems (e.g., life cycle, etc.), and just changes with their intensity and hardness make up a kind of DNA of these systems. It is therefore on the spot, just as in the case of biotechnology to ponder over the sustainability of the changes (innovation), and similarly, how in the world of biology, very carefully manipulate with DNA due to the possible occurrence of mutations, but these cease to have the characteristics of the original systems. It raises the questions, what are the limits of performance with regard to their sustainability, to avoid "negative mutation of systems" and their collapse into each other.

Keywords – system, technical system, technological system, performance systems, systems sustainability

I. INTRODUCTION

The technical system is maybe enough generic term, but, in principle, is so referred to various technical systems consisting of various entities, machinery and equipment. A significant feature of their functioning is the interconnection of "networks" of links, for example mass, energy and information. Part of the technical systems is their management-management subsystem; the effect of the whole system is regulated in its surroundings.

Technical system produces a file of the influences acting on the transition process, in the course of the transformation of materials, energy and information-to change the status of an input operand to the output operand.

A good representative of the transformation technical system is a production organization. Due to its nature, this systemic transformation can be described as a technical process.

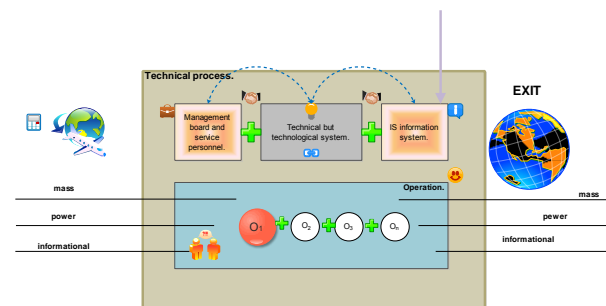


Fig. 1: Diagram of the process of displaying its system of transformations (technical process).

Technical system and for the operation of the system is activated, there are two elements in the process of dialectical unity. According to the course of processes, their property and known physical laws of technical systems apply technology and vice versa, the security right over the technical process (technology), is tied to the existence of a particular arrangement of the technical system. Technical systems are the source of the expected effects (results), which carry out the desired status change "operand" (raw materials, media, semi-product, product, etc.). Therefore it runs the state, dimensional, full TRANSFORMATION. The main functions of the system are the subject of the project's technical solutions/design, which is usually called-a system task. The nature of the system links shows that the elements are the source of system behaviour and the links between them are the bearer of this behaviour. A set of links is referred to as the structure of the system. Through the methods of structural analysis are identified the following characteristics of the structure of the system:

1. *existence/absence of links* between elements, correlation of selected elements, connections on

the system, completeness - link structure and its redundancy,

2. **orientation of the links**, relations of succession/relationship between elements in the system of prevention, the ways in the system, the availability of its elements, structural integrity and the degree of centralisation of the structure.
3. **the quality of links** and their parameters are then evaluated by the model.

Models of the structure of the system allow to assess its progress/arrangement of the links between different components of the system, regardless of the type of the elements covered by the concentration (in Fig. 1 are the basic types of structural elements), which are applied even in the design of technical systems.

TABLE 1

Characteristics system elements	1	2	3	4
Redundance = R	0	0,25	0	0
Compactness = Q	1	0,5	0,6	0,7
Centralization = C	0,7	0	1	0,7

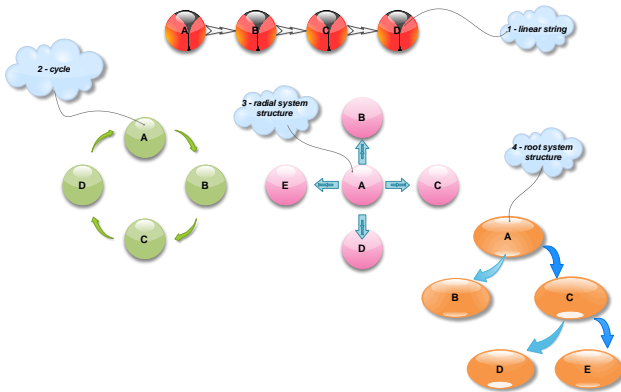


Fig. 2: The arrangement of the basic elements of the engineered systems with the values of structural redundancy (R), compact (Q) and centralization (C) from which we can build a complex structure of the system. Redundancy is that represented structure is complete and whether it is more than just the minimum number of links. An indicator of the structural compactness expresses the distance between elements of the structure, what is the value of Q higher; the proliferation of initiatives after the structural connections is faster. The degree of centralization of the structure expresses the relationship of "predecessor-successor" between particular points. In a highly centralized structure, the value of the centralization closing to one, and these structures are better able to provide a response to the input stimuli, operating from around the system.



Fig. 3: Features of the technical systems

II. SYSTEMS PERFORMANCE

The performance of the systems is, in principle summary product of performance of the processes. Under the term of the PERFORMANCE it is necessary to understand the properties of the individual processes of technical or technological system (*performance is therefore a measure of the magnitude of the results*). **Knowledge of these properties, sufficiently precisely diagnosed and continuously monitored, it is important for their operational control in order to fulfil the requirements for functionality, reliability, and stability of the systems.** Monitoring and measuring of performance is therefore an important task in particular for owners of processes, i.e., those processes outside the systems make decisions and implement them. Without the processed data from the results of performance measurement processes cannot be objective to control how the processes and systems. How to measure the physical, technical and technological properties are already relatively long known and contemporary diagnostic devices allow even high accuracy and operational reliability of the measurement.

For the time course of changes is important processing of diagnostic networks and IT tools. Mathematics and programming could assist us in compiling the models whose outputs may form so-called PERFORMANCE INDICATORS

The character of these indicators must be related to uniqueness of system in the ongoing processes; some may even have a universal character and can be used in a wide variety of measurements. By motivation in repeatedly from the assessment of organizational systems, it may be indicators, for example:

- a) transient time performance of functions,
- b) the performance of its utilization,
- c) the cost of implementation (energy consumption, operational and unused energy emissions, etc.)
- d) the share of mismatches with regard to the assumptions (mathematical models),
- e) the number of operational deviations,
- f) the level of competence of the complex processes,
- g) the use of available capacities, etc.

In addition to these, let's say "universal performance indicators", it is possible to propose specific indicators. These can be derived from indicators of productivity, compliance with the requirements, the yield of resources, etc., for example:

- the speed of response to measured and indicated disagreement,
- the speed of compilation of the system for innovation proposed in the course of the trial operation,
- the average response time to technical/technological stimulus,
- recovery of the physical capacities of the system processes,
- carried out repairs within 24 hours from their registration, etc

III. SUSTAINABILITY AND PERFORMANCE OF TECHNICAL SYSTEMS

The current world trend in the area of technical systems is very similar to the trends of economic globalisation, then simply put the focus on maximizing profit "at any cost". Let us try on the analogy with biological systems, with the most difficult – human. The help of anabolic steroids and dietary supplements is possible from a less physically fit man "to make" a muscle mass bloated "monster" daily charges his anatomical system, on the border of sustainability. The limits between the effective use of the biological functions and the collapse of the system of linkages of the various functional units of the body (heart, lungs, a set of soft tissue, etc.) are very thin. There are many examples of excess that "Rubicon" between life and death, between bodybuilders desiring for an unlimited growth of the volume of the mass of muscles [e.g., though Arnold Schwarzenegger as an adviser to the U.S. President for physical health, he has repeatedly enormous health problems with heart (sample of ideas in unlimited possibilities of American way of life!)].

An example of a similar practice is, for example, the automotive industry. Automakers compete in offer of the different assistance systems wannabe enhancing safety on the roads. However, what is the result? Adaptive cruise control for large supplement helps to prevent possible collisions to a certain speed limit. However, it does not help the "competitors" on the road, as it does not work at high speeds and at other drivers raises more idea "fuses" at their own carelessness. Therefore it raises a false sense of security and reduces operational alertness and attention. This contributes to the suppression of a sense of responsibility for the performance of activities that we carry out. This is true more generally for all systems cooperating with man as an administrator and managing systems. Therefore, it reduces attention and, in particular, responsibility for the execution of the activities. Many of the firms it says address by minimizing the influence and involvement of the human factor by introducing high concentrations of elements of automation and

mechanization. An accompanying phenomenon is high unemployment, and less need for and ability to invest in the higher performance of technical and technological systems. The company tries to minimize this phenomenon of higher concentrations of their production capacities, etc.

As it seems, this concept is a downward spiral. So obviously, we have got beyond the sustainability and performance enhancement raises the rather negative vectors in the social community structures and disproportionately burdens the environment and empties the source option of the Earth. We believe that as well as ecological and biological systems operating in the spiral of their life cycles, as well as the technical systems are limited in their life cycles, and therefore has a huge importance to the monitoring of the performance and setting of rational limits of the performance for all systems. It certainly slows down the innovation dynamics, however, which apparently is the capital source of diversification and resources enervation with national and international community. Excessive depletion of the resources and the possibilities of human community by a single aspect, the acceleration of consumption by the producers for the purpose of maximizing profits is clearly already beyond sustainability. The starting point is a return to consumption generated by NEED and not marketing accelerating by higher comfort and security at the expense of liability.

IV. THE ROLE OF METRICS, DIAGNOSING AND METROLOGY

In the world there are relatively a lot of models of monitoring and measuring the performance of business processes and systems, i.e. systems of assessing companies and institutions (just a random Maskell's production class worldliness, Gross's and Lurch's SMART, Kaplan's and Norton's Balanced Scorecard and Globerson's performance criteria). For an individual assessment of the performance of technical systems, in fact, there is not a complex system, so far, we process the same in assessing the reliability of complex/mountings systems, therefore, the whole system is so reliable how reliable/unreliable is the component with the lowest value

. This methodology, however, "deletes" from the game an important element of the functionality and stability of the systems i.e. LINKS and their properties. Closest to the physical nature of technical systems and the complexity of the assessment (a sort of holistic understanding, including the links between the elements of the system) is one of the already mentioned models, the system of performance criteria with a metric of measurable physical and technical properties under the control of the nature and robustness of the binding elements of the systems. To measure the technical and physical properties is available methodological and tool potential of metrology as well as for changes to these properties over time, so continuous monitoring of the aid of diagnostic parameters for assessing the performance of the networks. Performance

metrics should be established experimentally for a particular technical systems, that play an indispensable role as the designers of these systems, and their operational process "owners", this is indispensable for their teamwork. It is possible to motivate the choice of criteria for measuring performance of organizations, such as:

- *Validity (relevance)of measurement and the completeness of the measurements,*
- *Sufficient detail of measurements,*
- *Sufficient frequency and accuracy of measurement,*
- *The correct timing of measurement and consistency of data in time,*
- *The simple clarity of information,*
- *The responsibility for the results of the measurements, etc.*

V. CONCLUSION

This contribution is trying to appeal to developers and users of technical systems to a "stop" and a place of continual escalation on the performance of the systems have devoted greater attention to optimizing system performance based on a painstaking examination of the objectified user needs. For the most accurate interpretation of these needs, you need the required properties of the elements of the systems and the characteristics of their reciprocal links. For this purpose you can use the monitoring and diagnostic systems, working in real time, allowing objectively to the requirements corresponding to the setting up and management of technical and technological systems on the basis of sustainability based on needs.

Application of the combined voltage impedance spectroscopy for insulation diagnostics

V. Ďurman, J. Lelák, V. Šály

Institute of Power and Applied Electrical Engineering, Faculty of Electrical Engineering and Information Technology,
Slovak University of Technology Bratislava,
tel: +421 60291612, vladimir.durman@stuba.sk

Abstract— The paper discusses the possibilities of using the complex modulus measurements in the range of very low frequencies for investigation of phenomena appearing on the electrode-dielectric interface in transformer oil. It was found that the dominant process in this case is the electrode polarization. The results also proved that the process is non-linear. Useful information on the process can be derived by performing measurements with a superimposed dc-ac voltage

Keywords— electrode polarization; dielectric properties; transformer oil; slow polarization processes;

I. INTRODUCTION

Ordinary insulation systems are mostly created as many-layer structures. By investigating the system properties, we are dealing with phenomena originating at the layer interfaces. The basic interface in any system is the electrode-dielectric interface. At every interface the process of space charge accumulation appears. Each space charge influences the electric field inside the system. Therefore we must check the interface phenomena at dimensioning any insulation system. The interface phenomena are often manifested as slow polarization processes. Those are the processes with high relaxation time. The lower limit of its value is about 1 s. Monitoring of the slow processes is useful in praxis also for investigation of materials ageing. In experimental research of the slow phenomena we use the methods of dielectric spectroscopy both in the time domain and in the frequency domain. Measurement of a slow polarization is a time-consumption process. It requires an instrument with a long-term stability. Some obstacles may occur if the process is overlapped by conduction of the system. In this way we need to use some special procedures for the system evaluation.

II. THEORETICAL

The dielectric properties of materials are commonly characterized by semi empirical functions of the complex permittivity ε^* . In the range of very low frequencies a complex modulus $m^* = 1/\varepsilon^*$ is preferable used. By the complex modulus formalism the necessary dielectric diagrams are shifted to the region of higher frequencies, which make the data processing easier. As for the complex permittivity, recently, the universal dielectric response of Jonscher is preferred [1], but in the papers on dielectrics the Havriliak – Negami function is mostly used in the case

of polymer structures and also in the case of electrode polarization [2]. In a simple model situation with two-layer dielectric it is sufficient to use the famous Cole-Cole formula. The mentioned function can be written as follows:

$$C_0 \varepsilon^*(\omega) = C_0 \left(\varepsilon_\infty + \frac{\Delta\varepsilon}{1 + (j\omega\tau_0)^{1-\alpha}} \right). \quad (1)$$

Here ω is the angular frequency, ε_∞ is the optical permittivity of the dielectric, C_0 is the geometric or vacuum capacitance, $\Delta\varepsilon$ is the permittivity increment, τ_0 is the relaxation time and α is the shape parameter.

Two-layer dielectric is mainly created at the electrode surface in the system with blocking and noninjecting electrodes. The free cations in dielectric are accumulated near the negative electrode, creating a positive charge. A similar process runs near the positive electrode. The steady state of accumulation is given by the balance of concentration gradient and the Coulombic (electric) force [3]. The cations in dielectric and the negative charge at the electrode create so-called double layer. The layer is characterized by the Debye length:

$$L_D = \frac{1}{q} \left(\frac{\varepsilon_0 \varepsilon_R kT}{n_0} \right), \quad (2)$$

where q is the ionic charge, ε_0 is the vacuum permittivity, ε_R is the relative permittivity of material in absence of free charges, n_0 is the free ion concentration, k is Boltzmann's constant and T is temperature. In the case of non-polar material the value of ε_R equals to ε_∞ .

In some previous works [4-5] it was found, that the electrode polarization could be represented by a simple Debye model, i.e. the model according to (1) with zero value of parameter α . By using label L for the electrode distance and σ_D for the material conductivity we can write for the permittivity increment $\Delta\varepsilon$:

$$\Delta\varepsilon = \left(\frac{L}{2L_D} - 1 \right) \varepsilon_R. \quad (3)$$

For relaxation time τ_0 the next equation is valid:

$$\tau_0 = \frac{L}{2L_D} \frac{\varepsilon_0 \varepsilon_R}{\sigma_0}. \quad (4)$$

III. EXPERIMENT

The aim of experiments was to examine the properties of electrode interface in electric grade transformer oil. The oil was used as supplied with no additional refining. The oil specimen was placed in the measuring system consisting of nickel-coated plan-parallel electrodes, which were adjustable by means of a micrometric screw. The electrode area of the system was $2 \cdot 10^{-3} \text{ m}^2$. The measurements were performed at temperature of $21 \text{ }^\circ\text{C}$. The electrode spacing was set up to $1 \cdot 10^{-4} \text{ m}$. By our experiments we used the ModuLab MTS (Materials Testing System) made by the Solartron Analytical. The instrument works in the frequency range from $1 \text{ } \mu\text{Hz}$ to 1 MHz . The accuracy of the voltage and current measurement is 0.1% of reading $+ 0.05 \%$ of range. The instrument provides possibility of the combined voltage and current analysis in such a way, that the small ac components can be separated from the major dc ones for proper impedance calculation. To simulate the higher electric fields as can appear during the oil operation in transformer, in experiments we used relative low voltages applied on the thin layers of oil. The ac voltage on the specimens during measurements was 0.1 V . The ac voltage was combined with dc voltage aiming at detection of possible non-linear behavior of the interface.

IV. RESULTS AND DISCUSSION

At the beginning, the measured data of complex capacitance were treated graphically. The results can be seen in Figs. 1 – 2. The presence of polarization phenomena is evident from increasing trend of the real part of capacitance. Unfortunately, the relaxation maximum of the imaginary part of capacitance was not reached in the actual frequency range. Better information on the polarization parameters can be derived from the complex modulus diagrams. These are in Figs. 3 – 4. The diagrams are typical for the parallel RC circuit with deformed low-frequency tail. From the circuit analysis we know, that the parameter C can be easily calculated as the reciprocal value of the modulus real part at high frequency edge. The parameter R is then derived from the slope of the modulus imaginary part at high frequencies in the logarithmic scale. The next part of the impedance, which is connected in series with the mentioned RC circuit, can be calculated after subtracting the RC circuit data from the measured values of complex modulus. The whole process is illustrated in Figs. 5 – 6 for one selected set of data (measured at zero dc voltage). Here the measured data are marked as +, the RC circuit data as x, the data after subtraction as o. The data after subtraction were fitted with function according to (1). The sum of the fitting function and the RC circuit data is depicted in the mentioned figures as a line.

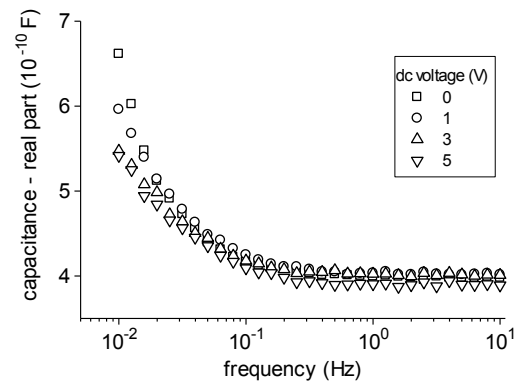


Fig. 1. The real part of oil capacitance with dc voltage as parameter.

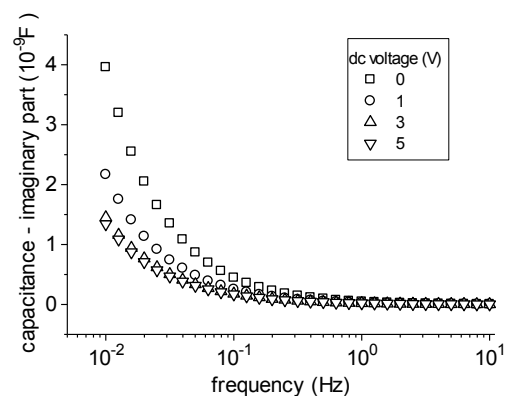


Fig. 2. The imaginary part of oil capacitance with dc voltage as parameter.

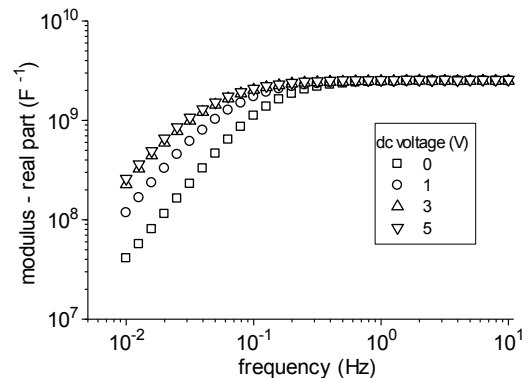


Fig. 3. The real part of oil modulus with dc voltage as parameter.

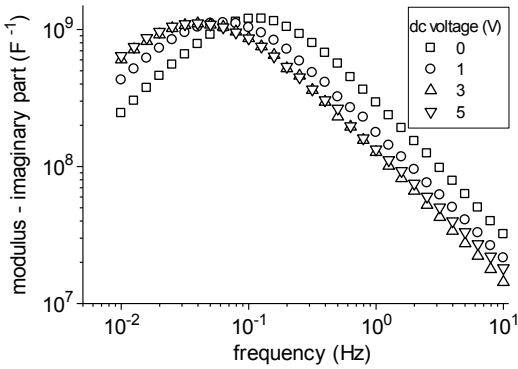


Fig. 4. The imaginary part of oil modulus with dc voltage as parameter

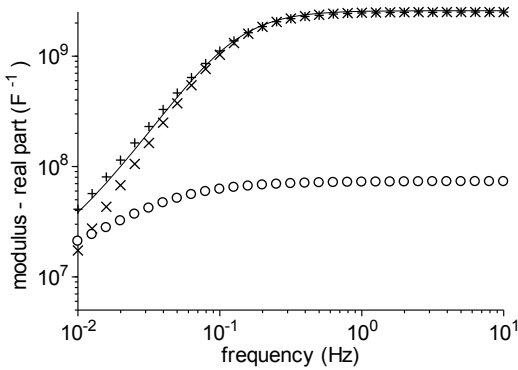


Fig. 5. The real part of oil modulus. Measured data as points, calculated data as line

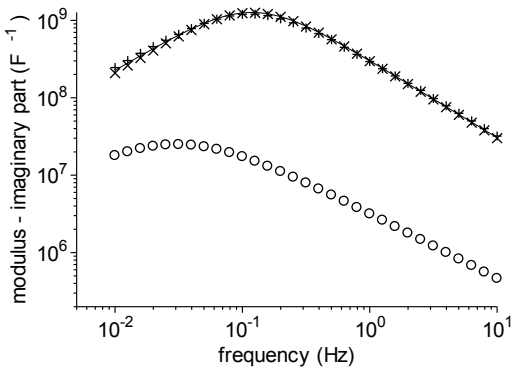


Fig. 6. The imaginary part of oil modulus. Measured data as points, calculated data as line

All necessary parameters derived from our measurements are summarized in Tab. 1. Except of the circuit parameters R , C and parameters from (1), there is also an estimation of the thickness of near-electrode layer with accumulated space charge (assigned as h). It was calculated from the parameter $C_0\epsilon_\infty$ and the electrode area.

TABLE I. SUMMARY OF THE CALCULATED RESULTS

U_{dc} (V)	R ($10^9 \Omega$)	C ($10^{-10} F$)	$C_0\epsilon_\infty$ ($10^{-8} F$)	$C_0\epsilon_s$ ($10^{-7} F$)	τ_0 (s)	α (-)	h ($10^{-5} m$)
0.0	3.34	3.98	1.37	1.05	58	0.15	0.29
1.0	5.32	4.04	0.41	1.08	343	0.15	0.94
3.0	7.52	4.02	0.30	1.07	442	0.15	1.31
5.0	7.46	3.93	0.22	1.08	1025	0.15	1.74

V. CONCLUSION

The results of our measurements reveal an existence of electrode process at the electrode interface of transformer oil. It was shown, that the process is non-linear i.e. it depends on the voltage. The calculated thickness of the near-electrode layer increases with voltage. In contrary to the theoretical knowledge about relaxation time (4), the layer thickness is in our case in direct proportion with the relaxation time. It means that the determining factor of (4) is the oil conductivity. While the charge is accumulated at the electrode, the charge mobility and also the conductivity decrease. On the other hand, the model cited in the theoretical part requires a constant charge level throughout the mentioned layer. This was not fulfilled as the dispersion parameter α has non-zero value, which implies a non-constant space charge profile. Calculation of the actual charge distribution and corresponding electric field will follow in our future work.

ACKNOWLEDGMENT

This work has been supported by the Slovak Research and Development Agency under the project No.: APVV-0181-11.

REFERENCES

- [1] A. K. Jonscher, "The universal dielectric response and its physical significance," *IEEE Trans. EI.*, vol. 27, pp. 407-423, 1992.
- [2] S. Emmert, M. Wolf, R. Gulich, S. Krohns, S. Kastner, P. Lunkenheimer, A. Loidl, "Electrode polarization effects in broadband dielectric spectroscopy," *Eur. Phys. J.*, vol. B83, pp. 157, 2011.
- [3] R. Coelho, "Sur la relaxation d'une charge d'espace," *Revue Phys. Appl.*, vol. 18, pp. 137-146, 1983.
- [4] R. J. Klein, S. Zhang, S. Dou, B. H. Jones, R. H. Colby, J. Runt, "Modeling electrode polarization in dielectric spectroscopy," *J. Chem. Phys.*, vol. 124, pp. 144903, 2006.
- [5] J. R. MacDonald, "Theory of ac space-charge polarizations effects in photoconductors, semiconductors, and electrolytes," *Physical review*, vol. 92, pp. 4-17, 1953.

Non-statistical measurement uncertainties

T. Panc, O. Tůmová, Z. Mačičková

Department of Technologies and Measurement, Faculty of Electrical Engineering, The University of West Bohemia,
Univerzitní 26, Pilsen, www.zcu.cz
tel: +420 377 634 567, email: panct@ket.zcu.cz,
tel: +420 37763 4507, email: tumova@ket.zcu.cz,
tel: +420 737 069 549, email: zmaci@students.zcu.cz

Abstract — this article deals with non-statistical measurement uncertainties. It is shown that uncertainties are not important only in the evaluation of the measurement result, but even before the measurement, i.e. the creation of a measurement procedure, selection of appropriate devices and methods. Most common influences, which cause measurement uncertainties, are categorized. The main attention is given to the method used for the influences size determination. In practice, this process can be source of serious errors. These errors can significantly affect value of the computed uncertainty, and thus the credibility of the whole measurement. Therefore, it is important to be able to identify and eliminate these errors.

Keywords — uncertainty; measurement; error

I. INTRODUCTION

The concept of measurement uncertainty can be encountered as a result of growing pressure on production quality more and more. The main objective of the evaluation of measurement uncertainty is to ensure confidence in the results of measurements. During the process of determining the uncertainties are also identified interferences, weaknesses and ways to improve, which will be specifically demonstrated in this article. Unfortunately described goals are not always being successfully fulfilled. The problem is generally low awareness of uncertainty, even between companies and people dealing with measurement. A role as well plays superficial understanding of the process of measuring and applied influences. However, there is a potentially more serious problem in the system determining uncertainties itself. It is the influence of subjectivity. If the calculation of uncertainty should have any predictive value, it is necessary to realize and fully understand the processes of direct measurement, the effects the surroundings on the measure, but also the manner in which we carry out analysis of uncertainties itself.

II. CLASSIFICATION OF THE EFFECTS

On the results obtained in the measurement affect wide range of effects. The first step in determining the size of given effects on the results of the measurement is their identification and division. They can be divided into two groups. First are those that can be identified and which have a deterministic effect. Other either cannot be identified at all or their effect is chaotic. This division determines how you can determine the level of influence of the measured value.

For definition of randomly variables are applied statistical methods, collectively known as Method A (formerly uncertainty type A). The procedure for determining the uncertainties by statistical methods is well defined in the standards. To do so, it is required repeated measurements under otherwise identical conditions. From the measured values is calculated mean value, which corresponds to the measurement result, while the uncertainty is determined by the size variance:

$$u_A = k_s \sqrt{\frac{1}{n(n-1)} \cdot \sum_{i=1}^n (x_i - \bar{x})^2} \quad (1)$$

,where n is count of measurement, k_s is multiplying coefficient used when less than 10 measurement are proceed, \bar{x} is mean value, x_i is value from one measurement.

The basic method of determining the statistical uncertainty is not complicated, although in specific cases, it is necessary to use more sophisticated statistical means and methods whose analysis is not the subject of this article.

III. NON-STATISTICAL SURVEY OF UNCERTAINTIES

All methods and procedures for determining the uncertainty of measurement without the use of statistical tools are referred to as methods B. As mentioned earlier, it is extremely important to the procedures, because they can also affect the procedures of statistical uncertainties evaluation. Unfortunately their determination is more complicated and more prone to subjectivity than the methods A.

Initial analysis of factors influencing measurements should be performed before the start of measurement. It is actually the first step in methods B - identification of influences. In very general terms one can say that everything takes effect on the performed measurement every time. Absolute majority of effects can not consider with equanimity, because their effect on the resulting value is negligible. Concurrently with the identification of the effects is therefore made a rough reasonable estimate of size of the effect on the measured quantity. For processing are so selected only factors with a significant influence on the measurement. Other elements are neglected. Here is hiding the possibility of error occurs, which can significantly affect the entire discovery process uncertainties. If it is based on miscalculations neglected impact that actually has a considerable influence on the measured value, then the resulting uncertainty does not reflect reality.

As mentioned before, the process of identifying the effects is crucial even for making measurements within the method A. It specifies to us which of the measurement parameters must be kept constant in order to observe the requirement "otherwise identical conditions." If are not maintained the same conditions, the uncertainty determined by method A come very high, effect inadequate to random processes, which brings us back and may warn us to the error in the evaluation by the method B and that was a major effect overlooked, wasn't kept constant, and therefore increases the uncertainty determined method A. But you cannot rely on this "warning". It is quite possible that undiscovered effect during the measurement methods A will not move, there will be no uncertainty grows, but during the other measurements occurs its change, which distorts the results.

After selecting the striking effects is necessary longer accurately determine the size of their effect on the measured quantity. It includes several sub-processes. The first is to set possible realistic limits of variations influence. Also here you can easily commit inaccuracies. For example we know that on measurement has effect the temperature, so we need to determine the real interval in which the temperature may vary during the measurement. Let us assume making measurements in indoor areas. If we consider the movements should be e.g. $-50\text{ }^{\circ}\text{C}$ to $+1000\text{ }^{\circ}\text{C}$, the uncertainty of this impact would be unacceptably high and would not correspond to the reality. If we consider temperature from 20 to $30\text{ }^{\circ}\text{C}$, we will be certainly closer to the reality. It may happen that we omit some relevant information, such as the space in which the measurement is made – if is the production with increased temperature, or conversely air-conditioned area, then identified insecurity, would also not comply, it would be too low!

One can also encounter fact that when trying to calculate the uncertainty, we find that we are able to determine not only the extreme limits, but actually the direction and specific size of the influence on the measurement result. In this case this is not uncertainty, but the systematic error that can be repaired in the result. Even with this error, it can be calculated as with the uncertainty, but it is absolutely inappropriate, because this significantly impairs accuracy. Understandably should be determined the measurement uncertainty of the impact and then uncertainty associated with made corrections. It is often, in an effort to simplify, neglected. Needless to say, often rightly so.

The next step is to determine the probability distribution of frequency of effect sizes within a given interval (θ). For this step it is necessary to have even more information than in the previous determination period. There are three methods of determining a probability distribution. The first and the most accurate is the long-term measurement of the impact of operating in an environment, in which the measurement takes place. Although this option provides the most objective the results, it is also very expensive and time consuming and is not practically used. The second option is an educated guess. It is made on the basis of sufficient information and a thorough knowledge of influence and his connections.

The degree of precision of this method is mainly determined by the quality of information and experience of the person conducting the assessment. The third method is based on determining the typical distribution. It is probably the most commonly used method. It uses the fact that the probability distribution is in typical effects well known and in most cases the same. Here we can make mistakes when actual measurement conditions significantly differ from those, for which is the characteristic distribution for a given influence determined. A typical example of this method is the application of a uniform probability distribution entirely to errors of digital as well as analog measuring instruments.

From the knowledge of the limit values of influence and probability distribution is determined the uncertainty caused by this influence:

$$u_{Bj} = \frac{Z_{jMAX}}{\theta} \quad (2)$$

,where Z_{jMAX} is error interval and θ is probability distribution constant.

This procedure is applied to all identified negligence effects.

Finally, it is necessary to determine to what extent the change affecting the quantity reflect (Y) on the change of the measured value (X). For this purpose the implementation of so-called sensitivity constant:

$$c_j = \frac{\Delta Y}{\Delta X} \quad (3)$$

There may be a problem if the sensitivity is not constant but it is a function of a variable, which may be mentioned in terms of sensitivity constant unacceptable simplification. Fortunately, this case occurs in practice only rarely and approximations using constant usually does not mean a problem.

When calculating the measurement results from several measured values, is necessary to calculate the resulting uncertainty based on the rules for propagation of errors in formulas, see [2]. At the same time occurs complication in the form of mutual correlations. Correlations can occur between the measured quantities and therefore between their uncertainties. Comprehensive evaluation of correlations is especially in complex systems very difficult task. Very often, when assessing the existence and size of the correlations, is used an educated guess. If this method should be at least fundamentally correct, then it's needed major experience and a considerable amount of information about the process and their interrelations. Correlations are often underestimated and in order to simplify the work is completely neglected. Not always is neglect appropriate and it can lead to a return of the gross inaccuracies of the resulting uncertainties. One could say that a qualified guess is correctly applied only in cases, where it is considered a case measuring only minimally differing from those measurements, to which were detected correlations analyses of the measured data. Analysis of correlation using the measured data is the only completely objective method of determining the existence and magnitude of correlation between individual effects.

Uncertainties mutually correlating members are determined by the relation:

$$u_f = \sqrt{\sum_{i=1}^n \left(\frac{\partial f}{\partial x_i}\right)^2 u_i^2 + 2 \sum_{j < k}^n r_{jk} \left(\frac{\partial f}{\partial x_j}\right) \left(\frac{\partial f}{\partial x_k}\right) u_j u_k} \quad (4)$$

,where f is the function describing relation between measured values, n is number of elements, r_{jk} is correlation coefficient, $u_{i,j,k}$ are individual uncertainties and $x_{i,j,k}$ are measured values.

After determining of all uncertainties, determine the sensitivity of the measured quantity on the influence and netting of mutual correlations, are all partial uncertainties from various influences summed up in vector:

$$u_B = \sqrt{\sum_{j=1}^n u_{Bj}^2} \quad (5)$$

Thereby is by method B finally established the overall uncertainty of measurement. This is further in vector adding to the uncertainty specified by method A:

$$u_C = \sqrt{u_A^2 + u_B^2} \quad (6)$$

And subsequently it added up more uncertainties from other factors measuring chain, until it is finally determined the overall uncertainty. If necessary, it is multiplied by the coefficient of expansion (k_u), which creates extended uncertainty:

$$U_C = k_u \cdot u_C \quad (7)$$

Extended uncertainty should be placed together with the result of each measurement. For more details about the expression and calculation of uncertainties, see the relevant standards and documents, like [3].

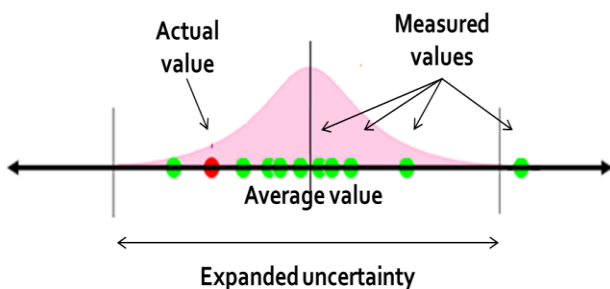


Fig. 1. Relationship between measured value, result of measurement (average value) and uncertainty

IV. RESUME

As you can see, the process of determining the non-statistical uncertainties is full of tasks that are highly prone to possible errors. In overall perspective we can say that the main reason is that a number of steps depend on a qualified assessment. The whole process is very subjective. In most cases, it is possible to eliminate subjectivity, but at the cost of the multiple complication of the entire measurement, the use of complex analytical and statistical methods, etc... This is for practical use quite inconvenient, time consuming and expensive. For these reasons, the subjectivity in determining the uncertainty of measurement

is practically impossible to avoid. In addition, there acts still one factor that has not been mentioned. It is the pressure on the evaluating person. Evaluation of uncertainty in measurement is performed frequently in order to demonstrate the quality of a product or service, obtaining certifications, etc. So usually there is pressure on favorable outcome of an uncertainty analysis, therefore practically finding the lowest uncertainty. For the same reason one can sometimes question the data in data sheets measuring instruments etc. It is clear that the aim of manufacturers is to sell the product, which entails exaggeration of its ability and unfortunately technical parameters. Not infrequently can be found the data sheets with incomplete data or with the data without these key conditions etc. All of this has once again an impact on the growth of subjectivity of the whole process and deformation of obtained results.

Referred findings may lead to the conclusion that, although the idea behind the system identification of uncertainties and the reasons for its use are good, it is a concept containing a number of systematic errors. This may result in a relatively easy to obtain, completely subjective results which would shift from the scientific issues, to pseudoscientific layer.

V. SOLUTION

A systemic solution of described problems leads to the creation of new normative documents that specifically mention uncertainties caused by this and that influence. It is a solution in specific and routine cases. Unfortunately, for various reasons, such data may be non-transferable and their applications may occur to the above errors. It is always necessary to carefully analyze and compare the conditions under which the data presented is valid, and in which it is performed for a specific measurement.

The most appropriate solution is to avoid the estimates and the constant scrutiny of the validity of the assumptions. Practically, this means a priori not to neglect various effects based on a subjective impression, so that the results cannot be affected, but rather verify this fact computationally, or better measurement. Most of the factors examined (interaction, probability distribution, limits, size and linearity dependencies) can be verified by measurement. As has been said, often it is not a measure in no way simple, quick and inexpensive; therefore it cannot be practically used. Possibility of experimental verification of proposition would never be condemned immediately; on the contrary it should be a major and integral part of all considerations.

Another important factor is the detailed knowledge of the performed measurements, its substance, used instruments, equipment and principles. It is the only way to correctly identify the influencing factors and correctly decide which can and which cannot be neglected. Overall, complete, relevant and detailed knowledge and information are very important. Many seemingly unimportant facts can have on the size measurement uncertainty surprising influence.

Last but certainly not least, is the ability to resist external pressures that can target a certain outcome of an

uncertainty analysis. You can easily affect the magnitude of the uncertainty by deliberate negligence of some of the important parameters without being obvious at first sight. Likewise, you can by "reasonable estimate" reach diverse numbers. Therefore, it is appropriate to replace the estimation with more suitable methods - measurement, data sheets, and results of similar measurements. A certain solution here is to undertake evaluation of uncertainties by an independent person / institution, or several persons / institutions.

Despite all efforts, you cannot subjectivity and therefore results "built on sand" completely avoid. But in accordance with these principles, it is possible to limit given influences on the minimum.

REFERENCES

- [1] O. Tůmová. Metrology and processes evaluation (Metrologie a hodnocení procesů). Prague: BEN, 2009.
- [2] H. Uhrová. Uncertainty of measurement and data processing. Physics Laboratory Exercises (Nejistoty měření a zpracování výsledků. Laboratorní cvičení z fyziky). Prague: Institute of Chemical Technology, Prague, 2001, pages 20-36.
- [3] EA Documents. Expression of the uncertainty of measurement in calibration (Vyjadřování nejistot měření při kalibracích). Prague: Czech Accreditation Institute - Public Service Company, 2001.
- [4] T. Panc, O. Tůmová, L. Kupka. Calibrating the contact temperature sensors without professional equipment (Kalibrace dotykových snímačů teplot bez profesionálního vybavení). Pilsen: The University of West Bohemia, 2012.
- [5] T. Panc, O. Tůmová. Evaluation of uncertainty of measuring chain for detecting the relative displacement and vibration of rotor (Vyhodnocení nejistot měřicího řetězce pro zjišťování relativního chvění a posuvu rotoru). Pilsen: The University of West Bohemia, 2012 unpublished.

Evaluation of mechanical parameters by the software for quality control

Markéta Růžková¹⁾ Olga Tůmová²⁾

Faculty of Electrical Engineering, University of West Bohemia, Univerzitní 26, 306 14 Pilsen, www.fel.zcu.cz

¹⁾ tel.: + 420 377 634 561, email: ruzkova@ket.zcu.cz

²⁾ tel.: + 420 377 634 563, email: tumova@ket.zcu.cz

Abstract - This article is focused on the statistical evaluation of mechanical parameters of metal retaining rings, which are the most expensive item in the construction of generators in the electrical engineering industry. The aim of this paper is to evaluate their mechanical parameters, whether they comply with the requirements which are imposed on them. The computer software for quality control are used for statistical evaluations, one of them is the STATISTICA[®].

The article deals with ways how to evaluate the parameters by using tools for quality control. This is to determine whether the process of supplier production is correctly set in the view of statistics. The basic guideline for the determination of the probability distribution of the process is descriptive statistics and the test of normality that proves that the measured values are in a normal distribution, and provides more options for data processing.

Keywords - quality control; statistical data processing; mechanical parameters; software; control charts;

I. INTRODUCTION

The statistical data processing is the most often used tool in the commercial sphere, in the data mining methods, in the science and engineering fields. Each producer tries to improve its production process. This can be simply achieved by using tools for quality control. The tools for quality control are used to evaluation and optimization the results of production. The software for the data evaluation is a tool for quality control. This article is focused on the implementation of statistical analysis of mechanical parameters of metal retaining rings.

II. SOFTWARE STATISTICA[®]

The computer software STATISTICA[®] is a comprehensive and integrated system for data analysis, including their graphical representation and a development of custom applications. It contains a wide range of basic and advanced analytical tools to be used in a variety fields (e.g. tools and analysis for data mining, business, social sciences, or engineering applications). All analytical tools, which are offered by this software, are available as a part of the integrated system. The needs and preferences of the user are very diverse, so the STATISTICA[®] offers one of the simplest and most flexible user environments. Therefore, the user does not

need any knowledge of the software technologies because it works automatically and intuitive. The outputs of the software are in the form of a protocol where the charts, tables, etc. are generated as a separate output graphic format.

III. INFORMATION ABOUT THE DATA

The data for processing were provided by company in the electrical engineering industry, which produces air-cooled generators and belongs to the world's major producers. The retaining rings are the highest stressed components within generators that demand high strength and ductility and a high corrosion resistance. Stressed material is due to stress in shrink fit, own weight, centrifugal loads of copper and a corrosion. Some of the most important parameters, or mechanical properties that were evaluated by mechanical tests and will be processed in this article, are the yield point R_p [MPa] and tensile strength R_m [MPa]. The measured values of each delivered retaining ring are listed by the producer in the delivery paper. The limit values for each type of machine that should not be exceeded are specified in the contract between the customer ("the producer of generators") and the supplier (producer of retaining rings). These data will be processed with regard to the required limits.

IV. STATISTICAL QUALITY CONTROL (SQC)

Statistical quality control is the application of statistical techniques in the quality control. SQC includes the use of regression analysis, tests of significance, acceptance sampling, control charts, distributions, and so on. Mechanical parameters as a yield point and tensile strength have been evaluated by the statistical computer software STATISTICA[®]. The results will be presented in the following chapters.

A. Descriptive Statistics

Descriptive statistics helps to pull useful information from data, whereas the probability provides, among others, a basic for inferential statistics. Descriptive statistics provides basic information about the tendency and variability of data. It is an analytical tool that generates a report of statistical criteria. The output of descriptive statistics is shown in the table 1.

TABLE I. DESCRIPTIVE STATISTICS

	Rp [MPa]	Rm [MPa]
Mean	1171,40	1204,39
Standard Error of Mean	1,56	1,29
Median	1172,00	1203,00
Modus	1163,00	1201,00
Standard deviation	25,61	21,27
Range	655,76	452,25
Minimum	1108,00	1152,00
Maximum	1245,00	1261,00
A number of values	271,00	271,00

This output has tabular values for the following:

- *Mean*: Arithmetic average of the data values. The mean of sample / population is the sum of all the responses / population divided by the *sample / population size* (the number of observation made or the number of items taken from a population).
- *Standard error*: The square root of the variance of sampling distribution of a statistic.
- *Median*: The data of *n* observations are ordered from smallest to largest. For an odd sample size, median is the ordered value at $(n+1)/2$. For an even sample size, median is the mean of the two middle ordered values.
- *Standard deviation*: A mathematical quantity that describes the variability of a response. It equals the square root of variance. The standard deviation of a sample (*s*) is used to estimate the standard deviation of a population (σ). (*Population*: The totality of items under consideration. *Sample*: A selection of items from a population).
- *Range*: For a set of numbers, the absolute difference between the largest and smallest value.
- *Minimum*: Lowest number in data set.
- *Maximum*: Largest number in data set.

B. Histogram

Histogram is a frequency diagram in which bars proportional in area to the class frequencies are erected on the horizontal axis. The histogram has the columns (categories) and the height of these columns corresponds to the frequency of each category. The width of each category corresponds to the class interval. The histogram provides a “visual test of normality”, that allows to identify the layout of values. As can be seen from the following histograms of the data (Fig. 1, 2) there is a normal distribution. Normal distribution is often useful to describe various physical, mechanical, electrical, and chemical properties. There is a histogram of a bell-shaped distribution, this shape is expected. The optimal number

of category in histogram is 8-12 (15). Any category should not be empty and any value must not be outside the category. Due to the large number of values in this case the number of category 15 was elected.

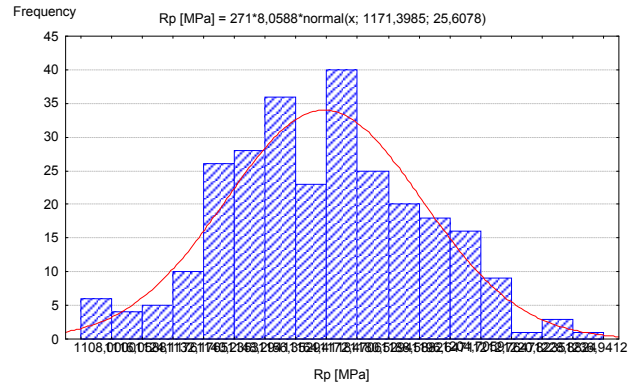


Fig. 1. Histogram of yield point

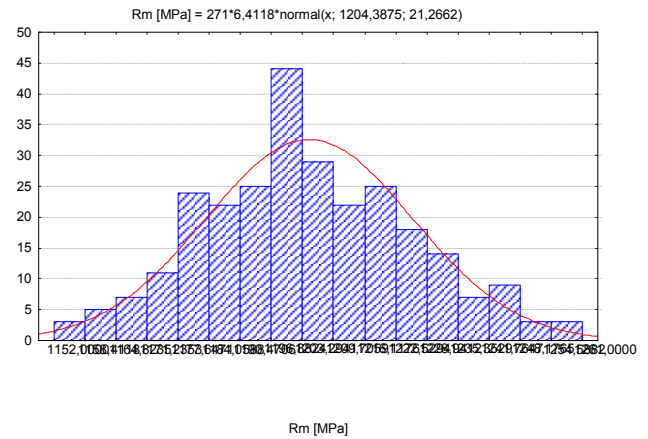


Fig. 2. Histogram of tensile strength

C. Normal Probability Chart

This type of chart is used to evaluate the normality of distribution. It provides a way how to examine the data, whether they are from the normal distribution. The selected variable is plotted against the values that correspond to the normal distribution. There is actually a normal distribution as the probability chart shows. There are not any anomalies (Fig. 3, 4). Therefore, if the observed values (plotted on the x-axis) have a normal distribution, all values should fall on a straight line that is displayed in the chart. If the values have not a normal distribution, the values should deviate from the line. If there is a problem in quality of spacing and the data create a clear pattern (e.g., shape of letter S, etc.), then it can be transform in some way before it will be used in procedures that provides a normality (e.g. logarithmic transformation is often used to modification the “ends” of the distribution).

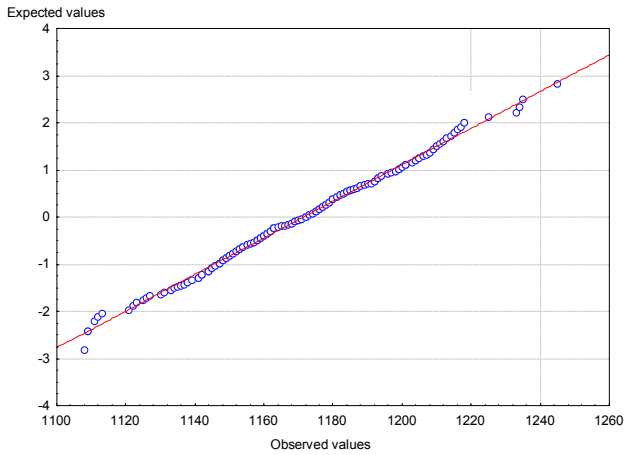


Fig. 3. Normal probability chart of yield point

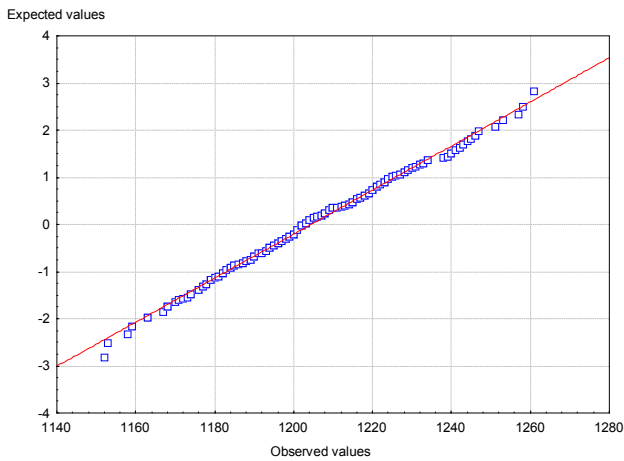


Fig. 4. Normal probability chart of tensile strength

The computer software STATISTICA® is based on the analysis of the probability density. It evaluates data to the y-axis, which represents the value of the σ (sigma). The probability density depends on the measured values that are related to the "width" of normal probability chart.

D. Control Chart

Control charts offer the study of variation and its source. Control charts can give not only process monitoring and control but also direction for improvements. Control charts are the most objective tool for quality control. They show that the producing process is set up correctly or incorrectly. In any production, the degree of quality has to be monitored to meet quality requirements.

There are two "enemies" of the production quality - the deviations from the requirements and excessive variability around these requirements. The software STATISTICA® provides the standard Shewhart control charts. Dr. Shewhart is credited with developing the standard control chart test based on 3σ limits to separate the steady component of variation from assignable causes. The type of chart can be selected in the software options (e.g. for individual values). The control limits or warning limits

can be set, if their values are known, if not, the data are evaluated automatically by the computer software. It means that SW sets tolerance (control) limits automatically on $\pm 3\sigma$ from the mean. The warning limits are set on $\pm 2\sigma$. It is a standardized procedure. If the limits are known, we set it manually. In this article there have been used both these options, so in the following figures the differences can be compared and evaluated. The producer indicates the minimum and maximum value of the yield stress and tensile strength, which may not be exceeded. These values are called lower and upper tolerance limit. The control charts are used to graphically illustrate that the production process is set up correctly in the view of statistics. That means that there are not any determinable causes of variability. The testing of metal retaining rings was carried out continuously, it is a continuous value. For this reason it has been used control chart by measurements. The charts for individual values were generated to make the results more accurate. As you can see from the charts in Fig. 5, 6 the process is set up correctly and the data values are in the tolerance limits which are set up by the producer. The upper tolerance limit is set to 1 280 MPa and the lower is to 1 100 MPa. The requirements for mechanical values are specified and easily achieved, however, the values can move closer to the upper limit.

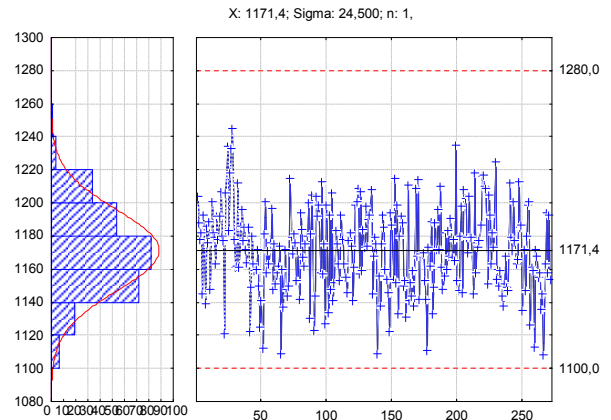


Fig. 5. Control chart (yield point)

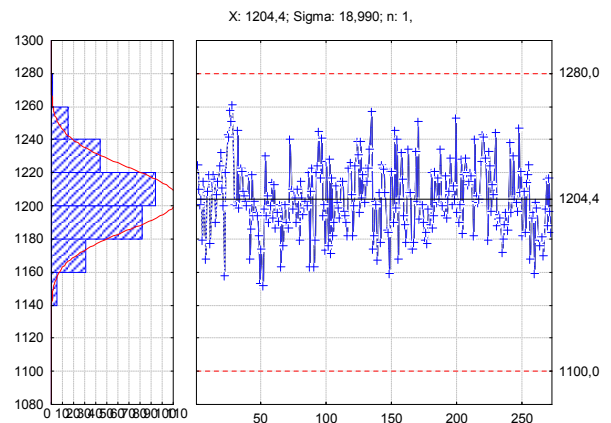


Fig. 6. Control chart (tensile strength)

In the Fig. 7, 8 are the charts with control limits $\pm 3\sigma$ from the mean and the tolerance limits are at the distance $\pm 2\sigma$ from the mean.

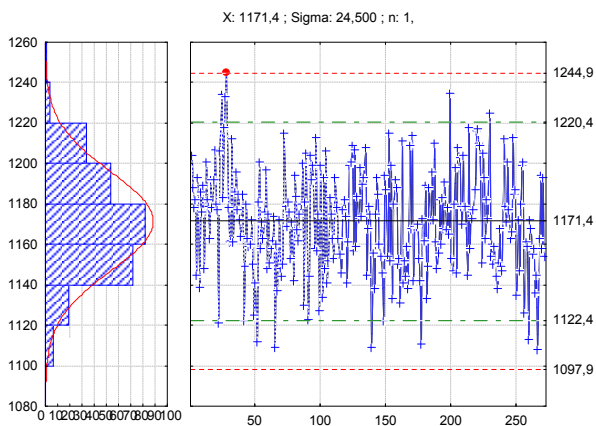


Fig. 7. Control chart with tolerance limits (yield point)

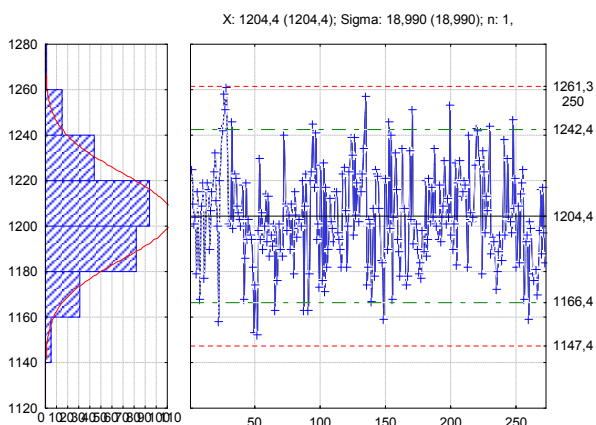


Fig. 8. Control chart with tolerance limits (tensile strength)

It would be possible to move the tolerance limits after evaluation of the difference between the tolerance limits and their possible shift. The requirements on the product would be tighten up. This would improve not only the quality, but also the prestige of the producer in the business.

V. CONCLUSION

The data that have been provided by the company of the electrical engineering industry are the mechanical parameters of retaining rings for generators. These have been analysed by the statistical computer software STATISTICA[®]. The monitored parameters - mechanical properties, are the yield point (Rp) and tensile strength (Rm). The main aim of this article is to get information about the data. Each of the parameters is the result of the material mechanical test. If we focus on the individual results, then the histograms demonstrate that it is a normal distribution. It is the expected result. This result has been confirmed by the test of normality. The normal probability chart has shown that the values have been on the straight line. The descriptive statistics has given the basic information about the measured data – about the mean, standard error of mean, median, modus, standard deviation, range, a number of values. The control charts are the most important results. The analysis clearly shows that the process is set up correctly. It does not exceed the specified limits. It is the result, which is achieved at the output.

Resulting from this the production process and the tolerance limit are set up correctly. The values of mechanical parameters have not been below the lower limit. It is the most important for the results of the mechanical tests. The higher values of mechanical properties are desirable for the components. Based on the results which have been provided by the software STATISTICA[®] we can say that the use of statistical computer software for data analysis is very useful. Thanks to it, it is possible to process the data and find the solutions for improve production.

REFERENCES

- [1] Forrest W. Breyfogle III, "Implementing Six Sigma: smarter solutions using statistical methods, 2nd ed.", John Wiley & Sons, Inc., Hoboken, New Jersey, 2003
- [2] J. Hendl, "Přehled statistických metod zpracování dat, analýza a metaanalýza dat", Portál, s.r.o., Praha, 2004
- [3] O. Tůmová, D.Pirich, "Nástroje řízení jakosti a základy technické diagnostiky", Západočeská univerzita v Plzni, 2003

Mathematical analysis of transformer insulation state

Miroslav Gutten¹⁾, Daniel Korenčiak²⁾, Milan Šebök³⁾, Mikołaj Bartłomiejczyk⁴⁾

Department of Measurement and Application Electrical engineering, Faculty of Electrical Engineering, University of Žilina, Univerzitná 1, 010 26 Žilina, Slovakia

¹⁾ tel: +421 41 513 2127, email: miroslav.gutten@fel.uniza.sk ,

²⁾ tel: +421 41 513 2135, email: daniel.korenciak@fel.uniza.sk

³⁾ tel: +421 41 513 2126, email: milan.sebok @fel.uniza.sk,

⁴⁾ Department of Electrical Transport Engineering , Faculty of Electrical and Control Engineering, Gdańsk University of Technology, ul. Sobieskiego 7, 80-216 Gdańsk, Poland, E-mail: mbartlom@ely.pg.gda.pl

Abstract—The paper is presenting mathematical model – TOPSIS and CI method, which was utilized on insulating state of distribution transformer to analyze and sensibility of individual measurements methods mutual comparison. We can uniquely determine importance of these measurements methods with this mathematical apparatus in these measurements methods in insulating state of transformers.

Keywords— transformers, insulation, composite indicator, TOPSIS method

I. INTRODUCTION

With regard to the development of the world and national economies, also control, maintenance and its analysis by mathematic calculations becomes an important sphere [1], [2], [19], [20], [26]. This sphere also includes power transformers, where their proper function has a positive impact on the trouble-free supply of electricity and heat for industries and households. It is therefore necessary, in the absence of scientific and research potential in distribution organizations, to achieve the objectives of the proposed activities, i.e. in-depth analysis of undesirable impacts on the state of devices, design of measurements and their verification, and design of new diagnostic procedures for improving reliability of power transformers.

In case we want to determine the real insulating state of a transformer and then lifetime of insulation, is necessary to analyze some measurements in individual types of assays and then determine their exactness and reliability with mathematical models. We can exactly prove the importance of these assays by mathematical and statistical models in the field of analysis of the insulating state of transformers [23], [24].

For mathematical analyzing these assays measurements we chose within the frame of comparison of the degree of sensitivity in single methods of the insulating state of distribution transformers 110/22kV:

- insulation resistance and absorption coefficient R_{60}/R_{15} ,
- dissipation factor and capacity: $\tan\delta$ and C ,
- relative change of short-circuit voltage dU_k .

II. DESCRIPTION OF CHOSEN MEASUREMENTS

The oldest and easiest method of inspecting the state of insulators is by means of insulation resistance measuring. The main disadvantage of this method is that insulation resistance does not only depend on the state of insulation but also on its type and dimensions. Insulation resistance method can be used to evaluate the state of insulation of electric device only on the basis of previous experience with the same insulation on the same devices.

The method is based on the following principle: change in insulator state causes change in time dependence of a current flowing through the insulator by direct voltage [8]. A current flowing through an insulator consists of a time-decreasing absorption element and stabilized element. The more water content there is in the insulation, more apparent increase of the stabilized element of a current is the observed comparing to the absorption element. The absorption element of a current has a low effect on the characteristics of time dependency in relation to the current as well as the resistance, and flattens with increasing humidity.

Utilizing this knowledge for evaluation of the insulation state does not require determining the full time dependence of a current. It is enough to determine the value of a current (resistance) in two different moments from the time of connection to direct voltage. The ratio of these two values defines the state of insulation and is called the polarizing index. Since it is a non-dimensional parameter, it does not depend on the dimension of insulation. Polarizing index is measured after 1 and 10 min or after 15 and 60 s.

So as to better illustrate the change in values of the polarizing index, it needs to be expressed by both elements of a current – absorption element i_a and stabilized element i_∞ .

The humid and contaminated insulation is determined by i_∞ , therefore numerator and denominator are very close values and their ration tends towards 1. On the other hand, the dry and clean insulation which is in good condition has a very low stabilized current and the time dependent element i_a is dominant. Thus, the fraction value is noticeably higher than 1. The absorption coefficient of new transformers before usage in operation should reach at least 1,3.

The measurements of the dissipation factor ($\text{tg}\delta$) and the capacities of transformer windings are used for additional determination of the insulation quality as whole or only of some parts of the transformer. The value of $\text{tg}\delta$ indicates presence of polar and ion compounds in oil and it also determinates the aging of oil. The degree of oil humidity can be measured by temperature dependence of $\text{tg}\delta$ [8].

Changes in the state of short-circuit voltage dU_k (impedance) express geometrical winding movements and their construction changes in transformers. This technical condition depends on the thermal and mechanical effects of short-circuit currents.

By means of measurement of short-circuit voltage we can identify the mechanical and insulating deformation of the winding of a transformer.

Absolute value of short-circuit voltages usually are not sufficient to qualify the condition of winding without knowledge of their evolution in time, so the analysis is based on comparison of values for a specified time of operation of a transformer.

III. COMPOSITE INDICATOR AND TOPSIS METHOD

A composite indicator (CI) is a mathematical aggregation of a set of individual indicators that measure a multi-dimensional concept. There are m compared alternatives; each alternative consists of n sub-indicators x_{ij} . For each alternative is evaluated CI. CI is used for the performance measurements, benchmarking, via providing an aggregated performance index in various fields such as Human Development Index, Road Safety Index [2], [3], [16]–[18].

$$\begin{matrix} \text{alternative 1} \\ \text{alternative 2} \\ \vdots \\ \text{alternative } m \end{matrix} \begin{bmatrix} x_{11} & x_{12} & \cdots & x_{1n} \\ x_{21} & x_{22} & \cdots & x_{2n} \\ \vdots & \vdots & \ddots & \vdots \\ x_{m1} & x_{m2} & \cdots & x_{mn} \end{bmatrix} \rightarrow \begin{bmatrix} CI_1 \\ CI_2 \\ \vdots \\ CI_m \end{bmatrix}$$

Fig. 1. CI construction of graphical representation.

The graphical representation of CI construction is illustrated on Fig. 1. There are m compared alternatives, each alternative consist n sub-indicators x_{ij} . For the each alternative is evaluated CI indicator. Sub-indicators usually have no common measurable units.

Generally, the structure of CI can by expressed by the equation:

$$CI = \sum_{i=1}^n w_i I_i \quad (1)$$

where w_i means weight assigned to indicator i .

The TOPSIS method is used to analyze a multi-criteria decision making problem with m alternatives with n criteria. In the TOPSIS method, the best alternative should have the shortest Euclidean distance from the positive ideal solution

(PIS) and the longest distance from the negative ideal solution (NIS). The PIS is a hypothetical solution which maximum values from the database of all alternatives, and the NIS is a hypothetical solution which minimum values from the database of all alternatives. TOPSIS defines an index called relative closeness to the PIS and remoteness from the NIS [7]. This index can be used as a CI of alternatives.

IV. ASSIGNING INDICATORS WEIGHTS BY FACTOR ANALYSIS

The values of the weights will be assigned by factor analysis. Factor analysis method is based on a reducing the dimensions of the problem, where the n dimensions are transformed into a p smaller number unobserved variables called factors. The idea of factor analysis can be described by the formula:

$$X = FY + E \quad (1)$$

where X – matrix of the input data, Y – matrix of uncorrelated common factors, F – matrix of factor loadings, E – matrix of the specific factors.

The dimensionality of matrix F depends on the selected number of the factors. Each factor explains a part of the variance of the input data.

The approach to the calculations of weight factors suggested in [2] consist the following steps:

Step 1: Define a number of factors:

Chosen factors should explain 70 – 80% of the variance of the input data. Usually there are 2 or 3 factors.

Step 2: Define squared factor loadings:

Squared factor loadings can be described by the formula:

$$u_{ij} = \frac{a_{ij}^2}{\sum_{k=1}^m a_{kj}^2} \quad (2)$$

where m – the numbers of the factors.

Step 3: Calculate preliminary weights:

The preliminary values of the weights can be expressed as:

$$w'_j = \frac{\max_k u_{kj}}{e'_k} \quad (3)$$

where e'_k is the relative variation explained in the data sheet:

$$e'_k = \frac{e_k}{e} \quad (4)$$

where e is total variation explained by chosen m number of the factors, e_k is variation explained by the k factor.

Step 4: Rescaling of the weights:

The final values of the weights are described by the formula:

$$w_j = \frac{w'_j}{\sum_{i=1}^m w'_i} \tag{5}$$

V. RESULTS OF THE CALCULATION

Assigning of the weights of the criteria by factor analysis was the first step of the calculation. Two factors in factor analysis were chosen: factor 1 represents the parameters R_{60}/R_{15} and C , and explains 38% of total variance; factor 2 represents the parameters dU_k and tangent delta, and explains 34% of the variance. The values of weights are presented in Table I.

TABLE I. TABLE STYLES CALCULATED VALUES OF THE WEIGHTS

Parameter	Weight
R_{60}/R_{15}	0,24
dU_k	0,36
tangent delta	0,17
C	0,22

Assigned weights of the criteria were applied to fuzzy TOPSIS model. Table II presents the results of the calculations as well as the data for four sub-indicators.

To investigate the impact of criteria weights was realized the sensitivity analysis – were calculated the values of CI for different sets of weights. The 11 experiments were conducted, the sets of weights are presented in Table III, and results of the sensitivity analysis are showed in Fig. 2. There is shown range of standard deviation of CI calculated for 11 sets of weights and CI calculated in previous part of paper.

It is noticeable, that the assigned values of CI are placed in the range of the standard deviation, what confirm the reliability of the fuzzy TOPSIS method. In Fig. 3 it is presented sensitivity analysis regarding the final outcome ranking – the technical condition of each transformer referred to the other transformers.

Better position in ranking means better technical condition – higher CI. The average position in sensitive analysis in every case is located closely to position based on the previous assigned value of CI. In some cases is visible significant between the maximal and the minimal position – fg. T8, T10, T12. It can be explained by the disproportion between several technical parameters of transformer. That fact indicates a prerequisite of ill-natured technical condition of transformer and can be used to identify a failure.

To investigate the accuracy of presented fuzzy TOPSIS method was realized the cluster analysis. Cluster analysis is a multivariate technique which informs about similarity in the data set. Clustering is task of assigning objects into groups – cluster. The objects in the same cluster are more similar to each other than to those in other clusters.

TABLE II. FOUR SUB-INDICATORS AND CI VLUES FOR THE 13 TRANSFORMERS

Tr	Sub-indicators				Results of the calculations		
	$\frac{R_{60}}{R_{15}}$	dU_k [%]	$\tan\delta$	C [pF]	d^+	d^-	CI
T1	1,36	0,47	0,0217	2881,4	0,53	0,41	0,43
T2	1,37	8	0,0186	4746,7	0,51	0,44	0,46
T3	1,58	4,5	0,0123	2996,5	0,12	0,81	0,87
T4	1,44	7,9	0,0075	2731,5	0,41	0,49	0,54
T5	1,31	42,7	0,0046	1957,5	0,74	0,21	0,22
T6	1,55	32,4	0,0135	3815,5	0,27	0,76	0,74
T7	1,25	0	0,0424	3940,0	0,75	0,35	0,32
T8	1,31	21,4	0,0177	4882,0	0,66	0,31	0,32
T9	1,30	8,95	0,0160	4235,3	0,64	0,39	0,38
T10	1,39	2,41	0,0122	2236,0	0,54	0,43	0,44
T11	1,38	8,93	0,0153	3825,2	0,51	0,43	0,46
T12	1,32	20,4	0,0126	4030,7	0,66	0,31	0,32
T13	1,31	3,64	0,0187	3775,0	0,64	0,39	0,38

TABLE III. SETS OF WEIGHTS FOR SENSITIVITY ANALYSIS

Parameter	R_{60}/R_{15}	dU_k	\tan	C
Set 1	0,25	0,25	0,25	0,25
Set 2	0,5	0,167	0,167	0,167
Set 3	0,167	0,5	0,167	0,167
Set 4	0,167	0,167	0,5	0,167
Set 5	0,167	0,167	0,167	0,5
Set 6	0,4	0,4	0,1	0,1
Set 7	0,1	0,4	0,4	0,1
Set 8	0,1	0,1	0,4	0,4
Set 9	0,4	0,1	0,1	0,4
Set 10	0,1	0,4	0,4	0,1
Set 11	0,1	0,4	0,4	0,1
Set 12	0,1	0,4	0,4	0,1
Set 13	0,24	0,36	0,17	0,22

The classification aims to reduce the dimensionality of a data set by finding the similarities between classes [2]. A dendogram is the result of method and illustrates the relationships between objects. On Fig. 4 is shown dendogram obtained by the clustering.

It is seen, that the location of the transformers on dendogram corresponds with the values of CI. Transformers with the similar value of CI are located near on the dendogram, e.g. T8 and T12, T9 and T13. The most “separately” located are cases T3, T6, T5 and T7. It may be explained by CI values: T3 and T6 got the best rating, T5 and T7 one of the worst. Thus, the position of points can be used as an indicator of transformer insulation condition.

VI. CONCLUSION

On the basis of summary results of the mathematical CI model, there can be set optimized modern techniques for the diagnosis of insulation state chosen oil transformers, thereby a higher quality of trouble-free distribution of heat and electricity will be achieved.

A composed indicator has been accepted as a useful tool in many non-technical areas, such economy, society, and environment [14], [15]. In this paper is presented application of CI in field of technical sciences. Beside this, other presented methods of MCDA (e.g. hierarchical clustering) can be used for evaluation the technical condition of electrical equipment.

ACKNOWLEDGMENT

This work was supported by the Grant Agency VEGA from the Ministry of Education of Slovak Republic under contract 1/0624/13.

REFERENCES

- [1] P. Zhou, B. W. Ang, K. L. Poh, "A mathematical programming approach to constructing composite indicators", *Ecological economics*, vol. 6, pp. 291-297, 2007.
- [2] M. Nardo, M. Saisana, A. Saltelli, S. Tarantola, A. Hoffman, E. Giovannini: „Handbook on constructing composite indicators: methodology and user guide”, *OECD Statistics Working Paper*, vol.3, 2005.
- [3] E. Hermans, "A methodology for developing a composite road safety performance index for cross-country comparison", PhD thesis, Universiteit Hasselt, 2009.
- [4] C. B. Alphonse, "Application of the analytic hierarchy process in agriculture in developing countries", *Agricultural Systems*, no. 53, pp. 97-112, 1997.
- [5] J. Jurčík, "Analysis of Insulating State on Transformer Model Using PDC Method", *Proceedings of 9th International Conference 2012 ELEKTRO Žilina-Rajecké Teplice*, 2012.
- [6] P. Hamalainen, O. Seppalainen, „The analytic network process in energy policy planning”. *Socio-Economic Planning Sciences*, vol. 20, no. 6, pb 399-405, 1986.
- [7] R. Ramanathan, „A note on the use of the analytic hierarchy process for environmental impact assessment”, *Journal of Environmental Management*, no. 63, pp. 27-35, 2001.
- [8] C. Kahraman, "Fuzzy Multi-Criteria Decision Making-Theory and Applications with Recent Developments", Springer, 2008.
- [9] T. Gwo-Hsung, H. Jih-Jeng, "Multiple Attribute Decision Making – Methods and Applications", CRC Press Taylor & Francis Group, 2011.
- [10] S. M. Hatefi, S. A. Torabi, "A common weight MCDA-DEA approach to construct composite indicators", *Ecological Economics*, vol. 70, pp 114-120, 2010.
- [11] B. Łazarz, H. Madej, A. Wilk, T. Figlus, G. Wojnar, "Diagnozowanie złożonych przypadków uszkodzeń przekładni zębatach", Wydawnictwo Instytutu Technologii Eksploatacji – Państwowego Instytutu Badawczego Katowice-Radom, 2006.
- [12] A. Wilk, H. Madej, T. Figlus, "Analysis of the possibility to reduce vibroactivity of the gearbox housing", *Maintenance and reliability*, no. 2, 2011.
- [13] Bartłomiejczyk M., "Análiza efektywnosti rekuperace trolejbusové dopravy metodou Monte Carlo". *XLIII. Sešit Katedry Elektrotechniky*. VŠB Ostrava, Ostrava 2010
- [14] S. Judek, J. Skibicki, "Wyznaczanie parametrów elektrycznych trakcyjnego układu zasilania dla złożonych warunków ruchu przy wykorzystaniu programu pspice", *Przegląd Elektrotechniczny*, no. 12, pp. 270-273, 2009.

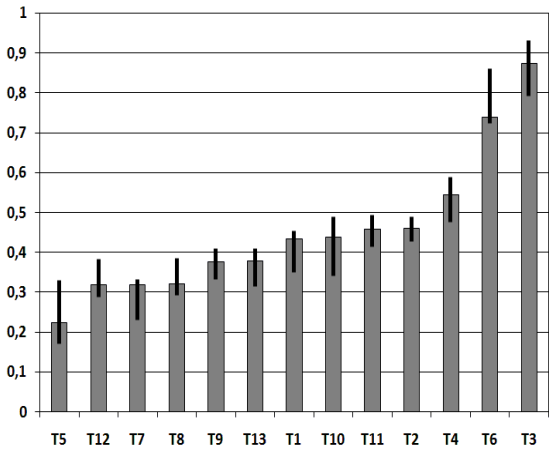


Fig. 2. The results of the sensitivity analysis - values of CI and standard deviation

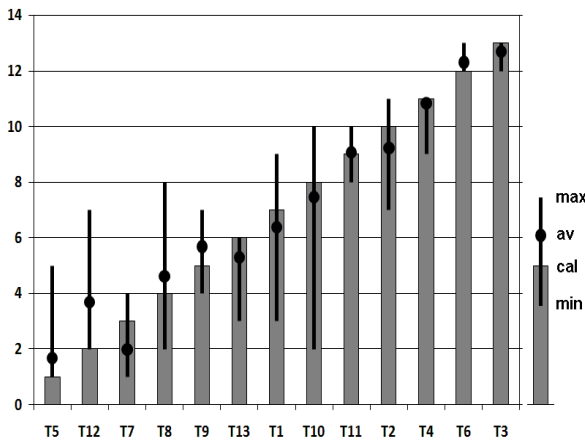


Fig. 3. The results of the sensitivity analysis - ranking of transformers, max, min, av - the highest, lowest, average ranking position obtained in sensitivity test, cal - position corresponding with CI value, better position means better CI value

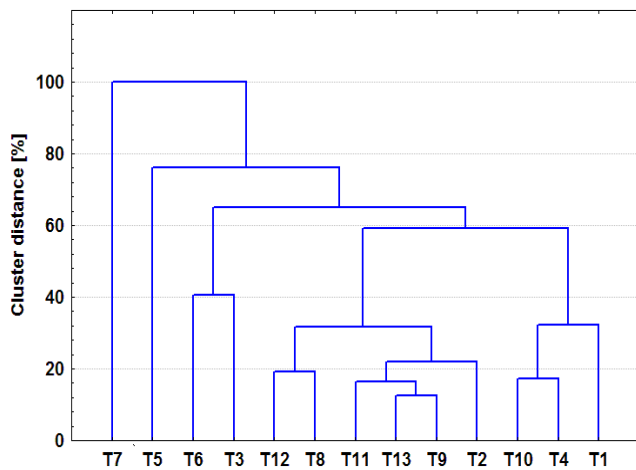


Fig. 4. Dendrogram based on hierarchical clustering

Analysis of Ignition Systems

Milan Šebök¹⁾, Miroslav Gutten²⁾, Ľubomír Ostrica³⁾ Daniel Korenčiak⁴⁾

Department of Measurement and Application Electrical engineering, Faculty of Electrical Engineering,

University of Žilina, Univerzitná 1, 010 26 Žilina, Slovakia

¹⁾ tel: +421 41 5132129, email: milan.sebok@fel.uniza.sk,

²⁾ tel: +421 41 5132110, email: milan.gutten@fel.uniza.sk,

³⁾ tel: +421 41 5132124, email: lubomir.ostrica@fel.uniza.sk,

⁴⁾ tel: +421 41 513 2135, email: daniel.korenciak@fel.uniza.sk

Abstract— Ignition systems even in its simplest form represent electrical systems which produce voltage waveforms in a form of pulses in complex shape. For the diagnosis of these systems is necessary to use such diagnostic systems, which allow to record these waveforms for next analysis. In the presented contribution we deal with possibilities of analysis and investigation of waveforms, primary and secondary circuit fully electronic ignition systems.

Keywords— DFS ignition systems, analysis, LabVIEW, high-voltage waveforms .

I. INTRODUCTION

Distributorless ignition system (DIS) is ignition system which distributes high voltage to each spark plug without using mechanic distributor. High voltage shall be achieved to create a spark at the spark plug igniting the mixture through a high-voltage coil (transformer). High-voltage outlets in distributorless ignition system are directly applied to plugs, thus increasing the number of ignition coils. An immediate flash-over in the cylinders is necessary to determine by a separate switch controlling of transformer primary circuits. In practice are used two solutions which differ in the number of ignition coils.

II. THE DFS IGNITION SYSTEM

Ignition system with coils with dual secondary windings DFS (Doppelfulen Spule) is ignition system where high voltage is transported directly on spark plugs and flash-over occurs at a certain moment on the two plugs at the same time. Fig.1 shows simplified scheme of the DFS system.

At some point of flash-over on two spark plugs at the same time a pulse of high-voltage appears on the secondary winding of the transformer, space between electrodes of the spark plug ionizes the electrical strength of the space exceeded by high voltage and current discharge flows through a spark. The engine operating parameter signals enter into the control unit by which the control unit is creating control pulses for the final stages of ignition coils (Fig.1). The operating signals are needed to calculate the specific moment in which the high-voltage pulse should occur.

In the fig.2 is an example of voltage waveforms (pulses) of the primary and secondary winding of the transformer.

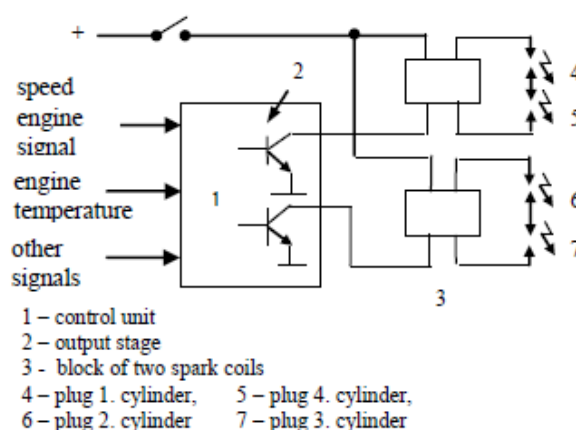


Fig. 1. Simplified scheme of the ignition DFS

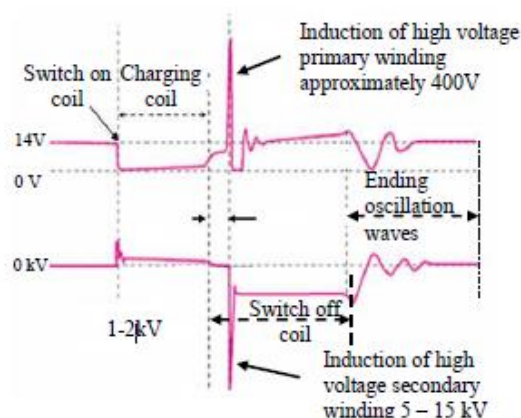


Fig. 2. The voltage waveforms of the primary and secondary winding of the transformer

The spark has to flash over in cylinder near the top dead center in compression stroke for right engine running.

III. THEORY OF PHYSICAL MODEL

In analysing the spark plug discharge problem, the spark plug current discharge channel is an overriding factor. As current i shooting through the unshielded centre electrode is the dominant ignition current, the discharge channel and the corresponding circuit model of the spark plug are shown below in Fig.3 [6].

In Fig.3, R_r is the series resistance and its value can be given by the manufacturers; r_g is the air-gap resistance of the spark plug; and C_q , C_r and C_p are the parasitic capacitances between the centre electrode and the shell.

Circuit is getting from the steady state into a new due to active element parameter changes i.e. connecting or disconnecting the voltage source or current.

Fig.4 shows the ignition system circuit model with the following simplifications: 1) the parasitic capacitances between the ignition system's modules are neglected and are finally added to the whole system; 2) the ignition coil circuit model is simplified here, which is expatiated in [7].

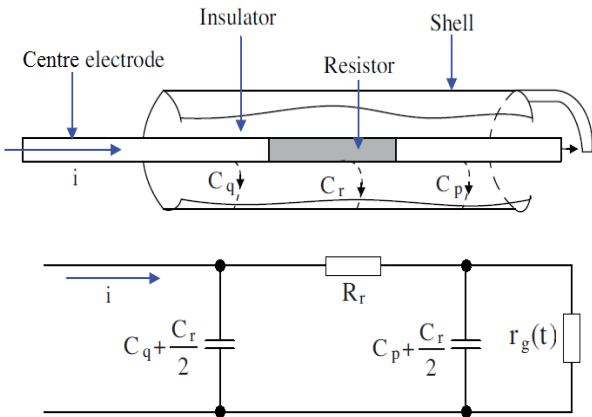


Fig. 3. The discharge channel and circuit model of the spark plug

From the equivalent circuit of the ignition on Fig.4 is obvious, that change in steady-state to another is associated with a change of electromagnetic energy $W(t)$ of circuit.

This can be distributed into electric field energy accumulated in the capacitor circuit and magnetic field energy accumulated in inductors

$$W(t) = \sum_{k=1}^{n_1} W_{ek}(t) + \sum_{k=1}^{n_2} W_{mk} \quad (1)$$

where n_1 is the number of capacitors and n_2 is the number of inductors.

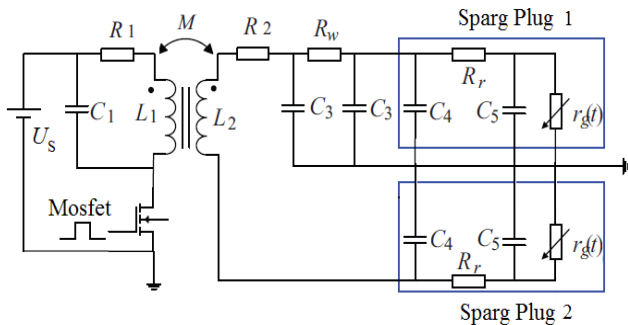


Fig. 4. The circuit model of the ignition system EFS [5]

In Fig.4 are valid there equations [5]:

$$C_4 = C_q + \frac{C_r}{2}, C_5 = C_p + \frac{C_r}{2}, C_3 = \frac{C_w}{2} \quad (2)$$

where U_S is voltage of the DC power supply, R_1 and R_2 are respectively the resistance of the primary and the secondary winding, L_1 and L_2 are respectively the inductance of the primary and the secondary winding, M is the coefficient of mutual inductance between the primary and the secondary winding, C_w is the parasitic capacitances between the high-voltage wire and the shell, and R_w is the resistance of the high-voltage wire.

IV. ANALYSIS AND MEASUREMENT OF HIGH-VOLTAGE WAVEFORMS OF IGNITION

The sides of primary coils are powered by the pulse voltage and switching by output stages to frame, or the ending degrees are integrated into module of coils. The control unit controls the switching and injection, and each coil is switched once per one cycle of the motor by control pulses Fig.5.

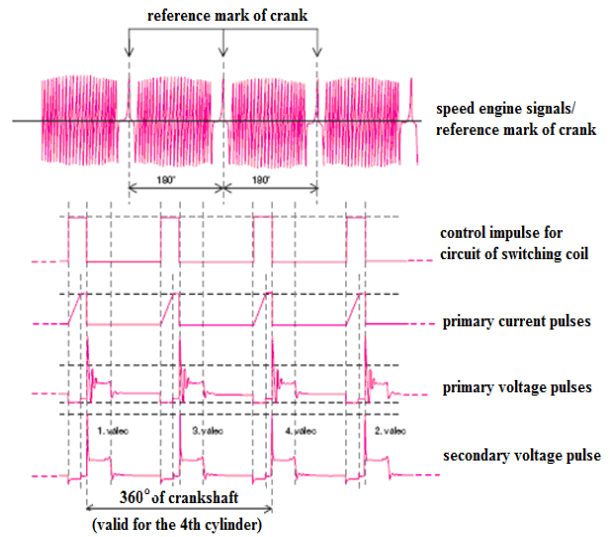


Fig. 5. Synchronization of switching and the emergence of high-voltage pulses

Synchronization of switching is taken away from the crank speed. Obviously for the synchronization are needed another signals for adaptation of the ignition immediate operating conditions (engine load signal, temperature and the intake air quantity, throttle position etc.). [4]

To the control unit are entering signals of engine operating variables. Ignition with EFS is not sufficient just with crank speed signals because each ignition coil receives one control pulse for two turns of crank but from the signal reference mark the control unit do not know whether the piston of cylinder is at the top dead center compression stroke or at exhaust stroke. It is not possible to decide whether the spark-over is conducted in the 1st or

4th cylinder and therefore is needed synchronization pulse which is a control pulse cam Fig.6.

On the basis of cam and crank signals the control unit is creating control pulses for final stages of each ignition coil Fig.5

In the secondary circuit coils is high-voltage diode connected. For each of the cylinders in the moment of switching the primary winding on the secondary side there is a high voltage pulse (1-2kV). In ignition systems with distributor and the cylinder located outside circuit is disconnected. This voltage do not shift air gap between the plug electrodes and thus undesirable spark on the spark plugs does not skip. [4]

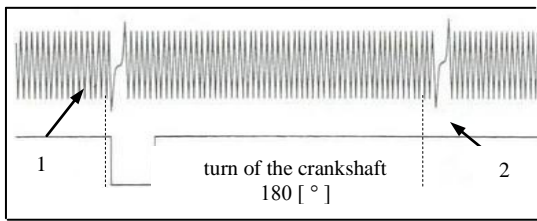


Fig. 6. Speed engine signal / reference mark of crank (1) and cam position signal (2).

In DFS system high voltage pulse of secondary circuit breaks dielectric area on the distance given by the sum of the distances of the electrodes connected distance given by the sum of the distances of the electrodes connected in series spark plugs in series and therefore there is no discharge. If the primary circuit switch off it incurred substantially higher voltage which breaks through the area between two electrodes of spark plug and that results in a spark.

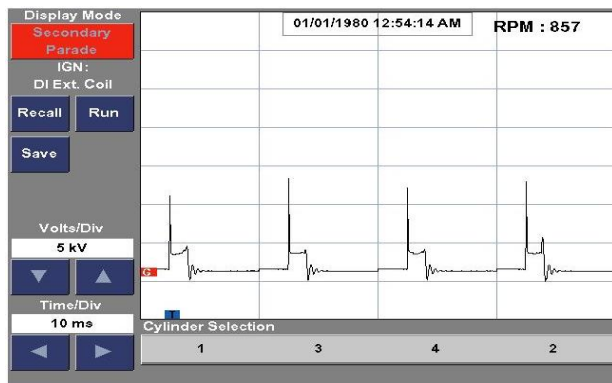


Fig. 7. Ignition pulses of cylinders in the DFS system

V. SIMULATION WAVEFORMS

For a deeper analysis can be used simulation by programming environment NI Labview, where you can set up through the mathematical model of such operations during the subsequent simulation of error conditions spark pulses Fig.8.

According to Fig.8 we can be divided into waveform for five periods, which we then mathematically spread (interval t_1 until t_5):

Interval t_1 : $u(t) = 0$

Interval t_2 : $u(t) = l \cdot \cos(n \cdot t) e^{-d \cdot t}$

l – the voltage in the steady state is voltage constant, n – determines the number of amplitudes, k – amplitude, d – specifies the attenuation.

Interval t_3 : $u(t) = a \cdot t + c_1$

a – is constant of inclination of the line, c_1 – determines the initial state (final state in the interval t_2).

Interval t_4 : $u(t) = \frac{1}{b\sqrt{\pi}} \cdot e^{-t^2/b^2} + c_2$

b – amplitude constant, c_2 – determines the initial state (final state in the interval t_3).

Interval $t_{5,1}$: $u(t) = -m \cdot t + c_3$

m – is constant of inclination of the line, c_3 – determines the initial state (final state in the interval t_4).

Interval $t_{5,2}$: $u(t) = k \cdot \cos(n \cdot t - h) e^{-d \cdot t} + c_4$

n – determines the number of amplitude, d – specifies the attenuation, h – shift of course, c_4 – determines the initial state (final state in the interval t_5).

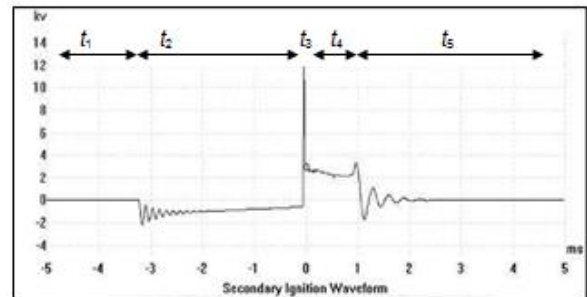


Fig. 8. Model of ignition voltage waveform

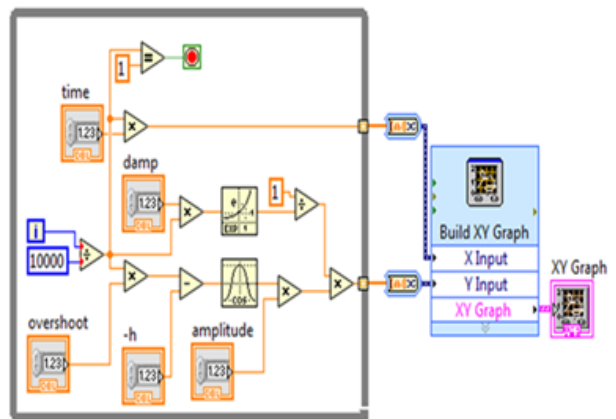


Fig. 9. The sequence of program in Labview

In Fig.9 is presented by sequence program of high voltage waveform ignition model EFS with a faulty diode and simulation graph on Fig.10, which shows the comparison of malfunctioning ignition coil – sinusoidal course with decreasing amplitude at switching on primary side of transformer and switching off secondary side of transformer the shutdown transformer (faulty diode) and graph with the end of burning sparkle without damped oscillations (correct operation of the ignition coil).

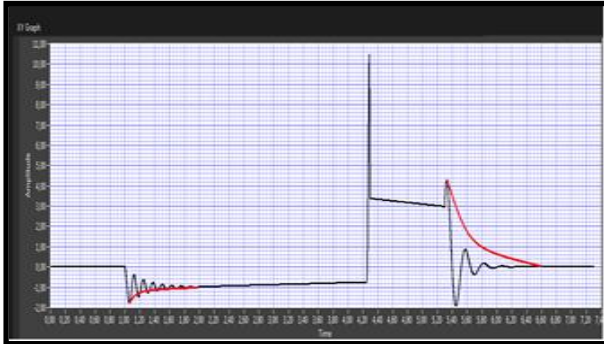


Fig. 10. Simulating spark waveforms during correct and incorrect operation

REFERENCES

- [1] Bosh, van den J., Duijm, N.: Outflow and Spray Release, In: VROM, Hague, 2005
- [2] Li, B., Zhao, Y., Sun, P.: The Study of Ambient Condition on the Performance of Marine Diesel Engine, In: Journal of Harbin Engineering University, Vol. 27/2006
- [3] Šebök, M.: Investigation of electrical properties of sensors and non-electrical quantities, In: PhD thesis, University of Zilina, 2007
- [4] Pulkrabek, W.: Engineering Fundamentals of the Internal Combustion Engine, In: Pearson Prentice Hall, Plateville, 2003
- [5] Wang, I.Q. et al.: Circuit model and parasitic parameter extraction of the spark plug in the ignition system, In: Turk J Elec Eng & Comp Sci, Vol. 20, No.5, 2012
- [6] Soldera, F.A., Mucklich, F.T., Hrastnik, Kaiser, K., T.: Description of the discharge process in spark plugs and its correlation with the electrode erosion patterns, In: IEEE Transactions on Vehicular Technology, Vol. 53, pp. 1257-1265, 2004
- [7] Jia, J., Wang, Q., Yu, J., Zheng, Y.: Wideband equivalent circuit model and parameter computation of automotive ignition coil based on finite element analysis, In: Application Computational Electromagnetics Society Journal, Vol. 25, pp. 612-619, 2010.
- [8] Tarimer, I., Güven, M., E., Arslan, S.: Computer aided design of an electromagnetic ignition coil for high speed benzene engines, In: Przegląd elektrotechniczny = Electrical Review, Vol. 87, 2011, No. 2, pp. 230-235
- [9] Šimko, M., Chupáč, M.: The theoretical synthesis and design of symmetrical delay line with surface acoustic wave for oscillators with single-mode regime of oscillation, In: Przegląd elektrotechniczny = Electrical Review, Vol. 88, 2012, No. 12A, pp. 347-350
- [10] Xianmin LI, Xi LU, Guangde HAN: The Design and Simulation Research of Mazda6 Hybrid Electric Vehicle, In: Przegląd Elektrotechniczny = Electrical Review, Vol. 88, 2012, No. 3b, ISSN 0033-2097, p. 44-47
- [11] Šimko, M., Chupáč, M.: Method of measurement of radio transmitters antenna systems. In: Przegląd Elektrotechniczny = Electrical Review, Vol. 86, 2010, No. 12, ISSN 0033-2097, p. 342-344

Acoustic investigation of magnetic fluid based on transformer oil TECHNOL

J. Kúdelčík¹⁾, P. Bury¹⁾, M. Šebök²⁾

Department of physics¹⁾, Department of measurement and applied electrical engineering²⁾,
Žilinská univerzita v Žiline, Univerzitná 1, 010 26 Žilina

¹⁾ tel: +421 41 513 2310, email: kudelcik@fyzika.uniza.sk, ²⁾ milan.sebok@fel.uniza.sk

Abstract— The structural changes in a magnetic fluid upon the effect of an external magnetic field and temperature were studied by acoustic spectroscopy. The attenuation of acoustic waves was measured as a function of magnetic field in the range of 0 - 300mT and as a function of temperature in the range of 15 - 30 °C. The strong influence of the steeped magnetic field on the acoustic wave attenuation was detected and its hysteresis was observed, too. In magnetic field, there are dominant interactions between the magnetic field and the magnetic moment of the nanoparticles. These interactions lead to the aggregation of magnetic nanoparticles and clusters formation. However, the temperature of magnetic fluids has very important influence on the obtained dependencies, where the mechanism of thermal motion acts against the cluster creation. The acoustic spectroscopy was used to study the anisotropy of transformer oil-based magnetic fluids upon the effect of an external magnetic field and temperature. The observed influences of magnetic field and temperature on the investigated magnetic liquids structure are discussed.

Keywords — magnetic field, transformer oil; magnetic liquid; acoustic attenuation.

I. INTRODUCTION

A transformer oil based magnetic fluids are colloidal suspensions of magnetic nanoparticles covered with a surfactant layer in transformer oils [1], [2] as shown in Fig. 1. Particles of this size are monodomain and interaction between them may lead to their agglomeration and subsequent sedimentation. To avoid these undesired side effects magnetic particles can be coated by a surfactant that produce entropic repulsion. The macroscopic magnetic properties of the magnetic fluid are determined by the orientation of magnetic moments of nano-particles in the external magnetic field. The transformer oil with magnetic nanoparticles that is usually used for both high voltage insulation and power electronics cooling is subjected to extensive research to enhance its characteristics. The magnetic fluids should have better insulating and thermal properties. These types of magnetic fluids can be considered to be the next-generation heat transfer fluid as they offer exciting new possibilities to enhance heat transfer performance compared to pure liquids. The dielectric breakdown strength of transformer oil, however, is strongly influenced by the aggregation effects of magnetic nanoparticles and can induce electric breakdown [4], [5].

One of the methods of studying changes in the magnetic fluid structure is based on the measurements of changes in the acoustic wave attenuation $\Delta\alpha$ under the influence of an external magnetic field [6]-[8]. The change of the acoustic attenuation of acoustic waves propagating through suspensions, in which magnetic nanoparticles constituting one phase are dispersed in a continuous second phase, can indicate characterized properties and structure of magnetic liquids. The interaction between the acoustic waves and the magnetic nanoparticles or clusters leads to additional attenuation of acoustic wave compared to that in the carried liquid.

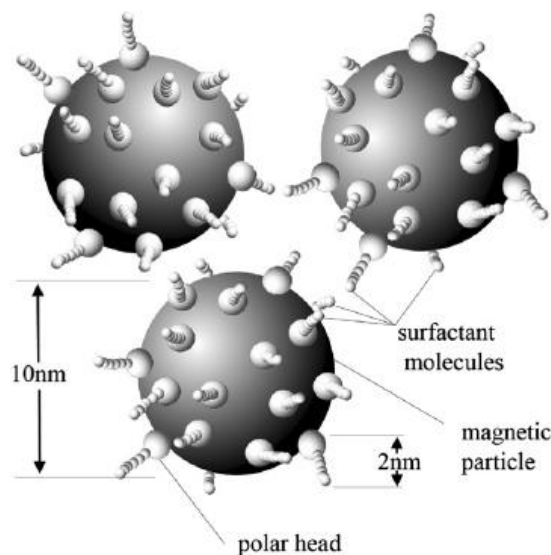


Fig. 1. Schematic sketch of the magnetic particles in a ferrofluid [3].

Under the effect of an external magnetic field the nanoparticles of magnetic fluid become arranged into clusters, forming chains stiffening the liquid structure. Acoustic wave propagation in magnetic fluid placed in magnetic field was studied by several authors both theoretically and experimentally [2], [6], [7]. There are also computer simulations by Satoh [8] or Mendelev [10] who investigated aggregation phenomena in a polydisperse colloidal dispersion of ferromagnetic nanoparticles. All these works suppose that chainlike clusters are formed along magnetic field direction, but clusters can have various shapes. These shapes depend on both particle-particle and particle-field interactions. The experimental measurements of the acoustic attenuation as a function of magnetic field were made by several works [6]-[16].

In this paper the authors study the influence of temperature on the changes of the acoustic attenuation in magnetic fluids based on transformer oil TECHNOL caused by the magnetic field. The dependence of the attenuation of acoustic wave on the angle φ between the direction of propagation and that of the magnetic field, known as the anisotropy of the attenuation of acoustic wave, were measured too.

II. EXPERIMENTAL SETUP AND RESULTS

The block diagram of the experimental arrangement is shown in Fig. 2. The measurements of the attenuation of the acoustic wave of frequency 12.65 MHz were carried out by a pulse method using the MATEC Pulse Modulator and Attenuation Recorder, model 7700 [6], [8]. An acoustic wave propagating in the thermostatted closed measuring cell ($1.5 \times 0.9 \times 1 \text{ cm}^3$, the temperature stabilized with an accuracy $\pm 0.2 \text{ }^\circ\text{C}$) inserted in an electromagnet undergoes a multiple reflection from the transducers and its subsequent echoes are recorded. Two selected adjacent pulses following separate paths reach a detector from where signals proportional to their amplitudes are fed to the MATEC receiver. The signal from the MATEC, which is proportional to the changes of the acoustic attenuation in the magnetic fluid, was recorded by oscilloscope and measured by a computer program. Computer program also control current source for electromagnet.

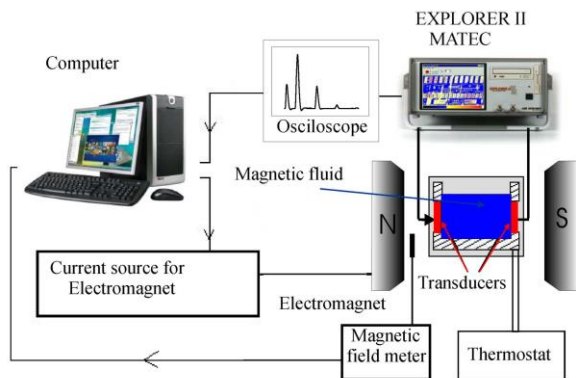


Fig. 2. Experimental setup.

Transformer oil TECHNOL was used as the carrier liquid for the preparation of magnetic fluids for the investigation by acoustic methods. The magnetic fluid (MF) used in experiments consisted of magnetite particles ($\text{FeO} \cdot \text{Fe}_2\text{O}_3$) with the mean diameter $a = 11.1 \text{ nm}$, coated with oleic acid as a surfactant. The volume concentration of magnetic particles was 0.5%. The basic properties of 0.5% MF TECHNOL were follow: the density 0.854 g/cm^3 and saturation magnetization 2.1 mT . The ideal magnetic particles interact with magnetic field, but not interact with each other. The degree of ideality is characterized by the coupling constant λ . For this type of MF with hydrodynamic diameter $d_h = 11.1 \text{ nm}$ is coupling constant $\lambda = 7.3$. The coupling constant determines the magnitude of dipolar attraction of neighboring grains. Large values of

coupling constant λ mean agglomeration of particles in larger structures – clusters, chains.

The acoustic attenuation depends on the magnetic field intensity, the rate of its changes and the temperature of magnetic fluid. Fig. 3 presents the attenuation change as a function of magnetic field B for the same sweep rate, which is parallel to k . Magnetic field was linearly increased ($2.2 \text{ mT per minute}$) to maximum value 100 mT (■ black color), 200 mT (● red color) and 300 mT (▲ blue color), respectively. The magnetic field after reach the maximum value and 1-minute pause decreased at the same rate.

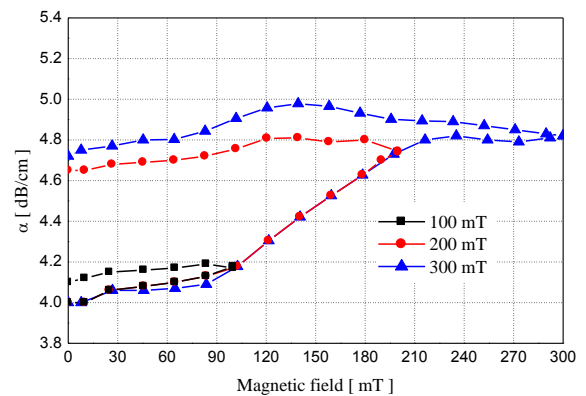


Fig. 3. Development of the acoustic attenuation in the magnetic field for 0.5% MF measured at $20 \text{ }^\circ\text{C}$ for different achieved maximum values of magnetic field (■ - 100 mT , ● - 200 mT , ▲ - 300 mT). Magnetic field increased and/or decreased at constant rate, 2.2 mT/min

The measurement of the change of acoustic attenuation as the function of external magnetic field (Fig. 3) showed that with increasing the magnetic field the acoustic attenuation also increases. This increase is caused by aggregation of particles to chain-like formation, what is the result of interactions between the magnetic field and the magnetic moment of the nanoparticles. The development of the attenuation of acoustic wave depends on the maximum of the external magnetic field and shows a hysteresis [6], [8]. At higher maximum magnetic field there were complicated structures like: long chains or clusters (structures as long as tens of nanometers [1], [10]-[12]). The process of agglomeration finished at around 210 mT and with next increasing magnetic field there were no important change of acoustic attenuation, yet. At degreasing magnetic field the value of acoustic attenuations varies very slowly, because lifetime of clusters was longer than time of decrease of the magnetic fluid. From 120 mT the magnetic field is insufficient to compensate clusters, which decay by thermal energy. But the structure does not return to the initial state after the magnetic field has been removed.

The acoustic attenuation was investigated in studied MF in the temperature range of $15 - 30 \text{ }^\circ\text{C}$ (Fig. 4). The obtained results indicate also the significant effect of temperature on the acoustic attenuation. For all measured temperatures the acoustic attenuation increases with increasing magnetic field. For the temperatures $20 \text{ }^\circ\text{C}$ and

25 °C the measurement of the acoustic attenuation shows the largest changes originated from the process of cluster creation and shows also higher hysteresis. At these temperatures the creation of cluster is more effective because Brown thermal motion is not so effective to destroy the clusters [5]. At the temperature 30 °C The influence of magnetic field on the acoustic attenuation happens small. Also in this type of measurement the changes of the acoustic attenuation show a hysteresis. This effect can be described by existence of clusters, which lifetime was longer than time of decrease of the magnetic fluid. The structure does not return to the initial state.

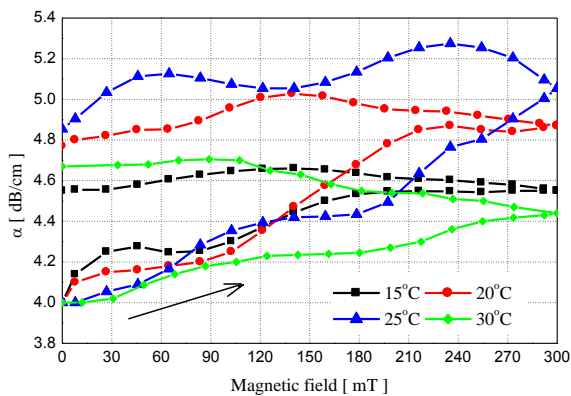


Fig. 4. The temperature influence on the acoustic attenuation in the magnetic field (■ 15 °C, ● 20 °C, ▲ 25 °C, ◆ 30 °C).

Fig. 5 presents the acoustic attenuation changes in the MF subjected to a jumped magnetic field 200 mT for 30 min and its behavior after removal magnetic field. The acoustic attenuation was measured as a function of time under the following conditions: the magnetic field increased in 10 second to 200 mT (A denotes switch on), then this value of the magnetic field was constant for 30 min and finally the field decreased to zero in 1 second (B is switch off). The area between A - B corresponds to the range of time in which the magnetic fluid was subjected to a constant value.

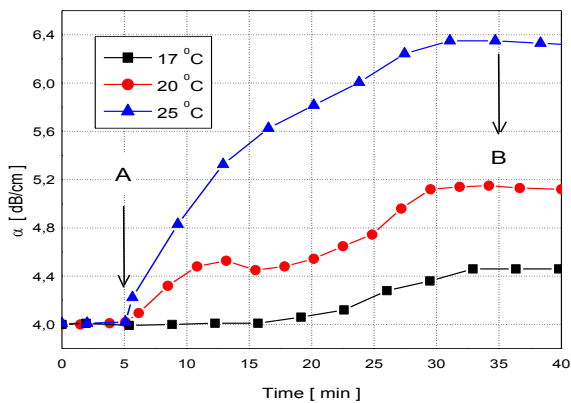


Fig. 5. Experimental data of the acoustic attenuation for jump change of the magnetic field to value 200 mT measured at temperatures ■ 17 °C, ● 20 °C and ▲ 25 °C. A denotes switch on and B switch of the magnetic field.

Fig. 5 presents the acoustic absorption change for pulse changes of the magnetic field: 200 mT during 30 min for three temperatures 17 °C, 20 °C and 25 °C. The change of the absorption coefficient occurred very slowly with increasing time. It can be seen that at after 25 minute the coefficient reaches constant values for all measured temperatures. From these results it can be said the processes of clustering had long timescale. After magnetic field switch off, the change of the acoustic absorption coefficient does not return to initial value and its value almost decreases not. This means that the clusters exist also after there is no magnetic field.

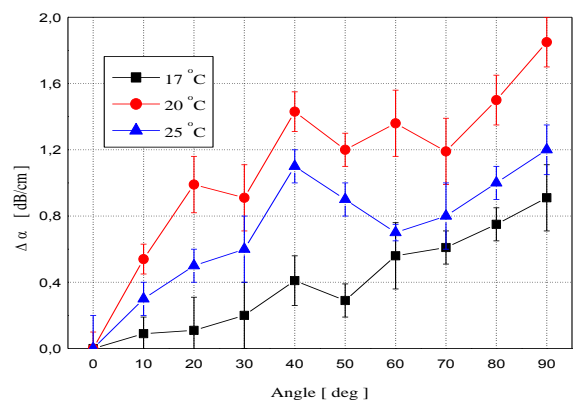


Fig. 6. Anisotropy measurement of the change of acoustic attenuation at 200 mT magnetic field for temperatures: ■ 17 °C, ● 20 °C, ▲ 25 °C.

The results of the anisotropy of acoustic attenuation in the magnetic fluid of the value 200 mT are shown in Fig. 6. The measurements were made in the dependence on the angle φ between the magnetic field B and wave vector k measured for various temperatures of MF. The results indicate a significant effect of temperature on the anisotropy of acoustic attenuation in MF. As it can be seen from the measurements the acoustic attenuation slowly increases with the angle φ . At angle $\varphi = 40^\circ$ are local maxima for temperatures 20 °C and 25 °C. The acoustic attenuation is higher in perpendicular case of the magnetic field B and wave vector k .

III. DISCUSSION

It is known that the interaction between the external magnetic field and the magnetic moment of the nanoparticle in magnetic fluids leads to the aggregation of nanoparticles to new structures [2], [7], [8], [12]. These structures enlarge with the magnetic field and this process has the influence on the value of the acoustic attenuation. In our previous works [7], [8] or other experimental works [6], [11] it was observed that the acoustic attenuation initially increases with increasing magnetic field. This effect can be explained by several parameters. One of is the time constant of creation of higher structures of nanoparticles. Others are temperature or viscosity of given magnetic fluids. However, following progress at higher magnetic field can be different depending on the structure changes caused by developing of cluster shape in individual cases.

The measured results show a strong influence of the acoustic attenuation on the value of magnetic field in magnetic fluid based on transformer oil TECHNOL (Fig. 3). When the magnetic field increases at a constant rate, the interactions between magnetic moment of the nanoparticle and the magnetic field leads to the aggregation of particles, chain-like shapes and later to clusters with radius hundreds of nanometers [7]. These structures cause the increase of the acoustic attenuation with increasing magnetic field. With increasing magnetic field α increases because of the viscosity of MF increases. Values of α are the result of an additional resonance absorption of ultrasonic wave by the spherical clusters formed in fluid. The temperature is next important factor which influences on the values of acoustic attenuation as is shown in Fig. 4. With the temperature is connected the thermal energy, which causes decay of clusters. With higher temperature speed of magnetic particles increases and molecules of transformer oil (Brown motion) and their collision with cluster can causes with higher probability its destruction. These effects agree with other works [6], [10] - [12].

The anisotropy of acoustic attenuation was investigated in the temperature range of 17–25 °C (Fig. 6). As it can be seen from the results there is the significant effect of temperature on the acoustic attenuation. The measurements show the largest changes coupled with the process of chains orientation in the direction of field. The slow increase of the change of acoustic attenuation with angle φ is connected with long time of lifetime of chain-like structures or clusters. Of course, there are also other effect influenced on the acoustic attenuation, like the radius of clusters and the length of their chains. At the temperature 20 °C the acoustic attenuation is higher. At other temperatures the anisotropy was smaller, where the main effect is caused by decrease of viscosity with the temperature [6], [10] or [16]. On the basis of the theory for the anisotropy published by Taketomi [13] it can be determined influence of translational vibrations and rotational degrees of freedom of clusters existed in MF in the presence of magnetic field.

IV. CONCLUSION

This study was focused on magnetic field induced changes of the structure of magnetic nanoparticles in transformer oil based magnetic fluids. The strong influences of both magnetic field and temperature on the structures were detected using acoustic spectroscopy. The observed behavior of the acoustic attenuation validated the process of aggregation of the magnetic nanoparticles into clusters on the one side and the role of thermal motion on their desintegrate. The study of the anisotropy showed the there is also important the orientation of magnetic field in the transformers.

ACKNOWLEDGMENT

This work was supported by projects VEGA 1/0624/13 and R&D operational program Centre of

excellence of power electronics systems and materials for their components No. OPVaV-2008/2.1/01-SORO, ITMS 26220120003 and No. OPVaV-2009/2.1/02-SORO, ITMS 26220120046 funded by European regional development fund (ERDF). The authors gratefully acknowledge Professor M. Timko from the Slovak Academy of Science (Košice) for sample of the magnetic fluid.



References

- [1] V. Segal and K. Raj, "An Investigation of Power Transformer Cooling with Magnetic Fluids", *Indian J. Eng. Mater. Sci.* 5 (6), pp. 416-422, 1998.
- [2] S. Odenbach, "Ferrofluids - magnetically controlled suspensions", *Colloids and Surfaces A: Phys. Eng. Aspects*, 217, pp. 171-178, 2003.
- [3] I. Sharifi, H. Shokrollahi and S. Amiri, "Ferrite-based magnetic nanofluids used in hyperthermia applications," *Journal of Magnetism and Magnetic Materials* vol. 324, pp. 903-915, 2012.
- [4] P. Kopčanský, L. Tomčo, K. Marton, M. Koneracká, I. Potočová and M. Timko, "The experimental study of the DC dielectric breakdown strength in magnetic fluids" *Journal of Magnetism and Magnetic Materials*, vol. 272-276, Part 3 (2004) 2377-2378.
- [5] J. Kúdelčík, P. Bury, P. Kopčanský, M. Timko "Dielectric breakdown in mineral oil ITO 100 based magnetic fluid", *Physics Procedia* 9, pp. 78-81, 2010.
- [6] J. Józefczak, "Acoustic properties of PEG biocompatible magnetic fluid under perpendicular magnetic field", *Journal of Magnetism and Magnetic Materials*, vol. 293, pp. 240-244, 2005.
- [7] J. Kúdelčík, P. Bury, J. Drga, P. Kopčanský, V. Závishová and M. Timko, "Comparison of Theories of Anisotropy in Transformer Oil-Based Magnetic Fluids", *Advances in electrical and electronic engineering*, vol. 11, no. 2, pp. 147-155, 2013.
- [8] J. Kúdelčík, P. Bury, J. Drga, P. Kopčanský, V. Závishová and M. Timko "Temperature Effect on The Structure of Transformer Oil Based Magnetic Fluids Using Acoustic Spectroscopy, *Acta Physica Polonica A* No. 5-6, pp. 1169-1171 (2012).
- [9] A. Satoh Three-dimensional Monte Carlo simulations of internal aggregate structures in a colloidal dispersion composed of rod-like particles with magnetic moment normal to the particle axis, *Journal of Colloid and Interface Science*, 318, pp. 68-81 (2008).
- [10] V.S. Mendeleev and A.O. Ivanov, "Ferrofluid aggregation in chains under the influence of a magnetic field", *Phys. Rev.* vol. 70, 051502, 2004.
- [11] A. Skumiel, "The effect of temperature on the anisotropy of ultrasound attenuation in a ferrofluid", *Phys. D: Appl. Phys.*, vol. 37, pp. 30733079, 2004.
- [12] Z. Rozynek et al, "Structuring from nanoparticles in oil-based ferrofluids", *European Physics Journal E*, 34, 28 DOI 10.1140/epje/i2011-11028-5 (2011).
- [13] S. Taketomi, "The Anisotropy of the Sound Attenuation in Magnetic Fluid under an External Magnetic Field", *J. Phys. Soc. Japan*, vol. 55, pp. 838-845, 1986.
- [14] P. Hockicko, "High Frequency Acoustic Spectroscopy of Perspective Materials for Electrotechnic", *AKUSTIKA*, Vol. 17, 2012.
- [15] J. Jurčík and M. Gutten, "Analysis transformer insulation by PDC method" *Pzegląd elektrotechniczny Electrical Review*, vol. 89, no. 1a, pp. 169-171, 2013.
- [16] A. Józefczak, T. Hornowski and A. Skumiel, "Temperature Dependence of Particle Size Distribution in Transformer Oil-Based Ferrofluid", *Int J Thermophys* (2011) 32:795-806, DOI 10.1007/s10765-010-0895-5.

Possibility of using simulation tools for the development of new nanocomposite materials

Michal Čermák¹⁾, Radek Polanský²⁾

¹⁾ University of West Bohemia/ Faculty of Electrical Engineering/ KET, Univerzitní 26, 306 14 Pilsen, Czech Republic

²⁾ University of West Bohemia/ Faculty of Electrical Engineering/ RICE, Univerzitní 8, 306 14 Pilsen, Czech Republic

¹⁾ tel: +420 377 634 551, email: czermak@ket.zcu.cz

²⁾ tel: +420 377 634 517, email: rpolansk@ket.zcu.cz

Abstract— Polymer nanocomposites filled by organically modified layered silicates, intercalated halloysite clay or carbon nanotubes are in the main scientific interest of polymer nanocomposite development and the results of the scientific research are beginning to apply in industrial practice. Despite the proven benefits, the nanocomposites are used to very specific applications nowadays. The reasons for the limited growth of nanocomposites are caused by unresolved challenges especially in the dispersion processing of nanoparticles into polymer matrix and sufficient oxidative and photo-oxidative stability that are key elements in the design of new insulation materials.

This article summarizes achieved information about possibilities of use of simulation tools, which can be helpful in design of new mixtures for LFHC (Low Fire Hazard Cables) and LOCA (Loss of Coolant Accident) cables. The article also demonstrates the possibility of prediction of basic mechanical properties by different simulation methods in the polymer nanocomposites compounds. Results of simulation are compared with experiment.

Keywords— *Nanocomposite; simulation of mechanical properties; polymer nanocomposite*

I. INTRODUCTION

Polymeric materials enhanced by nanoparticles such as microtubules, spherical nanoparticles or modified organoclay provide tremendous opportunities to change physical, chemical and optical properties of the origin polymer. Despite the proven benefits in improvement of the mechanical behaviour, the barrier properties and the flame retardancy of polymer nanocomposites are used in only a few applications and the use of this type of material is still limited. This fact is mainly caused by experimental complexity during the development of the new polymer nanocomposite. [1-4] However, computational and simulation methods together with their hardware tools have already reached the level that can be used in the field of designing materials over the last decade. Therefore the intense attention not only in the scientific community, but especially in the various industrial sectors involved in the design of new materials is currently devoted to possibilities of simulation of polymer nanocomposites. These methods significantly accelerate the development of new materials and thus help these methods to accelerate

the product launch to the commercial practice. However, making corresponding mathematical description of the designed polymer nanocomposites by modeling methods causes many difficulties and challenges. It is due to the incomplete description of the interaction of individual components of the polymer nanocomposites and also computational complexity of the research task. Computational modelling and simulation are currently particularly useful for polymer nanocomposites in solving the following problems:

- a) The thermodynamics and kinetics of the polymer nanocomposite.
- b) The study of the structure of polymeric system and the simulation of the dynamics of the system especially in the interphase interface and nanocomposite interface with the polymer matrix from molecular to macroscopic level.
- c) The study of rheological changes in polymer blends caused by the fulfilment of nanoparticles.
- d) The explanation of the mechanisms between nanoparticles and base polymer matrix, which cause changes in the properties of the resulting polymer nanocomposite. [5]

Possibilities of use of simulation methods and tools for cable industry are provided particularly in the development of the new polymer mixtures according to the input requirements, optional stabilization of mixtures and the prediction of the main processing properties (melt flow index, cohesion and homogenization), that can be useful during determining which way and how easily / hard will the pre-designed mixture technologically workable. Another important area of concern can be the prediction of the thermodynamic properties, the mechanical properties, the dielectric and structural behaviour of the mixtures at various conditions of stress.

Therefore, the purpose of this article is a brief introduction to the modelling and the simulations of polymer nanocomposites with a focus on the methods, which can be used for predicting the mechanical properties of these materials. The first part of the article presents the basic computational approaches to modelling

processes that are based on the descriptions of atomic interactions or continuity of observed parameters. Whereas the second part summarizes achieved information about polymer nanocomposite simulation with focusing on the methods of molecular modelling and shows some interesting results achieved by continuous modelling methods.

II. SIMULATION OF NANOCOPOSITE BEHAVIOUR

Properties of nanostructured materials can be determined by relatively large set of methods that come under different groups' length scale and time scale (Fig. 1). For the simulation of small object and computationally less demanding situations (< 1000 of atoms) the technique of computational chemistry (Quantum Mechanics - QM) is applied and this technique is capable of describing quantum-mechanical interaction between atom in step of iteration in matter of 10^{-15} s in the high-quality manner. Methods based on computational chemistry are used mainly for qualitative evaluation of the theoretical assumptions in the interface of the polymer matrix/nanocomposites. The mechanical properties (because of their macroscopic behaviours) have to be stimulated in the larger group of particles (> 1000 of atoms), hence the large length and time scale. By the reason of aforementioned simplified models that come under the discrete methods such as Nanomechanics (Molecular Mechanics – MM, Molecular Dynamics – MD, Monte Carlo – MC, truss simulation – TS) and also to the continuous methods such as Micromechanics (Eshelby, Halphin-Tsai, Rule-of-Mixtures, Mori-Tanaka) and Structural Mechanics (Finite Element Method - FEM, Boundary Element Method - BEM) are more or less used for the material prediction. [6, 7] In the comparison to the discrete methods the continuous simulation methods are based on the assumption of the existence of a continuum solved computing task and the interactions between the phases of the composites are generally neglected. These methods can be divided into the analytical and computational methods.

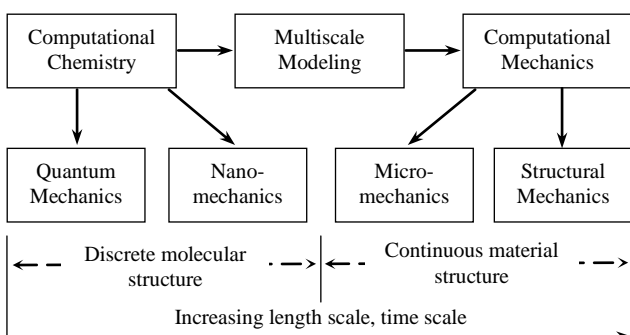


Fig. 1. Modeling methods and tools used for prediction of mechanical behaviour. [8]

The mechanical change of behaviour of the base polymer system by adding nanoparticles is the demonstration of several mechanisms of interactions. Firstly, the filler itself is able to influence the morphology of the polymer system and thus improve strength and toughness of the designed material. Secondly, these fillers

can inhibit the spread of micro-cracks during stress. Thirdly, the fillers can positively influence the interfacial conditions and appropriately adjust the structure by treatment of nanoparticles surface on the polymer matrix. The key parameters of nanoparticles that influence the mechanical behaviour of final material most are: the size of nanoparticles, the surface area, the shape and aspect ratio. Furthermore, dispersion of nanoparticles in the polymer matrix and its own interaction is also very important parameter. [9]

Appropriate simulation tools for prediction of the mechanical properties are the methods of the molecular modelling in nanoscale and mesoscale. For example QM, MD and MC (Fig. 2) methods are able to predict very well: the local load of the mixture, the interface properties, or the structural response to the mechanical stress. In addition, these methods are very well capable to predict the elasticity, thermal expansion, vibration energy frequency, the reaction temperature, dielectric constant of the mixture, the level of binding energy or glass transition temperature of the analysed system. [8] Therefore, the methods of molecular modelling are very powerful tools for prediction of the polymer nanocomposite behaviour.

However, the benefits resulting from the discrete description of the problem cause also some disadvantages, mainly consisting of the computational complexity of the task and the associated limitation of the amount of elements in the simulation and the site of the iteration step. These two variables determine the level of length scale and time scale and total computing time. Generally, the neglect of the particular amount of conformations of elements in the simulated system is caused by the rough iteration step or reduction of elements in the simulation. Therefore the simulation can have a low explanatory power. Regarding to aforementioned, it can be retreated from the discrete simulation and solve the problem by continuous models in some cases. But solving the problem by the continuous models causes significant simplification of the whole system, what can be seen on the Fig. 3.

Quantum Mechanics Motion of electron Schrödinger equation	Molecular Dynamics Motion of atoms Newtonian equation	Monte Carlo Motion of atoms Random walk
Electronic distribution Geometric structure Bonding, unbonding Total energy	Molecular structure Interaction at interface Thermodynamics prop. Intercalation kinetics Mechanical prop.	Nanoparticle surface Thermodynamics prop.

Fig. 2. Molecular modeling and simulation methods commonly used for polymer nanocomposites. [5]

The quality of results of continuous models are dependent on the periodicity and the number of different types of particles and with the increasing complexity of the system decreases the quality of the simulation results. A typical example of these kinds of materials are ternary and quaternary polymer nanocomposite systems used as a basic material in LFHC and LOCA cable systems, that find their application mainly in civil and industrial engineering and everywhere where the large number of people is expected.

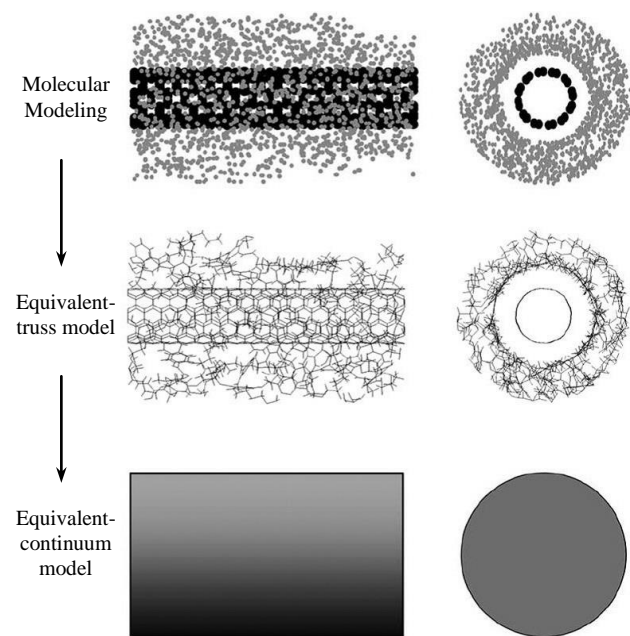


Fig. 3. The case study represented by molecular, equivalent-truss and equivalent continuum models. [10]

III. SIMULATED RESULTS

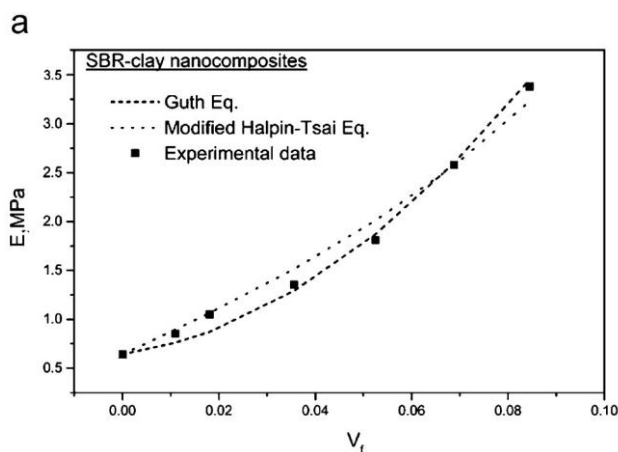
In two last decades, many attempts have been made in simulation of the mechanical behaviour of polymer nanocomposite. The research studies at present are mainly focussed to the simulation of the behaviour of polymer nanocomposite filled by carbon nanotubes and organoclays in varying degrees of intercalation even in the exfoliation form. The following table summarizes the results of simulations of the mechanical properties of selected polymer nanocomposites. The selection of studies was chosen in the possibility of applying the results to the cable industrial practise in the field of the design of new polymer nanocomposites mixture. Therefore, the results are focused on the simulation of mechanical properties using MD and some selected continuous methods.

As indicated above, the continuous models are very sensitive to the diversity of the investigated system. But Guth's studies and models (Guth eq. And Modified Halpin-Tsai; Fig. 4) suggest a shift in this field of simulations. In his models the reduction factors that are directly dependent on the morphology of the nanofiller are introduced. The simulation results and the experimental results achieved by this adjustment of models are similar. Especially better results in the simulation of properties of polyolefines and rubbers filled by varying degrees of

organoclay are achieved in comparison with the results of the classic model Halpin-Tsai. The quality of results of the Halpin-Tsain simulations are comparable with Guth's modified models only in polymer nanocomposites systems with the low-dose of the fulfilment of intercalated organoclay particles [11]. Studies that would be focused to the simulation of mechanical properties of multicomponent polymer nanocomposites are not available nowadays.

TABLE I. ACHIEVED RESULTS IN LITERATURE

Material system	Simulation Method	Predicted Properties	Conclusions of research
Carbon Nanotube/PE	MD, Mori-Tanaka	Elastic Modulus	The moduli of functionalized system were determined and compared with pure PE [12]
Carbon Nanotube/PE	MD	Elastic Modulus	The effect of crosslinking density on load transfer was validated. [13]
Carbon Nanotube/PE	MD	Stress-Strain	Results of MD simulation were compared with prediction of rule-of-mixtures techniques. [14]
Carbon Nanotube/PA	MD, Mori-Tanaka	Elastic Modulus	Critical length for maximum load was determined and the interface of nanocomposite was examined. [15]
Nanoclay/PA	MD, Halpin-Tsai	Elastic Modulus	The effects of distribution of the clay clusters on properties were determined and compared with Halpin-Tsai Simulation [16]
Nanoclay/PA	MD, Halpin-Tsai, Mori-Tanaka, FEM	Elastic properties	The multiscale simulation of PA reinforced by nanoclay was presented. [17]
Nanopart./PA	MD, Halpin-Tsai	Elastic Modulus	The interface effects of the nanoparticles on elastic properties on PA was studied [18]
Carbon Nanotube/Epoxy	MD	Interfacial Bonding	The changing of mechanical properties on loading of nanotubes were presented. [14]
Carbon Nanotube/PS	MD, Halpin-Tsai	Load Transfer	The effects of degree of crosslinking between nanotubes and PS on mechanical properties were studied. [19]



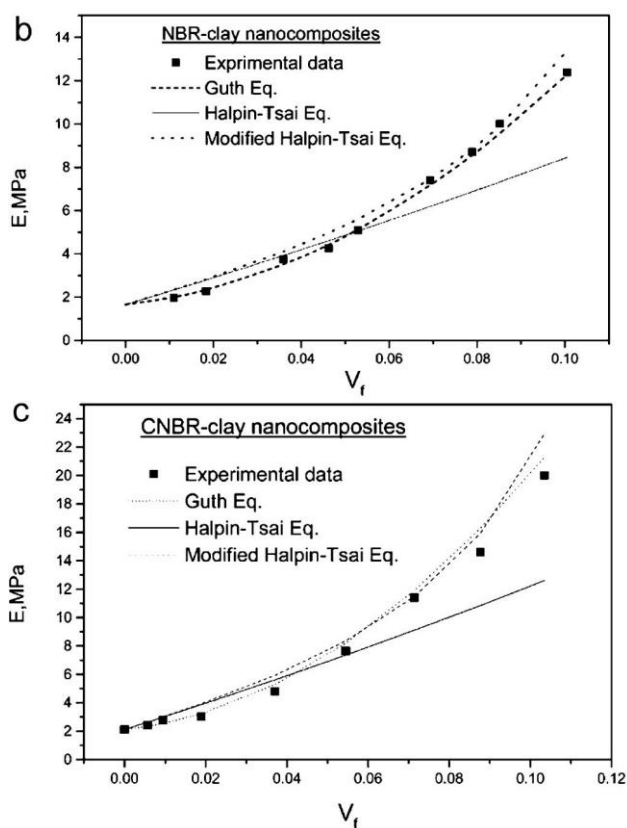


Fig. 4. The theoretical predictions of modulus of the a) SBR-clay nanocomposites, b) NBR-clay nanocomposites, c) CNBR-clay nanocomposites by three different continuous models in comparison of experimental results. [11]

IV. CONCLUSION

The computing modelling of molecular structures and simulation of their interactions came through a rapid development in the last twenty years. In particular, the area of drug development was the pioneer field of application of these methods and has brought unprecedented opportunities to accelerate drug development. These options are currently available for use in other sectors. The results that were presented in this article show that computer modelling in the simulation of polymer nanocomposites has its "infancy" behind and the use of these methods and techniques for the design of new compounds for cable industry have well-founded potential. Especially the discrete simulation methods such as the Molecular Mechanics, the Molecular Dynamics and techniques based on the Monte Carlo show the real use for development of polymer nanocomposites. Unfortunately, these models are very demanding on the computing performance. It is caused by the step size of iteration, which is in the matter of 10^{-15} s. So it makes impossible to computing complex problem and situations in more realistic time scale.

However, the results obtained and presented in this article concern by only binary polymer nanocomposites. The question arises, how much will be the results of the discrete and the continuous models affected by filling other compounds in the simulated mixture. The quality

level of output of simulation will be the key parameters for acceptance or rejection of the examined method.

ACKNOWLEDGMENT

This research has been supported by the European Regional Development Fund and the Ministry of Education, Youth and Sports of the Czech Republic under the Regional Innovation Centre for Electrical Engineering (RICE), project No. CZ.1.05/2.1.00/03.0094 and by the Student Grant Agency of the West Bohemia University in Pilsen, grant No. SGS-2013-026 "Material and Technology Systems in Electrical Engineering".

REFERENCES

- [1] H.R. Zweifel, D. Maier, M. Schiller, *Plastics additives handbook*, 6th ed.; Cincinnati, Ohio: Hanser Publications, 2009, p. 1222.
- [2] P., Kiliaris, C.D. Papaspyrides, "Polymer/layered silicate (clay) nanocomposites: An overview of flame retardancy," *Progress in Polymer Science*, vol. 35, no. 7, pp. 902-958, 2010.
- [3] M.C., Costache, J. M. Heidecker, "The influence of carbon nanotubes, organically modified montmorillonites and layered double hydroxides on the thermal degradation and fire retardancy of polyethylene, ethylenevinyl acetate copolymer and polystyrene," *Polymer*, vol. 48, no. 22, p. 6532-6545, 2007.
- [4] F. Gao, G. Beyer, Q. Yuan, "A mechanistic study of fire retardancy of carbon nanotube/ethylene vinyl acetate copolymers and their clay composites," *Pol.Deg.Stab*, vol. 89, no 3, 2005.
- [5] Q.H. Zeng, A.B. Yu. "Multiscale modeling and simulation of polymer nanocomposites," *Progress in Polymer Science*, vol. 33, no. 2, pp. 191-269. ISSN 00796700, 2008.
- [6] S.C. Glotzer, W. Paul, "Molecular and mesoscale simulation methods for polymer materials" *Annual Review of Materials Research*, vol. 32, no. 1, 2002.
- [7] D.P. Kroese, T. Taimre, Z. Botev, *Handbook for Monte Carlo methods*. Hoboken, N.J.: Wiley, 2011, pp. 743.
- [8] P.K. Valavala, G.M. Odegard, "Modeling Techniques for Determination of Mechanical Properties of Polymer Nanocomposites," *Reviews on Advanced Materials Science*, Vol. 9, no. 1, pp. 34-44, 2005.
- [9] N.M. Ghoniem, E.P Busso, N. Kioussis, H.C. Huang, "Multiscale modelling of nanomechanics and micromechanics: an overview," *Philos Mag.*, vol. 83, pp. 528, 2003.
- [10] G.M. Odegard, R.B. Pipes, P. Hubert, "Comparison of two models of SWCN polymer composites," *Compos Sci Technol*, vol. 64, 2004.
- [11] Y.P. Wu, Q.X. Jia, D.S. Yu, "Modeling Young's modulus of rubber-clay nanocomposites using composite theories," *Polym Test* vol. 23, pp. 903-9, 2004.
- [12] G.M. Odegard, "AIAA/ASME/ASCE/AHS Structures," *Structural Dynamics and Materials Conference*, Norfolk, Virginia, 2003.
- [13] S.J.V. Frankland, A.Caglar, D.W. Brenner *J. Phys. Chem.*, Vol. 106 pp. 3046, 2002
- [14] J. Gou, B. Minaie, B. Wang, Z. Liang and C. Zhang, *Computational Materials Science*, vol 31, pp. 225, 2004.
- [15] E.T. Thostenson and T.W. Chou, *Journal of Physics: Applied Physics* vol. 36, pp. 573, 2003.
- [16] L. Zhu, K.A. Narh, *Journal of Polymer Science Part B: Polymer Physics*, vol. 42, pp. 2391, 2004.
- [17] N. Sheng, M.C. Boyce, D.M. Parks, *Polymer*, vol. 45 pp. 487, 2004.
- [18] G.M. Odegard, T.C. Clancy, T.S. Gates, *Polymer*, vol. 46, pp. 553, 2005.
- [19] Y. Hu and S.B. Sinnott // *Journal of Materials Chemistry* 14 (2004) 719.

Implementation of Lean management for diagnostic processes

Jan Šimota¹⁾, Katarína Bandžáková²⁾, Jiří Tupa³⁾

^{1,2,3)} University of West Bohemia /Faculty of Electrical Engineering/ KET, Univerzitní 8, 306 14 Pilsen, Czech Republic, www. zcu.cz

¹⁾tel: +420 377 634 547, email: jsimota@ket.zcu.cz

²⁾tel: +420 377 634 548, email: bandk@ket.zcu.cz

³⁾tel: +420 377 634 008, email: tupa@ket.zcu.cz

Abstract - The paper deals with the implementation of the Lean management for improvement of the diagnostics processes. The goal of the Lean management is more flexible production with the same financial resources. This approach is a very efficient tool in identification and elimination processes and activities, which doesn't bring the value. The implementation of the Lean management in diagnostics area can improve efficiency and flexibility current processes. An important part of Lean management is implementation of detailed processes mapping and identification the parts of the processes, which bring the value added for customer. The process mapping can be realized with Value Stream Mapping methodology. The PDCA method is used for systematic improving of processes. The problems are solving with methods A3 Thinking and problem solving.

Keywords - Lean management, Value Stream Mapping, Value Stream Maps, PDCA, A3, 5S Implementation, Batch Size Reduction, Macro design

I. INTRODUCTION

Lean management is a method orientated at the production, flow values, elimination a waste etc. Most often is this method used in the production companies, but the use is in the research and development or in state sector, for example in the hospital or in the education etc. This paper deals with the implementation Lean management in the diagnostics, more precisely in the test laboratories. Model for implementation will be the Lean management in the hospital, more precisely in the clinical laboratory. [1] The goal of this paper is to present a case study, which compares the present situation in the diagnostic laboratory with the situation after implementation Lean management. For the implementation are used the tools of Lean management, they are Value Stream Mapping, PDCA (Plan-Do-Check-Act) and A3 thinking and problem solving.

II. LEAN MANAGEMENT

The roots of Lean Management have been applied at the company Toyota in Japan. The idea to change the mass production came in the 50's of the 20th century. The goal was that the production was more flexible and it didn't require big financial resources. It is a new style of leadership that is powered by the need for quality, speed, flexibility and a clear communication in many ways. It focuses on improving communication between the company and its customers, suppliers and company and between the company and its employees [2].

Diagnostics, as well as other industries, has strict standards under which are the measurements doing. Many of these standards can cause processes to be redundant and non-value-added; however, they must be performed to satisfy condition of standards. These activities fall into a third category –non-value-added, but necessary. These activities should not be excluded when driving improvement, but further ways to improve should be explored while adhering to standards.

An important part of Lean Management is the identification and elimination processes, which don't bring added value, such processes are wasteful. These processes or activities typically occupy 75-95% of the total time needed to implement the process. [1]

Lean Management has very wide application. It is not a tactic or a cost reduction program, but a way of thinking and acting for an entire organization. For differentiation are used the attribute, which determine in which area is used, for example Lean Production, Lean Marketing, Lean Audit, Lean Six Sigma etc. Lean can be implemented in the field of diagnostics, where it can achieve results as in manufacturing companies.

There are the five-step thought processes for guiding the implementation of Lean techniques:

1. Identify value from the standpoint of the end customer by product line.
2. Identify all the steps in the value stream for each product line and eliminating those steps that do not create value.

3. Make the value-creating steps occur in tight sequence and the product will flow smoothly toward the customer.
4. As flow is introduced, let customers pull value from the next upstream activity.
5. As value is specified, value streams are identified, wasted steps are removed, and flow and pull are introduced, begin the process again and continue it until a state of perfection is reached in which perfect value is created with no waste. [3]

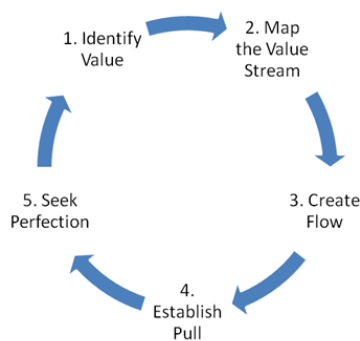


Fig 1.Principles of Lean Management [3]

III. LEAN MANAGEMENT IN DIAGNOSTICS

The application of Lean Management in diagnostics is the same as in any other manufacturing or non-manufacturing enterprise.

Lean Management in diagnostics is not just the method but also the thinking, which can bring the better results in diagnostics. Lean Management can improve the number of measurements, accelerate the preparation of measurements and effectively work with the results.

For the implementation of Lean management is critical clearly state the need for improvement from the beginning. There are five key steps that should be taken when starting the implementation towards a Lean management improvement.

1. Develop a burning platform for change
2. See the waste
3. Develop the lab's specific plan for improvement
4. Implement changes
5. Measure, monitor, and sustain

IV. METHODS

A. Value Stream Mapping (VSM)

VSM is a Lean manufacturing technique used to analyse and design the flow of information and materials required to bring a product or service to a customer. At company, where the technique originated (Toyota), it is known as “material and information flow mapping”. It can be applied to nearly any value chain. [4] This technique representing the value stream with symbols and numbers, and it is the key to understanding the

entirety of the transformation of raw materials into finished goods. [4]

B. Value Stream Maps

A value stream map illustrates the flow of materials and information as the product or service moves through the process.

C. Four steps to VSM

1. Define and pick the product or product family.
2. Create the “Current State” Value Stream Mapping (CSVSM).
3. Create the “Future State” Value Stream Mapping (FSVSM).
4. Develop an Action Plan to make the FSVSM the CSVSM. [5]

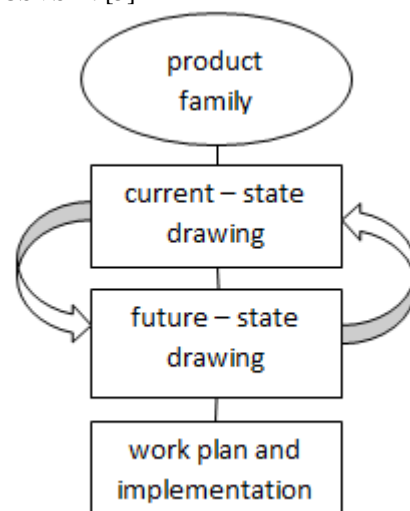


Fig 2. Initial Value Stream Mapping steps

V. PDCA (PLAN DO CHECK ACT) OR DEMING CYCLE

After mapping the selected processes is important to decide what changes will be made and what will be the consequences for the laboratory itself. The method of Lean Management is continually improving processes, which can be done using the PDCA. The four phases in the PDCA cycle involve:

- PLAN - Identifying and analysing the problem.
- DO - Developing and testing a potential solution.
- CHECK - Measuring how effective the test solution was, and analysing whether it could be improved in any way.
- ACT - Implementing the improved solution fully. [6]

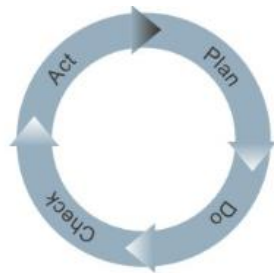


Fig 3. PDCA cycle [6]

VI. A3 THINKING AND PROBLEM SOLVING

An integral part of any process improvement is a solution to a problem that may occur. To solve problems you can use the method of A3 thinking and problem solving, which closely cooperates with PDCA. Method A3 is literally the communication tool that records the main results from the PDCA cycle. A3 is objective method to improve communication and resolve the problem. Unsurprisingly, they are called A3 because they fit on a single side of A3 (11 x 17 inch) sheet of paper. It is important to use a structured and comprehensive description of the problem, then analyse it in detail and propose solutions.

Steps of the A3 Problem Solving Process.

1. Identify a problem or need.
2. Conduct research to understand the current situation.
3. Conduct root cause analysis.
4. Devise countermeasures to address root causes.
5. Develop a target state.
6. Create an implementation plan.
7. Develop a follow-up plan with predicted outcomes.
8. Discuss plans with all affected parties.
9. Obtain approval for implementation.
10. Implement plans.
11. Evaluate the results. [7]

VII. CASE STUDY

The case study is focus on the using of Lean management tools in diagnostic laboratory. In the diagnostic laboratory is useful for the implementation to use the method 5s Implementation, Batch Size Reduction and arrange the work place by the method Macro design.

A. Implement the changes

Within the “House of Lean” there are multiple tools that could be implemented. Figure 5, represents some of core tools that could be implemented. It can be difficult at times to know

where to start; however, the value stream map can shed light on which tools to implement.

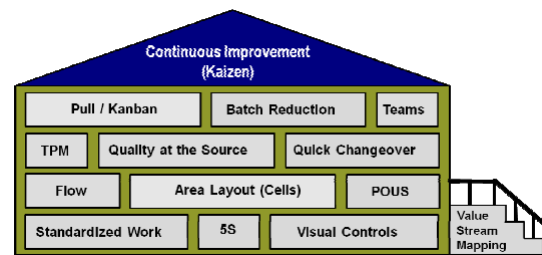


Fig 4. House of Lean [6]

To help understand which tools to implement, the chart below provides some guidance on when to use various Lean tools. It outlines some of the typical opportunities that exist in diagnostic laboratory today and the corresponding Lean tool(s) that could help drive improvement.

TABLE I. USING OF LEAN TOOLS

Opportunity	Lean Tool
Large amount of in process specimen	Batch Size Reduction, Teams
Redundant Work	Root cause analysis
Multiple Handling	Standard work methods
Inconsistency in tech or phlebotomist process	Standard work methods
Re-labeling or Insufficient sample volume	Quality at the Source
Not understanding current conditions or status	Visual Controls
Excessive travel / walking	Flow, Point of Use Storage, Area Layout
Excessive clutter and visual noise	5S Implementation

B. 5S Implementation

In many cases the improvement team determine 5S as first improvement opportunity to implement to the diagnostics processes. 5S is widely considered as the foundation for all other Lean Improvements. 5S is the name of a workplace organization method.

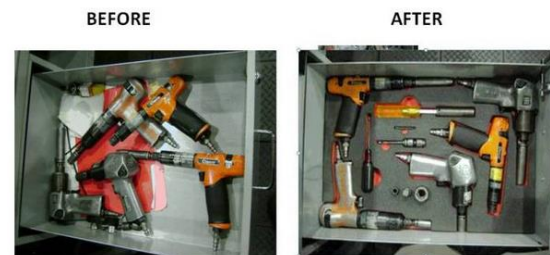


Fig 5. 5S implementation [6]

C. Batch Size Reduction

Evaluating and minimizing the batch size of various processes can yield substantial results. Large batch sizes lead to the potential for greater quality errors and increased lead time. By reducing batch sizes throughout the process, it can provide better agility to respond to customer demand. In addition, large batch sizes can result in downstream constraints in the process. By reducing batch sizes,

The influence of nano- and micro- fillers on heat transfer in electrical insulation system

T. Tomášková¹, M. Svoboda², P. Trnka³

Department of Technologies and Measurement, Faculty of Electrical Engineering, University of West Bohemia in Pilsen, Czech Republic, <http://www.zcu.cz/>

¹⁾ tel: +420 37763 4570, email: tomaskot@ket.zcu.cz

²⁾ tel: +420 37763 4532, email: michal88@ket.zcu.cz

³⁾ tel: +420 37763 4518, email: pavel@ket.zcu.cz

Abstract— This article describes the influence of nano- and micro- fillers on the properties of an electrical insulation system and heat transfer in electrical devices. Nano fillers may affect the fundamental properties of dielectric systems such as dielectric constant, dielectric strength, space charge, loss factor, resistance to partial discharge, thermal conductivity and heat transfer coefficient by convection. Heat transfer takes place in three ways by conduction, convection and radiation. Composites are used in electrical insulation system in applications where individual components or materials are not suitable. Using nano fillers can improve performance parameters of electrical equipment without necessity of design changes. The important matter is to study and mathematically describe the processes in high-voltage insulation systems, search for new materials which can improve dielectrics thermal properties and the overall efficiency of high-voltage electrical equipment.

Keywords— *electrical insulation system, dielectric constant, dielectric strength, space charge, loss factor, resistance to partial discharge, thermal conductivity*

I. INTRODUCTION

Electrical equipment is a complex system that is composed of several subsystems: mechanical, magnetic, electrical, ventilation and dielectric. Parameters of electrical equipment can be analyzed and modified but we must know the properties of the individual subsystems, of which the electrical equipment is assembled. For these reasons, it is necessary to pay close attention to thermal conditions in the electrical equipment, study and mathematically describe the processes taking place in high-voltage insulation systems. It is also important to study new materials which could improve the dielectric and thermal properties of electrical equipment. Nanomaterials, as state before can affect the electric, thermal and mechanical properties of dielectric systems.

II. HEAT TRANSFER IN ELECTRICAL DEVICES

With the increasing performance of electrical equipment, the great attention must be paid to the losses grow and therefore the issue of heat transfer. To prevent damage, it is important to handle the heat losses. Properly designed ventilation and dielectric system of electrical equipment can significantly affect their reliability, safety

and durability. It further reduces the weight of the electrical machine and thus the production costs. Before we analyze the influence of nano- and micro- fillers on the dielectric and thermal properties of a high - voltage insulation system, we must know the variants of cooling and heat transfer in electrical machines. By cooling of electric machines is meant taking away the heat caused by electromagnetic and mechanical losses. The cooling medium diverts heat loss. For the design of heating and cooling circuits, it is necessary to know the ways of heat transfer. Heat transfer is the sharing of energy between molecules and atoms (transfer of energy from a place with a higher temperature to a place with a lower temperature). Heat transfer takes place in three ways by conduction, convection, and emission (radiation).

A. Transfer of heat by conduction

The second Fourier's law is used to describe the spread of heat dissipation. The most commonly used form of Fourier's equation of heat conduction [1] is:

$$\frac{\partial T}{\partial t} = a \cdot \nabla^2 T + \frac{q_v}{c_p \cdot \rho} \quad (1)$$

Were: ∇^2 - Laplace operator

$$\nabla^2 = \frac{\partial^2}{\partial x^2} + \frac{\partial^2}{\partial y^2} + \frac{\partial^2}{\partial z^2} \quad (2)$$

T	is the temperature (K)
x, y, z	are the spatial coordinates
q_v	is the heat flow released intrinsic sources ($\text{W} \cdot \text{m}^{-2}$)
ρ	is the density ($\text{kg} \cdot \text{m}^{-3}$)
t	is the time (s)
a	is the thermal diffusivity ($\text{m}^2 \cdot \text{s}^{-1}$)
c_p	is the specific heat capacity ($\text{J} \cdot \text{kg}^{-1} \cdot \text{K}^{-1}$)
λ	is the thermal conductivity ($\text{W} \cdot \text{m}^{-1} \cdot \text{K}^{-1}$)

The thermal diffusivity of a material is a measure of how fast the material temperature adapts to the surrounding temperature (3). Thermal diffusivity of a material influences the penetration and speed of

temperature adaption under a varying thermal environment.

$$a = \frac{\lambda}{(\rho \cdot c_p)} \quad (3)$$

Thermal conductivity is a physical parameter of the substance, which depends on the temperature, pressure and chemical composition of the substance (4).

$$\lambda = \frac{P \cdot d}{S \cdot \Delta T} \quad (4)$$

The power P passes through the sample surface area S and thickness d , with the temperature difference ΔT on the inner and outer surfaces of the sample. Determination of thermal conductivity is simply, in the case of a homogeneous substance. The situation is complicated by heterogeneous substances. In these cases, the thermal conductivity is influenced by the processing technology. Values of thermal conductivity for different substances can be found in Table I [1], [2].

TABLE I. VALUES OF THERMAL CONDUCTIVITY

Substance	λ (W·m ⁻¹ ·K ⁻¹)
Gases	0 - 0,1
Liquids	0 - 1
Solid	0 - 400

B. Transfer of heat by convection

Transfer of heat by convection is the movement of various fluids of different temperature and different densities of internal energy. During convection heat exchange takes place, for example, fluid flow passes, or removes heat from the surface of the substance. Convection can be divided into natural and forced. What follows is the part, which is focused on heat transfer between the liquid and solid material. It can be described mathematically as the equality of the first Fourier's law and Newton's law [1], [2]:

$$q_{konv} = -\lambda \cdot \text{grad } t = \alpha_{konv} \cdot (T_{pov} - T_{tek}) \quad (5)$$

Were:

- q_{konv} is the convective heat flow (W)
- $\text{grad } t$ is the temperature gradient
- T_1 is the temperature of solid substances (K)
- T_2 is the temperature of the fluid flowing (K)
- α_{konv} is the coefficient of heat transfer (W·m⁻²·K⁻¹)

Coefficient of heat transfer determines the intensity of heat exchange between the fluid and the surface of solids. Equation which allows calculation α_{konv} contains physical properties of the liquid, the nature of the flow under certain conditions. A general criterion equation of heat transfer by convection describes the process of heat transfer by convection [1], [2], [3]. Coefficient of heat transfer depends on the properties and flow velocity of the fluid and also on the shape of the surface. Values of coefficient of heat transfer by forced and natural convection can be found in Table II [2], [4].

TABLE II. VALUES OF COEFFICIENT OF HEAT TRANSFER

Substance	α_{forced} (W·m ⁻² ·K ⁻¹)	α_{natur} (W·m ⁻² ·K ⁻¹)
Gases	25 - 250	2 - 25
Liquids	50 - 20 000	50-1 000

C. Transfer of heat by emission (radiation)

Radiation is the third way of heat transfer. Energy transfer is carried by electromagnetic waves as in case of light. There are two theories of the behavior of light - wave theory, where the light can describe classical electromagnetic theory and the quantum particle theory (interaction of light with matter, laser). Radiation in large electrical equipment does not apply so significantly as conduction and convection. With regard to the accuracy of the thermal calculations it can be neglected.

III. COMPOSITE MATERIALS

Composite material is a material made of two or more constituent materials with different physical and chemical properties. When they are combined, they form a material with characteristics different from the individual components [5], [6], [7].

A. Particle Reinforced Composites

Composite material that consists of particles of one material embedded in another material can be called particle composites. In most cases inorganic isometric particles are used. Their composition is varied for example calcite, oxides of silicon, aluminum and magnesium and mica. Particle fillers is changing mechanical properties (elastic module, toughness, hardness, density) matrix.

According to the size filler (reinforcement) composites can be divided into the nano, micro and macro composites. Nanocomposites can have reinforcing phase dimensions (length or diameter particles) in the units to tens of nm. Microcomposites have dimensions of reinforcement (transverse sizes of particles or fibers) from 10⁰ μm to 10² μm.

B. Fiber Reinforced Composites

Composites can be classified according to their fiber reinforced into short and long. In general, mechanical properties of the materials reinforced with the short fibers are better than the properties of unreinforced materials. Short fibers can be dispersed in a matrix of random or preferred orientation. Long fiber reinforced composite materials are lightweight, durable and rigid. Hybrid composite materials are made of different types of fiber reinforcement (fabric composed of carbon and aramid fibers). Fiber reinforced composites that include particulate fillers can be called hybrid composites. Composite materials can be divided into two - component and three - component. These composite materials may be reinforced with paper, fabric, glass fiber, PEN, PET foil. Phenolic, silicone, melamine and epoxy resins can be used for impregnation. Dielectric barrier (filler) provides electrical strength of the resulting composite (mica paper).

IV. PROPERTIES OF NANO- AND MICRO-COMPOSITES

Molecular motion in nanocomposites is limited by a strong link between a nanofiller and a matrix. The nanocomposites can have certain properties which are different from microcomposite materials. The shape, volume and dimensions of nano- or micro- fillers can affect many properties of the resulting material. Many scientific teams focused their research on electrical insulation composites with nanomaterial [8], [9], [10]. The aim is to influence the electrical and thermal properties by adding a certain amount of nanofillers.

A. The influence of fillers on electrical properties

When the polymer is filled with inorganic fillers of micrometer sizes (a few tens of percent), permittivity usually grows. Micro fillers have higher permittivity than an unfilled polymer and also cause interlayer polarization. When the polymer is filled with inorganic nanoparticles (a few of percent), we can observe a decrease in permittivity. If the nanoparticles are dispersed evenly, the mobility of the polymer chain may be limited.

Loss factor $\tan \delta$, depending on the fillers exhibits a different behavior. For example, nanofiller titanium dioxide (TiO_2) in epoxy base reduces the loss factor, especially at low frequencies about 0.1 to 1 Hz [10], and high temperatures. By contrast, nanofiller silica (SiO_2) has a lower value of $\tan \delta$ than pure epoxy resin at mains frequency and also shows an increase at frequencies above about 100 kHz [8].

In many cases there was a reduction in the space charge in composites with nanofillers [7], [8], [9]. Examples are nanocomposites of the base epoxy and inorganic isometric particles (TiO_2 , Al_2O_3 and ZrO_2), or composites of the base polypropylene (PP) and ethylene vinyl acetate (EVA) with filler layered silicate nanocomposites. When the filler has a micro - dimensions, the electric field of the space-charge is double [6].

B. The influence of fillers on thermal properties

Addition of filler with good thermal conductivity to the composite may increase its thermal conductivity. Materials with low thermal conductivity form a thermal barrier on the path of the heat flow from its beginning in the electrical equipment to the cooling medium. Table III shows the values of the thermal conductivity of the individual components of composite materials [7]. The value of laboratory prepared polyethylene nanofibers, which have a high thermal conductivity of about $104 \text{ W} \cdot \text{m}^{-1} \cdot \text{K}^{-1}$ [7] is remarkable.

TABLE III. VALUES OF THERMAL CONDUCTIVITY

Material	$\lambda (\text{W} \cdot \text{m}^{-1} \cdot \text{K}^{-1})$
Phenolic resin	0,35
Epoxy resin	0,3
Polyamide	0,21
Aluminum oxide	25 - 30
Zirconium oxide	3,76

V. EXPERIMENT

It is quite challenging to accurately measure the amount of heat that passes through some material. Therefore, a simple device for measuring heat transfer of material was created, which can be seen in Figure 1.



Fig. 1. Arrangement for thermal conductivity measurement.

Polystyrene PS as a thermal insulator ($0,04 \text{ W} \cdot \text{m}^{-1} \cdot \text{K}^{-1}$) was used for the production of the box with inner dimensions of $80 \text{ mm} \times 110 \text{ mm} \times 200 \text{ mm}$, which are pasted to each other. A sample of dimension $120 \text{ mm} \times 90 \text{ mm}$ is placed in the middle and divides the polystyrene box into two parts. In the inner part is hanged 10W resistor, which serves as a source of heat. The measuring sensors are attached to the both surfaces of the sample. Since polystyrene is a better thermal insulator and polystyrene walls are thicker than the samples used, most of the heat produced by the resistor passes through the sample. The thermal power of the resistor is equal to the energy released (heat) in a given time. Thermal conductivity of the sample was calculated from the measured data using an equation (4). Table IV shows the values of the thermal conductivity of the five samples.

TABLE IV. THE VALUES OF THE THERMAL CONDUCTIVITY AND LOSS FACTOR

The sample	$\lambda (\text{W} \cdot \text{m}^{-1} \cdot \text{K}^{-1})$	$\tan \delta$
Plain Epoxy	$8,63 \cdot 10^{-02}$	0,0144
Epoxy + Al_2O_3 25 %	$1,40 \cdot 10^{-01}$	0,0119
Epoxy + Al_2O_3 12,5 %	$1,21 \cdot 10^{-01}$	0,0153
Epoxy + Al_2O_3 6,25 %	$1,14 \cdot 10^{-01}$	0,0111
Epoxy + Al_2O_3 3,125 %	$1,07 \cdot 10^{-01}$	0,0122

The sample was made with the use of these materials: epoxy resin and aluminum oxide (Al_2O_3). In this research, an attempt was made to determine how the addition of fillers (Al_2O_3) affects the thermal and electrical properties (Fig. 3 and Fig. 4) of the sample. Five specimens were manufactured (the particular weight ratios are in tab. IV).

The thermal conductivity of the composite material is dependent on the dimensions and structure of the filler particles. The dimensions of the filler particles were approximately 0,1 mm (fig. 2). They were measured by a microscope Olympus SZX 10.

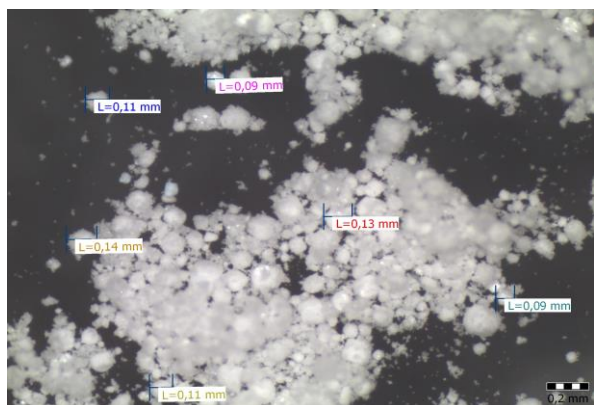


Fig. 2. The dimensions particle of the filler

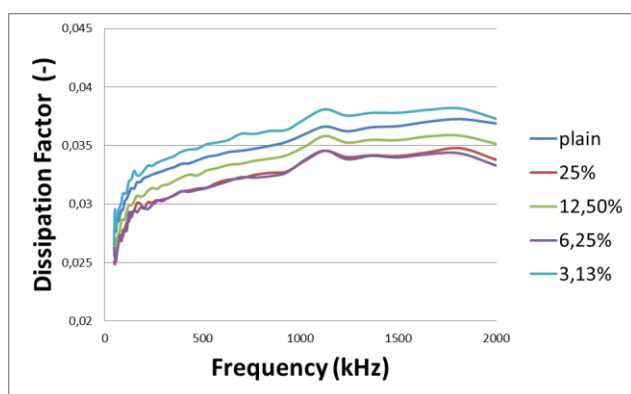


Fig. 3. Frequency dependence of $\tan \delta$ on samples filled by Al_2O_3

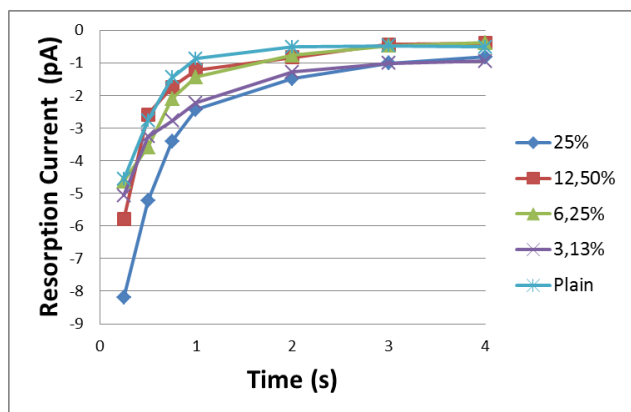


Fig. 4. Resorption currents on samples filled by Al_2O_3

VI. CONCLUSION

Temperature conductivity is an important parameter of electrical insulating system. This paper describes the impact of Al_2O_3 additive on thermal conductivity of epoxy resin. Thermal conductivity rises (as expected) with amount of Al_2O_3 (3,125 %, 6,25 %, 12,5 %, 25 %) The dimensions of the filler particles were approximately 0,1 mm. Measurement of the dependence of $\tan \delta$ and resorption currents was performed to check the impact to dielectric properties. The impact of fillers on the $\tan \delta$

dependence on frequency (about 5 kHz to 2000 kHz) was not observed. The resorption currents are clearly dependent on the filler concentration. This effect may be caused by the formation of space charge on inhomogeneities caused by accumulation of filler particles. After sample shortcutting thus it takes a longer time to release the free charge.

Acknowledgment

This research has been supported by the European Regional Development Fund and the Ministry of Education, Youth and Sports of the Czech Republic under the Regional Innovation Centre for Electrical Engineering (RICE), project No. CZ.1.05/2.1.00/03.0094 and supported by Student Grant Agency of the West Bohemia University in Pilsen, grant No. SGS-2012-026 "Material and Technology Systems in Electrical Engineering"

VII. REFERENCES

- [1] A., Macháčková, R., Kocich, Sdílení tepla a proudění, učební text, VŠB – Technická univerzita Ostrava ISBN 978-80-248-2576-2, [online] dostupné z: http://www.person.vsb.cz/archived/FMMI/STP/STP_FINAL_LAS_T.pdf, [cit. 11. 01. 2013]
- [2] M. Pavelek, Základy přenosu tepla, FSI VUTv Brně, Energetický ústav. Odbor termomechaniky a techniky prostředí, TERMOMECHANIKA. [online], dostupné z http://ottp.fme.vutbr.cz/users/pavelek/termo/15_Prenos.pdf, [cit. 21. 01. 2013]
- [3] O. Holeček, D. Šnita, Sdílení tepla, [online], [cit. 11. 01. 2013] dostupné z: <http://www.vscht.cz/uchi/ped/chi/chi.ii.uohy.k11.sdileni.tepla.pdf>
- [4] Sdílení tepla. 7/4/6. [online] dostupné z <http://www.vscht.cz/uchi/ped/bc05/07.sdileni.tepla.pdf>, [cit. 27. 01. 2013]
- [5] Classification of Composite Materials, [online] dostupné z http://www.ehow.com/list_7471987_classification-composite-materials.html, [cit. 27. 03. 2013]
- [6] T. Tomášková, "Perspektivní kompozity pro elektrotechniku," diplomová práce, ZČU Plzeň, 2012, vedoucí diplomové práce Doc. Ing Eva Kučerová, CSc.
- [7] T. Tomášková, M. Svoboda, P. Trnka, "Vliv nano- a mikroplniv na šíření tepla elektroizolačními systémy," in press.
- [8] J. Matoušek, "Modelování a chování složených soustav ve střídavém elektrickém poli," Brno: Vysoké učení technické v Brně, Fakulta elektrotechniky a komunikačních technologií, 2010. 60 s. [online], Diplomová práce, vedoucí Ing. Zdenka Rozsivalová, dostupné z: http://www.vutbr.cz/www_base/zav_prace_soubor_verejne.php?file_id=27654, [cit. 15.01.2013]
- [9] G.C. Montanari, D. Fabiani, F. Palmieri, D. Kaempfer, R. Thomann, R. Mulhaupt, "Modification of electrical properties and performance of EVA and PP insulation through nanostructure by organophilic silicates," IEEE Transactions on Dielectrics and Electrical Insulation, vol.11, no.5, pp. 754- 762, Oct. 2004
- [10] T. Tanaka, "Dielectric nanocomposites with insulating properties," IEEE Transactions on Dielectrics and Electrical Insulation, vol.12, no.5, pp. 914- 928, Oct. 2005

PD Series Prediction Based on Surface Charge Distribution Measuring by Matrix Method

P.N.Bondarenko¹⁾, O.A.Emelyanov, A.P.Gorlov, J.V.Shabanov, M.V.Shemet, I.N.Sorokoletov

St.Petersburg State Polytechnical University, Polytechnicheskaja st., 29, St.-Petersburg, Russia

<http://www.spbstu-eng.ru/>

¹⁾ tel: +7 921 978 35 83, email: bonpetnik@yandex.ru

Abstract— It is well known that during partial discharge (PD) the charge accumulates on the surface of dielectric barrier. This charge forms its own electric field and decreases the gap field. There is little information about quantitative estimation of the charge field role in the next PD evolution. So it is necessary to know the topology of the settled charge. This paper describes the matrix method of charge topology obtaining, topograms for some models being presented. The electric field has been calculated for the “needle-air gap-barrier-plane” model after each discharge. It has permitted to predict the following PD voltage. The calculated and experimental PD voltages have significant correlation.

Keywords — *partial discharge; charge distribution; probes matrix; field calculation; PD prediction.*

I. INTRODUCTION

This paper is devoted to the regularity problem of the PD series evolution for the general types of insulation defects. From the beginning of PD investigation it was considered as evident fact, that PD extinction is associated with charge accumulation on dielectric barrier. This charge forms the opposite field, decreases total field in the gap and leads to self-maintained discharge decay. That is why discharge repetition is possible only with voltage increasing. But this proposition is qualitative, and there is little information on quantitative estimation of charge role in PD development. As a result partial discharges are interpreted in experimental investigations as stochastic process rather than regular one. It is obvious that to solve the problem of PD series development prediction we need to measure not only the apparent charge of PD but (and it is more important) the local charge distribution on barrier surface. There are some methods which can be used for this purpose. First of all it is dust figure, then it is well known Kelvin probe, further it is the method based on Pockels' effect. Also the ultrasonic or laser probing of charge is used. Every method has its own advantages and limitations.

II. EXPERIMENTAL SETUP

In our investigations a new matrix method has been elaborated for surface charge spatial scanning measurement. Its application can be described on the base of charge study in the “needle-air gap-barrier-plane” model (Fig.1). High voltage (HV) is applied to the needle (1). When PD takes place in the air gap (at about 50-500 μm)

corresponding charge (2) settles on the barrier surface (3). Barrier is placed on the upper matrix structure surface which is built into the insulating plane (5). The matrix consists of $16 \times 16 = 256$ cylindrical probes which have a diameter of 0.35 mm and are disposed with a step 0.6 mm. Fig.1 represents only one row of 16 probes. Each probe is grounded through a capacitor of 150 pF.

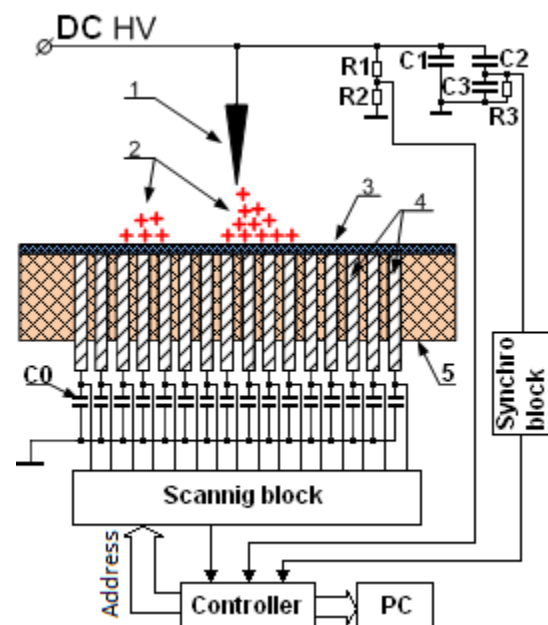


Fig.1 Block scheme of matrix method of the charge measurement.

The signals from each probe come to the Scanning block which multiplexes probes signal. The multiplexing begins with the appearance of PD when capacitive divider “C1, C2, C3, R3” forms a pulse which passes through the Synchro block to the Controller. The latter generates a binary address, corresponding to each probe, and Scanning block sends the analog signal from this probe to the Controller. The scanning duration is 2.56 ms. The high voltage signal comes to the Controller from a resistive divider “R1, R2” and is registered with PD simultaneously. The whole information consists of sequential number of PD, the PD ignition voltage and the array of 256 figures corresponding each probe potential comes to the personal computer PC. A special program has been created for data handling, including field calculation.

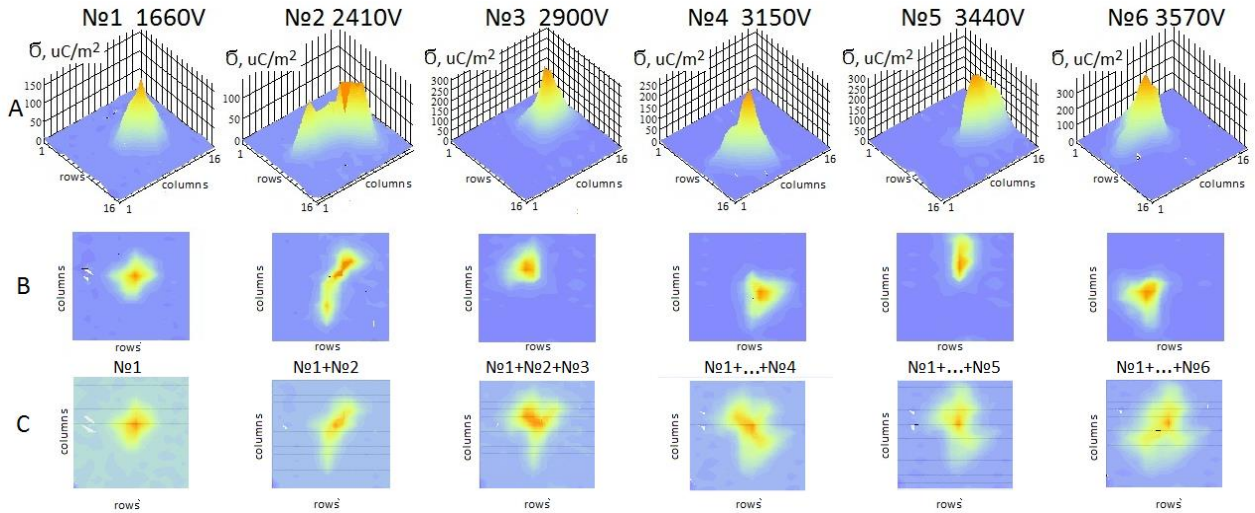


Fig.2 The charge density topograms of 6 PD for model “positive needle-air gap-barrier-plane” (A – 3D view of individual PD, B – top view of individual PD, C – top view of accumulated charge density).

III. EXPERIMENT RESULTS

In accordance with Fig.1 the investigation of charge topogram has been executed for positive polarity of the needle. The needle tip radius was 10 μm and the 100 μm polyethilenterephtalate (PET) film was used as a barrier. The air gap was 300 μm . The voltage was raised with a rate 50 V/s. Up to 3570 V six PD have been registered. The charge density topograms are presented in Fig.2.

3D views of individual PD are represented in the A row. The inception voltages for each PD (PDIV) are shown side-by-side with PD numbers. Top views are shown in B row. The summary views of charge densities are shown in C row. It can be seen that the charge spot of each next PD locates in another place. After receiving data about the distribution of the charge density the electric field calculation has been made by means of COMSOL Multiphysics v.3.5a software. The algorithm of this calculation consists of the following steps:

1. The evaluation of the maximum field strength vector ($\overline{E1}$) at the needle tip before the charge settling on the polymer surface; this module value is defined as a criteria of PD ignition $|\overline{E}_{crit}| = |\overline{E1}|$;
2. The determination of the field strength $\overline{EQ1}$ at the needle tip induced by the settled charge;
3. The calculation of the vectors sum module $|\overline{E1}_{sum}| = |\overline{E1} + \overline{EQ1}|$ (the module of the gap field vector will decrease);
4. The evaluation of a new applied voltage using the iteration method when summary gap field will be equal the critical value $|\overline{E1}_{sum}| = |\overline{E}_{crit}|$; this applied voltage is the voltage $U2'$ of the expected nearest PD or the predicted voltage;
5. The procedure is repeated for all PD.

The calculation result is presented in Fig.3.

The correlation coefficient has been evaluated as follows:

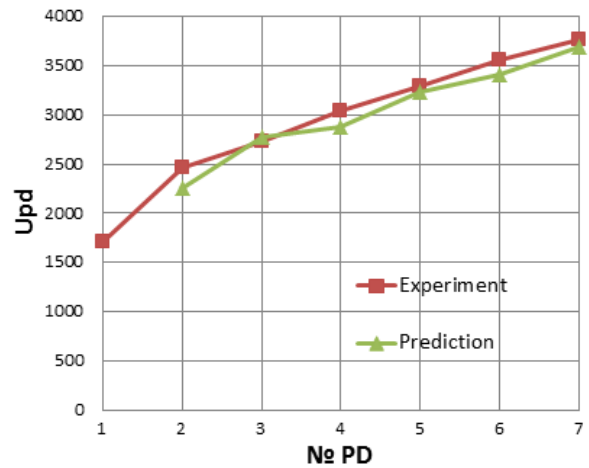


Fig.3 The comparison of the experimental and prediction appearances of six PD series with positive needle.

$$r_{xy} = \frac{\sum_i (x_i - M(x))(y_i - M(y))}{\sqrt{\sum_i (x_i - M(x))^2 \sum_i (y_i - M(y))^2}}, \quad (1)$$

where $M(x)$, $M(y)$ - mathematical expectation, x_i , y_i - current values.

For the experimental and prediction curves in Fig.3 $r_{xy}=0.97$, i.e. there is a significant correlation between these values.

The experiments with the negative polarity of the needle have been carried out in the same conditions. For the interval up to 3889 V twenty PD have been registered. The charge density topograms for six of them are presented in Fig.4. In contrast with the positive needle experiment the charge spots have accurate round forms and are located on the needle axis. The results of electrical fields computations and forecasted voltages of each next PD ignition are shown in Fig.5. The calculating algorithm was the same as in the case with the positive needle. The correlation coefficient is $r_{xy}=0.97$, i.e. there is significant correlation between this values too.

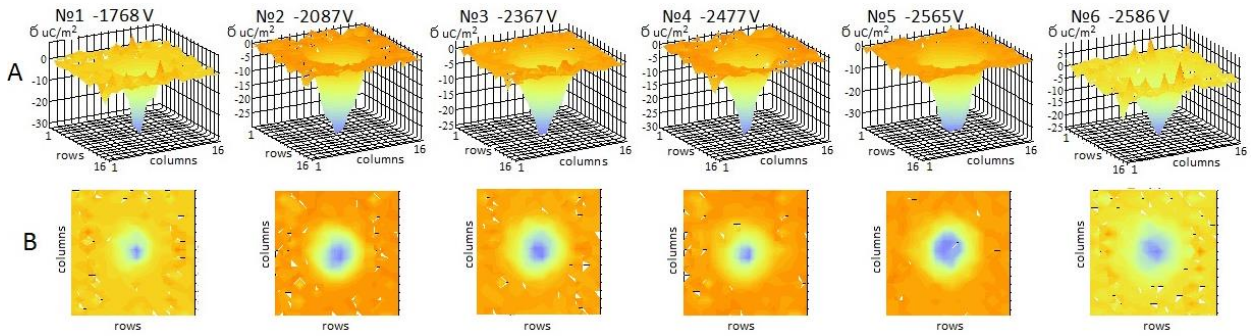


Fig.4 The charge topograms of 3 out of 11 series PD for model “negative needle-air gap-barrier-plane”.

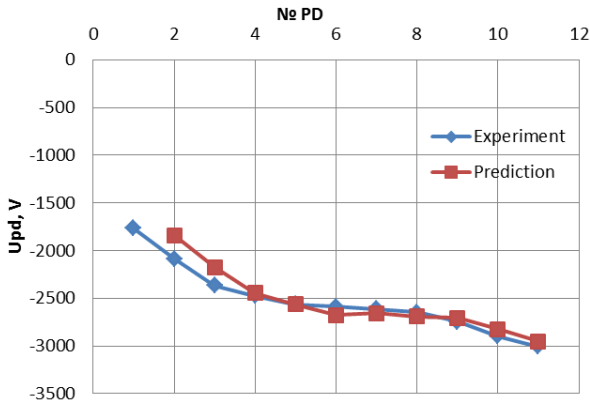


Fig.5 The comparison of the experimental and prediction appearances of eleven PD series with negative needle.

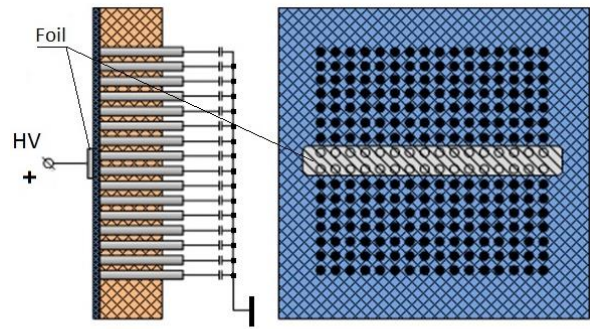


Fig.6 The scheme simulating the edge PD (a) and charge topogram sum after each of nine PD (b).

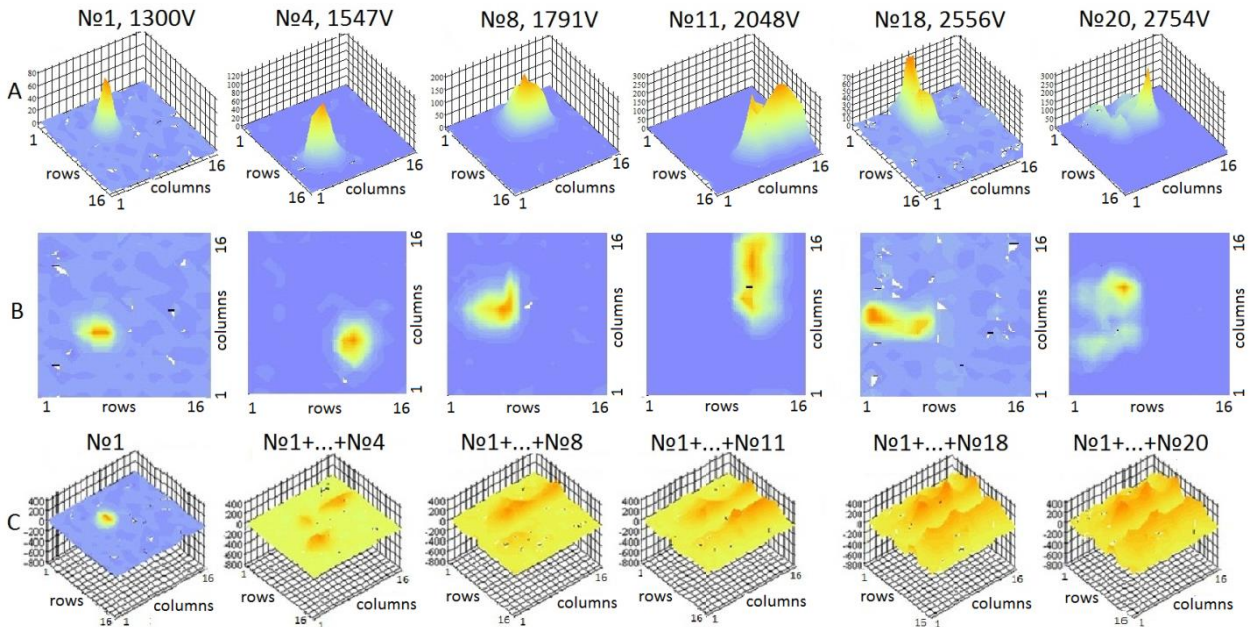


Fig.7 The charge topograms of 9 out of 20 series of edge PD with positive foil.

The next experiment was carried out for edge PD simulation. For this purpose a narrow aluminum annealed foil electrode (1.2 mm wide, 8 μm thick) was placed on the barrier surface above the matrix center (Fig.6).

The results of nine out of 20 PD registration are presented in Fig.7 (for positive foil). Three-dimensional views of individual PD are presented in the A row. The PDIV are shown side-by-side with PD numbers. The top views of individual PD are shown in the B row. The

summary charge density views are shown in C row. The discharges take place on both sides of the foil electrode.

Fig.8 shows the space charge distribution in the edge model with negative foil. For the interval up to -4804 V 39 PD have been registered, six of them are represented in Fig.8. Three-dimensional views of individual PD are shown in the A row. The top views of individual PD are shown in the B row. The top views of summary charge density distribution are shown in C row.

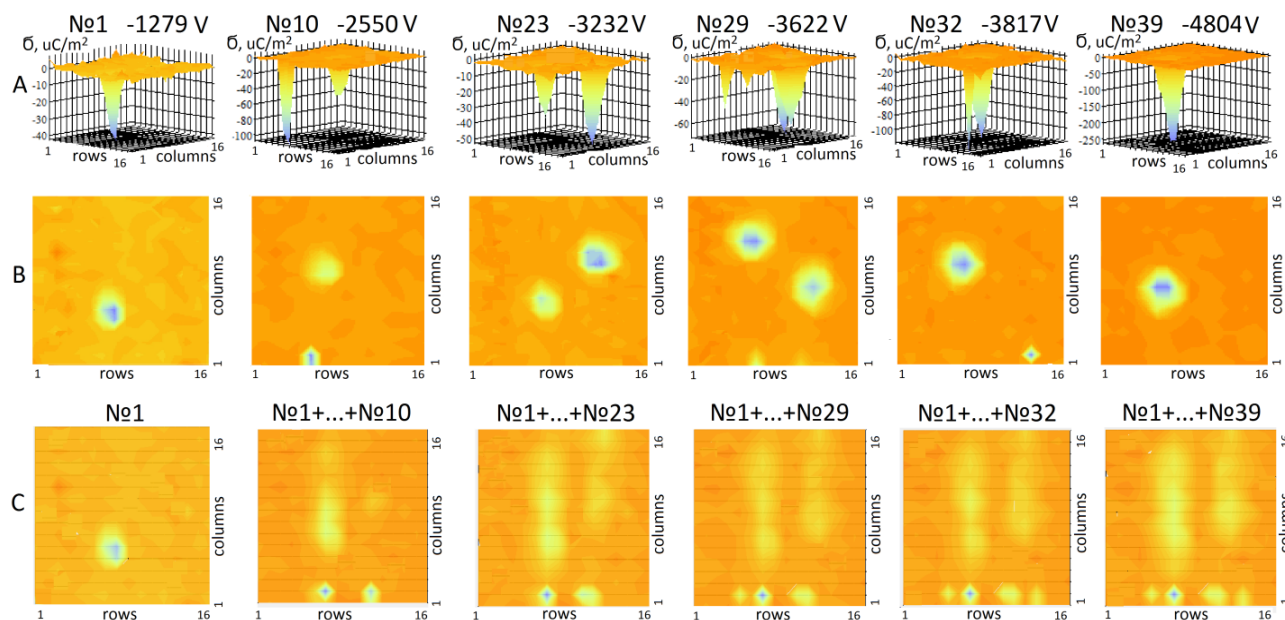


Fig.8 The charge topograms of 9 out of 39 series of edge PD with negative foil.

Sometimes several discharges occur simultaneously. It can be seen that there are very short voltage steps between the adjacent edge PD – they don't exceed 200 V.

IV. CONCLUSION

The represented matrix method gives a possibility to obtain detailed qualitative and quantitative information about the charge density distribution on the polymer barrier surface after PD. This method can be applied successfully to various models of insulation defects as it was shown by the example of an “edge PD” model and a “needle-air gap-barrier-plane” model. For the latter the settled charge field, the resulting gap's field and the expected value of each next PD ignition voltage have been computed. Strong correlation between the experimental and predicted voltages for PD successions has been marked.

REFERENCES

- [1] R. J. Van Brunt. Stochastic Properties of Partial-discharge Phenomena. IEEE Trans. on Electr. Ins., 1991, v.28, №5, 902-948.
- [2] Y. Murooka, S. Koyama. Nanosecond surface discharge study by using dust figure techniques. J. Appl. Phys., 1973, v.44, №4, 1576-1580.
- [3] J.C. Devins, S.I. Reynolds. Rotating probe electrometer. Rev. of Sci. Instr., 1957, v.28, №1, 11-13.
- [4] Akiko Kumada, Shigemitsu Okabe, Kunihiko Hidaka. Residual charge distribution of positive surface streamer. J. Phys. D: Appl. Phys. 42 (2009) 095209 (8pp).
- [5] F. Gégot, Th. Callegari, M. Aillerie, J. P. Boeuf. Experimental protocol and critical assessment of the Pockels method for the measurement of surface charging in a dielectric barrier discharge. J. Phys. D: Appl. Phys. 41 (2008) 135204 (10pp).
- [6] T. Takada. Acoustic and optical methods for measuring electric charge distributions in dielectrics. IEEE Trans. Dielect. and Electr. Ins., 1999, v.6, №5, 519-547.

Influence of technological factors on thermal and electrical properties of insulation systems for large rotating machines

Andrey Bezborodov¹⁾, Tatiana Shikova²⁾

St.Petersburg State Polytechnical University, Polytechnicheskaja st., 29, St.-Petersburg, Russia
<http://www.spbstu-eng.ru/>

¹⁾ tel: +7 921 743 62 16, e-mail: a.bezborodov85@gmail.com,

²⁾ tel: +7 921 776 35 14, e-mail: t_shikova@mail.ru.

Abstract — Insulation systems of large rotating machines are simultaneously subjected to electrical, thermal, mechanical and chemical stress. That is why composite or compound materials are widely used in this application. The combination of such materials creates the desired insulation system properties. The special technological parameter of insulation - density (PI) is introduced. Dependence of electrical properties (tg δ , Eps and breakdown strength) and thermal conductivity of composite insulation materials, which are commonly used in rotating machines from that parameter are discussed in this paper.

Keywords— Resin-rich mica tapes, insulation density, life time, thermal conductivity.

I. INTRODUCTION

In the next few years the predicted increase of the world power consumption up to 30000 billion kW·h is going to lead to an increase in the manufacture of generating electric equipment. So there is a necessity of increasing such parameters of electric machines, as there quality, durability and reliability. Today great attention is paid to the development and research of electrical insulation materials and systems, capable of retaining their properties at a high level under long term influence of such factors, as high operating temperature, intensity of the electric field, mechanical loadings and vibration. Having low thermal conductivity insulation forms a barrier for the heat flow from current conducting parts of the machine to the cooling medium. It results in the temperature gradient which leads to the degradation of the main electrical and mechanical characteristics of insulating materials causing the breakdown of the whole construction.

Along with using fillers with high thermal conductivity such as Boron Nitride and Dioxide Alumina there are other ways to increase thermal conductivity (λ) of the insulation system.

High voltage stator windings insulation of electrical machines is a composite material and it consists of the following components: mica paper, fiberglass and epoxy

resin. Thermal conductivity of the composite system depends on the thermal conductivity of each component and its contents. The lowest thermal conductivity in such system has epoxy resin (0,20 – 0,25 W/(m·K)). It is necessary to reduce the content of this component to increase the thermal conductivity of the insulation.

II. EXPERIMENT

There are several ways of changing the contents of the components in the Resin Rich technology: temperature change during the preheating stage and variation the number of mica tape layers used for groundwall insulation of the rotating machines.

The next stage after samples preparation was the process of termopressing that restricts the sample dimensions. It is known that with the increase of the initial tape layers number (in case overall thickness of the sample being constant) increases in the removed epoxy resin, which leads to an increase of the insulation system mechanical properties [1]. To estimate the required number of layers of tape a special technological parameter of insulation - density (PI) was introduced. Insulation density - the number of layers of the mica tape, per 1 mm thickness of the insulation ($PI = n / d$, where n - the number of layers of mica tape, and d - the thickness of the final insulation). Therefore it is interesting to evaluate the effect of the insulation density parameter on the electrical and thermal characteristics.

Thermal conductivity of multilayer planar samples with different values of the parameter PI was investigated. For convenience in this paper, relative value of the density parameter $PI = PI_i / PI_{max}$ is used. Where PI_{max} - the maximum, and PI_i - the current value of the parameter. Planar samples were made of a different number of mica tape layers, but after termopressing average thickness of the samples was from 2.1 up to 2.2 mm. That was achieved by using the restraints during hydrostatic pressing on industrial equipment (duration was 6 hours, temperature was 160 °C).

The dependence of the thermal conductivity coefficient of the temperature was obtained by means of the thermal conductivity measuring device IT - λ - 400.

The instrument operates on the principle of monotonous heating when during basic period of time the temperature field in the sample under test remains nearly constant. The heating speed is determined by the initial heater voltage (30 V) and the speed of its change. Both values are strictly constant. The thermal scheme is shown in Fig. 1.

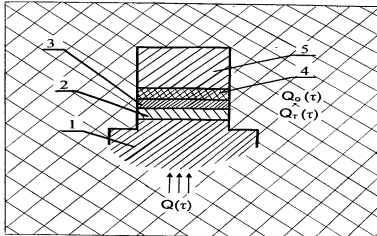


Fig. 1. Thermal scheme of the method.

Where:

1 - heated base, 2- plate of the calorimeter, 3- contact plate, 4- sample under test, 5- bar-condenser, $Q(\tau)$ - heat flows (W), $Q_T(\tau)$ - heat flows going through the medium section of the calorimeter plate 2 (W), $Q_0(\tau)$ - heat flows through the sample 4 and absorbed by the bar - condenser 5 (W), τ - time (s).

To determine the thermal conductivity during the experiment the differential of temperatures in the sample and the calorimeter plate was measured at the fixed points of temperature.

Taking into consideration the operating conditions of electrical insulation in electrical machines, the temperature range of thermal conductivity coefficient measuring was chosen from 25 °C up to 150°C.

The thermal conductivity coefficient was calculated as:

$$\lambda = \frac{h \cdot \vartheta_T \cdot k_T}{\vartheta_0 \cdot S \cdot (1 + \sigma_c) - P_k \cdot \vartheta_T \cdot k_T} \quad (1)$$

Where:

σ_c - correction of the heat capacity of the sample, ϑ_0 - temperature differential on the sample (K), S - area of the sample cross-section (mm^2), k_T - proportionality coefficient characterizing effective thermal conductivity of the calorimeter plate ($\text{W} \cdot \text{K}^{-1}$), ϑ_T - temperature differential in the calorimeter plate (K), h - sample thickness (mm), P_k - correction of the contact heat resistance of the sample ($\text{m}^2 \cdot \text{K} \cdot \text{W}^{-1}$).

Samples used in the measurements were made of standard Resin-Rich mica-containing tapes. In the experiments flat disk samples with the diameter $15,05 \pm 0,15$ mm and thickness (h) 1.3 to 2.1 mm were used. The experimental results (average results received in measuring of 5 samples) at the temperature 150 °C are presented in the Fig. 2.

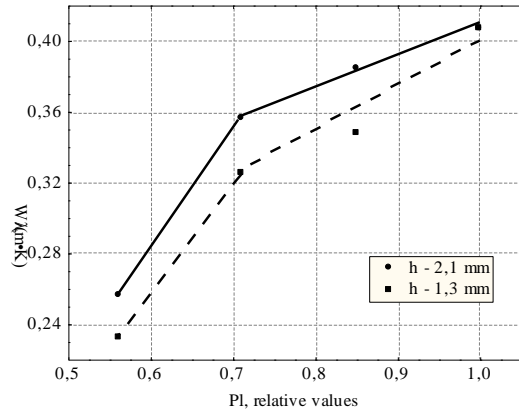


Fig. 2. Dependence of the thermal conductivity from the insulation density.

Analyzing the Fig. 2, one can come to the conclusion that change in the thickness of the samples did not lead to a significant change in λ . Increase of the parameter PI from 0,57 to 1,0 leads to the increase of the thermal conductivity at 150 °C. from 0,25 to 0,42 $\text{W}/(\text{m} \cdot \text{K})$. This effect is associated with a decrease in the mass fraction of epoxy resin (C_{er}) in insulation from 0,38 to 0,24 (Fig. 3). In this case, the form of the dependences $\lambda = f(PI)$ is maintained irrespective of the samples thickness. Moreover, the value of thermal conductivity - 0,42 ($\text{W}/(\text{m} \cdot \text{K})$), seems to be maximum for the insulation system, since further decrease of epoxy resin content is impossible. So the optimization of the process parameters (increase of the insulation density) can increase the thermal conductivity of the insulation system only up to a certain level. But having obtained this result, we can argue that the decline in the value of the parameter PI below 0.7 is unacceptable.

The assumption about the influence of the components content was verified by calculating the volume fraction of the components in insulation. This calculation show that a decrease in technological parameter PI below 0.7 in the insulation system leads to the fourth component - air. Sharp fall of the thermal conductivity at the slight change in C_{er} (Fig.3) can be explained by the fact that volume content of the air is about 30%.

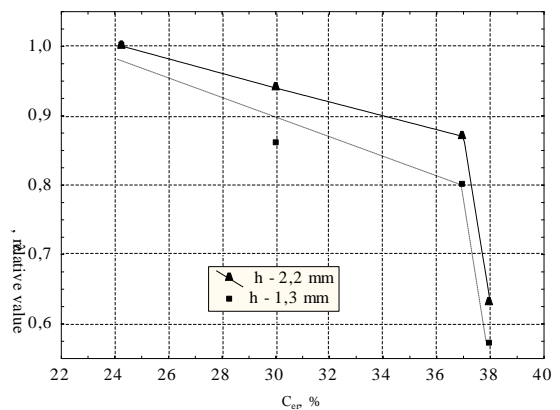


Fig. 3. Dependence $\lambda = f(C_{er}, \%)$.

Samples for measuring the dissipation factor ($\text{tg}\delta$) were created from risen-rich mica tape. Their size was 100 x 100 mm and thickness was from 2,1 to 2,2 mm. They were cured under the hydrostatic pressure 1 MPa at the temperature of 160°C.

The dissipation factor was measured by three-electrode system Vector 2.0. The results of this experiment are presented in Fig. 4.

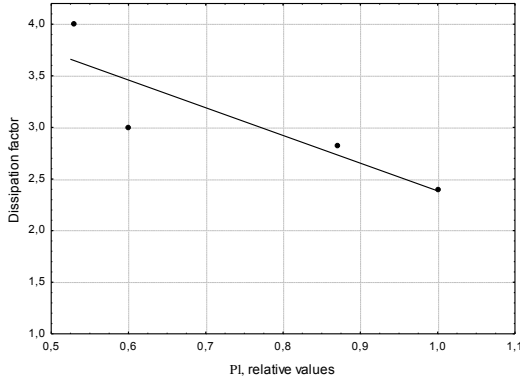


Fig. 4. Dissipation factor dependence from insulation density.

As one can see in Fig.4, the level of the dissipation factor is the highest within the samples with density 0,57. Decrease in $\text{tg}\delta$ dependence is primarily due to the fact that there is no low-molecular plasticizer in epoxy resin and the conductivity at the temperature to 155 °C does not change.

The second important electrical characteristic is a dependence of the permittivity on density. Analyzing the Fig.5, applying to all tested density interval (8,0 – 10,6) one can come to the conclusion that the character of the dependence $\epsilon=f(C_{\text{cr}})$ coincides with the dependence of $\lambda = f(C_{\text{cr}})$. With an increase of epoxy resin content in the samples up to 37-38%, which corresponds to the content of the epoxy resin in the original insulation tapes, a sharp decrease of the dielectric constant occurs. What could be due to the formation of air gaps in the samples structure.

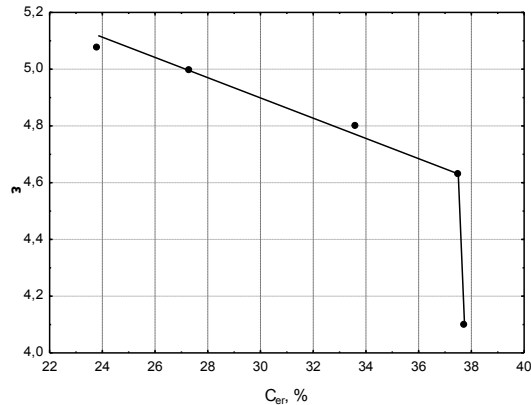


Fig. 5. Dependence $\epsilon=f(C_{\text{cr}})$.

The study of the samples integrity was carried out by fixing the weight gain during long-term exposure in the aquatic environment.

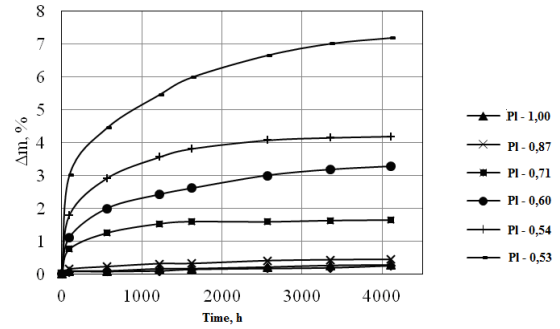


Fig. 6. Time dependence of samples moisture increasing.

After exposure in water for 4000 hours, the samples saturation occurs. In this case, the presented curves show that least dense samples (corresponding the values PI from 0,56 to 0,7), absorbed a lot of moisture. Attainment of saturation can be interpreted as filling all the air gaps with water. Volume occupied by the water was calculated (i.e. the volume of entrapped air). It was shown that the samples having the maximum density (PI = 1) contain less than 1% of air gaps. Least dense sample comprises not less than 10.7% impurities in its volume, which is equivalent of 0,16 mm thickness of air layer. But, apparently, these air gaps are dispersed throughout the sample.

The pore volume can also be calculated by considering the samples mass, mass of all mica tapes components and their density that can be determined by the hydraulic weighing. For the sample with the highest number of air gaps calculated value of C_{air} was 11.6%, which is well coincides with the experimental result (Fig.7).

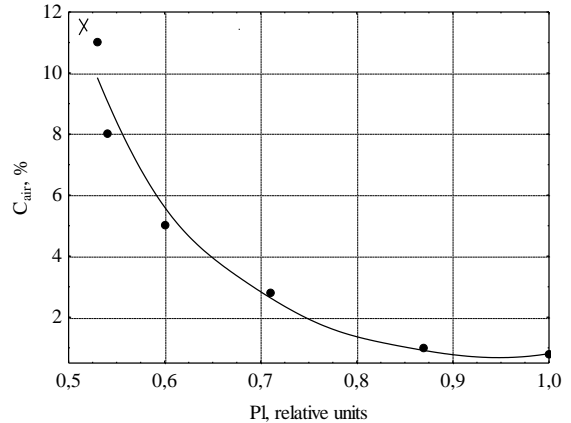


Fig. 7. Connection between content of air gaps in the sample and insulation density.

The third important parameter for the insulation materials that are commonly used in rotating machines, is their life time. The long-term breakdown strength was obtained by aging samples at voltage level of 7.5 kV(50 Hz) for 360 hours, further ascent with speed of 2 kV/24 hour up to 15kV (50 Hz) and exposure till its breakdown.

For the analysis of long-term breakdown strength, function of times distribution before breakdown for

insulation (τ) has been constructed. Empirical distributions of operating time values to refusal are described by two-parametrical Weibull distribution:

$$F(t) = 1 - \exp(-\tau/\tau_{63})^\beta, \quad (2)$$

Where:

τ - the time before breakdown; τ_{63} - the time constant (63 % kvantil for an operating time to breakdown); β - the shape parameter.

Statistical distributions of times before breakdown (on a likelihood paper of two-parametrical Weibull law) are presented in the Fig. 8.

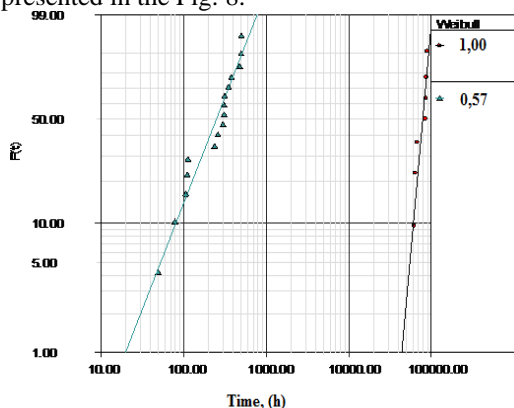


Fig. 8. Distribution of life time at U = 15 kV for samples.

From Fig.8 we can find out that destruction of several insulation layers of the samples with maximum density ($PI = 1$) does not lead to rapid destruction of the remaining layers under the interlaminar discharge. It is not so for the samples with lower density ($PI = 0,57$), which would be sensitive to any damage of the layers in the process of taping, and in the course of operation.

Decreasing in insulation density can negatively affect the life time of the isolation system.

Another milestone should be noted. In the case of non-compliance parameters preheating stage or its wrong choice, due to premature curing epoxy resin, parameter PI can be reduced even in the case of applying the required number of layers of mica tape. Therefore, all of the data on the impact parameter in PI insulation performance can be attributed to the description of the influence of premature curing (at the preheating phase) on the properties of the insulation.

III. CONCLUSION

This paper describes the possibility of increasing thermal conductivity and long-term breakdown strength by changing such parameter of the insulation as its density. Other find out that samples having maximum value of density, had maximum thermal conductivity - 0,42 (W/(m·K)) and life time - 8,7x104 hours. Increasing the insulation density allows to decrease dissipation factor and percentage of the air gaps. However, this question demands further research in view of (considering) different types of insulating mica tapes. Research work in this field will be continued.

REFERENCES

- [1] Shikova T.M. "Improvement of the system of the insulation of the large electrical machines from the resin-rich materials," *Electrotechnics*, vol. 3, pp.8-13, March 2007.
- [2] Polonsky Y.A., Bezborodov A.A., Kovalev A.G. "Measuring the thermal conductivity of the insulation materials, using in high voltage rotating machines," *Electrotechnics*, vol. 3, pp.15-19, March 2009.

Insulating liquids without negative impact on the environment

Vaclav Mentlik¹⁾, Pavel Trnka¹⁾, Jaroslav Černý²⁾

¹⁾University of West Bohemia, Univerzitní 8, 306 14 Pilsen, Czech Republic, www.zcu.cz

¹⁾tel: +420 377 634 406, email: mentlik@ket.zcu.cz

²⁾Institute of Chemical Technology Prague, Technická 5, 166 28 Prague, Czech Republic, www.vscht.cz

²⁾tel: +420 220 443780, email: Jaroslav.Cerny@vscht.cz

Abstract — Currently used electrical insulating liquids are due to their uneasy biodegradability and negative impact on the environment and human health problematic. Given by the need of elimination of the negative influence of electrical equipment on the environment it is necessary to develop a fluid from raw materials which are by their nature environment-friendly. They should be easily biodegradable so will not cause current difficulties and economical losses. A liquid emphasizing biodegradability and good electrical insulating properties at the same time is not in central Europe produced yet. Such a fluid should be technically equivalent to the currently used mineral fluids. Therefore, it is necessary to pay maximum attention to this area.

Keywords— *biodegradability; electroinsulating fluid; insulating mixtures; ester*

I. INTRODUCTION

Insulating fluids are undoubtedly an integral part of the insulation system of most power transformers, especially because the machine with the insulation system, which is represented by the liquid and solid components, allow the transmission of virtually limitless power.

Currently used liquids are however very problematic by their nature and especially by its uneasy degradability and negative impact on environment and human health. Opinions in areas of relationship of technical equipment and the environment that currently prevails, clearly leads to the search for ways how to eliminate the negative effects of such as devices on the environment. This of course determines the search for solutions enabling the development and production of fluids manufactured from raw materials which are by their nature environment-friendly and easily biodegradable and not causing current difficulties and losses experiencing while using actual insulating liquids.

It is essential to find ways of solving this issue and emphasize respect for the maximum utilization of domestic resources and sources of alternative or renewable energy in accordance with sustainable development programs.

Another aspect which has to be considered is the possibility to develop variation of liquids with different degree of biodegradability. In some less demanding areas may not be as consistent asset emphasis harmlessness of used liquid in link to the surrounding environment. Some areas do not strictly need harmless insulation liquid, because this topic is treated different way.

This will entail respecting economic aspects, as an indisputable advantage of these insulating liquids would be their lower price, and thus better economic acceptability. Currently, in addition to conventional oils or inflammable liquids in Czech Republic are not yet used fluids accentuating biodegradability simultaneously with excellent electrical insulating properties. It means that they are technically equivalent to currently used mineral fluids used in power electrical devices.

II. REQUIRED PARAMETERS OF NEW ELECTRICAL INSULATING FLUIDS

A new feature that is required is biodegradability. These fluids thus by their properties shall conform to products already introduced to the market but with considerable higher price. The issue of higher price also speaks against their application on market. The main limiting and required properties should be in accordance with the technical specifications for the new synthetic organic esters for electrical purposes [1] and should have electroinsulating properties in limits specified in Table 1.

TABLE I. REQUIRED PROPERTIES OF NEW ELECTRICAL INSULATING FLUIDS

parameter	unit	value
density	kg/dm ³	max 1
kinematic viscosity at 40 °C	mm ² /s	max 35
kinematic viscosity at 20 °C	mm ² /s	max 3000
breakdown voltage	kV/2,5 mm	45 - 50
dissipation factor tan δ	-	max 0,03
inner resistivity at 90 °C	GΩ.m	min 2
acid number	mg KOH/g	max 0,3
water content	mg/kg	max 200
flash point	°C	min 250
pour point	°C	max - 45
appearance	-	clear with no sediment

These parameters also reflect the nature of already existing products such as biodegradable and non-flammable transformer oil MIDELE 7131.

Oil that can be compared to new developed product is a product of COOPER, Wisconsin, USA distributed as Envirotemp FR3.

Important features of these two products are given in Table 2 for comparison.

TABLE II. CHARACTERISTIC FEATURES OF MIDEL AND ENVIROTEMP FR3

parameter	unit	MIDEL 7131	ENVIROTEMP FR3
characterization	-	ester-based transformer oil	natural based oil with antioxidant, additive and pigment
breakdown voltage	kV/2,5 mm	75	60
acid number	mg KOH/g	0,03	max 0,06
dissipation factor tan δ	-	0,03 (at 90°C)	0,02
flash point	°C	275	300
pour point	°C	-60	-18
water content	mg/kg	50	150

Interesting is the price range of presented fluids, when it should be noted that recent price of these oils (MIDEL and Envirotemp) is almost eight times higher than the price of today used mineral oil.

III. POSSIBLE WAYS IN NEW LIQUIDS RESEARCH

In accordance with the current level of knowledge new electrical insulating fluids can be obtained using two accesses. First, entirely new fluid manufactured from raw materials can be found while achieving optimum desired properties - in particular their complete biodegradability. The second, it is a possibility to prepare insulating fluid by mixing compounds, which have acceptable biodegradability considering the demands of the desired properties - the search for cheaper and acceptable variations.

While considering the new electrical insulating liquids one can turn attention to substances with good biodegradability as: alkyl esters, tri-alkylesters of citric acid, di-alkyls of malic acid, alkyls of ethoxylated alcohols and alkyl esters of selected amino acids. In these compounds, by the appropriate selection of alkyls during the synthesis of alkylesters, we can eliminate instability of natural triglycerides, and thus increase the thermal-oxidative stability. It is however necessary to address the problem of easy water binding by mentioned compounds, which is so far disadvantage. However it is a direction of research that can be worth for further fluids development.

IV. NEW ELECTRICAL INSULATING MIXTURES

As already stated, the other way to get new biologically degradable insulating fluids is to find suitable materials with proper physical and electrical properties and low price at the same time.. This access naturally require not only considerable experience in the field, but also the corresponding experimental verification of properties of mixtures in order to refine their performance. In the first phase were examined properties of mixtures whose, composition and basic physical properties - density and viscosity at 40 °C are shown in Table 3.

TABLE III. TESTED INSULATING MIXTURES

tested fluid	density 40°C kg.m ⁻³	kinematic viscosity at 40 °C mm ² .s ⁻¹
50% Radiolube 7388 + 50% Nivol N 108	0,8779	20,51
50% Di-2ethylhexyl Adipate + 50% Nivol ONP 18	0,8645	11,19
Zerol Ester 32 A	0,985	32
Zerol Ester 32 B	0,985	32
80% Zerol Ester 22 + 20% Nivol N 108	0,9457	15,77
50% Zerol ester 22 + 50% Nivol N 108	0,8995	15,67

These mixtures (Table 3) were subjected to measurement of temperature (20 - 90 °C) and frequency (150 Hz – 150 MHz bridge TETTEX) dependence of the dissipation factor tan δ . The results are presented in Figures 1 and 2.

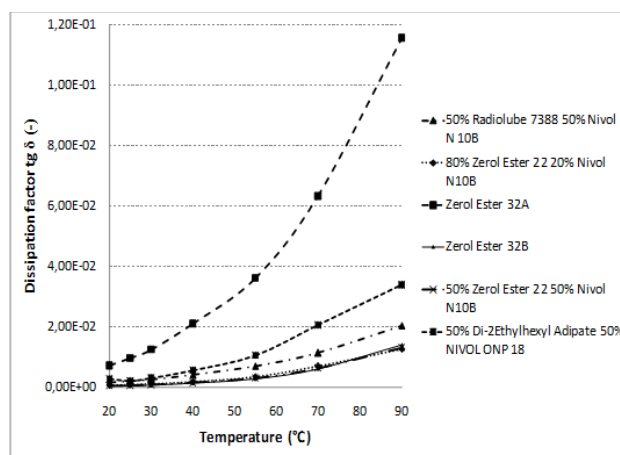


Fig. 1. Temperature dependence of the dissipation factor of measured liquids

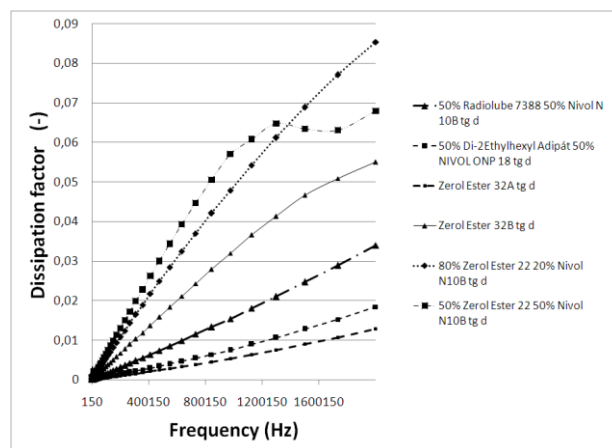


Fig. 2. Frequency dependence of the dissipation factor of measured liquids

From Figure 1 it is evident that the best dependencies have mixtures Zerol with Nivol, when the temperature dependence of the dissipation factor does not show a greater increase. Both mixtures with different ratios of the

two components (80 + 20, 50 + 50 % - Zerol + Nivol) prove almost identical dependence. Regarding the frequency dependence, Zerol and mixture of 50% di-2Ethylhexyl Adipate + NIVOL NP 18 have the lowest dielectric losses. Mixtures of Zerol + Nivol in both percentage variations showed higher losses. It is interesting to see a comparison of selected – best of prepared mixtures in the temperature and frequency dependence of the dissipation factor with the commonly used mineral oil Shell Diala DX. This comparison is captured in Fig. 3 and 4.

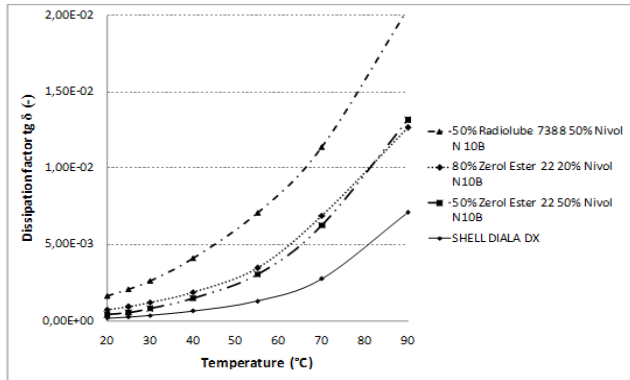


Fig. 3. Temperature dependence of the dissipation factor of selected monitored liquids compared to mineral oil Shell Diala DX

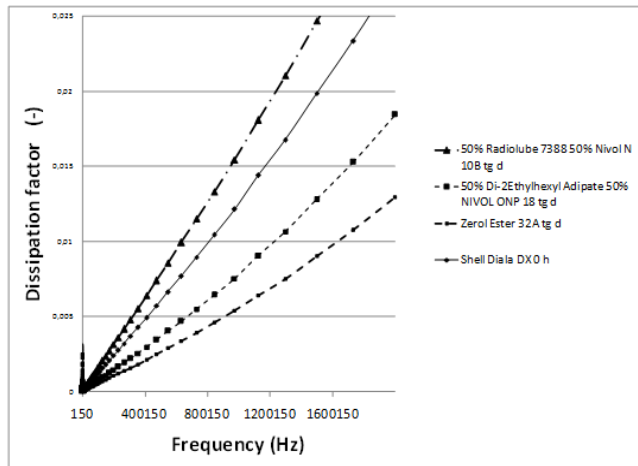


Fig. 4. Frequency dependence of the dissipation factor of selected monitored liquids compared to mineral oil Shell Diala DX

The temperature dependence shows that the mineral oil is the best from observed. The dependencies of mixtures Zerol and Nivol have the same trend as the dependence of Shell Diala DX. Their dielectric losses are however higher. Both mixtures, with different ratios of the components have virtually identical dependencies, however at lower temperatures is a mixture of 50 + 50 slightly better and the mixture of 80 + 20 has lower losses at 90 °C . Other mixtures have significantly higher dissipation factors than mineral oil. From frequency dependence it is evident that Zerol and mixture of 50% Di-2Ethylhexyl Adipate + NIVOL NP 18, are the best of all tested mixtures the best. They have lowest losses - having even better dependence than mineral oil Shell Diala DX. Mixtures of Zerol and

Nivol in both ratios did not show a suitable performance in frequency dependences.

In order to better assess the behavior of observed mixtures was measured frequency dependence of the test fluids at lower frequencies using dielectric spectrometer Novocontrol.

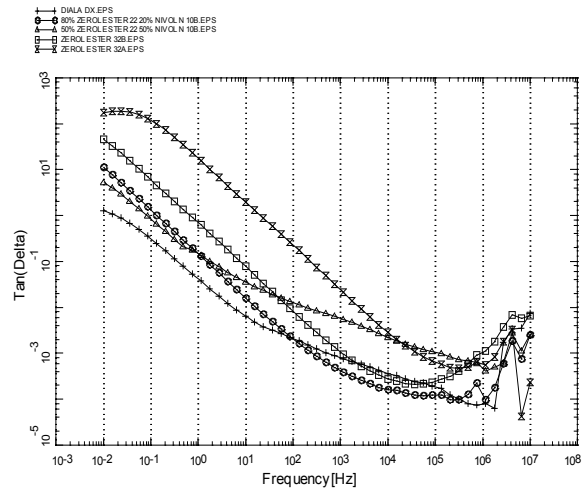


Fig. 5. Frequency dependence of the dissipation factor of selected monitored liquids compared to mineral oil Shell Diala DX

The sample of oil is placed in the small electrode system allowing to measure over a wide frequency range. The amount of liquid is only 40 μl . The identified dependencies are shown in the following figures 5 and 6. The dependence of mineral oil SHELL Diala DX is plotted fo

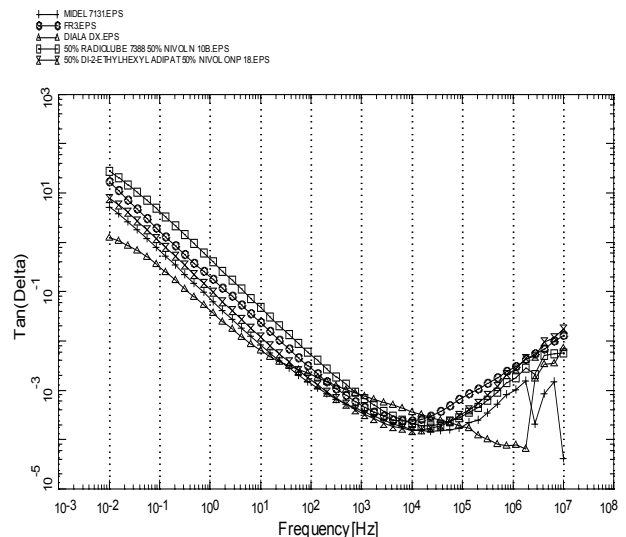


Fig. 6. Frequency dependence of the dissipation factor of selected monitored liquids compared to mineral oil Shell Diala DX

Figure 5 and 6 shows that fluids based on esters, and whether natural or synthetic have a characteristic course of dissipation factor. In the highest frequencies region measurement can contain an errors (Diala, Midel). From Figure 5 it is evident that the insulation mixture Zerol + Nivol - 50 +50% behaves in the observed frequency

domain as mineral oil, when the dependence of the dissipation factor is shifted towards higher values. On the contrary mixture Zerol + Nivol 80 + 20% (80% of the ester) shows a dependence similar to esters dependencies, when its characteristic is shifted downward towards better values. Interesting is the fact that in the area around the power frequency of 50 Hz curve of the dissipation factor of mineral liquid intersects with the curve of the mixture. The mixture exhibits lower dielectric losses than mineral oil at high frequencies. The different frequency dependences correspond to different chemical composition of the fluids.

By additional evaluation of the measurements can be obtained frequency dependence of permittivity of monitored fluids. This is shown in Figures 7 and 8.

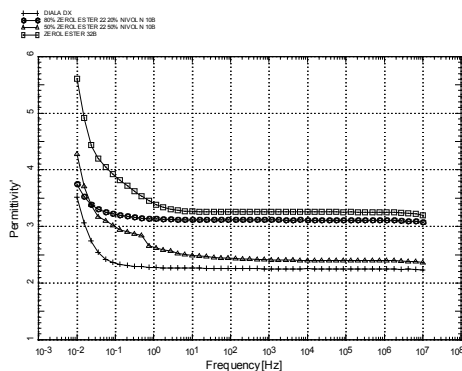


Fig 7. Frequency dependence of permittivity of Zerol and its mixtures with Nivol compared with Diala DX

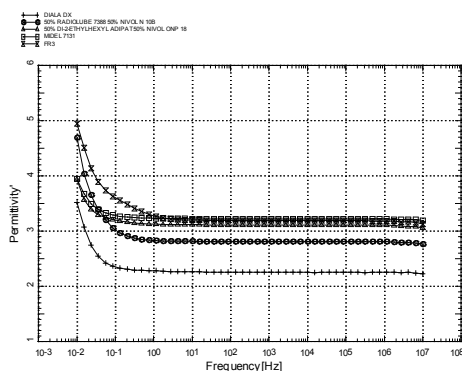


Fig 8. Frequency dependence of permittivity of monitored mixtures compared with Diala DX, Midel and FR3

For the industrial frequency of 50 Hz are summarized permittivity values in Table 4.

TABLE IV. PERMITTIVITY OF TESTED FLUIDS

fluid - mixture	permittivity
Diala DX	2,25
FR 3	3,17
MIDEL 7131	3,18
50% Radiolube 7388 + 50% Nivol N10 B	2,8
50% Di-2-Ethylhexyl Adipát +50% NivolONP 18	3,1
Zerol Ester 32 B	3,28

80% Zerol + 20% Nivol	3,1
50% Zerol + 50% Nivol	2,45

Figures 7 and 8 as well as Table IV shows the permittivity of measured new mixtures. The values of permittivity are higher than of the Diala DX oil. Their values however show appropriate value of this property.

The performed test of breakdown voltages of monitored liquids showed that the obtained values for the new mixtures are in some cases near commercial liquids, see Table V.

TABLE IV. ELECTRIC FLASHOVER VOLTAGES – kV/2,5 mm

fluid - mixture	flashover voltage	standard deviation	coefficient of variation %	A type uncertainty
FR 3	50,15	11,17	22,27	5,93
50% Radiolube 7388 + 50% Nivol N 10B	44,66	4,59	10,28	2,44
50% Di-2-EthylhexylAdip át+ 50% Nivol ONP18	14,67	3,95	26,96	2,1
ZerolEster 32 A	36,2	9,0	24,86	4,78
ZerolEster 32 B	35,78	7,98	22,31	4,24
50% Zerol + 50% Nivol	28,5	2,22	7,78	1,18
80% Zerol + 20% Nivol	45,87	6,23	13,58	3,31

V. CONCLUSION

Taking into consideration observed parameters, it can be stated that mixtures Zerol + Nivol and Radiolube + Nivol should be further studied in the future. Dielectric losses, dielectric constant and the value of flashover voltage here show suitable values. The prepared mixture should be subject to not only the physical but especially electric tests. The complete paper-oil system need to be tested respecting the active degradation effects - particularly temperature.

ACKNOWLEDGMENT

This research has been supported by project TA03020251 Environmentally friendly insulation liquids.

- [1] ČSN EN 61099 Technické podmínky pro nové syntetické organické estery pro elektrotechnické účely, Český normalizační institut,
- [2] Mentlík, V., Trnka, P.: Elektroizolační kapaliny šetrné k životnímu prostředí – úvodní studie. ZČU v Plzni. Prezentace TAČR 03020251. 31.5.2013[not published].

Influence of the Electrical and Environmental Test-Conditions on the Characteristic Parameters of Return Voltage Curve

I. Mladenovic¹⁾, Th. Scharrer¹⁾, Ch. Weindl¹⁾

University of Erlangen-Nuremberg, The Chair of Electrical Energy Systems
Cauerstr. 4 – Haus 1, 91052 Erlangen, Germany

1) tel: +49 9131 8529 518, email: ivana.mladenovic@fau.de

Abstract— Diagnostics of the electrical equipment, its efficiency, accuracy and reliability are of the highest importance for the economical and therefore profitable condition based asset management. In this article the focus will be on the return voltage measurement, a diagnostic method applicable to medium voltage paper insulated lead covered cables (PILC). The influence of the electrical and environmental test-conditions on the characteristic and diagnostic parameters of the return voltage curve have been investigated. Thereat the boundary conditions during the measurement procedure as e.g. duration of the polarization phase have been defined. Return voltage measurements have been performed on cable samples (PILC cables - 20kV, 150mm²) that were artificially aged within an accelerated aging experiment. The cable samples were differently pre-aged - from brand new, up to cables that had been in operation for 60 years. Measurements of the return voltage curves in different stages of the ageing process enabled an additional analysis of the influence of cable condition on the characteristic parameters.

Keywords— *medium voltage cable; PILC cable; diagnostics; aging; return voltage*

I. INTRODUCTION

Diagnostic systems for medium and high voltage (MV and HV) equipment have been intensively researched and developed in the last decades as the reliable knowledge of equipment condition enables the establishment of a high efficient investment and maintenance planning [1] [2]. The major asset in the European inner-city MV power networks are power cables with more than 50% share of paper insulated lead covered (PILC) cables. Although they are increasingly being replaced since the 1980s [3], due to their long life-time and their reliability, PILC cables still make up one of the backbones of the urban distribution networks in many parts of e.g. Europe or Northern America. However, there are still no established criteria for the evaluation of the cables condition and the estimation of the time to the next failure.

In order to point out the limits and characteristic values of the different diagnostic variables, an accelerated aging experiment on PILC cables has been carried out. For this purpose, a novel system, its hardware as well as the software components, called ICAAS (Integrated Cable

Accelerated Aging System) was developed and realized, [4] [5] [6]. The test samples are 150mm² PILC cables, with a nominal voltage of 20 kV, a length of ca. 45 m and variable service histories: from brand new cables, cables which were stored for 10 years to samples aged for 20, 40 and 45 years in the field operation. The aim of this project is the determination of suitable parameters describing the aging process of PILC cables by a constant monitoring of the relevant aging parameters and the commonly used diagnostic parameters: dissipation factor ($\tan\delta$) and partial discharges. During almost two years of the aging experiment, numerous studies have been carried out, where the influence of temperature, voltage, cable condition etc. on several diagnostic parameters have been investigated [7] [8]. Actually, the so formed knowledge databank consists of over 270.000 measurements and more than 900GB of data, [9].

In addition to the common parameters $\tan\delta$ and partial discharges, DC diagnostic methods have been performed in different stages of the aging experiment, [9] [10]. In this paper, the physical background of the return voltage method and its measurement principle, are presented. The influences of the different electrical (polarization time and/or voltage), thermal test-parameters and cable condition on the return voltage curve and p -factor as the related diagnostic parameter are shown.

II. THE PHYSICAL BACKGROUND OF THE DC DIAGNOSTIC METHODS

When a dielectric is exposed to an electric field several polarization processes with different relaxation frequencies occur. These are for example atomic (10^{14} Hz), orientation (10^8 - 10^{12} Hz) and boundary (1-103 Hz) polarization. Due to its low relaxation frequency, boundary polarization is primarily relevant for DC-applications like the return voltage measurement. It is typical for insulation systems which are composed of at least two dielectrics with different properties, for example the layered insulation of PILC cables which is built up by the two components paper and mass. The process of boundary polarization is characterized by a charging of the dielectric with the higher conductivity through the second dielectric and its lower conductivity.

III. BASIC PRINCIPLES OF RETURN VOLTAGE MEASUREMENT

By return voltage measurement (RVM), the specific behavior of the insulation described above can be used for diagnostic applications. For that purpose, the selected cable is firstly polarized by applying a DC-Voltage U_p for the time t_p , Fig. 1. After short-circuiting the cable for a time t_d in which the geometric capacitance is discharged and polarization processes with smaller time constants are eliminated, the curve of the return voltage is recorded.

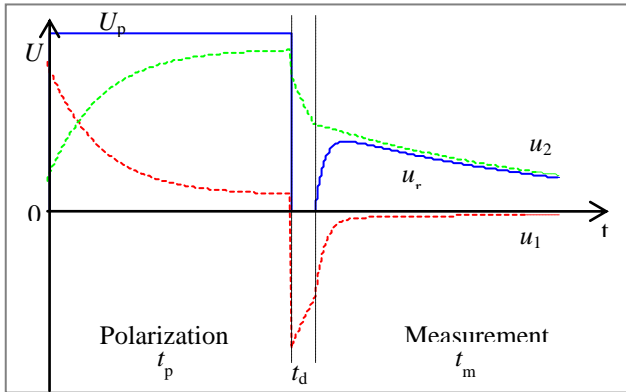


Fig. 1 Principal shape of the voltages during a return voltage measurement

The dominating polarization effect after the short circuit and therefore responsible for the occurrence of the return voltage is boundary polarization with its large time constant.

Due to their elimination by the short circuit those polarization processes with smaller time constants can be neglected in an equivalent circuit. Only boundary polarization has to be represented. An adequate equivalent circuit for the description of boundary polarization is the Maxwell model. It consists of two serial RC-elements (R_1 - C_1 and R_2 - C_2) that represent the dielectrics mass and paper with their time constants τ_1 and τ_2 , respectively.

Using Maxwell model, the curve of the return voltage is given by:

$$U_r(t) = U_s \cdot (e^{-t/\tau_2} - e^{-t/\tau_1}) \quad (1)$$

U_s represents the voltage over the capacitors C_2 , respectively C_1 directly after the release of the short circuit. The voltage U_s has a complex dependency on several parameters like the polarization voltage U_p , the ratios R_2/R_1 and C_2/C_1 , but not on the dielectric time constants directly. Likewise, the voltage U_s is influenced by the geometry of the cable and also by the temperature because of the temperature dependency of R_1 and R_2 .

It is well known that some parameters have a strong influence on the return voltage curve. For example, in [10] it is shown, how the cable temperature in the moment of measurement influences the curve shape and in this way also the parameters used for the further diagnostics conclusions.

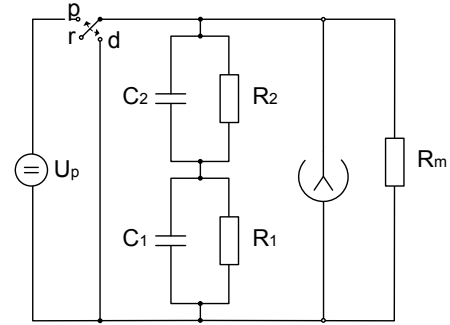


Fig. 2 Equivalent circuit according to the Maxwell model

The parameters usually taken for the evaluation of the return voltage curve and diagnostics are the voltage maximum U_m , the time of the voltage maximum t_m and the initial incline s of the curve:

$$U_m = U_s \cdot (\lambda^{1/(1-\lambda)} - \lambda^{\lambda/(1-\lambda)}), \quad (2)$$

$$t_m = \tau_1 \cdot \left(\frac{\lambda}{\lambda-1}\right) \ln \lambda, \quad (3)$$

$$s = \frac{U_s}{\tau_1} \left(\frac{\lambda-1}{\lambda}\right), \quad (4)$$

where λ presents the ratio of the two time constants τ_2/τ_1 .

Return voltage maximum U_m and the incline s are dependent on U_s , and therefore affected by all dependencies mentioned above. As time constant τ_1 is temperature dependent, cable temperature has also an effect on the parameters t_m and s . These dependencies impede a reliable evaluation of return voltage measurements on the basis of the three parameters U_m , t_m and s . For example measurements taken on the same cable sample in different seasons would lead to incomparable results only because of differences in the ambient or cable temperature.

To overcome these limitations and to ensure comparability, the p -factor has been introduced as a diagnostic parameter:

$$p = \frac{U_m}{s \cdot t_m} = \frac{\lambda^{1/(1-\lambda)} - \lambda^{\lambda/(1-\lambda)}}{\ln \lambda}. \quad (5)$$

As it can be seen in the equation above, p -factor is only dependent on the ratio λ of the time constants. With the voltage U_s , the dependencies on U_p and the geometry can be eliminated. The influence of temperature is minimized due to the fact that the variation of each of the time constants caused by different temperatures is nearly the same.

The progressive aging of the paper-mass dielectrics generally leads to a decrease of the dielectric time constants τ_1 and τ_2 . As a result of the physical aging processes and the degradation of the paper, water is generated and accumulated in the solid dielectric. This results in an increase of the conductivity and a change in the time constant of the paper. Because of that the two time constants are changing in different ranges and the progress of aging becomes visible by the p -factor.

IV. INFLUENCE OF THE ELECTRICAL PARAMETERS

A. Influence of the Polarization Time

Electrical parameters, like the polarization voltage and time (U_p, t_p) or duration of the short circuit phase (t_d), are adjustable parameters that can be controlled and selected to influence the measurement results in a suitable way for the diagnostic purposes, differing therefore to the undesirable environmental influences.

Numerous measurements have been carried out on the cable samples in the aging field as well as in an additional test-site, where the reserve-cable samples have been stored and prepared. The standard measurement parameters [9], are used, except for the parameter which is investigated for its influence on the return voltage curve.

In Fig. 3 the return voltage curves for variable polarization times (120s, 240s, 480s, 900s and 1800s) are shown. The presented curves were measured at 1kV polarization voltage and under comparable environmental circumstances with an average temperature of ca. 19°C and a relative humidity of ca. 50%.

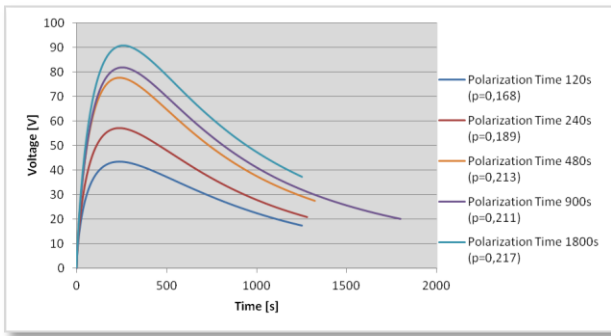


Fig. 3 RVM for variable polarization times

Correlating the characteristic parameters of the return voltage curve with the polarization time duration, it can be stated that t_m changes only slightly until U_m and s increase with the polarization time. The deviation of the directly measured U_m and t_m with a variable t_p is clearly visible in Fig. 4.

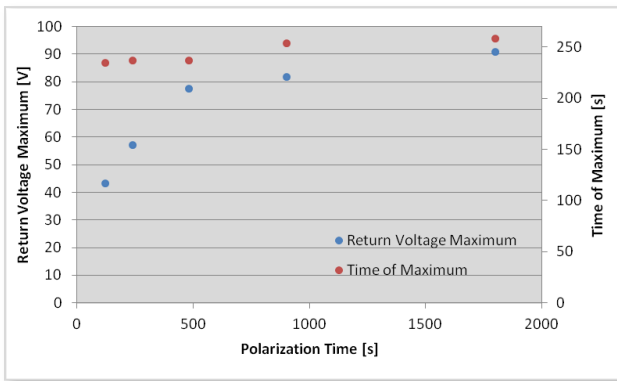


Fig. 4 Deviation of U_m and t_m for different durations of t_p

Moreover, the deviation of the p -factor is present by variable polarization times, but still very small for $t_p = 480s \rightarrow 1800s$.

Therefore, it can be concluded that the polarization time should not last less than 480s where the deviation especially of U_p is still significant, Fig. 3. Anyway, some average values of the characteristic parameters are obtained with 900s, which is overtaken in the field measurements as a standard t_p value.

B. Influence of the polarization voltage

To analyze the influence of the polarization voltage level, the polarization time was selected to be 900s and short circuit time 2s. The measurements were carried out under comparable and steady environmental conditions (average temperature of ca. 20,1°C and relative humidity of ca. 48%).

The maximal voltage U_m increases proportionally to the polarization voltage, Fig. 5, as it was expected based on the direct and linear proportionality of $U_r \sim U_s \sim U_p$. The effects on the initial incline s , which increases with U_p , can also be seen in Fig. 5. Only the time of maximum remains almost constant so that the p -factor changes less than the return voltage maximum. The p -factor varies between 0,206 for 0,5kV polarization voltage and 0,233 for 2kV polarization voltage. Accordingly the independency of p -factor of the polarization voltage could be confirmed. Measurements at 3kV had to be stopped due to too high return voltage levels.

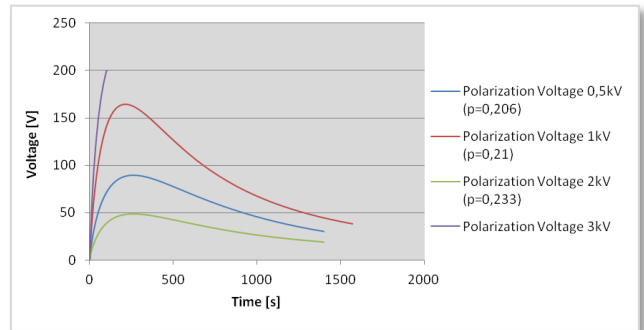


Fig. 5 RVM for variable polarization voltages

The standard values of the polarization voltage in field measurements are 1kV, 2kV and 4kV.

V. INFLUENCE OF CABLE CONDITION AND TEMPERATURE

In order to examine the effects of changes in the cable condition on the return voltage curves and on p -factor, measurements in ICAAS have been carried out before the aging experiment started in 2009 and after some time of artificial aging in 2012 at polarization voltages of 1kV, 2kV and 4kV and a temperature of ca. 23°C. The calculated p -factors for two different voltage levels (2kV and 4kV) are shown in Fig. 6. Additionally, in 2012 measurements have been performed at two different temperatures of ca. 11°C (marks colored blue) and ca. 23°C - both present in the field.

The cable samples of interest have been manufactured in 1987 and 1988 (service-aged cables – K10, K11, K12, K13 and K18), in 2000 (unused, stored cables – K14 and K15) and in 2008 (new cables – K16 and K17).

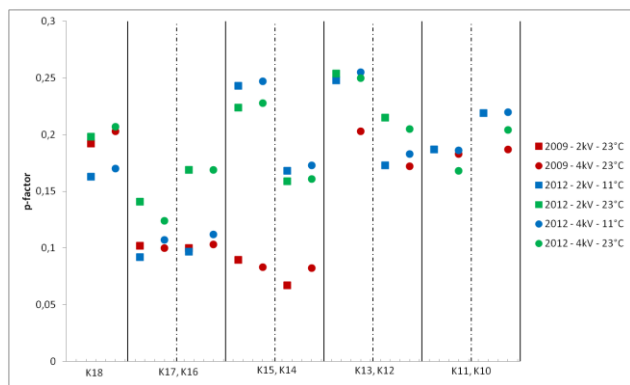


Fig. 6 Development of the p -factor during the ageing experiment and its dependency on temperature and voltage

Cable sample K18 has been exposed to electrical stress only. The p -factors before and after the aging process are nearly the same. The cable samples K10 to K17 have been aged both electrically and thermally. With the only exception of K12, the p -factors of these cables have increased due to the aging process. p -factor therefore can indicate the proceeding degradation of the insulation. In 2009, the p -factors were nearly identical for cables with the same service life. According to the absolute values of the p -factors after the artificial aging, it can be predicated that even the cable samples with one and the same operational history (from the same cable field line) age individually, for example K14 and K15.

As already mentioned and shown above, p -factor is assumed to be nearly independent of the polarization voltage. In Fig. 6 it can clearly be seen, that the dependence of the p -factor on the polarization voltage is negligible. In the majority of the cases, p -factor increases with the polarization voltage but only very slightly.

Regarding the influence of temperature, the behavior of p -factor is quite different. Comparing the blue and green marks which were taken at a temperature of 11°C respectively 23°C in Fig. 6, differences between the p -factor values can be seen for almost each cable sample. Although there is not a functional correlation visible, temperature seems to have a non-negligible influence on p -factor that is much more significant than the voltage dependency. Therefore, it is to be recommended to perform return voltage measurements at comparable temperature levels.

VI. CONCLUSION

One of the diagnostic methods applicable on the MV PILC cables is based on the return voltage measurement.

In this paper the behavior of the characteristic parameters of the measured return voltage curve and the derived diagnostic parameter p -factor at variable test conditions and cable condition have been presented and discussed.

Analyzing the influence of the polarization voltage level and duration on the p -factor, it was shown that polarization phase should not be shorter than 900s.

Moreover, the dependency of the return voltage on the polarization voltage level is well compensated by the derivation of p -factor. It is shown, that, first of all, temperature has a remarkable but not correlative influence on the parameters of the return voltage curve, like voltage maximum or initial incline. On the other hand, p -factor shows a much less intensive temperature dependency in comparison to the return voltage curve itself – but still not negligible.

It can be concluded that by return voltage measurements specific properties of the insulation system can be analyzed. By the usage of an intelligent parameter like p -factor the knowledge about aging processes and hence changing of the dielectrics electrical parameters can be improved.

ACKNOWLEDGMENT

The authors would like to thank the following cooperating companies for the financial and organizational support of the entire project: N-ERGIE AG (Germany), N-ERGIE Netz GmbH (Germany), N-ERGIE Service GmbH (Germany), Bayerische Kabelwerke AG (Germany).

REFERENCES

- [1] FGH - Forschungsgemeinschaft für Elektrische Anlagen und Stromwirtschaft e.V., "Asset-Management von Verteilungsnetzen - Komponentenverhalten und Analyse des Kostenrisikos," Mannheim, 2006.
- [2] FGH - Forschungsgemeinschaft für Elektrische Anlagen und Stromwirtschaft e.V., "Zustandorientierte Instandhaltung von Mittelspannungsnetzen," 2002.
- [3] H. S. and S. W., "Bewertung von Investitionsalternativen bei MS-Kabelnetzen," *EW – Das Magazin für die Energie Wirtschaft*, vol. 15, pp. 28-35, 2007.
- [4] I. Mladenovic and C. Weindl, "Artificial Aging and Diagnostic Measurements on Medium-Voltage, Paper-Insulated, Lead-Covered Cables," *IEEE Electrical Insulation Magazine*, vol. 28, no. 1, pp. 20-26, January/February 2012.
- [5] I. Mladenovic, C. Weindl and C. Freitag, "New System for MV-Cable ageing under controlled conditions," in *Congrès international des Réseaux électriques de Distribution 2009, CIREDD*, Tschech Republic, 2009.
- [6] I. Mladenovic and C. Weindl, "Determination of the Environmental Conditions for the Accelerated Ageing of MV-PILC Cables," in *9th International Conference on Properties and Applications of Dielectric Materials, ICPADM*, China, 2009.
- [7] I. Mladenovic and C. Weindl, "Dependencies of the PD- and $\tan(\delta)$ -Characteristics on the Temperature and Ageing Status of MV PILC Cables," in *Electrical Insulation Conference - EIC*, Annapolis, USA, 2011.
- [8] I. Mladenovic and C. Weindl, "Influence of the thermal stress on the diagnostic parameters of PILC cables," in *CMD*, Tokyo, Japan, 2010.
- [9] I. Mladenovic, "Determination of the Remaining Lifetime of Paper Insulated Lead Covered Cables based on the Diagnostics of Partial Discharges and the Dissipation Factor," Erlangen, Germany, 2012.
- [10] C. Weindl, I. Mladenovic, T. Scharrer and R. Patsch, "Development of the p -factor in an Accelerated Ageing Experiment of the MV PILC Cables," in *10th International Conference on Solid Dielectrics, ICSD*, Germany, 2010.

Comprehensive Approach to Management of Service Lifetime of Power Generation Equipment

Ing. Pavel Cvešpr, Ph.D.

I @ C Energo, a.s., Vaculikova 1a, 628 00 Brno, Czech Republic, www.ic-energo.eu
tel: +420 545 549 443, email: pcvespr@ic-energo.eu

Abstract— A necessary condition for the effective control of the modern production technologies is the availability of quality information concerning an operated system, processed continuously on a process basis throughout the whole time of a system's actual technical life. The aim of the paper is to present the LTOs (Long Term Operation suite) information system as the comprehensive tool for saving, processing and evaluating of this information for the purpose of determining the controlled aging trends and an expected year of equipment end of life, primarily with regard to its lifetime extension beyond the project limit.

Keywords— Diagnostics, maintenance, expected year of equipment end of life/remaining useful life

I. INTRODUCTION

The maintenance and repairs of power generation equipment place high demands not only in relation to the provision of qualifications and materials, but they also require quality and timely information about the equipment behaviour collected during its operation. The successful maintenance management involves use of this information for optimum planning and repair management and establishment of corrective measures to reduce random maintenance (maintenance after failure).

Each piece of equipment operated in the technological process sends signals about its “state of health”, which need to be correctly interpreted and, depending on the level of importance, forecasts or corrective measures should be made to recover the set operating parameters. With regard to the strategy of commissioning and operating fully loaded equipment running in a unit arrangement, it is also important to learn about the extent of risk of operation with the designed parameters and the prediction of end of life of the equipment.

The crucial questions that worry equipment owners in relation to its remaining useful life and equipment operators in relation to its reliability are as follows: How long can a piece of equipment be operated safely and effectively while maintaining the requirements on its operability? What is the

technical condition of the monitored parts of equipment and what is their remaining useful life? When should an outage be planned? What will its scope be? Does it pay to repair the equipment or is a new investment needed? A qualified answer to all these questions is absolutely necessary for the correct assessment of the state of all important equipment, while without a reliable database only practicable with great difficulty, if possible at all.

The aforementioned facts give diagnostics a role which integrates sources of information, procedures of data processing and a presentation of conclusions, with the aim of understanding the ageing of operated systems and the ambitions to manage their service lifetime.

II. LIFETIME MANAGEMENT

The process of lifetime management comprises a complex whole of interrelated activities, which determines the procedures, activity sequences, roles, responsibilities, inputs and feedback for the defined equipment units. It includes a description of equipment and degradation mechanisms affecting it, an overview of programmes – the work procedures relevant to lifetime management, defining of limits restricting further operation, expected outputs etc. The result is the prediction of the remaining useful life of equipment.

Equipment lifetime management is at the heart of the process of Asset management, whose aim is to provide the required equipment function in the desired quality. In order to provide the required function it is very important to learn about the effects of ageing on the equipment and adopt feasible corrective measures before the function is lost. The basic goals of life management are as follows:

- optimize the operation, maintenance and service life of systems, constructions and components
- maintain the required level of performance and safety of the unit and at the same time maximize returns on the investments over the planned length of life of the production equipment/unit
- allow for an early detection of the causes and mitigation of the consequences of ageing for the equipment units relevant to safety and operability

- prepare materials/data for optimum utilization of the technical life of equipment,
- furnish proof of maintaining the safety reserves and the remaining useful life of critical equipment/unit components to the regulatory authorities,
- optimize the preventive maintenance programme so that it supports the management of critical equipment ageing,
- create a schedule for replacement (modernization)/repair of the equipment no longer fit for continued operation based on safety, economic or other reasons
- enable service extension for a system, component or construction beyond the original project life while at the same time providing the safety of operations – the goal of the LTO Programme (Long Term Operation), Fig. 1.

More detailed information could be found in [1], [2].

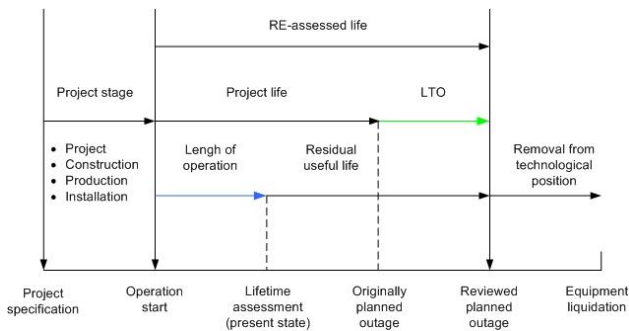


Fig. 1: Life cycle of operated equipment

III. GRADED APPROACH TO LIFETIME MANAGEMENT

All the power generation equipment units are divided into three categories based on their safety, technological and economic importance and the strategic outlook regarding their future operation. For each category, the lifetime management is defined based on individual procedures.

Category 1 - Lifetime management based on the defined Lifetime management programme. This applies to the equipment for which preservation of the safety function is conditioned by equipment integrity and whose potential failure is unacceptable with regard to long-term operation or from the economic point of view.

Category 2 - Lifetime management based on the Preventive maintenance. This category includes equipment for which the possibility of functionality failure can be allowed in certain cases. For the most part, these units are replaceable.

Category 3 - Lifetime management based on the Corrective maintenance. This category includes the remaining equipment whose possible failure does not result in safety-related or immediate technological (production)

impacts or serious economic impacts. The failure of equipment is permissible.

Table 1: Categorization of equipment units from individual areas based on their number

Category	Mechanical	Electrical	Construction
1	42.3 %	1.8 %	4.9 %
2	15.6 %	8.9 %	3.3 %
3	31.5 %	55.8 %	47.1 %
Other	10.6 %	33.5 %	44.7 %

IV. LIFETIME MANAGEMENT MATRIX

The method of solving the impacts of ageing and degradation mechanisms on relevant equipment and its components is described by a 'Lifetime management matrix' [1] which is created individually for each category and type of monitored equipment. It represents a relation between the monitored equipment, the degradation mechanisms affecting it, the methods of degradation identification and the limit values. It provides a decisive input for a SW solution of the problems relating to determining of equipment lifetime.

V. LTO SUITE

LTOs [3] is designed as a modular system consisting of a database, an application core (the Equipment Register, Documentation and protocols, Planning and Diagnostics), a security module, an integration-analytical layer (IA layer), a presentation layer and an interface of the cooperating small SW applications.

The database (see Fig. 6) is created as a central data store (CDS) on the ORACLE basis which contains static and dynamic data.

The static data is the basic descriptive data on the equipment. It includes name of equipment, its label data and designed parameters.

The dynamic data on the unit in question is continuously gathered during its operation on the technological position. This mainly involves operation data (temperature, pressure, flow volume,...), data from the off/on – line diagnostics and data from inspections and reviews, archived according to the set mode.

As for the equipment newly put into operation it is very important to record its 'zero status' (initial state) (Fig. 5). This mainly includes storage of the results of guarantee measurements and tests. Without this information it is impossible to determine the level of material degradation, the end-of-life year or operate equipment with an acceptable degree of risk until failure.

The Equipment Register module is the basic module of the LTOs system. It keeps records of equipment units and gauges including their technical parameters. All the

information flows needed for activities of the other modules pass through this module.

The Planning module is used to plan diagnostics, inspection and examination activities on the production equipment and to plan calibration of gauges. The output of the module is short-term and long-term plans generated based on the knowledge of life cycles and the data of the latest completed examination for the relevant diagnostic method. This information enters the Documentation and Protocols module.

The Documentation and Protocols module performs automated processing of data from the protocols that result from the completed plan of inspection activities. The protocol data is saved in the CDS for further use mainly by the Diagnostics module.

The Diagnostics module provides tools for monitoring and archiving of values of the parameters describing the condition of turbines, pressure parts of boilers and steam pipelines, steel and civil structures, desulphurization technologies and electrical installations. The module generates databanks from monitoring lifetime of the main production equipment (including the operation and material diagnostics).

The IA layer is used to integrate and analyze the results from the individual controlled ageing programmes directed toward relevant units, and from other information sources following the rules set by an appropriate Lifetime Management Standard. It is enabled to insert a final statement of an expert (see tab. 2) in charge of lifetime management of a given equipment unit.

The presentation layer allows for creating specific-purpose outputs over the structured data stored in the CDS. To create the outputs an automated query system (abbreviation ADS in Czech) is used, which is an I&C Energo product designed for nuclear power plants.

Table 2: Assessment grades

Assessment grade	State	Action Planned diagnostics interval
A	Excellent	leave as it is/extend
B	Satisfactory	leave as it is
C	Satisfactory with a comment	consider reduction
D	Unsatisfactory	reduce interval
E	Unacceptable	shut down immediately

LTOs is designed as a typical client-server application. It allows for collecting information about equipment in the needed depth of breakdown, evaluating this information and proposing measures to meet the expected level of operation reliability.

VI. INFORMATION PROCESSING

Information is processed using procedures within a special Diagnostics calculation module. The needed methods for algorithms relating to the individual procedures for some parts of the technology were developed within the grants managed by the Ministry of Industry and Trade and are included in the individual standards for Lifetime Management.[1]

Fig. 2 shows a view of the integration – analytical layer which aggregates all the available information on the operated equipment or its components in the followed time period. It enables an expert to make a final statement on the equipment lifetime and consult it with the equipment operator / owner through an “approval work-flow“.

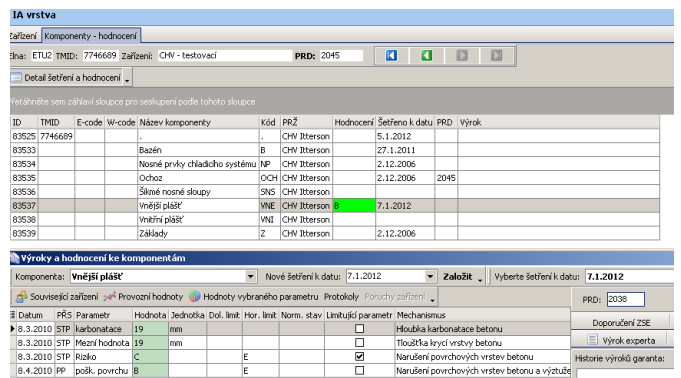


Fig. 2: Evaluation of cooling towers diagnostics in IA layer

Fig. 3 represents one of the graphic outputs of the Diagnostic module in the area of monitoring vibrations of rotary machines. The measured vibration values and completed diagnoses are continuously saved in the CDS. Each area of the equipment has their specific outputs defined.

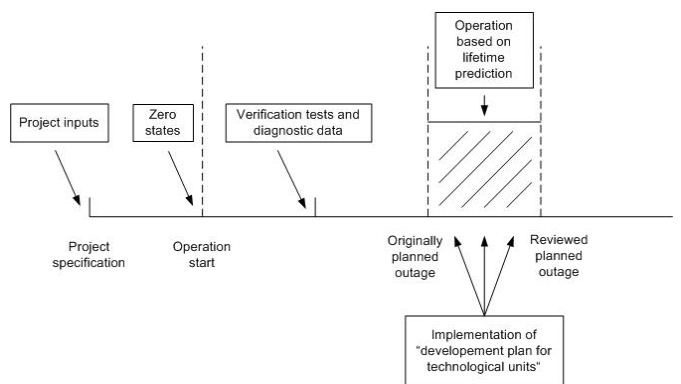


Fig.5: Milestones in the Lifetime management process

A view of the data store for operation values presents an example of TG 230 MW turbo generator (see Fig. 4).

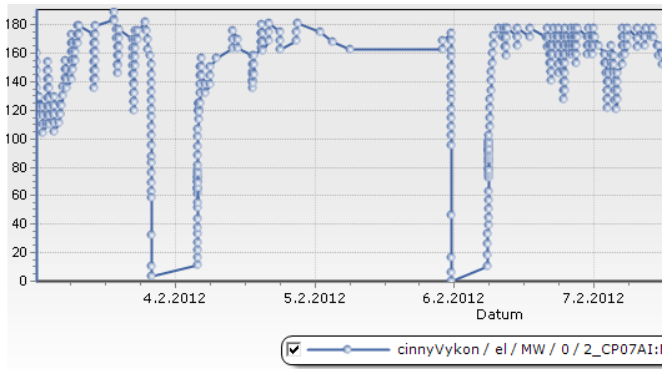


Fig. 4: Time course of a quantity monitored on TG

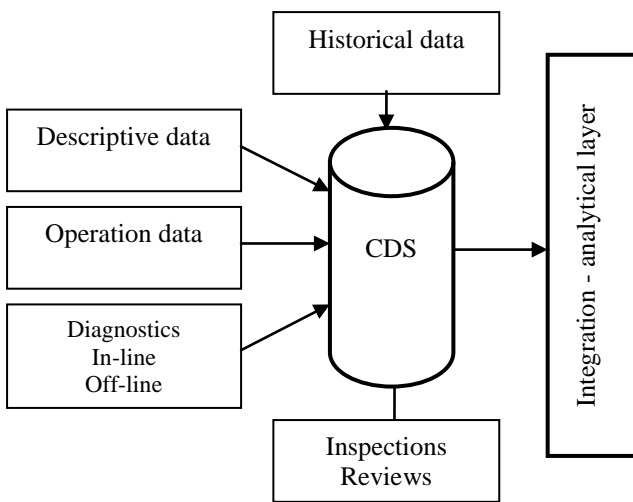


Fig. 6: Central data store – inputs i

VII. CONCLUSION

A SW solution of the aforementioned problems provides a unified approach to information on the technical condition of equipment, its operation, maintenance and diagnostics, which provides enough information for a qualified assessment of equipment. The use of CDS information makes it possible to substantially reduce the risk of unpredictable faults, evaluate the state of equipment and describe the risks of its operation around the expected (designed) year of its life end.

VIII. ACKNOWLEDGEMENTS

In addition, you can express thanks, or you may omit this part completely.

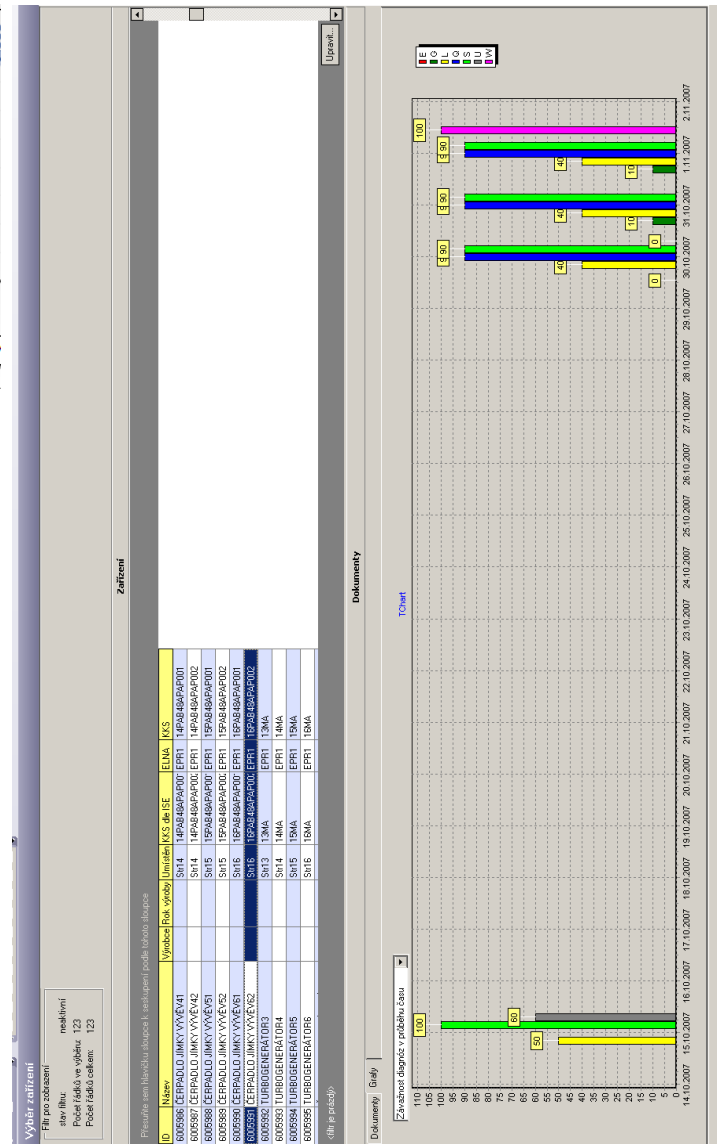


Fig. 3: Evaluation of level of seriousness of diagnoses in time while conducting vibrodiagnostics of a pump

IX. REFERENCES

- [1] Standard ST006r01, Lifetime Management of ČEZ Power Plants. Praha: ČEZ, May 2010.
- [2] Work procedure PP 330r02, Recording and Assessment of Condition and Lifetime Management of Assets. Praha: ČEZ, May 2010.
- [3] Target concept (Project documentation) SW solution, implementation of LTO. Supplied by I &C Energo, 2011

Detection and Visualisation of SF₆

Ing. Václav Straka

“TMV SS”, Studánková 395, 149 00 Praha 4, Czech Republic, www.tmvss.cz

¹⁾ tel: +420 272 942 720, email: info@tmvss.cz ,

Abstract — Gas SF₆ (Sulfur hexafluoride) is increasingly used as insulating medium, not only at HV but also at high-voltage. In significant number of applications is not easy to detect the leakage by using only a “sniffer”. This identification is not effective enough due to vastness of area. In some cases is not even possible to use this due to the HV area. The solution for not only those cases could be used special infrared camera. This article describes the characterization of concept as well as particular visitation examples.

Keywords — SF₆; thermocamera; FLIR

I. DETEKTION OF LEAKAGE SF₆ FROM TANGS

The high-voltage tangs are constructing not only with regards to effective quality but also to minimized leakage of insulation medium, in this case called SF₆. Potential leakage could have a bad impact on the environment (greenhouse effect) but also on safety and reliable process of element filled SF₆. Leakage detection of gas is used when the leakage is detected (low pressure in tangs) for localization of the critical place and following repair. The detection is also use as method to verify the tightness before putting into operation or before any repair. For this diagnostic is possible to use several methods and equipment.

A. „Mechanical“ methods of leakage detection

Although it seems paradoxical, these methods come into consideration at the time of failure of usual methods (“sniffers”). It is a method of coating tangs compartments into plastic strips or painting soapy foam. Typically aim either concentrate outflow into a small space (in the case of plastic belts) or the formation of bubbles in the case of using soapy water.

B. Detector of gas leakage

In these days for standard instrument could be taken “sniffer”. There are two types, standard and infrared. The standards are quite cheap; however their negative attribute is sensitivity on SF₆, humidity and running wind. The infrared version is not sensitive either to humidity or running wind, however allows automatic quantification of concentration gas leakage. Both concepts have common ability, which is necessary to measure in the place of leakage. When the measurement is done more further the measurement is less accurate.

C. Monitoring of gas leakage

For enclosed places is construct monitoring of gas leakage. This works on identical principal as infrared “sniffer”. Usually they are used in GIS, warehouse of SF₆

or places with great amounts of elements isolated in gas. For example it could be high-voltage switchboard. The priority of monitoring is to protect the workers. The elements isolated in gas are monitored for detection of pressure loss.

D. Visualization of gas leakage

The newest trend is system for visualization. The first system was made to emit laser equipment, in these days not produced any more. It was used for attenuation of the reflected signal from the background, so the leakage was shown. However this type has not become as much popular probably due to its size or the price. Another produced system was based on the acoustic signal emitted by equipment. Also in this system the reflected background is needed, however doesn't show accurate localization and require to measure in a quite short distance. Also this principle has not succeeded. The newest trends are infrared cameras works in long-waves. The system use reduced signal in very narrow long-waves zone, which is typical especially for SF₆. This article is mainly focusing to this system.

II. VISUALIZATION OF LEAKAGE SF₆ BY THERMOCAMERA FLIR GF306

By using thermo camera FLIR GF306 a leakage of SF₆ was detected in 220 kV measured transformer voltage. Thermo camera FLIR GF306 is owned in Czech and Slovak republic only by company “TMV SS” spol. s r.o.

A. FLIR GF 306

Tomographic camera FLIR GF 306 could be used for:

- Radiometric quantitate measurement (appraisal temperature fields with specific temperature points)
- Non radiometric quantitate measurement/imaging leakage of gases.



Fig. 1. Camera FLIR GF 306

Selection of technical specification GF 306:

Field of view: 24° x 18° /0, 3 m
 Detector: Cooled (Stirling cooler)
 Mosaic detector QWIP,
 320x 240 pixels
 Spectral wide: 10 – 11 μm
 Wide of measured temperature: - 40 °C až + 500 °C
 Temperature sensitivity: < 25 mK při + 30 °C
 Increase display resolution: Filter to lower humming mode
 HSM (High Sensitivity Mode)
 Wide of working temperature: - 20 °C až + 40 °C
 Weight (including battery): 2, 48 kg

Thanks to the spectral wide of this camera and also to sensitivity together in use with mode called HSM is possible to display chosen gases (SF6, ammonia, ethylene and 21 more). It is used in a specific wave-length where are some gasses, partly or fully non transparent. For example, from spectral permeability hexafluoride sulphur SF6 – as picture 2. This gas is possible to display for example as a smoke in place of leakage SF6.

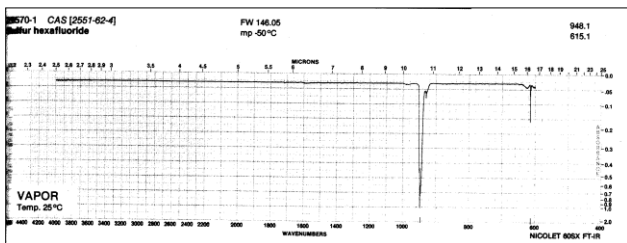


Fig. 2. Spectral permeability of SF₆

B. 220 kV CT

Localization, monitoring and visualization of SF6 have been done by one pole CT TAG 245, the manufacture called Nuova Margini Galileo/Italy, which was made in 1995. CT is isolated in gas SF6 (pressure 0, 50 MPa, operational pressure is 0, 4 MPa in 20 °C temperature,

weight of SF in CT is about 7,5kg.) CT is built from those base parts mentioned below:

- Lamp from aluminum alloy (include secondary terminal connection, two input gas valve and unit for measuring pressures)
- Porcelain isolator
- Head from the aluminum alloy (include safety valve, change of primary conversion and two covers, which protect change of primary conversion)
- Copper primary clamp (connected to the head)
- Secondary windings (in upper part of CT)

The high of CT is 3330 mm. The CT head is connected to support isolated by flange (8 – 12?) connecting with screw and nut (M 12?).



Fig. 3. 220kV CT TAG 245

C. Performed measurements

1) 15.09.2011

The weather during the measurement – sunny, temperature about 20 °C, gusty winds about 1m/s coming from the west. The out coming terminals were situated south-north.

By camera GF was controlled all the CT. The leakage of gas was measured in the head of CT on the out coming terminal towards to the transporter 220/110 kV. The leakage of SF6 on the CT was performed in 6m distance. During the measurement the CT was normally working. The responsible operator put out the CT of operation and built a fence in the 19.9. The service organization has screwed in the nuts on flange in CT of two coils (connection of supported isolator and head of CT). Finally

was performed a check of tightness by “sniffer” – no leakage were found.

2) 21.09.2011

The weather – clouded, temperature of the air was about 17°C, similar gusty wind as at the day on 15.9.2011.

By the camera GF 306 was again found a leakage SF6 on the ground in a similar place where it was aimed in September 15th 2011. Further measurements with the camera GF 306 was performed from the platform of scaffold. The SF6 leakage was not detected in the flange but on the body of the head! - See Figures 4 to 6. By “sniffer” (WIKA SF6-IR-Leak) was found the place of leakage so afterwards an approximate size of a crack / hole could be found. From Figures 4 and 5 it can be seen that the leakage from the hole is probably shape of circular and the size is less than about 0.5 mm! (This calculation was based on the known size / diameter of the probe body “sniffer”, respectively by the internal diameter of the probe, where the gas sucks. The size is about 3 mm). By searching the leakage using “sniffer” was verified on the flange at a distance of 10 cm from the leak concentration were measured SF6 of 80 ppmv, which is about 195 mm from the leak where no values were measured in ppmv SF6.

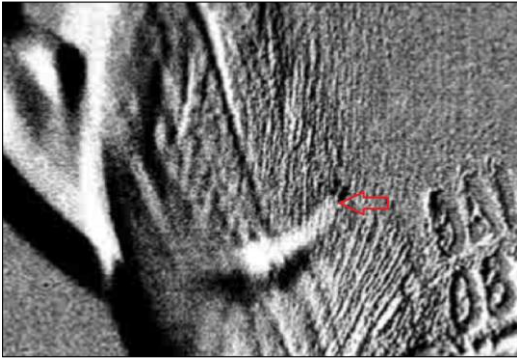


Fig. 4. Termogram of leakage



Fig. 5. Place of leakage – probe of sniffer



Fig. 6. Place of leakage (above flange)

Fig. 7.

III. CALCULATION OF LEAKING SF₆

A. Calculation based on filled gas

This calculation was based on the information of the provider, that the CT is filled up about 3-4 kg.

About 3, 5 kg/year = 3500 g/year ≈ 9, 6 g/day ≈ 0, 4 g/hour ≈ 6, 7 mg/min ≈ 0, 1 mg/sec = 100 μg/s

Note: Please note, the calculation is only informative, there is no taken into consideration either weather, change of temperature, pressure act.

B. Calculation based on leakage gas

Those sources for the calculation of ppm_v g/year provided Dr. Roland Kurte from company WIKA, who used in the example IEC 60068-2, which describe all the leakage [Pa.m³/s].

In the measurement in 21.09.2011 was measured a concentration 1700 ppm_v SF₆ by “shiffer” WIKA in a 3m distance from the crack

In a case of measured leakage 1700 ppm_v SF₆

$$\begin{aligned} \text{is:} \\ L = x \cdot 5,996 \cdot 10^{-7} \text{ [Pa.m}^3\text{/s]} &= 1700 \cdot 5,996 \cdot 10^{-7} \\ \text{[Pa.m}^3\text{/s]} &= 1,014 \cdot 10^{-3} \text{ [Pa.m}^3\text{/s]} \end{aligned}$$

Weight m [g] is described as follows:

$$m = x \cdot 1,142 \text{ g/year} = 1700 \cdot 1,142 \text{ g/ year} = 1941,4 \text{ g/ year} = 1,941 \text{ kg/ year}$$

When comparing the weight of leaking gas respectively filled SF6 (ie is about 3.5 kg / year) and the conversion of the measured weight at 1,700 ppmv ie about 1.91 kg / year, these values are listed in kg / year. The measured concentration ppmv SF6 is based on the distance from the detected leak. At a distance of 10 cm from the leak has been measured at 80 ppmv SF6!

IV. EVALUATION AND CONCLUSION

From the provided measuring follows:

- GF 306 sensitivity is sufficient to identify locations of leaks of SF6 filled device, even when the device is in normal operation mode and from safe distance. The visualization leakage has been verified in concentration of 23ppm.

- although sensitivity of sniffer WIKA is relatively high, in some case of searching leakage SF6 220 kV MTP to Rz XXX could be mechanically scanned using the probe MTP because leakage of SF6 is on the MTP.

REFERENCES

- [1] FLIR – GF 603
- [2] Records from measuring done on substation 220 kV CT, Jiří Svoboda, “TMV SS” spol. s r.o.

Online Hot Spot Calculation in Power Transformers

Michal Svoboda¹⁾, Pavel Trnka²⁾

University of West Bohemia, Faculty of electrical engineering, Univerzitní 8, 306 14 Plzeň, www.fel.zcu.cz

¹⁾ tel: +420 377 634 516, email: michal88@ket.zcu.cz,

²⁾ tel: +420 377 654 518, email: pavel@ket.zcu.cz

Abstract— Permanent availability is one of the key parameters of electrical energy. To ensure its permanent availability it is necessary to perform diagnostics and maintenance actions. Especially high voltage transformers and generators must be monitored. Diagnostic tests describe the state of operated machines and thus enable operators to make decision about maintenance.

The main degradation mechanism that affects the life of power transformers is the temperature. Especially hot spot temperature has to be monitored and evaluated. This paper presents the procedure of online computation of hot spot temperature on the basis of online diagnostics. Hot spot temperature can be further used for online residual life calculation.

Keywords— power transformer; hot spot temperature, online calculation; residual life

I. INTRODUCTION

Power transformers are one of the main equipment of power systems, thus they are responsible for continuous supply of electrical energy. In order to ensure reliable operation of the oil-immersed power transformer, there is an urgent need to accurately assess the state of its insulation system. The diagnostics is the key to obtain important data for evaluation of the state of insulation system. In operation, transformers are subjected in set intervals to offline diagnostic measurements to assess the degree of aging. On the basis of these measurements the remaining lifetime is estimated [1].

The insulation system of power transformer is based on two compounds. The first one is the transformer oil, which is both an electrical insulation and cooling media. The oil samples can be taken during the prophylactics or they can be taken during machine operation. In case when the oil parameters do not fulfill the requirement or required criteria, the oil can be regenerated.

The second compound of power transformer insulation system is the paper. This term stands for a number of materials which may vary in parameters. However the chemical structure is always based on cellulose chain.

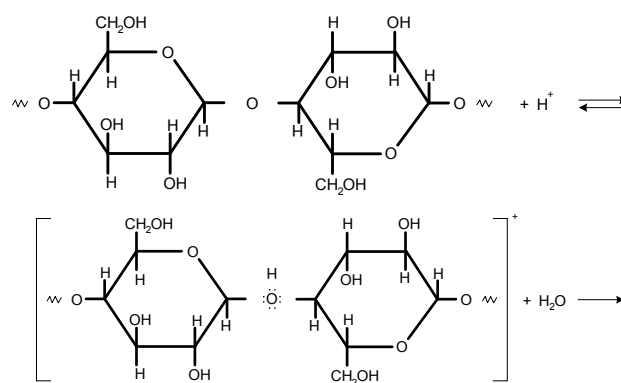
II. AGING PHENOMENA

Ageing is an irreversible deleterious change to the service ability of an insulation system. Aging factors can be divided into four main types (mechanical, electrical,

thermal and environmental influences). These factors are catalysts of chemical reactions which creates irreversible changes. The liquid component of the transformer insulating system is mostly represented by mineral oil. It is a mixture of light hydrocarbons prepared by distillation of naphthenic oil.

Various oxygenated organic compounds are created by oxidative aging. These molecules are polar and they are dissolved in oil. Organic acids react with the metal parts of the transformer, which etch and thus contaminate the oil. During by the oxidation reaction water and carbon dioxide are generated as by-products. Aging products deteriorate the electrical properties of the oil, either when it is dissolved or colloidal particles. Insulation resistance of transformer oil decreases and the likelihood of breakdown increases. The strong electric field deforms these nonpolar particles and aligns them together into strings formation, which enables flashover between phases or between phase and grounded parts of the machine [2].

To increase electric strength and reduce electrical insulation distances in transformers, various materials based on cellulose are used. These materials are commonly denoted as transformer paper Cellulose is a polysaccharide mixture, where the dominant monomers are glucose molecules. Degradation factors (especially temperature) cause cleavage of long polysaccharide chains into smaller units. As an examples it is possible to mention hydrolysis of glycosidic bonds, the reaction scheme is shown in Fig. 1 Exposition to moisture and acidic environment (which is provided by degradation reactions transformer oil) leads to chain cleavage and loss of mechanical strength of the paper.



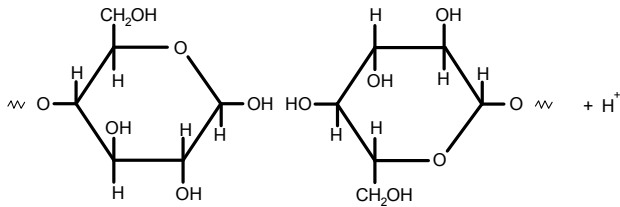


Fig. 1. The hydrolysis of transformer paper [3]

The hydrolysis is not the only reaction influencing cellulose. Transformer paper is subjected to further oxidation or cross-linking reactions where the fiber strength is decreasing. Paper became fragile and due to vibration (mechanical stress) it decays.

III. MODELING OF PAPER-OIL INSULATION SYSTEM ENDURANCE

Temperature can be considered as the main factor that gradually degrades the insulation system of transformers. For simple modeling of the insulation resistance of the oil-paper can therefore be used only temperature. The first description of dependence of reaction rate on temperature was denoted by Arrhenius in 1889 [4]:

$$k = A \cdot e^{\left(\frac{-E_a}{R \cdot T}\right)}, \quad (1)$$

where: k is reaction rate, A is a preexponential factor (s^{-1}) E_a is activation energy ($J \cdot mol^{-1}$), R is the universal gas constant with the value $8.314 J \cdot K^{-1} \cdot mol^{-1}$ and T is temperature (K)

Arrhenius law in direct relation to the life of transformers insulation system was presented by Montsinger in 1930 [5]. It states that an increase in temperature of every eight degrees Celsius halves the lifetime of transformer paper.

If higher precision is necessary, a combination of temperature and electric field can be considered. Models proposed by Falou (2) [6] or Ramu (3) [7] can be denoted as an example.

$$\tau_{(E,T)} = e^{\left(\frac{A_1 + A_2 \cdot E + \frac{B_1}{T} + \frac{B_2 \cdot E}{T}}{T}\right)} \quad (2)$$

$$\tau_{(E,T)} = e^{\left(\frac{a_1 + \frac{a_2}{T} + b_1 \cdot \ln(E) + \frac{b_2 \cdot \ln(E)}{T}}{T}\right)}, \quad (3)$$

where: $\tau_{(E,T)}$ is the lifetime and $A_1, A_2, B_1, B_2, a_1, a_2, b_1, b_2$ are constants which must be determined experimentally. It should be noted that all mentioned above applies to mineral oils, but not generally for other insulating fluids such as synthetic esters.

For the evaluation of the state of the insulation system it is necessary to consider its weakest spot, or the most stressed areas. The thermosiphon effect (the natural convection of liquids caused by heat differences) is advantageous in case of cooling; however, it is not advantageous from the viewpoint of degradation. The

hottest oil is gathered in upper parts of transformer and thus it affects local insulation elements more. The temperature distribution in the transformer tank is shown in Fig. 2, where T_{OU} stands for temperature of upper oil layers, T_{WU} is temperature of upper winding part and T_{HS} is the hot spot temperature. Symbols g and H are further discussed in eq. (4).

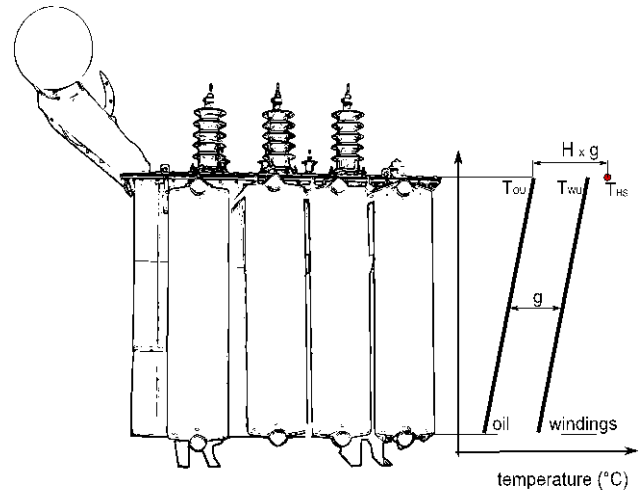


Fig. 2. The temperature distribution in transformer tank

Temperature increases with height, i.e. the hottest oil is just below the lid. However the hottest place in the transformer, denoted as hot spot temperature T_{HS} is elsewhere. Hottest place is directly on the upper layers of winding, because the paper also acts as a heat insulator and restricts the heat transfer from the windings to the oil. Hot spot temperature can be estimated by three ways:

- Fiber optical measurement
- Static calculation
- Dynamic calculation

A. Fiber optical measurement

The thermal sensors are attached to the end of optical fibre (or the fibre itself can work as thermal sensor) and placed between insulated conductor and spacer. Optical signals are transmitted to the terminal block located on the transformer lid.

The greatest disadvantage of this method is the risk of discharge along the optical fiber. The material of the optical fiber or its supporting structure has a different dielectric constant than transformer oil, which cause nonlinear distribution of the electric field. The sensors must be placed in upper part of transformer, which is close to the bushings.

B. Static calculation

The static calculation of hot spot temperature is based on transformer design and temperature rise test. Procedure of hot spot temperature calculation is given in standard IEC 60076 [8]. The input parameters to calculation are the temperature of the oil in the upper layer (T_{OU}) and the

current (I). Hot spot temperature is then calculated using the formula:

$$T_{HS} = T_{OU} + H \cdot g \cdot \left(\frac{I}{I_N}\right)^y, \quad (4)$$

where: H (-) is a hot spot factor, g (°C) is the difference between winding and oil temperature at rated conditions, I_N (A) is rated current and y (-) is correction coefficient used in case when prescribed loading is not reached during the temperature rise test. In case the temperature rise tests are not known, other option of calculation are possible [8], [9].

C. Dynamic calculation

Dynamic calculation is based on the solution of differential equations. The principle of the calculation is the same as in previous case. The advantage is particularly higher accuracy in transients.

$$T_{HS} = T_{OU} + \Delta T_{HS}, \quad (5)$$

where: ΔT_{HS} (°C) is the temperature gradient between the hot spot place and the oil in the upper tank.

$$\Delta T_{HS} = \Delta T_{H1} - \Delta T_{H2}, \quad (6)$$

Differential equations for hot spot temperature rise are easily solved as the sum of two differential equations:

$$k_{21} \cdot \left(\frac{I}{I_N}\right)^y \cdot \Delta T_{HR} = k_{21} \cdot \tau_w \cdot \frac{d\Delta T_{H1}}{dt} + \Delta T_{H1}$$

$$(k_{21} - 1) \cdot \left(\frac{I}{I_N}\right)^y \cdot \Delta T_{HR} = \frac{\tau_o}{k_{22}} \cdot \frac{d\Delta T_{H2}}{dt} + \Delta T_{H2} \quad (7)$$

Where: k_{21} (-) k_{22} (-) are constants of the thermal model, τ_o (min), τ_w (min) is the time constant of the oil and winding ΔT_{HR} (°C) is the temperature gradient between the hot spot place and the oil in the upper layer of the container at rated load and y (-) is winding exponent. These parameters are described in the standard IEC 60076-7 in Annex C.

IV. PROGRAM FOR ONLINE CALCULATION OF HOT SPOT TEMPERATURE

A simple program is being developed at our department. The program enables online temperature measuring and further hot spot calculation. The values of hot spot temperature are used for online computation of residual life of an insulation system. The program was compiled in LabView development environment. The structure of the program is shown in Fig. 3.

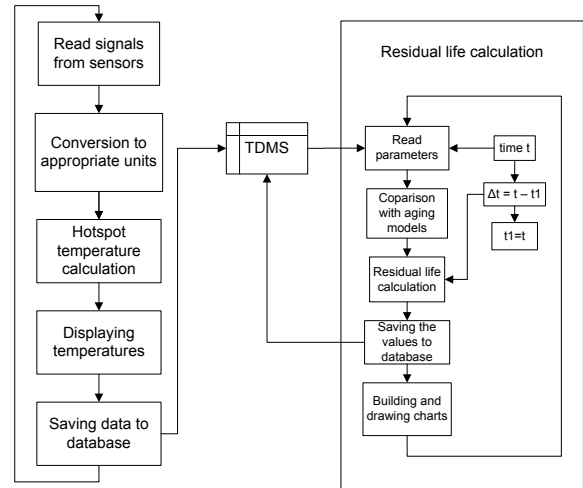


Fig. 3. The structure of presented program for hot spot calculation and further relations to residual life calculation

The program first reads the temperature from the sensor. It is possible to use various types of temperature sensors; in this case a thermocouple type K was used. The output signal is thus a voltage proportional to temperature. Subsequently, using the conversion table voltage is converted to temperature. The hot spot temperature is calculated based on the current loading. The loading is only simulated at this time. The hot spot temperature is calculated using the relationship (4). The hot spot temperature is the basis for determining the relative aging speed and further the residual lifetime of insulating system.

A screenshot of interface is on Fig. 4. Measured and calculated parameters are displayed.

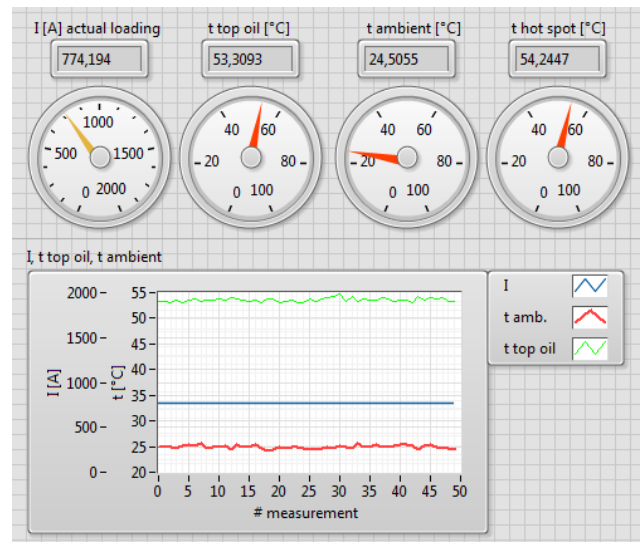


Fig. 4. Screenshot of program interface

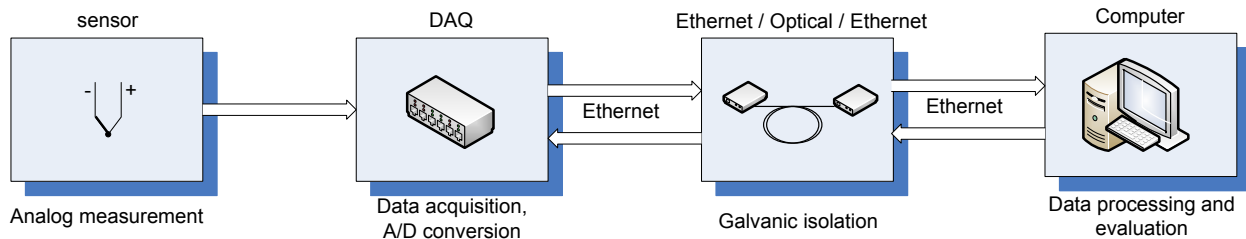


Fig. 5. Schematic representation of measuring circuit

The measured and calculated data are stored in a TDMS database. This database is divided into smaller files so that they can be opened and viewed in common spreadsheet applications. If measurements are performed with high frequency, the program must handle large amounts of data, which are then difficult to evaluate

Measuring chain is built modularly. For data acquisition was used system CompactDAQ – manufacturer National Instruments, which consists of a chassis and modules. Wide range of modules for different parameters is available. The manufacturer also offers several chassis, with one or more free slots for modules. In this way it is possible to configure and install the system according to particular application needs, or it is possible to expand it in future.

The chassis communicates with a computer via ethernet interface. The chain was appended by Ethernet/optical converters in order to electrically separate the local network from a high-voltage area. Optical fiber eliminates the possibility of voltage flashover to the local network and it is also resistant to electromagnetic interference.

Input data can be transferred into the program in various ways. LabView allows communication with the measuring equipment using industrial computer buses (GPIB, Modbus, RS232, USB, PCI, Ethernet, etc.). So any other diagnostic equipment fitted with data output can be deployed.

V. CONCLUSION

Temperature is one of the most important degradation factors of transformer insulation system. In order to predict the state of insulation or its lifetime, it is necessary to determine the place which is affected by highest stress (the temperature in this case). Often the hot locations are unavailable for direct measurement, so it is necessary to calculate demanded values.

A methodology of hot spot temperature calculation on the basis of online temperature measurement is proposed

in this paper. The hot spot temperature is further used for residual life estimation.

ACKNOWLEDGMENT

This research has been supported by the European Regional Development Fund and the Ministry of Education, Youth and Sports of the Czech Republic under the Regional Innovation Centre for Electrical Engineering (RICE), project No. CZ.1.05/2.1.00/03.0094, project TA03020251 Environmentally friendly insulation liquids and supported by Student Grant Agency of the West Bohemia University in Pilsen, grant No. SGS-2012-026 "Material and Technology Systems in Electrical Engineering"

REFERENCES

- [1] B. Patel, Z.D. Wang, J.V. Milanovic, P. Jarman, "A comparative review of transformer reliability on a individual and population scale and an assessment of reliability methodologies," 2012 International Conference on Condition Monitoring and Diagnosis (CMD), pp.870-873, Sept. 2012
- [2] V. Barborka, "Diagnostika transformátorových olejů v návaznosti na prodloužení životnosti transformátorů", in *Elektro odborný časopis pro elektrotechniku*, no. 07, July 2002.
- [3] M. Ďurovič a kol. "Restaurování a konzervování archiválií a knih, Pasek, 2002.
- [4] V. Mentlík, J. Pihera, R. Polanský, P. Prosr, P. Trmka, „Diagnostika elektrických zařízení“, BEN – technická literatura, Praha 2008.
- [5] Montsinger, V. M., "Loading Transformers By Temperature," in *Trans. American Institute of Electrical Engineers*, vol.49, no.2, pp.776,790, April 1930
- [6] Gjerde, A.C., "Multifactor ageing models - origin and similarities," in *IEEE Electrical Insulation Magazine*, , vol.13, no.1, pp.6,13, Jan.-Feb. 1997
- [7] T. S. Ramu, "On the estimation of life of power apparatus insulation under combined electrical and thermal stress", in *IEEE Trans. Electrical Insulation*, Vol. 20, No. 1, pp. 70 - 78, Feb. 1985
- [8] IEC 60076-7 "Power Transformer -Part 7: Loading Guide for Oil-Immersed Power Transformers", Dec. 2005
- [9] IEEE Guide for Loading Mineral-Oil-Immersed Transformers and Step-Voltage Regulators," IEEE Std C57.91, pp.172, March 2012

Temperature Correlation of C and Tg δ Based on Real Response of Measured Object

Ing. Václav Straka

“TMV SS”, Studánková 395, 149 00 Praha 4, Czech Republic, www.tmvss.cz

¹⁾ tel: +420 272 942 720, email: info@tmvss.cz ,

Abstract — Parameter C and tg delta are the most used indicator within diagnostic isolating systems. This article including all examples from professional experience is mainly referring to the area of performing transformers and bushings, even when the process and methods are applied to any dielectric isolating system. The primary goal of this article is to point on the fact that temperature relation based only on a measured values and standard parameters and not sufficient and may cause some incorrect results. This article points to actual method how to be able to measure a temperature correction curve directly in any fields.

Key words – dielectric spectroscopy; power transformer; high-voltage

I. INTRODUCTION

The main element is a transformer. Its function is to transform voltage into a required value before transferring electric power. This is the most important part between production and usage of electric energy.

Damage of transformer may cause power failure in populating or industrial area. In this case it would be a great financial loss not only for distributors but even for wholesale as they would be force to stop all the producing. Therefore is very important to prevent from such as situations by regular control and maintenance of transformers.

Transformer frequency diagnostic is suitable process for detection of any effect in transformer.

Low-frequency diagnostic (dielectric spectroscopy in frequency domain) is a method especially focuses on detection and measurement of moisture in transformer paper isolation and also in a paper barrier regardless temperature of the environment or the equipment.

In the past years were presented a different type of diagnostics method based on variable fervency. The main subject of this article is a temperature relation in measured values. Further in this article will be describe two different methods FDS and “classic” high voltage measurement.

II. DIELECTRIC SPECTROSCOPY IN FREQUENCY DOMAIN - FDS

One of the new methods of diagnostic different isolation systems is dielectric spectroscopy based on frequency reliance. The principle is to monitor elements responses (polarization) based on frequency changes in

wide area. This method could be used for diagnostic of electric equipment, device and elements. Further in this article will be introduced applications particularly in power transformers, high voltage cables isolated in paper and also in cross linked polyethylene. This method could be used in other applications such as winding of electric devices (generator or engine), equipment’s transformer with oil filling etc. Introduced will be also primary concept of method FDS – frequency domain spectroscopy.

III. DESCRIPTION OF METHOD

Method FDS is used for diagnostic of equipment; in Czech Republic is very popular IDAX 206, IDAX 300 or IDA 200. It is based on generator of sinusoids voltage $140V_{ef}$ in range of frequency 10 kHz up to 0,0001 Hz. It is compactible device of 6 kg weight. Device’s performance is sufficient for diagnostic of power transformers and paper isolating cables (for application on cables with isolation cross linked polyethylene can be connected external high voltage unit). The base of this function is a measuring of generate voltage and current coming from measured device presented in required values (Z , $\cos \varphi$, $\tan \delta$, c , ϵ' , ϵ'' , $\Delta\epsilon$ and others possible values). In some cases if you monitor only $\tan \delta$ you cannot evaluate the whole picture of measured sample as mentioned further in this article. The device uses a third protective electrode usually connected to tank of transformer or to cable isolation. Thanks to frequent sensitivity of ammeter and signal filtration can the device works in area with a strong electromagnetic induction without any problem. The device accuracy has been compared with regular high voltage equipment’s 10kV and 20kV without any differences. Significant advantage is a wide frequency area allowing quite extensive diagnostic in different parts measured sample.

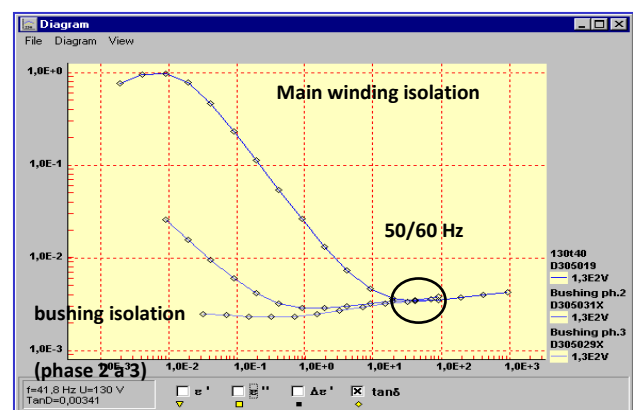


Fig. 1. Picture 1 – frequency dependency $\tan \delta$

IV. APPLICATION

Further to this method is important to mention chosen application including type of mode measured values.

V. POWER TRANSFORMERS

On the power transformer all isolating status could be measured. For example; between each of windings, between windings and ground or diagnostic bushing etc. By this diagnostic can be determinate $\tan \delta$ in 50 Hz and correct compensation, as well as moisture paper isolation and oil conductivity regardless of transformer temperature. The purpose is a measuring in frequency range 1 kHz up to 0, 0001 Hz where each of element (temperature, oil conductivity, paper isolation moisture and construction layout) that effect measured values has different impact in a different frequency (see picture number 2). This gives us possibility to take each impact and separate it, so we could make a different measuring in a different condition, for example in temperature 20⁰ C.

The picture below displays chart of main windings isolation. Moisture of paper isolation is shown particularly by shape of a curve especially at the end points and also by the steepness in the middle part. Oil conductivity in the chart is 45° therefore any change of moisture will change horizontally and construction of transformer will change vertically. The temperature has impact on all movements in horizontal way. Therefore it allows when the temperature is known convert excessive $\tan \delta$ to nominal temperature without any risks of incorrect direction – see picture number 3

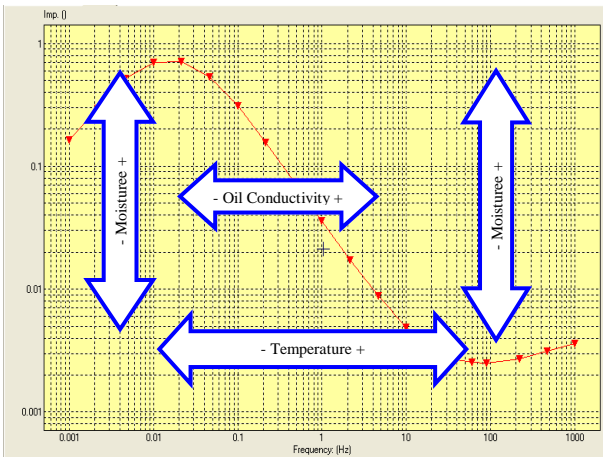


Fig. 2. Picture 2 – vlivy na korekci tan δ

In picture 2 is evident that without any knowledge of curve (i.e. only measuring in one point) in closes environment it’s impossible to convert tan δ in 50 Hz into selected temperature because a directive could either has positive or negative value based on combination of conductivity, moisture and temperature. Wide frequency zone allows shaping curve beyond the border of measurement.

When comparing this method to a “classic” diagnostic method the great advantage is interpretation based on conduction of transformer, short time of measuring,

repeatable of testing, low sensitivity of electromagnetic induction against DS and also easy understanding and formability of measuring results.

However it’s necessary to mention the voltage non-linear that is not possible to calculate from those provided information. Based on capacity of measured samples it not possible to construct accurate equipment, which would be able to generate voltage in kV in frequency range from 1 kHz.

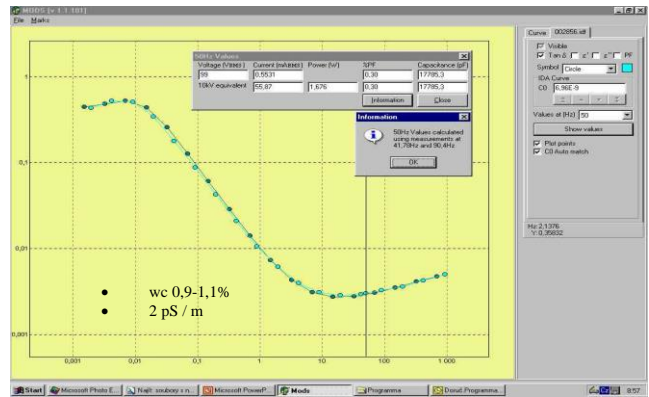


Fig. 3. Picture 3 quantification of humidity

In the case we need to show process with a different humidity in the same time as oil conductivity see the picture 3 showing a chart. On the chart is not shown only quantification of values on level 50 Hz but also the content of humidity in paper isolation, in this case windings isolation. In this instance the humidity is evaluate based on the same values between measured respond (the curve) and theoretic model, that could be expressed as conductivity and humidity (oil isolation resistance). In the same way the measured values could be corrected into nominal temperature.

VI. FREQUENCY VERSUS TESTING AND DIAGNOSTICS IN HIGH-VOLTAGE

The high-voltage is standard method used in transformers, windings and isolation systems. Usually the monitored parameters are resulting high voltage value and absolute values. In same cases of testing isolating system has not got any relative temperature therefore the measured values needs to be adjusted into the measured temperature.

VII. THE USUALL METHOD OF TEMPERATURE CORRECTION

This is usually provided by correction of standard curves. In practise they seem to show more than theoretic because their responses are not only linear but also are individual characteristics of actual element. Standard temperature correction curve are shown in picture 4.

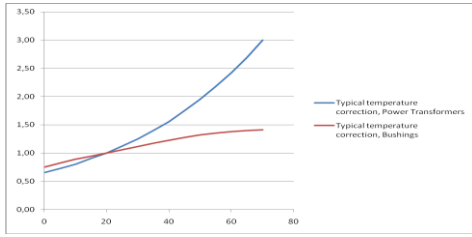


Fig. 4. Picture 4 Standard temperature correction curve

VIII. REAL PROCESS IN PRACTISE

The solution is performed by multi-point measuring in adequately wide frequency area so that the correction is not only estimated, however it's based on the real process. The example of frequency process is shown in picture 5. In terms of temperature reliance, each characteristics behaves very similar like in method FDS. This allows simulation of processes or values measured in the past. In the following picture is shown process of different samples, which were tested in artificially created temperature.

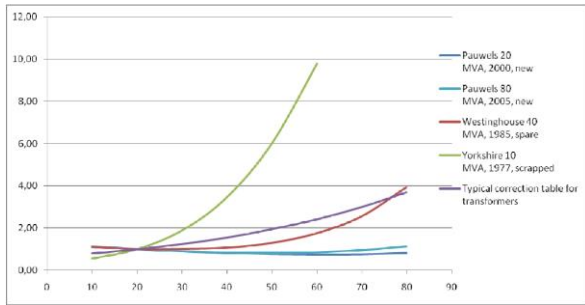


Fig. 5. Picture 5 – real process in transformers

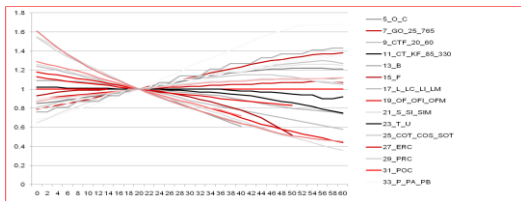


Fig. 6. Picture 6 show identical measurement in windings.

IX. SOLUTION FOR MEASUREMENT IN FIELD

In practise is not possible to obtain individual characteristics of each element. Another aspect, which is important to mention is characteristics variability in compliance with degrades or wear of equipment. Therefore it's necessary to ascertain the characteristic before each measurement. This method is usable in variable frequency in area waveform frequency. This measuring is shown in picture 7.

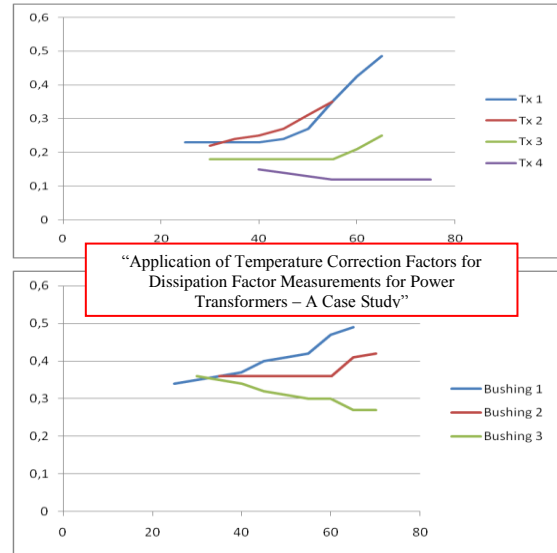


Fig. 7. Picture 7 variable frequency in area waveform frequency

X. VALIDATION OF CORRECTION CURVES

In practise each element is inspected for different temperature and validated. The results of validation are shown on the table below.

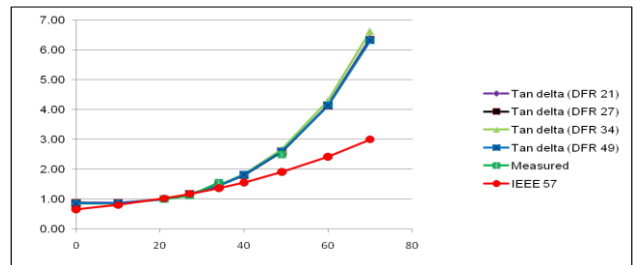


Fig. 8. Picture 8 correction characteristics

Temp. (°C)	Cap. (pF)	Tand (%), measured	Individual Corr. factor	ITC tand (%) @20°C	IEEE C57.12.90	IEEE tand (%) @20°C
21	1978	0.329	1.04	0.31	1.02	0.32
26	1976	0.367	1.20	0.31	1.14	0.32
34	1978	0.516	1.53	0.34	1.37	0.38
49	1974	0.832	2.70	0.31	1.91	0.44

Fig. 9. Picture 9 calculation

The correction characteristics were get from a chart and used for calculation. Concurrently were used a "standard" correction constant. You can see this process has led to different and incorrect results. The only reliable process is individual temperature correction. In present days this process is presented in only one device called DELTA 4000 made by company Megger.

XI. CONCLUSION

Frequency diagnostic of power transformers provide possibility to get more of diagnostics methods. Offer wider spectrum of diagnostics methods of humidity in paper isolation and also of diagnostic mechanics of deflection. Each of above mentioned method helps to provide quicker and effective estimation of actual state of transformer and its humidity for further operation. The purpose of this article is to provide all the information of new methods to the reader.

A new chapter is field high-voltage testing is added of frequency dependency. It's a new process, which is very suitable for using in field. In the present practise of using single correction curves can be considered as the introduction of systematic errors in the measured results.

REFERENCES

- [1] Straka Václav, CIREC 2003, Selected methods of diagnostics of electrical machines, appliances and components - dielectric spectroscopy in the frequency domain

Experiences in Online Condition Monitoring System for Power Transformers

Bartłomiej Dolata¹⁾, Jan Dončuk²⁾, Felix Mamutov¹⁾, Jiří Velek²⁾

¹⁾ ALSTOM Grid GmbH, Rheinstrasse 73, Mönchengladbach, Germany, www.alstom.com

²⁾ CEPS, a. s., Elektrarenska 774/2, Prague 10, Czech Republic, www.ceps.cz

¹⁾ tel: +492 161 944 480, email: bartłomiej.dolata@alstom.com,

²⁾ tel: +420 211 044 220, email: doncuk@ceps.cz

Abstract — The target of modern monitoring systems is to increase the operational reliability of transformers and to achieve a reduction of the life cycle cost. Utilities and other operators of electrical networks nowadays are forced to reduce their costs in terms of operating and maintenance of the installed equipment. The decision of cost reduction can be supported by the use of online monitoring and due to change over from time-based to condition-based maintenance. The monitoring of all major components of the transformer is an important prerequisite in order to acquire knowledge of the operating conditions of power transformers. Another important aspect is the possibility to correlate all measurement and analytical values, or even different transformers in the substation. The monitoring system MS 3000 provides a comprehensive online condition monitoring and diagnosis of power transformers. The paper deals with CEPS' experiences in online condition monitoring for power transformers.

Keywords — power transformer; monitoring system; system architecture; data management; central monitoring system

I. INTRODUCTION

In the course of the ongoing development and extension of smart grids, more and more intelligent devices are applied in order to observe critical assets, to support the operators in accurately timed maintenance activities and to ensure reliability from energy generation to transmission and distribution.

Since power transformers are essential for electrical energy transformation and thereby of prime importance for electrical grids, their continuous operation is a top priority concern. Sudden outages would lead to huge costs due to rapid troubleshooting measures, replacements and consequential charges for power supply disruptions.

II. MONITORING SYSTEM OF POWER TRANSFORMER

In recent years numerous power transformers of CEPS network have been equipped with the online condition monitoring system. The using of various sensors and their integration into only one system allows for the knowledge of significant information about the current status of the power transformer or many transformers in substation. The installed monitoring system is providing extensive information about the active part, bushings, OLTC or cooling system of the transformers.

MS 3000 is a comprehensive monitoring system which allows for a permanent observation and a meaningful

analysis of power transformers. Based on complex sophisticated algorithms and standard calculations the system enables the user to optimize transformer maintenance and provides the operators with the capability of immediate reaction on any events.

Due to a highly modular system design, specific solutions strongly tailored to customers' requirements can be realized. MS 3000 features detection and observation of a broad range of operation related quantities like voltages, load currents, temperatures, gas contents, partial discharges, positions of tap-changers and their power consumptions etc.

MS 3000 performs calculations incorporating input values and resulting in computed prognosis of probable faults and in evaluation of present transformer states. Thereby it closely supports the operators in scope of the servicing process. Furthermore, the system automatically generates warnings and alarms and is able to send appropriate messages via email or SMS.

Different relationships between transformer-specific quantities are considered in order to give the user an extensive overview of the condition of the four main transformer parts, namely the active part, the bushings, the cooling unit and the tap-changer. In case of abnormalities MS 3000 provides information about possible reasons and recommendations depending on the affected transformer part and the kind of fault, based on an integrated expert knowledge module. Implemented calculations like determination of the present hotspot, the aging rate and the lifetime consumption or the evaluation of gas contents according to widely recognized methods – like IEC ratio method, Doernenberg's method, Rogers's method etc. – are an integral part of MS 3000. But beyond that, proprietary algorithms can be applied in order to determine changes of bushing capacitances, perform thermal model calculations, analyze on-load tap-changers during the switching and recognize defective fans and cooling groups.

III. ARCHITECTURE AND DATA EXCHANGE OF MONITORING SYSTEM

Binary and analogue signals generated by intelligent sensors and simple relays are fed in by the use of field bus technology. Therefore cubicles with bus modules are installed at transformers and wired with signal generating devices. For the supervision of several transformers different bus architectures can be built up including star,

ring and line topologies based on both copper and optical fiber connections.



Fig. 1. Example of the the MS 3000 installed at CEPS transformer

All acquired data is transmitted to the MS 3000 IED (Intelligent Electronic Device) – which can be installed inside a transformer cubicle or inside the control room module – for processing. For exchange of data MS 3000 supports standardized process control protocols like IEC 60870-5-101, IEC 60870-5-104, IEC 61850 or Modbus and can be flexibly configured for desired data sets to be transmitted. Both is possible, to share information with a process control system and to feed in data from other devices e. g. comprehensive sensors or further monitoring systems.

IV. VIZUALIZATION OF HISTORICAL DATA IN MONITORING SYSTEM

All data detected and calculated by MS 3000 as well as all occurred alarms and warnings are stored in historical databases and are available for later analysis. Though the data can be directly analyzed by the use of MS 3000 tools it is also possible to export it in the CSV format in order to process information with other programs. The MS 3000 IED provides a web-based HMI (Human-Machine-Interface), thus realizing a very comfortable access to the monitoring system from any standard PC with installed web browser and residing in the same network. By the use of the MS 3000 web pages present values of various transformer-specific and system-specific quantities can be visualized. Web visualization of the CEPS transformer’s actual condition is shown in Fig. 2 and the historical monitoring data in Fig. 3.

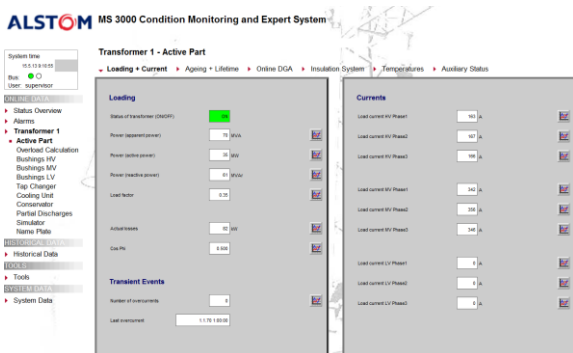


Fig. 2. Web visualization of active part section of CEPS transformer

Furthermore, historical data can be displayed in the form of lists or graphs allowing the user to add comments for any available data point. Sophisticated tools give the user the possibility of extended analysis. By means of the DGA Tool it is possible to evaluate the transformer insulation condition and to store online and offline measured gas values for the observed transformers. By the use of the Report Generator transformer-related PDF-reports for user-defined data sets and periods of time can be automatically generated.

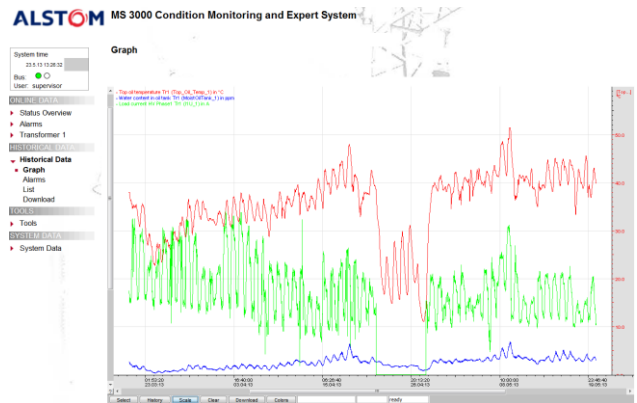


Fig. 3. Web visualization of transformer historical monitoring data

V. MEASUREMENTS REALIZED IN CEPS MONITORING SYSTEMS

There are specific technical requirements regarding an online power transformer condition monitoring system given by CEPS. Various quantities related to transformer’s present condition and their operation are monitored. Voltages, currents, temperatures, moisture, gas dissolved in oil and quantities characterizing the actual condition of the OLTC, bushings and cooling system are detected by means of special sensors and processed in terms of advanced analysis.

The operational voltage is measured as phase to earth for HV and MV side and visualized as phase to phase voltage. For the voltage detection the sensor is connected to the measuring tap of the bushing via the voltage adapter. The measuring principle is based on capacitive voltage divider. The operational currents are obtained by the use of current transformers installed at the bushings. These currents are scaled to the range of 0 to 1 A and transformed to the range of 0 to 20 mA by means of the current transducer located in the monitoring cubicle. Usually primary, secondary and tertiary currents are detected. Voltages and currents are consequently used for the calculation of the different quantities like loading factor, apparent, real and reactive power, etc. Besides that, various additional calculations are performed according to the IEC 60076-7 standard (e.g. hot-spot, rate of ageing and life time consumption) and advanced algorithms.

Temperatures of the oil are detected using Pt100 sensors with three-conductor connections. Typical temperature measurement is realized on the top of the transformer’s tank – top oil temperature. An optional temperature measurement is realized on the bottom of the transformer’s tank – bottom oil temperature, which is

useful in case of the ODAF cooling system. Temperatures at the inlet and outlet of the cooling unit are measured and are used for analysis of the cooling unit performance. The temperature sensor Pt100 located at the monitoring cubicle is used for the measurement of the ambient temperature.

Various binary signals are fed into the monitoring system by the use of the floating relay contacts. These are used for the additional information of operational status of different devices. The switching status of pumps and fans is used to detect their state and to determine the operation time. The information of the switching status of the cooling unit is considered for the calculation of the thermal model of the transformer.

Since the moisture is one of the ageing factors and has big impact on the oil-paper insulation system of the power transformer it is important to monitor the present water content in oil. A capacitive thin film sensor is usually used for online measurement of the water content in oil. The principle is based on the change of the capacitance depending on the content of the moisture in the liquid insulation system. The sensor is usually connected via flange and installed at the transformer (Fig. 4 left side). Both the measured water content in oil and the oil temperature are used for the determination of the moisture in insulation paper.



Fig. 4. Moisture and gas sensors (left) and Buchholz gas sensor (right)

The detection and analysis of gases dissolved in oil is meaningful for transformer condition assessment. Each thermal, electrical and combined fault is accompanied by the generation of a significant amount of distinctive combustible gases. Thus, gases dissolved in oil are key identifiers of possible faults. Knowledge of the content and type of gases allows effective identification and recognition of faults in power transformer. Simple gas sensors or multi-gas sensors can be used for the detection of the gases dissolved in the oil. Simple gas sensors usually detect hydrogen as the key gas of each thermal or electrical fault or total TDCG value of combustible gases dissolved in the oil. Multi-gas sensors can detect wide range of gases dissolved in the oil. These allow more precise analysis of the insulation and deeper view of the present transformer condition. CEPS² has already many simple gas sensors in use and performs offline laboratory dissolved gas-in-oil analysis DGA every year. In case of the steep gradient of the fault gases, online DGA will be used to confirm the gradients and therefore the multi-gas sensor will be installed on the particular transformer.

In case of oil immersed transformers with conservators, the Buchholz relay is used as a protective and safety device. It is obvious that free gases come up into the Buchholz relay installed in the pipe between the top of the transformer and the conservator. If the gas amount exceeds critical limit the Buchholz relay performs an emergency switch off of the transformer. For the online determination of the Buchholz gas amount a special sensor has been developed. The sensor is installed between the degassing valve of the Buchholz relay and the conservator. The sensor is shown in Fig. 4 on the right side.

By means of the change of the bushing capacitance (ΔC) the online condition of the bushing insulation can be assessed. For the determination of ΔC the monitoring system evaluates present voltages and considers initial capacitances. The signal decoupling is realized by the use of the special bushing adapter and voltage sensor which is based on capacitive voltage divider. Fig. 5 shows the installed voltage sensors and adapters.

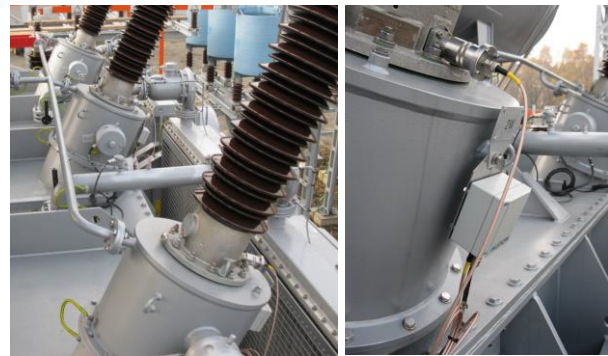


Fig. 5. Bushing's monitoring (left) and voltage adapter and sensor (right)

For the assessment of the OLTC different parameters are monitored. The monitoring system considers present OLTC position, oil temperature and moisture inside the OLTC conservator, number of switching operations as well as power consumption of the motor drive.



Fig. 6. Power consumption of motor drive sensor (left) and water content in oil sensor(right)

Based on the correlation of the power consumption of the motor drive and the change of present position of the OLTC the evaluation of the OLTC condition is realized. The information is used for detection of mechanical faults. Additionally to the standard OLTC monitoring the contact

wear out model can be integrated. Fig. 6 shows installed sensors for the measurement of power consumption and water content in oil.

VI. CEPS CENTRAL MONITORING SYSTEM OF POWER TRANSFORMERS

The analogue and digital signals from the sensors are connected to the bus terminals inside the MS 3000 monitoring cubicle installed at the transformer. The signals are transferred to the server (IED) via field bus. The intelligent electronic device is connected to CEPS' local area network (LAN) based on Ethernet. All the data generated by MS 3000 can be visualized on each standard PC connected to CEPS' LAN by use of appropriate IP address. For a highly efficient data processing and storage all monitoring systems are connected to the CMST (Central Monitoring System of Transformers) giving the user a global overview of present transformer conditions and allowing for comfortable data evaluation. The architecture of the CMST is shown in Fig. 7.

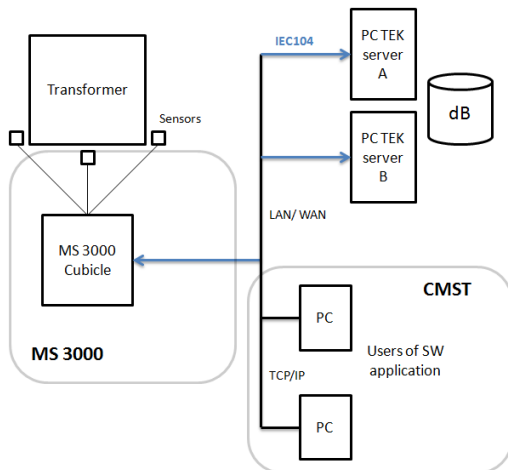


Fig. 7. Architecture of the CEPS' Central Monitoring System of Transformers

Monitoring system's data is transferred to database servers (two servers in case of data backup) via communication protocol IEC 60870-5-104 (historical reasons). The Central Monitoring System is a software application installed on each CEPS' computer which enables each employee to see the actual condition of all CEPS' power transformers. Advantages are mainly one application for all transformers, unified data visualization and their following analyses independent of the monitoring devices. Experience gained during the condition assessment of the power transformers can be easily used in assessment of the similar events which occur on the other transformers. This approach also enables sharing of these experiences with other users. The overview visualization of CEPS' CMST is shown in Fig. 8.

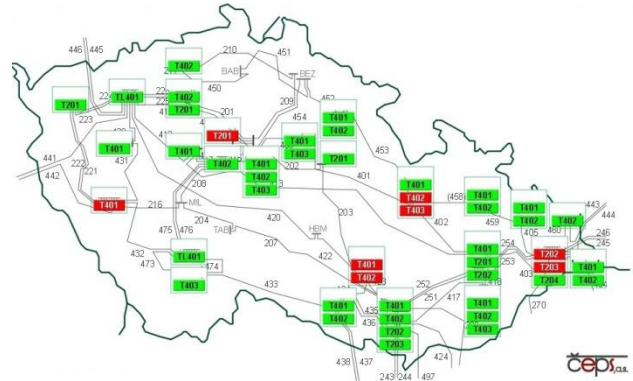


Fig. 8. CEPS' Central Monitoring System of Transformers

The present state of all CEPS' transformers connected to the CMST can be visualized at the same time. The actual condition is given by the particular color of the transformer's name. Green color represents failure-free condition and red highlight symbolizes warning/alarm condition. After clicking on the particular transformer, current status of the subsystem is shown and particular quantity is also highlighted by red color. This warning/alarm condition is usually shown when the quantity exceeds the threshold value which can be set by means of the visualization software of the online monitoring system. Fig. 9 shows an example of data visualization in CEPS' CMST.

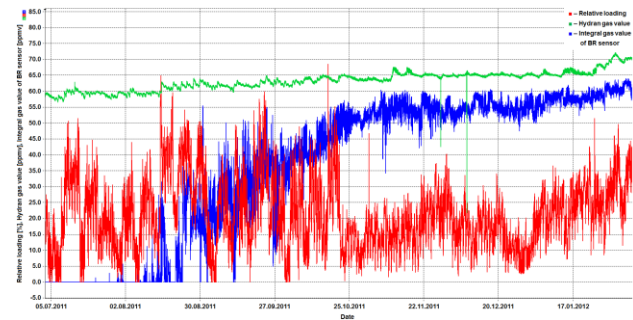


Fig. 9. Visualization of the data in CEPS' Central Monitoring System of Transformers

Today each new CEPS power transformer is equipped with the MS 3000 online monitoring system, however only selected data are integrated into the CMST and stored permanently. In case of any kind of anomaly or message, the transformer, particular subsystem and the monitored quantity are highlighted by the red color on the CMST visualization. Each warning/alarm message generated by the MS 3000 is visualized too. In this case, CMST enables a link to the web interface of the particular MS 3000 monitoring system for detailed analysis and further explanations.

VII. CONCLUSION

The experiences with online monitoring systems have shown that valuable information about actual condition of the observed transformers can be gained. The application of numerous sensors provides additional advantageous information concerning the ageing of insulation like dissolved gas in oil or water in oil content as well as status of OLTC or cooling unit condition. The using of the CMST as centralized data solution provides clearly represented information about the current status of the power transformer network. All this brings enormous benefits in transformer data management, data distribution as well as maintenance of a single transformer or even transformer float.

REFERENCES

- [1] Technical brochure No. 343 "Recommendations for condition monitoring and condition assessment facilities for transformers." CIGRE WG A2.27, April 2008. 27 p.
- [2] Technical brochure No. 227 "Guidelines for life management techniques for power transformers." CIGRE WG 12.18 Life Management of Transformers, 2002. 125 p.
- [3] J. Velek, J., et al. Monitorování stavu a životnosti silových transformátorů v PS ČEPS, a. s. In: Nové výzvy elektroenergetiky v ČR a SR. Skalský Dvůr: Národní komitét CIGRE ČR a SR, 2010.
- [4] M. J. Heathcote. The J & P Transformer Book: A Practical Technology of the Power Transformer. 13th ed. Burlington, MA: Newnes, 2007, 974 p. ISBN 978-075-0681-643.
- [5] M. Wang, A. J. Vandermaar, K. D. Sristava. Review of condition assessment of power transformers in service. IEEE Electrical Insulation Magazine. November/December 2002, Vol. 18, No. 6, p. 12-25.
- [6] MS 3000: Comprehensive on-line condition monitoring, diagnostics and expert system for power transformers - Manual 1.0, Revision date 14. 3. 2012. ALSTOM Grid. Monchengladbach, Germany, 2012. 262 p.
- [7] S. Tenbohlen et al. Enhanced diagnosis of power transformers using on- and off-line methods: Results, examples and future trends. In CIGRE Session 2000: 12-204. Paris (France): CIGRE, 2000. 8 p.
- [8] T. Stirl, R. Skrzypek, S. Tenbohlen, R. Vilaithong. On-line condition monitoring and diagnosis for power transformers their bushings, tap changer and insulation system. In: International Conference on Condition Monitoring and Diagnosis. CMD 2006, Changwon, Korea, 2006. 4 p.
- [9] M. Rosner, J. Weenen, X. Hao. Benefits of comprehensive and interactive on-line monitoring and expert systems for power transformers. In: International Conference on Condition Monitoring and Diagnosis. CMD 2008, Beijing, China, 2008, 5 p.
- [10] J. Dončuk, V. Mentlík, J. Velek. Condition assessment of power transformer using gas detection methods. Przeglad Electrotechniczny. Vol 2013, No 1a, p. 164 - 168
- [11] J. Dončuk. Možnosti hodnocení stavu transformátorů. Pilsen, 2011. Thesis for the final state doctoral exam. 60 p. FEE UWB Pilsen.
Supervisor: Václav Mentlík.

Intelligent measuring diagnostic system for estimation of operational state of high voltage rotating and non-rotating electrical machines

Ing. Pavel Ryška, Ph.D., Ing. Pavel Justiz

Orgrez, a.s., Division of Electrical Laboratories, Vítkova 17, 186 00 Prague 8, CZ, www.orgrez.cz

Ing. Radek Sedláček, Ph.D., Doc. Ing. Josef Vedral, CSc.

CTU in Prague, Faculty of Electrical Engineering, Technická 2, 166 27 Prague 6, CZ, measure.feld.cvut.cz

Abstract — Reliability and trouble-free operation of existing and newly installed high voltage generators and transformers forming the basis of the power system of the Czech Republic depend to a great extent on the quality of their insulation systems. Therefore diagnostics of insulation systems with respect to their current state is very important. One of the most effective diagnostic methods is the galvanic method of measurement of partial discharges supplemented with dissipation factor measurement. This article focuses on the diagnostic system under development, which will enable to measure dissipation factor, energy and frequency of partial discharge occurrence. Based on measured results the related software will help to determine probable time between failures of power equipments. This procedure will result in significant economic savings in terms of inspections, repairs and shutdowns of equipments.

Keywords — partial discharges, measurement, insulation system, diagnostics, rotating and non-rotating electrical machines, charge calibration

I. INTRODUCTION

There are a lot of non-destructive methods used for condition assessment of HV machine insulation systems. Acoustic, chemical, visual methods or thermography are of non-electrical character. Capacitance and dissipation factor measurement of electrical machine winding insulation and measurement of partial discharges using coupling device at the terminals of test machine are examples of electrical methods. The differentiating character of partial discharge measurements allows localized weak points of the insulation system to be identified. Partial discharge (PD) measurement has gained acceptance all around the world because long-term monitoring of a PD level and its statistical evaluation can also predict a residual lifetime of electrical machines and can be effective for increase the reliability of electrical power transmission and distribution. It helps to better scheduling of economical investments in the area of maintenances and renovations.

PD measurement can be performed directly by detection of induced charge or indirectly by detection of physical quantities such as discharge light, mechanical vibration, ultrasonic waves or chemical changes of SF₆ gas caused by arcing during presence of discharges. All measuring methods used for PD are listed in [1]. Among

other things, this paper deals with galvanic method of PD measurement. The principle of the method is based on voltage pulses measurement between terminals of the test electrical machine. However, a suitable HV coupling capacitance standard together with coupling device must be used for PD signal separation from AC HV supplying tested machine. A great advantage of that method consists in possibility to use it for on-line and off-line testing. The test circuit is shown in Fig. 1.

Typical pulse width is in range a few nanoseconds till a few microseconds. Direct digitalization of PD current impulse is illustrated in Fig. 2.

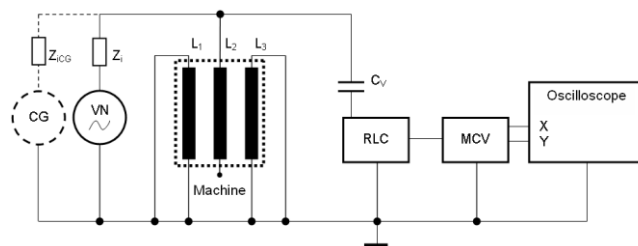


Figure 1: Test circuit for galvanic method of PD measurement (VN – HV power supply (25 kV/50 Hz), C_v – coupling capacitance (100 pF), RLC coupling unit, MCV – PD meter)

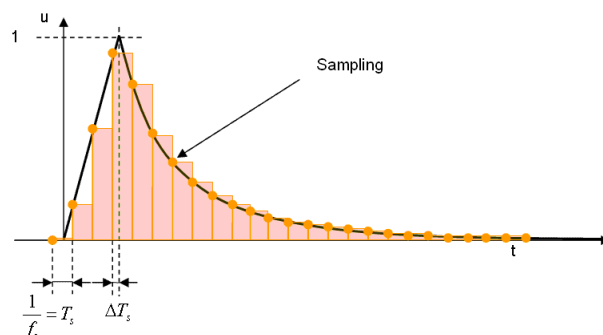


Figure 2: Direct digitalization of PD current impulses (sampling rate: 50 MSA/s ($T_s = 20$ ns), AD converter resolution: 14 bits, dynamic range of measuring chain: min. 60 dB)

According to results of performed experiments the pulse width is independent of overvoltage but increases rapidly with increasing gap or thickness of dielectric material. Main followed parameter of the PD analysis is apparent charge q and its phase angle ϕ regarding period of testing high voltage.

II. PD METER

Basic concept of intelligent measuring diagnostic system for PD measurement using galvanic method can be seen in Fig. 3. The block structure of the PD meter is shown in Fig. 5.

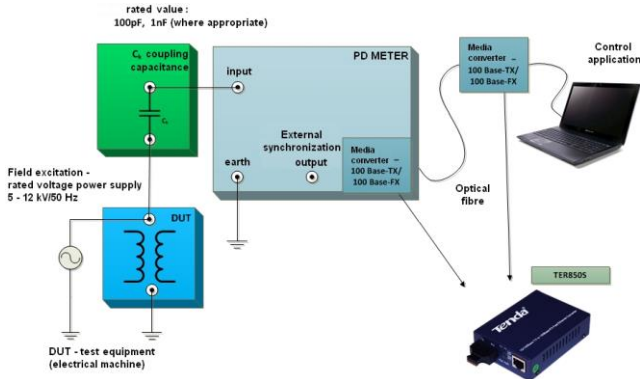


Figure 3: PD measurement concept

At present, owing to the availability of fast digital electronics, there is a possibility to implement hardware that provides fully digital signal processing with PD signal. Apparent charge calculation is performed just in time domain using summation of discrete samples forming each PD event. The PD meters should work with the frequency bandwidth 30 kHz - 500 kHz [3], in some case the frequency bandwidth should be extended up to 2 MHz [4]. A new PD meter enabling to sample the PD signal at frequency of 50 MSa/s was designed and constructed. The whole PD meter is battery-operated device, which does not have any controls and is fully controlled by a computer. To ensure sufficient security the Ethernet link connection between PD meter and control computer is realized by optical fiber.

For any PD event evaluation of is very important PD localization concerning period of testing voltage. There are two different ways to perform it. One possibility of synchronization is via external optically coupled input. The Second one is derived by means of complex coupling devices, which includes zero-cross circuit working in the whole range up 100 V_{RMS}. The functional sample of PD meter was designed and constructed at ČVUT in Prague.

III. COUPLING DEVICE

Essential integral part of each PD meter is auxiliary input circuit, so-called coupling device. The main purpose of this complex coupling device is to separate PD signal from exciting testing 50 Hz voltage. Generally speaking, the coupling device behaves like high-pass filter having cut-off frequency approximately a few kHz, so that power frequency 50 Hz would be suppressed.

The maximal level of the PD signal is 10 V_{RMS}. The maximal input voltage of coupling device is 100 V_{RMS}, frequency range from 10 kHz to 10 MHz.

IV. CHARGE CALIBRATOR

Before starting actual measurement using the PD meter, there is a necessity to pass calibration procedure. The concept of calibration of PD meter is presented in Fig. 4. The block structure of the charge calibrator is shown in Fig. 6.

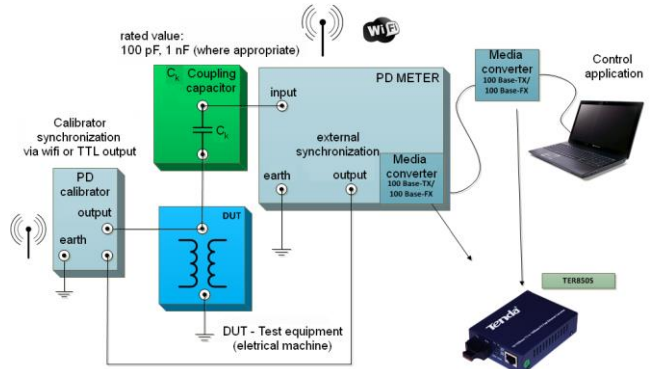


Figure 4: Concept of PD meter calibration

For this reason a new smart charge calibrator controlled by microcontroller was designed and constructed.

The calibrator is capable to generate charge pulses in the range from 100 pC to 100 nC. In addition to charge size users should set certain number of pulses generated per each half period in range from 1 to 16. There is a possibility to change width of generated pulse. The rising edge of charge pulse is less than 100 ns, falling edge can be set in four different values: 1 μs, 5 μs, 10 μs and 50 μs. The principle of calibrator is not complicated. Reference voltage is used for charging reference capacitors. After charging the reference capacitor in proper time, this capacitor is discharged by means of given reference resistor through analogue switch. A voltage/current convertor is implemented at the output stage. Due to this fact the calibrator is equipped with current output.

V. EXPERIMENTAL MEASUREMENT

The results achieved during experiment in the ORGREZ laboratory and carried out with the PD meter are presented in Fig. 7.

It was verified that the complex coupling device and the PD meter operate correctly. The whole measuring system is still being developed, particularly as regards main software for control and displaying of the results.

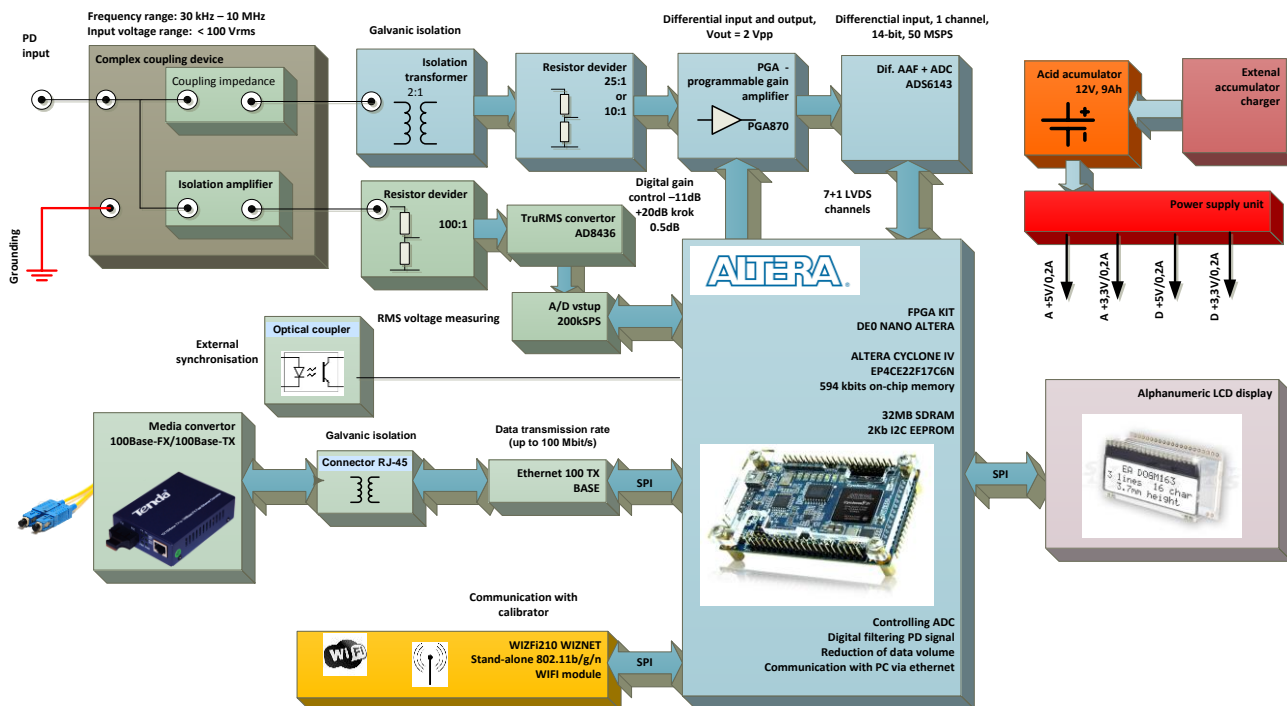


Figure 5: Block structure of the PD meter

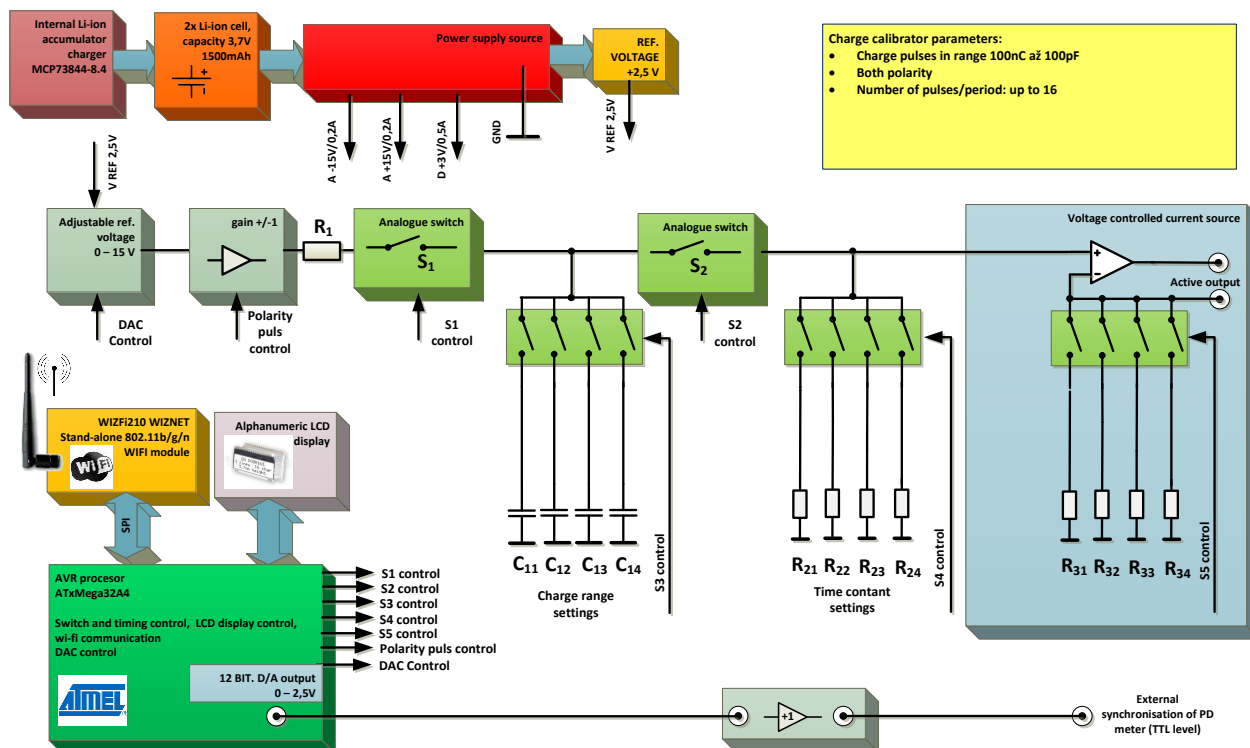


Figure 6: Block structure of the charge calibrator

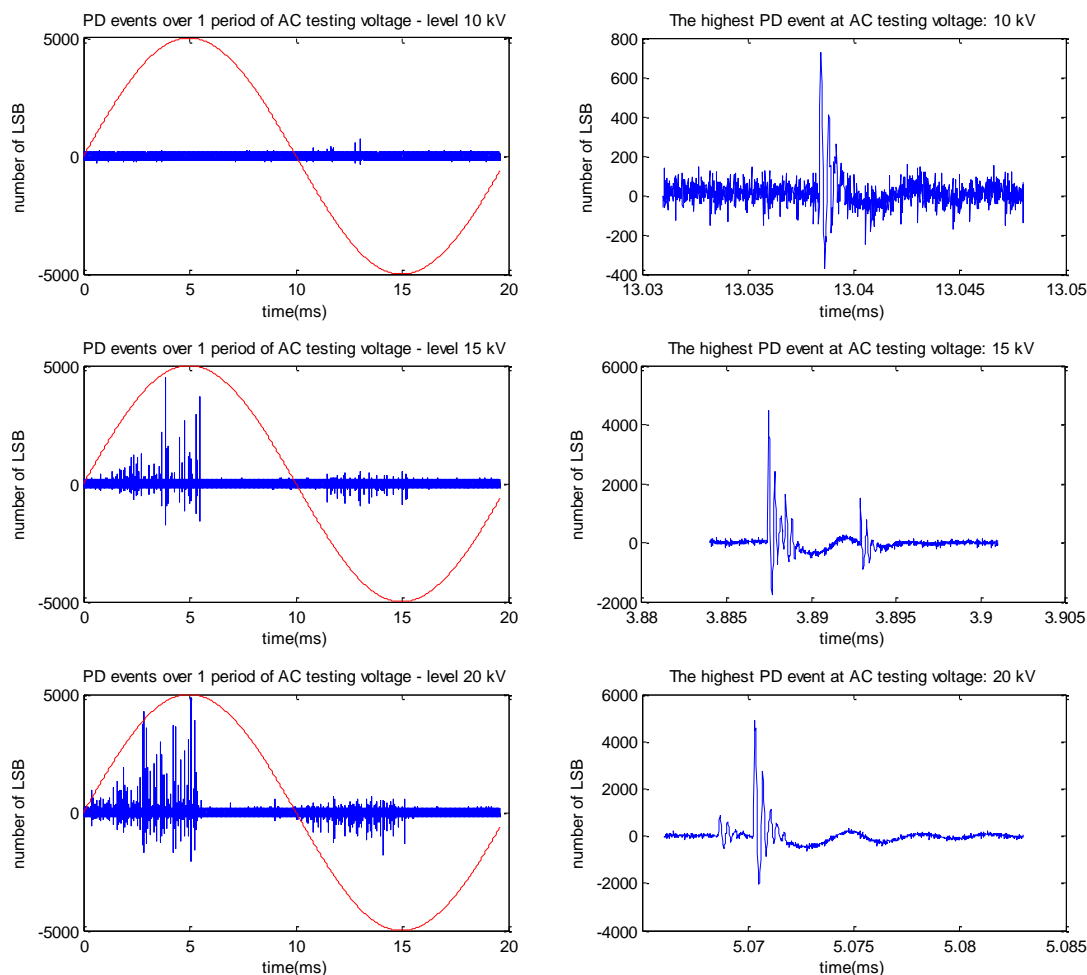


Figure 7: Characteristics achieved from the measurements using the PD meter

VI. CONCLUSION

In this paper, the concept of the PD diagnostic measurement system and wideband PD meter are described. There are also presented newly developed sophisticated coupling device and smart charge calibrator that should be used before each PD measurement. The control software is still under development. The first testing was performed in accredited laboratory. The future work will be concentrated on improvement of frequency bandwidth of coupling device and implementation of algorithm for the PD analyses in field-programmable gate array (FPGA).

ACKNOWLEDGMENT

This paper was created thanks to the support of the Technology Agency of the Czech Republic within the framework the second ALFA sub-programme, No. TA02010311 “*Intelligent measuring diagnostic system for estimation of operational state of high voltage electrical rotary and non-rotary machines*”.

REFERENCES

- [1] M. Hikita, S. Okabe, H. Murase, H. Okubo, “Cross-equipment Evaluation of Partial Discharge Measurement and Diagnosis Techniques in Electric Power Apparatus for Transmission and Distribution,” *Dielectrics and Electrical Insulation*, IEEE Transactions on , vol.15, no.2, pp.505-518, April 2008.
- [2] IEC/TS 60034-27, “Off-line partial discharge measurements on the stator winding insulation of rotating electrical machines”, CEI/IEC 60034-27:2006
- [3] IEEE Trial-Use Guide to the Measurement of Partial Discharges in Rotating Machinery, IEEE Std 1434-2000, 2000.
- [4] IEC 60270, “High-voltage test techniques - Partial discharge measurements”, CEI/IEC 60270:2000.
- [5] D. Koenig, Y. Narayana Rao: *Partial Discharge in Electrical Power Apparatus*, VDE Verlag, Germany, 1998, ISBN: 3-8007-1760-3.
- [6] W. Pfeifer, T. Brosche, W. Hiler, E. Frauer: *Novel Characterization of PD Signals by Real-Time Measurement of Pulse Parameters*. *IEEE Transaction on Dielectrics and Electrical Insulation*, Vol.6, No.1, February 1999.
- [7] K. Zálaiš: *Částečné výboje v izolačních systémech elektrických strojů*. Praha, Academia, 2005, ISBN: 80-200-1358-X.
- [8] V. Mentlík, J. Pihera, R. Polanský, P. Prosr, P. Trnka: *Diagnostika elektrických zařízení*. BEN, 2008, ISBN: 978-80-7300-232-9.
- [9] J. Vedral, M. Kříž: *Digital Signal Chains in Partial Discharge Measurement*. *IEEE International Workshop on Intelligent Data Acquisition and Advanced Computing Systems IDAACS 2009*, Rende Cosenza, Italy, 2009, pp. 82-86, ISSN: 978-1-4244-4882-1.
- [10] J. Vedral, M. Kříž, “Signal Processing in Partial Discharge Measurement”, *Metrology and Measurement Systems*, vol. XVII, No.1, pp.55-63, 2010.

Transformer Fleet Management as Approach for Risk Based Asset Management

S. Kornhuber¹⁾, O. Kouzmine²⁾, S. Schreiter³⁾

ABB AG, Trafoweg 4, 06112 Halle (Saale), Germany, www.abb.de

¹⁾ tel: +49 345 5686 133, email: stefan.kornhuber@de.abb.com,

²⁾ tel: +49 345 5686 228, email: oleg.kouzmine@de.abb.com,

³⁾ tel: +49 345 5686 102, email: sebastian.schreiter@de.abb.com,

Abstract— Power Transformers are key assets as a part of electrical transmission as well as distribution networks, but the installed base is aging and a part of them have been reaching the design life time at current time. Furthermore the changing in the power generation, changing in the power streams and increasing of the demand leads to a certain higher and dynamic load level of the aged infrastructure. If transformers fail unexpected the network operators have to take care about this situation quite fast, but a full replacement can take often months and involves a certain amount of money. Additional also a fault at easy replaceable or repairable components can lead to a catastrophic damage at the transformer itself. To manage the investments of reparations and replacements a good and consistent overview about the health status and the related risk to the power network of the transformer fleet is necessary. Periodic measurements, permanent monitoring of key values and diagnostic interpretation based on the measurement results are only one part of the input facts, but there are important input values missing. For a suitable and reliable overview of the transformer fleet an impact survey with the operator (impact of a failure to the network / costs) and a check of the possible next steps based on the installed transformers is necessary. With this kind of information a risk matrix and a suggestion for the next steps can be prepared for budget requests by the asset management.

Keywords— power transformers, asset management, fleet management, condition assessment, diagnostics

I. INTRODUCTION

The investments in electrical power networks have been increased in Europe by the end of the 2nd World War. Furthermore the increasing industrialization and the increasing electrical power demand (and the increasing of the need of reliable power supply) led to big investments. Beside the investments in the grid infrastructure also investments in power transformer were done. As shown in fig. 1 the peak of the main part of the population is approx. 40 years old. In a worldwide view the average of transformers of the industry are approx. 30 years and of the utilities approx. 40 years old. [1]

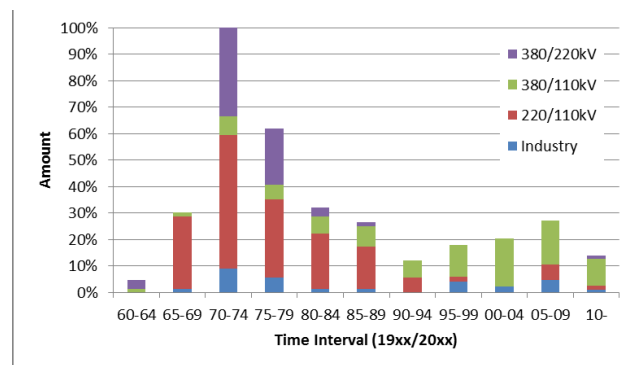


Fig. 1. Transformer population of a German TSO [2]

Power transformers are designed for a long lifetime, whereby on the other side the investments in power transformers are quite high from the financial prospective. Also the lead times for power transformers are quite long. Beside the careful design of power transformers the materials are also related to the well-known aging processes whereby the failure rate will increase over time. The failure rate over time (also known as bath-tube curve) describes the failure rate over time. In fig 2 typical bath-tube curves are shown for power transformer for industrial usage, for step-up transformer at power plants and for utility usage shown. A significant difference of the knee point can be observed.

Valuable failure statistics are available at the utilities as well as in network communities. Actual the CIGRE working group A2.37 is working on a new data basis for the failure statistic survey and published the first results in [4] and [3]. According to this first results the winding, tap changers and the bushing failures were identified as a main part as shown in fig. 3.

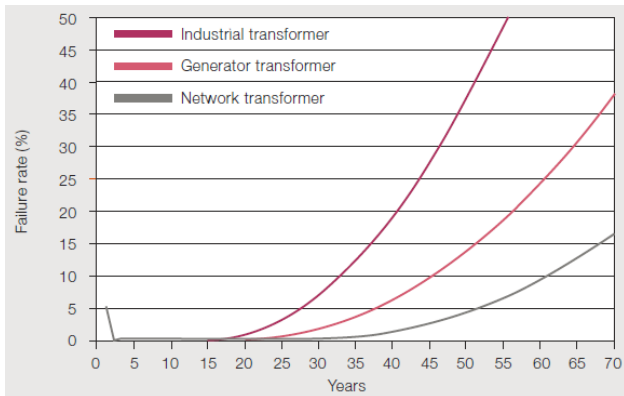


Fig. 2. Development of the transformer failure rate in three different applications (bath-tube curve) [1]

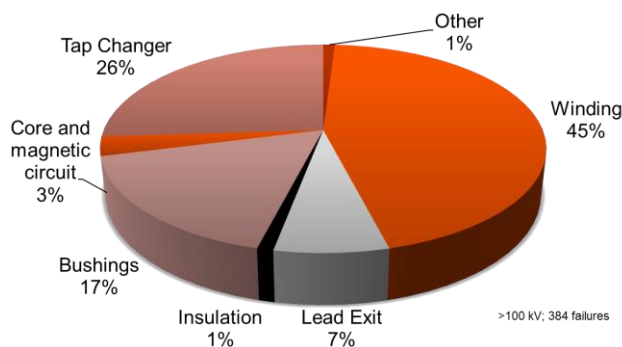


Fig. 3. Failure distribution of transmission transformers [3]

According to [4] nearby of 65% of the failed surveyed transformers have been repaired onsite or in a factory. In 60% of the scrapped transformers a winding defect was involved. In [4] also a calculation of the possible failure rate according to the collected data is shown, which harmonizes quite suitable with fig. 2.

II. MAINTENANCE STRATEGIES

By covering the situation of aging infrastructure and the knowledge of the failure rate of the assets a suitable strategy has to be applied. Following common maintenance strategies are well known and used over several years:

- IBM - Incident Based Maintenance: If an asset fails the asset is repaired or scrapped.
- TBM - Time Based Maintenance: At defined time intervals condition assessment and maintenance tasks (sometimes based on the results of the condition assessment) are done.
- CBM - Condition Based Maintenance: Based on the results of the condition assessment maintenance tasks are planned and applied.
- FCM - Forecast Based Maintenance: Based on the results of the condition assessment, the further development and the further usage of the unit assessment maintenance tasks are planned and applied.

- RCM - Reliability Centered Maintenance: Overall strategy by estimating the reliability of the whole network based on the reliability of the single assets (which can be estimated by condition assessment) and the further usage and demand.
- RBM - Risk Based Maintenance: Additional to the condition of the asset also the effects of an outage are considered. Therefore the risk is calculated by a product of costs and recurrent.

Beside the strategies the effects to the whole network has to be considered and reflected. [5]

A. Condition Assessment Measurement Methods

For the assessment of the condition of power transformers following different methods are well known an established.

During the normal site review or time based maintenance program a visual inspection maybe included. During the visual inspection the condition - based on a visual overview - is evaluated. This includes the condition and tightness of the tank, the condition and tightness of valves, breather, bushings, surge arrestors, leads and radiators, the assessment of the oil level and the oil temperature (if possible also the winding temperature), the functionality of fans, the visual functionality of OLTCs and . If necessary also an inspection by using an infrared camera can be done.

One of the most important condition assessment tool of a power transformer is the analysis of the oil. The analysis of the chemical and physical properties (SOT - standard oil test) as well of the dissolved gases (DGA test) is mostly done on a regular basis and well standardized (IEC 60422 and IEC 60599). With this methods the electrical and physical properties of the oil, the condition of the cellulose can be evaluated and possible indications of failures can be found. By using the Furan analysis the condition of the cellulose materials (degree of polymerization – DP), like pressboard and paper, can be estimated. These evaluations can be mostly done, when the unit is in operation.

By providing the transmission ratio measurement the transmission ratio of the transformer is evaluated and compared with the nominal values of the rating plate. The static resistance measurement provides information about the winding resistance as well as all connections between the points of the measurement. This includes all connections between the bushing, the tap changer and inter-winding connections. Beside the presented static resistance measurement also a dynamic resistance measurement can be provided. With the dynamic resistance measurement the dynamic behavior of the OLTC during the switching process can be examined.

By the usage of the Frequency Responds Analysis (FRA) of transformers deviations of the mechanical set up of the winding could be observed. With the measurement of the no load losses and short circuit losses at reduced voltages it is possible to recognize differences to original measured values (e.g. commission or other assessments), which indicates changes in the iron circuit (no load losses)

or in the mechanical setup of the winding (short circuit impedance).

With the measurement of the insulation resistance the resistive and polarization behavior of the insulation is evaluated. The capacitance and dielectric loss factor measurement of the bushings and the main capacitance of the transformer are widely used. The measurement of the dielectric responds (FDS or PDC measurement) of the whole insulation system provides necessary information for the evaluation of the moisture in the cellulose.

If an indication for Partial Discharge events (e.g. as result of the DGA of the oil) is available a partial discharge measurement by using the UHF method or the electrical method according to IEC 60270 can be applied for closer evaluation.

Additionally to the shortly described assessment possibilities additional methods are described in the literature.

Beside the condition assessment by the use of manual measurements automatic permanent monitoring systems are available at the market. The most common systems are such for the monitoring of condition of bushings, partial discharge, oil moisture, or different types of DGA in oil.

B. Cost involvement of Condition Assessment

Based on the different strategies different cost involvements have to be considered for the preventive maintenance and condition assessment tasks. It has to be considered that for a full transformer survey at the voltage level of 110 kV up to two days for measurements per transformer has to be planned and the transformer has to be disconnected from the power grid. Based on the results of the assessment further tasks have to be considered, like maintenance, on-site repair or factory repair. For this reason a long term view over the whole asset gives the benefit for a suitable planning considering reduced costs, planning for long term outages for factory repair or replacing by a new unit and technical view about the asset.

For the installation of permanent monitoring systems direct costs of the monitoring system as well of the installation of the monitoring system, but also indirect costs like such to keep the system running, maintenance, data infrastructure and permanent data evaluation are involved.

III. FLEET MANAGEMENT STRATEGY FOR POWER TRANSFORMERS

A. Motivation for fleet management

As discussed in the introduction of this paper power transformers are a key component of the electrical power network and the uninterruptible usage has to be ensured in electrical power depending community. Nevertheless most probably a time-based replacement of power transformers will not take place due to the high investment costs. For this reason a strategy for the right life elongation methods and replacements at the right economical and technical point has to be done. To oversee this problem as well to get a suitable base for decision a proper fleet management should be introduced in the asset management.

As discussed in the introduction the main investments were taken in the 60s and 70s at this example. Considering that the total numbers of units haven't decreased in a significant way, a certain portion of transformers is currently in the area of increasing failure rates related to the bath-tube curve. To keep the failure rates at a low level an optimized maintenance and tasks for live elongation has to be implemented. At the same time liberalization and deregulation of the electrical power market and the related the upcoming competition and regulated transmission rates leads to decreasing budgets for maintenance. With this changed economic driven focus a time based maintenance for keeping the general failure rate very low cannot be financed and a risk related budgeting (and tasks) per unit has to be set up.

Beside the replacement or repairing costs after an unforeseen outage of a power transformer a total cost calculation has to take place. A non-negligible part has to be covered in terms of revenue losses, payments for adequate power supply (during the outage) or not supplied energy costs, which can reach easily times of the repairing or replacement costs of the power transformer unit. Furthermore also the different public law or contract situation has to be considered in the total costs view. Contractual penalties could reach up to 100 times of the price of the delivered electrical energy [1].

Additional to the cost and law related topics also the technical situation of a power transformer unit has to be considered. On the one hand side the life time and much more important the remaining life time of the core components (active part) has to be evaluated as well as the remaining components. It has to be considered that some components are not more in production for power transformers, which were designed e.g. 50 years ago. Furthermore environmental responsibility aspects have to be considered for the technical decisions.

To consider the dimensions an analysis of the situation of the power transformer fleet as well also a risk consideration has to be implemented. By the usage of both dimensions a short, mid and long term planning can be arranged.

B. Process of fleet management

The proposed process contains various subtasks, which are described in the following paragraphs. It is important to see this process as an infinite cycle process, which includes also the evaluation of the effects of an unexpected outage (failure) and the risk assessment.

The process provides an updated (actual) planning tool for the short-, mid- and long term view based on the evaluation of the effect of an outage and considers also implicit the economic view.

C. Description of the transformer fleet

As a start of the process the transformer fleet should be described and defined. Also an introduction of suitable categories and attributes could be helpful.

D. Evaluation and homogenization of available historical data of the fleet

For the implemented transformers the historical measuring data, maintenance reports, design documents, commission reports, failure reports and so on should be organized and found. These kinds of documents will exist most probably not in a harmonized and electronic form. Especially for trending analysis and calculations a harmonization and digitizing have to be done.

E. Evaluation of effects of unexpected outage (failure)

For each unit the total costs of an unexpected outage should be evaluated. This consist the direct and indirect monetary costs as well also non-monetary cost, which should be weighted with close monetary value. This process is important at the start of the fleet management, but it is also necessary to update this if changes in influences are available.

F. Development and Application of Condition Assessment

Based on the historical data, the previous condition assessments and the evaluation of the effects of unexpected outage a proper condition assessment program should be developed. This condition assessment program should not only consider the technical parameter, but should also consider the total costs of the condition assessment. Based on the developed program the measurement task should be applied. Furthermore based on onsite measuring results maybe directly additional measurements should be applied.

G. Evaluation of the Risk Level

Based on the effects of failures as well as the results and estimation from the condition assessment the related risk level can be evaluated. The main dimensions of the risk assessment are the failure costs and the failure probability.

H. Recommendation for Maintenance / Repair Activities, Replacement

If a reduction of the risk level is necessary a proper maintenance / repair program or a replacement strategy has to be developed. For the maintenance / repair program an optimized cost / benefit ratio of the activities should be reached.

IV. PRACTICAL EXPERIENCE OF THE IMPLEMENTATION OF PROPOSED FLEET MANAGEMENT STRATEGY

The discussed and presented fleet management strategy is used for several different transformer fleets over several years. In the following paragraphs one example for an implemented fleet management is presented and discussed.

A. Reasons for Fleet Management

In a typical electrical power grid several transformers with different individual properties, condition, age and importance are installed. For all this transformers different types of information are available at different places. To enable a risk based maintenance it is necessary to get an overview about the transformer and there individual condition and needs. Therefore the necessary information must be available consistently (see step "Evaluation and homogenization of available historical data of the fleet")

Furthermore, in case of a failure information of the failed transformer must be available immediately to enable well based decision about the next steps. Therefore, the practical implementation of the fleet management in a software based system needs to include all kind of historic and actual data available.

B. Transformer Fleet Ddatabase

The developed database system includes all historic and actual data, provides an overview over the next maintenance- and diagnostic actions as well as an overall risk assessment for each transformer of this fleet.

This database is based on standard tools and can be used by different users and easily adapted and improved for different usage and purposes. The main page of this database system is shown in fig. 4.

Ergebnisse		Übersicht							
Sortierung aufheben		Geräteart	Fabriknummer	Zustand	Wichtigkeit	Handlungsbedarf	Nächste Standarduntersuchung	Nächste DGA	Nächste Furananalyse
Leistungstransformator	1234	7.3	9	8	05.11.2012	05.11.2012	05.11.2012		
Leistungstransformator	1235	6.5	3	4	05.11.2012	05.11.2012	05.11.2012		
Leistungstransformator	1236	5.2	2	3	05.11.2012	05.11.2012	05.11.2012		
Leistungstransformator	1237	4.7	1	2	05.11.2011	05.11.2011	05.11.2011		
Leistungstransformator	1238	9.2	7	8	05.11.2011	05.11.2011	05.11.2011		
Leistungstransformator	1239	3.5	6	4	05.11.2011	05.11.2011	05.11.2011		
Leistungstransformator	1240	2.1	5	3	05.11.2011	05.11.2011	05.11.2011		
Leistungstransformator	1241	1.9	4	2	05.11.2011	05.11.2011	05.11.2011		
Leistungstransformator	1242	7.4	7	7	05.11.2010	05.11.2010	05.11.2010		
Leistungstransformator	1243	6.2	6	6	05.11.2010	05.11.2010	05.11.2010		
Leistungstransformator	1244	5.4	5	5	05.11.2010	05.11.2010	05.11.2010		
Leistungstransformator	1245	4.7	4	4	05.11.2010	05.11.2010	05.11.2010		
Leistungstransformator	1246	9.2	4	7	05.11.2012	05.11.2012	05.11.2012		
Leistungstransformator	1247	3.2	9	6	05.11.2012	05.11.2012	05.11.2012		
Leistungstransformator	1248	2.1	3	2	05.11.2011	05.11.2011	05.11.2011		
Leistungstransformator	1249	1.5	2	1	05.11.2010	05.11.2010	05.11.2010		
Leistungstransformator	1250	5.7	1	3	05.11.2010	05.11.2010	05.11.2010		

Fig. 4. Overview of the transformer fleet (main page)

The main page gives an overview about all units of this fleet and indicates the next necessary maintenance and diagnostic measures. In the additional pages the technical data of the units and there components can be accessed. Finally the results of the different investigations as discussed in II.A are shown. All findings are concluded to an overall risk assessment for each unit and can be shown in correlation to the importance of the unit. This total overview indicates how to spend the maintenance budget for the most risky and important units.

UW 1, Tr 1

Allgemeine Daten	
Umspannwerk:	UW 1
Betriebsmittel:	Tr 1
kennzeichnung:	
Hersteller:	ABB
Typ:	TSSN 7651
Fabriknummer:	1234
Baujahr:	1987
Alter:	24
Geräteart:	Leistungstransformator
Leistung[MVA]:	200
Zustand:	7.3
Wichtigkeit:	8
Handlungsbedarf:	8
nächste Standarduntersuchung:	05.11.2011
nächste DGAuntersuchung:	05.11.2011
nächste Furananalyse:	05.11.2011
Besonderheiten:	keine

Verfügbare Dokumente		
Bilder	Gesamtansicht	Ansicht Bild 1 Bild 2 Bild 3 Ordner
Visuelle Inspektion	aktuelle Visuelle Inspektion	
Ölanalysen	aktuelle Ölanalyse	
Messungen	aktuelle Messung	
Expertisen	aktuelle Expertise	
Vorhandene Unterlagen	neustes Dokument	

Fig. 5. Detailed view of one transformer

Additionally the database allows a deep view for each unit in an individual transformer page as presented in fig. 5. Beside the technical data of the transformer all relevant historic and actual data can be stored for later use. Especially the historic trends for single or multiple results of the oil analysis and electrical measurements can be created.

C. Outcome and Benefit for Asset Management

Using the described database enables to create a maintenance plan according to individual risk and importance for all units within a transformer fleet, ensures the consistent and complete structure of all relevant data and provides a solid basis for decision in case of a failure of one unit quickly.

The presented database is in use at several utilities including up to 100 units of different voltage- and power levels per system.

V. CONCLUSION

Due to the fact of the aging infrastructure and the aging of the power transformers on the one hand side and the changes in the economic situation due to the liberalization and deregulation on the other side it is important to find an optimized way for a suitable maintenance and condition assessment as well as a well selected and planed strategy for repairs and replacement of power transformers.

The proposed fleet management strategy is an infinite circular process model and allows a continuous overview and actualized overview about the transformer fleet. The benefit for the asset management is, that a planning based on this data can be done for short-, mid-, and long term activities by considering the condition and the risk of their power transformer fleets.

The successful practical evaluation of the proposed process is done at different fleets and the practical experience is discussed at one example.

REFERENCES

- [1] T. Westman, P. Lorin, P. A. Ammann, "Fit at 50", ABB Review 1 / 10, pp 63-69, 2010
- [2] U. Sundermann, „Flottenmanagement von Transformatoren aus Sicht eines Übertragungsnetzbetreibers“, Transformer Life Management 2012
- [3] S. Tenbohlen, J. Jagers, G. Baston, B. Diggin, M. Krüger, P. Manski, B. Desai, J. Gebauer, J. Lapworth, A. Mcintosh, A. Mikulecky, P. Müller, C. Rajotte, T. Sakia, S. Yukiyasu, „Transformer Reliability Survey: Interim Report“, Electra No. 261, pp. 46-49, April 2012
- [4] S. Tenbohlen, F. Vahidi, J. Gebauer, M. Krüger, P. Müller, "Assessment of Power Transformer Reliability", XVII International Symposium on High Voltage Engineering, Hannover, Germany, August 22-26, 2011
- [5] C. Sumereder, "Analyse und Bewertung von Betriebsmitteln in der Hochspannungstechnik", Habilitation Graz University of Technology, 2010

Influence of end corona protection on dissipation factor

Stauber J.¹⁾, Birner T.²⁾, Bezděkovský J.³⁾, Krupauer P.⁴⁾

BRUSH SEM s.r.o., Edvarda Beneše 564/39, Doudlevice, 301 00 Plzeň, Czech Republic, www.brush-sem.cz

¹⁾ tel: +420 603 197 278, email: jiri.stauber@brush.eu,

²⁾ tel: +420 378 210 466, email: tomas.birner@brush.eu,

³⁾ tel: +420 378 210 488, email: jiri.bezdekovsky@brush.eu,

⁴⁾ tel: +420 734 785 327, email: petr.krupauer@brush.eu,

Abstract— This article deals with an influence of the end corona protection (ECP) on dielectric dissipation factor (DF) value measured on a stator winding. The losses in a slot part of insulation take effect during DF measurement with guard rings (according to CSN EN 50209) on stator bar insulation. The influence of ECP takes effects during measuring of “global” DF. The potential is controlled by surface semi conductive layers lying on insulation in place of the highest gradient. The effect of the ECP is that there are losses which are added to the losses in the main wall insulation. Both losses create together global losses of a stator bar insulation system (and also complete winding). The losses in the area of the ECP are significantly higher than the losses in the slot part insulation. In this article we mention a qualitative and (for a concrete example) also a quantitative comparison of the DF in the whole insulation system. At the same time there is a discussion about an impact on the interpretation of some diagnostic measurement of loss factor provided on a generator.

Keywords— stator bar; stator winding; dissipation factor (DF); ECP (End corona protection); OCP (Outer corona protection); dielectric losses

I. INTRODUCTION

The dissipation factor of a stator bar (or coil) insulation is measured according to the standard CSN [1], or according to IEEE [2]. In both cases the measurement is done with the guard rings. The measurement according to [1], [2] includes only dielectric losses in the slot part insulation of stator bars/coils. In case that the dissipation factor is measured on wound stator, it is not possible to measure according to a standard (it is not possible to apply a guard ring on every single bar). The global dissipation factor does not include only dielectric losses in slot part, but also losses in the area of end corona protection (ECP).

This article deals with an influence of the end corona protection (ECP) on the value of the global dissipation factor measured on the wound stator. During measurement of the global dissipation factor on the wound machine, there is influence of the ECP, which controls the potential of electric field in the area where the stator bar leaves a slot. The potential is controlled by surface semi conductive layers in the area of the highest gradient. In consequence of ECP on the slot exit, there are losses that are added to dielectric losses from main wall insulation. Both losses

together create the global dielectric losses of stator bar insulation (and complete winding).

II. ESTABLISHMENT OF DISSIPATION FACTOR BY MEASUREMENT ON WOUND STATOR

During measurement of dielectric losses on a wound stator (Fig. 1), one electrode of the Schering bridge is connected to the stator winding copper, the other electrode is connected to the stator body (magnetic core) plus other unmeasured phases.

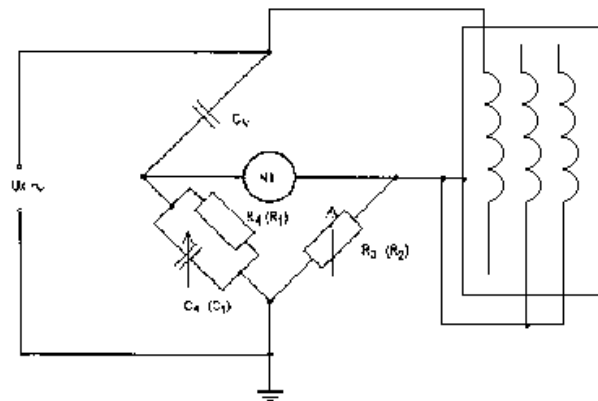


Fig. 1. Schering bridge - masurment of DF on one stator phase (stator winding ungrounded)

In this case the measurement shows the global dielectric losses. It means losses in slot part insulation plus losses in ECP area. On the wound stator we cannot separate the losses in slot part from losses in ECP. It would be necessary to apply a guard ring on each stator bar (on slot exit) and then to ground each guard ring. This is practically impossible. Evaluation of ECP influence is possible to establish only on the single bar (before insertion into the stator). We can measure dielectric losses in OCP area and separately losses in ECP area as it is shown below.

III. ESTABLISHMENT OF LOSSES IN OCP AREA

During measurement of dielectric losses according to standards [1], [2], only the Outer Corona Protection (OCP) is connected to a measurement part of the Schering bridge – see the equivalent circuit of stator bar in Fig.2 and Schering bridge configuration Fig. 3.

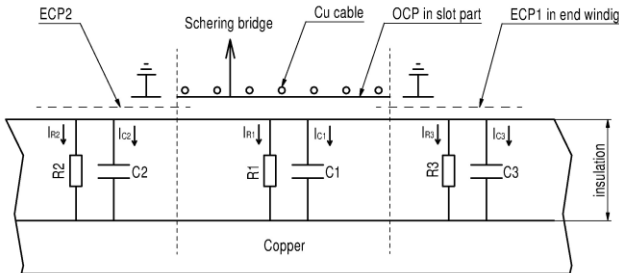


Fig. 2. Equivalent circuit of stator bar – measurement with guard rings

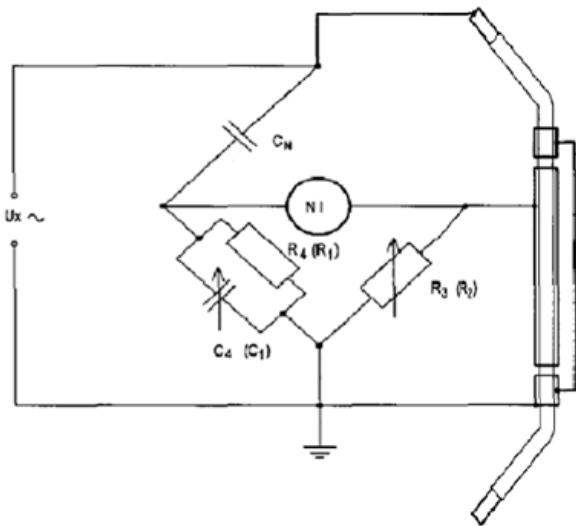


Fig. 3. Schering bridge – measurement according to a standard with guard rings

In this case capacity C1 and resistance R1 are measured. The resistance R1 reflects the dissipation factor only in area of OCP (only slot part). The losses which are in the ECP area are shielded (the guard rings lead the losses out of the Schering bridge).

IV. ESTABLISHMENT OF LOSSES IN ECP AREA

We can measure the losses in endwinding area (ECP on slot exit) thanks to exchange measurement electrode for a guard ring. Then the OCP works as a guard ring – see Fig. 4 and Fig.5. The losses in the slot part (OCP) are shielded and only the losses in ECP (slot exit) take effect. The current I_2 flowing to the ECP runs through the capacity C2, resistance R2 and also through axial resistance R_p . The losses in resistance R_p are much higher than the losses inside insulation (resistance R2). In this case the losses include both dielectric losses in insulation and losses in ECP on slot exit.

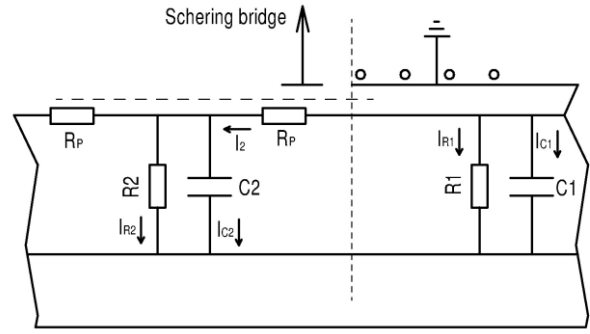


Fig. 4. Equivalent circuit of stator bar – exchange of measuring parts

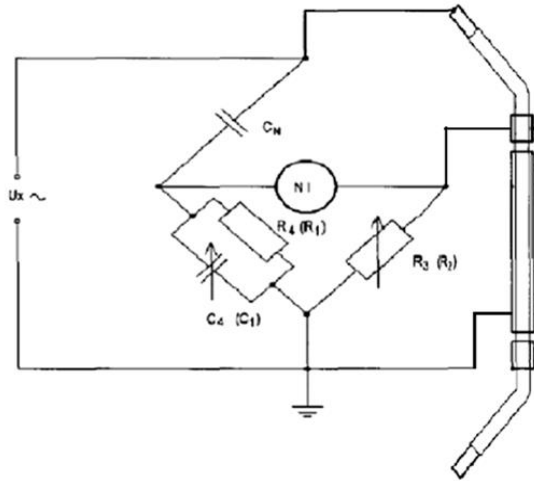


Fig. 5. Schering bridge – measurement of losses in ECP

V. ESTABLISHMENT OF GLOBAL LOSSES ON STATOR BAR

The global losses include both dielectric losses in slot insulation and losses in ECP on slot exit. The global losses are measured without the guard rings. The equivalent circuit is in Fig.6. Fig. 7 shows Schering bridge configuration for measurement without guard rings.

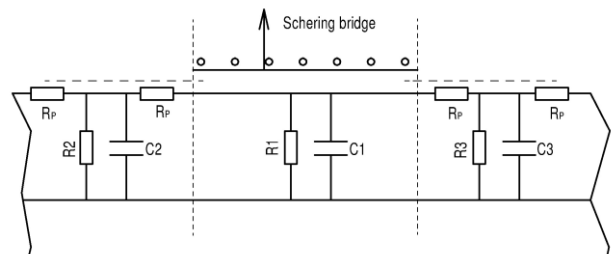


Fig. 6. Equivalent circuit of stator bar without guard rings; Resistance R1 corresponds to dissipation factor $\text{tg}\delta_1$; R2 corresponds to $\text{tg}\delta_2$; R3 corresponds to $\text{tg}\delta_3$

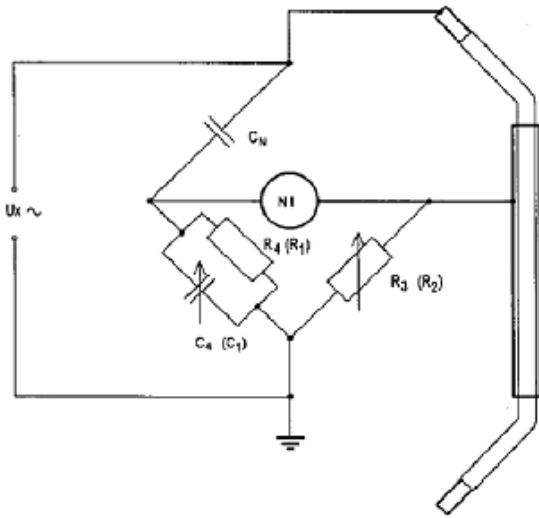


Fig. 7. Schering bridge – measurement without guard rings

Fig. 8 shows (for one particular example) statistical evaluation of measured losses on some stator bars insulation for 3 versions of measurement.

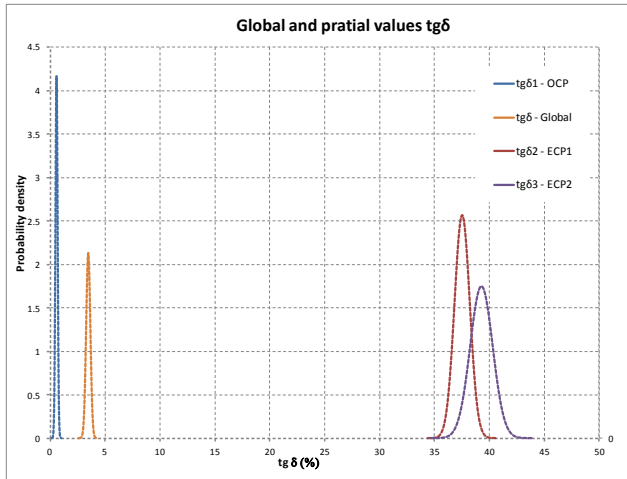


Fig. 8. Probability density function of dielectric losses (global, OCP, ECP)

On the basis of the equivalent circuit (see Fig. 6) we can measure the partial capacity and dissipation factors. Then we can derive an equation for calculation of the global dissipation factor (including both dielectric losses in OCP and losses in ECP on slot exit).

$$tg\delta_c = \frac{C1 \times tg\delta1 + C2 \times tg\delta2 + C3 \times tg\delta3}{C1 + C2 + C3} \quad (1)$$

When we calculate value of the global dissipation factor $tg\delta_c$ (Fig. 9 $tg\delta_{Calculate}$) according to equation (1), we get values that are lower than values measured according to Fig 6, Fig. 7. It is because the length of the OCP is longer due to the guard rings (see Fig 9).

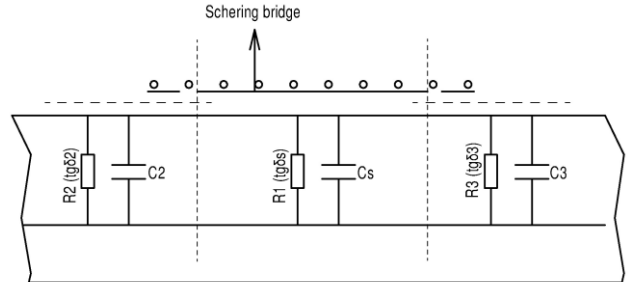


Fig. 9. Equivalent circuit of stator bar - the OCP is longer due to guard rings

If we measure the dissipation factor $tg\delta_s$ according to Fig. 9 (conductive connection of guard rings with the OCP), then we will get values of dissipation factor comparable with calculation $tg\delta_{calculate}$ (see Fig. 10). In Figure 10 there is for comparison the global value of dissipation factor $tg\delta_{Global}$ measured according to Fig. 6 and Fig. 7. For summary it is presented a value of dissipation factor $tg\delta1$ measured according to Fig. 2 and Fig. 3.

Simultaneously it is possible to see the impact of the change in ECP length on the dissipation factor of a stator bar and on a complete generator.

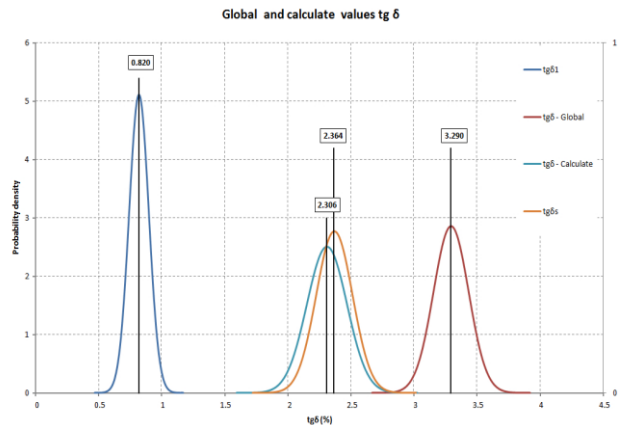


Fig. 10. Probability density function of measured values $tg\delta1$, $tg\delta_{Global}$, $tg\delta_s$ and calculated value $tg\delta_{Calculate}$

The files of calculated $tg\delta_{Calculate}$ and measured $tg\delta_s$ values were tested to meet hypothesis tests for parameters of normal distribution functions. At significance level $\alpha=0,05$ the tested hypothesis was not rejected for tests of dissipation and mean value. It is possible to say that the files vary neither in dissipation nor mean value.

VI. WATT LOSSES IN DIELECTRIC INSULATION SYSTEM

The capacity of insulation in slot part of each single stator bar is in range of nF (nano Farad). The effective current through insulation system in slot part is in range of microA. So the power losses in slot part are very low - in range of 1 Watt.

The power losses calculated from the global dissipation factor are in range of 10 Watts. The power dielectric losses calculated for wound stator are still less than 1% of Joule losses in stator copper wires.

VII. CONCLUSIONS

The dissipation factor measured on ECP on slot exit is in range 10-45% (the value depends on manufacturing technology in ECP area and kind of ECP). The losses in ECP are significantly higher than losses in main wall insulation.

The partial capacities and partial dissipation factors (in ECP and in OCP) are dependent on the dimensions of the stator bar. The dimensions (and the partial capacities) significantly influence the global dissipation factor of winding. The longer the slot part is (OCP), the lower influence of ECP is on the global dissipation factor. Simultaneously the modification of ECP (resistance selection, number of grades, length of ECP) will significantly influence the dissipation factor in ECP area and also influence the value of dissipation factor of one stator bar or winding.

The entire mentioned above have got a fundamental impact on the evaluation of measurement of dissipation

factor of wound machine. Changes of dissipation factor in insulation system are overlapped by changes in ECP area. The influence of the ECP is amplified by a fact that the resistance of the semi conductive layer depends markedly on voltage gradient and temperature. This has got an impact on the interpretation of results from diagnostic measurement of dissipation factor of wound stator.

The influence of ECP on the global dissipation factor is a reason why it is not possible to determine a limit value of dissipation factor for a generator [4].

The dielectric loss is a property of any particular insulation material and its chemical composition. It is not an indicator of insulation quality. For maintenance tests on complete windings, the initial DF measured is irrelevant. A significant amount of deterioration has occurred if the DF has increased by 1% or more from initial value. It is necessary to observe the tendency of dissipation factor (tendency vs. voltage, tendency vs. time).

REFERENCES

- [1] ČSN EN 50209:1999, "Test of insulation of bars and coils of high-voltage machines"
- [2] IEEE Std 286-200, "IEEE Recommended Practice for Measurement of Power Factor Tip-Up of Electric Machinery Stator Coil Insulation"
- [3] F.T. Emery, "Basic of Power Factor Measurement on High Voltage Stator Bars & Stators Windings", IEEE Electrical Insulation Magazine, May/June 2004-Vol.20, No.3
- [4] Technical Specification 2/1651/CD, "Dielectric dissipation factor measurement on stator winding insulation of rotating electrical machines", Project IEC 60034-27-3 TS Ed 1

Aspects of partial discharge behaviour – voltage dependence

Petr Mráz¹⁾, Václav Mentlík²⁾, Josef Pihera³⁾, Rainer Haller⁴⁾

Faculty of Electrical Engineering, University of West Bohemia,
Univerzitní 8, Pilsen, Czech Republic, www.zcu.cz

¹⁾ email: pmraz@ket.zcu.cz, ²⁾ email: mentlik@ket.zcu.cz

³⁾ email: pihera@ket.zcu.cz, ⁴⁾ email: rhaller@kee.zcu.cz

Abstract— This paper deals with fundamentals of partial discharge (PD) behaviour and it is especially focused on PD voltage dependence. Mostly is assumed that the PD activity is strongly connected with the value of the test voltage i.e. with raising test voltage the PD activity should be increased too. It will be shown, that dependent on the type of PD source the voltage dependence of PD behaviour can be very different. The paper describes and explains general behaviour of three fundamental types of PD – external discharges, surface discharges and internal discharges. Conclusions to a deeper understanding of PD test results are described.

Keywords— partial discharges; gliding discharge; internal PD; corona; voltage dependence

I. INTRODUCTION

Partial discharge (PD) measurements became one of the wide spread used diagnosis method in condition evaluation of electrical devices especially in case of high voltage devices. Nowadays it is easy to buy commercial measuring tool, but the core issue is how to perform PD measurement, how to evaluate the measured data and which reasonable conclusions should be made. Additional to that depending on the diagnosis task some problems of connection the measuring system to the test object or the choice of the right sensors have to be solved. Basic instructions and some recommendations for solving these problems are made in the relevant standards and guides [1-3]. For interpretation of PD activity evaluated by the measured PD parameters very often the dependency on the applied test voltage is used. The common existing evaluation for this kind of measurement is that with increasing test voltage the PD parameters are increased too and the measured values are more or less linear dependent on the applied test voltage. In the paper is shown, that the PD parameter depending on the applied test voltage could have a different behaviour caused by different PD sources. The described investigations were made with some well-known basic (artificial) PD sources, which are typical for relevant defects in electrical apparatus, such as transformers, rotating machines, switchgears/ GIS or cables. The PD activity was evaluated by the PD parameter Q_{IEC} (apparent charge) as well as PRPD patterns according to the recommendations mentioned above. The obtained results should give a contribution to a better interpretation of measured PD activity under real test conditions.

II. TEST AND MEASUREMENT CONDITIONS

A. Test objects

For the measurement three basic test arrangements were chosen simulating typical corona -, gliding – and internal discharges (table I). First one was needle-plane arrangement (table I.-A) to simulate corona discharge. Brass needle tip shape was 24 μm before electrical stress and lower brass circular electrode has diameter 75 mm, gap distance was 10 mm.

Gliding discharge phenomenon was measured according to the arrangement which is shown in table I.-B. Top electrode had circular shape and its diameter was 50 mm. Lower electrode had circular shape as well and its diameter was 75 mm. Insulating material was represented by block made of Poly(methyl methacrylate) (PMMA). Dimensions of this insulating material were 140x140 mm, thickness 10 mm. Top electrode was pressed to the insulating material by constant and defined pressure, which was ensured by spring located in a holder system of the top electrode.

Internal partial discharges were measured according to arrangement shown in table I.-C. The top (high voltage)-electrode had a circular shape with a diameter of 50mm. The ground-electrode was circular shaped too (diameter 75mm). The top-electrode was pressed to the dielectric material by a constant and defined pressure, which was given by a spring located in a holder system of the top electrode. The whole test setup was completely immersed into transformer oil to suppress the gliding discharge on

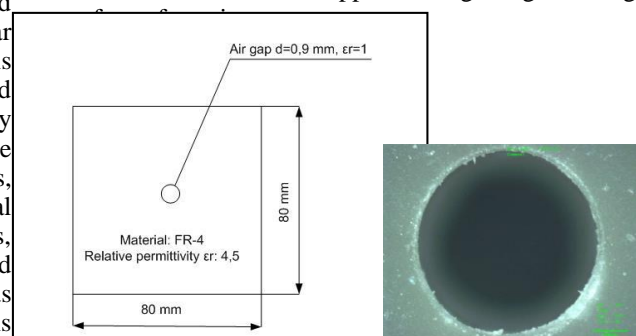
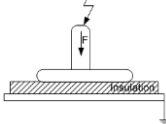
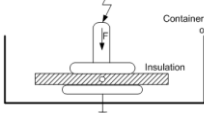


Fig. 1. Diameters of internal PD sample and microscopic view [15]

The dielectric material was realized by sheets of FR4 (FR4 is a composite material composed of woven fibreglass cloth with an epoxy resin binder that is flame

resistant) with dimensions of 80 x 80 mm and thickness of 3 x 0.6mm. The diameter of cavity was 0.9 mm round shape and was measured microscopically by Stereomicroscope Olympus SZX10, see figure 1. [15]

TABLE I. TEST ARRANGEMENTS OVERVIEW

A	Corona Needle-plane	
B	Gliding discharge	
C	Internal discharge	

B. Test circuit

Measurement was performed using a test circuit according to IEC 60270 (fig. 2), [2]. It consists of a 50 Hz-power transformer (0-50 kV), coupling capacitor (C=1000pF), measuring impedance (Z=50Ω) and partial discharge analyser PD SMART¹. The whole test circuit was located into a shielded test room, where a PD sensitivity of less than 1 pC was reached at a test voltage value up to 30 kV.

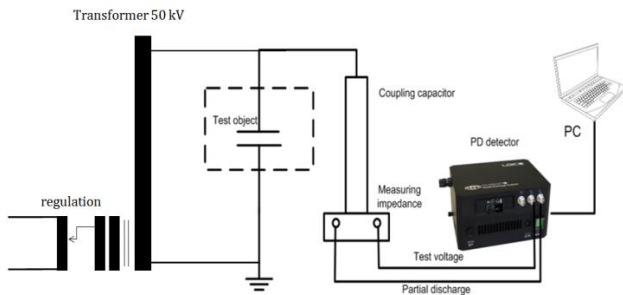


Fig. 2. Test circuit

C. Test procedure

The test procedure was carried out in two stages (fig.3, 4).

FIRST STAGE

Increasing the test voltage up to U_i (inception voltage), measuring the Q_{IEC} -value, increasing the test voltage up to $1.2 U_i$, decreasing the test voltage to $0.8 U_e$ (extinction voltage) and repeating the procedure 5 times. For evaluation an averaging of the measured values was made.

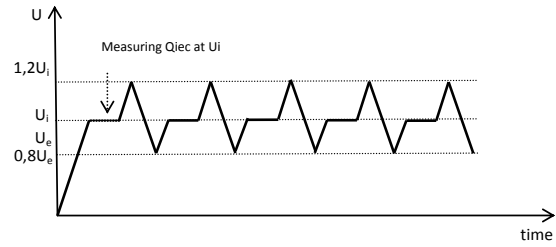


Fig. 3. First stage measurement (principle)

SECOND STAGE

For measuring of any time-dependencies of PD- values the $Q(t)$ - behaviour was measured in the second stage procedure according to Fig.3. Time dependence of corona discharge was set to 15 minutes at 350 % U_i (self extinguish phenomenon). Decreasing test voltage from 350% U_i to U_e with 35 % U_i steps – measuring Q_{iec} and PRPD (Phase resolved PD characteristics or Φ -q-n) and Φ -q diagrams for each voltage step. Time dependence of gliding discharge was 5 minutes at 135 % U_i . Decreasing test voltage from 135 % U_i to U_e with 0,5 kV voltage-steps and time dependence of internal partial discharge was 10 minutes at 120 % U_i . Decreasing test voltage from 120 % U_i to U_e with the same (0,5 kV) steps.

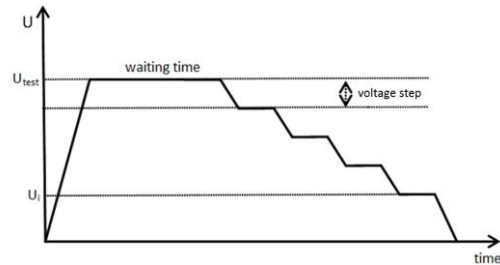


Fig. 4. Second stage measurement (principle)

III. EXPERIMENT RESULTS

A. Corona discharge

TABLE II. MEASURED VALUES FOR CORONA DISCHARGE

Average Inception voltage U_i	1,56 kV
Average Apparent Charge at inception voltage Q_{iec}	37,8 pC
Average extinction voltage U_e	1,43 kV

There are four phases of corona to breakdown development [4-8]

First phase ($U_{test} = U_i \sim 1,6 \text{ kV}$)

If AC voltage is applied to the needle, pulses can be observed in negative half sinus wave. These pulses have relatively small amplitude (depending on the tip shape), high repetition rate and they are time- stable. This phenomenon is called Trichel pulses. They are caused by fast transfer of electrons from voltage electrode (needle) to ground electrode (plane). Electrons leave behind

¹ LDIC PD fully digital measuring system (DOUBLE LEMKE)

themselves slow positive ions, which create space charge around the tip and suppress the electron's movement for a certain time. If the ions are moved away, the next pulse is possible (fig. 5).

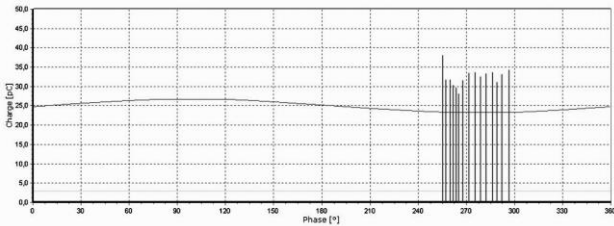


Fig. 5. Φ -q diagram - first phase of corona

- Second phase ($U_{\text{test}} = 200 \% U_i \sim 3,1 \text{ kV}$)

Increasing of test voltage causes that the range of the Trichel pulses over the voltage (or the area of phase angle) gradually spreading - between the electrodes flow more and more electrons- avalanches, a higher PD repetition rate could be measured too (fig. 6).

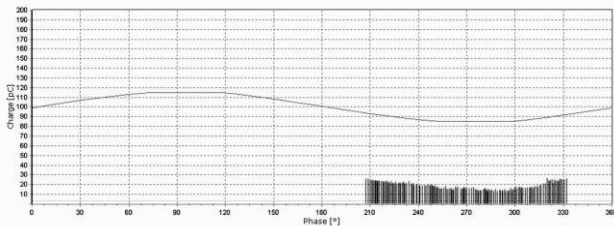


Fig. 6. Φ -q diagram - second phase of corona

- Third phase ($U_{\text{test}} = 263 \% U_i \sim 4,1 \text{ kV}$)

With higher value of test voltage a special PD behaviour can be observed, so called "pulses less area". It is located in the middle of Trichel pulses cluster (fig.7). With common partial discharge detectors no PD pulses can be observed in this area. In fact the repetition rate of pulses in this area is so high, that common PD analysers are not able to recognize them.

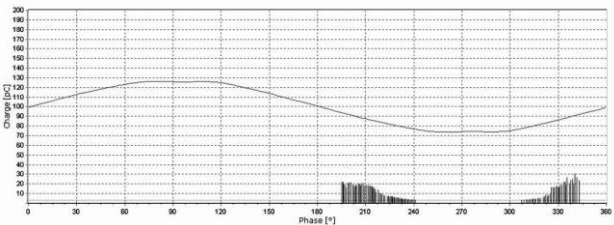


Fig. 7. Φ -q diagram - third phase of corona

- Fourth phase ($U_{\text{test}} = 350 \% U_i \sim 6 \text{ kV}$)

If the test voltage is increased even more - close to breakdown voltage - high energy pulses occur in positive half sinus wave of test voltage. These pre-breakdown or onset streamers are typical with their high charge resp. energy levels (significantly several times higher than Trichel pulses) and with their instability - this is a phase very close to breakdown. These pulses are located in positive half sinus wave of test voltage (needle) because this arising instable conduct channel consists of positive

streamers. This fourth phase can be very easily turned to the breakdown thanks to their instability. In that case onset streamers can be observed in both polarities of test voltage. Fourth phase is characterized by an audible (acoustic) effect (fig. 8, 9).

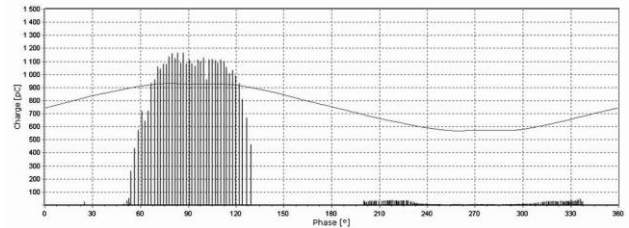


Fig. 8. Φ -q diagram - fourth phase of corona

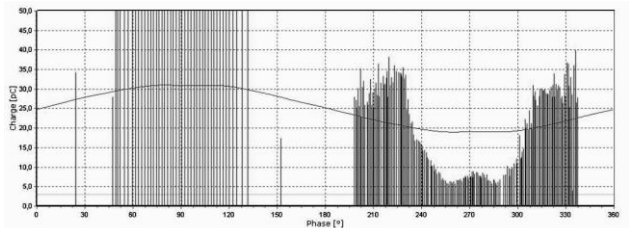


Fig. 9. Φ -q diagram - fourth stage of corona - zoom to negative half sinus wave

The charge- voltage dependency shows the typical characteristics of this PD behaviour (fig. 10). In the first phase a quasi constant charge level over the voltage will be obtained. Therefore, this behaviour was in the past particular used like a high- voltage- calibrator [3]. It should be noticed, that the level of measured charge is dependent on the tip- radius. The described phenomenon is valid only in a certain range of test voltage. If the voltage is increased, the stability of the charge value is lost (see fig. 10 - higher dispersion).

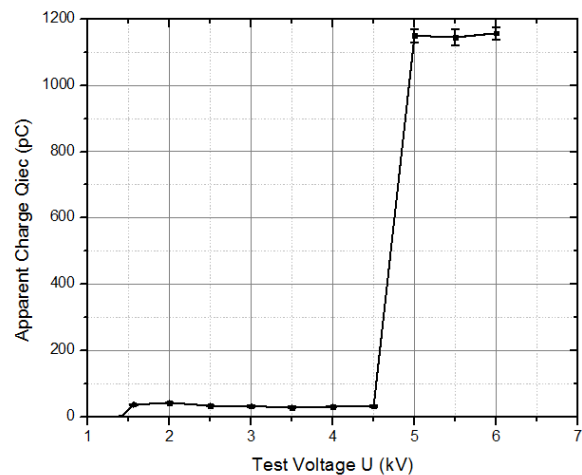


Fig. 10. Charge- voltage dependence of corona

B. *Gliding discharge*

TABLE III. MEASURED VALUES FOR GLIDING DISCHARGE

Average Inception voltage U_i	7,1 kV
Average Apparent Charge at inception voltage Q_{iec}	1310 pC
Average extinction voltage U_e	6,8 kV

Figure 11 shows the typical PD behaviour of gliding discharge at Φ -q-n diagram. There is no phase shift during test voltage increasing. Gliding discharge activity is characteristic by two symmetric triangle diagrams, one is in positive half sinus wave and the second is on the negative half sinus wave of test voltage. The peaks are at 60° of phase in positive half sinus wave, respectively in 240° of phase in negative half sinus wave. In some cases the cluster in negative half sinus wave of test voltage can have smaller amplitude of charge. Only the size (the level of apparent charge) of diagram is changing with voltage increasing.

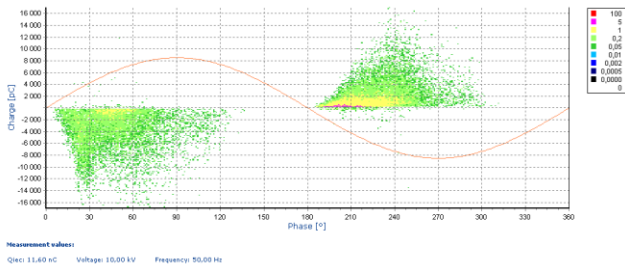


Fig. 11. Φ -q-n / PRPD pattern for gliding discharge

At the same time the charge- voltage dependency is typically for gliding discharges (fig.12), [9-13]. All values are in the nC- range, with relative high dispersion behaviour, the PD activity is monotonously increased at higher test voltage.

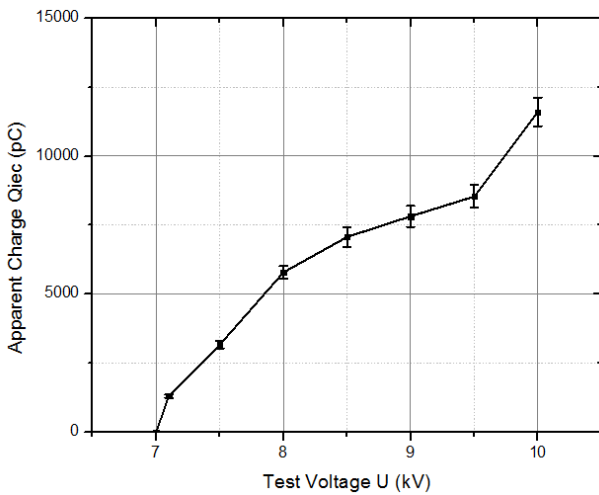


Fig. 12. Charge- voltage dependency of gliding discharge

C. Internal discharge

TABLE IV. MEASURED VALUES FOR INTERNAL DISCHARGE

Average Inception voltage U_i	3,65 kV
Average Apparent Charge at inception voltage Q_{iec}	240 pC
Average Extinction voltage U_e	3,1 kV

The typical PD behaviour of an internal cavity is characterized by a hysteresis at test voltage up and down (fig. 13). It is supposed, that the avalanche of fast electrons in the cavity let the slow ions behind itself. [15]

The ions then create space charge and it receives on the inner surface of the cavity. It causes deformation of the original electrical field.

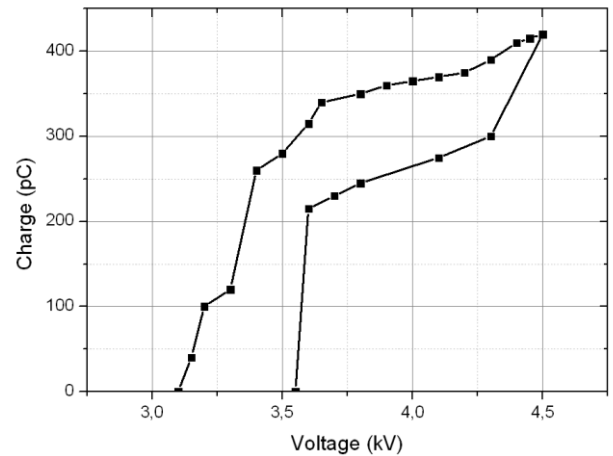


Fig. 13. Charge- voltage dependency of internal discharge (inception and extinction voltage area)

Space charge has an opposite field influence in comparison with the external field, the resulting field within the cavity is weaker. Therefore in comparison with the inception voltage the extinction voltage is lower caused by the space charge inside the internal defect. In some cases this behaviour can be used for identification of the existing PD sources.

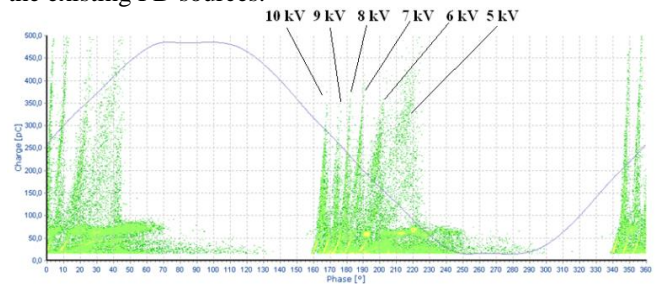


Fig. 14. Φ -q-n / PRPD pattern for internal discharges at different test voltages

A typical PD behaviour can be obtained by measuring the PRPD- pattern (fig. 14), [14-19]. There are two symmetrical clusters in both half sinus waves and with higher test voltage the PD activity “cluster” (so-called rabbit ears) is shifted to a lower phase angle and at the same time the PD activity is limited to a smaller “phase-area”.

Even the charge- voltage dependency shows a characteristic behaviour (fig. 15). After the PD inception and small increasing of the test voltage the PD activity expressed by the measured charge is even quasi unchanged at higher test voltages. It should be noticed, that the dispersion of the charge values is much higher than at corona- PD’s, the value of the charge is determined by the size of the cavity. In case of several cavities with different size also levels of inception voltages can be changed. Also this typical behaviour

could be used in some cases for a better identifying of the existing PD sources.

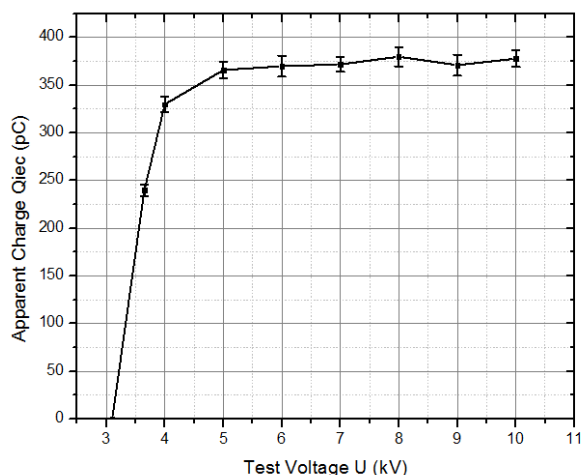


Fig. 15. Charge- voltage dependency of internal discharge

IV. CONCLUSION

In the paper some aspects of PD evaluation are discussed – in detail the charge- voltage behaviour and accompanied PD parameters- of basic PD arrangements typical for real existing PD defects. The obtained results confirm that each type of PD defect has its specific PD behaviour and especially its charge- voltage dependency. Not all of them have a monotonously increasing PD activity at higher applied test voltage. As example the Corona PD activity has a special charge- voltage characteristic, which is characterized by Trichel pulses up to final pre-breakdown onset streamers. Gliding discharges in general have more or less linear increasing character of PD activity with rising test voltage, caused by linear increase of electrical field inhomogeneity. Internal discharges have first part of charge- voltage characteristics similar to the corona, but higher dispersion of measured values but then it differs. Despite of another physical background of PD activity of internal defects is strongly dependent on size and filling material of cavity. Therefore, it is not convenient to evaluate the PD activity only by an absolute value of apparent charge or by generalized charge- voltage behaviour. Consequently, for a better evaluation of measured PD results and, at the same time, a better interpretation of the PD activity a more complex observation and enhanced evaluation of the PD values seems to be necessary.

ACKNOWLEDGMENT

This research has been supported by the Student Grant Agency of the West Bohemia University in Pilsen, grant No. SGS-2012-026 "Material and Technology Systems in Electrical Engineering"

REFERENCES

- [1] Lemke, E. et al; "Guide for Partial Discharge Measurements in Compliance to IEC 60270," CIGRE-WG D1.33, 2008
- [2] IEC 60270 "High-voltage test techniques - Partial discharge measurements"
- [3] Kreuger, F.H.; "Partial Discharge Detection in High- Voltage Equipment," Butterworths, London, 1989
- [4] G. W. Trichel, "The Mechanism of the Negative Point to Plane Corona Near Onset," Phys. Rev., Vol. 54, pp. 1078-1084 (1938).
- [5] Edin, Hans. Partial Discharges Studied with Variable Frequency of the Applied Voltage. Stockholm, Sweden, 2001. PhD thesis. Kungl Tekniska Högskolan.
- [6] Gardiner, P.S.; , "Some characteristics of negative point-plane corona," Electrical Engineers, Proceedings of the Institution of , vol.125, no.5, pp.467-468, May 1978
- [7] Van Brunt, R.J.; Misakian, M.; Kulkarni, S.V.; Lakdawala, V.K.; , "Influence of a dielectric barrier on the stochastic behaviour of Trichel-pulse corona," Electrical Insulation, IEEE Transactions on , vol.26, no.3, pp.405-415, Jun 1991
- [8] Van Brunt, R.J.; , "Physics and chemistry of partial discharge and corona. Recent advances and future challenges," Dielectrics and Electrical Insulation, IEEE Transactions on , vol.1, no.5, pp.761-784, Oct 1994
- [9] Junhao Li; Wenrong Si; Xiu Yao; Yanming Li; , "Partial discharge characteristics over differently aged oil/pressboard interfaces," Dielectrics and Electrical Insulation, IEEE Transactions on , vol.16, no.6, pp.1640-1647, December 2009
- [10] Berg, G.; Lundgaard, L.E.; , "Discharges in combined transformer oil/paper insulation," Dielectric Liquids, 1999. (ICDL '99) Proceedings of the 1999 IEEE 13th International Conference on , vol., no., pp.144-147, 1999
- [11] Beroual, A.; Kebbabi, L.; , "Analysis of cumulative number and polarity of creeping discharges initiated at solid/liquid interfaces subjected to AC voltage," Electrical Insulation and Dielectric Phenomena, 2009. CEIDP '09. IEEE Conference on , vol., no., pp.380-383, 18-21 Oct. 2009
- [12] Kiiiza, R.C.; Niasar, M.G.; Nikjoo, R.; Wang, X.; Edin, H.; Ahmed, Z.; , "Comparison of phase resolved partial discharge patterns in small test samples, bushing specimen and aged transformer bushing," Electrical Insulation and Dielectric Phenomena (CEIDP), 2012 Annual Report Conference on , vol., no., pp.88-91, 14-17 Oct. 2012
- [13] Hudon, C.; Belec, M.; , "Partial discharge signal interpretation for generator diagnostics," Dielectrics and Electrical Insulation, IEEE Transactions on , vol.12, no.2, pp. 297- 319, April 2005
- [14] Welsch, A.; Haller, R. Partial Discharge Diagnostics for Localisation of Defect Parts in Gas Insulated Medium Voltage Switchgear. XV International Symposium on High Voltage Engineering. 2007, Ljubljana, Slovenia
- [15] Kornhuber, Stefan; Boltze, Matthias; Haller, Rainer; Mraz, Petr; Pihera, Josef; , "PD behaviour of basic test arrangements under different measurement conditions," Condition Monitoring and Diagnosis (CMD), 2012 International Conference on , vol., no., pp.557-560, 23-27 Sept. 2012
- [16] Gross, D., W. „Locating partial discharge using acoustic sensors”, HighVolt Kolloquium '11, May 19-20, 2011, Dresden, Germany, pp. 99-106
- [17] Bodega, R.; Morshuis, P.H.F.; Lazzaroni, M.; Wester, F.J.; , "PD recurrence in cavities at different energizing methods," Instrumentation and Measurement, IEEE Transactions on , vol.53, no.2, pp. 251- 258, April 2004
- [18] Gross, D.W.; Fruth, B.A.; , "Characteristics of phase resolved partial discharge pattern in spherical voids," Electrical Insulation and Dielectric Phenomena, 1998. Annual Report. Conference on , vol., no., pp.412-415, vol. 2, 25-28 Oct 1998
- [19] Das, S.; Purkait, P.; , "φ-q-n pattern analysis for understanding partial discharge phenomena in narrow voids," Power and Energy Society General Meeting - Conversion and Delivery of Electrical Energy in the 21st Century, 2008 IEEE , vol., no., pp.1-7, 20-24 July 2008

Electrical field distribution along stator bars in dependence of lengths semiconductive stress grading tapes

Ondřej Krpal¹⁾, Eva Kučerová²⁾

Faculty of Electrical Engineering, University of West Bohemia, Univerzitní 8, Czech Republic, www.fel.zcu.cz

¹⁾ tel: +420 377 63 4545, email: ondrej.krpal@ket.zcu.cz ,

²⁾ tel: +420 377 63 4515, email: kucerova@ket.zcu.cz

Abstract — Places of occurrence are located on the surface of the stator bars or coils either between stator core or in the end-winding near the end of the stator core. To suppress the undesirable effect of partial discharges the conductive armor tapes and semiconductive tapes are applied. In machines operating above 6 kV with absence of the protection the partial discharge activity can lead to gradual damage of the insulation ending in its breakdown. The gradient of electrical field distribution along stress grading surface varies in dependency on its length.

In this article the method of measuring electrical field distribution is described as well as the gradient increase of electrical field along the stator coil in dependency on the length of the semiconductive stress grading tape.

Keywords— synchronous generator; semiconductive stress grading tape; electrical field; partial discharges; end-winding

I. INTRODUCTION

The distribution of electric potential in the end-winding in high voltage rotating machines is unequal and therefore there must be applied materials which reduce the electric field gradient. Thus the occurrence of surface discharges is minimized. These materials are called stress grading system, semiconductive stress grading tape, anticorona protection or non-linear resistance grade. The name is based on its non-linearity of the electric current on voltage (fig. 1). These protections are applied with 2 cm overlap over conductive (slotted) protection.

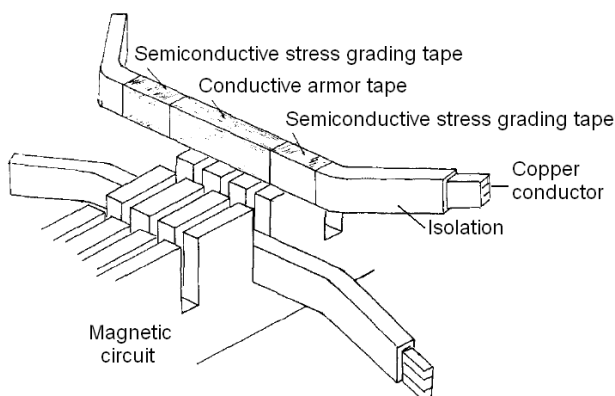


Fig. 1. Arrangement of the stator bars in synchronous generator [2]

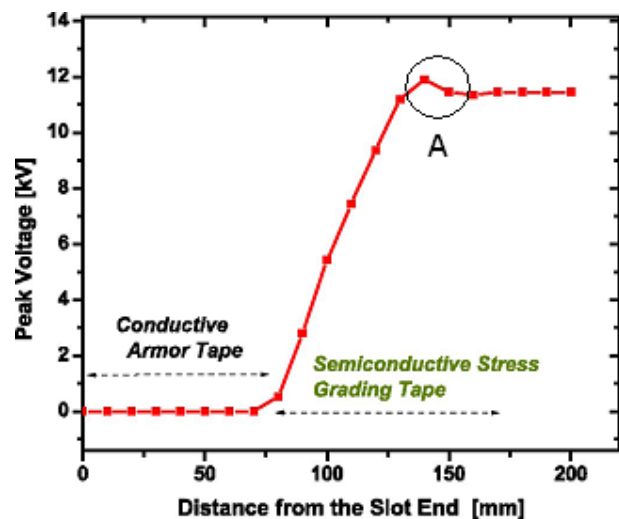


Fig. 2. Theoretical curve of the potential distribution along the stator bar [6]

The figure 2 shows the theoretical curve of potential distribution along the stator bar. There is a slight voltage decrease in the middle of the semiconductive stress grading tape.

II. SAMPLES OF THE STATOR BAR

A. Manufacturing of the stator samples

To manufacture the samples of stator coils the steel rods with dimensions 36 x 12 x 1200 mm were used. First, the steel was mechanically machined by sandpaper, then cleaned with acetone and was thus deprived of dirt and grease. The thickness and width of the bars was measured at five points from the edge (ie 280 mm, 440 mm, 600 mm, 760 mm and 920 mm). Thus, the rods were prepared and then placed into the winding machine.

The pull of the tape winding was set to 60 N and the individual rods were wrapped by insulation Relanex 45,033 in 12 layers with half overlap and the last 13th layer was applied to the contact. The beginning and end of the insulation was cut into a length of 1070 mm. At the center of the insulation conductive protection used for slot

part was placed in the middle of the bar of a length of 300 mm (Fig. 3).

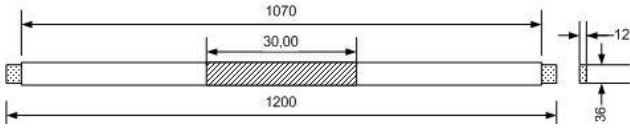


Fig. 3. Sample of the stator coil

These bars were taped by Eltafilm 76,000 – separation tape. Moreover, before inserting it into the press machine, each rod was wrapped up by separating foil. The ends of the foil were tied to prevent any outflow of resin during gelation and curing.

Curing itself lasted about 160 minutes. First, the press machine was preheated at 60 °C, after the rods were inserted and pressed and the temperature raised to 110 °C. After 15 minutes, the jaws were squeezed and the temperature was increased to 165 °C for 80 minutes. Then the press machine was cooled back to 60 °C. The curing process of the first sample is shown in Figure 4. Figure 5 shows the curing machine.

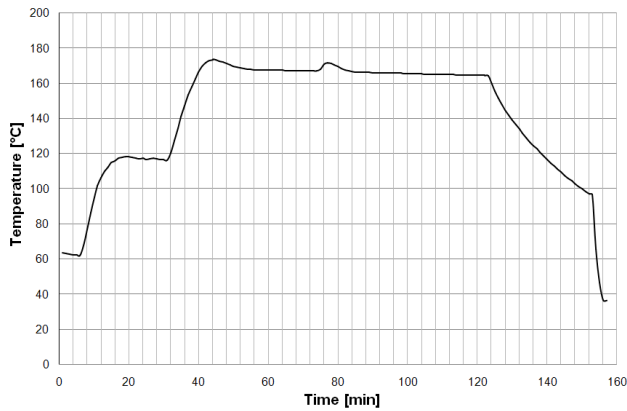


Fig. 4. Curve of the stator bar curing



Fig. 5. Curing machine

After curing, the separation film was removed from the samples and also redressed the separation from tape. Again, the width and thickness in the above-mentioned distances from the edge of the steel rod were measured. The average width of the insulation thickness was 3.46 mm, height 3.49 mm insulation. Compressibility insulation width was calculated to be 30.07% and high compressibility 29.36%.

III. MEASUREMENT

A. Measuring of the losses factor and relative permittivity

To optimize these protections there were produced samples of stator bars and measured nondestructive electrical insulation properties (losses factor and relative permittivity – results are shown in Fig. 6). Insulation was designed to prevent its breakdown at test voltage 3·Un (i.e. in our case up to about 55 kV) for one minute. Semiconducting protection was then applied in two combinations which were then compared to each other based on the stress distribution along the bar.

Measurement of losses factor and relative permittivity was carried out on an automatic bridge (Figure 7). Capacities C_X (sample) and C_N (normal capacity) are high voltage, capacity C_M and C_R are low voltage. Dissipation factor $\tan \delta$ is determined from the phase angle between the voltages that appear on the capacitors C_M and C_R .

Two shielding electrodes were placed on the sample of the stator bar 3.5 mm from the ends of the conductive tape. In the middle of conductive tape stuck sensing copper electrode. The steel bar is then connected to an AC voltage with a frequency of 50 Hz. The voltage increases in steps of 3 kV, in the range of 3 kV to 18 kV. The measured 25 values were averaged.

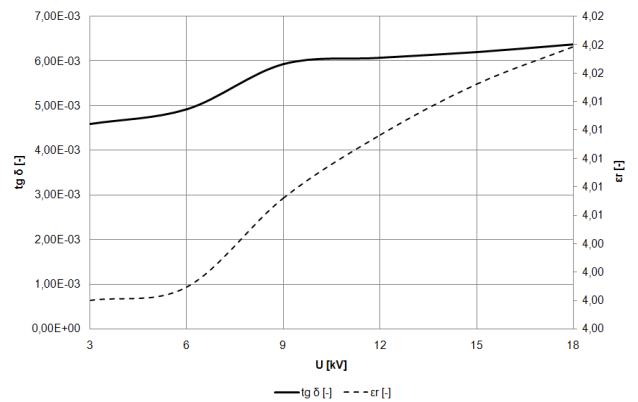


Fig. 6. Measurement of relative permittivity and losses factor

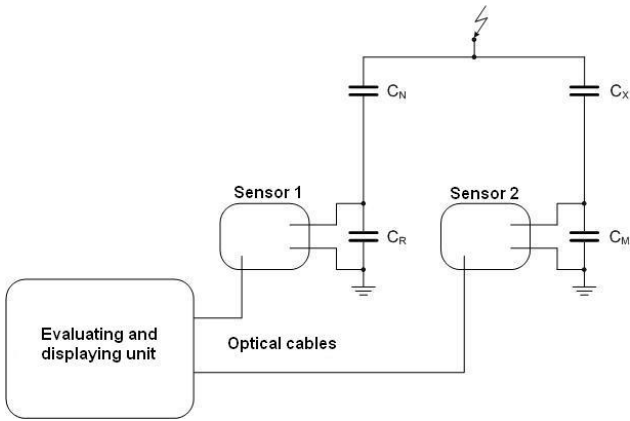


Fig. 7. Automatic bridge for measuring dielectric losses [1]

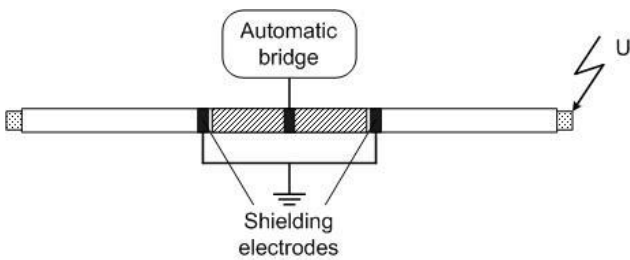


Fig. 8. Sample prepared for measuring the losses factor and relative permittivity

B. Measuring of the electrical field distribution along the stator bar

Samples were equipped by semiconductive stress grading tape (Akasic Tape 4b). First the tape was lapped by the tape and then placed in an oven.

The tapes were lapped in two lengths – 12 cm and 15 cm from the conductive armor tape.

The curing process of the semiconductive stress grading tape is shown in picture 9. The temperature was increased from 22°C up to 120°C, then 120°C was kept for 120 minutes. After that the oven was turn off and temperature decreased back up to 22°C.

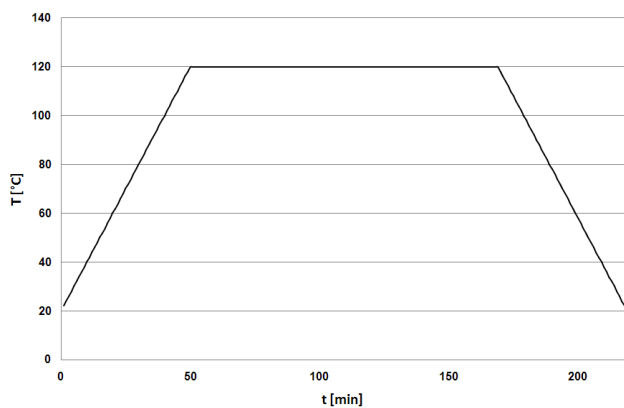


Fig. 9. Curing of the semiconductive stress grading tape

The grounding electrode was placed on the conductive armor tape. The high voltage was connected to the steel bar. The measuring was carried out in several voltage levels. From 5 kV up to 55 kV with the steps of 5 kV. The voltage was measured in every centimeter from the conductive armor tape and thus we have got the graphs showing voltage dependency on the distance from the magnetic core (conductive armor tape) – Figure 11.

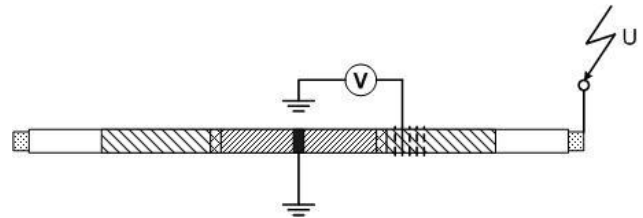


Fig. 10. Arrangement of the measuring

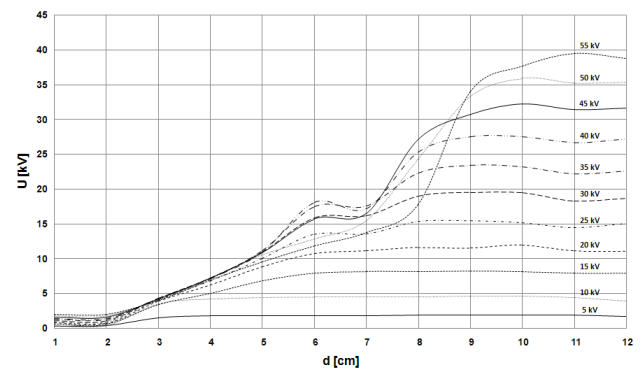


Fig. 11. Voltage dependency on the distance from the magnetic core (12 cm length of the semiconductive stress grading tape – Akasic Tape 4b)

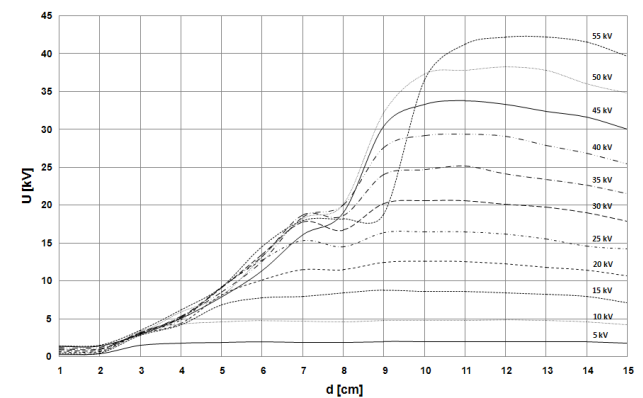


Fig. 12. Voltage dependency on the distance from the magnetic core (15 cm length of the semiconductive stress grading tape – Akasic Tape 4b)

IV. DISCUSSION

From the graphs it is noticeable that up to 30 kV the curves meet the theoretical assumption and in the middle of the semiconductive stress armor tape there is the voltage decrease as well as is seen in the figure 2. From

the voltage of 30 kV, the curves show ripples. The decrease can be caused by appearing of partial discharges and increase of the surface currents.

V. CONCLUSION

Surface discharges are undesirable effect which is harmful to the insulation of the stator bar and can lead to damage. This can cause shutdown of the whole machine and economical losses. The semiconductive tapes minimize surface discharges and protect insulation against such damage.

ACKNOWLEDGMENT

Thanks to Mr. Ing. Zdenek Bezděk, Ph.D. from the company COGEBI, PLC in Tábor, where all the samples were manufactured.

Thanks to Mr. Libor Zelénka from the company SILENT-CZECH LLC for provision of the semiconductive stress grading tapes.

This work was supported by the Student Grant Agency of the West Bohemia University in Pilsen, grant No. SGS-

2012-026 "Material and Technology Systems in Electrical Engineering"

REFERENCES

- [1] MENTLÍK, Václav, et al. *Diagnostika elektrických zařízení*. Praha: BEN, 2008. 440 s. ISBN 978-80-7300-232-9.
- [2] ROBERTS, A. Stress Grading for High Voltage Motor and Generator Coils. *IEEE*. 1995, 1, s. 26-31.
- [3] ZÁLIŠ, Karel. *Částečné výboje v izolačních systémech elektrických strojů*. Praha: Academia, 2005. 135 s. ISBN 80-200-1358-X.
- [4] MALAMUD, R.; CHEREMISOV, I. Anti-corona Protection of the High Voltage Stator Windings and Semi-Conductive Materials for Its Realization. *IEEE*. 2000, 1, s. 32-35.
- [5] MALAMUD, R.; SCHUMOVSKAYA, G.; STEPANOVA, T. The Development of Semiconducting Materials for Anti-Corona Protection Designs of Generator High Voltage Winding and their Testing at Cryogenic Temperatures. *IEEE*. 2008, 1, s. 420-423.
- [6] ESPINO-CORTES, Fermin P., Edvard A. CHERNEY a Shesha JAYARAM. Impact of Inverter Drives Employing Fast-Switching Devices on Form-Wound AC Machine Stator Coil Stress Grading. [online]. 2007, roč. 23, č. 1, s. 16-28 [cit. 2013-02-19]. Dostupné z: http://ieeexplore.ieee.org/xpls/abs_all.jsp?arnumber=4068210

VPI process optimization

Michal Rok¹⁾, Radim Zahradníček²⁾, Tomáš Barták³⁾, Lubomír Kousal⁴⁾

Škoda ELECTRIC a.s., Průmyslová 4, Plzeň, Czech Republic, www.skoda.cz

¹⁾ tel: +420 378 181 283, email: michal.rok@skoda.cz,

²⁾ tel: +420 378 181 224, email: radim.zahradnicek@skoda.cz,

³⁾ tel: +420 378 181 067, email: tomas.bartak@skoda.cz,

⁴⁾ tel: +420 378 181 283, email: lubomir.kousal@skoda.cz

Abstract— the purpose of this paper is to give a practical view on the problem of VPI process validation. On-line measurement of capacity during the VPI (Vacuum Pressure Impregnation) process allowed its detailed study and revealed time savings. Based on these time savings was suggested reduction some phases of the process. Since optimized VPI process have to be verified to prove that quality of insulation system wasn't affected we had to found suitable method. Common approach is to use destructive testing. This analysis of the traction motor is very expensive and time consuming. We have tried to find an alternative solution which would be more cost-effective. Result was suggestion of non-destructive diagnostic consists of on-line measurement of the capacity and partial discharges measurement on finished stators. Measurement was performed on the two sets of stators. First set was impregnated by a standard process and second one by optimized process. Measurements results of both stator sets were compared and evaluated.

Keywords— VPI process, partial discharge, capacitance measurement

I. INTRODUCTION

VPI technology is very important process in the production of traction motors for many years. Main purpose of VPI technology is to remove all air from stator insulation and fill it up by impregnation resin.

VPI process consists of 6 phases. The first phase is called reached a vacuum. The purpose of this phase is brought to vacuum in the autoclave with an inserted stator for impregnation. The length of this phase is given by power of vacuum pumps. Next phase is called a dry vacuum. The dry vacuum is used to complete elimination air and moisture in the stator insulation before the impregnation. This phase usually takes from 30 to 60 minutes. Next phase is called flooding. While keeping the vacuum in the autoclave resin is slowly supplied until an inserted stator is completely flooded. Length of this phase is limited by efficiency of VPI equipment. Next phase is called wet vacuum. This phase is used to complete elimination of air bubbles from resin and stator insulation. Phase usually takes 60 minutes. After that the process continues from vacuum to overpressure phase. Pressure is increased gradually until set value is reached. Length of this phase is given by efficiency of VPI equipment. Last phase is called keeping overpressure. Length of overpressure phase is set individually and depends on the

size of the inserted stator. It's the longest phase of the VPI process. After keeping overpressure resin is pumped back into the storage tank. Pressure in autoclave is decreased to atmospheric and autoclave is opened. Impregnated stator is placed in an oven and rotary cured.

The length of individual phases VPI process depends on the specific application. Usually is for the VPI process validation used method based on destructive tests. Destructive tests are very detailed. Complete stator is cut in small segments which are than deeply analyzed. Destructive tests are very time consuming and expensive.

We have tried to find an alternative method using non-destructive testing to validate optimized parameters of the VPI process. Watching capacitance during the VPI process gives us a basic overview of the quality of an impregnated stator. Thanks to this was possible to focus on each phase of the VPI process. Analysis of the time behaviour of capacitance can reveal possible reserve. Optimized parameters must be experimentally validated.

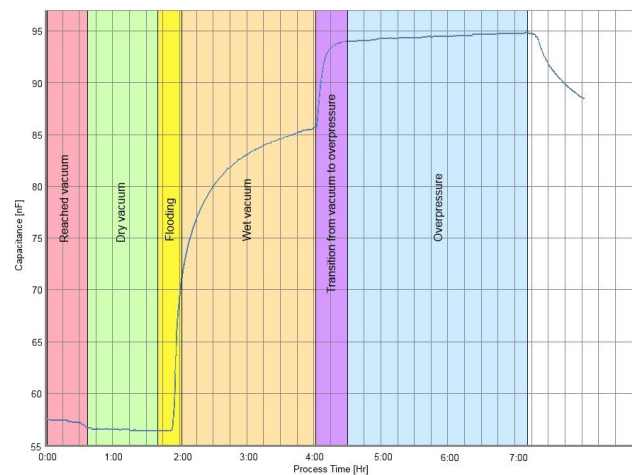


Fig. 1 Graph of capacitance during the VPI process

II. EXPERIMENT DESCRIPTION

Quality of impregnation evaluation is based at two measurement, capacitance and partial discharges. Comparison of partial discharge measurement of stators impregnated by standard and optimized process reveals possible change in quality of VPI.

Experiment was carried out on the stator with weight 2300 kg and output power 1280 kW. Insulation system is applicable for temperature class 200. For coil is used copper conductor wrapped by polyimide tape. For insulation is used mica tape with aramid fibres and glass cloth as carrier. In end winding is additionally used glass-polyester cover tape. The stator is impregnated by silicon resin.

Capacitance of stators typically reaches at the begin of process approximately 56 nF. On the end of process capacitance has approximately 95 nF. Time savings of VPI process is possible in dry vacuum and keeping overpressure phases only. Other phases (reached vacuum, flooding, wet vacuum and transition to overpressure) are limited by efficiency of VPI equipment or there isn't place to time savings.

Optimization was divided in to 2 steps. First step was to analyze capacitance data. We have looked at capacity behaviour of 18 stators and compared it to each other. Average values of capacitance and standard deviation are in tab. 1.

TAB. 1 COMPARISON OF CAPACITANCE

	After dry vacuum	After overpressure
\varnothing [nF]	55,83	95,05
δ [nF]	0,31	0,29

Average values of the capacitance of the wet vacuum and overpressure phases have standard deviation of 0.3 nF. Based on capacitance measurement we have decided to adjust process parameters in such way that capacitance value in these phases will not be changed more than one standard deviation.

Second step was determined the particular time savings from capacitance time behaviour. Typical time behaviour of capacitance during process is in fig. 1. At the end of the dry vacuum phase is value of capacitance more than 17 minutes constant and remain constant even in first 12 minutes of next phase (wet vacuum). This mean that phase of wet vacuum was finished with big time reserve. This phase was reduced by 15 minutes. Next possible reduction is in phase of overpressure. There is on the end of phase almost constant value of capacity. We had set that capacitance must not change more than 0.3 nF after finish of process. This capacitance value corresponds approximately to 60 minutes. Thanks to this optimizing in process we have reached reduction of 15 min in phase dry vacuum and 60 minutes in phase overpressure. Comparison between standard and optimized parameters is in tab. 2.

TAB. 2 COMPARISON OF PARAMETERS

	Dry vacuum	Overpressure
Standard parameters	1 h	3 h
Optimized parameters	45 min	2 h

III. USED METHODS

The experiment consists of two measurement methods. First method was measuring of capacitance during VPI process. We have used programmable automatic RLC meter Fluke PM6304. The instrument is connected directly to measured stator inside the autoclave. Capacitance is measured between winding and iron core and recorded from closing of autoclave until its opening. Data are recorded continually to a computer during the process. Results of measurement are saved as html file in which is possible to find exact values of capacity, pressure and temperature at any time.

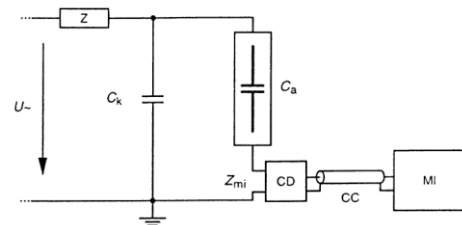


Fig. 2 Partial discharge measurement circuit [1]

Second method was measuring of partial discharge. We have used global method, which detects level of partial discharges across the measured object. This can roughly estimate the overall degree of impairment of the insulation system, creation of local defects or determine the type of discharge activity. [4]

Measuring circuit consists of detection impedance Z_{mi} , coupling capacitor C_a and detector CD. Diagram is in fig. 4.

The measured parameters were the inception voltage U_i , extinction voltage U_e , apparent charge Q_{iec} and average discharge current I . The inception voltage of partial discharge is voltage at which partial discharge in measured object we can detect first. The extinction voltage of partial discharge is voltage at which repetitive partial discharge in measured object don't already appear. The apparent charge, known as Q_{iec} is according to standard EN 60270 defined as the quantitative determination largest repeatedly occurring levels. Value Q_{iec} corresponds to peak value of the apparent charge sited with largest number of pulses. Average current of partial discharge is integral value, which is determined as the sum of the absolute values of the apparent charge Q_{iec} for a certain time interval. [2, 3]

Measurement was performed by Faculty of Electrical Engineering at University of West Bohemia by equipment from company Doble – Lemke. At first measured values were ignition and extinction voltage. After that we measured dependence of largest repeatedly occurring partial discharge magnitude (Q_{iec}) and average discharge current (I) on voltage. From 3 kV to 5 kV with step 0.5 kV and voltage was reached after 60 s.

IV. MEASUREMENT RESULTS

In experiment were measured 16 pieces of stator. 8 pieces (numbers 1 – 8) were impregnated by standard VPI process and 8 pieces (numbers 9 – 16) were impregnated by optimized VPI process. First was measured capacitance. Results are in fig. 3 and fig. 4. We were focused on values after dry vacuum and after overpressure phase.

Standard process average value of capacitance was after dry vacuum phase 55.93 nF and after overpressure phase 94.93 nF. We have reached average value in optimized process 55.81 nF after dry vacuum phase and 94.71 nF after overpressure phase. As you can see the conditions we have set were fulfilled. The difference of average values is lower than one standard deviation (0.3 nF).

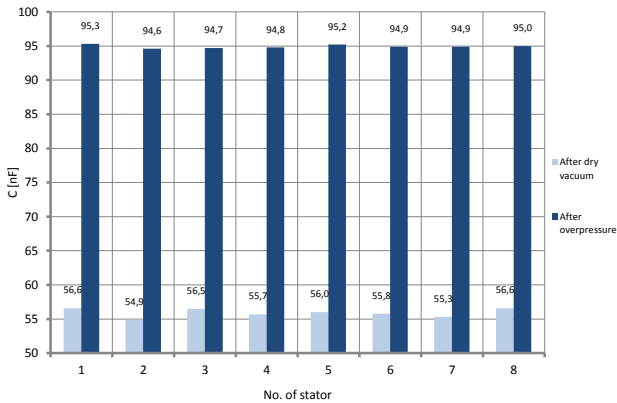


Fig. 3 Capacitance values (Standard VPI process)

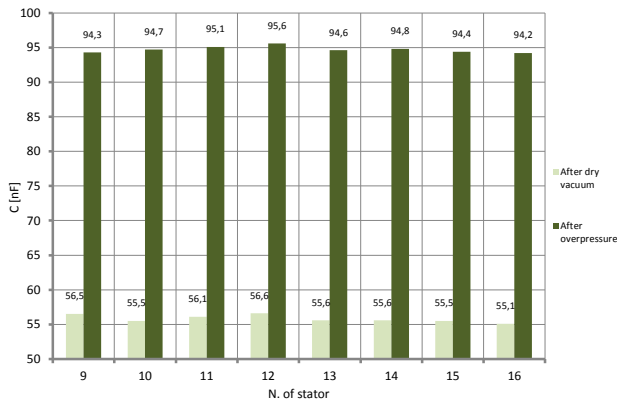


Fig. 4 Capacitance values (Optimized VPI process)

Second measurement was partial discharges. The measured values of inception and extinction voltage are in fig. 5 and fig. 6. Average value of inception voltage (U_i) was 2.18 kV in the standard process. Average value of extinction voltage (U_e) was 1.93 kV. Average values in the optimized process are lower – 1.98 kV and 1.73 kV. Measurement of partial discharge is very sensitive to various types of ambient noise and power supply quality. These influences can easily superpose to the measuring equipment. As you can see in fig. 5 stator number 7 and 8 we measured lower inception and extinction voltage than

at other stators. This effect could be caused by fact that measurement was performed in different day so conditions wasn't the same.

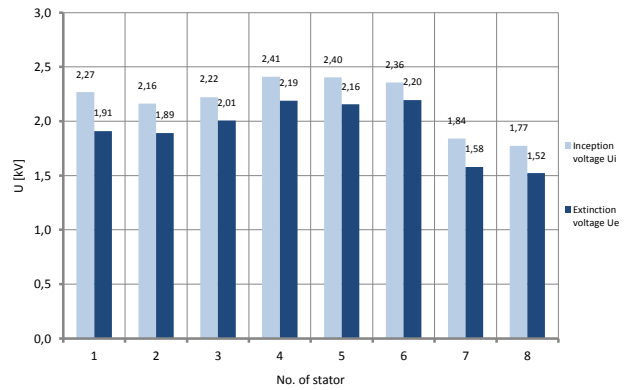


Fig. 5 Inception and extinction voltage (Standard VPI process)

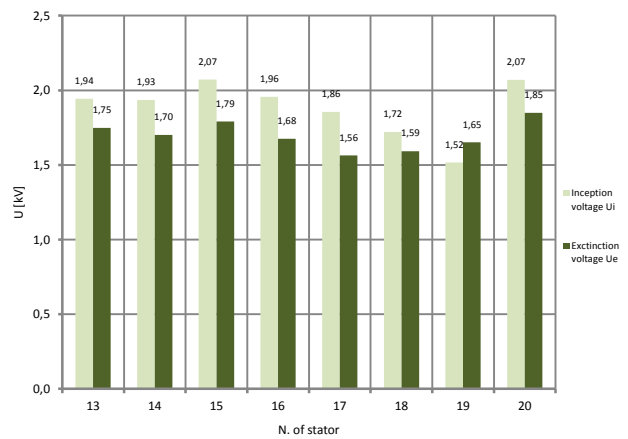


Fig. 6 Inception and extinction voltage (Optimized VPI process)

Next measured value was apparent charge Q_{iec} . According to EN 60270 this is the parameter on its basis are partial discharges evaluated. If we compared the level of Q_{iec} in fig. 7 (standard VPI process) and fig. 8 (optimized VPI process) it seems to be approximately the same. But thanks to the large variation of values it couldn't be precisely evaluated. A similar situation also occurs in the average current discharge (fig. 9 and 10).

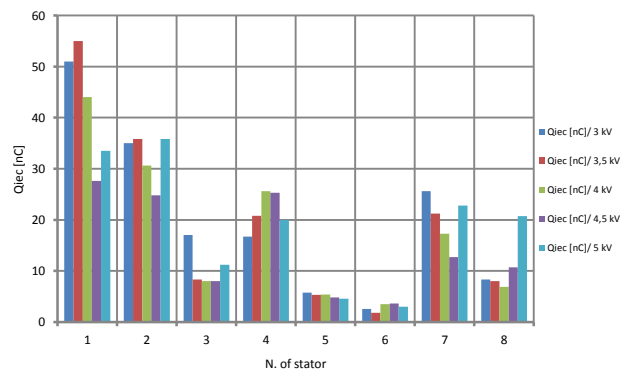


Fig. 7 Dependence apparent charge Q_{iec} on voltage (Standard VPI process)

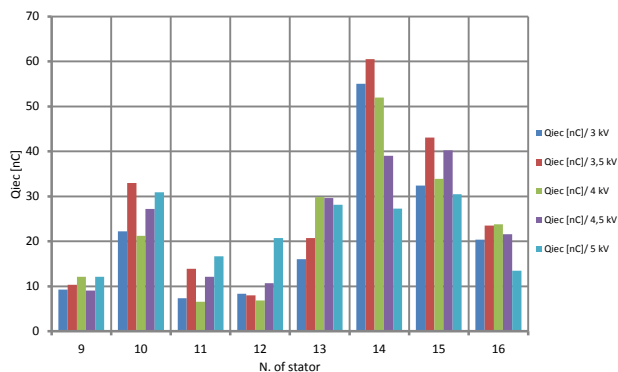


Fig. 8 Dependence apparent charge Q_{iec} on voltage (Optimized VPI process)

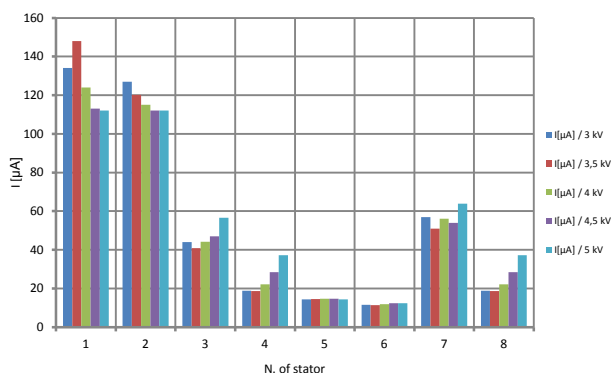


Fig. 9 Dependence average discharge current I on voltage (Standard VPI process)

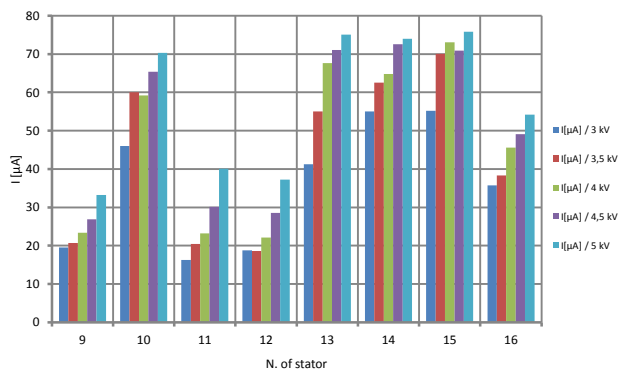


Fig. 10 Dependence average discharge current I on voltage (Optimized VPI process)

V. CONCLUSION

This experiment was designed to non-destructive verification of changes in our VPI process. In the first step was analyzed capacitance time behaviour of stators.

Values showed us that there are some time savings that could be optimized. In second step were designed optimized parameters of VPI process. Third step was to verify optimized process with using partial discharge measurement. We have compared discharge activity of stators impregnated by standard and optimized process. Measurement was carried out in cooperation with the Faculty of Electrical Engineering at University of West Bohemia.

The measured values of inception and extinction voltage seem to be decreased by about 0.3 kV between the standard and the optimized VPI process. It is a signal that optimized process could have an impact on the quality of impregnation. Unfortunately, a large variation in the values of apparent charge and average current partial discharges haven't demonstrated that optimized VPI process can reliably put into practice. We decided that we won't use optimized parameters. The measured data together with the behaviour of the stators in operation will be the subject of further research.

VI. REFERENCES

- [1] MENTLÍK, Václav, Josef PIHERA, PROSR a Pavel TRNKA. *Diagnostika elektrických zařízení*. Praha: BEN - technická literatura, 2008. ISBN 978-80-7300-232-9.
- [2] ČSN EN 60270. *Technika zkoušek vysokým napětím – Měření částečných výbojů*. Prosinec 2001. Praha: Český normalizační institut, 2001.
- [3] MRÁZ, Petr, Josef PIHERA a Václav MENTLÍK. *Partial discharge measurement - state of the art* [online]. Plzeň, 2012 [cit. 2013-05-09]. Dostupné z: http://home.zcu.cz/~pmraz/ELEN/ELEN_Mraz_Mentlik_Pihera.pdf. Příspěvek. FEL ZČU Plzeň
- [4] PRSKAVEC, Ing. Ladislav. *Částečné výboje ve strojích točivých: Výbojová činnost v zařízeních vn a vnn* [online]. Praha, 2002 [cit. 2013-05-10]. Dostupné z: http://poli.feld.cvut.cz/~xprskave/pdf/2002_06_PVCZ_Castecne_vyboje_ve_strojich_tocivych.pdf. Akademická práce. ČVUT.

DC Diagnostics of Solar Cell Parameters

O. Szabó², Milan Perný¹, J. Lelák¹, V. Šály¹, M. Váry¹, S. Flickyngerová², E. Vavrinský²

¹Institute of Power and Applied Electrical Engineering, Faculty of Electrical Engineering and Information Technology, Slovak University of Technology Bratislava, tel: +421 60291884, milan.perny@stuba.sk

²Institute of Electronics and Photonics, Faculty of Electrical Engineering and Information Technology, Slovak University of Technology Bratislava, tel: +421 902128844, ondro.szabo@gmail.com

Abstract— We present the automated measurement system developed in order to measure basic DC parameters of solar cells, particularly on definition of parasitic series and shunt resistances, in this paper. The system is based on the application of KEITHLEY 2440 and Oriel solar simulator class AAA. PC data acquisition and LabVIEW software is used. Various methods which use different calculating procedure and measurement under illumination or in the dark are applied.

Keywords— PV cell parameters; LabVIEW; parasitic resistances;

I. INTRODUCTION

The aim of this work is the development of measuring workplace designed for computerized measurement of DC parameters of photovoltaic (PV) cells. Basic PV parameters can be obtained directly from the I - V characteristics of illuminated solar cell. Parameters are: short-circuit current (I_{sc}), open circuit voltage (V_{oc}), current and voltage at maximum power (I_m , U_m), fill factor (FF) and efficiency (η). Other important parameters which reflected the quality of the solar cell, are parasitic resistances, i.e. series (R_s) and parallel resistance (R_{sh}). There are several methods for the calculation of parasitic resistances. These methods can be divided into procedures working with I - V characteristic measured in the dark or on illuminated solar cells or their combinations and using corresponding mathematical apparatus.

II. MEASURING WORKPLACE

Measuring workplace is designed so that the entire measurement process can be remotely controlled by a PC computer without affecting the source meter. Simple block diagram of workplace is shown in the Fig.1. Four-quadrant source meter Keithley 2440 is designed for precise I - V characteristics measurement of various semiconductor structures. Controlling software with data saving and different analysing algorithms for solar cell parameters was designed in graphical programming environment – LabVIEW. Additionally, the software includes several special methods to determining of series and parallel resistances. Solar simulator ORIEL class AAA was used for the measurement of illuminated photovoltaic cells. This simulator offers defined quality in spectral characteristics, reliability for reproducing of incident solar spectrum at the earth's surface and homogeneity of illuminated area.

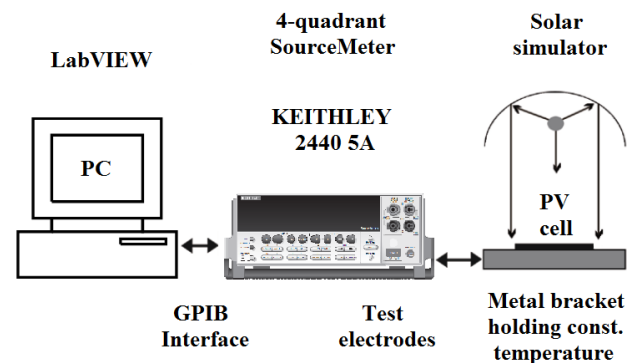


Fig. 1. Block diagram of PV workplace.

III. AUTOMATED MEASUREMENT CYCLE

Automated measurement cycle of illuminated PV cells using source meter offers advantage in more precise determination of I_{sc} . One of the quality indicators of photovoltaic cells is the fill factor (FF) which is equal to ratio of $P_m/V_{oc}I_{sc}$. Only a part of incident radiation is converted into electrical energy. Proportion of output power P_m of photovoltaic cell to light power P_{in} is called efficiency η . The measured I - V characteristic and P - V characteristic are shown in the Fig.2.

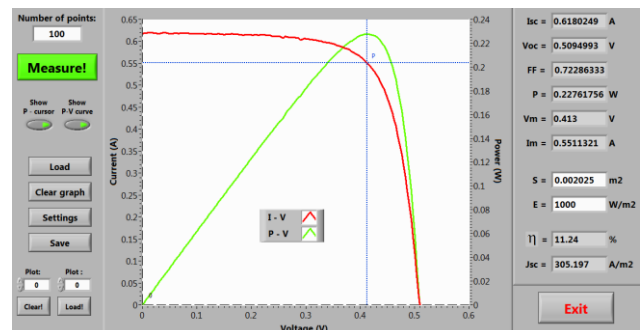


Fig. 2. Graphical user interface (GUI) with measured I - V and P - V characteristics.

IV. PARASITIC RESISTANCE MEASUREMENT METHODS

I - V CHARACTERISTICS MEASURED IN DARK

Roderick's method [1] determines the series resistance R_s using I - V characteristic measured in the dark, positively biased. The calculation is based on the fact that

for larger load in forward direction the influence of solar cell series resistance R_s must be taken into account. Shockley equation is then passed into the form

$$I = I_0 \left(e^{\frac{e(V-I.R_s)}{mkT}} - 1 \right) \quad (1)$$

The impact of the series resistance R_s is reflected in graphical dependence $InI = f(V)$ as a deviation from linear shape (Fig.3). The diode factor m and saturation current I_0 could be calculated from the straight line.

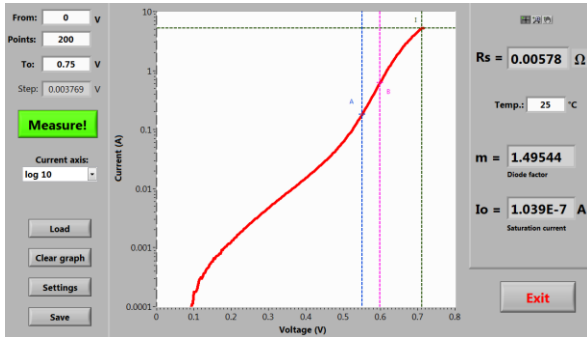


Fig. 3. Roderick's method [1] used for calculating of serial resistance R_s .

Parallel resistance R_{sh} , using method **Wolf's - Rauschenbusch's** [2], could be calculated from the reverse I-V characteristics measured in the dark. R_{sh} corresponds to slope of straight line set by points A and B (Fig. 4).

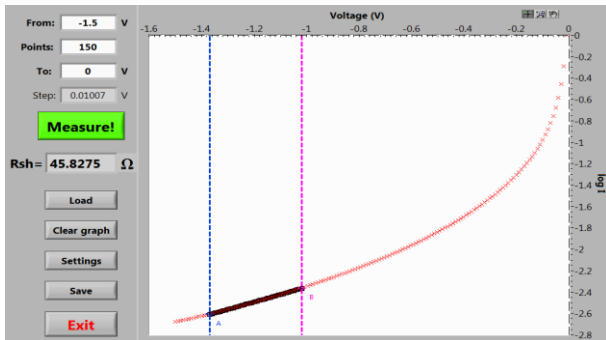


Fig. 4. Wolf's - Rauschenbusch's method [2] used for calculating of R_{sh} .

Cabestany's and Castaner's method [3] for calculating of series resistance R_s is based on measurement of two or more forward I-V characteristics obtained in dark. One measurement, in our case, is usually done without external resistor ($R_{ext1} = 0 \Omega$) while the second measurement includes the external resistor, (e.g. normal resistance $R_{ext2} = 0.1 \Omega$ in our case) connected to the solar cell in series. One should choose currents I_1 and I_2 at selected constant voltage V_a as shown in Fig. 5.

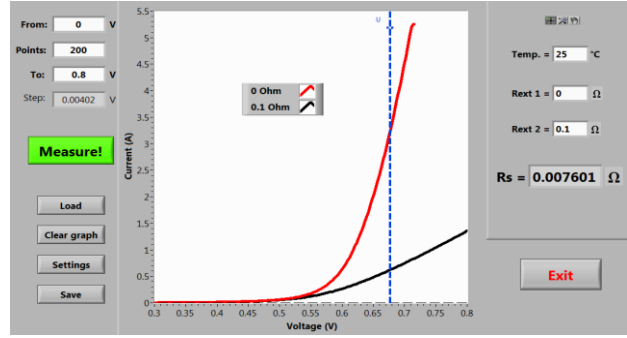


Fig. 5. Cabestany's and Castaner's method [3] used for calculating of serial resistance R_s .

Then the expression for R_s can be written in the form

$$R_s = \frac{\frac{kT}{e} \ln\left(\frac{I_2}{I_1}\right) + I_2 R_{ext2} - I_1 R_{ext1}}{I_1 - I_2} \quad (2)$$

ILLUMINATED I-V CHARACTERISTICS

Charles's et al. method [4] is numeric method for analysis of the I-V characteristics of PV cells at constant solar irradiation.

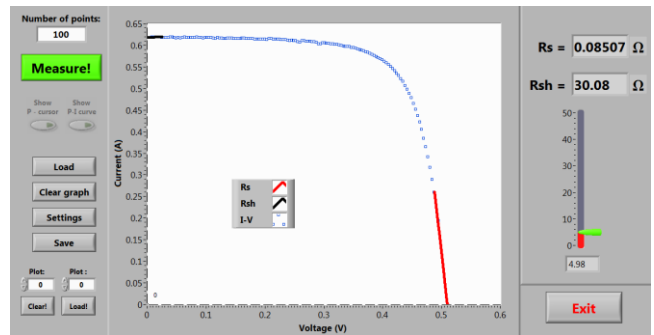


Fig. 6. Method of Charles's et al. [4] used for calculating of R_s and R_{sh} resistance.

This method can determine the series R_s and parallel R_{sh} resistance from the slope of tangent line at boundary points V_{oc} , I_{sc} (Fig. 6). Precise mathematical description goes beyond this contribution.

Wolf's - Rauschenbusch's method [2] calculates series resistance from at least two I-V characteristics measured at different light intensities. R_s is determined from the slope of the line passing through maximum power points.

Araujo's and Sanchez's method [5] is experimental method when the series resistance is calculated from the area (S) defined by the axes and the I-V characteristic. The calculation of the series resistance requires also knowing diode factor m which can be determined e.g. by using the Roderick's method [1] (Fig.3). Final equation for calculating the series resistance is

$$R_s = 2 \left(\frac{V_{oc}}{I_{sc}} - \frac{S}{I_{sc}^2} - \frac{mkT}{e} \frac{1}{I_{sc}} \right) \quad (3)$$

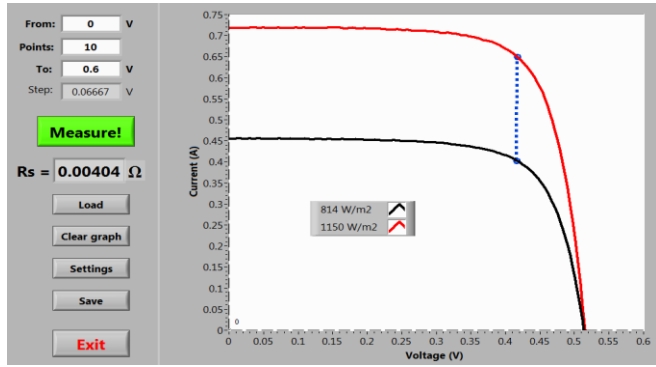


Fig. 7. Wolf's - Rauschenbusch's method [2] used for calculating of R_s .

Cape and Zehr [6] proposed a very simple approximate method for calculating the R_s from the basic PV parameters V_{oc} , I_{sc} , V_m and I_m . Calculation of the series resistance is defined as

$$R_s = \frac{V_{oc}}{I_{sc}} - \frac{V_m}{I_m} \quad (4)$$

COMBINED METHODS

Rajkanan's and Shewchun's method [7] for determining of series resistance R_s is based on measuring the illuminated I-V and forward dark I-V characteristics. Mathematical derivation and theoretical background of this method can be found in the relevant literature [7]. For calculating of R_s using this method, the measurement V_{oc} , I_{sc} at light conditions is required and the voltage V_d in the dark when current of the magnitude equal to I_{sc} flows through the cell.

$$R_s = \left(\frac{V_d - V_{oc}}{I_{sc}} \right) \quad (5)$$

V. EXPERIMENTAL RESULTS

A model calculation was carried out on crystalline silicon solar cells with the pn junction. Measured and calculated parameters are as follows: Solar cell area $S = 0.002025 \text{ m}^2$, irradiation intensity $E = 864 \text{ Wm}^{-2}$, diode factor: $m = 1.41$, saturation current $I_0 = 12.1 \text{ nA}$, efficiency $\eta = 14.78\%$, short current density $J_{sc} = 307.89 \text{ A} \cdot \text{m}^{-2} = 30.79 \text{ mA} \cdot \text{cm}^{-2}$, open-circuit voltage $V_{oc} = 0.586 \text{ V}$.

TABLE I. CALCULATED VALUES OF R_s .

Applied method	R_s (Ω)
Roderick [1]	0,0058
Cabestany - Castaner [3]	0,0076
Charles [4]	0,085
Wolf - Rauschenbach [2]	0,017
Araujo - Sanchez [5]	0,013
Cape - Zehr [6]	0,073
Rajkanan - Shewchun [7]	0,123

TABLE II. CALCULATED VALUES OF R_{sh}

Applied method	R_{sh} (Ω)
Wolf- Rauschenbach [2]	45,8
Charles [4]	30,1

VI. EFFECT OF TEMPERATURE

The output power of solar cells and the shape of the I-V characteristics are influenced by the temperature of the solar cells. The developed GUI application allows to display I-V characteristics obtained at different temperatures (with the temperature as a parameter). Increasing temperature reduces the width of the band gap of semiconductor. Slightly increase in short-circuit current occurs but significant decrease of the open circuit voltage is observable (shown in Fig. 8). Reduction of the maximum output power supplied by the cell at constant radiation intensity, and thus the reducing efficiency of photovoltaic energy conversion was observed with increasing temperature.

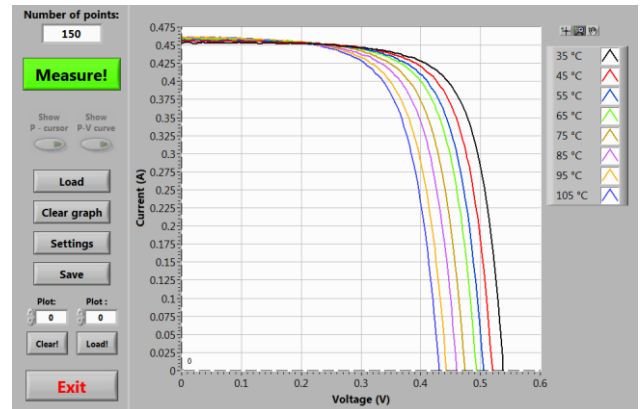


Fig. 8. Illuminated I-V characteristic measured at different temperatures.

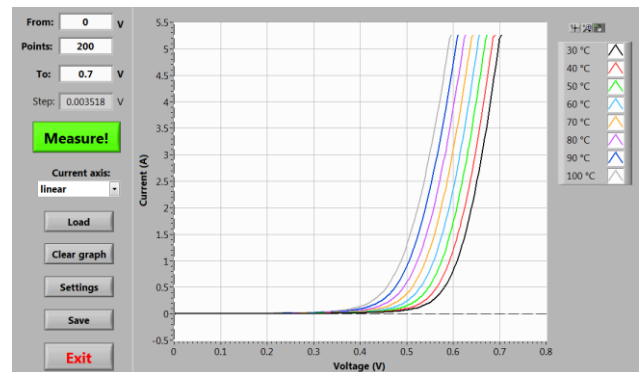


Fig. 9. Dark I-V forward characteristic measured at different temperatures.

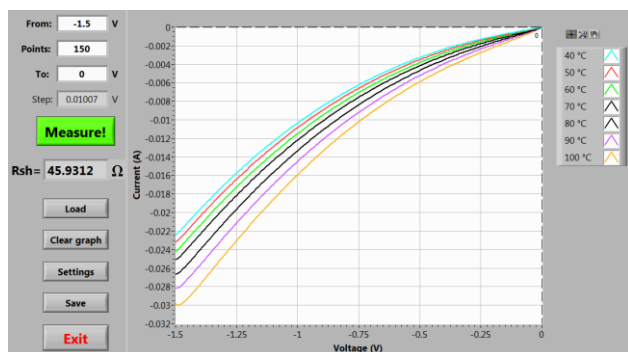


Fig. 10. Dark I-V reverse characteristic measured at different temperatures.

The slightly change of R_S value with temperature (within the temperature range 300-380 K) was observed in our case of Si cell with the basic semiconductor resistivity $1 \Omega \cdot \text{cm}$. Growth of parasitic series resistance R_S is influenced by the temperature resistance of the metallization which leads to a linear increase with temperature. Parallel resistance R_p decreases with increasing temperature [8].

VII. CONCLUSION

In conclusion we can say that by measuring of series and parallel resistances of solar cells we can obtain important information about their quality which can be used for next optimizing of the technology process. From the analysis of each method results that the most accurate method for determining of the R_s is Rajkanan - Shewchuna method [7], because this method calculates with non-linear characteristic of front layer surface and substrate resistance, therefore it is suitable especially for precise laboratory measurements. In contrast Cape's and Zehr's method [6] is very simple and is suitable especially for approximate calculating of R_s value. The aim of this

study was to provide an overview of the issues and propose Graphical User Interface (GUI) for PC control of the measuring device and the subsequent efficient processing of the measured data not only for laboratory use but also for educational purposes.

ACKNOWLEDGMENT

These publications are the result of implementation of the project: "Increase of Power Safety of the Slovak Republic" (ITMS: 26220220077) supported by the Research & Development Operational Programme funded by the ERDF.

REFERENCES

- [1] Rhoderick, E. H.: Metal – Semiconductor contacts. Oxford, Clarendon Press 1980, s. 7.
- [2] Wolf, M., Rauchenbach, H.: Series resistance effects on solar cell measurements. *Adv. Energy Conv.*, 3, 1963, s. 455.
- [3] Cabestany, J., Castaner, L.: A simple solar cell series resistance measurement method. *Rev. Phys. Appl.*, 18, 1983, s. 565.
- [4] Charles, J. P., a iní.: A practical method of analysis of the current – voltage characteristics of solar cells. *Solar Cells*, 4, 1981, str. 169.
- [5] Araujo, G. L., Sanchez, E.: A new method for experimental determination of the series resistance of a solar cell. *IEEE Trans. Electr. Dev.*, ED-29, 1982, č. 10, s.1511.
- [6] Cape, J. A., Zehr, S. W.: Effect of temperature variation in concentrator cell series resistance measurements. In: *Proc. 14th IEEE Photovoltaic Specialists Conference 1980*, s. 449.
- [7] Rajkanan, K., Shewchun, J.: A better approach to the evaluation of the series resistance of solar cells. *Solid State Electr.*, 22, 1979, s. 193.
- [8] Dušička, P., Hutňan, M., Jelemenský, E., Kolláth, E., Packa, J., Šály, V., Šulek, P.: *Obnoviteľné zdroje energie : Biomasa - slnko - voda*. - Pezinok : Renesans, s.r.o., 2011. - 304 s. - ISBN 978-80-89402-37-3

Department of Technologies and Measurement
On-line journal for electrotechnics and electronics

electr  **scope**

www.electroscope.zcu.cz

Executive redactors

doc. Ing. František Steiner, Ph.D.
and Ing. Josef Pihera, Ph.D.

**Journal is registered on the list of reviewed journals
published in the Czech Republic**

AUGUST 23-28 2015

University of West Bohemia in Pilsen, Czech Republic

ISH

19th International Symposium
on High Voltage Engineering

TOPICS OF INTEREST

1. Electromagnetic fields

computation, measurements, environmental effects

2. Transient voltages

lightning, switching, repetitive impulses, surge arrester, insulation coordination, overvoltage protection

3. High voltage and high current testing techniques

test procedure, evaluation

4. Advanced materials and insulation systems

outdoor, indoor, solid, liquid and gas insulated, nanodielectrics

5. Diagnostics and monitoring

partial discharges, evaluation procedures, knowledge rules, data mining, applications

6. HVDC technologies and applications

design problems, testing and measuring techniques

IMPORTANT DATES

Abstract Submission Deadline

November 30, 2014

Abstract Acceptance Notice

January 31, 2015

Full Paper Submission Deadline

April 15, 2015

Full Paper Acceptance Notice

May 15, 2015

Early Bird Registration Deadline

May 31, 2015



www.ish2015.org



Proceeding of the International Conference

Diagnostika '13

Conference on Diagnostics in Electrical Engineering CDEE 2013

Held in Parkhotel Pilsen, September 2 – 4, 2013

By DTM, FEE, UWB

Publisher: University of West Bohemia in Pilsen

All the papers were reviewed by conference advisory board. This publication was published using the manuscripts supplied by their authors. All mistakes in manuscripts there could be changed, nor could the English be checked completely. The readers are therefore asked to excuse any differences in this publication which may have arisen from the above causes.

Pilsen 2013

Editor: doc. Ing. Pavel Trnka, Ph.D.
Cover design: Václav Boček
Name: Diagnostika `13
Publisher: University of West Bohemia in Pilsen
Print: Tribun EU s.r.o., 2013
ISBN 978-80-261-0210-6